SEISMIC DESIGN OF REINFORCED CONCRETE BEAM-COLUMN JOINTS WITH FLOOR SLAB

A thesis

submitted in partial fulfilment

of the requirements for the Degree

of

Doctor of Philosophy in Civil Engineering

at the

University of Canterbury

by

(Patrick) Pak Chiu Cheung

University of Canterbury
Christchurch, New Zealand

1991

ABSTRACT

Beam-column joints are addressed in the context of current design procedures and performance criteria for reinforced concrete ductile frames subjected to large earthquake motions. Attention is drawn to the significant differences between the pertinent requirements of concrete design codes of New Zealand and the United States for such joints. The difference between codes stimulated researchers and structural engineers of the United States, New Zealand, Japan and China to undertake an international collaborative research project. The major investigators of the project selected issues and set guidelines for co-ordinated testing of joint specimens designed according to the codes of the countries. The tests conducted at the University of Canterbury, New Zealand, are reported. Three full-scale beam-column-slab joint assemblies were designed according to existing code requirements of NZS 3101:1982, representing an interior joint of a one-way frame, an interior joint of a two-way frame, and an exterior joint of a two-way frame. Quasi-static cyclic loading simulating severe earthquake actions was applied. The overall performance of each test assembly was found to be satisfactory in terms of stiffness, strength and ductility. The joint and column remained essentially undamaged while plastic hinges formed in the beams. The weak beam-strong column behaviour sought in the design, desirable in tall ductile frames designed for earthquake resistance, was therefore achieved. Using the laws of statics and test observations, the action and flow of forces from the slabs, beams and column to the joint cores are explored. The effects of bond performance and the seismic shear resistance of the joints, based on some postulated mechanisms, are examined. Implications of the test results on code specifications are discussed and design recomendations are made.

ACKNOWLEDGEMENTS

The research work reported in this thesis was carried out in the Department of Civil Engineering of the University of Canterbury, New Zealand, as part of the United States/New Zealand/Japan/China collaborative research project on the seismic design of reinforced concrete beam-column joints. Financial support from the following organisations in New Zealand is gratefully acknowledged : the Building Research Association of New Zealand, the Ministry of Works and Development, the University Grants Committee, the University of Canterbury, and the US/NZ Cooperative Science Programme. Pacific Steel Ltd, Auckland, kindly provided the steel reinforcement.

I wish to express my deepest gratitude to Professor T. Paulay and Professor R. Park under whose supervision this project was undertaken. Thanks are extended to the technical staff of the Civil Engineering Department, especially to Messrs N.J. Hickey and G.W. Sims for their valuable contributions to the experimental work. Messrs S.L.K. Pasa and A.M. Bell took part in the work on the first test unit. Other technical staff members provided assistance under the excellent management of Mr G.E. Hill. Also acknowledged are Mrs V.J. Grey for draughting work, Mr L.H. Gardner for photographic processing and Mrs D.L. Forbes for typing the manuscript.

Fellow postgraduate students and visitors from different countries have made life in the testing laboratories an enjoyable experience. Their help is also appreciated. I owe a great deal to Mr J. Restrepo for his assistance in the testing of the second unit and constructive discussions. Also thanks are due to Mr Dai Ruitong, Dr X. Zhao, Dr Pam Hoat Joen, Messrs L.L. Dodd and F. Yanez. Mr L.M. Meggett, a senior lecturer at the University of Auckland, gave some useful suggestions on the design of the loading rig.

Finally, I would like to thank my wife and my parents for their understanding, encouragement and support during the past years.

TABLE OF CONTENTS

NOTATION

(Symbols which are used in illustrations and tables and are self-explanatory may not be listed here.)

A_g	=	Gross area of column section
A_{jh}	=	Total area of effective horizontal joint shear reinforcement
A_{jv}	=	Total area of effective vertical joint shear reinforcement
A_s, A'_s	=	Area of tension and compression reinforcement respectively
A_{sc}	=	Area of reinforcement in one face of column
b_c	=	Overall width of column
b_e	=	Effective flange width of T or L beam
b_w	=	Width of beam web
c	=	Neutral axis depth in beam or column section
C_c, C'_c etc	=	Compression stress resultant in concrete
C_j	=	Joint shear participation factor = $V_{jh}/(V_{jx} + V_{jy})$
C_s, C'_s etc	=	Compression stress resultant in reinforcement
C_x, C'_x etc	=	Compression force in x-direction
C_y	=	Compression force in y-direction
D	=	Diagonal compression force
$D_1 \ldots D_7$	=	Observed horizontal movement of test column measured by dial gauges
d_b	=	Nominal diameter of reinforcing bar
D_c	=	Diagonal compression force resisted by concrete strut mechanism in joint core
d_m, d_n	=	Slip of beam bar inside joint core
D_s	=	Diagonal compression force resisted by truss mechanism in joint core
E_c	=	Modulus of elasticity of concrete, MPa
E_s	=	Modulus of elasticity of steel, MPa
f	=	Shape factor used in estimating shear deflection
f'_c	=	Compressive strength of concrete, MPa

f_r = Modulus of rupture of concrete, MPa

f_s, f'_s etc = Stress in reinforcing bar

f_{sx}, f_{sy}, f_{xx}, f_{xy} = Stress in slab bar

f_u = Ultimate strength of reinforcement, MPa

f_y = Yield strength of reinforcement, MPa

f_{yh} = Yield strength of horizontal joint reinforcement

f_{yv} = Yield strength of vertical joint reinforcement

$f_{y,o}$ = Estimated overstrength of reinforcement

$f_{y,m}$ = Measured yield strength of reinforcement

$h_1 \ldots h_5$ = Distance between potentiometers above beam and beneath beam

h_b = Depth of beam

h_c = Overall depth of column in the direction of horizontal shear to be considered

h'_c = Reduced depth of column

h_s = Thickness of floor slab

H_x = Horizontal shear force in x-direction

I_{cr} = Moment of inertia of cracked concrete section

I_e = Effective moment of inertia

I_g = Moment of inertia of uncracked gross concrete section

jd = Internal level arm between resultant forces

K_f = Ratio of steel compression force to total compression force

$K_{theoretical}$ = Computed stiffness of idealised elastic structure

K_{test} = Measured stiffness of test specimen

L' = Length of part of beam

ℓ_1, ℓ_2 = Shear span of beam from centreline of column

ℓ'_1, ℓ'_2 = Shear span of beam from column face

ℓ_j = Length of diagonal of an instrumented joint panel

ℓ_c = Storey height or height of column between points of support of test specimen

ℓ'_c	=	Clear height of upper or lower column from beam face of test specimen
M	=	Structural material factor
M_1, M_2	=	Bending moment at beam sections 1 and 2
M_a	=	Maximum moment in member at stage at which the deflection is being computed
m_A, m'_A etc	=	Bending moment in slab
M_{bz}	=	Bending moment in transverse beam at an interior joint about z-axis
M_{ci}	=	Ideal (nominal) flexural strength of a column section based on specified material properties
M_{code}	=	Column centre-line moment derived from code-specified lateral forces
M_{col}	=	Design moment at critical section of a column based on capacity design procedure
M_{cr}	=	Bending moment at first cracking
M_{des}	=	Design column moment for a test unit
M_{ez}	=	Bending moment in edge beam at an exterior joint about z-axis
M_i	=	Ideal (nominal) flexural strength of a beam section calculated using either specified or measured material properties of steel and concrete
M_i^*	=	Maximum ideal flexural strength considering contribution of all slab reinforcement parallel to the beam
M_{max}	=	Maximum column moment relevant to M_{des}, assuming beam and all slab reinforcement in tension having reached strain hardening
M_s	=	Bending moment in the plane of floor slab
M_{ty}	=	Torsional moment about y-axis
M_u	=	Dependable flexural strength of beam section, calculated as M_i multiplied by a strength reduction factor ϕ
n	=	Coefficient representing code restrictions on storey drift
p	=	Uniformly distributed vertical forces on a joint core
P_1, P_2	=	Vertical force applied at a beam end
P_e	=	Minimum design axial load in compression on column
P_i	=	Theoretical beam tip force based on ideal flexural strength of beam section

R_j	=	Reaction force inside joint core
$R_a \ldots R_d$	=	Distance between centre-line of a beam sub-region and beam tip force
r_s	=	Space ratio
S	=	Structural type factor
$S_1 \ldots S_5$	=	Distance of a pair of potentiometers from column face or adjacent pair
T, T'	=	Tension force in reinforcement (subscripted)
T_h	=	Tension force in hoop reinforcement
T_j	=	Tension force inside joint
T_s	=	Tension stress resultant in reinforcement
u_1, u_2 etc	=	Unit bond force
u_b	=	Average bond stress
u_{bo}	=	Average bond stress including overstrength of bar in tension
u_o, u_o'	=	Unit bond force including overstrength of bar in tension
V	=	Storey shear force
V_b	=	Vertical shear force in beam
V_c, V_c'	=	Horizontal shear force in column
V_{ch}	=	Horizontal joint shear strength assigned to concrete strut mechanism
V_{code}	=	Horizontal seismic force as specified by loadings code
V_{col}	=	Design shear force for column
V_{cv}, V_{cv}^*	=	Vertical joint shear strength assigned to concrete strut mechanism
$V_{dependable}$	=	Dependable storey shear strength of test specimen, calculated as V_i multiplied by a strength reduction factor ϕ
V_i	=	Ideal storey shear strength of test specimen calculated according to code design recommendations
V_i^*	=	Ideal storey shear strength of test specimen calculated assuming full participation of floor slab reinforcement in tension
$V_{i(test)}$	=	V_i based on measured material properties of steel and concrete

$V_{i(design)}$	=	V_i based on specified material properties of steel and concrete
V_{jh}	=	Horizontal shear force across a joint
v_{jh}	=	Nominal horizontal shear stress in a joint
V_{jv}	=	Vertical shear force across a joint
V_{jx}, V_{jy}	=	Horizontal joint shear force in x and y directions respectively
v_{jv}	=	Nominal vertical shear stress in a joint
V_s	=	Shear force in the plane of slab
v_s	=	shear flow
V_{sh}	=	Horizontal joint shear strength provided by horizontal joint shear reinforcement
V_{sv}	=	Vertical joint shear strength provided by vertical joint shear reinforcement
V_x	=	Shear force in x-direction
X, x	=	Horizontal displacement (subscripted)
z, z_1, z_2	=	Moment lever arm between compression and tension stress resultants in a beam
α	=	Inclination of potential failure plane in a joint core
α'	=	Inclination of reaction force in an exterior joint core
β	=	Area ratio of bottom to top reinforcement in beam
γ_1, γ_2	=	Joint shear strain
γ	=	Total joint shear strain
Δ	=	Displacement (subscripted) or prefix to defined symbol to indicate an increment in that quantity
Δ^*	=	Displacement observed when three-quarters of ideal strength is attained
Δ_1, Δ_2	=	Deformation of joint diagonal
Δ_{B1}, Δ_{B2}	=	Observed vertical displacement of beam end
Δ_c	=	Total horizontal displacement of test column
$\Delta_{c,b}$	=	Horizontal displacement of column from contribution of beam deformations

$\Delta_{c,c}$	=	Horizontal displacement of column resulting from contribution of column deformations
$\Delta_{c,j}$	=	Horizontal displacement of column resulting from contribution of joint shear distortion
Δ_e	=	Elastic displacement
ΔP	=	Additional vertical force applied at beam end due to tension flange action
ΔT_c, $\Delta T_c'$ etc	=	Bond force transmitted from reinforcement over certain length
Δ_x	=	Displacement in x-direction
Δ_y	=	Yield displacement
δ	=	Prefix to defined symbol to indicate an increment in that quantity
$\delta_{1,b}$, $\delta_{2,b}$	=	Vertical displacement of beam resulting from contribution of beam deformations
$\delta_{1,c}$, $\delta_{2,c}$	=	Vertical displacement of beam resulting from contribution of column deformations
$\delta_{1,j}$, $\delta_{2,j}$	=	Vertical displacement of beam resulting from contribution of joint shear distortion
δ_{cs}	=	Horizontal displacement of test specimen resulting from movement of loading rig
ϵ_1, ϵ_{g1} etc	=	Strain at location 1
ϵ_s	=	Strain in reinforcement
ϵ_y	=	Yield strain
Θ, Θ'	=	Angle of rotation
Θ^*	=	Angle of relative rotation
Θ_s, Θ_s'	=	Angle of in-plane distortion of slab panel
κ	=	Inclination of joint diagonal to the horizontal
$\theta_1 \ldots \theta_5$	=	Rotation of beam section
λ_o	=	Materials overstrength factor relevant to specified properties
$\lambda_{o,m}$	=	Materials overstrength factor relevant to measured properties
μ	=	Displacement ductility factor applicable to a test specimen
μ_Δ	=	Displacement ductility factor applicable to a structure
ν	=	Amplification factor to allow for inelastic deformations

ξ_b	=	Bond strength factor allowing for bi-directional seismic effect
ξ_m	=	Bond strength factor allowing for beam moment effect
ξ_p	=	Bond strength factor allowing for axial column load effect
ρ	=	Area ratio of top beam reinforcement
ρ'	=	Area ratio of bottom beam reinforcement
ρ_s	=	Area ratio of slab reinforcement
ρ_{sh}	=	Area ratio of horizontal joint reinforcement
ρ_t	=	Area ratio of total column longitudinal reinforcement
υ, υ_1, υ_2	=	Stress ratio applicable to beam bars
ϕ	=	Strength reduction factor
ϕ_o	=	Beam overstrength factor
$\psi_1 \cdots \psi_5$	=	Beam curvature
ψ_1^*	=	Beam curvature with correction
ψ_y	=	Yield curvature
ω	=	Dynamic moment magnification factor

REFERENCES

1. Park, R. and Paulay, T., "Reinforced Concrete Structures", John Wiley & Sons, New York, 1975, 769 pp.

2. CND/EERI, "El-Asnam, Algeria Earthquake of October 10, 1980", Reconnaissance and Engineering Report, Earthquake Engineering Research Institute, Berkeley, California, January 1983.

3. Sauter, F., "The San Salvador Earthquake of October 10, 1986 - Structural Aspects of Damage", Earthquake Spectra, Professional Journal of the Earthquake Engineering Research Institute, Vol.3, No.3, August 1987, pp. 563-584.

4. NZS 3101:1982, "Part 1: Code of Practice for the Design of Concrete Structure", 127 pp., and "Part 2: Commentary on the Design of Concrete Structures", 156 pp., Standards Association of New Zealand, Wellington, 1982.

   (Note: Amendment No.1 was issued in December 1989, but for the purposes of this report, reference is made to the 1982 edition.)

5. ACI Committee 318, "Building Code Requirements for Reinforced Concrete (ACI 318-83)", 111 pp., and "Commentary on Building Code Requirements for Reinforced Concrete", 155 pp., American Concrete Institute, Detroit, 1983.

   (Note: For the purposes of this report, reference is made to the 1983 edition. There are some minor changes in the 1989 edition, ACI 318-89 / ACI 318R-89, 353 pp.)

6. NZS 4203:1984, "Code of Practice for General Structural Design and Design Loadings for Buildings", Standards Association of New Zealand, Wellington, 1984, 100 pp.

7. Applied Technology Council, "Tentative Provisions for the Development of Seismic Regulations for Buildings", Publication ATC3-06, June 1978, 505 pp., (Special Publication 510, National Bureau of Standards, U.S. Department of Commerce, Washington D.C.).

8. ICBO, "Uniform Building Code", International Conference of Building Officials, Whittier, California, 1985 Edition, 817 pp.; 1988 Edition, 926 pp.

9. SEAOC, "Recommended Lateral Force Requirements and Tentative Commentary", Structural Engineers Association of California, San Francisco, 5th Edition, 1988, 200 pp.

10. Blume, J.A., Newmark, N.W. and Corning, L.H., "Design of Multistorey Reinforced Concrete Buildings for Earthquake Motions", Portland Cement Association, Chicago, 1961, 318 pp.

11. Paulay, T., "Development in the Design of Ductile Reinforced Concrete Frames", Bulletin of the New Zealand National Society for Earthquake Engineering, Vol.12, No.1, March 1979, pp. 35-48.

12. Park, R., "Ductile Design Approach for Reinforced Concrete Frames", Earthquake Spectra, Professional Journal of the Earthquake Engineering Research Institute, Vol.2, No.3, May 1986, pp. 565-619.

13. "CEB Model Code for Seismic Design of Concrete Structures", Bulletin d'Information, Comite Euro-International du Beton, No.165, April 1985, 58 pp.

14. "Papers Resulting from Deliberations of the Society's Discussion Group on Seismic Design of Ductile Moment Resisting Reinforced Concrete Frames", Bulletin of the New Zealand National Society for Earthquake Engineering, Vol.2, No.2, June 1977, pp. 69-105; Vol.10, No.4, December 1977, pp. 219-237; Vol.11, No.2, June 1978, pp. 121-128.

15. Paulay, T., "Deterministic Design Procedure for Ductile Frames in Seismic Areas", Reinforced Concrete Structure Subjected to Wind and Earthquake Forces, Special Publication SP-63, American Concrete Institute, Detroit, 1980, pp. 357-381.

16. Paulay, T., "Developments in the Seismic Design of Reinforced Concrete Frames in New Zealand", Canadian Journal of Civil Engineering, Vol.8, No.2, June 1981, pp. 91-113.

17. Paulay, T., Park, R., and Priestley, M.J.N., "Reinforced Concrete Beam-Column Joints under Seismic Actions", Journal of the American Concrete Institute, Vol.75, No.11, November 1978, pp. 585-593.

18. Paulay, T. and Park, R., "Joints in Reinforced Concrete Frames Designed for Earthquake Resistance", Research Report 84-9, Department of Civil Engineering, University of Canterbury, Christchurch, 1984, 71 pp.

19. Park, R., "Ductility Evaluation from Laboratory and Analytical Testing", State of the Art Report in Special Theme Session SG on Ductility Evaluation and Design of Concrete Structures and Elements, Proceedings of the 9th World Conference on Earthquake Engineering, Tokyo/Kyoto, 1988, Vol. VIII, pp. 605-616.

20. Bertero, V.V., "Ductility Based Structural Design", State of the Art Report in Special Theme Session SG on Ductility Evaluation and Design of Concrete Structures and Elements, Proceedings of 9th World Conference on Earthquake Engineering, Tokyo/Kyoto, 1988, Vol. VIII, pp. 673-686.

21. Priestley, M.J.N. and Park, R., "Strength and Ductility of Concrete Bridge Columns Under Seismic Loading", Structural Journal, American Concrete Institute, Vol.84, No.1, January-February 1987, pp. 61-76.

22. Popov, E.P., "Seismic Behaviour of Structural Subassemblages", Journal of the Structural Division, American Society of Civil Engineers, Vol.106, No.ST7, July 1980, pp. 1451-1474.

23. Kitayama, K., Otani, S. and Aoyama, H., "Earthquake Resistant Design Criteria for Reinforced Concrete Interior Beam-Column Joints", Proceedings of Pacific Conference on Earthquake Engineering, Wairakei, New Zealand, 1987, Vol.1, pp. 315-326.

24. 2/DZ 4203, "Second Draft for Comment, General Structural Design and Design Loadings for Buildings", Standards Association of New Zealand, Wellington, 1989.

25. Bertero, V.V., "Seismic Behaviour of Structural Concrete Linear Elements (Beams, Columns) and Their Connections", Bulletin d'Information, Comite Euro-International du Beton, No.131, April 1979, pp. 123-212.

26. Sattary-Javid, V. and Wight, J.K., "Earthquake Load on R/C Beams: Building versus Single Beam", Journal of Structural Engineering, American Society of Civil Engineers, Vol.112, No.7, July 1986, pp. 1493-1508.

27. Paulay, T. "A Critique of the Special Provisions for Seismic Design of the Building Code Requirements for Reinforced Concrete (ACI 318-83)", Journal of the American Concrete Institute, Vol.83, No.2, March-April 1986, pp. 274-283.

28. ACI-ASCE Committee 352, "Recommendations for Design of Beam-Column Joints in Monolithic Reinforced Concrete Structures", Journal of the American Concrete Institute, Vol.82, No.3, May-June 1985, pp. 266-283.

29. Park, R. and Milburn, J.R., "Comparison of Recent New Zealand and United States Seismic Design Provisions for Reinforced Concrete Beam-Column Joints and Test Results from Four Units Designed According to the New Zealand Code", Bulletin of the New Zealand National Society for Earthquake Engineering, Vol.16, No.1, March 1983, pp. 3-24.

30. Applied Technology Council, "Seismic Resistance of Reinforced Concrete Shear Walls and Frame Joints: Implications of Recent Research for Design Engineers", Publication ATC-11, 1983, 184 pp.

31. ACI Committee 318, "Building Code Requirements for Reinforced Concrete (ACI 318-77)", American Concrete Institute, Detroit, 1977, 102 pp.

32. ACI-ASCE Committee 352, "Recommendations for Design of Beam-Column Joints in Monolithic Reinforced Concrete Structures", Journal of the American Concrete Institute, Vol.73, No.7, July 1976, pp. 375-392.

33. Meinheit, D.F. and Jirsa, J.O., "The Shear Strength of Reinforced Concrete Beam-Column Joints", CESRL Report No.77-1, Department of Civil Engineering, University of Texas at Austin, Texas, January 1977, pp. 271.

34. "AIJ Standard for Structural Calculation of Reinforced Concrete Structures" (in Japanese), Architectural Institute of Japan, Tokyo, 1982.

35. "Design Guidelines for Earthquake Resistant Reinforced Concrete Buildings Based on Ultimate Strength Concept" (draft translated by S. Otani), Architectural Institute of Japan, Tokyo, 1988.

36. Hanson, N.W. and Connor, H.W., "Seismic Resistance of R.C. Beam-Column Joints", Journal of the Structural Division, American Society of Civil Engineers, Vol.93, No.ST5, October 1967, pp. 533-560.

37. Cook, D.R.L., "The Design and Detailing of Beam-Column Joints", Master of Engineering Report, Department of Civil Engineering, University of Canterbury, Christchurch, 1984, 284 pp.

38. Kurose, Y., "Recent Studies on Reinforced Concrete Beam-Column Joints in Japan", PMFSEL Report No.87-8, Department of Civil Engineering, The University of Texas at Austin, Texas, December 1987, 164 pp.

39. Beckingsale, C.W., Park, R., and Paulay, T., "Post Elastic Behaviour of Reinforced Concrete Beam-Column Joints", Research Report 80-20, Department of Civil Engineering, University of Canterbury, Christchurch, 1980, 359 pp.

40. Suzuki, N., Otani, S., and Aoyama, H., "The Effective Width of Slabs in Reinforced Concrete Structures", Transactions of the Japan Concrete Institute, Tokyo, Vol.5, 1983, pp. 309-316.

41. Suzuki, N., Otani, S. and Kobayashi, Y., "Three-Dimensional Beam-Column Subassemblage Under Bidirectional Loadings", Proceedings of 8th World Conference on Earthquake Engineering, San Francisco, 1984, Vol.VI, pp. 453-460.

42. Joglekar, M., Murry, P., Jirsa, J. and Klinger, R., "Full Scale Tests of Beam-Column Joints", Earthquake Effects on Reinforced Concrete Structures US-Japan Research, Special Publication SP-84, American Concrete Institute, Detroit, 1985, pp. 271-304.

43. Leon, R. and Jirsa, J.O., "Bidirectional Loading of R.C. Beam-Column Joints", Earthquake Spectra, Professional Journal of the Earthquake Engineering Research Institute, Vol.2, No.3, 1986, pp. 537-564.

44. Paultre, P., Castele, D., Rattray, S. and Mitchell, D., "Seismic Response of Reinforced Concrete Frame Subassemblages - A Canadian Perspective", Canadian Journal of Civil Engineering, Vol.16, No.5, October 1989, pp. 627-649.

45. Durrani, A.J. and Zerbe, H.E., "Seismic Resistance of R/C Exterior Connections With Floor Slab", Journal of Structural Engineering, American Society of Civil Engineers, Vol.113, No.8, August 1987, pp. 1850-1864.

46. French, C.W. and Boroojerdi, A., "Contribution of R/C Floor Slabs in Resisting Lateral Loads", Journal of Structural Engineering, American Society of Civil Engineers, Vol. 115, No.1, January 1989, pp. 1-18.

47. Ammerman, O.V. and French, C.W., "R/C Beam-Column-Slab Subassemblages Subjected to Lateral Loads", Journal of Structural Engineering, American Society of Civil Engineers, Vol.115, No.6, June 1989, pp. 1287-1308.

48. Yoshimura, M. and Kurose, Y., "Inelastic Behaviour of the Building", Earthquake Effects on Reinforced Concrete Structures US-Japan Research, Special Publication SP-84, American Concrete Institute, Detroit, 1985, pp. 163-201.

49. Dai, R. and Park R., "A Comparison of the Behaviour of Reinforced Concrete Beam-Column Joints Designed for Ductility and Limited Ductility", Research Report 87-4, Department of Civil Engineering, University of Canterbury, Christchurch, 1987, 65 pp.

50. Park, R. and Dai, Ruitong, "A Comparison of the Behaviour of Reinforced Concrete Beam-Column Joints Designed for Ductility and Limited Ductility", Bulletin of the New Zealand National Society for Earthquake Engineering, Vol.21, No.4, December 1988, pp. 255-278.

51. Leon, R.T., "Shear Strength and Hysteretic Behaviour of Interior Beam-Column Joints", Structural Journal, American Concrete Institute, Vol.87, No.1, January-February 1990, pp. 3-11.

52. Park, R. and Hopkins, D.C., "United States/New Zealand/Japan/China Collaborative Research Project on the Seismic Design of Reinforced Concrete Beam-Column-Slab Joints", Bulletin of the New Zealand National Society for Earthquake Engineering, Vol.22, No.2, June 1989, pp.122-126.

53. MacGregor, J.G., "Free Body Diagrams, Mechanical Models, and Experimental Evidence", Concrete International: Design and Construction, American Concrete Institute, Vol.11, No.6, June 1989, pp. 72-78.

54. Schlaich, J., Schaefer, K. and Jennewein, M., "Toward a Consistent Design of Reinforced Concrete Structures", Journal of the Prestressed Concrete Institute, Vol.32, No.3, May-June 1987, pp. 74-150.

55. Collins, M.P. and Mitchell D., "Shear and Torsion Design of Prestressed and Non-Prestressed Concrete Beam", Journal of the Prestressed Concrete Institute, Vol.25, No.5, September-October 1980, pp. 32-100.

56. ACI committee 318, "Building Code Requirements for Reinforced Concrete (ACI 318-56)", American Concrete Institute, Detroit, 1956.

57. Vecchio, F.J. and Collins, M.P., "The Modified Compression-Field Theory for Reinforced Concrete Elements Subjected to Shear", Journal of the American Concrete Institute, Vol.83, No.2, March-April 1986, pp. 219-231.

58. Collins M.P. and Mitchell, D., "A Rational Approach to Shear Design - The 1984 Canadian Code Provisions", Journal of the American Concrete Institute, Vol. 83, No.6, November-December 1986, pp. 925-933.

59. Paulay, T., "Equilibrium Criteria for Reinforced Concrete Beam-Column Joints", Structural Journal, American Concrete Institute, Vol.86, No.6, November-December 1989, pp. 635-643.

60. Popov, E.P., "Bond and Anchorage of Reinforcing Bars Under Cyclic Loading", Journal of the American Concrete Institute, Vol.81, No.4, July-August 1984, pp. 340-349.

61. Milburn, J.R. and Park, R., "Behaviour of Reinforced Concrete Beam-Column Joints Designed to NZS 3101", Research Report 82-7, Department of Civil Engineering, University of Canterbury, Christchurch, 1982, 107 pp.

62. ACI Committee 317, "Reinforced Concrete Design Handbook - Working Stress Method", Special Publication SP-3, American Concrete Institute, Detroit, 3rd Edition, 1965, 270 pp.

63. Soesianawati, M.T. and Park, R., "Flexural Strength and Ductility of Reinforced Concrete Columns with Various Quantities of Transverse Reinforcement", Proceedings of Pacific Conference on Earthquake Engineering, Wairakei, New Zealand, 1987, Vol.1, pp. 65-76.

64. Birss, G.R., Paulay, T. and Park, R., "The Elastic Behaviour of Earthquake Resistant Reinforced Concrete Interior Beam-Column Joints", Research Report 78-13, Department of Civil Engineering, University of Canterbury, Christchurch, 1987, 96 pp.

65. Paulay, T. and Scarpas, A., "The Behaviour of Exterior Beam-Column Joints", Bulletin of the New Zealand National Society for Earthquake Engineering, Vol.14, No.3, September 1981, pp. 131-144.

66. Collins, M.P. and Mitchell, D., "Prestressed Concrete Basic", Canadian Prestressed Concrete Institute, Ottawa, 1987, 614 pp.

CHAPTER 1

JOINTS UNDER SEISMIC ACTIONS

1.1 INTRODUCTION

It is only in recent years that the attention of structural engineers has been drawn to the critical role of beam-column joints in reinforced concrete frames designed for earthquake resistance [1]. Although engineers placed more emphasis traditionally on beams and columns, concern for joint failures is becoming more justified as a result of field observations reported on recent events, such as the El-Asnam earthquake[2] and the San Salvador earthquake [3]. While current concrete design codes in New Zealand [4] and the United States [5] contain provisions pertinent to the seismic design of beam-column joints, it is to be noted that some significant differences exist in the design approach and detailing requirements. The aim of this report is to examine the various issues regarding beam-column joints and to present additional experimental and analytical findings.

1.2 DESIGN CRITERIA

For building structures in seismic regions, the ductile design approach has been almost universally accepted as a rational solution to achieve economic and adequate seismic resistance. This is evident from the adoption of the design approach for ductility in various building codes [6,7,8,9]. With respect to reinforced concrete multistorey frames, the approach led to what is popularly known as the "strong column-weak beam" concept whereby plastic hinges are designed to form in the beams rather than the columns. The aim is to prevent plastic hinges forming in columns, so as to avoid adverse "soft-storey" mechanisms. The application to the design of reinforced concrete moment resisting frames has been well covered in the engineering literature [1,10,11,12] and detailed provisions have now been written into concrete design codes or standards [4,5,13]. In New Zealand a further step has been taken in which the use of a deterministic "capacity design" method [12,14,15,16] is recommended in the codes [4,6] to quantify the

design actions in structural members. Calculations additional to those routinely used are required.

Beam-column joints in moment resisting frames are usually subjected to large shear forces due to lateral earthquake forces. This is illustrated in Fig.1.1 for typical interior and exterior planar frame joints. The situation becomes critical under large cyclic reversals of earthquake actions, under which the joints are prone to extensive cracking. In the ductile design approach, inelastic lateral displacements are expected to take place. Adjacent beams develop their maximum possible flexural strengths, forming plastic hinges. Meanwhile the parts of the column above and below a joint should preferably remain elastic. Thus the primary attention must be focused on the capability of each joint in transmitting the necessary shear forces, both horizontally and vertically across the possibly cracked core of such a joint, without jeopardising the desired ductile response of the frame. Therefore the joint should be considered as an integral part of the column. Design criteria for joints in the seismic environment of New Zealand have been suggested some years ago [17,18] as follows :

(1) The strength of a joint should not be less than the maximum strength of the weakest member it connects. This is to eliminate the need for repair in a relatively inaccessible region, and to prevent significant energy dissipation by joint mechanisms which undergo strength and stiffness degradation when subjected to cyclic loading in the inelastic range.

(2) The capacity of a column should not be jeopardised by possible strength degradation within the joint due to cyclic inelastic displacements. The joint is an integral part of the column and therefore it should not be a prime souce of energy dissipation.

(3) During moderate seismic disturbances, a joint should preferably respond within the elastic range. Joint deformations should not significantly affect stiffness and hence storey drift.

(4) The joint reinforcement necessary to ensure satisfactory performance should not cause undue construction difficulties.

There is evidence that these suggestions are viewed with reservations by some researchers outside New Zealand.

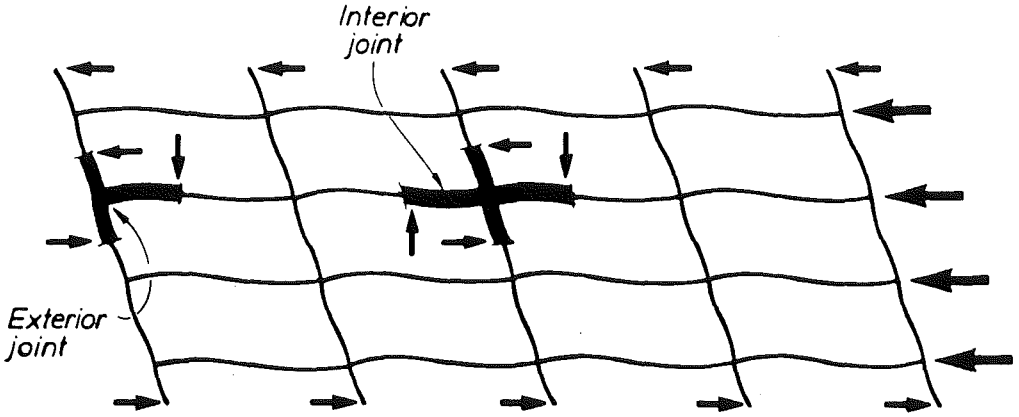

Fig.1.1 - Exterior and interior beam-column joint assemblies of a ductile moment resisting frame subjected to lateral forces

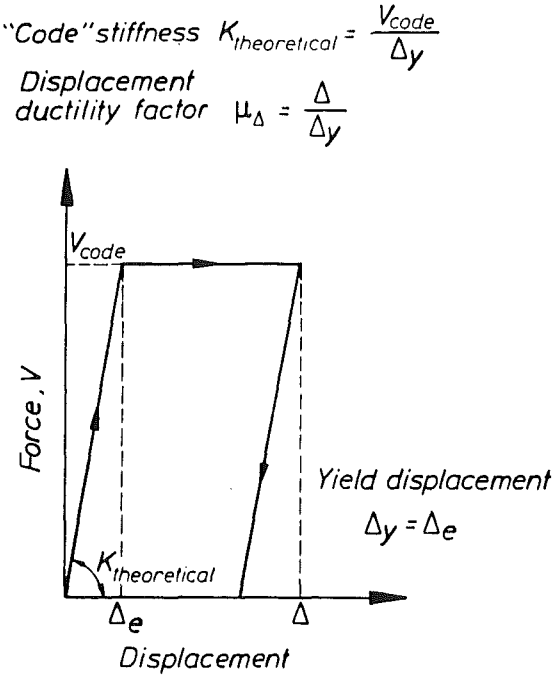

Fig.1.2 - Idealised force-displacement relationships for a bilinear elasto-plastic structure under code design seismic force

1.3 PERFORMANCE CRITERIA

1.3.1 General

The ductility demanded of a structure during earthquake actions is usually determined in terms of the magnitudes of inelastic deformations which may be expected. These magnitudes, when expressed in terms of ductility factors, are related to the stiffness of the structure in the elastic state, the strength of the structure and the severity of the earthquake.

A measure of the ability for plastic deformations is the displacement ductility factor, μ_Δ, which in this case is defined as the ratio of the maximum horizontal displacement, normally taken at the top of the structure, Δ, to the horizontal displacement at first yield, Δ_y, i.e.

$$\mu_\Delta = \frac{\Delta}{\Delta_y} \tag{1.1}$$

For fully ductile structures, seismic codes currently in use [6,7,8,9] imply generally a ductility factor ranging from five to seven. At maximum displacement, the development of a certain minimum strength (i.e. lateral force carrying capacity) is required.

An idealized bilinear perfectly elastoplastic response of a ductile structure under lateral forces, often used in design, is shown in Fig.1.2. In this case the displacement at yield, Δ_y, is well defined. In accord with the ductile approach, the yield displacement is identical to the maximum elastic displacement, Δ_e, of the structure when subjected to the action of the code design seismic force V_{code}. The displacement ductility factor of Eq.(1.1) is explained graphically in Fig.1.2. In corollary, the "code" stiffness, $K_{theoretical}$, is the computed elastic stiffness of the ideal structure. Stiffness criteria imposed by building codes are usually expressed by the interstorey limitations, generally known as drift limits. They are to be discussed in Section 1.3.2.

It is well accepted that the ideal response assumed above is in fact not attainable in a reinforced concrete structure. There are various reasons for this. For example, (a) plastic hinges may not form simultaneously in members of a structure, (b) longitudinal reinforcing bars at different depths

in the section of a member may yield at different load levels, and (c) cracking in members occurs progressively. A more realistic representation of the force-displacement response of reinforced concrete structures observed in laboratories is shown by the solid curved line in Fig.1.3. It is evident then that the definition of Δ_y is ambiguous. In fact various definitions have been adopted over the years by engineers and a need for "standardisation" has been voiced such as by Park [19] and Bertero [20].

To take into account the non-linearity of the elastic response, the usual approximation made in New Zealand [18,21] in the experimental determination of the yield displacement is to use the secant of the force-displacement relationship passing through the point when 75% of the ideal strength V_i of the test structure is attained. This is shown in Fig.1.3. Line OA is used to define the test structure's real stiffness K_{test}. This could then be compared with the estimated "code stiffness", $K_{theoretical}$, applicable to the ideal structure. The yield displacement, $\Delta_{y,test}$, for the test structure, is then determined by extending in Fig.1.3 this assumed linear response from A to B. This enables the displacement ductility factor μ for the test structure to be defined. The ideal strength, V_i, is based on the material properties measured at the time of testing and as calculated by traditional methods [1].

It may be argued that the above mentioned method of defining stiffness is arbitrary. However, this method is considered realistic, in that the stiffness is defined in terms of the post-cracking response of the test structure, which becomes relatively linear. It has been adopted over many years at research institutions in New Zealand [18,21]. It allows a practical evaluation of stiffness degradation in conjunction with ductility demand and also allows consistent comparison of different test results to be made.

A property that needs to be appreciated in the evaluation of structural earthquake resistance, is hysteretic response. This has been traditionally associated with the energy dissipation capacity of a structure by considering the shape of the force-deformation hysteresis loops [18,22]. Recent studies [19,23] suggest that some variations in hysteresis loop shape will not have a major influence on the inelastic dynamic response of a structure when subjected to severe earthquake excitation. That is, hysteresis loops showing some pinching or stiffness degradation caused by, for instance, inelastic deformations due to shear and bond mechanisms, will not necessarily

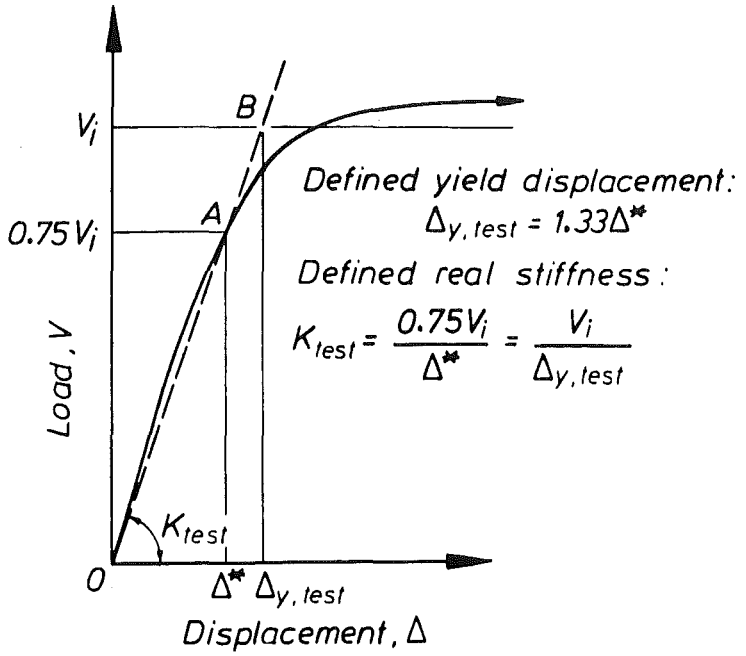

Fig.1.3 - Determination of yield displacement and stiffness for test structures

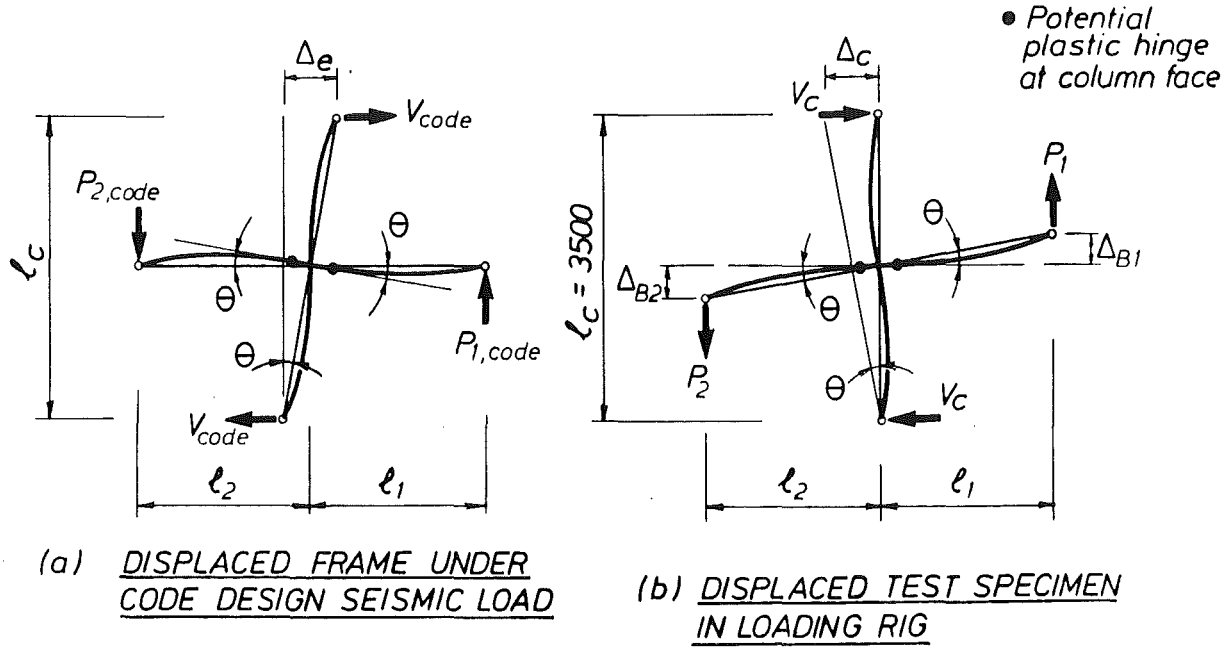

Fig.1.4 - Simulation of interior beam-column joint assembly by test specimen

lead to significantly larger inelastic displacements, providing that the structure has some damping of viscous type and is capable of some further damping by hysteretic energy dissipation. However the inelastic response of structures with a short fundamental period of vibration depends to a much larger extent on hysteretic energy dissipation. Thus the extent to which shear and bond mechanisms should be permitted to participate in the hysteretic behaviour is still a controversial matter. Furthermore there is no doubt that it is easier to repair damage occurring due to inelastic flexural deformations at a well detailed plastic hinge of a member than to repair damage resulting from inelastic shear and bond mechanisms.

1.3.2 Stiffness Criteria

As mentioned in Section 1.3.1, drift limits imposed by seismic requirements of building codes [6,7,8,9] can be interpreted in terms of interstorey displacements, Δ_e, calculated for the frame behaving elastically under code design seismic force V_{code}, shown in Fig.1.2 for an ideal bilinear elastoplastic structure. In Fig.1.4(a), a sub-frame is shown displaced laterally by an amount Δ_e due to the effect of V_{code}. Drift limits usually take the following form [6,7] :

$$\Delta_a = \nu\Delta_e \leq n\ell_c \tag{1.2}$$

where Δ_a = maximum allowable storey drift.

ν = amplification factor to allow for inelastic deformations, i.e. ductility demand with typical values of 1 to 6.5.

Δ_e = computed interstorey displacement for the elastic structure when subjected to the lateral seismic force used to determine the required strength of the components.

ℓ_c = storey height.

n = a coefficient principally to limit non-structural damage and hazard to occupants, typically 0.010 to 0.015 [7].

The above requirement implies that the storey drift calculated for the elastic multistorey frame, subjected to the lateral seismic design forces, in term of the percentage of the storey height, should be limited to

$$\frac{\Delta_e}{\ell_c}\,(\%) \leq \frac{100\ n}{\nu} \tag{1.3}$$

For code-designed frames, typical values for the storey drift given by Eq.(1.3) are in the range of 0.17 to 0.75%. The larger value is applicable to frames of limited ductility situated in areas of low seismic risk.

In New Zealand the current loadings code [6] specifies that for a fully ductile reinforced concrete frame, with non-structural elements having been separated, n = 0.01 and $\nu = 2/SM$, where S = structural type factor = 0.8, and M = materials factor = 0.8, so that $\nu = 3.13$. Hence the allowable interstorey drift of a structure behaving elastically subjected to code design forces is

$$\frac{\Delta_e}{\ell_c} \leq 0.32\%$$

This criterion controls the minimum acceptable stiffness for the structure under consideration. This code limit, currently under review, is compared to those set by other codes [7,8,9] as listed in Table 1.1.

A current draft revision of the New Zealand code [24] suggests that the maximum interstorey horizontal deflection in the severe seismic limit state should not exceed 3% of the interstorey height, unless it can be shown that greater drift can be tolerated by both structural and non-structural elements without causing danger to life. A fully ductile structure is assumed to be associated with a maximum displacement ductility factor of $\mu_\Delta = 6$. Hence for a storey in which $\mu_\Delta = 6$ the elastic stiffness limitation, using the assumptions of Section 1.3.1, becomes :

$$\frac{\Delta_e}{\ell_c} = \frac{3\%}{6} = 0.5\%$$

It is evident that this increased maximum drift limit would relax the current stiffness restriction. This matter is still currently under review by the code committee.

Table 1.1 - Code interstorey drift limitations for ductile reinforced concrete frames

	NZS 4203(1984)[6]	ATC 3-06 (1978)[7]			UBC(1985)[8]	UBC(1988)[8] & SEAOC (1988)[9]	
		Group I	Group II	Group III		h_t < 19.8m T < 0.7 sec	h_t > 19.8 m T > 0.7 sec
n	0.01	0.015	0.015	0.010	0.005	0.04	0.03
v	$\frac{2}{SM} = \frac{2}{(0.8)(0.8)} = 3.13$	$C_d = 6$			$\frac{1}{K} = \frac{1}{0.67} = 1.49$	$R_w = 12$	
Δ_e / ℓ_c	0.32%	0.25%	0.25%	0.17%	0.34%	0.33%	0.25%

Note : Symbols used are adopted directly from the text or pertinent codes

- n = a coefficient, when multiplied by the storey height, to give the allowable storey drift
- C_d = deflection amplification factor
- h_t = total height of building frame
- K = horizontal force factor
- ℓ_c = storey height
- M = structural material factor
- R_w = reduction factor used in determining seismic design base shear
- S = structural type factor
- T = fundamental elastic period of vibration, in seconds
- Δ_e = interstorey lateral deflection calculated for the elastic structure under design seismic forces
- v = amplification factor

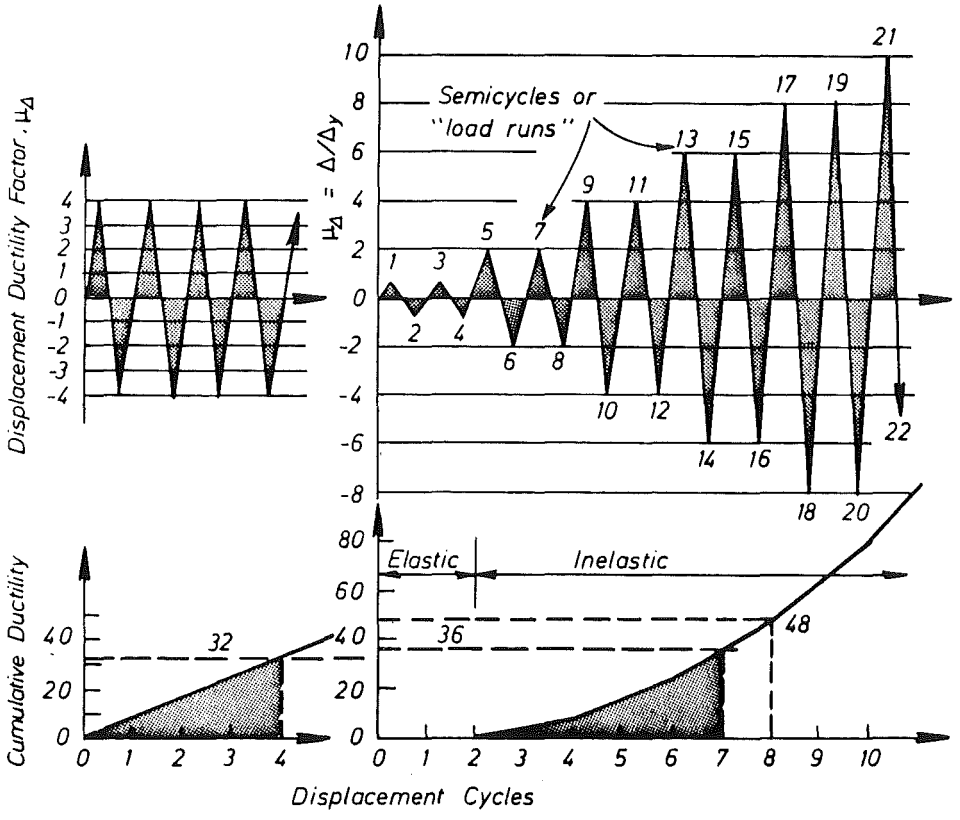

Fig.1.5 - Displacement criteria for assessing performance under simulated seismic actions in New Zealand

1.3.3 Criteria for Adequate Ductility

As stated before, structural systems intended to dissipate seismic energy by flexural yielding are required to have adequate ductility. Specified ductility factors, as shown in Fig.1.2, do not describe a force-displacement relationship, which would affect the structures' ability to dissipate energy, nor the effects of repeated reversing cyclic displacement. To clarify the intents with specified values of ductility factors, a performance test, based largely on engineering judgement, has been in use in New Zealand. According to the current New Zealand loadings code [6] a ductile structure should be able to undergo four cycles of loading to a displacement ductility factor of four in each direction, implying a cumulative displacement ductility factor demand of $\Sigma\mu = 32$. Furthermore, after those four cycles, the reduction in strength of any individual component should not exceed 30%, while that of the whole structure should not exceed 20%.

The draft replacement code [24] proposes that this criterion should apply to any structure, using the envisaged maximum ductility factor assigned to that type of structure. Hence ductile moment resisting reinforced concrete frames should be capable of undergoing four cycles of lateral loadings to a displacement ductility factor of six in each direction without the load carrying capacity reducing by more than 20%. The implied cumulative displacement ductility demand becomes $\Sigma\mu = 48$.

Figure 1.5 shows two simplified displacement histories commonly used in New Zealand for assessing structural performance of test models under quasi-static cyclic loading in a laboratory. The pattern shown in Fig.1.5(a) conforms with the current code [6] recommendations. The alternative displacement history in Fig.1.5(b) has become popular because more useful information can be extracted while moderate ductility demands are imposed. It is seen that the current NZS 4203 [6] demand is exceeded in cycle 7 while that of the proposed replacement code [24] specification is attained in cycle 8.

In seeking suitable displacement criteria it should be borne in mind that displacement cycles so selected cannot realistically follow the response of a structure to an actual major earthquake. For example, short period structures will be subjected to larger number of cycles of seismic deformation during a severe earthquake than long period structures. Instead, a relatively simple displacement criterion is sought which loads the structure to

reasonable displacement levels in the inelastic range for a number of cycles to enable an assessment to be made as to whether the performance of the structure is likely to be satisfactory during a major earthquake.

1.3.4 Performance Criteria for Isolated Test Specimens

The advantages and disadvantages associated with testing of complete full-scale structures as opposed to individual structural members have been discussed [25]. Laboratory testing of structural elements and assemblies, under quasi-static cyclic loading following simplified displacement histories similar to those described in Section 1.3.3, is still considered to be a very efficient experimental research procedure. An isolated test specimen (Fig.1.4(b)) is normally considered to be representative of a subassembly of a structure. Hence the performance observed may be consistently related directly to that of the prototype structure from which the test specimen is extracted [19,22]. It is often assumed, as for example in code specifications for storey drift limits, that inelastic displacements throughout the structure are constant multiples of the displacements obtained from elastic analyses. This can lead sometimes to significant underestimates of ductility demands on components. This is because the deformed shape of the plastified structure can be significantly different from that of the elastic system. Fig.1.6 illustrates the example of a frame, developed as a complete plastic mechanism. It is seen that plastic hinge rotations at the lower floors can be larger than what would be indicated by an overall displacement ductility factor that is expressed in terms of the lateral deflection at roof level. An analytical study [26] suggests that specimens simulating the behaviour of beams at different locations within a building should undergo different displacement histories. In the assessment of the performance of joints, such possible increases in local ductility demands should also be borne in mind.

In Fig.1.4, an interior beam-column joint test assembly is shown simulating a prototype building frame under seismic actions. It is assumed that the flexural strengths of the beam sections at both sides of the column develop simultaneously while undergoing equal rotations. It follows then that the yield displacement of the test specimen, $\Delta_{y,test}$ should also satisfy the intents of the storey drift limits expressed in Eq.(1.3). In New Zealand environment [6], this becomes

$$\Delta_{y,test} = \Delta_e \leq 0.0032\ell_c \qquad (1.4a)$$

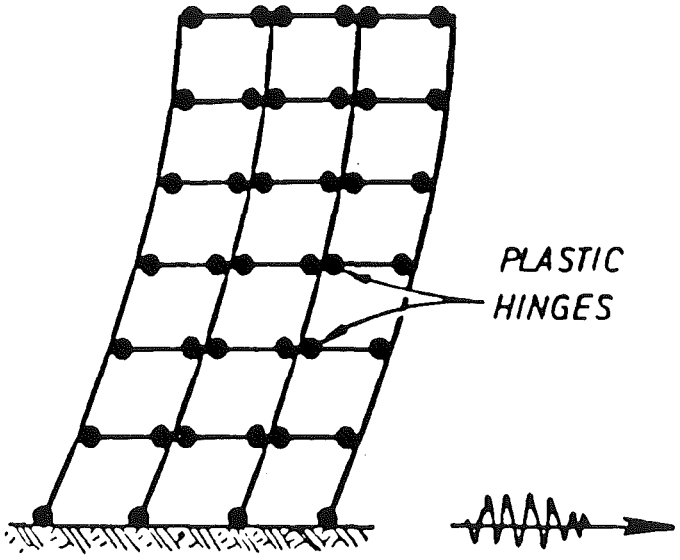

Fig.1.6 - The deflected shape of an inelastic frame under earthquake attack

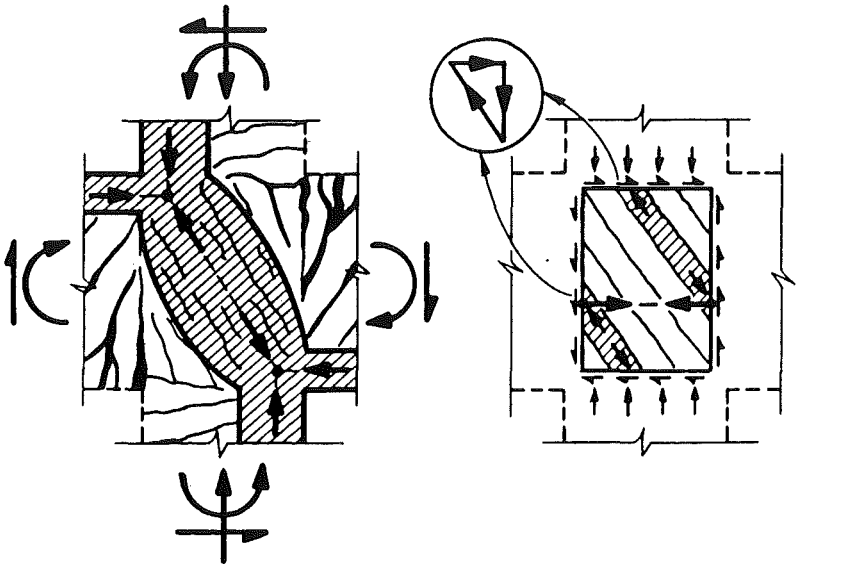

Fig.1.7 - Fundamental mechanisms of shear transfer in an interior beam-column joint

Eq.(1.4a) corresponds to the case when the dependable strength, $V_{dependable}$, based on specified material properties, is attained to resist code level force, V_{code}. This dependable strength is related to the theoretical ideal strength based on specified material properties in design, $V_{i(design)}$, by a strength reduction factor $\phi = 0.9$ [6]. That is

$$V_{dependable} = 0.9\ V_{i(design)} \qquad (1.5a)$$

However, the ideal strength of the test assembly, $V_{i(test)}$, based on measured material properties, is usually used to determine $\Delta_{y,test}$. Consequently the stiffness requirements should be adjusted by the ratio

$$\frac{V_{i(test)}}{V_{dependable}} = \frac{V_{i(test)}}{0.9\ V_{i(design)}} \qquad (1.5b)$$

The limiting interstorey deflection, relevant to the behaviour of the prototype frame subjected to code lateral forces, as inferred from the test assembly, should then be

$$\Delta_{e,test} = \frac{\Delta_{y,test}}{V_{i(test)} / 0.9\ V_{i(design)}} \leq 0.0032\ell_c \qquad (1.4b)$$

The yield displacement of the isolated test specimen, $\Delta_{y,test}$, can be determined according to the method suggested in Section 1.3.1 and Fig.1.3. The quasi-static cyclic load histories can then follow those recommended in Section 1.3.3.

1.4 CODE PROVISIONS

The current New Zealand concrete design code NZS 3101:1982 [4] devotes a full chapter to the design and detailing of beam-column joints. The formulation of design procedure for seismic effects was based on considerations of two mechanisms, postulated to explain the resistance of shear forces in joint cores [1,17]. As Fig.1.7 shows, one mechanism transfers shear forces via a diagonal concrete strut, while the other mechanism consists of a diagonal compression field which necessitates joint shear reinforcement. Fig.1.7(b) is also known as truss mechanism. Unless the axial compression on the column is large, the truss mechanism, enabling large bond forces to be

transmitted within the joint, was considered more effective. Consequently, according to this code a considerable amount of transverse reinforcement is required in joint cores. The proposed CEB Model Code [13] has similar requirements. For convenient reference, the relevant design provisions of NZS 3101 [4] are summarised in Appendix A.

In the major seismic codes [5,7,8,9] of North America, however, significantly different provisions have been made for the design of beam-column joints. The ACI 318 code [5] has been widely accepted as the reference for other codes with respect to structural design in concrete. The differences between seismic provisions for joints of NZS 3101 [4] and ACI 318 [5] have been discussed on several occasions [12,18,29].

The formulation of the ACI requirements was largely based on successive recommendations of ACI-ASCE Committee 352 on Joints and Connections in Monolithic Concrete Structures. Its latest report on beam-column joints appeared in 1985 [28]. Comparisons of NZS 3101 [4] with earlier ACI-ASCE 352 draft reports have also been made [18,29]. A project undertaken by the Applied Technology Council of the United States has resulted in another report, ATC-11 [30]. In the ATC report, past and current provisions of ACI 318 and ACI-ASCE 352 are compared with those of NZS 3101. Detailed comparisons are therefore not repeated in this report.

In summary, the NZS 3101 provisions are based on a rational model considering the contributions from concrete and joint reinforcement according to two mechanisms as shown in Fig.1.7. Earlier editions of ACI 318 (1977) [31] and ACI-ASCE 352 (1976) [32] took a similar but more simplistic approach. However, current ACI 318 [5] and ACI-ASCE 352 [28] recommendations have adopted a fundamentally different approach. This is based on the simple assumption that a joint can carry a specified maximum horizontal shear stress if the concrete within the joint core is adequately confined. It emphasises the presumed role of confinement by transverse reinforcement and beams that frame into a joint. It ignores the issue of controlling diagonal tension and mechanisms of shear transfer across the joint. Provided the specified maximum horizontal shear stress in the joint core is not exceeded, only the amount of transverse reinforcement, in form of hoops or ties, to satisfy confining requirements for adjacent columns needs to be placed in the joint. This procedure, based on empirical evidence [33], that joint shear strength is not

sensitive to joint core shear reinforcement is still open to debate as will become evident in Chapter 2.

There were no explicit code requirements for the joint design in Japan [34]. Reinforced concrete buildings in Japan have been traditionally designed to have very large earthquake resistance. This normally resulted in large size columns. Damage to the joint regions was scarcely observed in past earthquakes. However, with the gradual adoption of ductile design approach, some design guidelines [23,35] are being formulated. These appear to follow an approach similar to that of ACI 318 and ACI-ASCE 352.

1.5 LITERATURE REVIEW

The first study on beam-column joints was published in 1967 [36]. Since then research and laboratory testing have been carried out at various countries, particularly in North America, Japan and New Zealand. Results and interpretations by engineers led to the successive formulation of code recommendations referred to in Section 1.4. Apart from the background information given in the commentaries to NZS 3101 [4], and ACI-ASCE 352 [28], a thorough critical review was provided by Paulay and Park [18] and Cook [37] mainly in terms of New Zealand's performance criteria. A project undertaken by ATC [30] resulted in more than fifty technical papers and research reports having been summarised. In 1987, Kurose [38] made an extensive survey of related work done in Japan. However, it is difficult to make direct comparison of test results when the tests involve different load histories and different definitions of reference stiffness.

The majority of the earlier experiments were on joints of planar frames. Some tests involved unloaded transverse beams. However the results from these were not considered further in New Zealand in view of the skew earthquake actions to be taken into account. Beckingsale [39] found that the performance of space frame test unit was inferior to that of planar frame unit. Recent tests [40-47] began to include the effects of cast-in-place floor slab to more realistically simulate building frame responses. In a US-Japan cooperative research programme on earthquake engineering, a full scale seven-storey building structure was tested [48]. It was found that the measured base shear of the building under one-way loading was 50% higher than that theoretically estimated. It can be concluded from these tests that a

considerable part of the floor slab acted together with the longitudinal beams. However, little progress had been made with respect to theoretical aspects of the mechanisms of floor slabs and joint behaviour. Some attempts have been made by Paulay and Park [18] and Cook [37]. This topic will be dealt with in Chapter 7. Amongst others, studies of anchorage requirements of beam bars in interior joints and related tests have been carried out by Kitayama et al [23], Dai and Park [49,50] and Leon [51].

1.6 INTERNATIONAL COLLABORATIVE RESEARCH PROJECT

In view of the significant differences between the concrete design codes of New Zealand [4] and the United States [5,28] with respect to the seismic design of beam-column joints, a collaborative research project, to address the problem, was initiated by the University of Canterbury and the University of Texas at Austin. Subsequently a number of research engineers from New Zealand, the United States, Japan and China contributed to the project. The first two meetings were held in California in July 1984 and in Tokyo in May 1985, respectively, and issues regarding design philosophy and detailing requirements were raised and discussed. It was then agreed that the principal investigators from each country would undertake space frame beam-column joint tests. The design of the test specimens were to be according to the country's current concrete design code requirements. To enable comparisons of test results to be made, guidelines on the general dimensions of specimens and loading histories were agreed to by consensus. The third meeting was held in Christchurch in August 1987 and the fourth (final) one in Hawaii in May 1989. Details on the meetings have been reported in New Zealand by Park and Hopkins [52]. Research papers presented at the meetings will be published in a Special Publication Volume by the American Concrete Institute.

This thesis summarises the tests of three full-scale beam-column-slab joint assemblies, conducted in the structures laboratory of the Department of Civil Engineering, University of Canterbury, Christchurch, New Zealand, from 1986 to 1988. With the exception of one test unit by Beckingsale [39], previous studies in New Zealand considered beam-column joint assemblies of planar frames. The effects of transverse beams and floor slabs have not been investigated previously in New Zealand.

CHAPTER 2

DEVELOPMENTS IN BEHAVIOURAL MODELS OF JOINTS

2.1 INTRODUCTION

In the early days of the development of design procedures in reinforced concrete, many design rules, for example for shear, were formulated based on empirical conclusions drawn from the observed results of test specimens. As a result, such empirical rules had to be restricted to the narrow range of parameters studied. Inexperienced design engineers could possibly apply these rules to situations for which they are not applicable. Unless the engineer possesses a thorough understanding of structural behaviour and of the reasons for possibly unsatisfactory response, a rational design cannot be made in situations which are outside the range simulated in those experiments. For this reason, designs based on rational models have been advocated from time to time [53,54,55].

A rational and general, yet very simple, strength design procedure for members subjected to flexure with or without axial load was established over thirty years ago [1,56]. Recently, as a consequence of significant advances in the understanding of the mechanisms involved in developing the shear strength of reinforced concrete members [55,57], it became possible to replace the traditional collection of empirical equations for shear design by rational procedures based on clear, simple and verifiable principles [58]. For the design of beam-column joints, simple but rational procedures have been developed in New Zealand [4] and adopted in Europe [13]. However, code provisions for beam-column joints in North America [5,28] still rely on an empirical approach.

To assist in obtaining a better understanding of the behaviour of beam-column joints in ductile frames designed for earthquake resistance, this chapter is devoted to a study of behavioural models. An explanation of the mechanisms of shear and bond resistance in joints is offered. Rational models, using elementary laws of statics, are emphasised throughout. For convenience in illustration, an interior joint of a typical planar frame under

lateral seismic actions is taken as example. However, the principles can be readily extended to exterior joints.

2.2 EQUILIBRIUM CRITERIA

Under the horizontal earthquake actions, moments and shear forces are generated in the beams and columns of a building frame (Fig.1.1). These members in turn introduce internal stress resultants to joint cores, as shown in Fig.2.1, resulting in horizontal and vertical shear forces across the joints. The symbols for stresses and stress resultants are readily identified in Fig.2.1 and further details are given in the list of symbols. Within an uncracked joint core, internal diagonal tensile and compressive stresses, shown as f_t and f_c, are generated. Diagonal cracking of the core concrete may follow. Unless adequate resistance is provided, it is inevitable that diagonal cracking will eventually cause joint failure, usually along a corner to corner failure plane.

Consider the external and internal actions at a typical interior joint of a planar frame (Fig.2.1(b)). For simplicity, axial loads on the columns and beams are omitted. The ductile design approach implies that plastic hinges form in the framing beams, generally at the column faces. When this condition is reached, the horizontal shear force V_{jh} across the mid-depth of the joint core is

$$V_{jh} = T_1 + C_{c2} + C_{s2} - V'_c = T_2 + C_{c1} + C_{s1} - V''_c \qquad (2.1)$$

whereas the vertical joint shear force V_{jv} is

$$V_{jv} = T' + C''_c + C''_s - V_{b1} = T'' + C'_c + C'_s - V_{b2} \qquad (2.2a)$$

In the case of the common multilayered arrangement of column reinforcement, the derivation of the vertical stress resultants is more cumbersome. By taking into account the distances between the various stress resultants and the member dimensions, the following approximation for design purposes is allowed in New Zealand [4]

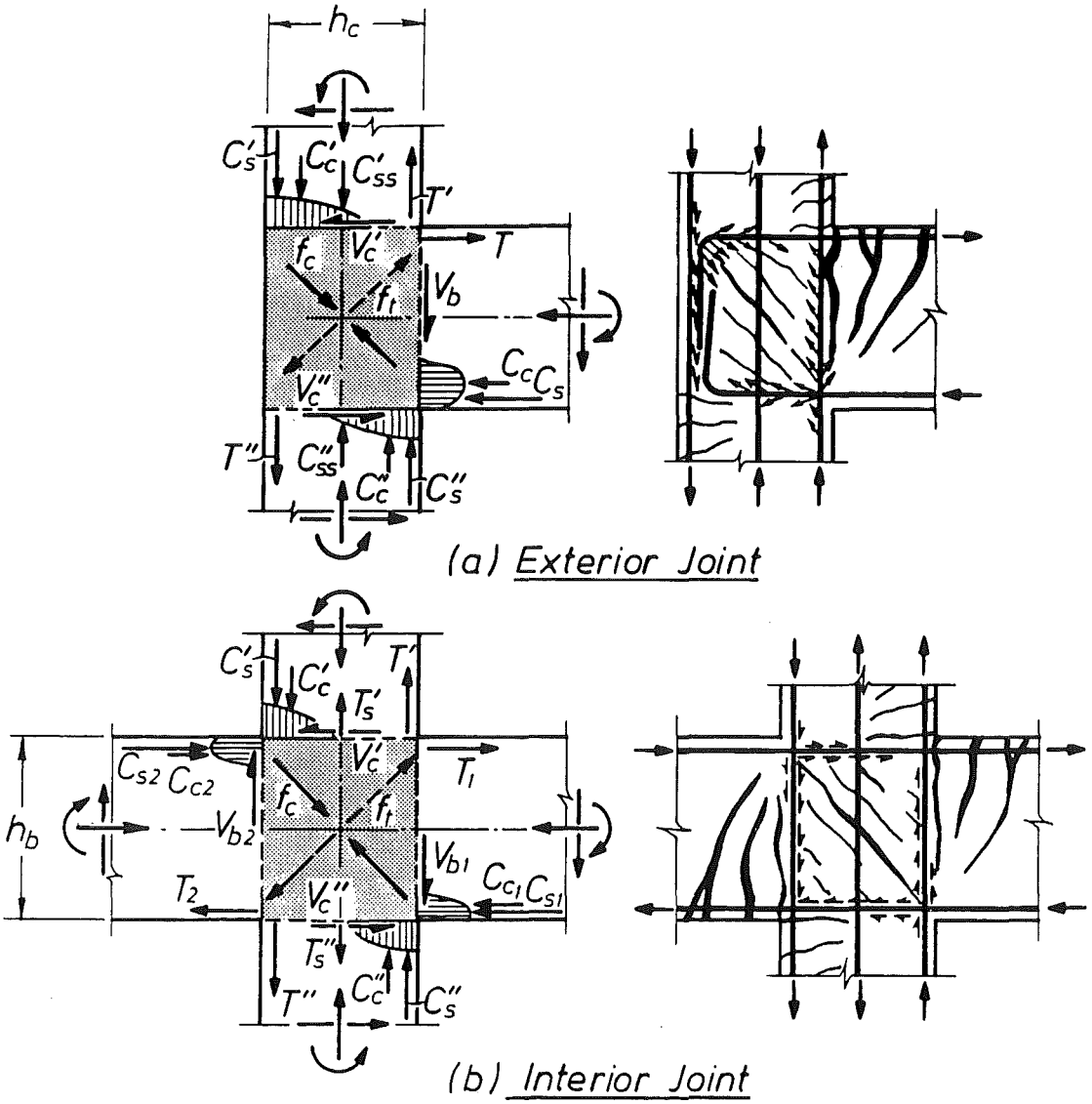

Fig.2.1 - Forces acting on beam-column joints under seismic actions

$$V_{jv} \approx V_{jh} \frac{h_b}{h_c} \tag{2.2b}$$

where h_b and h_c are the beam and column depths respectively.

For building frames with a regular layout, usually the beam shear forces as well as the column shear forces at the opposite sides of a joint core are similar. For this case it may be assumed that

$$V_{b1} = V_{b2} = V_b$$

and $$V'_c = V''_c = V_{col}$$

Then it is evident that Eq.(2.1) can be written as

$$V_{jh} = T_1 + T_2 - V_{col} \tag{2.3}$$

The joint shear forces for such a case are shown in Fig.2.2(a) with external forces identical to those in Fig.2.1(b). Actions at an exterior joint (Fig.2.1(a)) can be similarly considered, except that only one beam exists.

As mentioned in Section 1.4, two principal mechanisms (Fig. 1.7) to transfer shear forces in beam-column joints have been postulated. They will be reviewed in Section 2.3. To illustrate the need for these mechanisms, equilibrium considerations have been recently used by Paulay [59] to facilitate understanding of joint behaviour. From established principles of shear in diagonally cracked concrete, the phenomenon of "tension shift" [1] is used to explain the existence of tensile forces in the bars inside a joint core which is dominated by seismic actions. In the example interior joint core (Fig.2.2(a)), from elementary laws of statics the equilibrium of the beam-joint free body (Fig.2.2(b)) requires that the horizontal joint shear force must be equal to the sum of the horizontal tension forces, ΣT, generated in the beam bars and in the horizontal ties in the core [59]. In this model, it is assumed that the beam and column shear forces at the opposite sides of the joint core are identical and in equilibrium. Similarly it can be demonstrated that, in the absence of axial load on the column, the vertical joint shear force is equal to the total tensile forces generated in the vertical bars.

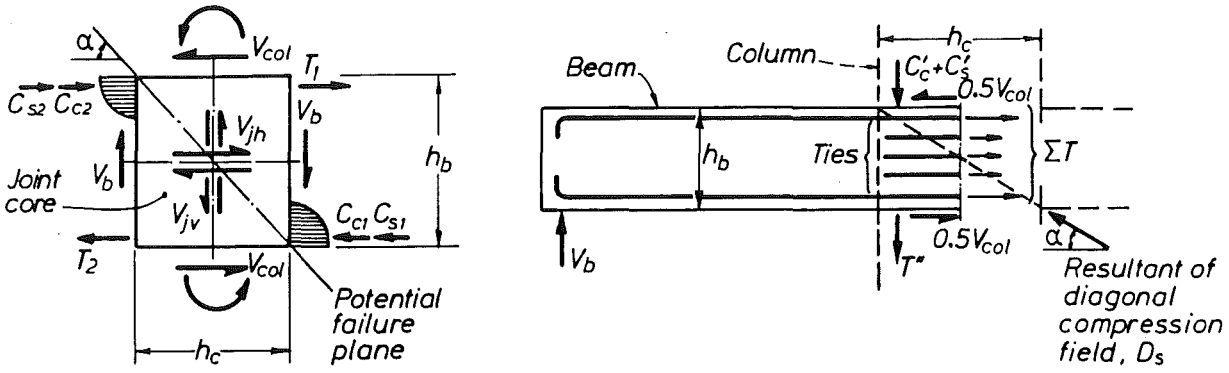

Fig.2.2 - Equilibrium criteria for an interior joint core

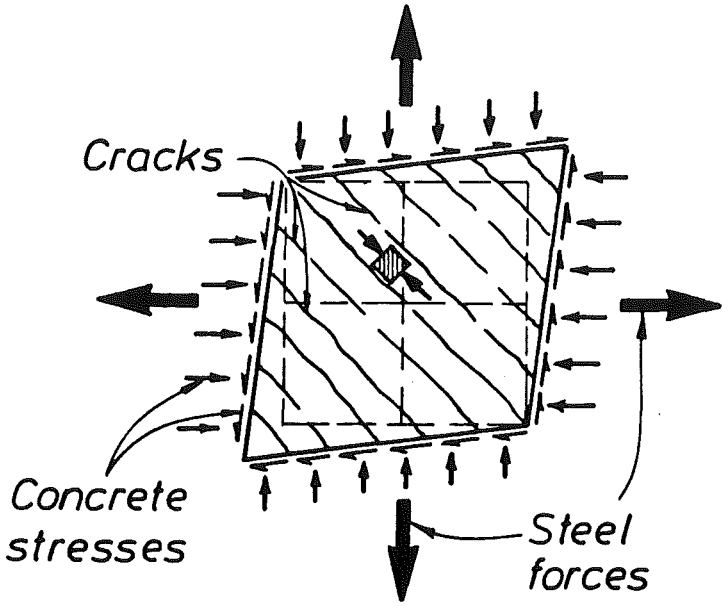

Fig.2.3 - Diagonal compression field induced by shear deformations in a diagonally cracked core of a beam-column joint [59]

Consideration of shear deformations (Fig.2.3) shows that shear stresses applied to the boundaries of a joint core can be transferred by means of a diagonal compression field. In comparison to the tensile strains in the reinforcement, diagonal concrete compression strains are generally negligible. Hence, as Fig.2.3 suggests, there is a tendency for the joint core to dilate as seismic actions continue.

2.3 SHEAR RESISTING MECHANISMS

2.3.1 Review of Strut and Truss Mechanisms

In a joint core, isolated as a free body (Fig.2.2(a)), external forces from the beams and columns must be resisted within the joint core. The external and internal forces at a typical interior joint are redrawn in Figs.2.4(a) and (b). Two principal mechanisms of shear resistance have been postulated [1,17] and further examined [18,29]. Some essential points are re-stated here for completeness of the discussion.

The first mechanism consists of the contribution of concrete compression and shear forces around the joint. A diagonal concrete strut (Fig.2.4(c)) sustaining a compressive force D_c, is assumed to be inclined at an angle and close to that of the potential diagonal failure plane (see also Fig.2.2). The diagonal force is mobilised primarily by concrete compression forces (denoted by C_c with superscripts in Fig.2.4(c)) at two corners. Forces labelled as ΔT_c (with superscripts) are bond forces transmitted from the reinforcement approximately over lengths within the shaded area. The strength of this mechanism, sustaining the diagonal force D_c, is sometimes referred to as the "shear carried by the concrete". The conventional notation V_{ch} and V_{cv} is used to represent the horizontal and vertical joint shear resistances respectively.

The second mechanism consists essentially of the contribution of the vertical and horizontal reinforcement inside the joint core. In Fig.2.4(d), V_{sh} and V_{sv} are horizontal and vertical forces transferred by bond from the beam and column bars. Primarily these bond forces are assumed to be transmitted to the core concrete mainly outside the diagonal concrete compression zones of Fig.2.4(c). In Fig.2.4(d) these forces are idealised as uniformly distributed shear flow. Despite extensive cracking in the joint

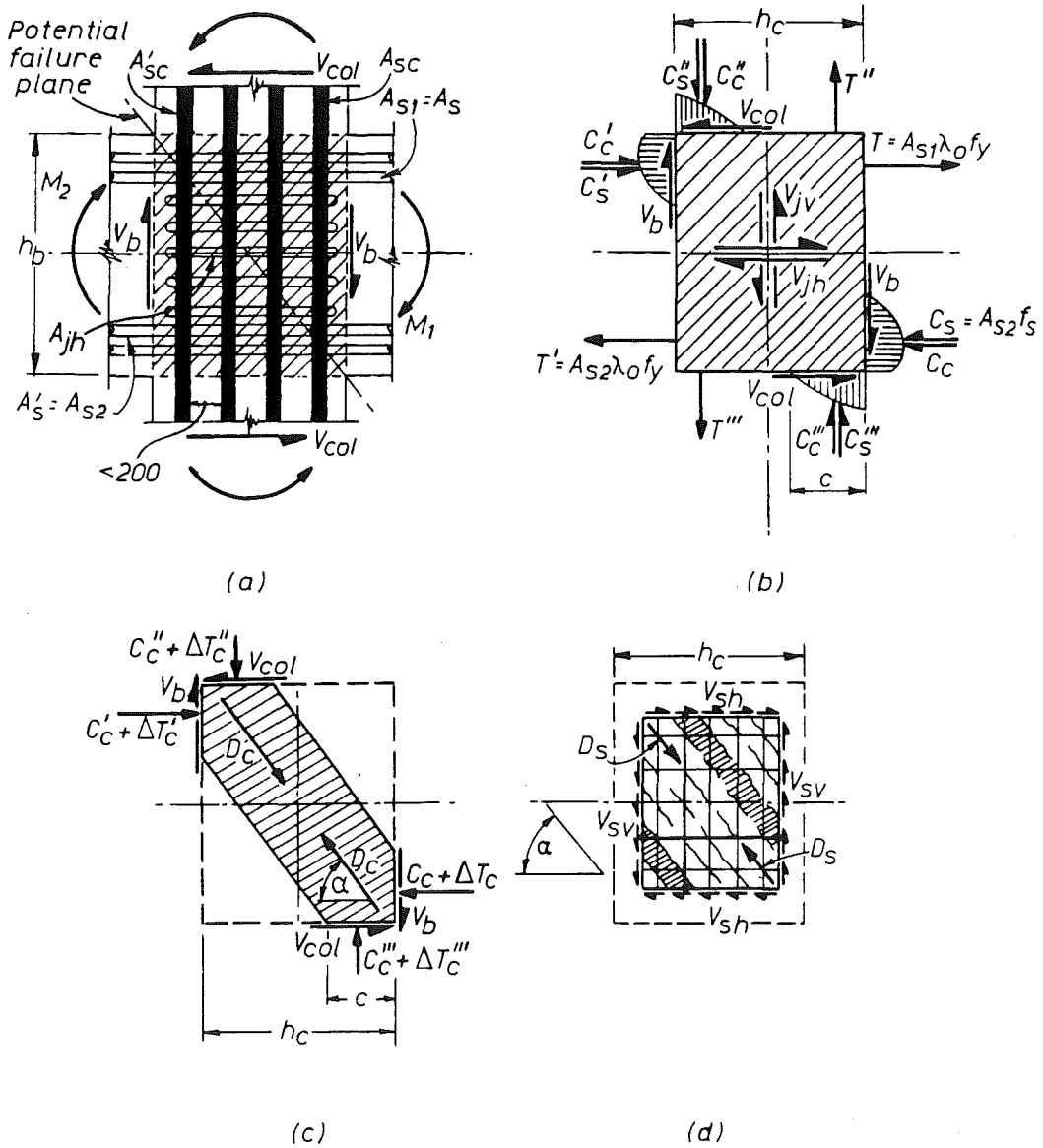

Fig.2.4 - Principal mechanisms of shear resistance of an inelastic interior joint core [17]

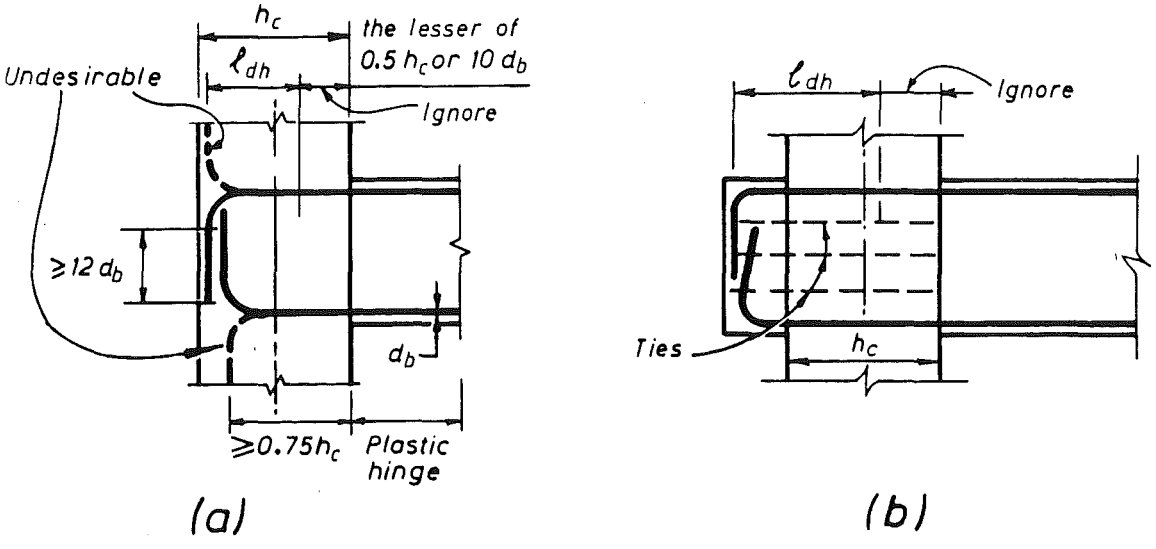

Fig.2.5 - Detailing requirements for longitudinal beam bars in exterior beam-column joints [4]

core, a diagonal compression field D_s can be sustained to resist the forces, if adequate lateral resisting forces at the boundaries are provided through the existence of the joint core reinforcement. The truss mechanism generating this compression field action involves horizontal reinforcement (normally in the form of joint hoops), vertical reinforcement (normally in the form of column intermediate bars) and diagonal concrete struts (two of which to illustrate a complete load path are shown shaded in Fig.2.4(d)). This mechanism is also known as the "shear carried by the shear reinforcement" and V_{sh} and V_{sv} denote the horizontal and vertical components of the total joint shear forces.

The above discussion refers to actions in a conventionally reinforced concrete beam-column joint. Other parameters, such as axial loads on the column and beams, or relocation of beam plastic hinges away from the column faces, may have adverse effects or may make beneficial contributions to the shear resistance. However the basic mechanisms are assumed to remain unchanged.

As cyclic inelastic loading progresses under severe earthquake actions, flexural cracking of the beams at the column faces become more severe. Flexural cracks may not close again upon moment reversals unless the beam bars, situated in the compression zones, slip or yield extensively. It was suggested [17] that the contribution of the concrete compression zones in the beams, shown as C_c and C_c' in Fig.2.4(b), would be significantly reduced. As a result, most or all of the beams' flexural strengths would have to be provided by steel couples provided by the top and bottom reinforcement. Flexural yielding, perhaps developing the overstrengths of the bars, results also in bond deterioration along the beam bars. Under these adverse conditions, the horizontal component of the diagonal compression strut mechanism, i.e. D_c in Fig.2.4(c), will diminish. Diagonal tension cracking in the joint core in alternating directions due to seismic actions can cause some degradation of the effectiveness of the strut mechanism. Eventually the horizontal core shear resistance may be transferred from the strut (D_c) mechanism to the truss (D_s) mechanism. By considering this particular situation the current New Zealand concrete design code [4] assumes, with some exceptions, V_{ch} to be zero. Consequently a considerable amount of horizontal joint reinforcement is required.

As for the vertical shear resistance of the joint core in frames proportioned in accordance with capacity design principles, the need for vertical reinforcement is reduced significantly. This is because in a ductile frame so designed, the columns are expected to remain elastic. Both the strut (D_c) and truss (D_s) mechanism are considered effective. Also the stresses in the compression zones of the column sections can be assumed to provide partial contribution to the joint truss mechanism. Detailed design provisions [4] can be seen in Appendix A.

The actions in an exterior joint are similar to those discussed before. However, the conditions are less critical because only one beam acts in this case (Fig.2.1(a)). With the proper detailing of bars provided, as shown in Fig.2.5, the diagonal concrete strut mechanism will be enhanced by the end hooks of the beam bars (Fig.2.1(a)). Hence the code [4] allows reduction in requirements for horizontal joint shear reinforcement.

2.3.2 Bond Mechanisms

The brief review in Section 2.3.1 implied that the bond response of the longitudinal bars, both in beams and columns play a very important part in the shear behaviour of a joint. While bond stresses introduce shear to the joint they also activate the two shear resisting mechanisms, the contributions of which in turn depend on the relative magnitudes as well as variations of bond stresses. These relationships are reviewed further using the interior joint of a ductile frame (Fig.2.1(b)) as an example.

For convenience the external actions on and shear forces across the joint core are redrawn in Fig.2.6(a). It is assumed that there is only one layer of bars in the top (Fig.2.6(b)) and in the bottom of the beam. However the following discussions can be readily extended to include any number of bars. Idealized changes in bar stresses across the joint core during the formation of plastic hinges at the column faces are shown in Figs.2.6(c) to (e).

The bond condition of the top beam bar (Fig.2.6(b)) of area A_s is quantified by unit bond force, u_1, assuming a uniform distribution of bond forces across the joint core, i.e.

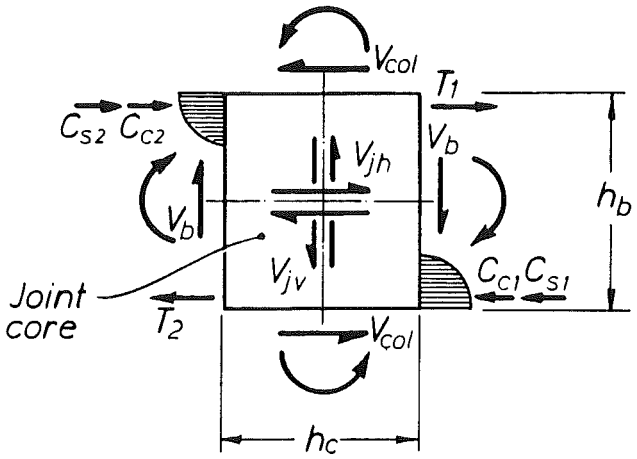

(a) Forces at Interior Joint Core

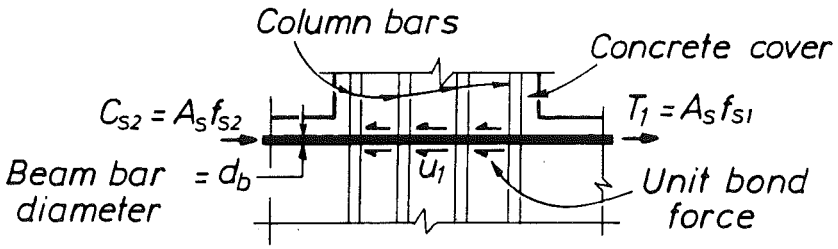

(b) Top Beam Bars with Area A_s

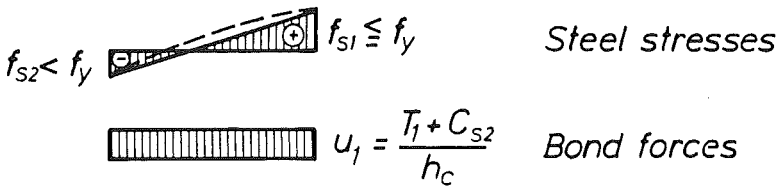

(c) When $|C_{c2}| > 0$, $|C_{s2}| < |T_2|$

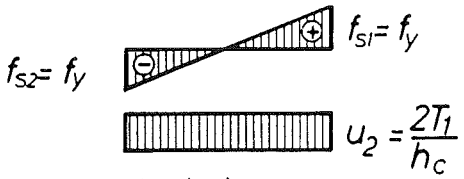

(d) When $|C_{s2}| = |T_1|$, C_{c2} May Be Zero

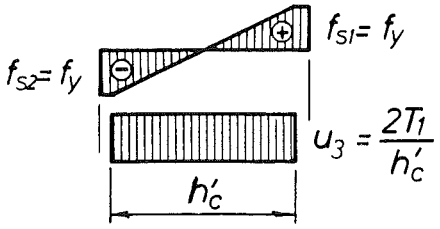

(e) After Some Yield Penetration

Fig.2.6 - Behaviour of a top beam bar with perfect bond across joint core during formation of plastic hinges

$$u_1 = \frac{T_1 + C_{s2}}{h_c} \tag{2.4}$$

where the forces T_1 and C_{s2} are tensile and compressive forces of the bar and h_c is the depth of the joint (column). An alternative and commonly used way of expressing the bond condition, is in terms of the average bond stress, i.e.

$$u_b = \frac{T_1 + C_{s2}}{\pi d_b h_c} \tag{2.5}$$

where d_b is the bar diameter. In reality the bond distribution around a bar within a joint is not uniform [1]. However, acceptably simple models, incorporating such complexities have yet to be developed for practical use [60].

During the initial stage of stressing to the attainment of ultimate flexural strengths of beam sections, the top bar stress at the right hand side of the column is f_{s1} in tension while that at the left hand side is f_{s2} in compression (Fig.2.6(b)). It can be easily shown [1] that while f_{s1} will reach the yield strength f_y of steel, the compression stress f_{s2} will in general remain elastic, since the concrete compression force C_{c2} (Fig.2.6(a)) also contributes to the flexural compression strength. Assuming perfect bond in the core, the unit bond force (or shear flow) in this case is u_1, in Fig.2.6(c), where the corresponding assumed longitudinal linear stress variation over the length h_c is also shown. A more realistic variation of steel stress, in the form of a curved broken line, is also shown in the same figure. Similar conditions apply to the bottom beam bars with area A'_s irrespective of whether the beam is symmetrically (i.e. $A_s = A'_s$) or unsymmetrically (i.e. $A_s > A'_s$) reinforced. No inelastic strains are assumed to have occurred within the joint.

A joint core under the conditions described above is classified as an elastic joint. Relevant quantities are redrawn in Fig.2.7. The two postulated shear resisting mechanisms (Section 2.3.1) in such a joint are shown qualitatively. The average bond force is assessed to have developed over a reduced core depth h'_c, because the concrete cover at the right hand side of the column is considered to be ineffective in developing bond resistance because of cracking. It can be seen in Figs.2.7 (a) and (b) that a significant portion of the bond forces of the top and bottom bars must be

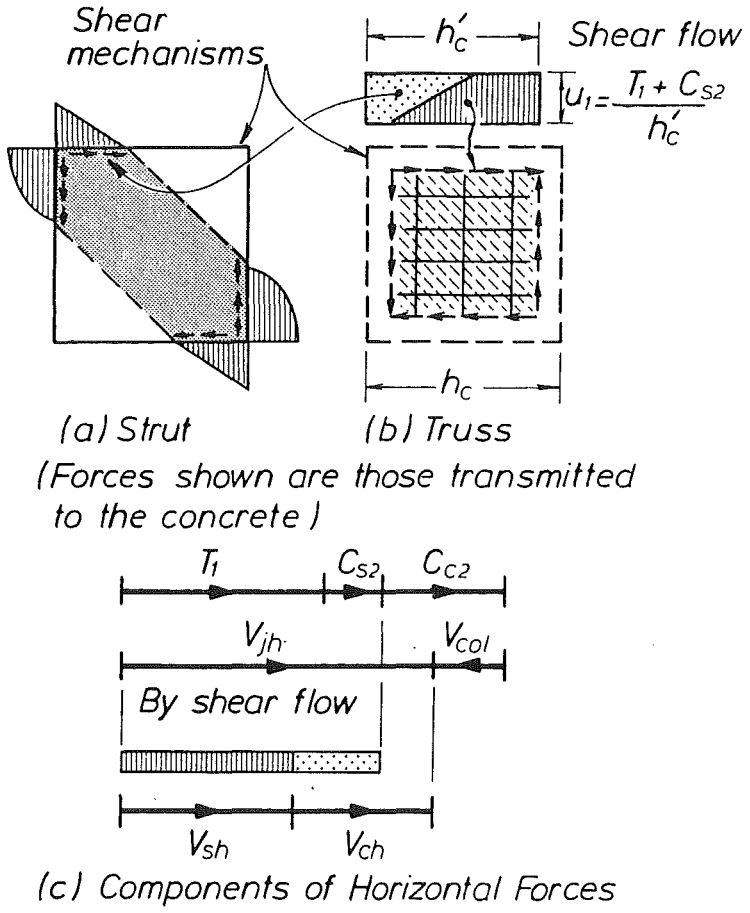

Fig.2.7 - Bond and shear mechanisms in an elastic joint core

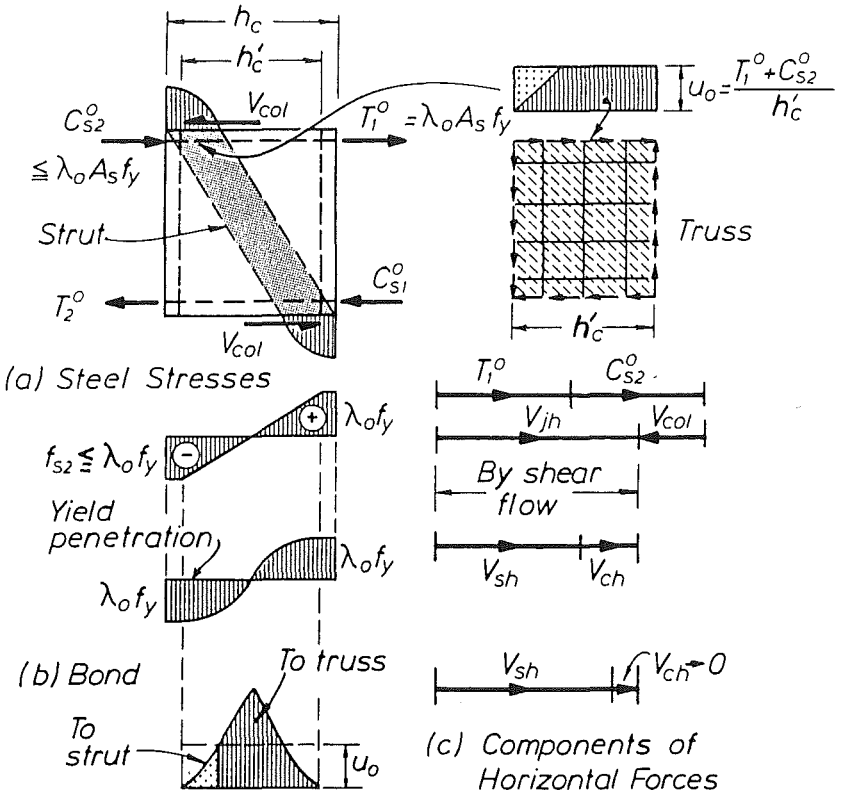

Fig.2.8 - Bond and shear mechanisms in an inelastic joint assuming perfect bond and strain hardening of beam bars

transmitted to the concrete core strut mechanism (shown shaded). Fig.2.7 also suggests that part of the flexural concrete compression force C_{c2} (see Fig.2.6(a)) is utilized to balance the shear force introduced from the column, V_{col}, and the remainder is transmitted to the diagonal strut in Fig.2.7(a). By comparing the relative magnitudes of the horizontal tension, compression and shear forces, for example along the top of the joint, a reasonable estimate of the effectiveness of the two mechanisms can be made (Fig.2.7(c)). Evidently the truss mechanism V_{sh} does not resist the entire joint shear V_{jh}. The shear resistance provided by the strut mechanism V_{ch} is shown to be very considerable. Hence the demand for joint reinforcement is moderate. Since joint deformations depend essentially on the steel strains of the truss mechanism, it follows that joint deformations are small in this case.

In a moderate earthquake, cyclic moment reversals will reduce the contribution of the concrete to flexural compression forces, such as C_{c2} (Fig.2.6(a)) at the column faces.

Consider moment cycles causing flexural cracks and subsequent concrete spalling at the upper left corner of the joint core (Fig.2.6(a)). In the subsequent cycle, the crack may not close. This will depend on the degree of the magnitude of ductility demand and also on the relative magnitudes of A_s and A'_s. This has been briefly discussed in Section 2.3.1. If A_s is greater than A'_s, then, even though the bottom bar yields in tension, the compression force $C_{s2} = T_2$ may not be large enough to cause the top cracks to close. Thus the compressive steel stress $f_{s2} \leq (A'_s/A_s)f_y$ is less than yield. The moment of resistance is thus provided by a steel couple. However when A'_s is greater than A_s, the large tensile force in the bottom bars should cause the top bars to yield in compression and thus the cracks should close. Hence the concrete compression force C_{c2} is not zero. A critical common case, to be considered, is that when $f_{s2} = f_y$ as shown in Fig.2.6(d). The resulting unit bond force becomes $u_2 > u_1$. With the decrease in magnitude of C_{c2} the contribution of the strut mechanism in Fig.2.7(a) is reduced. Its magnitude is more appropriately shown in Fig.2.8. Consequently the contribution of the truss mechanism must increase in order to resist the same total joint shear. This should cause larger joint deformations to take place. A joint in such case is classified as being in transition to an inelastic joint. In Fig.2.6(e), yield penetration is considered when the bond resistance of the cover concrete at both sides of the column is destroyed. The average unit bond force $u_3 > u_2$ is assumed distributed over a reduced core depth h'_c as shown. A further

reduction in the effectiveness of the strut mechanism is to be expected. Hence the contribution of the truss mechanism V_{sh} becomes more significant. The relative magnitude of V_{sh} is somewhere between that shown in Fig.2.7 for the elastic joint and that in Fig.2.8 for an inelastic joint to be discussed in the following paragraph.

An important consideration of inelastic joints should include the strain hardening of the beam bars in tension, normally expected to take place under more severe earthquake actions. This is shown in Fig.2.8. The top beam bar is assumed to be subjected to a tensile stress of $\lambda_o f_y$, where λ_o is a materials overstrength factor allowing for strain hardening and difference in material properties from those specified. In New Zealand, λ_o varies from 1.40 for Grade 380 steel to 1.25 for Grade 275 steel [4]. The bar in compression at the left hand side of the joint is expected to develop a stress less than $\lambda_o f_y$. The stress diagram in Fig.2.8(a) considers the worst case. As yield penetration into the joint core proceeds and is further aggravated by concrete disintegration due to spalling and crushing, the idealised linear stress variation is more realistically represented by the curved line. The average bond is given by $(T_1^\circ + C_{s2}^\circ)/h_c'$ as illustrated in the figure. However, in conformity with the non-linear stress variations, the bond distribution is more likely as shown in Fig.2.8(b). It is seen that the contribution of the strut mechanism is further reduced. In the extreme case V_{ch} is taken as zero. The entire joint shear is then resisted by the truss mechanism. It should be noted that a considerable portion of the compression force in the beam bars C_{s2}°, is required to equilibrate the column shear force V_{col}, and that this mechanism too involves bond forces. Again the joint deformations depend on the extent of the deformations associated with the truss mechanism, in particular the tensile strains in the joint reinforcement. Since perfect bond is assumed, stresses and strains of the beam bars at the centre of the joint should be nearly zero. Also the total elongation of the beam bars over the distance h_c or h_c' should be negligible.

The last paragraph summarises the basic assumption of the approach taken by the current New Zealand concrete code [4] on joint design. The aim when drafting these code provisions in the late 1970's was to enable a beam-column joint, such as shown in Fig.2.8, to sustain the very large bond forces, transmitted by beam bars, and thereby to enable the flexural overstrength of adjacent beam plastic hinges to be developed primarily by steel couples. Moreover, this aim was motivated by the desire to fulfill the conditions

incorporated in the seismic provisions of most concrete codes [4,5], namely to ensure the development of adequate curvature ductility at sections of plastic hinges. These provisions stipulated that a minimum amount of flexural compression steel, typically $\rho' \geq 0.5\rho$, be used in plastic hinges, in order to reduce the depth of the flexural compression zone and thereby to increase curvature ductility capacity. The flexural compression reinforcement, to be effective, must thus be able to develop significant compression, ideally up to a stress of $\lambda_o f_y$, as shown in Fig.2.8(a). Hence the intent of the New Zealand code provisions was to enable joints to be developed that are capable of sustaining adjacent plastic hinges in beams or columns, the behaviour of which can be predicted by universally accepted and codified principles of flexural theory. If this cannot be achieved, code provisions to ensure adequate curvature ductility in plastic hinges become meaningless.

When axial compression on a column is large (Fig.2.9), the code assumed that the strut mechanism can be enhanced, because the compression from the increased stress block in the column section enables larger bond forces from the beam bars to the strut to be introduced. Moreover it can be assumed that in this case some diagonal tensile stresses are possible in the joint core. As a consequence the load on the truss mechanism V_{sh} was assumed to be reduced. Hence less transverse reinforcement in the joint core would be required.

The foregoing discussions assumed that perfect bond exists. The longitudinal beam bars are thus well anchored in the joint core so that maximum tensile and compressive forces can be assumed to develop at the column faces at the same time. Beam bar elongations are negligible because the difference in the tension and compression forces is small.

In reality the bond between a beam bar and the core concrete is imperfect. Local bond-slip may take place [60]. Corresponding, somewhat idealized, bar stress and bond variations are shown in Fig.2.10, assuming small axial compression on the column. As the top beam bars slip in the joint core, flexural cracks at the upper left corner of the core close, thus activating the concrete compressive force C_{c2} and consequently reducing the steel compressive force C_{s2}. Bond forces are seen to be concentrated in the left half of the core. There is considerable elongation of the beam bar by virtue of the non-symmetrical stress distribution. This will cause "fixed end rotations" of beams at column faces, as reported by Bertero [25]. Frame

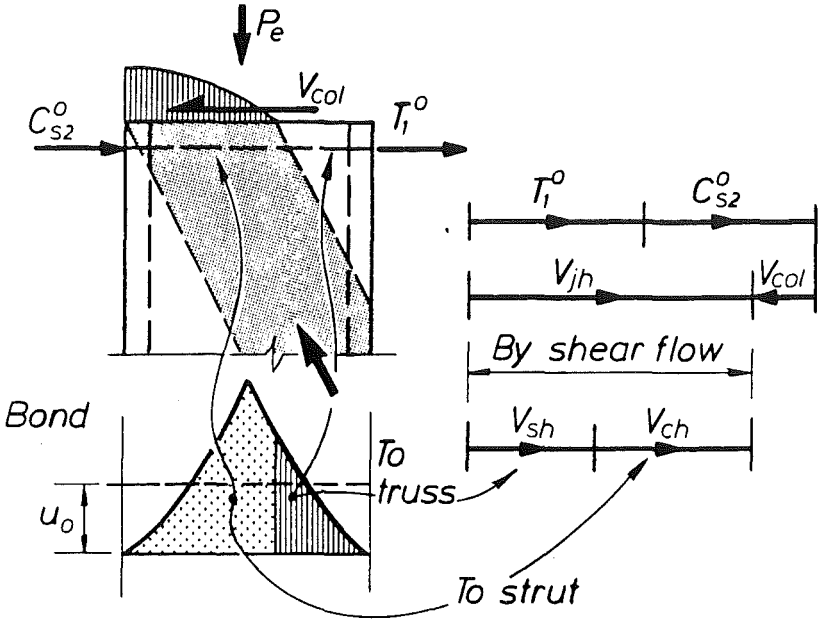

Fig.2.9 - Inelastic joint with large axial compression load on column

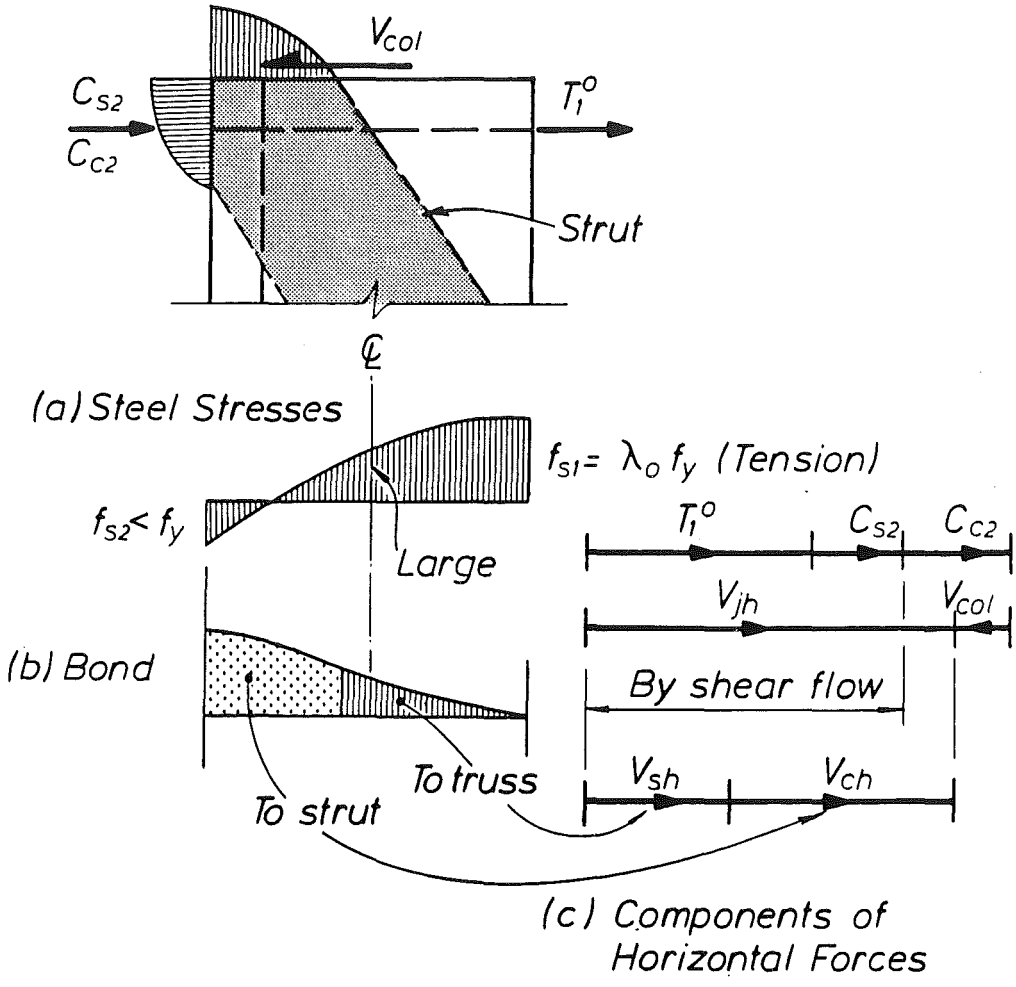

Fig.2.10 - Inelastic joint with imperfect bond along beam bars

flexibility is thus increased. However, there is the benefit of having the strut mechanism being re-mobilised.

In the extreme case, when the bond breaks down, beam bars slip freely through the joint core. In that case they will be anchored in the adjacent beams. Corresponding bar stresses and bond variation is shown in Fig.2.11. As the force vectors suggest, the concrete compressive force C_c becomes very large, thus further mobilising the strut mechanism. Both the shear input by bond and the resistance by truss mechanism diminish. Deformations of the joint core will be small. Yet because of very large elongations of the beam bars within the joint core (Fig.2.11) significant increase of frame flexibility will ensue. There will be no compression reinforcement in the beam at the column faces and crushing of the concrete in the beams at the column faces may occur. This behaviour does not comply with that of energy dissipation mechanisms expected in frames designed for ductile response. Large frame displacements, i.e. storey drifts, must be expected at the application of small lateral forces, till the large gaps, shown in Fig.2.11, close upon displacement reversal.

The foregoing discussion of joint response suggests that to ensure a reasonable energy dissipation in ductile frames, adequate bond resistance within beam-column joints must be maintained. It is convenient to use the unit bond force u_1 (Eq.2.4) or the average bond stress u_b (Eq.2.5) as reference parameter to gauge the severity of bond conditions for design purposes. With reference to the stress conditions of Fig.2.6(d), the total force acting on the beam bar within the joint core is $2T_1 = 2A_s f_y = 2f_y \pi d_b^2/4$. This is assumed to be resisted by the summation of bond stresses over the bar's surface area, i.e. $u_b \pi d_b h_c$. Thus the average bond stress is calculated as

$$u_b = \frac{1}{2} f_y \frac{d_b}{h_c} \qquad (2.6a)$$

In Japan, this parameter is referred to as the "bond index" [23].

The New Zealand concrete code [4] requirements for bond within an interior joint core are expressed in terms of bar diameter to column depth (i.e. d_b/h_c) ratios for two steel grades (see Appendix A). A more general expression could in fact be shown [18,27] to be

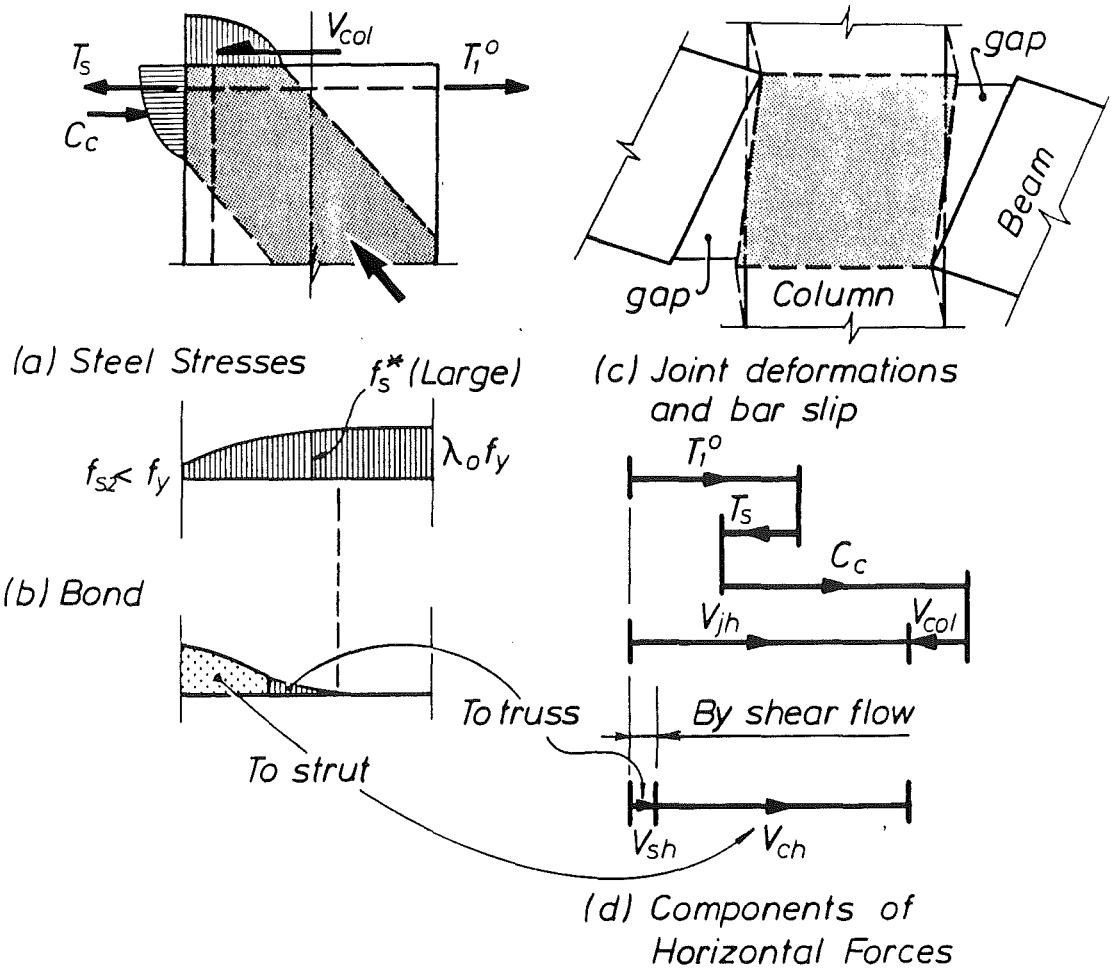

Fig.2.11 - Inelastic joint with bond failure of beam bars

$$R = f_y \frac{d_b}{h_c} \leq 11 \qquad (2.7)$$

and this will be used as a reference stress factor when comparing the bond performance of various test units.

By applying Eq.2.6(a), it follows that NZS 3101[4] implies a restriction on the bond stress to be

$$u_b \leq 5.5 \text{ (MPa)}$$

When strain hardening of the beam bar is considered (Fig.2.8), Eq.(2.6a) can be rewritten as

$$u_{bo} = \frac{1}{2} \lambda_o f_y \frac{d_b}{h_c} \qquad (2.6b)$$

With the materials overstrength factor being in the range $1.25 \leq \lambda_o \leq 1.40$ [4], it is seen that

$$6.9 \leq u_{bo} \leq 7.7 \text{ (MPa)}$$

It can be shown that the bond stresses u_b and u_{bo} derived above exceed considerably the allowable stresses associated with the code requirements for development length [4,5]. It has been pointed out [27] that the limitation according to Eq.(2.7) represents a compromise with some bond deterioration during inelastic seismic response being tolerated. Based on the favourable test results obtained recently, Park and Dai [50] propose further relaxation to take into account the benefit of higher strength concrete by specifying

$$u_{bo} \leq 1.53 \sqrt{f'_c}$$

where f'_c is the concrete compressive strength in MPa. This is restricted to cases where $f'_c \geq 20$ MPa. In Japan, Kitayama et al [23] suggest that u_b should not exceed $1.6\sqrt{f'_c}$.

2.3.3 Review of Bond Strength Requirements

The previous discussion pointed out that the current NZS 3101 provisions[4] place rather severe limitations on usable bar diameters in beam-column joints. At the expense of some loss in the quality of frame performance it appears that some relaxation of anchorage requirement in joints is justified.

In Chapter 1, performance criteria for test specimens, with due considerations given also to practical situations, have been discussed. Against these criteria, three sets of results of tests recently conducted at the University of Canterbury by Beckingsale et al[39], Milburn and Park[29,61] and Dai and Park[49,50] are re-examined with special attention being paid to the bond conditions of beam bars.

Using symmetrically reinforced beams, Beckingsale's Units B12 and B13 had D19 beam bars of Grade 275 steel through a column depth of 475 mm. Hence the R factor (Eq.(2.7)) was 11.4. Measured compressive strengths of concrete cylinders were 34.6 MPa for Unit B12 and 31.4 MPa for Unit B13 at the time of testing. Strain hardening of the bars in tension commenced at a displacement ductility factor of $\mu = 4$ corresponding to an interstorey drift of approximately 2.4%. Complete bar slippage was recorded, however, at $\mu = 6$ at a drift of 3.7%. The maximum compressive stresses in the beam bars at column faces, estimated by conversion from measured strains, were at the yield level. This implied that the compression reinforcement participated efficiently as intended, but some concrete remained effective in compression. It appears that stress conditions similar to those depicted in Fig.2.10 prevailed.

For beam-column assembly with unsymmetrically reinforced beams, the R factor of Beckingsale's Unit B11 was still 11.4. Concrete strength was 35.9 MPa. Slip failure of the bottom bar occurred at ductility $\mu = 6$ at an interstorey drift exceeding 3.5%. As the area of the bottom reinforcement was only half of that of the top, the bottom bars were more severely strained. However, strain-hardening of beam bars appeared to have started only at a ductility of $\mu = 4$ (drift of 2.4%). The maximum stress of the bottom bars in compression did not exceed the yield level.

Milburn's Unit 1 with R = 10.8 had beams symmetrically reinforced. Concrete compressive strength was 41.3 MPa. No bar slip failure was reported.

The report states that cracks at the beam sections under compression closed completely at a ductility of $\mu = 2$ at an interstorey drift of about 1.8%. Strain hardening of the bars in tension commenced at $\mu = 4$ at a drift of about 3.5%. Some pinching in the load-displacement response curves was reportedly caused by the "delayed crack closure in the compression region". On the other hand, the decrease in the measured tensile strains was not large enough to subject the bar to strain hardening in compression. It is more likely that local bond-slip of the bars caused the cracks to close, resulting in conditions similar to those shown in Fig.2.10.

Dai and Park tested four units with different beam reinforcement and R factors. Measured concrete strengths ranged from 36.2 MPa to 45.9 MPa. All four units gave satisfactory performance even though NZS 3101 requirements were not fully met. Significant slippage of bars was noted only at interstorey drifts exceeding 3%. However, it appears that even at lower displacement levels, some local bond-slip of beam bars took place. Beam bars in compression did not appear to have reached strain-hardening.

From the review of these selected test results, it is evident that the worst cases considered in NZS 3101[4], as described in Section 2.3.2, do not necessarily materialize in a building frame. This is particularly the case when practical limits on interstorey drifts are considered.

Designers will aim at using reinforcing bars of larger size and lesser amounts of joint reinforcement to mitigate congestion of reinforcement in joints. There is thus a need to relax relevant code requirements if they prove to be unduly conservative. The previous discussions suggest that perfect bond of bars anchored in joints is difficult to attain. However, some deterioration in bond performance in case of extreme seismic events, appears to be acceptable. For this reason, bond strength requirements are re-considered in the following two separate cases.

(a) Interior joint assemblies with symmetrically reinforced beams

This case is shown in Fig.2.12(a). Equal areas of top and bottom reinforcement in the beams, i.e. $A_s = A_s'$, are assumed. With concrete compressive forces existing, as represented by C_{c1} and C_{c2} in Fig.2.12(b), it follows from previous discussions that the maximum compressive stresses in the bars are not greater than the yield strength of the steel, f_y. When maximum

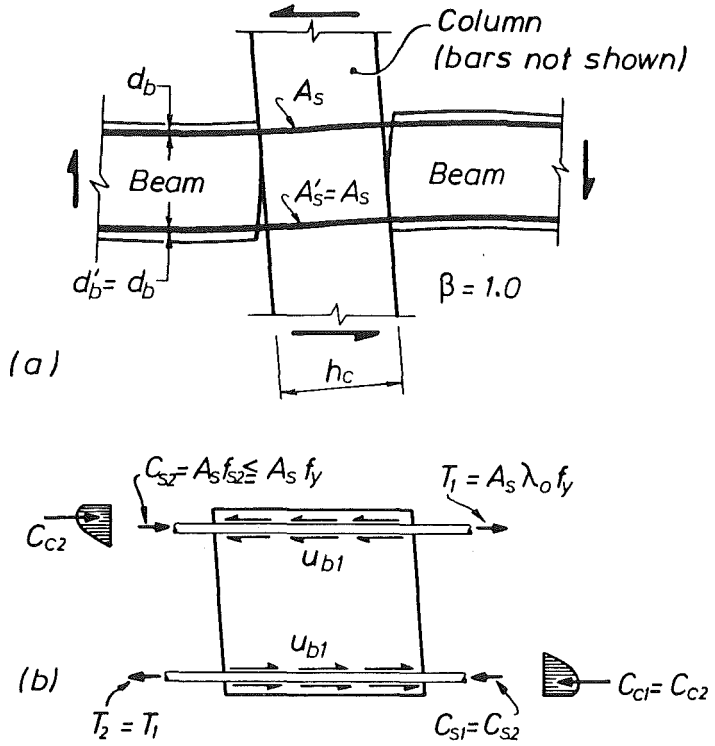

Fig.2.12 - Actions and forces along beam bars at joint assembly with symmetrically reinforced beams

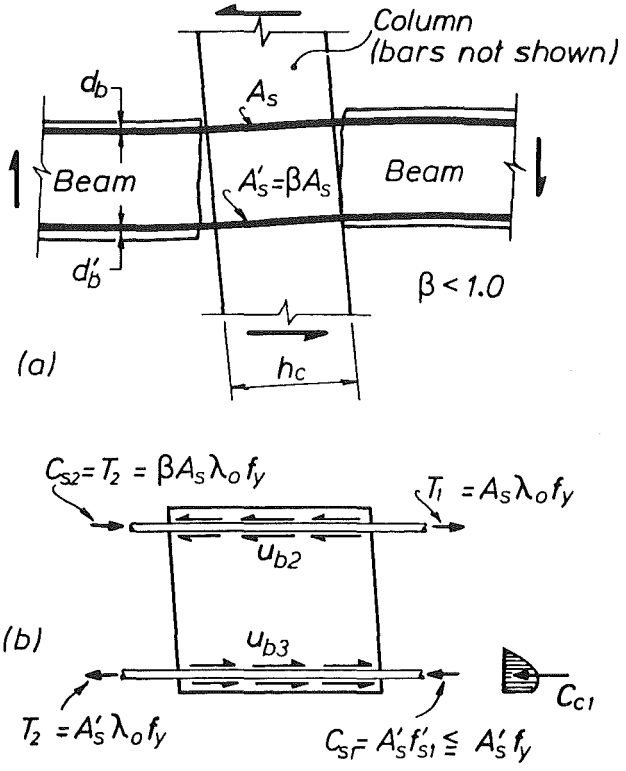

Fig.2.13 - Actions and forces along beam bars at joint assembly with unsymmetrically reinforced beams

stresses are attained in the top beam bar, the following equilibrium equation can be written to obtain the bond stress u_{b1},

$$A_s f_y + A_s \lambda_o f_y = \pi d_b u_{b1} h_c$$

and hence with R given by Eq.(2.7)

$$u_{b1} = \frac{(1 + \lambda_o)}{4} R \qquad (2.8)$$

Expressions for the bottom beam bars are identical since $d_b' = d_b$.

(b) Interior joint assemblies with unsymmetrically reinforced beams

With unsymmetrically reinforced beam sections as shown in Fig.2.13, stress conditions are different from those in case (a). However, it is shown that the bottom beam bars are subjected to the same bond conditions shown in Fig.2.12 so that $u_{b3} = u_{b1}$. While the large tensile force T_1 in the top bars should cause the bottom bars to yield in compression and close the cracks, local bond-slip of the bottom bars could as well mobilise the concrete compression force C_{c1} at the same time and thus reduce the bar stresses. This hypothesis comes from the review of the test results presented in earlier paragraphs. Strain hardening of beam bars in compression was not recorded. It is therefore concluded that the maximum level of the compressive stress in this case is also f_y.

For the top bar, it is assumed that no concrete compression force is developed at the upper left corner of the joint (Fig.2.13(b)) since T_2 is not large enough to cause the top bar to yield and hence to close the crack. The compression force C_{s2} shown thus represents the worst possible case. The bond stress u_{b2} is as follows :

$$\beta A_s \lambda_o f_y + A_s \lambda_o f_y = \pi d_b u_{b2} h_c$$

and hence

$$u_{b2} = (1 + \beta) \frac{\lambda_o}{4} R \qquad (2.9)$$

where $\beta = \frac{\rho'}{\rho} = \frac{A'_s}{A_s}$

The above two models will be re-examined in Chapter 8 in light of experimental findings.

2.3.4 Evaluation of Strut Mechanism from Bond Distribution

In Section 2.3.2 it was proposed that local bond-slip of beam bars inside an inelastic interior joint core would re-distribute the horizontal internal compression forces at the column faces (see Fig.2.10) and therefore re-mobilise the concrete strut mechanism to resist joint shear. Further in Section 2.3.3, a review of previous test results suggested that such re-distribution and re-mobilisation would occur in practical situations. These phenomena would be accelerated if bond strenth requirements are relaxed as outlined in Section 2.3.3. Because of the inseparable interrelationship between bond and shear phenomena within a joint, a more comprehensive assessment of the likely contributions of bond performance to joint mechanisms is therefore presented in this section. The distribution of bond forces along a beam bar anchored within a joint will continually change as earthquake forces increase and the structure passes through stages of elastic response into the inelastic range, eventually approaching the state corresponding to the maximum ductility demand. It is impractical to describe bond phenomena corresponding with each stage of seismic response. For design purposes, by necessity a compromise must be made in describing a pattern of bond force distribution which is both realistic and reasonably conservative when applied in the assessment of joint shear strength.

Fig. 2.14 refers to the same beam bar discussed in Section 2.3.2 but now considered being embedded in a relatively deep joint (column), corresponding with a very small value of $R = f_y d_b / h_c \ll 11$ (Eq.(2.7)). Although an unlikely case to arise in normal construction, it cannot be disregarded. Moreover a study of such case would give some insight to joint behaviour.

Under simultaneous tension and compression forces on opposite sides of the joint of Fig.2.14(a), steel stresses and bond forces are distributed in assumed patterns shown by broken and full lines in Figs.2.14(b) and (c). Because the factor R is small, the development lengths required for tension

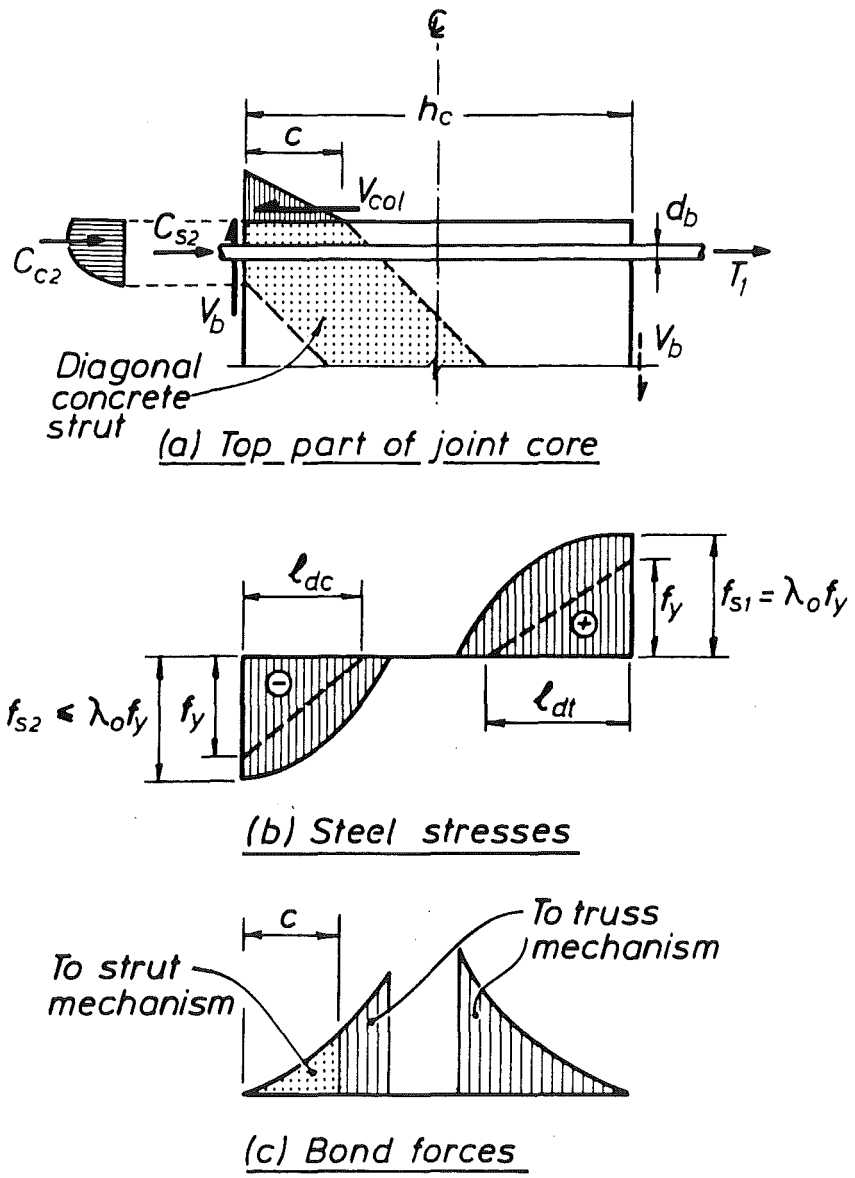

Fig.2.14 - Assumed actions in an inelastic interior joint with perfect anchorage of beam bars

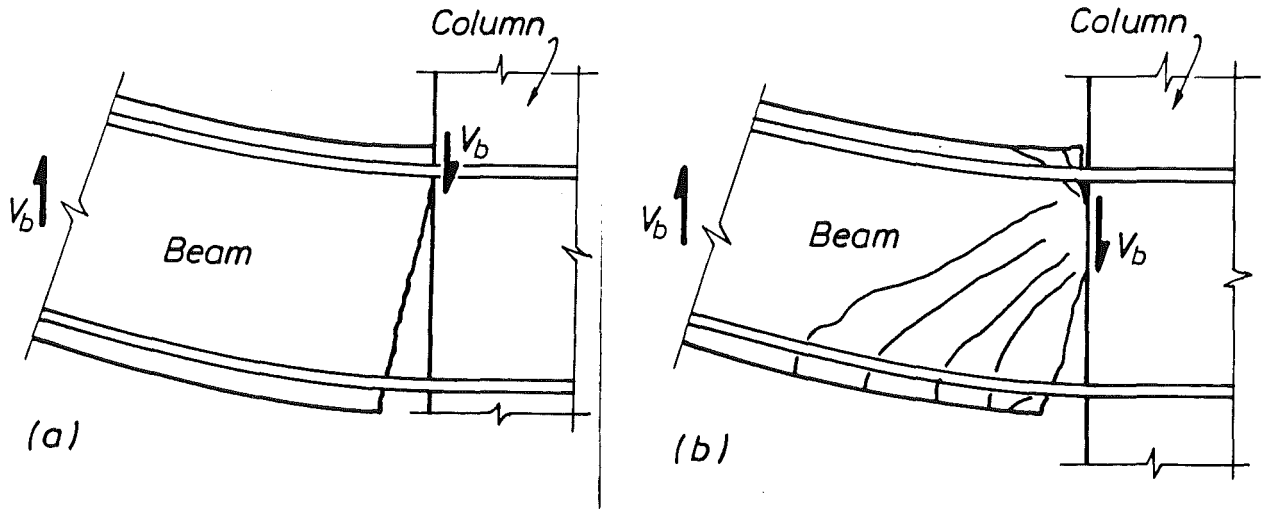

Fig.2.15 - Change of flexural compression zone in a plastic hinge after load reversals

and compression, ℓ_{dt} and ℓ_{dc} as suggested by codes [4,5] and indicated in Fig.2.14(b), can be easily provided. At the attainment of bar overstrength $\lambda_o f_y$, the development length might increase slightly. It is shown that h_c is much larger than the sum $(\ell_{dt} + \ell_{dc})$ so that even with yield penetration caused by reversed cyclic actions, the strain and stress of the beam bar in the centre of the column remain zero. Thus it is possible that some strain hardening of the beam bar in compression can be approached, resulting in $f_{s2} \leq \lambda_o f_y$. This very conservative assumption, shown in Fig.2.8, suggests then that the contribution of the diagonal strut may become negligibly small. Probable distributions of bond forces are shown in Fig.2.14(c).

Although not directly relevant to the consideration of bond mechanisms, it is necessary to recall a certain aspect of shear resisting mechanisms in beams using truss analogy [1]. Since sliding shear failure in the plastic hinge of a beam is not desired, the vertical beam shear force V_b shown in Fig.2.14(a) should be resisted primarily through the presence of horizontal concrete compression forces, for instance C_{c2}. This compression may be established when the beam deforms to achieve large plastic curvature, which enables concrete to resume contact between cracks above the top layer compression reinforcement. When a flexural concrete compression force C_{c2} is mobilized (Fig.2.14(a)) further increase of compression stresses in the top layer bars is not necessary. If the beam shear is relatively small, which is common when gravity load on a beam is significant, the concrete compression force C_{c2} in this case may be sufficient to enable the beam shear force to be transmitted by a mechanism as implied in Fig.2.15(a). However, when the beam shear V_b is large because seismic actions dominate, under large curvature ductility demand some sliding shear displacement occurs while compression forces are generated in the top bars (Fig.2.15(b)). Because of the previously imposed large residual tensile strains in these bars causing some spalling of the cover and bond deterioration over the yield zone, contact between previously formed crack faces below the top bars is established. As Fig.2.15(b) suggests vertical shear from the beam to the joint may be transmitted while some cracks across the top beam bars may still be open.

The mechanism hypothesised in Fig.2.15(a) is more efficient when the concrete cover and the beam width are large. In prototype construction concrete cover is normally in the range 30 to 40 mm. Cast in place floor slabs further ensure that a flange in compression is available to each beam.

As for the bottom part of the joint where the amount of bottom beam reinforcement is usually less than that at the top, conditions for developing the strut mechanism V_{ch} are more favourable. The much larger top tension forces, say T_1 in Fig.2.6, will easily close the bottom gap and introduce C_{c1}. Even when symmetrically reinforced beam is used, significant compression force C_{c1} is still likely to take place for the reasons just discussed. Hence it is concluded that this case needs not be considered further.

From the discussions in this and earlier sections, it becomes evident that the compressive stress in a beam bar, shown as f_{s2} in Fig.2.14, must be rather small. The maximum possible value is f_y, the yield strength in compression.

A realistic situation in building construction is represented by a value of $R \geq 11$ (Eq.(2.7)). The bar stress distribution in a "realistic" joint core (Fig.2.16 (a)) is qualitatively shown in Fig.2.16(b). The total of the code-specified anchorage lengths, ℓ_{dt} and ℓ_{dc} shown in Fig.2.14(b), are likely to exceed the column depth h_c. To illustrate the mechanisms involved in developing the anchorage of the beam bar which is being strained within the joint, detail '0' in Fig.2.16(a) sketches a rib at the centre line of the joint being displaced by over a gap of length x. This displacement results from some microcracking as well as crushing of the concrete surrounding the rib, thereby mobilising the "passive" bearing forces sustained by sound concrete behind the rib. The total anchorage force to be relied on is primarily the sum of these bearing forces over the anchorage length. Frictional resistance between the bar's surface area and the surrounding concrete can be ignored [1,60]. After force reversals and yield penetration into the joint core, there will be numerous gaps at the ribs throughout the joint. It can be expected that the gap length x at the centre will be the smallest.

When the seismic actions are reversed to push and pull the bar of Fig.2.16(a) to the left-hand side, even a relatively small force will be able to move the bar to the left by a distance x without significant resistance being experienced. This rigid-body movement of the beam bar over the distance x is the "local bond-slip" referred to in this report. Only after this movement x has taken place can bond start to develop with the rib of Fig.2.16(a) bearing against the left surface of the gap. As the applied forces increase, and bond in other regions of the joint deteriorate the gap

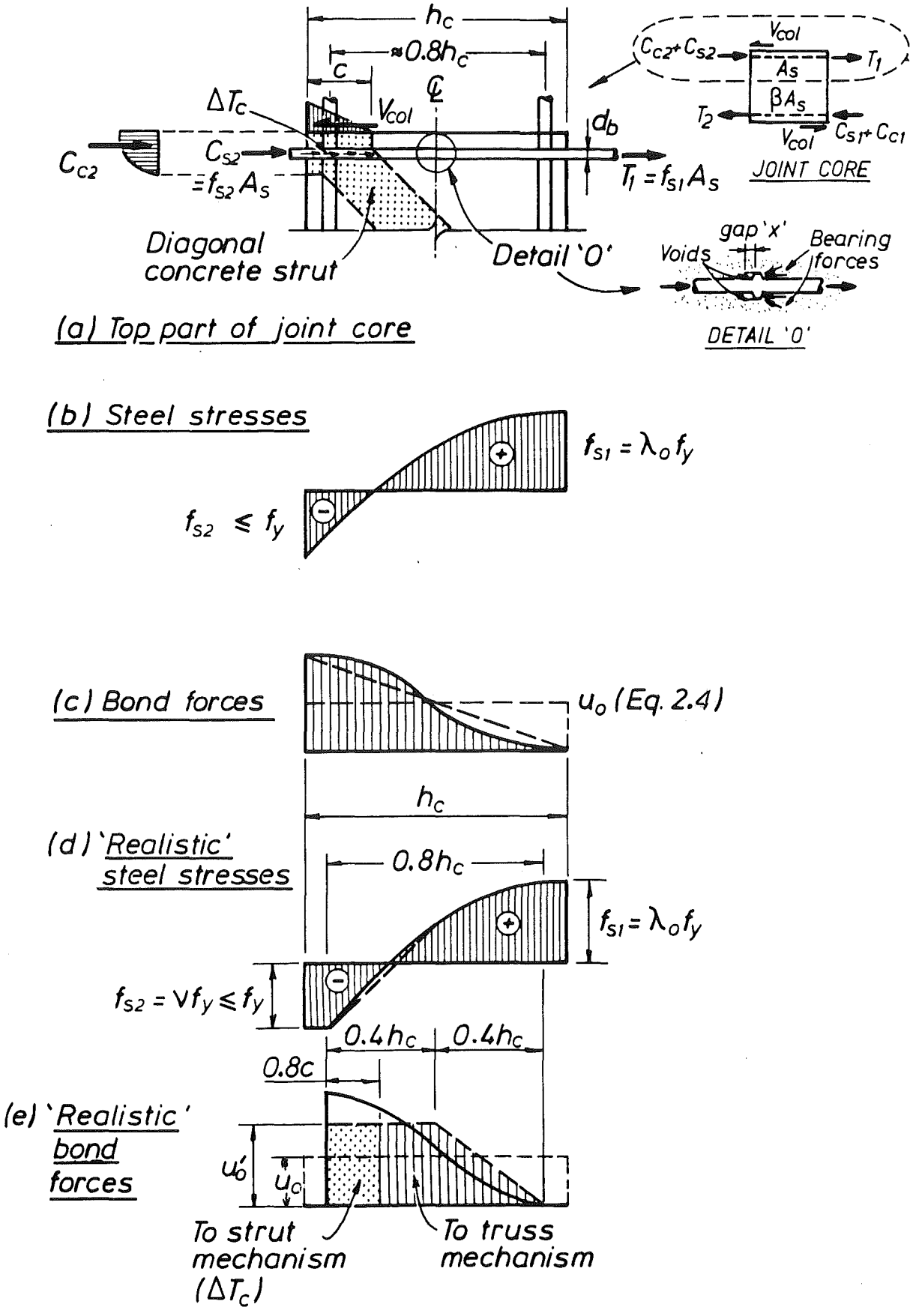

Fig.2.16 - Assumed actions in an inelastic interior joint with imperfect anchorage of beam bars

"x" should become larger. Therefore cyclic inelastic reversed loading of the beam bar can be expected to increase the slip progressively.

In a typical inelastic interior joint, such as the one of Fig.2.16, both the "local bond-slip" and the development of concrete compression forces at column faces via the mechanisms illustrated in Fig.2.15 can take place. These two actions ensure that the horizontal concrete compression C_{c2} is significant and accordingly the compressive steel stress f_{s2} is reduced to less than f_y. These conclusions imply that the traditional assumption of flexural section analyses, whereby strains in each fibre are the same for both the steel and the concrete, is grossly violated at the beam-column interface.

A possible distribution of unit bond forces within the joint core (Fig.2.16(a)) is suggested by the solid curved line in Fig.2.16(c). This distribution is the same as that shown in Fig.2.10. A simplified distribution is denoted by the sloping dashed straight line in Fig.2.16(c). The other extreme is a uniform variation represented by the horizontal broken line. The latter case is the same as the unit bond force defined by Eq.(2.5).

Yield penetration and bond deterioration of beam bars as a result of inelastic cyclic response are inevitable. Hence it is prudent to ignore the anchorage provided by the cover concrete at either face of the joint. The effective column depth, assumed lying between the centres of the outermost layers of column bars, is typically $0.8\ h_c$ (Fig.2.16(a)). A realistic steel stress distribution of Fig.2.16(b) is simulated with the pattern suggested by the curved line in Fig.2.16(d), with the corresponding bond distribution represented by the solid curved line in Fig.2.16(e). A coefficient $\nu \leq 1.0$ is introduced to recognize that f_{s2} does not exceed f_y. The steel stress distribution is further simplified by assuming linear variation over a length of $0.4\ h_c$ inside the joint core, as indicated by the dashed straight line in Fig.2.16(d). The resulting bond distribution, considered to be conservative for the purpose of estimating joint shear strength, is shown by the two dashed lines in Fig.2.16(e).

Adopting the assumed bi-linear bond distribution of Fig.2.16(e) for the joint core, the effective unit bond force u'_o, and the anchorage force ΔT_c introduced to the diagonal concrete strut over an assumed effective depth of 0.8c in recognition of yield penetration, can be derived as

$$u'_o = (T_1 + C_{s2})/0.6\ h_c \qquad (2.10)$$

and

$$\Delta T_c = 0.8c\ (T_1 + C_{s2})/0.6\ h_c \qquad (2.11)$$

By considering equilibrium of the horizontal forces in Fig.2.16(a), the shear resistance provided by the concrete strut mechanism is now estimated as

$$V_{ch} = C_{c2} + \Delta T_c - V_{col} \qquad (2.12)$$

It is necessary to determine c in Eq.(2.11) before ΔT_c can be found. While a column is usually proportioned on the basis of its ultimate strength, the capacity design procedure [1,6] effectively ensures that the columns above and below a floor behave elastically. Using traditional elastic stress analysis of cracked sections [62] it is found that, depending on the column reinforcement ratio ρ_t, the minimum practical values of the neutral axis depth c for sections with peripheral distribution of flexural reinforcement range between $0.25\ h_c$ and $0.35\ h_c$. Incorporating the beneficial effect of axial compression load on interior columns, it is therefore proposed that c be estimated by

$$\frac{c}{h_c} = 0.25 + \frac{0.8P_e}{f'_c\ A_g} \qquad (2.13)$$

where P_e is the minimum design compression load on a column and A_g is the gross sectional area. Eq.(2.13) and Eq.(2.11) intentionally underestimate the value of ΔT_c. Hence the final results can be generalised for applications in design. The influence on shear strengths of joints will be assessed in Chapter 8 after a study of the experimental results in this project.

2.4 CONFINEMENT AT JOINTS

As mentioned in Section 1.4, the ACI code provisions [5,28] emphasise the need for confinement of joint cores by framing beams and transverse joint reinforcement. In the review presented in Section 2.3, this aspect has not been considered. The following sections attempt to assess the relevance of confinement action to joint core behaviour. For this purpose some of the perceived fundamental principles of mechanisms of concrete confinement are restated.

2.4.1 Confinement of Linear Members by Transverse Reinforcement

The traditional role of transverse reinforcement, particularly in compression members, is to provide significant passive lateral pressure to the confined core when ductility demands arise. This pressure is mobilized by Poisson effects and is transverse to the applied external load. Confinement so achieved may then result in two very desirable features of the inelastic response of concrete[1]. Firstly, it can convert the relatively brittle material to a ductile one. Secondly, it may enhance compression strength so that, for example, the loss of the contribution to resistance of spalled concrete outside a confined core may be more than compensated for within the core. While the need for confinement of the end region of a column, subjected to axial compression and bending, often exists above or below a joint of a ductile frame, inelastic concrete compression strains due to these actions do not arise within a joint core. This is because under seismic actions, particularly when plastic hinges develop in beams on both faces of the column, the sense of either column or beam bending moments changes inside the joint core. For illustration, idealised moment patterns in a linear model structure, and realistic moment variations in a real structure with beam and column depths taken into consideration, are shown and compared in Fig.2.17. It is evident that moments within the joint will always be less critical. Hence the need to confine a joint core to the same extent as an adjacent potential plastic hinge region of a column does not appear to be justified. Nevertheless, as a conservative measure, this practice has been in use also in New Zealand [4] by specifying a minimum amount of reinforcement according to the confinement provisions.

There are many situations when the integrity of the concrete, subjected to tensile strains in one or several directions, is to be preserved. One of these is the restriction on diagonal splitting cracks, which may develop in the non-prismatic diagonal strut within the joint. Usually empirical or nominal amounts of reinforcement, often called basketing reinforcement, are used for this purpose. However, such reinforcement can seldom be associated with mechanisms of confinement.

A particular feature of transverse reinforcement in terms of the mechanism of confinement, briefly reviewed here, is that it does not resist any quantifiable external action. Its contribution to the inelastic response of concrete depends only on the imposed compression strain due to external

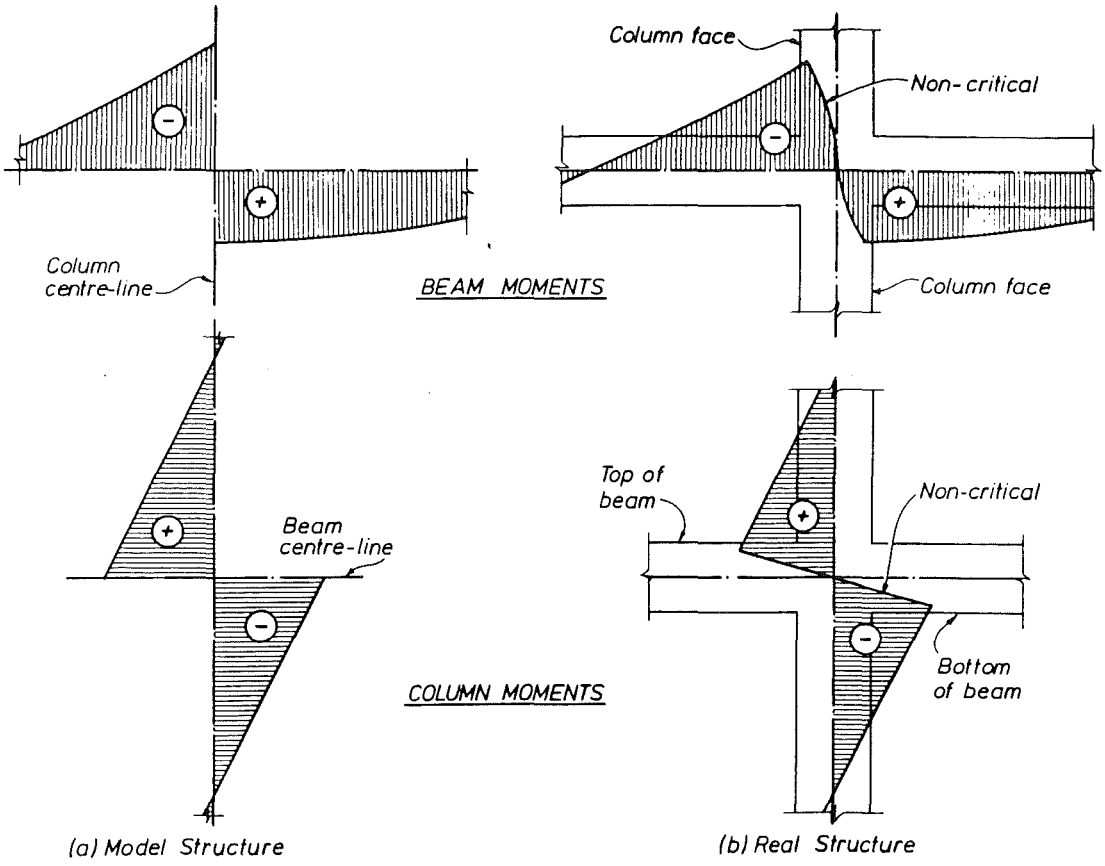

Fig.2.17 - A comparison of moment patterns for model and real joint assemblies

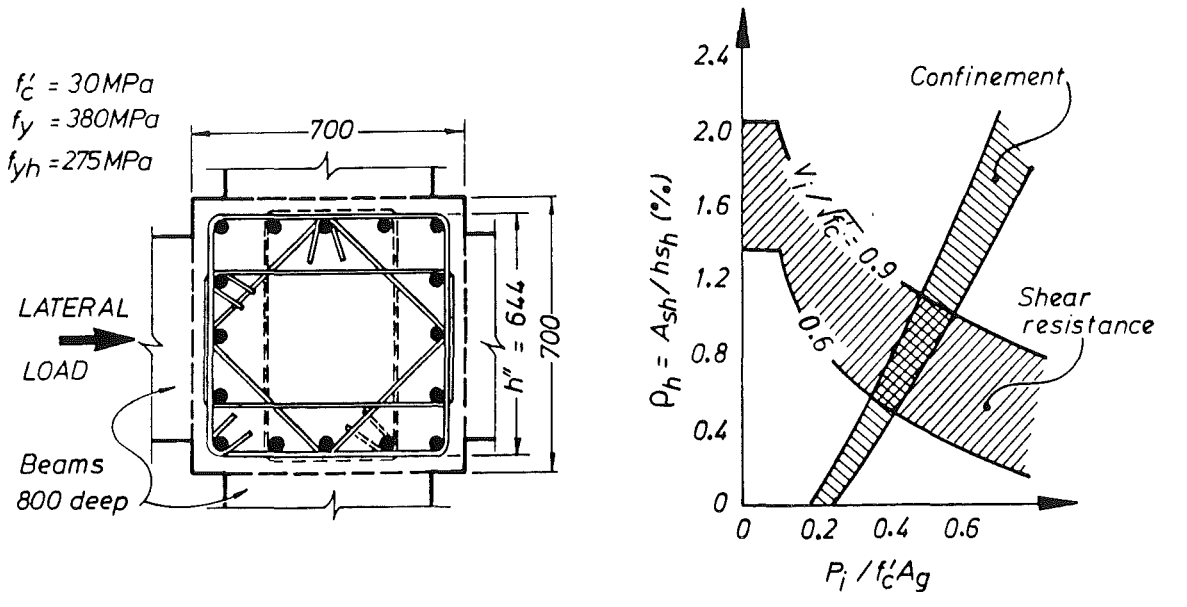

(a) Section of Example Column (b) Requirements for Transverse Reinforcement

Fig.2.18 - Requirements for transverse reinforcement in the plastic hinge region of an example column [27]

actions, such as bending moment and axial compression applied to a column, and on the volume of compressed concrete so affected and hence to be confined.

2.4.2 Confinement of Joint Cores by Beams

The degree of joint confinement afforded by adjacent beams may be studied with the aid of the example joint in Section 2.3 which has already been discussed in some detail. For an inelastic joint in which the beam bars function with perfect bond (Fig.2.8), cyclic moment reversals will gradually reduce the horizontal concrete compressive forces at the vertical faces of the column. It has been suggested in Section 2.3.2 that these forces may become ineffective in developing the strut mechanism of shear resistance. Thus the possibility of any significant horizontal confinement can be ignored.

Even when horizontal compression exists such as in an elastic joint (Fig.2.7) or an inelastic joint with imperfect bond along beam bars (Fig.2.10), no confinement of the core concrete, in terms of the previously stated definition, will arise. In fact for the inelastic joint (Fig.2.10), as a consequence of steel stresses and corresponding strain variations along the beam bars, the joint depth must increase. The beam bars tend to stretch the joint horizontally.

In the extreme case of a near complete breakdown of beam bar anchorage as indicated in Fig.2.11, tensile stresses will prevail over the entire embedded length of the bars. As seen in Fig.2.11 very large concrete compression force C_c is generated. This may then be viewed as significant confinement of the joint core afforded by adjacent beams. Indeed the concrete in the cores of such joints is usually not in distress. The likelihood of a shear failure along a diagonal tension failure plane is greatly diminished. However, the significant elongation of the beam bars and the associated slip will result in extremely poor hysteretic response. Such joints are not desired in ductile frames.

It may be argued that transverse beams improve the confinement around a joint core. However, the effects of diagonal earthquake attack on a structure need to be considered. Accordingly, it is to be expected that adverse stress conditions occur simultaneously in both principal directions of a two-way frame. Joint conditions in terms of confinement must be worse in such joints than in joints of one-way frames, unless bond failure of beam bars

within the joint cores, implied in Fig.2.11, is considered to be acceptable.

2.4.3 Confinement of Joint Cores by Transverse Reinforcement

As stated earlier, concrete compression stresses in the joint core, also part of a column, are seldom, if ever, critical. As seen in Fig.2.17 typically column bending moments at the level of the centre of joint are negligibly small. Poisson effects due to inelastic flexural actions do not arise. Hence significant confining stresses in horizontal ties or hoops are not mobilized.

Yet it may be claimed that the joint core is confined because the transverse reinforcement, anchored at the boundaries of the joint, is often highly stressed and it may even yield. The confining pressure so developed is, however, primarily associated with the mechanism of shear, as shown in Fig.1.7(b) and Fig.2.4(d), rather than with Poisson effects. If beam and column bars are efficiently anchored in the joint core, large shear forces, introduced at the four edges of the joint core necessitating the development of the diagonal compression field shown in Fig.2.3, are introduced to the diagonally cracked concrete (see also Fig.2.8). If bond transfer is poor, as Fig.2.11 indicates, only insignificant shear forces at the boundaries of the joint will be developed and hence only small shear deformations (Fig.2.3) will result. These deformations will not mobilize the tensile strength of transverse reinforcement that may have been provided. Thus it is suggested that the primary and indeed predominant role of transverse reinforcement in a joint core is its contribution to shear strength rather than to a confining mechanism.

2.4.4 Confinement of Joints by Floor Slabs

The mechanism of slab contribution, adjacent to a joint, in terms of flange action of beams, is examined in considerable detail in Chapter 7. However, test results suggest that after significant inelastic displacement excursions, there will be very little, if any, physical contact between the concrete in the joint core and that in the slab which surrounds it. When during a seismic attack, compression stresses are introduced to the joint core by a slab, acting as a compression flange, this can occur only on one side of the column. On the opposite side of the column, the slab having full depth cracks is clearly in tension. Thus at the level of a floor slab no

confinement of the joint core can be expected when ductile response controls frame behaviour.

2.4.5 Trends in the Demand for Transverse Reinforcement in Columns

(a) Shear reinforcement

It is generally accepted that in the potential plastic hinge regions of beams or columns without axial load, the entire shear resistance should be assigned to transverse (web) reinforcement. However, as axial compression load on a column is increasing, concrete shear mechanisms, other than the traditional truss, are also mobilized. When the design for shear is based on a diagonal compression field [55], the demand for transverse reinforcement can be readily shown to be reduced because of the reduced inclination of diagonal struts with respect to the member axis. Thus, as Fig.2.18(b) shows qualitatively, for a given shear, as measured by shear stress v_i, the demand for transverse (shear) reinforcement in the example column of Fig.2.18(a) reduces as the axial compression load increases [27].

(b) Confining reinforcement

When no or very small axial load is present, little confinement of the compressed concrete in the plastic hinge of a column is required, even when large curvature ductilities are to be developed. However, as the axial compression load, and hence the depth of the flexural compression zone, increase, confinement of the compressed concrete, to enhance its strain capacity, is of great importance. The general trend according to a recent study by Soesianawati and Park [63] for a range of curvature ductility demands is shown in Fig.2.18(b). The important task of providing effective lateral support to compressed bars in columns, will require considerable amounts of transverse reinforcement in the end regions of columns. This is often the controlling requirement, not shown in Fig.2.18, when axial compression loads on the column are relatively small.

(c) Relevance to joint cores

If it is accepted that, apart from anchorage criteria, shear resistance is the most important aspect of joint design, then the corresponding demand for transverse reinforcement, as shown in Fig.2.18(b) is

relevant. This means that the largest demand for shear reinforcement arises when axial load on the column, and hence on the joint core, is small.

Confining requirements clearly show a reverse trend. Only for column axial loads of moderate intensity might shear and confining requirements in a column lead to similar demands for transverse reinforcement. It must be recalled, however, that the need for confining reinforcement, shown in Fig.2.18(b) arises in columns outside the joint and not within the joint. On the other hand, the shear stress intensities implied in Fig.2.18(b) are those typical in beam-column joints rather than outside of it.

CHAPTER 3

TEST PROGRAMME

3.1 INTRODUCTION

As reported in Section 1.6, three full-scale reinforced concrete beam-column joint assemblies with floor slabs were designed in compliance with the current New Zealand concrete code [4] and tested under simulated earthquake loading. The structural dimensions and loading history followed the guidelines of the collaborative research project. Each of the three assemblies tested represented typical joint in three-dimensional building frames. The three assemblies were as follows :

Unit 1D-I : Interior beam-column-slab joint of a one-way frame.
Unit 2D-I : Interior beam-column-slab joint of a two-way frame.
Unit 2D-E : Exterior beam-column-slab joint of a two-way frame.

The aim of the tests was to examine the behaviour of the test assemblies under the simulated effects of a major earthquake so as to assess the structural adequacy in terms of the performance criteria described in Chapter 1. In particular, the effects of bidirectional loading and of the presence of transverse beams and floor slabs were to be investigated.

3.2 TEST UNITS

Details of the three Units, as constructed, are shown in Figs. 3.1 to 3.3. The Units were to simulate full-scale joint assemblies in frames of 3.5 metres storey height. The beam shear span provided in the Units was only about two-thirds of the distance to the midspan of an assumed prototype which had a beam span of 6 m. Also, the cantilever span of the one-way slab of Unit 1D-I, which modelled the topping slab of a ribbed floor system, was slightly less than one-third of an assumed prototype which had a 6 m span between two frames. The seismic load simulation is not considered to have been affected by these small changes. More significant effects, however, could have been due to the reduction in slab width participating as a beam flange. Because of this reduction some D10 slab bars parallel to but away from the beams of each

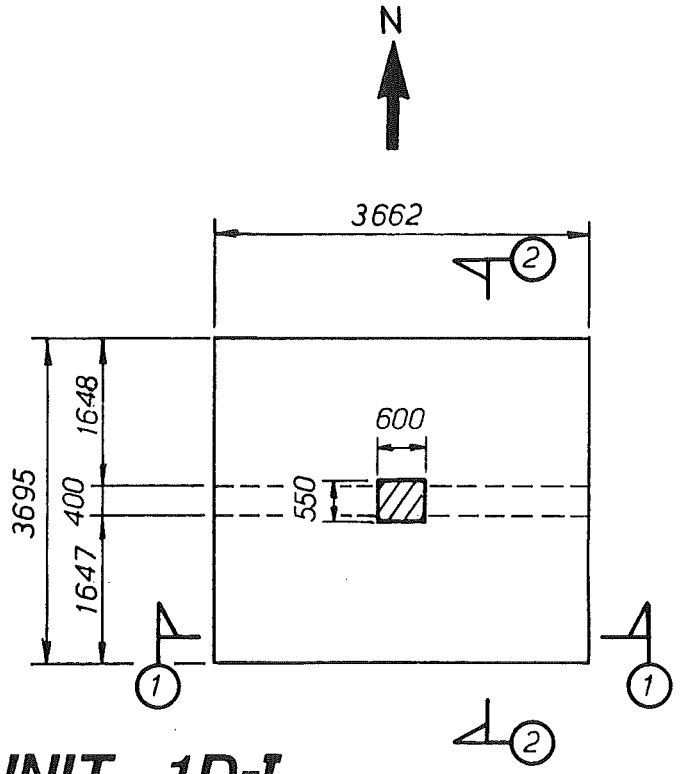

UNIT 1D-I PLAN

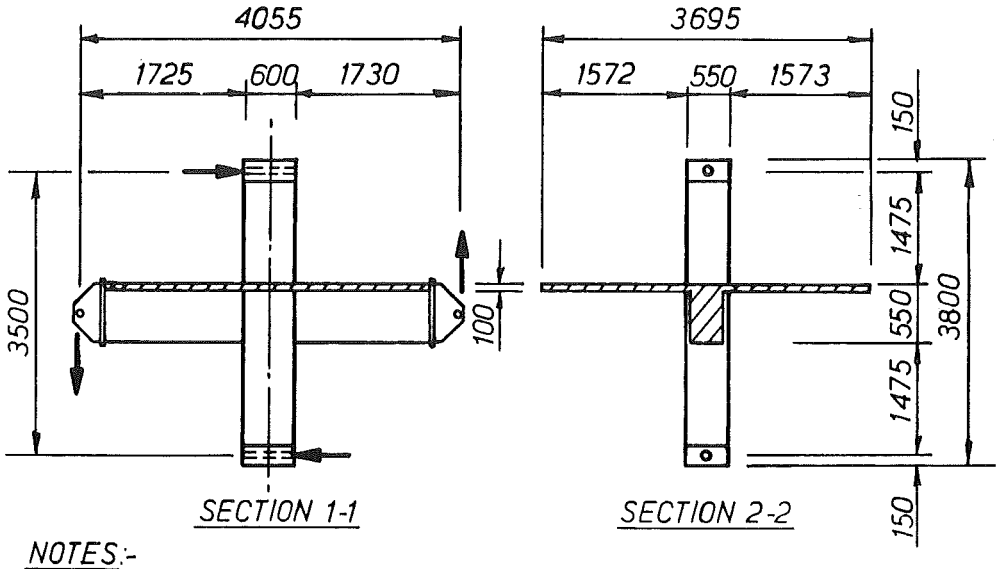

NOTES:-

1. Specified concrete strength at 28 days to be 30 MPa
2. Concrete cover to main reinforcement of beams and columns to be 40mm
3. Grades of reinforcing bars to be as follows: R = Grade 275 round bars
   D = Grade 275 deformed bars
   HD = Grade 380 deformed bars

(a) GENERAL ARRANGEMENT OF TEST UNIT 1D-I

Fig.3.1 - Details of Unit 1D-I

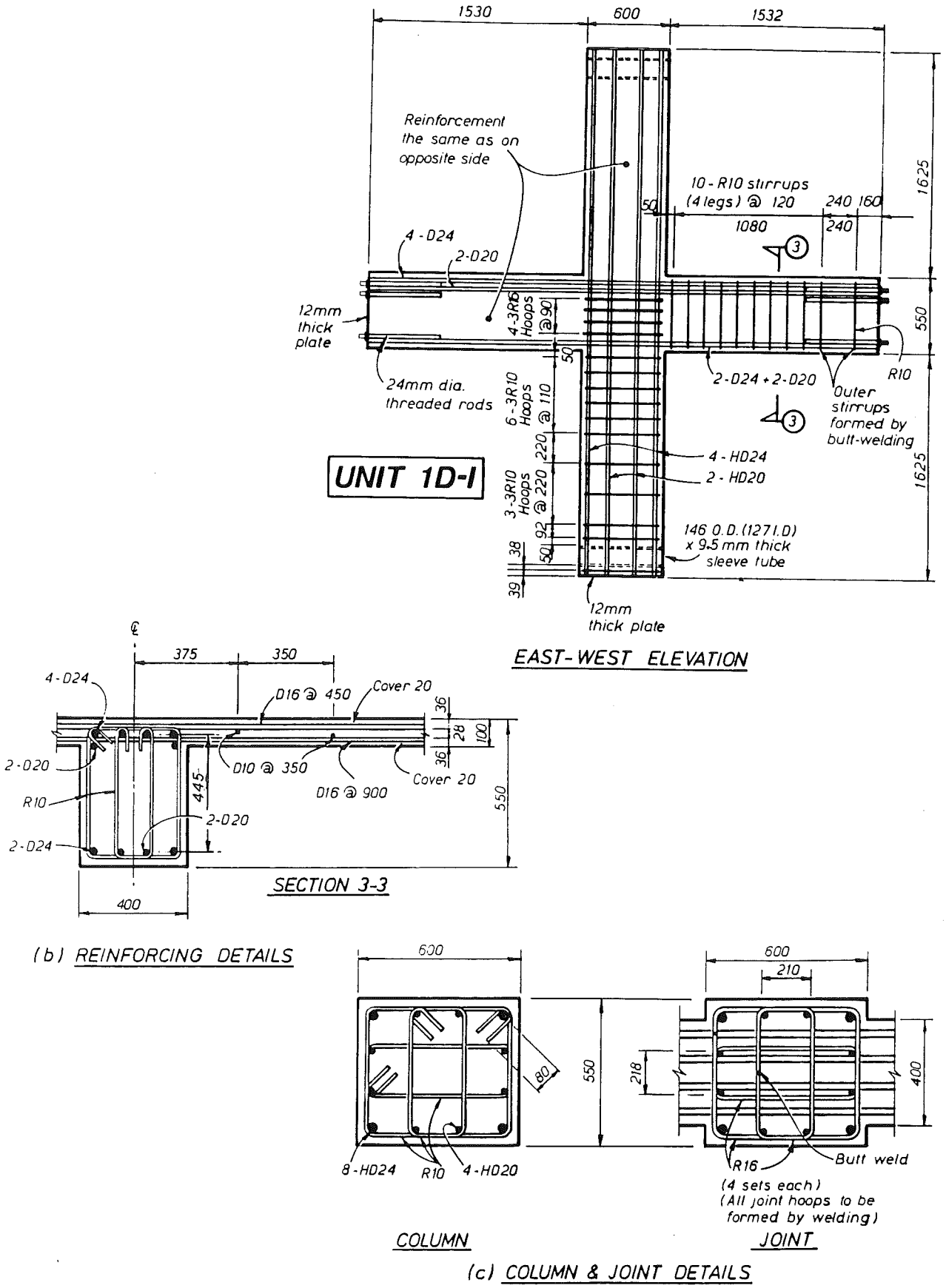

Fig.3.1 - Details of Unit 1D-I (continued)

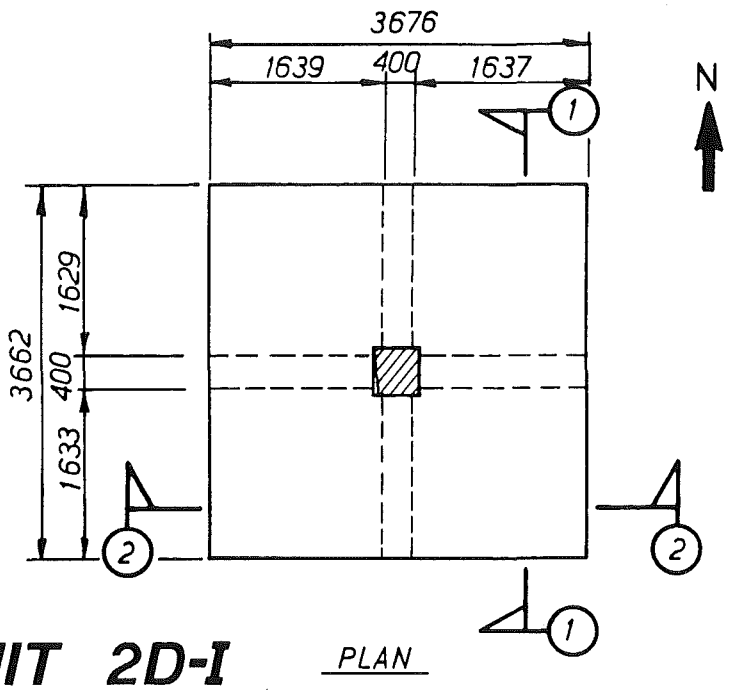

UNIT 2D-I PLAN

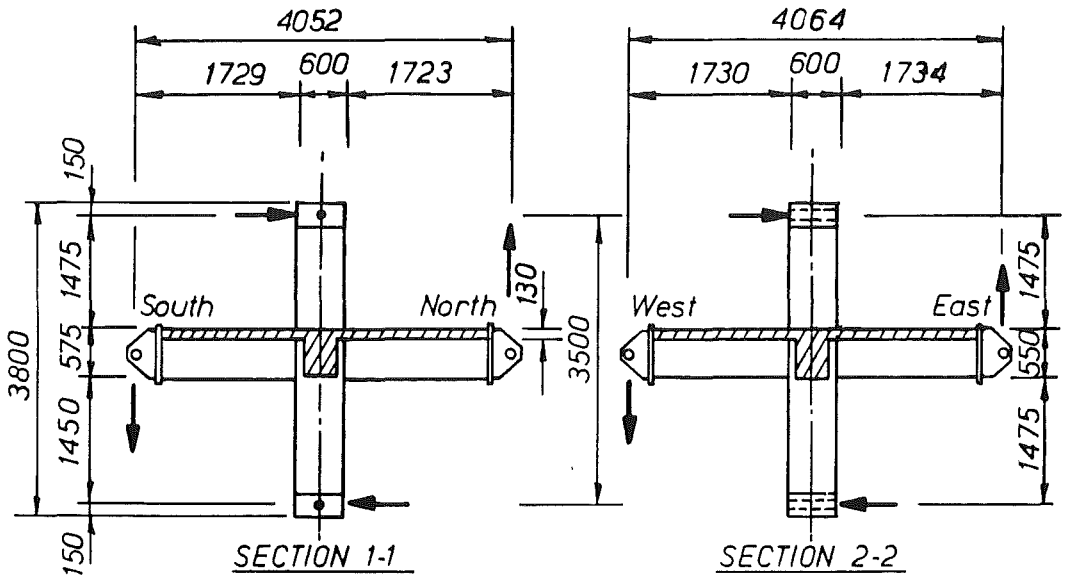

NOTES: 1. Specified concrete strength at 28 days to be 30 MPa

2. Unless otherwise noted concrete cover to main reinforcement to be as follows:
   40mm for beams & columns
   20mm for slabs

3. Grades of reinforcing to be as follows:
   R : Grade 275 round bars
   D : Grade 275 deformed bars
   HD : Grade 380 deformed bars

(a) GENERAL ARRANGEMENT OF TEST UNIT 2D-I

Fig.3.2 - Details of Unit 2D-I

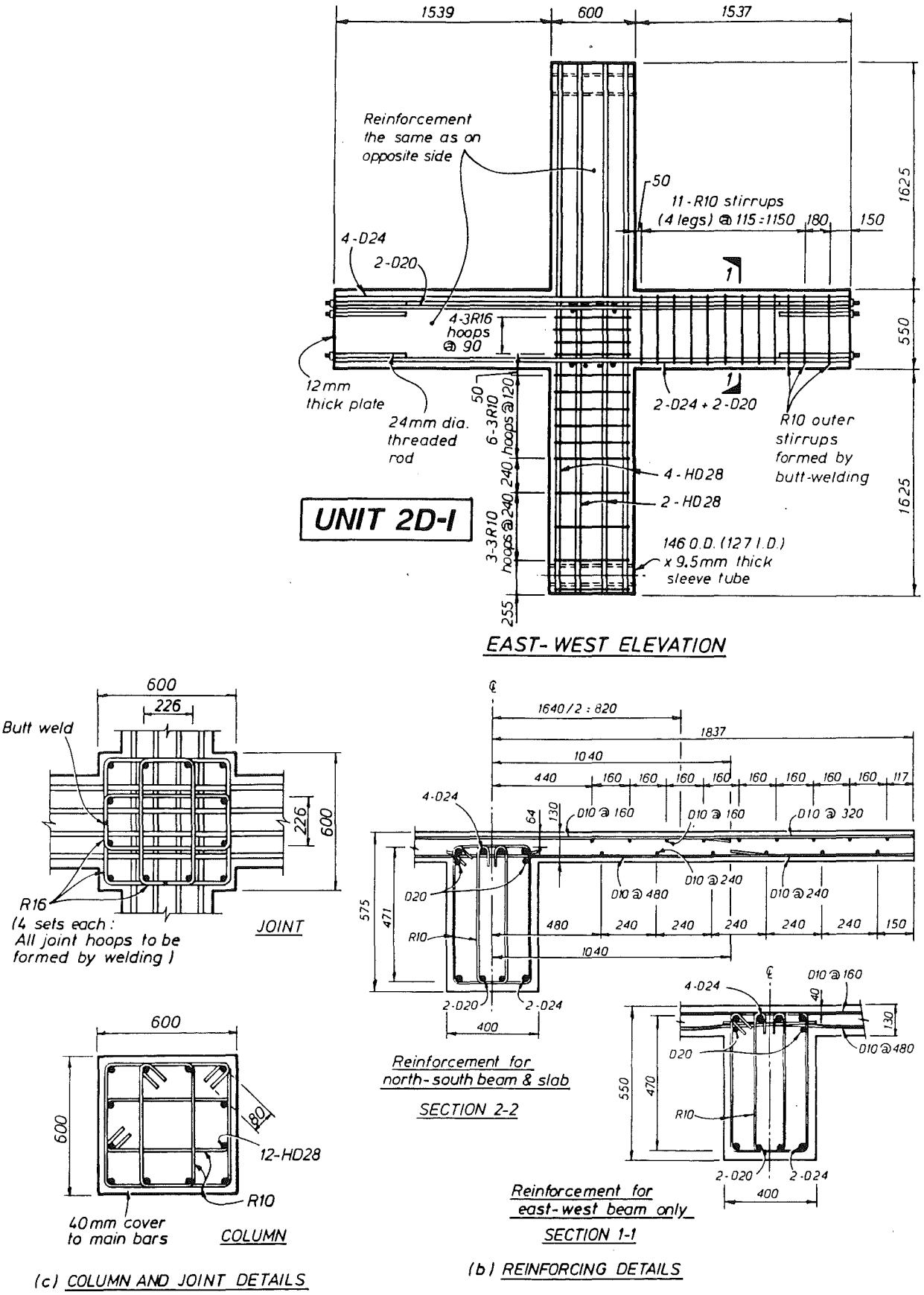

Fig.3.2 - Details of Unit 2D-I (continued)

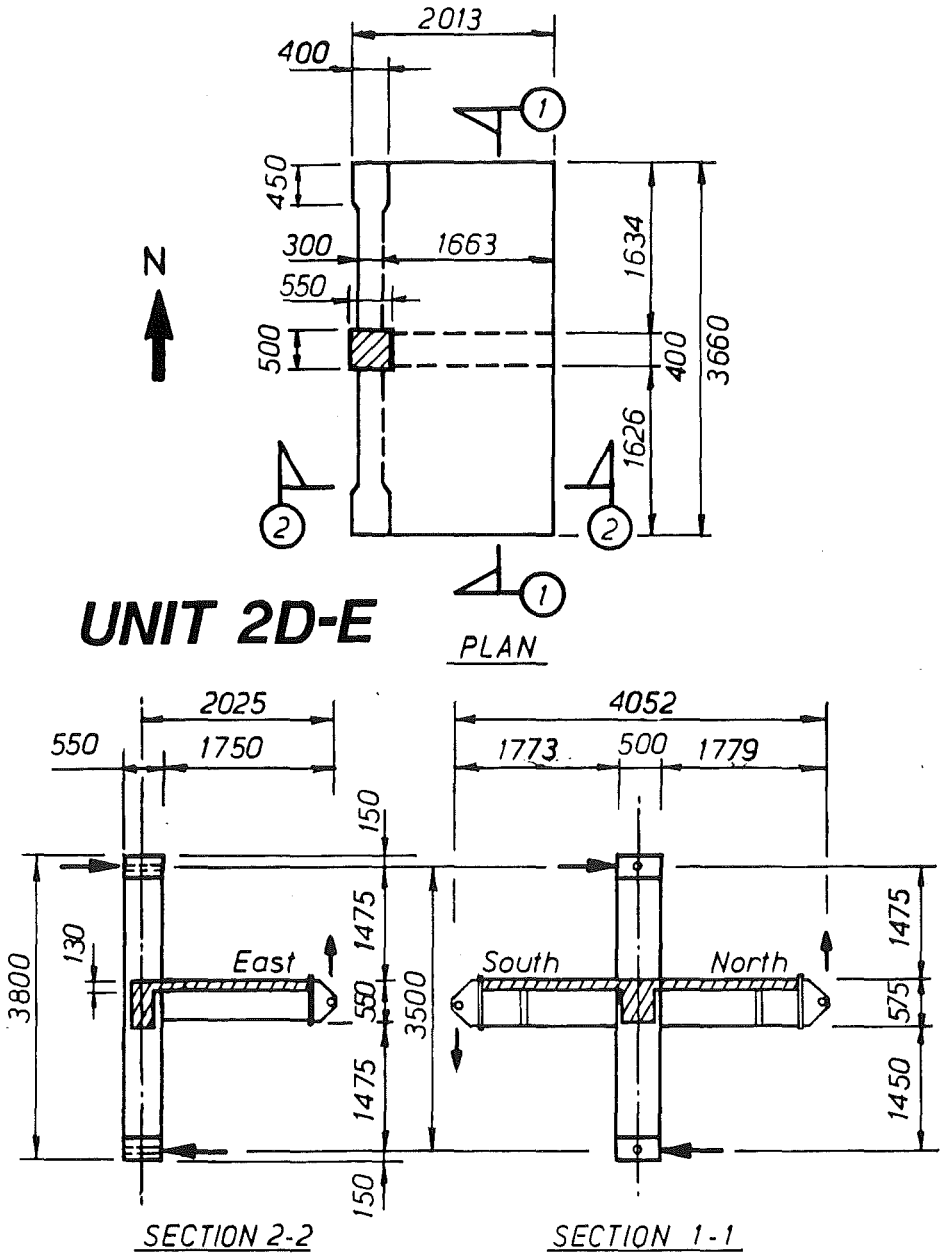

NOTES:

1. Specified concrete strength at 28 days to be 30 MPa
2. Unless otherwise noted concrete cover to main reinforcement to be as follows :
   40mm for beams & columns
   20mm for slabs
3. Grade of reinforcing bars to be as follows :
   R - Grade 275 round bars
   D : Grade 275 deformed bars
   HD : Grade 380 deformed bars

(a) GENERAL ARRANGEMENT OF TEST UNIT 2D-E

Fig.3.3 - Details of Unit 2D-E

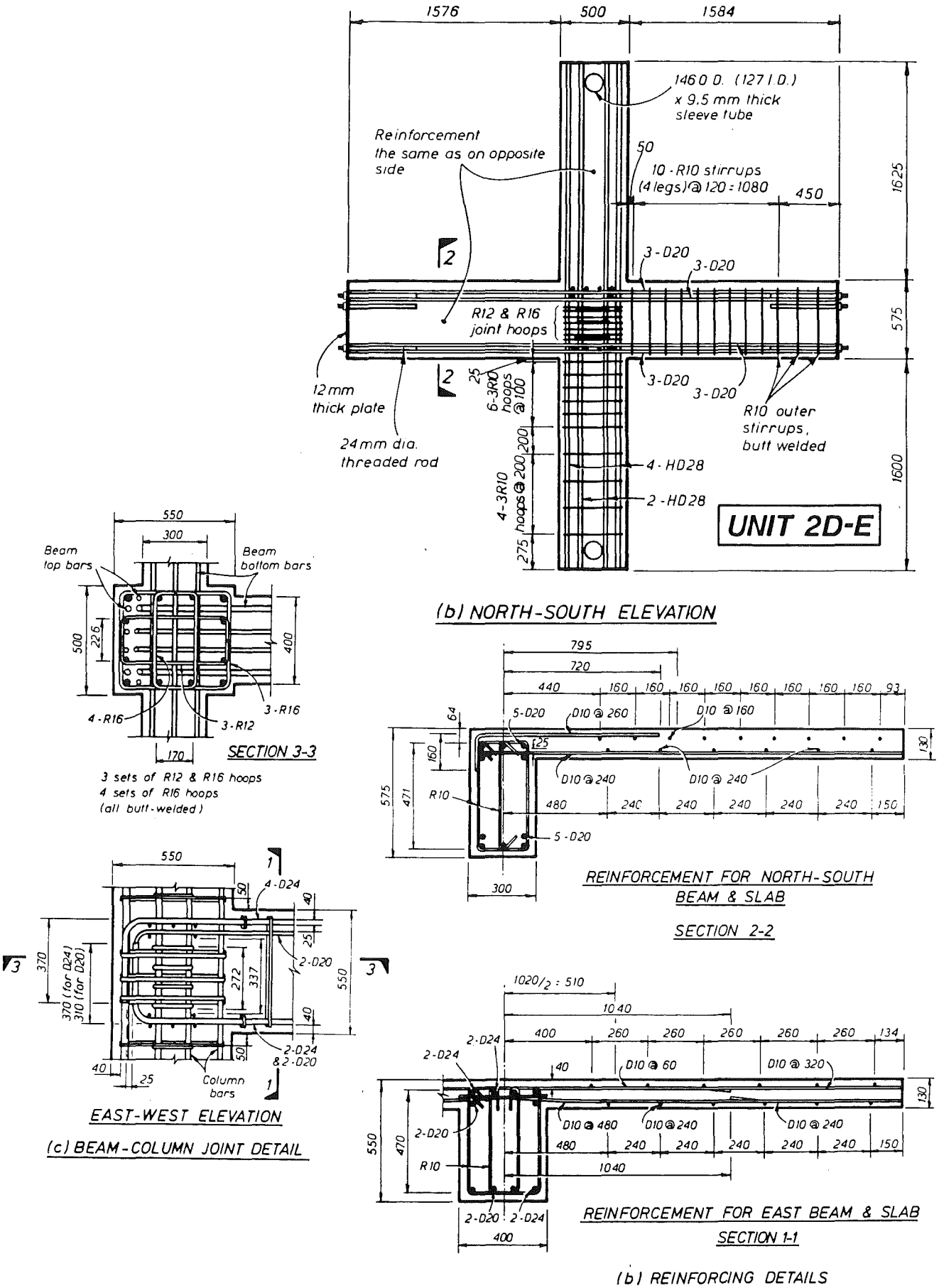

Fig.3.3 - Details of Unit 2D-E (continued)

Unit, which would have been placed in the larger prototype structure, had to be omitted. The action of this slab reinforcement, as possible tension reinforcement of the beams, was therefore not fully modelled. Apart from this omission, the layout of the slab reinforcement in each test assembly followed closely that of prototype construction. For Unit 1D-I (Fig.3.1), D16 bars were used for the slab transverse reinforcement so as to model the top flexural reinforcement of a ribbed one-way floor. These bars were placed in two layers in order to safeguard against a possible separation of the longitudinal beams from the slab.

The reinforcing details are shown in Figs. 3.1, 3.2 and 3.3, and the main reinforcement ratios are summarised in Table 3.1. Further details of slab bar arrangements can be seen in Figs.3.14 to 3.16 which show the positions of strain gauges. Design calculations for the three Units in accordance with NZS 3101 [4] and based on specified material properties are given in Appendices B.1, C.1 and D.1.

In the joint core of each test assembly, reinforcement was placed to resist the total design horizontal shear forces acting across the joint core, as is required by the New Zealand concrete design code [4] when the axial load level on the columns is less than $0.1f'_cA_g$. Thus a considerable quantity of horizontal hoops was necessary in each joint core. A smaller amount of transverse reinforcement would be required in the joint core if the ACI building code [5] was followed. The New Zealand code requirement is based on previous observations [39] that, when the axial load on the column is low, at large inelastic cyclic displacements the shear resistance provided by the diagonal concrete compression strut across the joint core diminishes, while that by a truss mechanism formed by the joint core reinforcement becomes dominant. When the axial column load is large this degradation of the diagonal compression strut mechanism is not so marked. To examine the worst case of joint core behaviour, no axial compression was applied to the upper columns of the test assemblies.

Initially all beams were designed to be of equal measured length from the centre of each Unit. After concreting and placing in position of the load transfer plates and pins, the shear span of the beams were found to be slightly different (Figs.3.1 to 3.3). During the test, the beam end-displacements were adjusted so as to achieve equal rotations for the two beams, as shown in Fig.1.4(b).

Table 3.1 - Summary of reinforcement ratios of test units

Unit		1D-I	2D-I	2D-E
Slab(1)	Thickness	100mm	130 mm	130 mm
	EW top	0.224%	0.377%	0.232%
	EW bottom		0.252%	0.252%
	NS top	0.447%	(Same as EW)	0.377%
	NS bottom	0.223%		0.252%
East/West Beam	Size	400 mm x 550 mm	400 mm x 550 mm	400 mm x 550 mm
	Top	(2-D10 slab bars included) 1.34%	(8-D10 slab bars included) 1.58%	(2-D10 slab bars included) 1.34%
	Bottom	0.77%	0.77%	0.77%
North/South Beam	Size	None	400 x 575 mm	300 x 575 mm
	Top	None	(8-D10 slab bars included) 1.57%	(4-D10 slab bars included) 1.30%
	Bottom	None	0.73%	1.03%
Column	Size	600 (EW) x 550 (NS) mm	600 x 600 mm	550 (EW) x 500 (NS) mm
		1.48%	2.05%	2.69%
Joint(2)		1.62%	(EW & NS) 1.62%	(EW) 1.25% (NS) 1.66%

Notes : (1) Reinforcement ratio of slab is expresseed in terms of gross concrete area.
(2) Reinforcement to resist vertical joint shear forces is provided by the intermediate longitudinal bars of the column.
(3) Notation : D10 = Grade 275 deformed bar of 10 mm diameter

Table 3.2 - Summary of ratios of bar diameter to beam or column depth of test units

Unit	1D-I	2D-I	2D-E	
Beam (Grade 275 steel)			North/South	East
Max. bar dia., d_b	24 mm	(identical to 1D-I)	20 mm	Anchorage length of hook exceeded code specified development length
Column depth, h_c	600 mm		500 mm	
d_b/h_c	1/25		1/25	
NZS 3101 limit	1/25		1/25	
Column (Grade 380 steel)				
Max. bar dia., d_b	24 mm	28 mm	(identical to 2D-I)	
Beam depth, h_b	550 mm	550 mm		
d_b/h_b	1/22.9	1/19.6		
NZS 3101 limit	1/20	1/20		

When constructing each Unit, the column and beam reinforcing cages were first fabricated on the floor and then lifted into the vertical testing position with the column pins in place. After the timber formwork has been erected, slab bars were fixed. Concrete was placed in two pours, a construction joint being made across the column section at the top of the slab. The second pour was carried out about a week after the first one. The concrete of the slab was cured by covering with damp hessian sacks for seven days. Upon removal of the formwork the concrete surface was inspected. The whole test unit was then given a coat of flat white paint to facilitate observation of cracking. Figures 3.4(a) to (c) show the Units under construction and Figs.3.5(a) to (c) show the test set-up at the end of the three tests.

Other important features of the design of the Units are summarised as follows :

1. The longitudinal reinforcement in the webs of all east-west beams (east beam only in Unit 2D-E) were kept identical. This enabled a direct comparison of the behaviour of exterior and interior joints.

2. The ratios of the diameter of the longitudinal bars to beam or column depth are listed in Table 3.2. They satisfied the current New Zealand code requirements [4] for ductile detailing.

3. In estimating the design shear forces applied to the beams and columns of a Unit, it was assumed that all the longitudinal beam and effective slab bars in tension were stressed to 1.25 times the specified yield strength of the steel (that is, to 1.25 x 275 MPa in this test series). With the use of these enhanced beam flexural strengths, it was the intention to eliminate flexural failure in the columns and shear failure in the beams and columns. Generally, the quantity of transverse reinforcement in the beams and columns was governed by limitations on the maximum tie spacing for concrete confinement and stability of compression reinforcement.

4. The design actions on the columns were estimated from the beam flexural overstrengths just mentioned, and supplemented by a dynamic magnification factor, ω. The test units are representatives of

(a) Column-beam reinforcing cages in position, with beam formwork partially erected (Unit 1D-I)

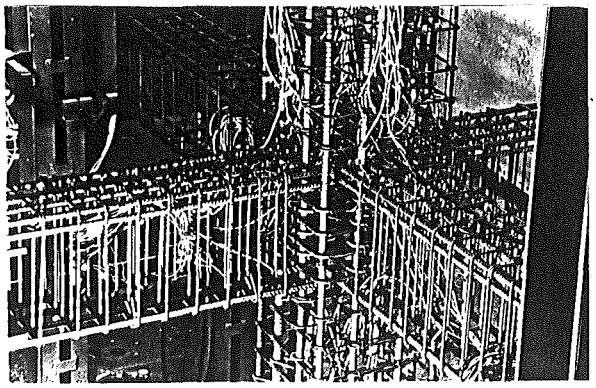

(b) Column-beam reinforcing cage in position with formwork to be erected (Unit 2D-I)

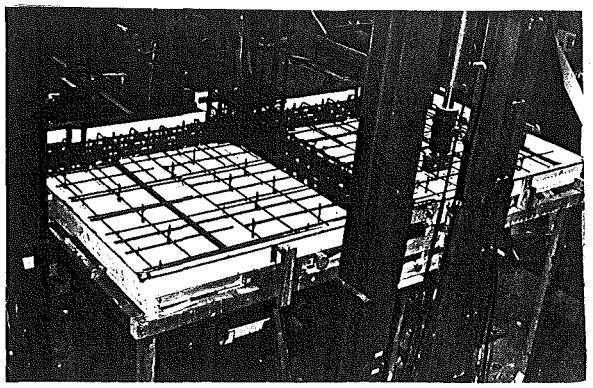

(c) Slab reinforcement and formwork completed, ready for first concrete pour (Unit 2D-E)

Fig.3.4 - Beam-column joint test assemblies under construction

(a) View from north-east at completion of test (Unit 1D-I)

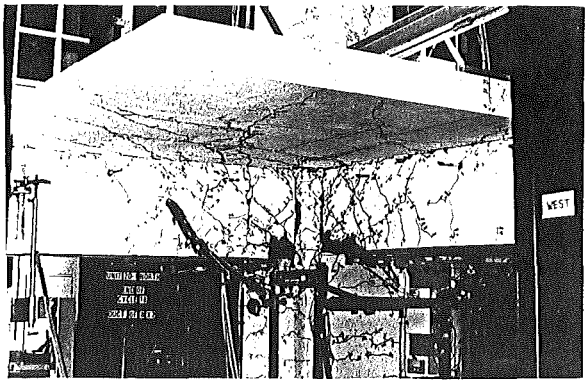

(b) View from north-west at the end of cycle 18, having attained a ductility of eight in both north-south and east-west directions (Unit 2D-I)

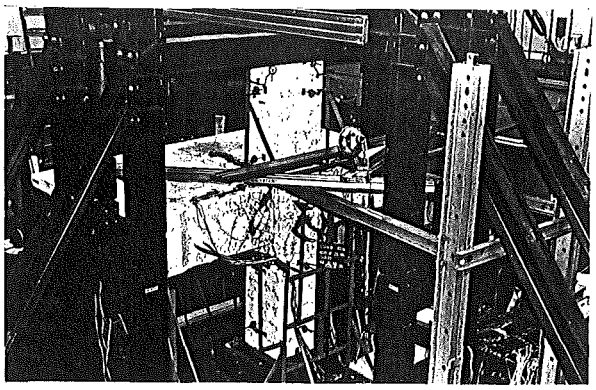

(c) View from north-west at the end of cycle 16, having attained a ductility of eleven in both north-south and east-west directions (Unit 2D-E)

Fig.3.5 - Test set-up of beam-column joint assemblies

members near the top of a multi-storey building where gravity induced axial loads on columns are rather small, but then the dynamic attack due to the higher modes of vibration may be more significant [4]. In a medium rise ductile frame, the recommended values of ω would be of the order of 1.6 for one-way frames and 1.7 for two-way frames. In this test series, however, the minimum values were adopted, resulting in $\omega = 1.3$ for Unit 1D-I and $\omega = 1.5$ for Units 2D-I and 2D-E. Thus when the code [6] design earthquake moment derived for a column is M_{code}, the final design column moment M_{col} becomes [4]

$$M_{col} = \omega\phi_o M_{code} - 0.3 h_b V_{col} \qquad (3.1)$$

where ϕ_o = overstrength factor = 1.25/0.9 = 1.39
h_b = depth of beam
V_{col} = column design shear force

Eq.(3.1) provides for adjustment to translate centre-line moments to those at the critical sections (i.e. beam top or soffit).

The design calculations in Appendices B.1, C.1 and D.1 are those generally used in routine design of prototype structures in New Zealand. To highlight the principles of the capacity design procedure [4], the resulting provided flexural strengths of the columns, shown as M_{ci} in Table 3.3, are compared to the required strengths when flexural plastic hinges form in the framing beams. All strengths were estimated according to the ACI stress block method [5] as explained in Section 3.8, on the basis of specified material properties and taking the strength reduction factor $\phi = 1.0$. In Table 3.3, the columns moments (1) to (3) are referred to those at the top and soffit of the beams. When column moments are compared to beam moments at a joint, a space ratio r_s needs to be introduced to take into account the physical dimensions of the joint core. In Table 3.3, however, the ratios M_{ci}/M_{des} and M_{ci}/M_{max} are identical to those referred to the extrapolated moments at a nodal point which is the centre of a joint. A space ratio is therefore not needed. The consequent moment ratios listed in Table 3.3 are comparable to the enhancement coefficient 1.25ω, with the values of ω as suggested in the last paragraph.

Table 3.3 - Comparison of design and provided flexural strengths of columns on the basis of specified material properties

Unit		1D-I	2D-I		2D-E	
		EW	EW	NS	EW	NS
(1)	M_{des} (kNm)	274.1	306.1	321.0	157.5	230.8
(2)	M_{max} (kNm)	383.1	468.6	486.0	255.9	325.7
(3)	M_{ci} (kNm)	474.7	700.4	700.4	626.9	560.3
	$\frac{M_{ci}}{M_{des}}$	1.73	2.29	2.18	3.98	2.43
	$\frac{M_{ci}}{M_{max}}$	1.24	1.49	1.44	2.45	1.72

Notes : (1) M_{des} is the column moment when the positive and negative flexural plastic hinges form in the beams, with the effective tension flange width of the beam as assumed by the New Zealand code NZS 3101:1982 and tensile steel stress f_y = 275 MPa.

(2) M_{max} is the maximum column moment when all beam and slab bars in tension have reached strain hardening with steel stress as 1.25 x f_y = 1.25 x 275 MPa.

(3) M_{ci} is the nominal (ideal) flexural strength of the column with steel stress based on f_y = 380 MPa.

(4) Compressive strength of concrete at 28-day is specified as f'_c = 30 MPa.

For the second and third test units, further considerations with respect to biaxial bending of columns need be given. As the beam strengths of Unit 2D-I in both directions are practically identical, the column may be subjected to $\sqrt{2}$ times the storey shear corresponding with unidirectional attack. By considering the fact that the theoretical flexural strength of a typical square column section on a diagonal is of the order of 90% of that corresponding to principal axes, the unidirectional attack of design moments, due to M_{code}, should be magnified by

$$\frac{\sqrt{2}}{0.9}\ (1.25/0.9) = 2.18$$

This is close to the code's recommendation of $\omega\phi_o = 1.5(1.39) = 2.08$

It can be seen that the columns, in particular that of Unit 2D-E, were considerably reinforced as a result of practical considerations. The design was somewhat unrealistic because, to represent the test situation, no axial load on the columns was considered. In the real structure, some axial compression would be expected and hence the required reinforcement contents in prototype columns could probably be less than those used in these tests.

5. The design shear forces across the joint cores were also estimated by assuming that the effective flexural reinforcement of the beam reached a stress level of 1.25 times the specified yield strength of the steel. The horizontal and vertical joint shear forces are listed as V_{jh} and V_{jv} in Table 3.4 and are compared with the shear resistance provided by the horizontal and vertical joint reinforcement, V_{sh} and V_{sv}. In accordance with code [4] recommendations, the intermediate longitudinal bars of the column were considered to be effective in resisting vertical shear in the joint cores. For horizontal shear, the joint hoops present in each Unit provided resistance almost identical to the design shear force.

6. To predict the theoretical ideal (nominal) strengths and stiffness of the Units for the purpose of comparison in testing, the ideal flexural strengths of the beam sections were calculated using the measured material properties of the concrete and steel. The ACI code [5] method, which assumed an equivalent rectangular compressive

Table 3.4 - Comparison of required joint shear forces with shear resistance provided by reinforcement of units according to the New Zealand concrete design code NZS3101:1982

Unit		1D-I	2D-I	2D-E	
Horizontal shear force			(EW & NS)	(EW)	(NS)
(a) Design	V_{jh} (kN)	1212	1350	764	1041
(b) Provided (nominal)	V_{sh} (kN)	1061	1061	678	874
(c) Provided (actual)	V_{sh} (kN)	1273	1273	807	1046
Vertical shear force					
(d) Design	$0.4V_{jv}$ (kN)	444	518	479	
(e) Provided (nominal)	V_{sv} (kN)	478	936	936	

Notes :

(a) Design horizontal shear force V_{jh} is given by the resultant horizontal force acting either above or below a horizontal plane at the mid-depth of the joint core. V_{jh} was calculated assuming the beam longitudinal bars reaching a stress of 1.25 f_y, where f_y = 275 MPa, as specified. It is considered that all of V_{jh} is to be resisted by the horizontal shear reinforcement. The nominal joint core shear stress $V_{jh}/b_c h_c$ was less than $1.5\sqrt{f'_c}$ MPa, the maximum allowed (NZS3101) in all cases.

(b) Provided (nominal) shear resistance of horizontal joint core reinforcement is $V_{sh} = A_{jh} f_y$, assuming f_y = 275 MPa, as specified.

(c) Provided (actual) shear resistance of horizontal joint core reinforcement is $V_{sh} = A_{jh} f_y$, where f_y = measured yield strength of steel used in tests.

(d) Design vertical shear force for vertical reinforcement is $0.4V_{jv}$, where V_{jv} is given by the resultant vertical force acting on one side of a vertical plane through the joint core. $0.4V_{jv}$ is to be resisted by the vertical shear reinforcement and $0.6V_{jv}$ is to be resisted by the concrete diagonal compression strut.

(e) Provided (nominal) vertical shear resistance of intermediate column bars is $V_{sv} = A_{jv} f_y$, assuming f_y = 380 MPa, as specified.

stress block for concrete with a maximum concrete compressive strain of 0.003, was adopted. Since the floor slabs and beams were cast monolithically, they were expected to act integrally as T-beams. For negative bending moment producing tension in the top bars, the New Zealand code [4] considers that all longitudinal bars placed within a certain slab width can act as tension reinforcement for the beam. The flange width is assumed to vary depending on the structural configurations, and is illustrated in Fig.3.6. These New Zealand code recommendations were followed in the design calculations. For T-beams subjected to positive bending moment under seismic conditions, the effective width of the flange in compression was assumed in all cases to be twice the column width, as shown in Fig.3.7. Calculations showed that for positive bending moment, larger widths would not increase the moment capacity significantly. Flexural strength values estimated using other assumptions are to be discussed in Section 3.8 and shown in Appendices B.3, C.2 and D.2.

7. The ideal (nominal) strength of a Unit subjected to seismic loading is attained when a positive moment plastic hinge occurs in the beam at one face of the column and a negative moment plastic hinge occurs in the beam at the other face of the column (Fig.1.4(b)). In the figures of Chapters 5 to 7 showing the measured lateral force-lateral displacement hysteresis loops, this ideal strength is denoted as V_i and is used as reference value for the normalised scale V/V_i. An alternative case assumes that all longitudinal slab bars over the full width of the slab yield in tension and contribute to the negative moment flexural strength of the beam. The sum of this possible negative moment strength and the positive moment strength, defined as above, gives the theoretical maximum strength denoted in terms of the lateral forces applied to the column as V_i^* in the hysteresis figures. Gravity load effects were not simulated. The effect of the self-weight of beams and slabs was considered insignificant.

8. Units 2D-I and 2D-E were to simulate full-scale joint assemblies of a prototype two-way frame. Therefore some features of both specimens were made similar, the most obvious being the slab thickness (both

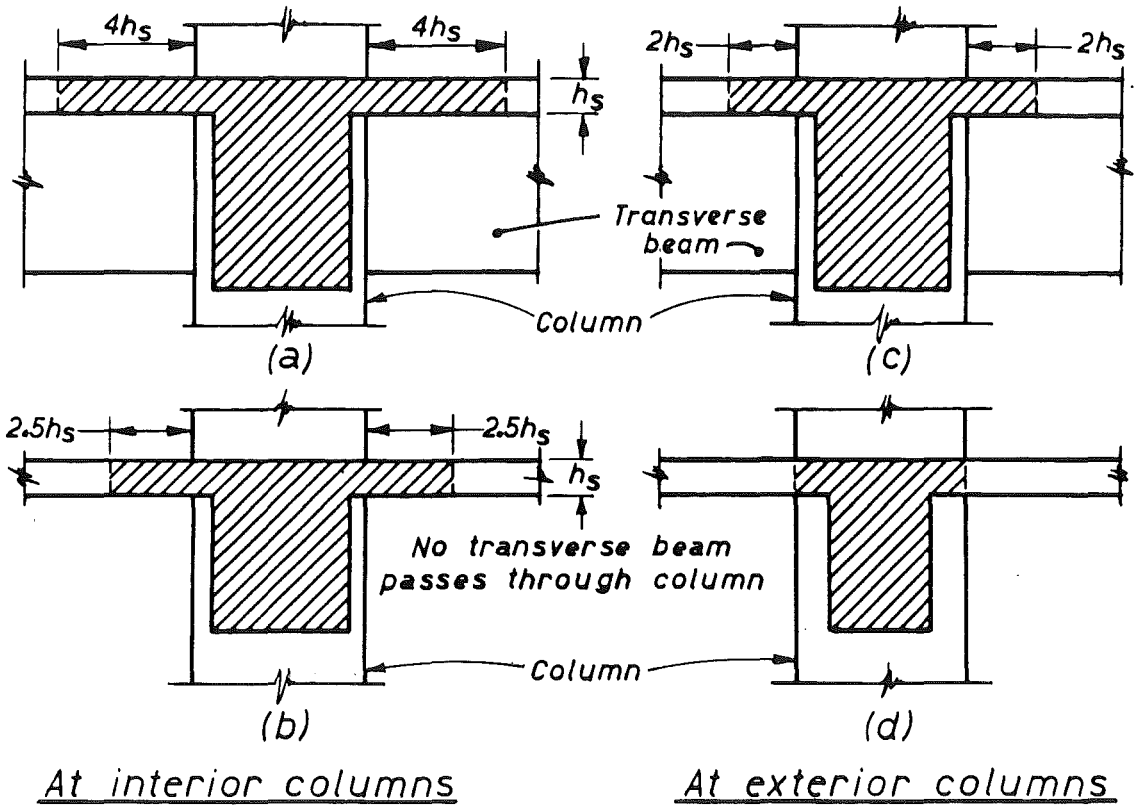

Fig.3.6 - Effective width of T-beam subjected to negative bending moment, within which the slab flexural reinforcement is considered as being fully effective in tension, as recommended by NZS 3101:1982 [4]

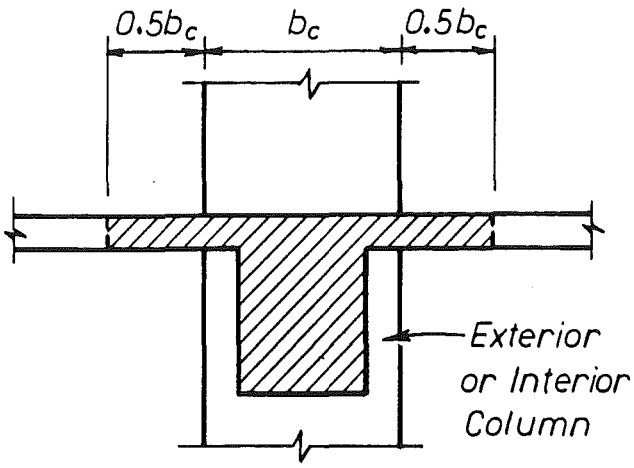

Fig.3.7 - Assumed effective width of T-beam subjected to positive bending moment causing compression in the slab

being 130 mm) and the east beam dimensions (as pointed out in point (1)). However, a significant deviation arose in the layout of the east-west slab reinforcement of Unit 2D-E. This followed that of a prototype edge slab. In the north-south direction, the (continuous) slab reinforcement arrangements of both Units were the same. Differences may be seen in Fig.3.2(b) and 3.3(b), as well as in Figs.3.15(b) and 3.16(b). Furthermore, in recognition of the smaller gravity load and lateral force imposed on the perimeter frame of the model building, the size of the N-S spandrel beams of Unit 2D-E was reduced accordingly (Fig.3.3). Similar considerations were given to the column. To enable installation of the standard steel load transfer plates to Unit 2D-E, ends of the north and south beams were widened to 400 mm (Fig.3.3(a)). The enlarged ends were adequately reinforced to prevent any failure at these locations.

3.3 MATERIAL PROPERTIES

3.3.1 Reinforcing Steel

The tensile properties of the reinforcing bars used were obtained by testing under monotonic loading in an Avery Universal Testing Machine with the strain being measured by a Baty mechanical extensometer of 50.8 mm gauge length. Table 3.5 lists the experimental results.

3.3.2 Concrete

Concrete was obtained from a commercial ready-mix plant. The maximum aggregate size was 20 mm. As can be seen from Table 3.6, which summarises the properties, a wetter concrete was used for the upper column pours in view of the difficulty in placing concrete in a restricted space. Although the cylinder strengths measured were below the specified limit of 30 MPa, it was found during the tests that the upper columns were structurally not inferior to the lower columns.

Table 3.5 Measured properties of reinforcing steel of test units

Grade of Steel	Grade 275 (MPa)							Grade 380(MPa)		
Bar Size	R10	R12	D10	R16	D16	D20	D24	HD20	HD24	HD28
Yield Strength, f_y(MPa)	315	320	326	330	318	300	283	482	500	432
Yield Strain, ε_y	0.0014	0.0013	0.0018	0.0015	0.0014	0.0013	0.0013	0.0024	0.0024	0.0018
Ultimate strength, f_u(MPa)	432	466	441	503	482	459	437	650	669	602

Notation : R10 = plain round bar of 10mm diameter

D20 = deformed bar of 10mm diameter

HD20 = deformed high strength bar of 20 mm diameter.

Table 3.6 - Measured properties of concrete of test units

Test Unit	1D-I		2D-I		2D-E	
Pour	1	2	1	2	1	2
Slump (mm)	75	150	50	100	75	150
f'_c at 28 Day (MPa)	43.5	25.3	35.5	25.1	43.5	25.3
Age at Test	80 days	71 days	130 days	126 days	80 days	71 days
f'_c at Test (MPa)	38.0	26.4	37.0	27.4	38.0	26.4

Notes : (1) Pour 1 included lower column, beams, slab and joint; pour 2 was for upper column only.

(2) f'_c = compressive strength of 100mm dia.x 200mm concrete cylinder

3.4 LOADING RIG

The configuration of the loading rig is shown in Fig.3.8. It consisted of two pairs of steel frames comprising diagonal struts, horizontal struts and vertical columns, all connected by high-strength friction grip bolts. In order to apply vertical forces at the beam ends either upwards or downwards with double-acting jacks, steel reaction beams to support the jack forces were to be fixed between the vertical columns. Pins were provided to enable the top and bottom of the concrete column to rotate in two perpendicular directions. The beam ends were also able to rotate and move laterally in the plane of the frame while the jacks were kept in a vertical position. Thus no axial forces were introduced to the beams. All forces were transmitted to the strong floor of the laboratory. The rig was designed to enable unidirectional or bidirectional (i.e. orthogonal east-west and north-south) simulated seismic forces to be applied without any alterations to the rig. In the test for Unit 1D-I, jacks at the east and west ends only were needed. For two-way joints, additional jacks were required at the north and south ends.

The way the column ends could rotate in two perpendicular directions can be seen from the details in Fig.3.8. Rotation of each column end was made possible by a steel box frame made up of four rectangular hollow sections joined by butt-welding. Each column end had a steel cap with the east and west sides bearing against the box frame. Tolerance was provided so that the column could still rotate in the north-south direction about the 126 mm dia. pin. On the other hand, the two 99 mm dia. pins allowed the box frame and the concrete column to rotate together in the east-west direction. The ends of the 126 mm dia. pin was machined to have vertical edges so that it could move vertically in the slots of the bearing plates. The photographs in Figs. 3.4 and 3.5 show the rig from different angles.

3.5 INSTRUMENTATION

3.5.1 Measurement of Forces

Load cells were used to measure the beam end forces by connecting each in series with a hydraulic jack (Fig.3.8(b)). Electrical resistance strain gauges were arranged in double circuits to give two outputs. The first

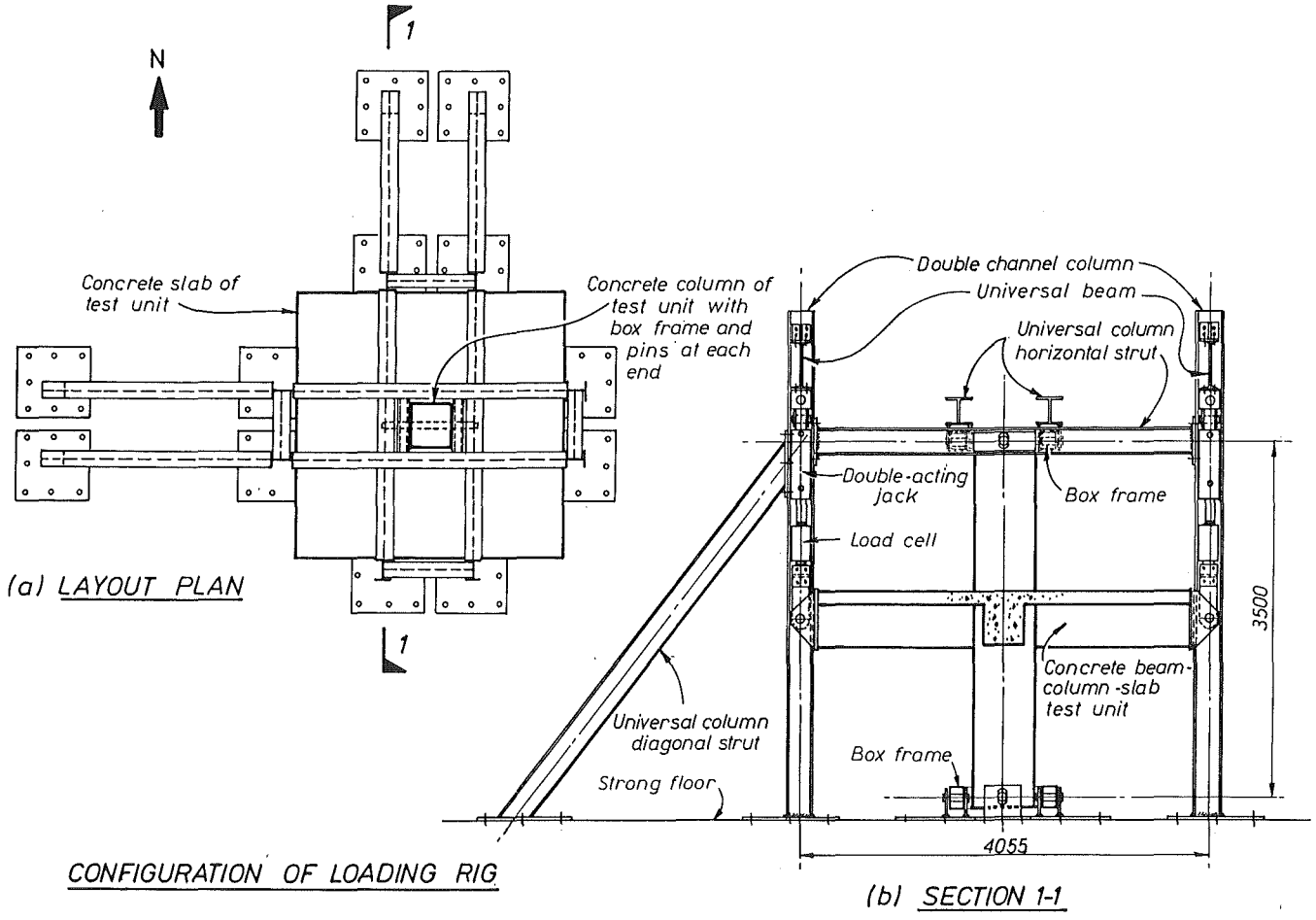

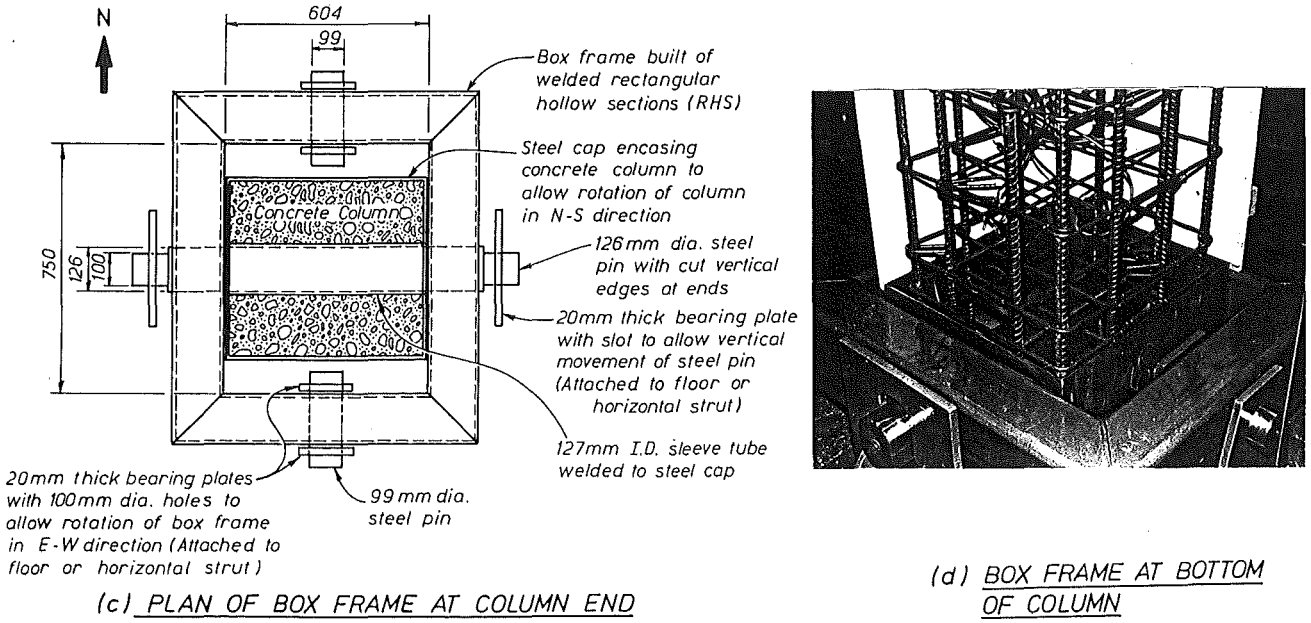

Fig.3.8 - The loading rig

output from each load cell was read directly using a Budd Strain Indicator against which the load cell had been calibrated in an Avery testing machine. The second output was used to drive the Y-axis of a Hewlett-Packard Pen Recorder, the X-axis of which was driven by the signal from a linear potentiometer that measured the beam vertical displacement. It was then possible to obtain an instantaneous plot of force-displacement relationship for each beam. This, however, served only as a reference in monitoring the overall progress of the test since the measured beam deflection included also the component due to the sidesway of the loading rig. It was necessary to correct the beam deflection values after measuring the lateral column deflection, as explained in Section 3.5.2. The force-displacement curves for the beams were then replotted.

3.5.2 Measurement of Displacements

To measure the beam deflections, joint distortions, and beam curvatures in the plastic hinge regions at the column face, linear potentiometers were used. For Unit 1D-I, they were installed as shown in Fig.3.9. Two potentiometers at the north face of the joint panel are not shown. All were connected to a 200-channel Solartron Data Transfer Unit which recorded voltage readings in punched paper tape. Each of the two linear potentiometers used with the pen recorder to monitor beam displacement were also connected in parallel with a Hewlett-Packard Digital Volt Meter (DVM). Reading from the DVM manually gave immediately the value of the gross beam deflection. Corrections were then made to obtain the real beam deflection by deducting the component due to horizontal column movement caused by deformations within the loading rig.

Five pairs of top and bottom potentiometers were used to measure curvatures of each beam within 825 mm from the column face. Each pair of potentiometers was attached to two steel rods embedded in the concrete of the beam. For fixity during concreting, all steel rods had to be tied to the main beam bars. It appeared inevitable that movements of these bars would be included in the potentiometer readings. To measure beam movements relative to the column, horizontal steel rods were embedded in the column so as to provide stationary targets for the potentiometers. This also alleviated the effect of spalling of the column concrete on the potentiometer readings. The rods were at least 90 mm above the top or bottom surface of the beam.

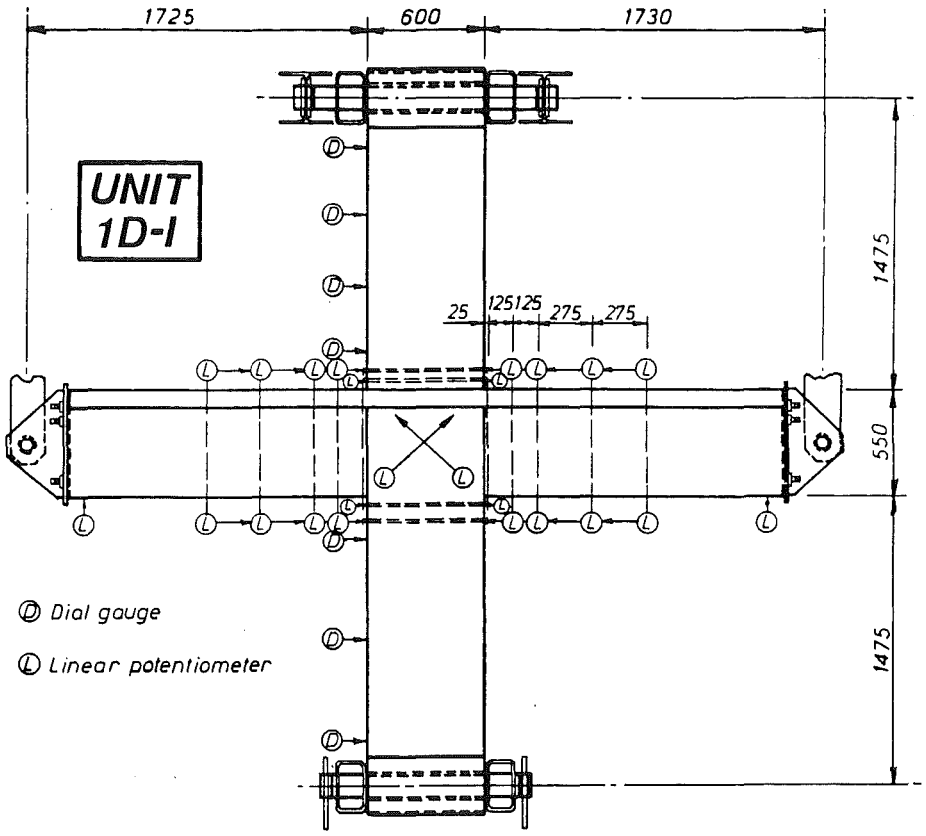

Fig.3.9 - Positions of linear potentiometers and dial gauges for Unit 1D-I

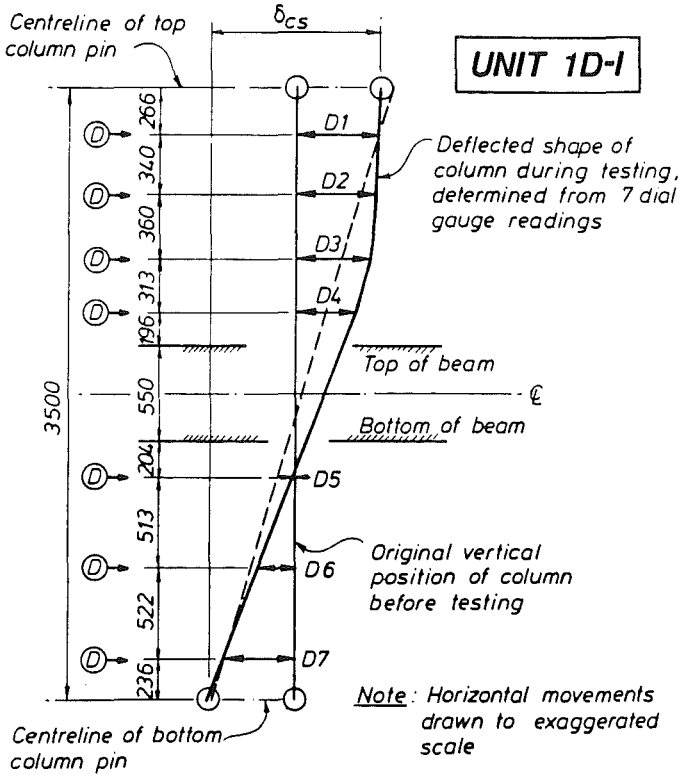

Fig.3.10 - Determination of horizontal east-west column movement from dial gauge readings (Unit 1D-I)

The horizontal east-west movement of Unit 1D-I was determined by the dial gauges shown in Fig.3.9. Direct measurements of movements of the column top or bottom 126 mm dia. pin were not taken because the pin was allowed to move inside the 127 mm dia. sleeve tube (see Fig.3.8(c)). Furthermore, placing a dial gauge in line with the top pin would occupay more space, causing obstruction to crack marking. As shown in Fig.3.10, the four dial gauge readings along the upper column, D1 to D4, and the three readings along the lower column, D5 to D7, gave information on the deformed shape of the column. The data were not sufficient and were not intended to be used to determine the curvatures of the column. Using the dimensions given in Fig.3.10, the movement of the centre of top pin relative to the bottom pin, δ_{cs}, could be reasonably estimated by

$$\delta_{cs} = (D1 + D7) + (D1 - D2)\frac{266}{340} + (D7 - D6)\frac{236}{522} \qquad (3.2)$$

To check the out-of-plane (north-south) movement of the test unit, additional dial gauges at the north face of the column, and at the vertical sides of the beam ends, were installed. They are not shown in Fig.3.9 but could be seen in the photograph of Fig.3.5(a). It was concluded that the tolerances provided in the rig allowed the test unit to undergo a small amount of horizontal out-of-plane movement and rigid body rotation about the column. However, this rotation was considered insignificant.

Displacement measurements for Units 2D-I and 2D-E followed the same principles just described. Further details are given in the following chapters on test results. Measurements were registered with respect to north-south (N-S) and east-west (E-W) directions. Figs.3.11 and 3.12 depict the actual positions of the dial gauges which monitored column movements. Because of difficulties with instrumentation, joint distortions for Unit 2D-I in both directions and Unit 2D-E in the E-W direction were not measured. However, it was possible to place two linear potentiometers diagonally at the exposed west face of the joint of Unit 2D-E, thus recording the shear distortions in the N-S direction. The arrangement was similar to that shown in Fig.3.9. In the tests of Units 2D-I and 2D-E, results were read through a CEDACS data acquisition system. It used an analogue-to-digital converter which was connected to a personal computer to control the scanning and record the signals.

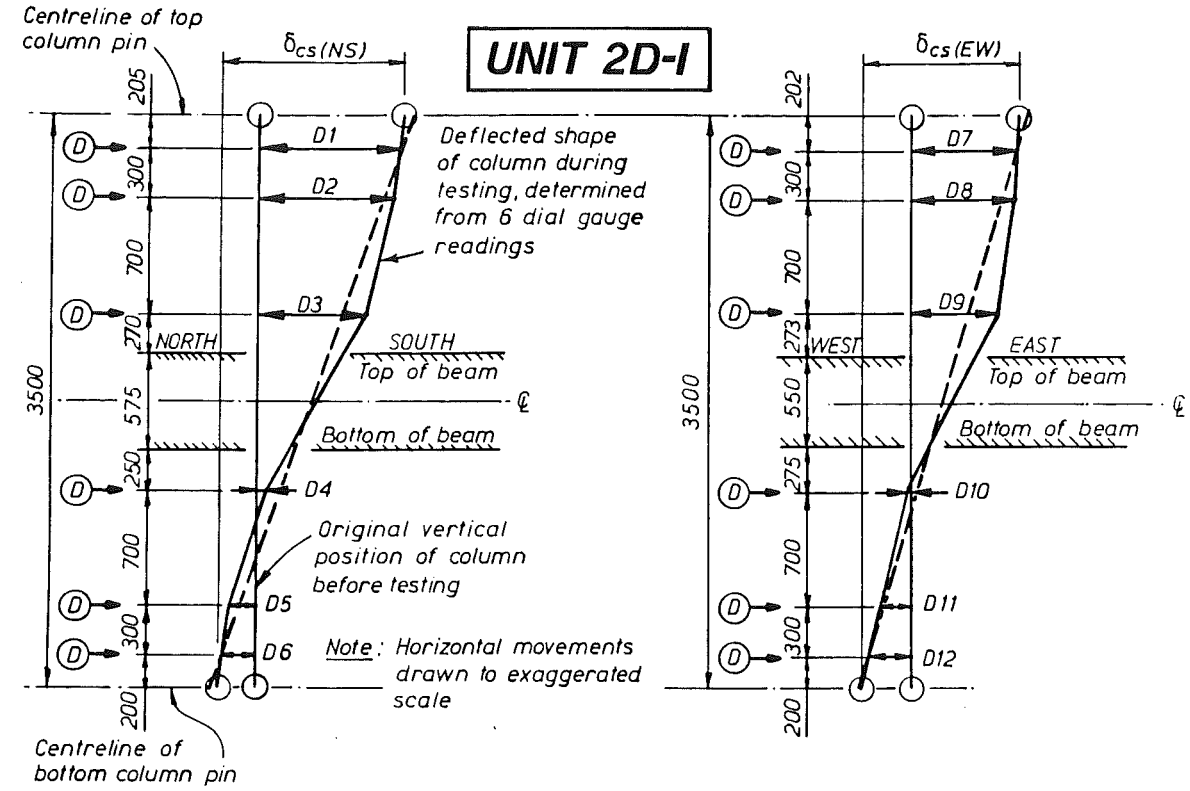

Fig.3.11 - Determination of horizontal column movement from dial gauge readings (Unit 2D-I)

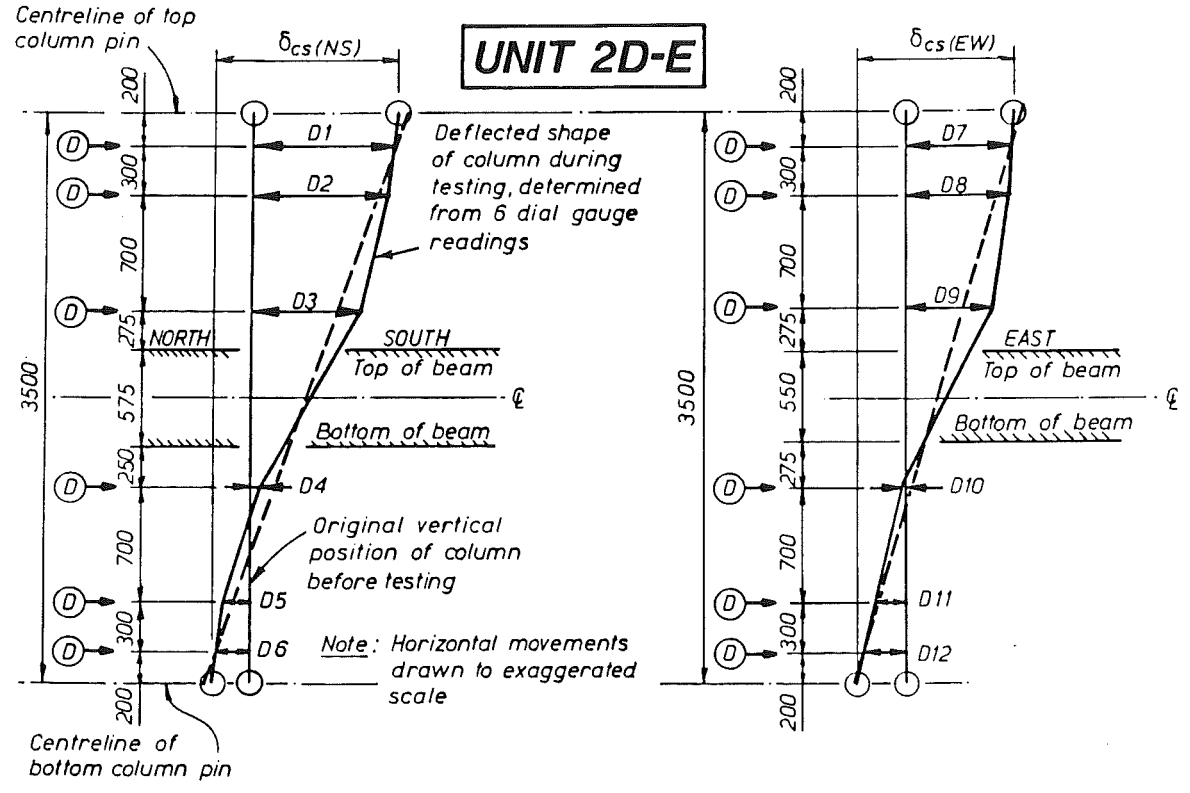

Fig.3.12 - Determination of horizontal column movements from dial gauge readings (Unit 2D-E)

Further instrumentation was conducted on Unit 2D-E as illustrated in Fig.3.13. Four linear potentiometers were placed perpendicular to the west face joint area in order to measure the rotations of the joint about the horizontal N-S axis (Fig.3.13(c)). Rotations about their longitudinal axes to estimate twist and horizontal lateral movements of the three beam ends were similarly monitored as shown in Figs.3.13(a) and (b).

3.5.3 Measurements of Reinforcing Bar Strains

A total of 503 Showa 120-ohm electrical resistance strain gauges (type N11-FA-120-11) were used to monitor strain variations along the reinforcing bars in the beams, column, slab and horizontal hoops in the joints. Figs.3.14 to 3.16 show the positioning, while Table 3.7 summarises the distribution of the gauges. Recognising that the reinforcing bars would in fact be subjected also to some bending rather than to tension or compression only, the strain gauges were fixed to the bars along their "neutral axis", so that bending strains would not be recorded. Hence the strain gauges for the beam, column and slab bars were placed at the sides of the bars.

For joint hoops of Unit 1D-I, the gauges were positioned at the undersides to avoid the effects of bowing out of hoops due to lateral expansion of the concrete in the joint core. During reduction of test data, it was found that noentheless irregularities of gauge readings did exist. It is possible that bending deformations occurred in the horizontal ties due to dowel action when diagonal cracks crossed these bars. Subject to the availability of enough channels for recording data, a pair of strain gauges at each location were considered desirable.

Like the linear potentiometers, all strain gauges of Unit 1D-I were read through the 200-channel Solartron Data Transfer Unit. There was a practical constraint on the number of strain gauges which could be used.

An improvement in the second and third tests was possible with the employment of the CEDACS data acquisition system which could accommodate more channels. With Unit 2D-I, the middle two sets of joint hoops had strain gauges fixed to both the top and the underside of each leg. Strains were taken as the average of the readings of each pair. In the construction of

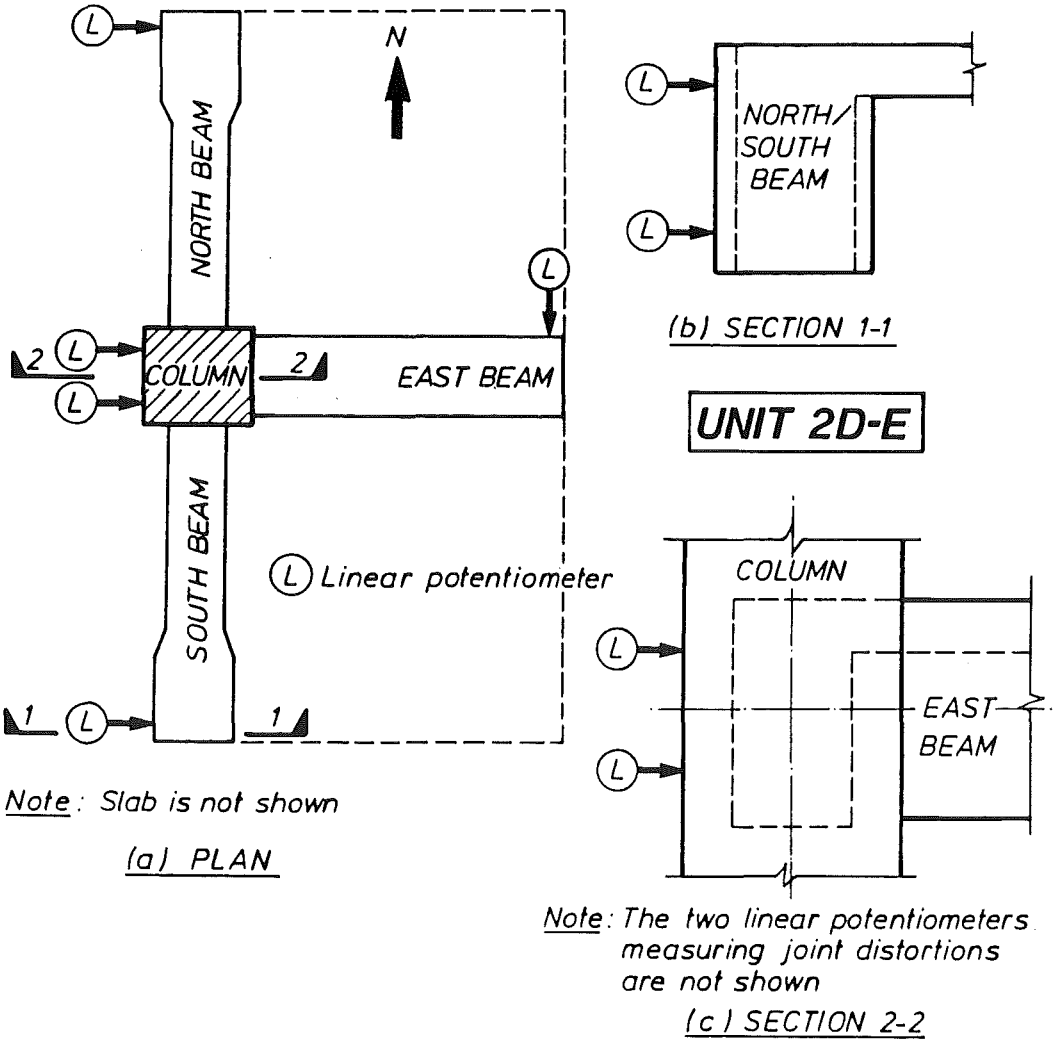

Fig.3.13 - Linear potentiometers to measure lateral movements of beam ends and joint of Unit 2D-E

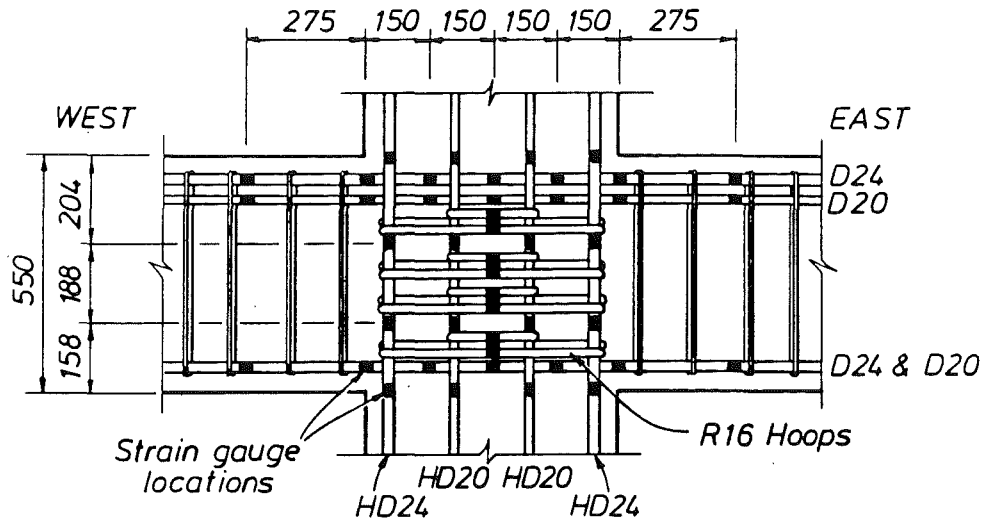

UNIT 1D-I

(a) BEAM-COLUMN JOINT

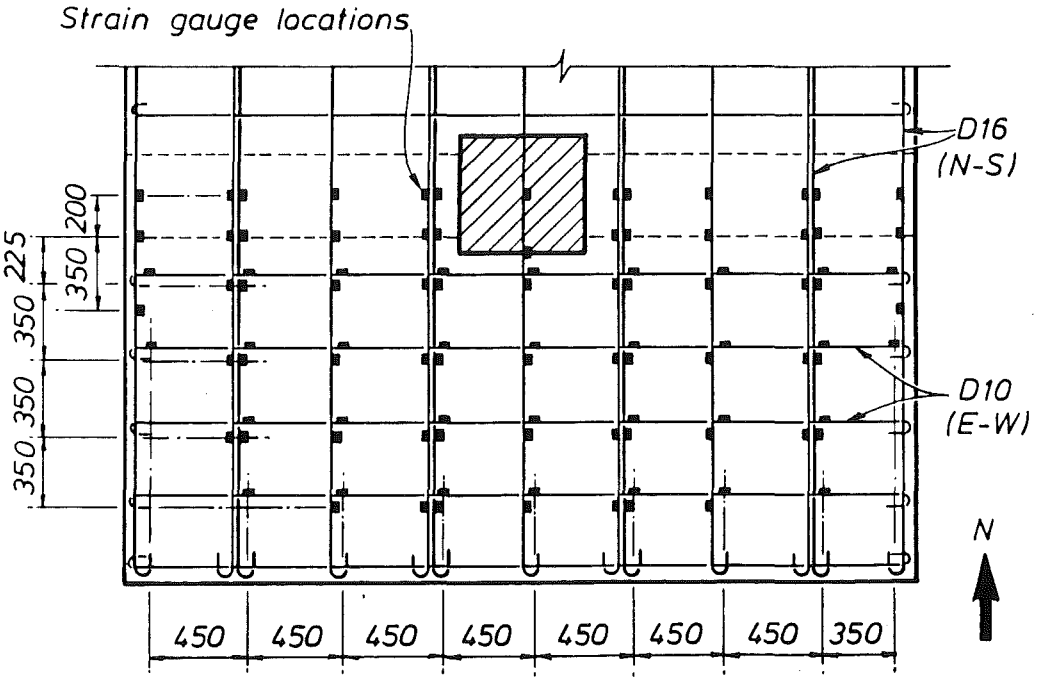

(b) SLAB

Fig.3.14 - Positions of electrical resistance strain gauges (Unit 1D-I)

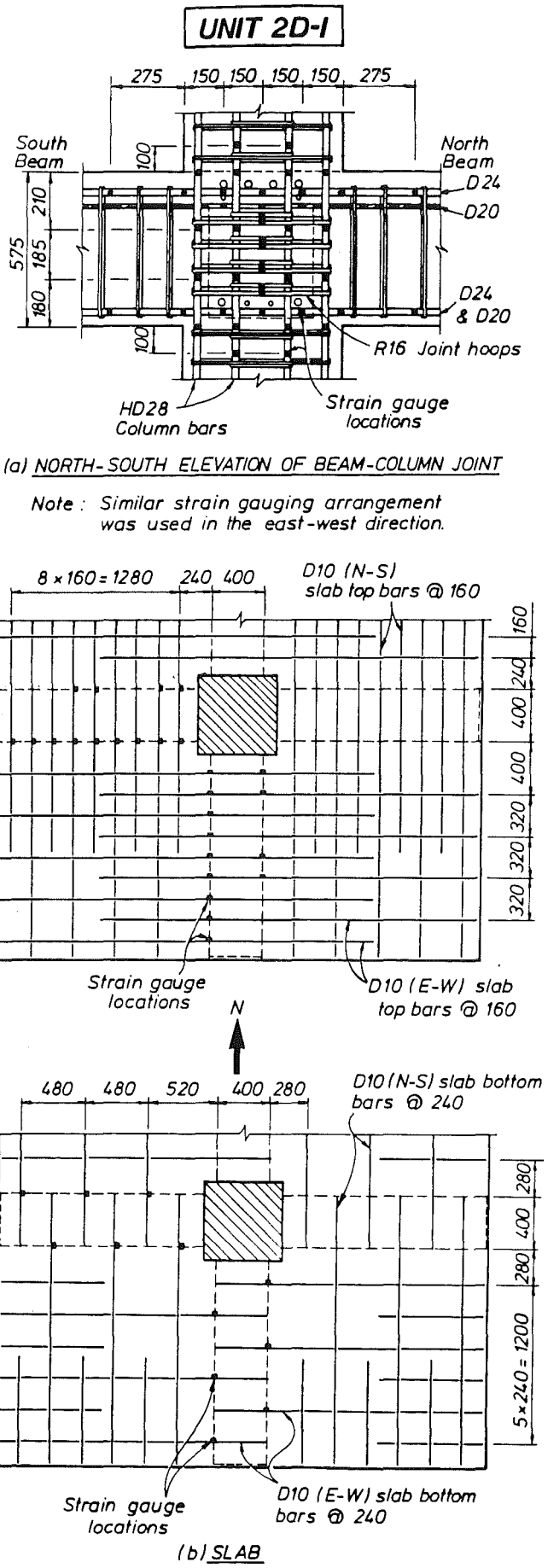

Fig.3.15 - Positions of electrical resistance strain gauges (Unit 2D-I)

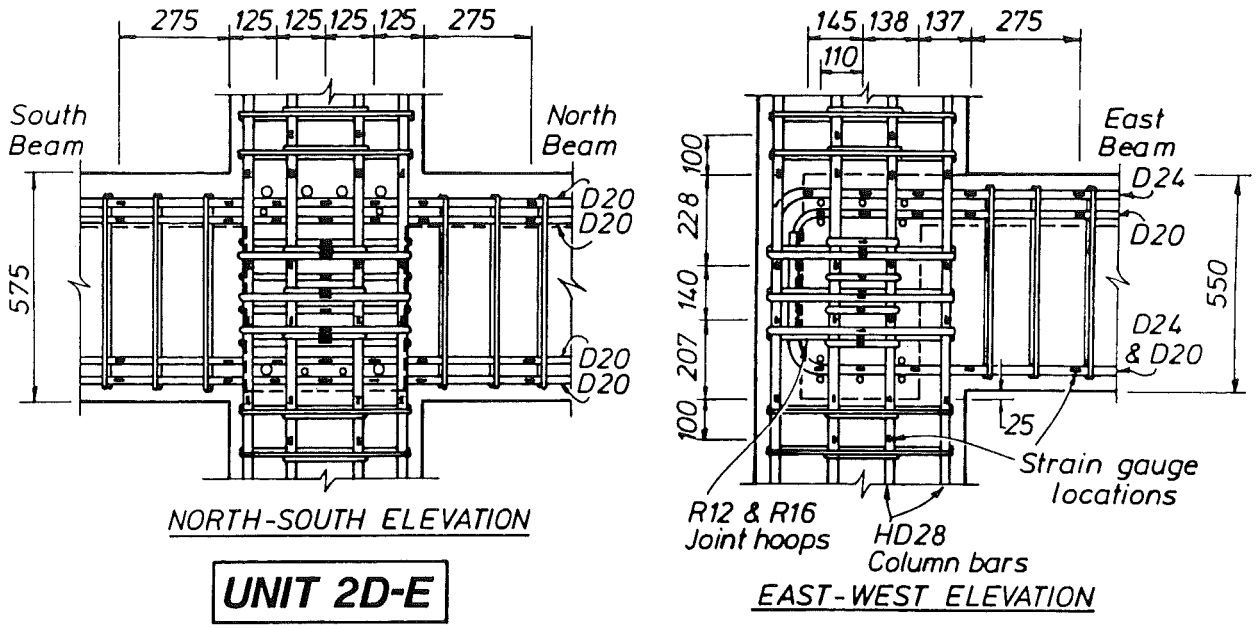

(a) BEAM-COLUMN JOINT

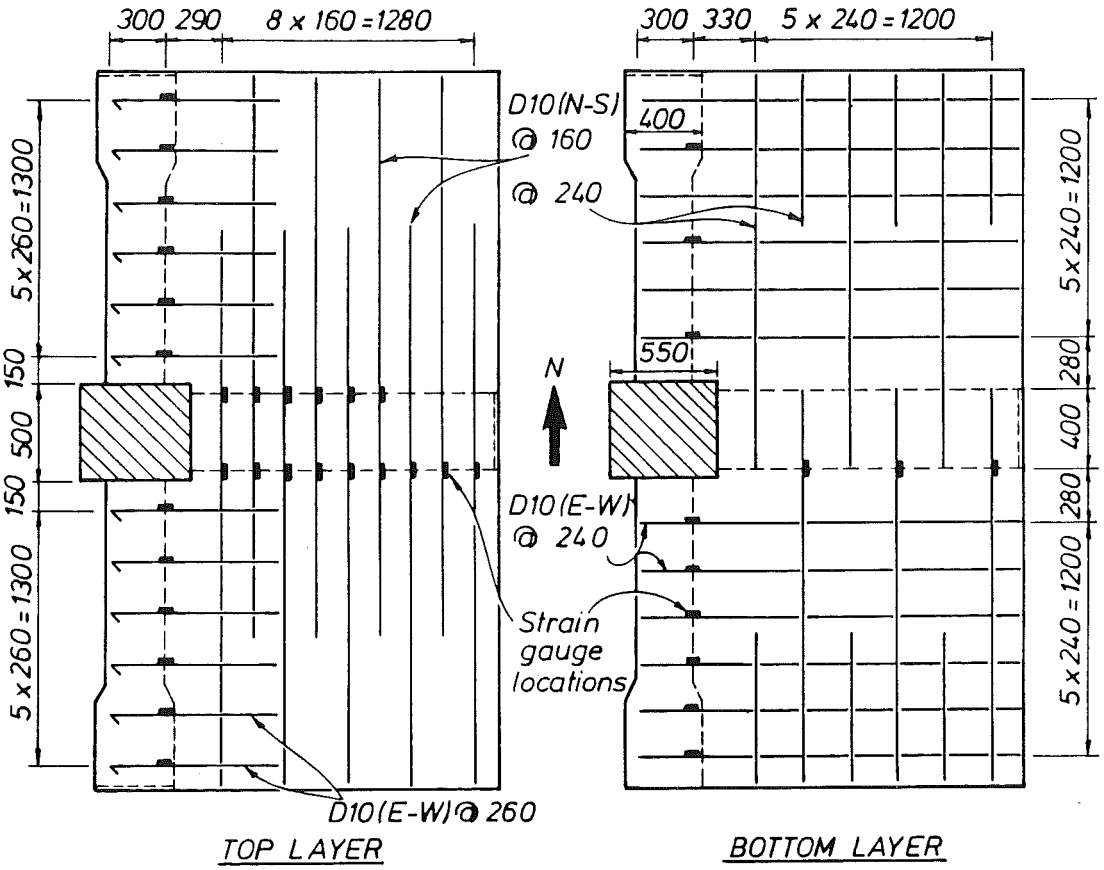

(b) SLAB

Fig.3.16 - Positions of electrical resistance strain gauges (Unit 2D-E)

Table 3.7 Distribution of electrical resistance strain gauges

(a) Unit 1D-I

Components	No. of Strain Gauges
Beam Longitudinal Bars (D24 and D20)	28
Column Longitudinal Bars (HD24 and HD20)	16
Slab Longitudinal Bars (D10)	36
Slab Transverse Bars (D16)	68
Joint Horizontal Hoops (R16)	14
Total	162

(b) Unit 2D-I

Components		No. of Strain Gauges
North-South Beam Longitudinal Bars (D24 and D20)		28
East-West Beam Longitudinal Bars (D24 and D20)		28
Column Longitudinal Bars (HD28)		36
North-South Slab Bars (D10)	Top Layer	13
	Bottom Layer	6
East-West Slab Bars (D10)	Top Layer	13
	Bottom Layer	6
Joint Horizontal Hoops (R16)	North-South	18
	East-West	18
Total		166

(c) Unit 2D-E

Components		No. of Strain Gauges
North-South Beam Longitudinal Bars (D20)		28
East Beam Longitudinal Bars (D24 and D20)		20
Column Longitudinal Bars (HD28)		48
North-South Slab Bars (D10)	Top Layer	15
	Bottom Layer	3
East-West Slab Bars (D10)	Top Layer	12
	Bottom Layer	9
Joint Horizontal Hoops (R16)	North-South	14
	East-West	14
(R12)	North-South	6
	East-West	6
Total		175

Unit 2D-E, this method was applied to each instrumentated leg of all the joint hoops.

Early in the tests strains in the beam and slab bars exceeded tensile yield strains. Bond-slip of beam bars was found significant. The validity of beam bar strains measured by strain gauges is to be discussed in Section 3.10. Slab bar strains are discussed in their pertinent sections. Strains of column bars were considered not affected because these bars remained essentially elastic. So were strains in the joint ties because they were subjected to tensile actions only.

3.6 TEST PROCEDURE

Before any forces were applied to a test unit, two complete sets of readings from the instrumentation were taken to check repeatability. The application of forces at the two beam ends were co-ordinated manually to give equal rotations of the beams. Had the loading spans of the east and west beam been equal, equal displacement could have been applied. In each load run, several force increments were made before the maximum was reached so as to provide data for plotting continuous force-displacement curves. This was necessary because considerable horizontal movement in the plane of the unit was caused by the sway of the steel loading frame. From readings of the dial gauges monitoring the movement of the upper and lower columns, the horizontal rigid body movement of the test unit was found according to the method described in Section 3.5.2. The corresponding component of beam end deflection due to this movement was then subtracted from the gross measured beam deflection.

After the maximum force or ductility level had been attained in each load run, unloading of the beams was carried out by load control by removing equal proportions of the maximum force for that load run for the relevant beam. Where the residual deflections of the two beams were not equal at the commencement of a load run, the imbalance was corrected at the initial stages of the load run by applying more displacement to the beam having the greater residual deflection until the two beam rotations about the zero line were equal.

A complete set of readings was taken at every increment and the true deflections of both beams were calculated immediately in order to determine how much adjustment the following increment required. At the peak of each load run, cracks on all faces of the test unit were marked with felt-tip pens on the white painted surface, using a different colour for each direction of loading. Photographs were taken normally at the peak of each run, but also at other stages when it was felt necessary. Because of the large size of the test unit, much time was spent on crack marking and photographing. At best only one cycle of loading could be completed in one day.

As discussed in Section 3.4, in this test series, beam deflections were to be imposed while the column ends were held in position. The equivalent column sidesway, Δ_c, and shear, V_c, obtained by considering the geometrical relationships shown in Fig.1.4(b) are

$$\Delta_c = \left(\frac{\Delta_{B1} - \Delta_{B2}}{\ell_1 + \ell_2} \right) \ell_c \qquad (3.3)$$

and

$$V_c = \left(\frac{P_1 \ell_1 - P_2 \ell_2}{\ell_c} \right) \qquad (3.4)$$

where Δ_{B1} = beam displacement at right-hand end
Δ_{B2} = beam displacement at left-hand end
ℓ_1 = length of right-hand beam
ℓ_2 = length of left-hand beam
ℓ_c = total height of column
P_1 = beam force at right-hand end
P_2 = beam force at left-hand end.

Upward acting forces and displacements, imposed on the right-hand beam as shown in Fig.1.4(b) and causing positive (sagging) beam moments, are taken positive, while downward loads and displacements, causing negative (hogging) beam moments, are taken negative.

3.7 LOADING SEQUENCE

3.7.1 Cyclic Load History

The quasi-static cyclic loading histories followed for the three Units are depicted in Figs.3.17 to 3.19. In each test, the first two load cycles were to impose a lateral force of about one-half of the theoretical ideal strength, V_i, as defined in Section 3.2. The intention was to examine the testing facilities, including the rig. This arrangement had been found very useful to the personnel carrying out the test in that the loading system and instrumentation could be examined and where necessary improved. As equal beam rotations were to be imposed in all cycles, these two initial small-load cycles allowed the personnel to practice the co-ordination of load application at the two beam ends.

The first yield displacement, $\Delta_{y,test}$, and the real stiffness, K_{test}, of each test unit were determined in the first half of the third load cycle by extrapolation from the measured displacement at 75% of V_i (see Section 1.3 and Fig.1.3). Subsequent cycles were displacement controlled with increasing imposed displacement ductility factors $\mu = \Delta/\Delta_y$ and enabled observation of the performance of the units at low as well as high ductilites. The stages at which the cumulative ductility demand limits of $\Sigma\mu = 32$ (see Fig.1.5) were satisfied, are shown in Figs.3.17 to 3.19. A continuation of the test beyond these limits gave an idea of the potential of the unit for larger ductility demands and helped to identify the causes of eventual failure or loss of resistance of the unit. It is seen that each unit was subjected to a displacement history much more severe than that envisaged by the recommended (Section 1.3) performance criteria.

Bidirectional loading was imposed to Units 2D-I and 2D-E, as in a manner shown in Figs.3.18 and 3.19. For instance, in run 13 of cycle 7, Unit 2D-I (Fig.3.18) was first displaced to $\mu = 2$ in the east-west direction. Then it was displaced in the north-south direction to $\mu = 2$, while maintaining the east-west deflected position. As north-south loading was progressing, the east-west resistance dropped, while displacement corresponding with the intended ductility was maintained. This phenomenon will be discussed in some detail in the next section. Besides giving easier control during the test, such a loading method permitted observations of the behaviour in two separate directions to be made, while also achieving biaxial effect. Unloading took

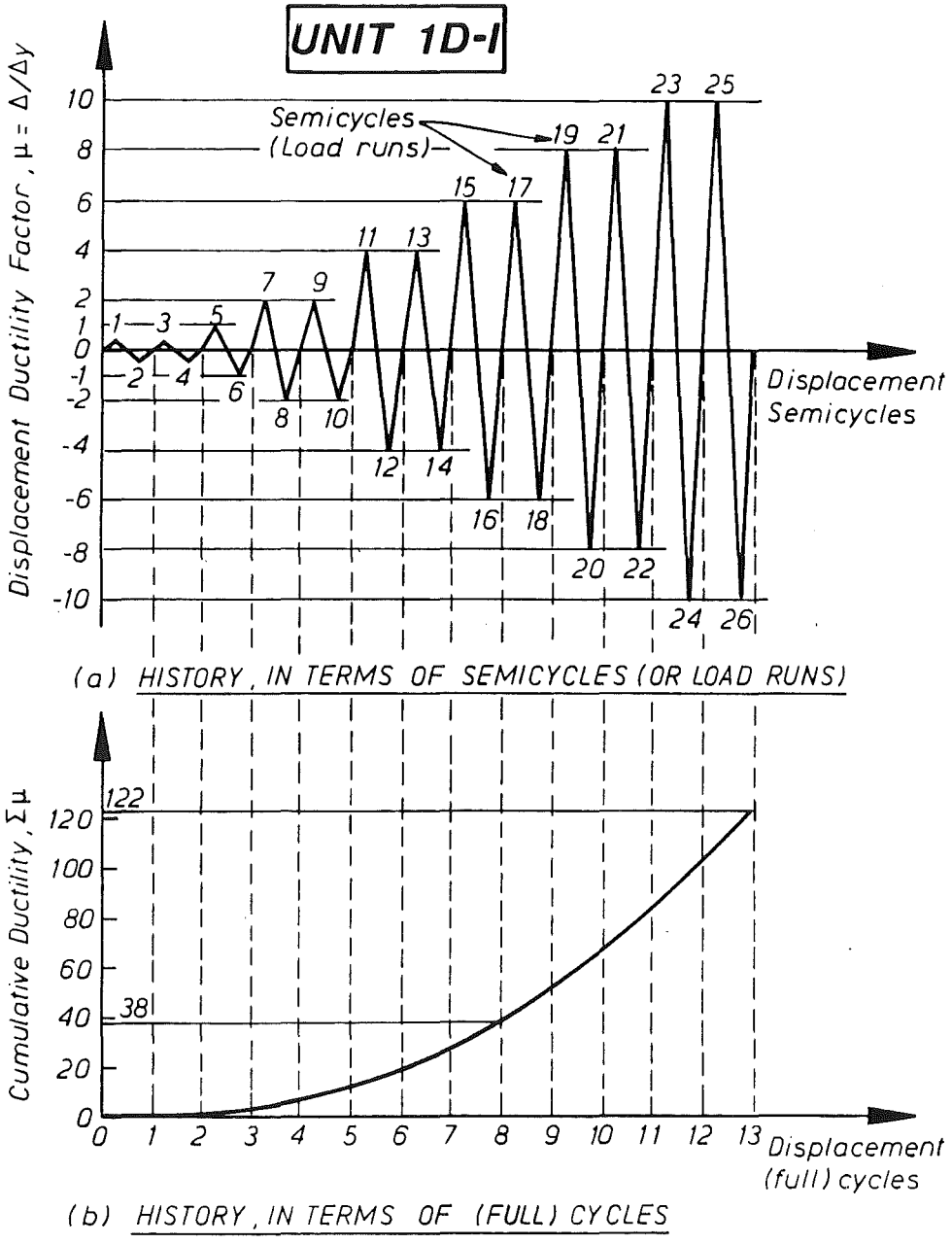

Fig.3.17 - Quasi-static cyclic loading history for Unit 1D-I

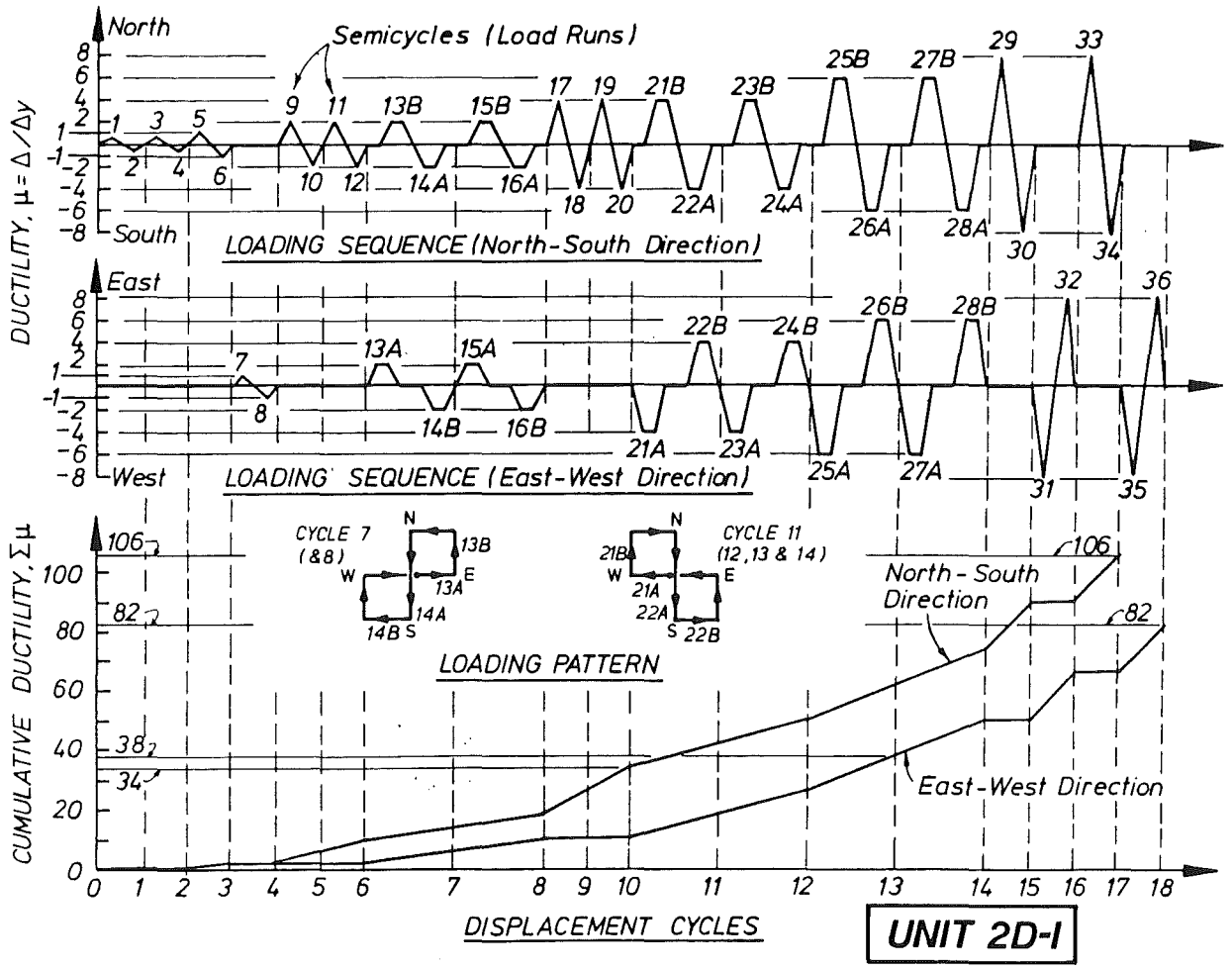

Fig.3.18 - Quasi-static cyclic loading history for Unit 2D-I

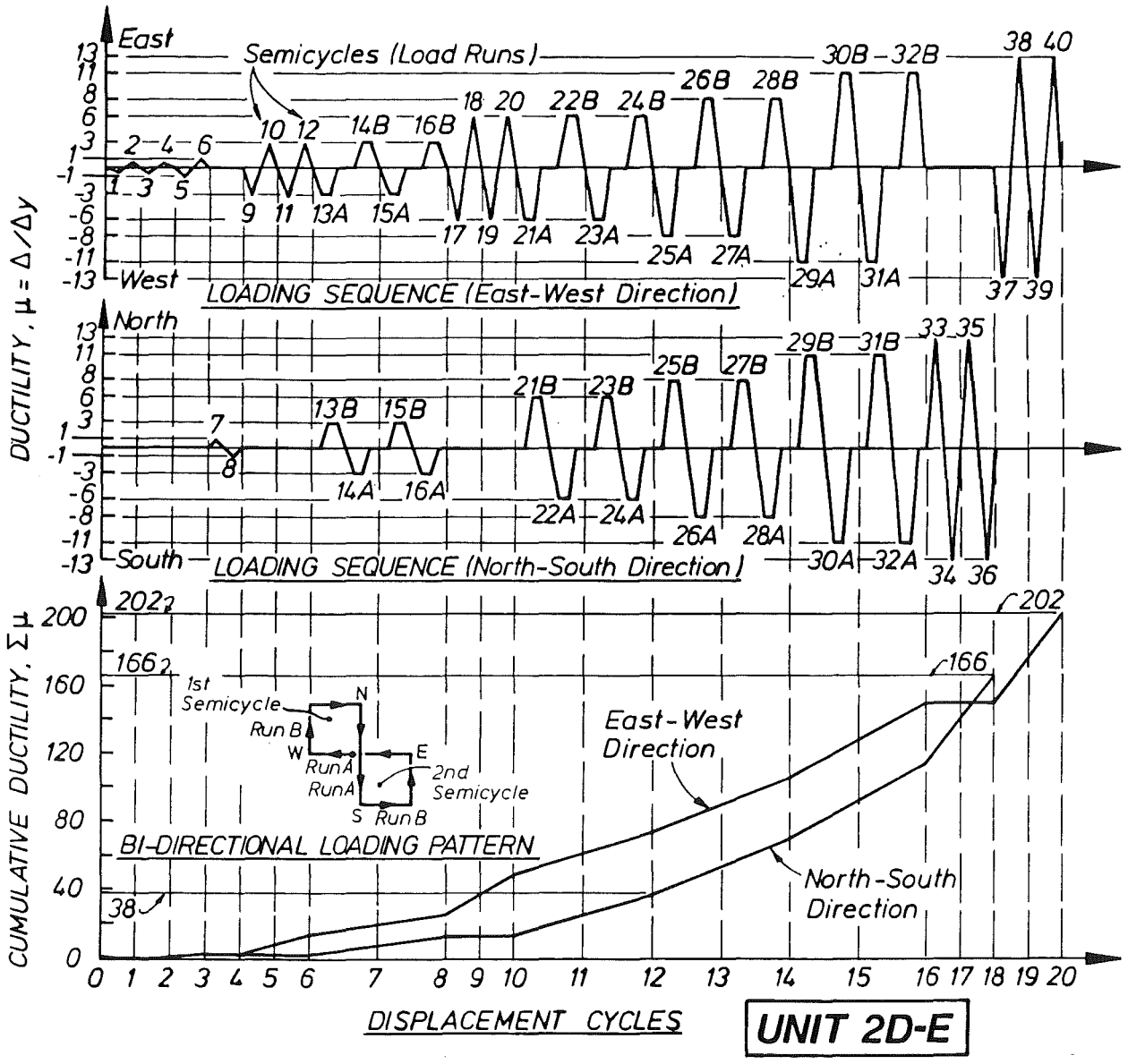

Fig.3.19 - Quasi-static cyclic loading history for Unit 2D-E

place in the east-direction first, followed by that in the north-south direction. Cycle 11 and thereafter had a reversed sequence pattern, as shown in Fig.3.18. The intention was to avoid excessive twisting of the test specimen. However, at the end of the test, it was concluded that this was not really necessary. The fixing arrangements at the beam ends and column ends could in fact accommodate considerable movements without affecting the test. Therefore a single biaxial pattern was adopted when testing Unit 2D-E (Fig.3.19).

For Unit 2D-E, loading was applied principally in the east-west direction (that is, perpendicular to the spandrel beam), for the sake of studying the behaviour of an exterior joint. The values for $\Delta_{y,test}$ and K_{test} were obtained for when the east beam was displaced downwards. Although they were more critical, the results were still significantly different from those found for Unit 2D-I. In order to make a more meaningful comparison of the behaviour of Unit 2D-E with that of the other two Units, the subsequent imposed ductilities, shown in Fig.3.19, were revised to give similar storey displacements also for Unit 2D-E.

3.7.2 Correlation between Force and Displacement Orbits

The special interaction effects of biaxial loading pattern employed in this test series are revealed in the hysteretic response diagrams in the following chapters. However for illustration purposes here, the force-displacement response in cycle 7, i.e. load runs 13 and 14, of Unit 2D-I are taken as example and drawn in the form of storey (or column) shear and displacement orbits in Fig.3.20.

At the end of cycle 6, a stage at which the unit had been subjected to two complete cycles of uni-directional north-south displacement corresponding to ductility of $\mu = \pm 2$, a zero load state was re-established. The column remained practically in its zero (before test) position in the east-west direction but it accumulated in the north-south direction a residual deflection of -8.4 mm. Points A and A' in Fig.3.20 represent this stage. Cycle 7 started eastwards to a peak storey shear of 251 kN at a displacement of 33.7mm or $\mu = 2$ EW (points B and B'). During this load run, called 13A, the test unit also moved northwards by 1.6mm. Then load run 13B with $\mu = 2$ NS was imposed to a peak load of 240.7 kN and a displacement of 33.5 mm. As N-S loading was progressing, the EW storey shear kept gradually decreasing by 17%

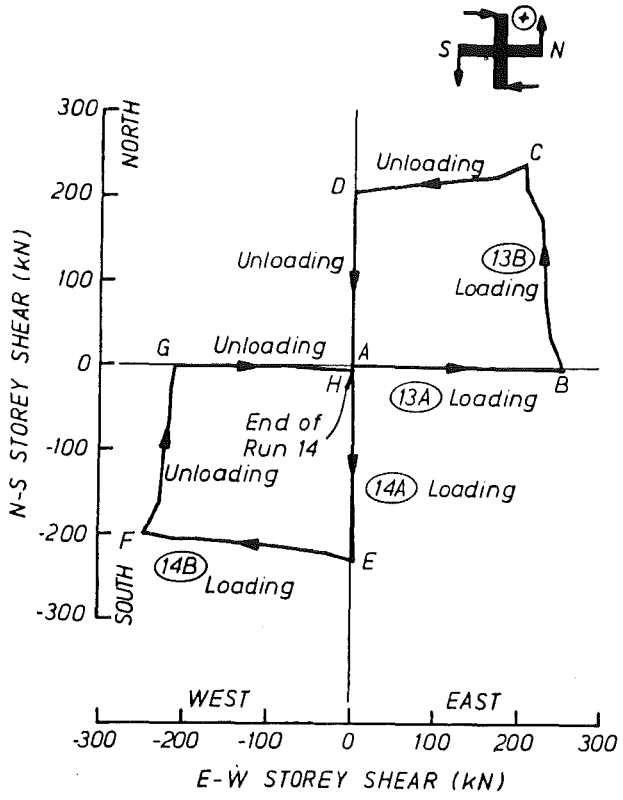

(a) SHEAR ORBIT

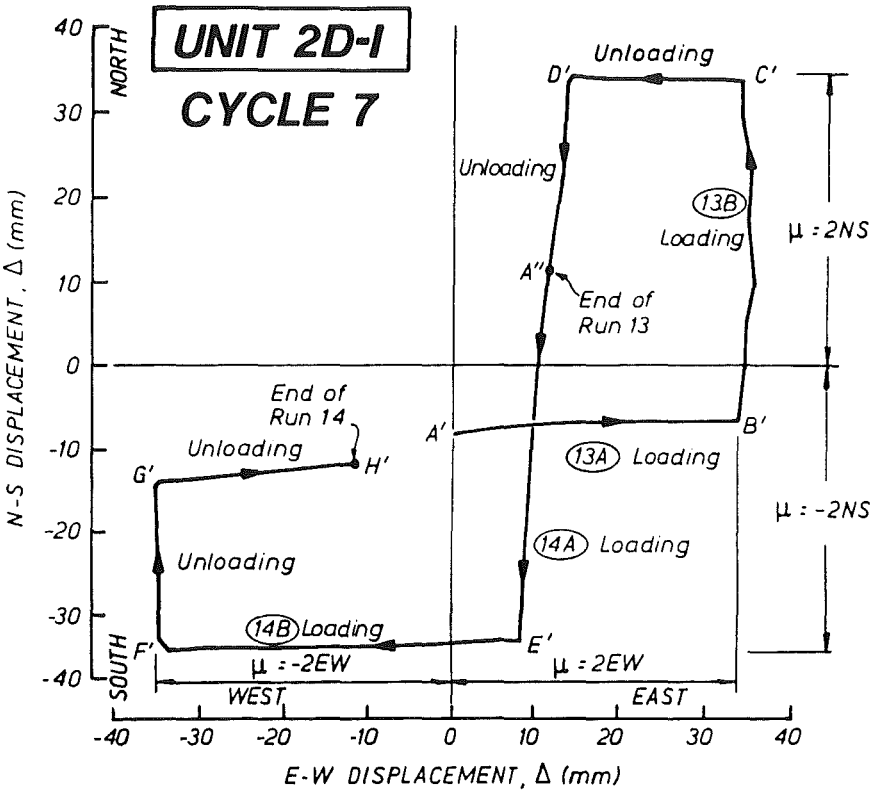

(b) DISPLACEMENT ORBIT

Fig.3.20 - Typical storey shear and displacement orbit diagrams

to a final value of 207.6 kN at a corresponding displacement of 34.2 mm (points C and C' in Fig.3.20).

Unloading took place in the east-west direction first, then north-south, until zero load (point A) was reached. The corresponding displacement point A", shown in Fig.3.20(b), indicates that there was a permanent deformation of 11.4 mm (N) and 11.6mm (E) at the end of run 13. Load run 14 took a different path, but features of the response were the same. The load and displacement orbits followed were AEFGH and A"E'F'G'H' respectively, as seen in Fig.3.20. Point H' shows again that as a result of permanent plastic deformations the unit was 11.7mm (S) and 11.6mm (W) away from its zero position at the end of cycle 7.

As Fig.3.20(a) shows, during imposed N-S displacements there was always some reduction of resistance in the E-W direction in spite of the large displacement in that direction being kept approximately constant. Similar response was observed when displacements were varied in the E-W direction.

There are two possible reasons for the observed drop in peak shear during orthogonal loading and unloading. The first is relaxation in the hydraulic jacks and creep in the specimen. The other is the contribution of the slab in tension to the flexural strength of the beams during biaxial displacements. These issues will be discussed further in detail in the following chapters.

A change in peak displacement, intended to remain constant, usually a slight increase during orthogonal action, was unavoidable. When the inelastic behaviour of such units is being studied, slight unintended changes in displacements were not considered to have had any effect upon the characteristics of overall response and hence the validity of conclusions.

The unit's observed movements from its "zero-load" position during orthogonal loading was also studied. For instance, in run 14A (Fig.3.20(b)), the unit moved unintentionally by 3.6 mm to the west, as indicated by points A" and E'. Some small E-W shear developed as well (point E in Fig.3.20(a)). This phenomenon became more significant subsequently at larger ductilites. However, the hysteretic curve for run 14B (Chapter 5) suggests that the unit "adjusted" itself during the initial loading increments. The overal stiffness of the unit in run 14B appears to have matched that during unloading, i.e.

curve 13A. This initial shift in displacement or shear was compensated by a slightly larger initial stiffness. It was considered that the overall behaviour of the unit had not been affected. In fact, curves 13A and 14B in Fig.5.10 could have been drawn continuously without a "kink" in between.

It may be argued that, to better simulate earthquake motions, the test unit should have been brought back to its original, before test (zero) position at the end of each cycle. In this case, some storey shear forces would have been required to keep the specimen in this desired "zero" position. This would have posed testing difficulties while also complicating the behaviour of the unit. The present testing procedures enabled direct comparisons of test results with those of Unit 1D-I and other projects [39,49] to be made. Moreover, energy dissipation capacity in either of the directions is more easily interpreted when using this displacement history. After all, when reinforced concrete structures, designed for ductility, are subjected to significant earthquake motions, permanent deformations are to be expected after earthquake motions ceased.

3.8 PREDICTION OF IDEAL STRENGTHS

3.8.1 General

The ideal (nominal) flexural strengths of the beam sections at column faces, $(\pm)M_i$, were calculated for various possible cases described in Section 3.8.2. These strength properties and the corresponding theoretical beam tip forces, $(\pm)P_i$, estimated on the basis of measured rather than on specified material properties, are summarised in tables of Appendices B.3, C.2 and D.2. Larger possible moments and associated forces for negative bending, when all longitudinal slab bars may be stressed in tension, are denoted by asterisks in superscript. As can be seen in Figs.3.1 to 3.3, which show the as-built dimensions, the shear spans of two beams on opposite sides of a column were slightly different. Hence the predicted vertical forces at the opposite ends of identically reinforcing beams were not exactly identical. In all cases, the self-weight effects of the beams and slabs on the test results were considered insignificant, and hence they were ignored.

It is necessary to consider the cases when flexural overstrength is developed. As inelastic displacements continue, steel bars in tension may

attain a stress level above the measured average yield stress f_y. The material overstrength factor relevant to a beam section and used in capacity design [4], based on a specified yield strength of f_y = 275 MPa, is λ_o = 1.25. For comparison in these tests based on measured yield strength, $f_{y,m}$, the following relationships are adopted :

$$f_{y,o} = \lambda_o f_y = \lambda_{o,m} f_{y,m} \tag{3.5}$$

so that

$$\lambda_{o,m} = \lambda_o \frac{f_y}{f_{y,m}} \tag{3.6}$$

where $f_{y,o}$ = estimated overstrength of steel
$\lambda_{o,m}$ = material overstrength factor relevant to measured strength

For the north-south spandrel beams of Unit 2D-E, only D20 bars were used. Thus $\lambda_{o,m}$ was taken as 1.15 for this case. As for Unit 2D-E in the east-west direction and Units 1D-I and 2D-I, the value of $f_{y,m}$ was taken as the average of the measured yield strengths of D20 and D24 beam bars. Thus for these cases, $\lambda_{o,m}$ = 1.18. The overstrength moments and vertical tip forces corresponding with these factors are referred to as $(\pm)M_{io}$ and $(\pm)P_{io}$ respectively, when necessary.

The ideal strength of a test unit is defined in terms of the lateral force at the column ends. This is denoted as either V_i or V_i^*, following the definitions given in point (6) in Section 3.2. The values of V_i and V_i^* vary, depending on the values of $(\pm)M_i$ adopted.

3.8.2 Flexural Strengths

For a reinforced concrete beam subjected to monotonic loading, the flexural strength is traditionally determined from considerations of strain compatibility and the equilibrium of internal forces developed in both the concrete and the reinforcing bars. The concrete compressive stress block is conveniently replaced by an equivalent stress rectangle [1, 5]. This method, generally known as the ACI method, is considered sufficiently accurate for design purposes regardless of whether the beam section is singly or doubly reinforced. Under the application of earthquake-type cyclic forces, however, the situation may be quite different.

It was reasoned in Section 2.3.1 that under seismic actions into the inelastic range of the beam's capacity, the contribution of the concrete to flexural resistance of doubly reinforced sections should diminish. The seismic strength, M_i, of a beam, particularly having equal amounts of top and bottom reinforcement, can then be readily evaluated as follows :

$$M_i = A_s f_y (jd) \qquad (3.7)$$

where A_s = total area of reinforcement in tension
f_y = yield strength of steel
jd = internal lever arm approximated as the distance between centroids of top and bottom reinforcement in beam

In routine design of building frames in many countries, beam sections are likely to be proportioned, using charts based on the ACI or a similar method, to provide the flexural resistance required for code design seismic forces. These techniques are traditionally based on beam response to monotonic loading. Strengths so computed would generally be somewhat larger than corresponding values derived from the "seismic approximation" of Eq.(3.7), as can be seen in Appendix B.2. Also in Appendices B.3, C.2 and D.2, ideal strengths based on measured material properties and on the ACI method, using different assumptions for the effective width of a flange, b_e, in tension or compression (Fig.3.21), have been evaluated. Relevant assumptions are described in the following paragraphs. The maximum dependable strain of concrete in compression is assumed to be 0.003.

From the computation of flexural strengths, it is easily seen that the "seismic approximation" of Eq.(3.7) has the advantage of being simple to use. In New Zealand where the "capacity design" approach (see Section 1.2) has been well established, this approximation is accepted as a routine procedure in design offices. In the capacity design method [4], materials overstrength factors λ_o and dynamic magnification factors ω are specified to estimate the maximum probable design actions in structural members. Sufficient strengths are to be provided by proper detailing so that the chosen means of energy dissipation can be maintained. In the design of ductile frames, these enhancement factors ensure that flexural failure in the columns and shear failure in the columns, beams and joints are eliminated. This concept has been repeatedly emphasised in Section 3.2 and Appendices B.1, C.1

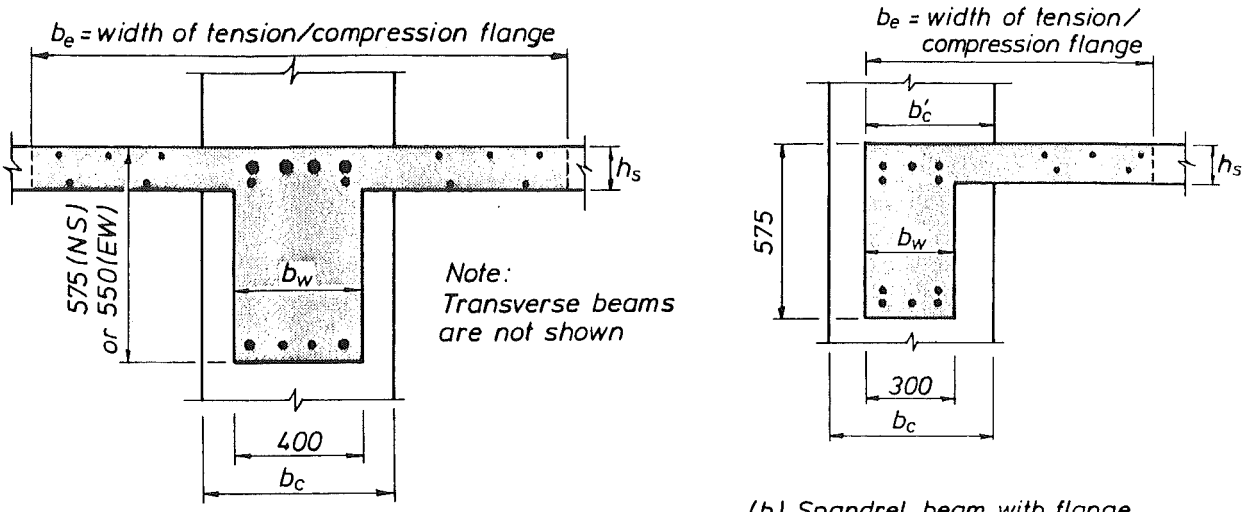

(a) Beam with flanges on both sides

(b) Spandrel beam with flange on one side only

(c) Effective width of compression flange ("positive" flexure $+M_i$)

Case	b_e (mm)	Unit 1D-I	Unit 2D-I	Unit 2D-E	
		East-West	East-West & North-South	East	North-South
a	zero	(flexural strength is estimated by pure steel couple)			
b	b_w	400	400	400	300
c	b_c	550	600	500	(b'_c=)425
d	$2b_c$	1100	1200	1000	700
e	Code*	1500	1500	1500	800
f	$3b_c$	1650	1800		975

* b_e is estimated according to NZS 3101 recommendations for T-beam design relevant to mid-span, monotonic, positive bending action.

(d) Effective width of tension flange ("negative" flexure $-M_i$)

Case	b_e (mm)	Unit 1D-I	Unit 2D-I	Unit 2D-E	
		East-West	East-West & North-South	East	North-South
g	b_c+th_s	(t=2.5) 1050	(t=4) 1640	(t=2) 1020	(t=4) 945
h	(full slab width)				

Fig.3.21 - Effective flange widths of T-beam and L-beam sections under flexure

and D.1. As illustrated in point (4) in Section 3.2, it follows then that some underestimation of the beams' flexural strengths using the above approximation should not jeopardise the desired seismic resistance of the designed ductile frame under small or moderate ductility demands.

Since the floor slabs and beams are cast monolithically, they act integrally as T-beams or L-beams as shown in Fig.3.21. Under negative bending, some slab bars will participate in beam bending action, with the tensile forces transmitted across the flange into the beam web by shear in the flanges. The ACI code [5] does not specifically cover this effect. However, other sources [1,4] suggest that some longitudinal bars placed in the slab within a certain distance from column faces be included as effective tension reinforcement. The design recommendations were based on engineering judgement rather than on experimental data. As shown in Fig.3.6, in the design of this test series the New Zealand code [4] was followed as a reference. At large ductilites, all longitudinal slab bars in tension may possibly yield. However, it is felt that only some of these bars will contribute to the beam's negative flexural strength at a column face. This limitation originates from considerations of shear transfer across the slab, and from biaxial loading effect. Chapter 7 examines the assessment of the number of bars considered to be effective as tension reinforcement in the full slab width.

For T-beam subjected to positive bending moment, there are recommendations [4, 5] for estimating the effective width of flanges in compression. Though the wording is not very explicit, the design of T-beams under mid-span, monotonic, positive bending action is inferred. In seismic conditions, the width of the compression flange at a beam-column junction should be much smaller. This is partly due to the fact that under seismic attack the slab is subjected to compression strain at one face of the column, while large tensile strains must prevail simultaneously at the opposite face of that column. Therefore for the prediction of positive flexural strengths, with the top fibres of the beam section in compression, five cases (Fig.3.21(c)) are considered in addition to case (a) which uses $b_e = 0$ to represent the action of only a steel couple (Eq.3.6). Case (b) assumes that b_e is the same as the beam web width, b_w, while case (c) uses the column width, i.e. $b_e = b_c$. The last three cases consider even larger flange widths in compression. In case (d), b_e is equal to two column widths, i.e. the column itself plus one-half column width on each side of the column (see also Fig.3.7). Case (e) follows code recommendations [4,5] for T-beam design

intended for mid-span action. The final case (f) uses the largest assumed effective width extending over three column widths. Despite the various values of these effective widths, the ideal flexural strengths for cases (d), (e) and (f) are very similar, because the internal lever arm remains essentially constant. The maximum difference is only 4%. For convenience, case (d) was taken as representative when considering flanges in compression.

For the evaluation of strength due to negative bending, causing tension in the top fibres of the beam section, case (g) follows the code recommendation [4], as shown graphically in Fig.3.6. It has been known (Section 1.5) that as imposed ductility increases, the effective width in tension also extends. This will be discussed in Chapter 7. At this stage, case (h) is assumed which gives the maximum possible negative moment when, irrespective of anchorage conditions, all slab bars crossing the critical section are assumed to have developed tension yield stress and are thus assumed to conribute to the flexural strength.

The reference strengths, V_i and V_i^*, mentioned in Section 3.2, are derived from a combination of cases (d) and (g), and of cases (d) and (h) respectively.

In this test series, most of the beams contained amounts of top reinforcement about 60% in excess of the bottom reinforcement. Thus a steel couple may be expected to resist positive seismic moment. On the other hand, when the direction of moment is reversed (i.e. to negative bending), the bottom bars in compression should yield because a large tensile force is developed in the top beam reinforcement with larger area. This should occur already when a moment less than the previous maximum is applied, after which the previously formed flexural cracks in the bottom of the beam section will close. The concrete then carries the required additional compression force. These two features have been compared with experiments when using beams with rectangular sections [1]. Since the test units were designed to simulate earthquake dominated frames, where beam plastic hinges due to both directions of earthquake loading were expected to form at column faces, it is considered useful to assess the response of the test units in terms of the idealised seismic strengths at thse sections, as just discussed. Therefore the strengths of the various beam sections in this test series are also estimated according to a "mixed" approach, i.e. combining cases (a) and (g) or (h). In Appendices B.3, C.2 and D.2, combinations of various cases are listed.

3.9 DISPLACEMENT COMPONENTS

3.9.1 General

As described in Section 3.6, earthquake actions were simulated by applying vertical forces to the test units at the beam ends while the equivalent storey (column) displacements and shears were calculated according to Eqs.(3.3) and (3.4). The storey displacement was a combination of the elastic and inelastic deformations of the various structural members of a planar frame, namely, the left and right hand beams, the upper and lower columns, and the joint core. With reference to Fig.3.22 showing a joint assembly in the east-west direction, the total storey displacement, Δ_c, is composed of three components as follows :

$$\Delta_c = \Delta_{c,b} + \Delta_{c,c} + \Delta_{c,j} \qquad (3.8)$$

where $\Delta_{c,b}$ = storey displacement from the contribution of beam deformations (Fig.3.22(a))

$\Delta_{c,c}$ = storey displacement from the contribution of column deformations (Fig.3.22(b))

$\Delta_{c,j}$ = storey displacement from the contribution of joint shear distortion (Fig.3.22(c))

Among the three components, those deformations which were considered significant were measured in the test. The other were estimated by calculations based on some traditional models. They are discussed in the following paragraphs.

3.9.2 Deformations of the Beams

As the applied force increased, plastic hinges formed in the beams at the column faces. The rotations in the plastic hinge regions accounted for a major part of the beam end deflections, $\delta_{1,b}$ and $\delta_{2,b}$ (Fig.3.22(a)). As illustrated in Fig.3.9 five pairs of potentiometers over a length of 825 mm (i.e. 1.5 times the beam depth h_b) of each beam measured the rotations. From these the average curvatures of the region were derived. For convenience in this report the region is referred to as the 1.5 h_b region and represented by

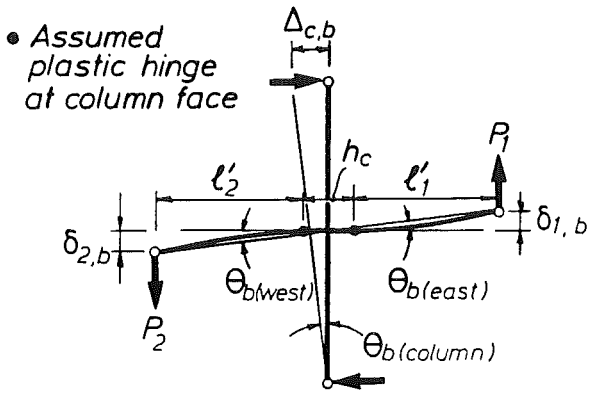

(a) ELASTIC AND INELASTIC DEFORMATIONS OF BEAMS

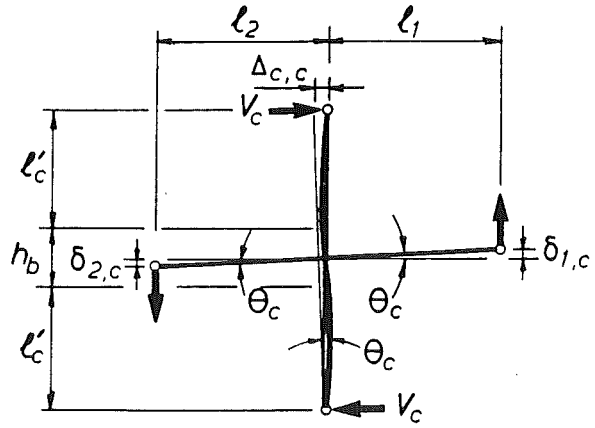

(b) ELASTIC DEFORMATION OF COLUMN

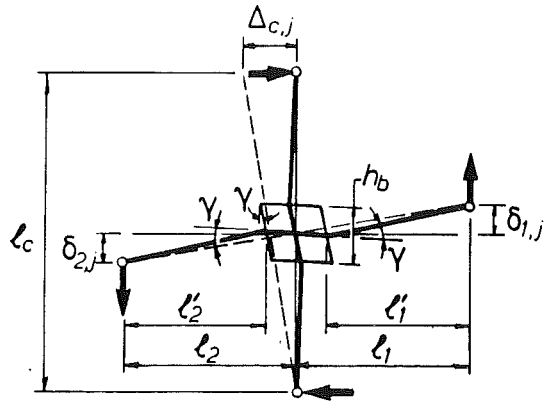

(c) BEAM AND COLUMN DISPLACEMENTS DUE TO ELASTIC SHEAR DISTORTION OF JOINT CORE

Fig.3.22 - Components of deformations in test unit in E-W direction

the abbreviations p.h. in the equations. To illustrate the computations for the region, Fig.3.23 shows in exaggeration the shape of the east beam having positive curvature under upward displacement. Fig.3.23(a) shows the before test situation. As the beam deforms under upward force, the segments undergo positive rotations in association with changes in distance from the column face, shown as ΔS and $\Delta S'$ in Fig.3.23(b). In agreement with the sense of curvatures and rotations, increases in distance are taken as positive. The rotations of the segments are then given by

$$\Theta_1 = (\Delta S_1 - \Delta S_1')/h_1 \tag{3.9a}$$

$$\Theta_2 = (\Delta S_2^* - \Delta S_2^{*\prime})/h_2 \tag{3.9b}$$

$$\Theta_3 = (\Delta S_3 - \Delta S_3')/h_3 \tag{3.9c}$$

Both Θ_1 and Θ_2 include bar deformations and slip within the joint. The average curvature of the first segment from the column face, over a gauge length of S_1, is defined as

$$\psi_1 = \frac{\Theta_1}{S_1} = \frac{\Delta S_1 - \Delta S_1'}{h_1}\,\frac{1}{S_1} \tag{3.10a}$$

In the test this segment was made as close as possible to the column face, with S_1 = 25mm. Therefore the apparent large curvature was primarily caused by the bar elongation and any local bond-slip within the joint. The value of ψ_1 so obtained were extremely large because S_1 was small when compared with the column depth h_c. A more realistic estimate of the curvature in this region could be made by assuming that strains at the column centre were zero. In this case, the average curvature of the first segment, relative to the column centre, defined as ψ_1^*, would be of the order of $S_1/(0.5h_c + S_1) = 0.077$ times ψ_1 when h_c = 600mm. Alternatively, ψ_1^* may be expressed by the following equation

$$\psi_1^* = \frac{\Theta_1}{0.5h_c + S_1} = \frac{\Delta S_1 - \Delta S_1'}{h_1}\,\frac{1}{(0.5h_c + S_1)} \tag{3.10b}$$

The average curvature of the second segment over a gauge length of $(S_2^* - S_1) = S_2$ is

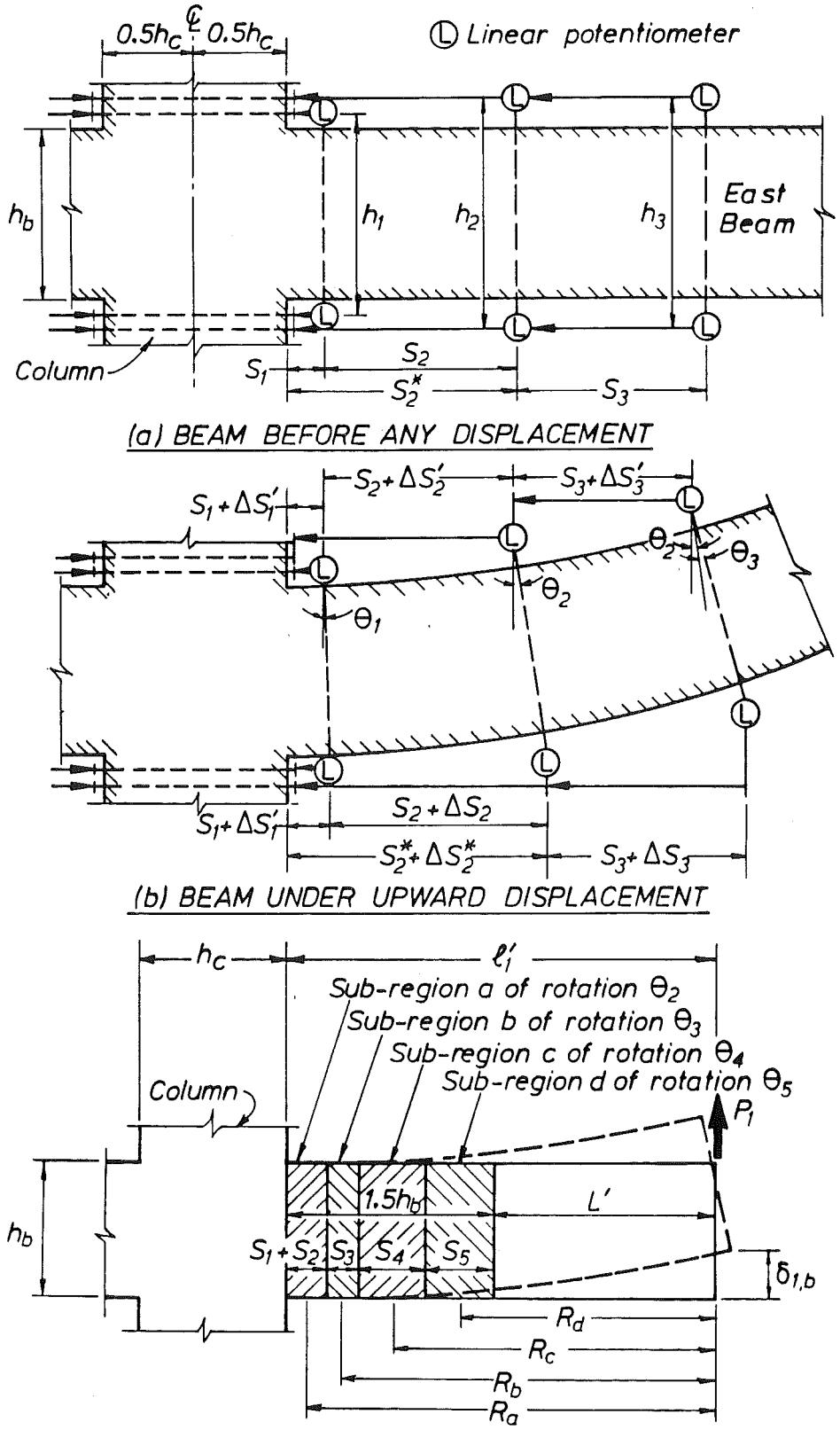

Fig.3.23 - Elastic and inelastic deformations of east beam

$$\psi_2 = \frac{\Delta S_2 - \Delta S_2'}{h_2} \quad \frac{1}{S_2} \tag{3.10c}$$

while the curvature of the third segment over a gauge length of S_3 is

$$\psi_3 = \frac{\Delta S_3 - \Delta S_3'}{h_3} \quad \frac{1}{S_3} \tag{3.10d}$$

Curvatures of other segments were determined in a similar way. The curvatures so obtained, and plotted at the centre of each gauge length for all load runs at their peaks are shown for all beams in the following chapter. As mentioned, the average curvatures of the first segments were determined according to Eq.(3.10b). At low ductilities, the observed curvature distributions shown in the figures are consistent. At high ductilities, however, ψ_1^* generally were smaller than ψ_2. This could be explained as a result of the spreading of plastic hinges, with ever increasing inelastic steel tensile strains from the column faces into the beams. The variations of beam bar strains will be discussed in Section 3.10. Some other irregularities in the curvature distributions were probably caused by crack developments within the gauge length. As mentioned in Section 3.5.2 the potentiometer readings might have been affected also by movements of the beam bars. The lack of a high degree of precision in these curvature measurements is not considered to have affected the validity of the assessment of beam behaviour.

The component of east beam delfection due to rotation in the 1.5 h_b (i.e. p.h.) region was calculated as follows :

$$\delta_{1,b(p.h.)} = \Theta_2 R_a + \Theta_3 R_b + \Theta_4 R_c + \Theta_5 R_d \tag{3.11}$$

where the sysmbols are defined in Fig.3.23(c). It is not necessary to inlcude Θ_1 here because Θ_2 (Fig.3.23(b)) has already incorporated the bar elongations and slip within the joint.

For the remaining length of the east beam, outside the 1.5h_b region, it was assumed that the flexural deflection, $\delta_{1,b(flx)}$ was elastic and hence this was estimated by

$$\delta_{1,b(flx)} = \frac{P_1 L'^3}{3E_c I_e} \tag{3.12}$$

where P_1 = applied force at the beam end
L' = length of the beam outside the $1.5h_b$ region (Fig.3.23(c))
E_c = modulus of elasticity of the concrete
I_e = effective moment of inertia according to Eq.(3.13) or (3.14)

In estimating flexural deflections, approximate allowance was made for the effects of cracking of the concrete on the stiffness of the beams and of the column. It was assumed, as in routine building design, that the effective moments of inertia I_e are

$$\text{for beams} \quad I_e = 0.5\, I_g \tag{3.13a}$$
$$\text{for columns} \quad I_e = 0.5\, I_g \tag{3.13b}$$

where I_g is the moment of inertia based on uncracked gross concrete area. In computing I_g for the flanged beams, the effective widths of the overhanging parts were taken as one half of those normally assumed for strength calculation [4] for compression flanges in the mid-span region. The relatively small I_e value assumed for the column was intended to recognize the absence of axial compression.

Alternatively, the following expression, recommended by the codes [4,5], was also used to determine the effective moments of inertia for beams and columns

$$I_e = \left(\frac{M_{cr}}{M_a}\right)^3 I_g + \left[1 - \left(\frac{M_{cr}}{M_a}\right)^3\right] I_{cr} \tag{3.14}$$

where I_{cr} = moment of inertia of the cracked section transformed to concrete
M_{cr} = moment at first cracking
M_a = maximum moment in member at stage at which the deflection is being computed

No instrumentation had been set up to measure the shear deformations in the beams. Visual observation during the test and measurement of the sliding along the cracks in the plastic hinge regions indicated that the final

inelastic shear displacement in each beam was about 3 mm. Exact measurements at high ductilities were not possible because of the spalling of concrete. However, an estimate was made of the elastic shear deformation, $\delta_{1,b(sh)}$, of the east beam. As the final value is relatively small compared to overall displacement, it was approximated by taking twice the shear deflection of an uncracked member [1]. That is

$$\delta_{1,b(sh)} = \frac{P_1 \, f \, \ell_1'}{0.2 \, E_c b_w h_b} \tag{3.15}$$

where f = shape factor (1.0 for T sections, 1.2 for rectangular sections)
ℓ_1' = shear span of beam from column face (Fig.3.23(c))
b_w = width of beam web
h_b = depth of beam.

In summary, the above relationships for the east beam can be expressed to give the total beam distortions as

$$\begin{aligned} \delta_{1,b} &= \delta_{1,b(p.h.)} + \delta_{1,b(flx)} + \delta_{1,b(sh)} \\ &= \delta_{1,b(p.h.)} + \delta_{1,b(others)} \end{aligned} \tag{3.16a}$$

In a similar way, the deflection components of the west beam (Fig.3.22(a)) are as follows

$$\begin{aligned} \delta_{2,b} &= \delta_{2,b(p.h.)} + \delta_{2,b(flx)} + \delta_{2,b(sh)} \\ &= \delta_{2,b(p.h.)} + \delta_{2,b(others)} \end{aligned} \tag{3.16b}$$

Because the beams were not symmetrically shaped and reinforced, the east and west beam deflections (Fig.3.22(a)) were not necessarily equal. As equal beam rotations were deliberately imposed in the test (see Fig.1.4), some corrections had to be made after considering other deformation components, as discussed in the following two sections.

The rotations measured in the $1.5h_b$ regions using linear potentiometers (Fig.3.9) were further analysed to study the extent of elongations and local bond-slip of the beam bars within the joint. With reference to Fig.3.24, east segment A corresponds to the region measured by

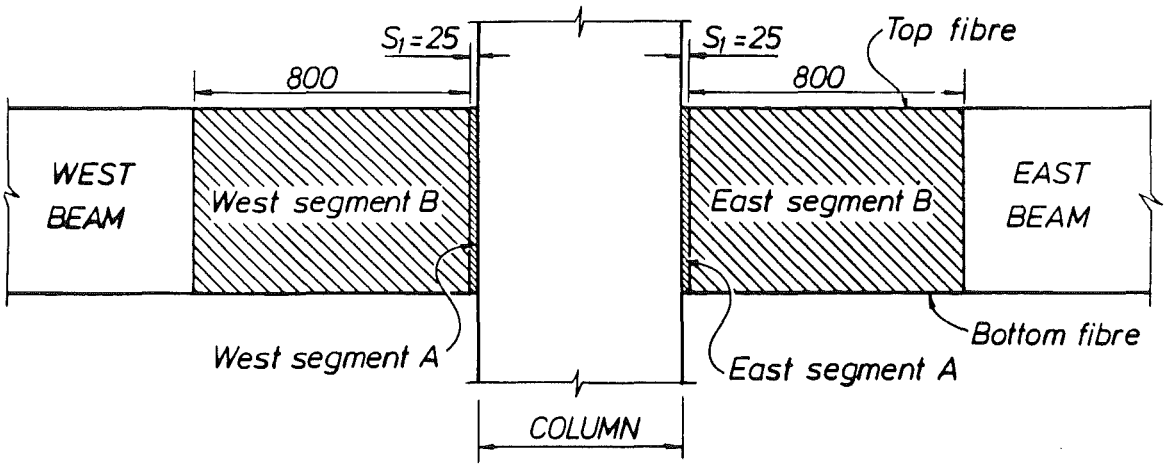

Fig.3.24 - Longitudinal movements of beams over two distinct segments

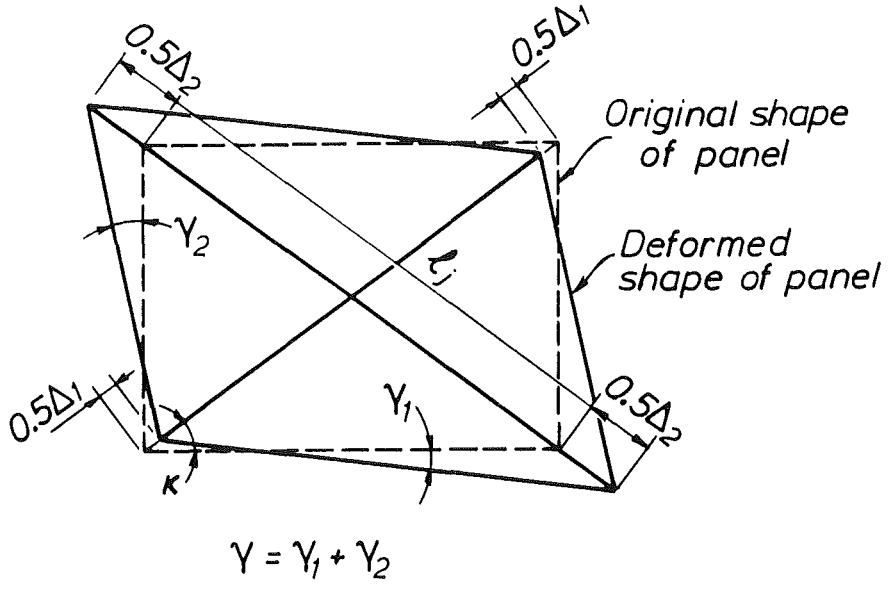

Fig.3.25 - Shear distortion of joint panel

the pair of potentiometers closest to the column (Fig.3.9) over a length of S_1 = 25 mm. It follows that movements in the east segment B of length 800 mm (Fig.3.24) can be determined as the sum of the movements measured in sub-regions a, b, c and d (Fig.3.23) less that measured in segment A. From the data recorded in the linear potentiometers, the movements of the top and bottom fibres of the east beam (Fig.3.24), and similarly of those of the west beam, could be readily calculated. The changes in length of segments A and B are plotted for comparison for each test unit.

Additional information, useful for structural design, is the growth in length of beams during plastification, caused by accumulation of residual tensile strains in the longitudinal beam bars. In building frames, this results in expansion of bay lengths, unless columns can offer some restraint. Lengthening of the beams in this test series was estimated by considering the increase in the total length of segments A and B.

3.9.3 Deformations of the Column

As shown in Fig.3.22(b), the column of the test unit deformed under the action of storey shear, V_c. Since the column was not designed to develop plastic hinges, it was assumed to remain elastic throughout the test. This assumption was subsequently found to be justified. The elastic flexural and shear deformations, $\Delta_{c,c}$, were not measured, but using column properties they were estimated, by applying Eqs.(3.12) and (3.15), as twice the deflection of the half-column. That is

$$\Delta_{c,c} = 2 \left(\frac{V_c \ell_c'^3}{3E_c I_e} + \frac{V_c f \ell_c'}{0.2E_c b_c h_c} \right) \qquad (3.17)$$

where ℓ_c' = shear span of half-column (Fig.3.22(b))
b_c = width of column
h_c = depth of column.

The associated beam deflections, $\delta_{1,c}$ and $\delta_{2,c}$, as a result of column action, were found from the geometrical relationship (Fig.3.22(b)) to be

$$\delta_{1,c} = \Delta_{c,c} \left(\frac{\ell_1}{\ell_c} \right) \qquad (3.18a)$$

$$\delta_{2,c} = \Delta_{c,c} \left(\frac{\ell_2}{\ell_c} \right) \tag{3.18b}$$

3.9.4 Deformations due to the Joint Shear Distortion

On the north and south faces of the joint area of Unit 1D-I as well as the west joint face of Unit 2D-E, linear potentiometer readings enabled the approximate joint core distortion to be measured. From the geometry shown in Fig.3.25, the total joint shear strain, γ, is obtained thus

$$\gamma = \gamma_1 + \gamma_2 = \frac{\Delta_2 - \Delta_1}{2\ell_j} \left(\tan \kappa + \frac{1}{\tan \kappa} \right) \tag{3.19}$$

where the measured displacements Δ_1 and Δ_2 are taken as positive when the diagonal length ℓ_j elongates and negative when it shortens. The shear strains, γ_1 and γ_2, are positive as shown in the figure, and κ is the angle of inclination of the joint diagonal to the horizontal.

The components of displacement due to this joint strain γ are computed as follows, using the symbols shown in Fig.3.22(c)

$$\text{(east beam)} \quad \delta_{1,j} = \ell_1' \gamma - \ell_1 h_b \gamma / \ell_c \tag{3.20a}$$

$$\text{(west beam)} \quad \delta_{2,j} = \ell_2' \gamma - \ell_2 h_b \gamma / \ell_c \tag{3.20b}$$

$$\text{(column)} \quad \Delta_{c,j} = \left(\frac{\delta_{1,j} - \delta_{2,j}}{\ell_1 + \ell_2} \right) \ell_c \tag{3.20c}$$

The potentiometer rods embedded in the concrete were located between the top and bottom layers of the beam bars and also between the outermost layers of the column longitudinal bars. It was therefore assumed that the joint shear strains measured did not include the effects of the deformations of the beam or columns bars within the joint core due to bond deterioration.

3.9.5 Total Deformations

The components discussed in the previous three sections can now be summed up. The various deflection components at all loading stages can be

expressed as percentages of the total experimental east beam deflections, Δ_{B1} (Fig.1.4(b)) at each stage of the loading. The relationship is as follows

$$\Delta_{B1} = \delta_{1,j} + \delta_{1,c} + \delta_{1,b(p.h.)} + \delta_{1,b(others)} + \delta_{1,b(unaccounted)} \qquad (3.21)$$

The last item in the equation is the deformation unaccounted for. It is the difference between Δ_{B1} and the other four items in Eq.(3.21). Eq.(3.21) can be applied to obtain similar relationships for the west beam and the column. As mentioned earlier, equal beam deflections were imposed in the test unit. Since $\delta_{1,b(p.h.)}$ and $\delta_{2,b(p.h.)}$ were not equal, $\delta_{1,b(unaccounted)}$ and $\delta_{2,b(unaccounted)}$ therefore had different values. Inelastic shear deformations in the beams are included in the "unaccounted" portions.

Joint shear strains were not measured for Unit 2D-I in both directions and Unit 2D-E in the N-S direction, because of lack of access to the joint force. Joint distortions for these two units will be discussed when presenting the test results in the following chapters.

3.9.6 Prediction of Stiffness

As discussed in Section 1.3, the theoretical stiffness of a structure, $K_{theoretical}$, is implied in most building codes in terms of the interstorey deflection, Δ_e, calculated for the frame behaving elastically under code design seismic forces, V_{code}. In Fig.1.2, the value for Δ_e is used to define the yield displacement Δ_y.

For each test unit, it was assumed that the maximum dependable flexural strengths of the beam sections at both sides of the column in a principal directions had developed simultaneously (see Fig.1.4) while undergoing equal rotations. P and V were the corresponding beam and column forces found by back calculation, details of which are given in Appendices B, C and D. Force and displacement relationships are expressed in Eqs.(3.3) and (3.4). The three major components of deflections, shown in Fig.3.22 and by Eq.(3.8), have been discussed in some detail in the preceding sections. The same principles can be used to estimate the deflection Δ_e. However, for easy reference in the calculations in the appendices, the method is summarised as follows.

(1) Deformations of the Beams

The elastic flexural and shear deformations of the beams (Fig.3.22(a)) are estimated by applying Eqs.(3.12) and (3.15) respectively, using the appropriate beam properties and the total beam lengths. Hence

(for right-hand beam) $$\delta_{1,b} = \frac{P_1 \ell_1'^3}{3E_c I_e} + \frac{P_1 f \ell_1'}{0.2E_c b_w h_b} \qquad (3.22a)$$

(for left-hand beams) $$\delta_{2,b} = \frac{P_2 \ell_2'^3}{3E_c I_e} + \frac{P_2 f \ell_2'}{0.2E_c b_w h_b} \qquad (3.22b)$$

There are two methods of calculating the effective moment of inertia I_e of a section, as given by Eqs.(3.13) and (3.14). The result from Eq.(3.14) is considered to be more accurate.

In the test, equal rotations are to be deliberately imposed to the beams. The equivalent storey sway is therefore assumed to be the average of $\delta_{1,b}$ and $\delta_{2,b}$. That is, from Eq.(3.3),

$$\Delta_{c,b} = \left(\frac{\delta_{1,b} - \delta_{2,b}}{\ell_1 + \ell_2} \right) \ell_c \qquad (3.23)$$

It should be noted that this method neglects the effect of "fixed end rotations" of beams at column faces (see Section 2.3.2) due to bond slip, if any, and elongation of the beam bars caused by dominant tensile strains inside the joint core. This effect becomes more significant as the beam depth increases.

(2) Deformations of the Column

The elastic flexural and shear deformations of the column (Fig.3.22(b)) are estimated according to Eq.(3.17).

(3) Deformations due to the Joint Shear Distortion

It was not attempted to predict even approximately joint distortion. According to previous tests [39,61], shear distortion of joints which are

properly reinforced contributes between 10% and 20% of the total beam deflection. Accordingly, a 20% of column deflection due to joint distortion is assumed here. That is

$$\Delta_{c,j} = 0.20\ \Delta_e \tag{3.24}$$

(4) Total Deformations

The components are summed up (Eq.3.8) to give the total equivalent storey (column) deflection Δ_e, which is also defined as yield deflection Δ_y, (Eq.1.2) as repeated below,

$$\Delta_e = \Delta_y = \Delta_{c,b} + \Delta_{c,c} + \Delta_{c,j}$$

(5) Stiffness

The theoretical stiffness of a test unit is then given by (see Fig.1.2)

$$K_{theoretical} = \frac{V_{code}}{\Delta_e} \tag{3.25}$$

3.10 ASSESSMENT OF BEAM BAR STRAINS AND SLIPS

The relationship between the strain results read from the strain gauges and those derived from linear potentiometer readings are illustrated with the aid of the example east beam in Fig.3.23. The essential details are reproduced in Fig.3.26(a). Also shown are the positions of the strain gauges on the bottom layer D24 beam bar. The following discussions refer to the strains at the level of this layer. The observations are also applicable to the strains along the top layer of bars. For exterior joint assembly, where the west beam does not exist, only slight modifications are necessary.

When the east beam in Fig.3.26(a) is displaced upwards, the increases of the lengths of the five segments S_i at the beam bar level, ΔS_i, are determined from the readings of the linear potentiometers (see Fig.3.23). This is based on the assumption that the potentiometer rods moved together with the beam bars. The corresponding average strains for a segment is given by

$$\epsilon_i = \Delta S_i / S_i \tag{3.26}$$

Note that the ΔS_i defined in this section are slightly different from those used in Section 3.9.2 (see also Fig.3.23(b)) in which ΔS_i referred to the length changes at the potentiometer levels.

The above expression for $\epsilon_1 = \Delta S_1 / S_1$ implies that the strain inside the column is zero. A more realistic estimation should include strain variations inside the column (joint) where bond must be developed, as has been discussed extensively in Section 2.3. An ideal strain distribution inside the joint, assuming perfect anchorage of the beam bar, is suggested in the lower part of Fig.3.26(b) by the dashed straight line 1. Also shown is the dashed line 2 for the ideal strain distribution in the beam, away from the column, due to flexural action only. For this latter beam strain distribution, however, it has been explained, with reference to the "tension shift" phenomenon [1], that the strains do not vary linearly when diagonal cracks form under shear. Hence the dotted curve 4 represents a more realistic distribution of tensile steel strains in the east beam. Similarly, because of the large shear inside the joint core, the dotted curve 3 should replace line 1. Attention is drawn to the three particular strains marked as ϵ_{g1}, ϵ_{g2} and ϵ_{g3} in Fig.3.26(b). They are expected to be the same as those measured by strain gauges g_1, g_2 and g_3 (see Fig.3.26(a)) respectively. Also strain ϵ_{g1} should be small in comparison to ϵ_{g3}.

For segment 1, a strain ϵ_1^* (Fig.3.26(b)) is shown to replace ϵ_1 in order to incorporate the "realistic" strains developed inside the joint core ϵ_1^* is assumed uniformly distributed over the short length S_1. The elongation Δs_1 is then given approximately by the shaded area 1 bounded by the horizontal strain line ϵ_1^* and the dashed straight line 1. It is assumed that the strain at the column centre is zero when the relatively larger strain ϵ_{g3} or ϵ_1^* is involved. The magnitude of area 1 is thus $\epsilon_1^* S_1 + 0.5\, \epsilon_1^*\, h_c/2$. Hence

$$\epsilon_1^* = \frac{\Delta S_1}{S_1 + 0.25 h_c} \tag{3.27}$$

It can be seen that ϵ_1^* so determined should not differ significantly from ϵ_{g3} if the measured ΔS_1 does not include any bar slip.

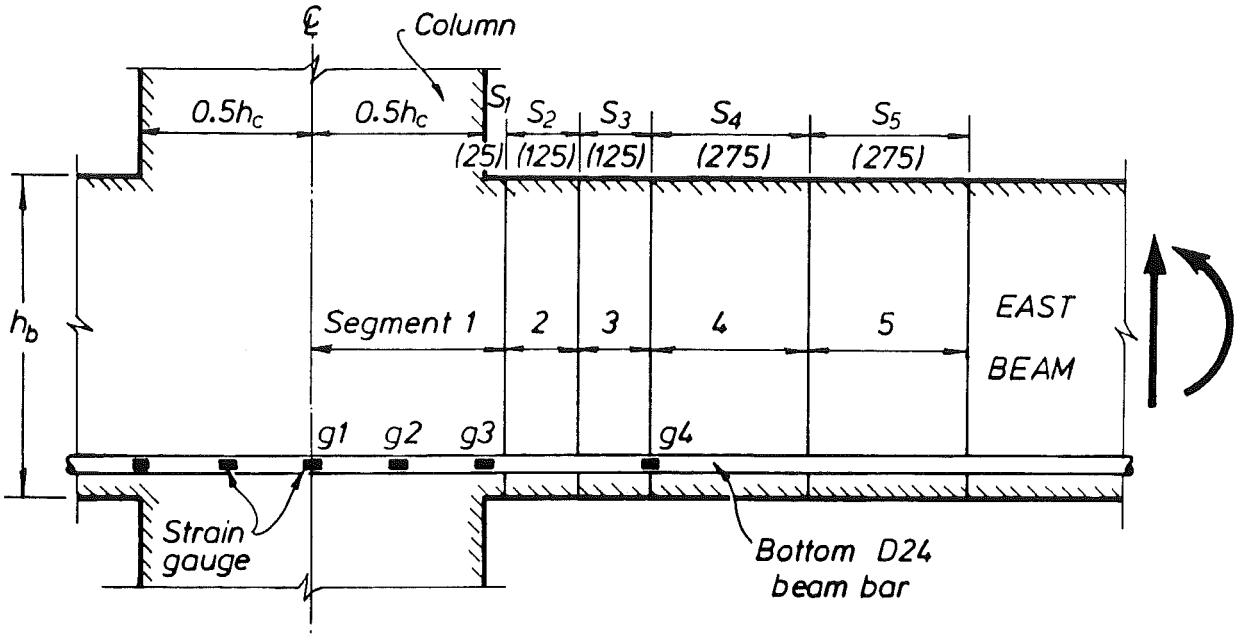

(a) Measurements for East Beam Deformations

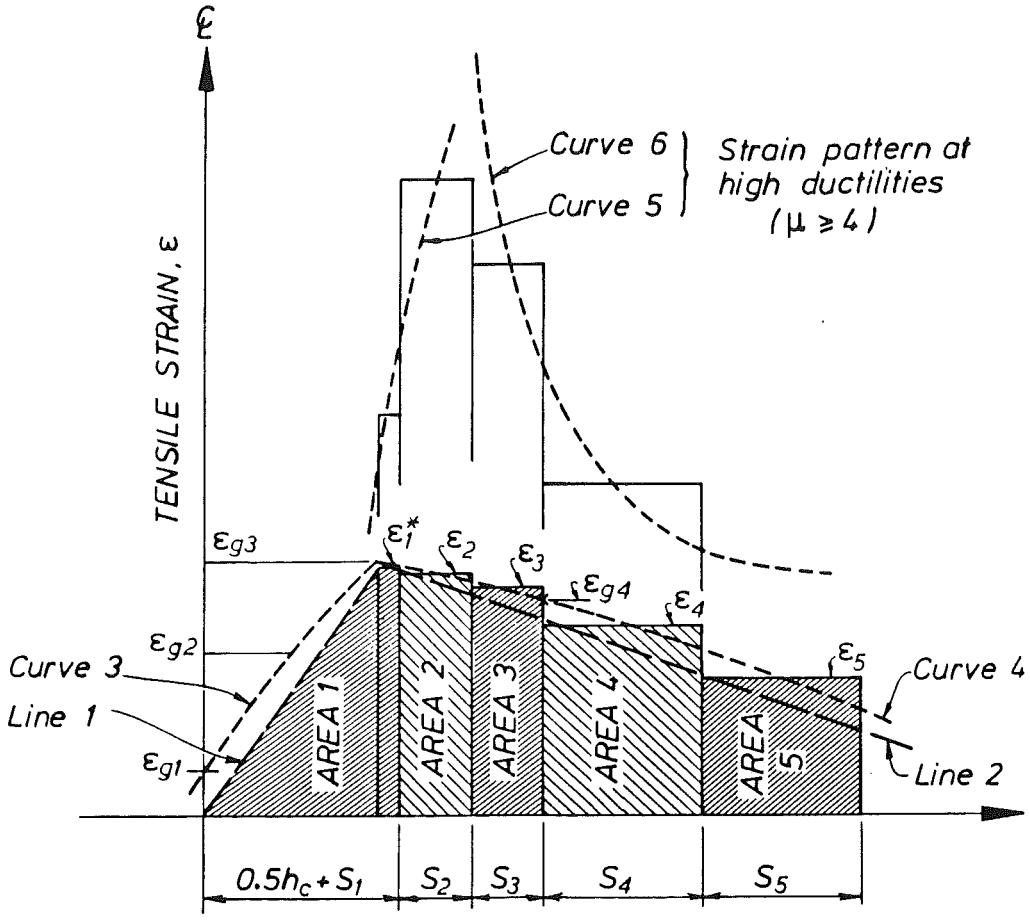

(b) Strain Distribution along Bottom Beam Bar

Fig.3.26 - Different beam strain patterns observed in tests

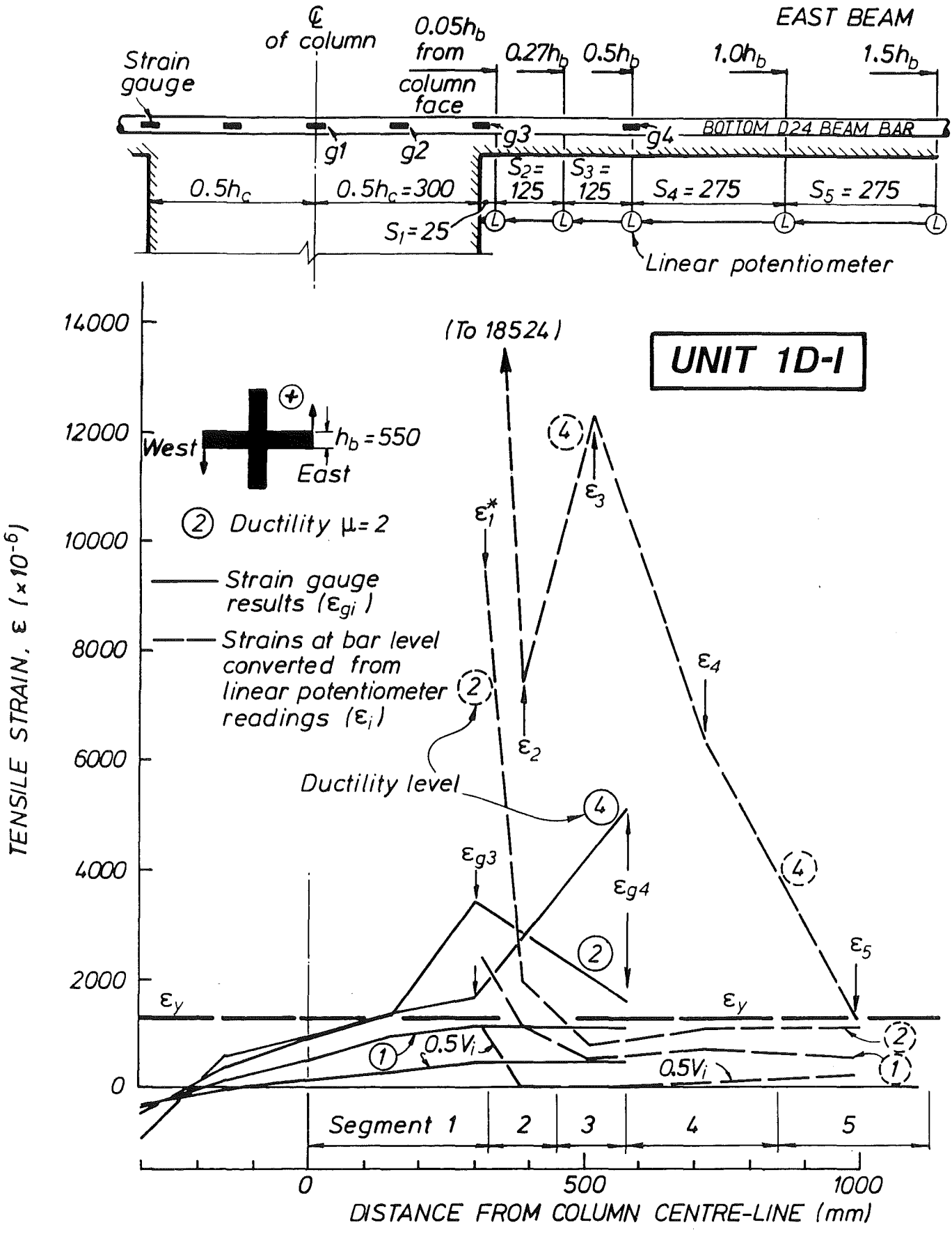

Fig.3.27 - Strain distributions at bottom beam bar level of Unit 1D-I

Other strains ϵ_2 to ϵ_5 defined according to Eq.(3.26) and derived from measured elongations are also indicated in Fig.3.26(b). The shaded areas 2 to 5 correspond to the measured elongations ΔS_2 to ΔS_5 respectively. The strain measured by the gauge g_4, ϵ_{g4}, should normally have a value between ϵ_3 and ϵ_4. Curves 5 and 6 will be referred to later in this section.

Corresponding results for the three test units are given in the following chapters. However, for the purpose of discussion in this section, some of the relevant results for Unit 1D-I are presented in Fig.3.27, which can be related directly to Fig.3.26. The solid lines in Fig.3.27 indicate strains obtained from strain gauge readings while the dashed lines represent strains derived from linear potentiometer readings.

In the elastic cycles (i.e. the first two cycles to approximately one-half of the ideal strength V_i) and the first inelastic cycle to displacement ductility of $\mu = 1$, Fig.3.27 shows that the strains (solid lines) followed the distributions as expected. Anchorage of the bottom beam bar was provided predominantly in the left half of the column. Similar values of ϵ_{g3} and ϵ_{g4} confirm the effect of diagonal cracks. On the other hand, strains determined from linear potentiometers were quite irregular. This was evidently affected by the non-uniform formation of flexural-shear cracks in the beam. In particular, the strain ϵ_1^* was much larger than the measured gauge strain ϵ_{g3} at ductility $\mu = 1$. It is noted that ϵ_1^* included the effect of bar slip within the joint core.

At the peak of $\mu = 2$, it was found that $\epsilon_{g3} = 0.34\%$ which was far less than $\epsilon_1^* = 0.95\%$, while $\epsilon_{g4} = 0.16\%$ was between $\epsilon_2 = 0.2\%$ and $\epsilon_5 = 0.11\%$. The elongation ΔS_1 was 1.67 mm. If strain gauge g_3 functioned properly, there should have been a bar slip of the order of $1.67\ (0.95 - 0.34)/0.95 = 1.1$ mm. Yet this rigid body movement of the beam bar could have caused the strain gauge to give erratic readings.

Effects of bar slip within the joint core became more obvious in the cycle to $\mu = 4$. While ϵ_{g3} read 0.17%, ϵ_1^* amounted to 1.85% corresponding with an elongation over segment 1 (Fig.3.27) of $\Delta S_1 = 3.27$ mm. Although ϵ_2 at $\mu = 4$ was measured to be 0.75%, it increased rapidly to 2.91% in the second cycle to the same ductility. In comparison with $\epsilon_3 = 1.23\%$ and $\epsilon_4 = 0.63\%$, $\epsilon_{g4} = 0.52\%$ was found to be considerably smaller. It becomes apparent at this

stage the bar slips caused the electrical resistance strain gauges to give unreliable readings.

Comparisons were made with previous tests conducted at the University of Canterbury [39,61,64] in which bar strains were measured in similar beam-column joint test units by DEMEC (demountable mechanical) gauges. In the inelastic range, average steel tensile strains over 100mm length at column faces consistently exceeded 1%, with the values eventually reaching 3% to 4%. These are significantly larger than the strains measured in this project by electrical strain gauges. When the ACI stress block method was used to calculate the theoretical flexural strengths of beam sections (see Section 3.8), the resulting tensile strains in beam bars were of the order of 2%. As can be seen in the test results presented in Fig.3.27 and the following paragraphs, beam bar strains measured by electrical resistance strain gauges seldom exceeded 1%. It is therefore considered that beam bar strain gauge results in this project were useful only up to a ductility level of $\mu = 2$ or when the horizontal longitudinal movement measured over a segment length was not more than 2 mm. It is considered that thereafter strains were more reliably predicted using linear potentiometer results.

It was stated that in determining ϵ_1^* from Eq.(3.27), slip of the beam bar was included in the quantity ΔS_1. Therefore the value of ϵ_1^* obtained by this method should be much larger than ϵ_2 or ϵ_3 (see the dashed lines in Fig.3.27). On the other hand, the realistic value of ϵ_1^*, if slip had been excluded, should only be slightly larger than ϵ_2 as is implied by curve 4 in Fig.3.26(b). However, the test results consistently showed a reverse trend with increasing imposed ductilities. The strains ϵ_2 and ϵ_3 determined according to Eq.(3.26) were much larger than ϵ_1^* estimated by Eq.(3.27). For instance, in the second cycle to $\mu = 4$, the strains converted from linear potentiometer readings were 1.53% (ϵ_1^*), 2.91% (ϵ_2) and 1.12% (ϵ_3) respectively. This trend is generalised in Fig.3.26(b) by the dotted curves 5 and 6. It is believed that strain hardening of the beam bar in the plastic hinge region started from the column face and propagated to the free end of the beam. Since there were no other reliable measurements to determine the real value of ϵ_1^* (slip excluded), a compromise is taken to estimate this "real" ϵ_1^* as

$$\epsilon_1^* \approx \frac{\Delta S_2 + \Delta S_3 + \Delta S_4}{S_2 + S_3 + S_4} \qquad (3.28)$$

This assumption implies that the strain at the column face is the same as the average strain over the plastic hinge of a length equal to the beam depth h_b.

The results from Eq.(3.28) were used to estimate beam bar slips. The assumed strain distributions inside a column (joint) are summarised in Fig.3.28. It is necessary to consider two strain patterns. Negative (compression) strains in a beam bar exist only at low ductilities, say at $\mu = 2$ as shown in Fig.3.28(a). At higher ductilities ($\mu \geq 4$), large residual tensile strains prevail even when the beam bar is in compression (Fig.3.28(b)). This phenomenon was discussed in Section 2.3.3. To simplify computations, the following idealisations are also made :

(1) The strains vary linearly inside the joint core.
(2) Yield penetration into the joint core is ignored.
(3) At high ductilities (Fig.3.28(b)), the strain at the centre of the column is assumed to be zero.

The local bond-slips of the longitudinal beam bars were estimated as follows. In Fig.3.29, horizontal movements of the outer boundaries of both the west and east segments 1 are shown to an exaggerated scale at the m^{th} load increment with negative ductility being imposed, and at the n^{th} load increment with positive ductility. Again the discussion is restricted to changes at the bottom bar level. According to the discussions in Section 2.3.4, slip can be taken as the displacement of the original centre of a beam bar in the joint core from the centre of the column. In this report slip is taken as positive for movement to the east, but in the following discussion sign conventions are not considered.

At the m^{th} load increment (Fig.3.29(a)), the bar slip to the west is shown as d_m. The movements of segment 1, as indicated by linear potentiometer measurements ΔS_{1m}^{E} and ΔS_{1m}^{W}, include this bar slip as well as the change in length of $(2S_1 + h_c)$ of the bar due to strains developed.

When the imposed ductility to the same level is subsequently reversed at the n^{th} load increment (Fig.3.29(b)), the bar slips to the east from its previous position by an amount of $d_m + d_n$ (shown in exaggeration). Final movements of the segments 1 are measured by linear potentiometers as ΔS_{1n}^{E} and ΔS_{1n}^{W} with reference to the before-test positions. These measurements again are a combination of beam bar slip and elongation or shortening of the

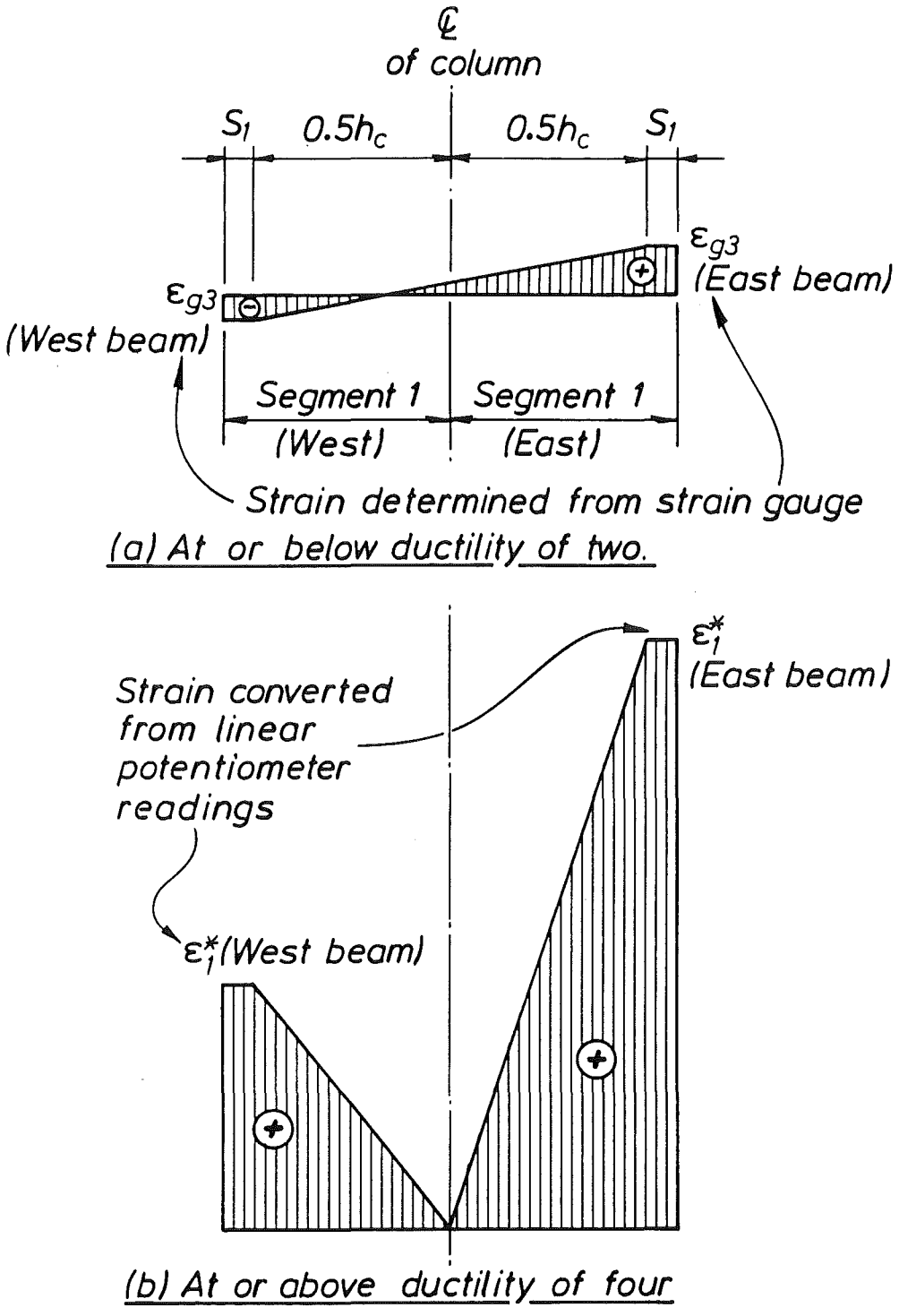

Fig.3.28 - Assumed strain distributions along bottom beam bar

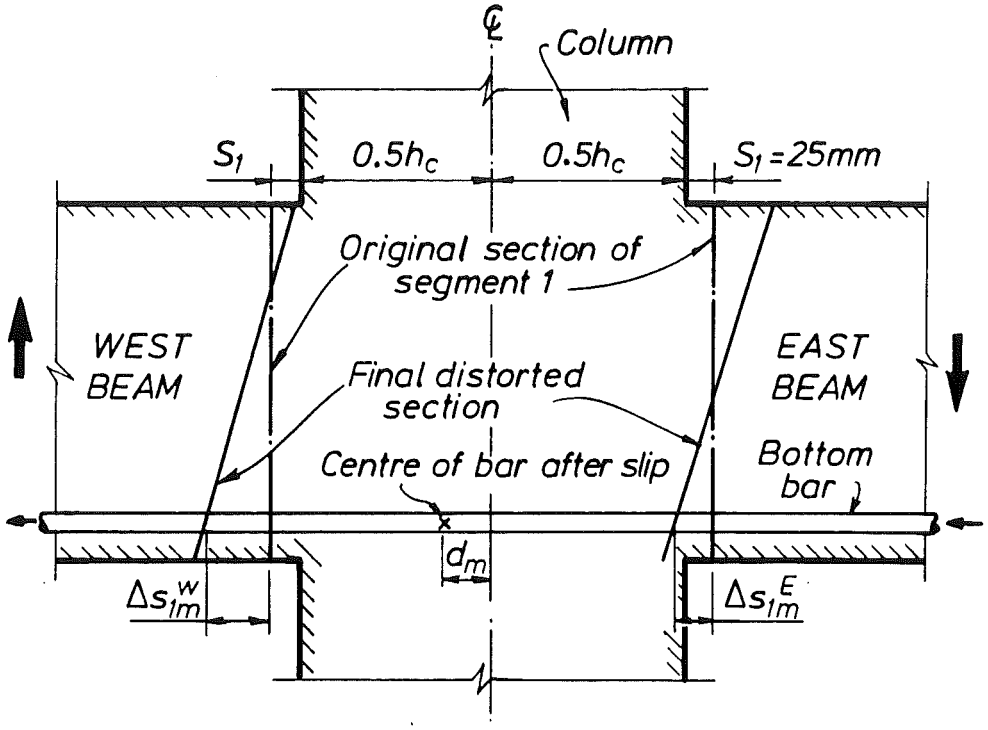

(a) At the m^{th} load increment

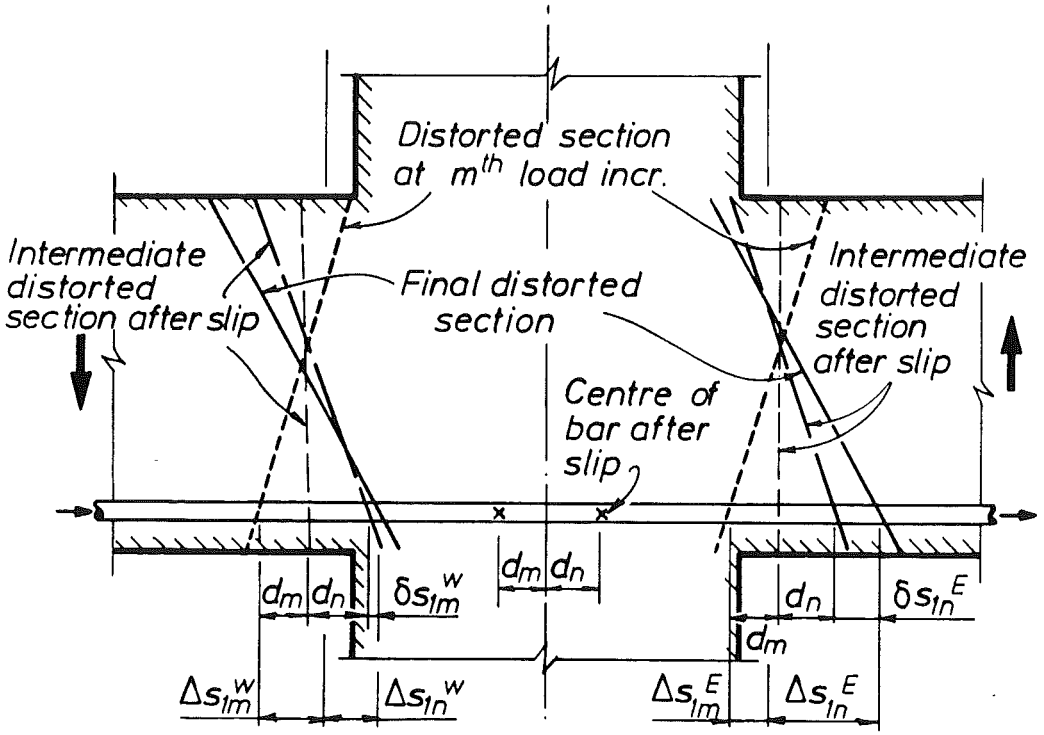

(b) At the n^{th} load increment

Fig.3.29 - Movements of bottom beam bar with slip

bar in virtue of the strains developed. The elongation and shortening, shown as δS_{1n}^{E} and δS_{1n}^{W} in Fig.3.29(b), can be estimated as the difference in the shaded areas under the strain distribution of either Fig.3.28(a) or 3.28(b), the strains being measured at the m^{th} and n^{th} load increments. Hence referring to Fig.3.29(b),

$$\text{(for east beam)} \quad \Delta S_{1m}^{E} + \Delta S_{1n}^{E} = d_m + d_n + \delta S_{1n}^{E} \qquad (3.28a)$$

$$\text{(for west beam)} \quad \Delta S_{1m}^{W} + \Delta S_{1n}^{W} = d_m + d_n + \delta S_{1n}^{W} \qquad (3.28b)$$

The distortions shown in Fig.3.29(b) are based on the tensile-compressive strain distribution pattern of Fig.3.28(a). It must be noted that at higher ductilities, the strain pattern of Fig.3.28(b) prevails.

From Eqs.(3.28a) and (3.28b), the slip at the n^{th} load increment, d_n, can be calculated because other quantities are known. There will be two values of d_n, one from Eq.(3.28a) and one from Eq.(3.28b). They may not be identical because of experimental errors involved and the approximations taken for the strains. Therefore for estimation of the slip at the following load increment, the average of the two d_n values is taken.

CHAPTER 4

TEST RESULTS OF UNIT 1D-I

4.1 GENERAL BEHAVIOUR

The test took about four weeks to complete with thirteen cycles of loading up to a displacement ductility factor of ten having been attained. The overall performance of the test unit was satisfactory in terms of strength and ductility capacity. As illustrated by the photographs in Figs. 4.1 to 4.6 and also Fig. 3.5(a), plastic hinges developed in the beams at the two column faces while fine flexural cracks in the column over the whole height were present. This indicated that the column remained essentially elastic. The desired behaviour of a ductile frame, i.e. a "strong column - weak beam" mechanism, was therefore achieved in this test. In the joint area, uniformly distributed diagonal cracks formed generally at an angle close to 45°. This could be reasoned to have resulted from the principal tensile strains in an uncracked body, under zero axial load. Joint cracks closed on load reversals and the cover concrete remained intact till the end of the test.

Cracks in the slab were not densely distributed. In addition to the photographs previously shown, Fig. 4.7 gives the pattern of the major cracks at the top surface of the slab. These cracks have been numbered for convenience as they are referred to in subsequent discussions. Except for the few cracks extending from the column, all slab cracks originated from the top flexural cracks of the beams. Cracks may be grouped into four types, namely,

(1) extensions of beam flexural cracks which were formed when the top fibres of the beams were in tension;
(2) transverse cracks coinciding with the slab bars placed perpendicular to the beams, normally as extensions of type 1 cracks;
(3) beam-slab interface cracks along the edges of the beams or sometimes along the edges of the reinforcing cages within the beams; and
(4) diagonal cracks extending from flexural cracks at the top of the beams to the east and west edges of the slab.

For instance, the cracks running in the north-south direction and labelled as W1N, W1S, W5,W8 amd E9 in Fig. 4.7 belong to type 2.

To supplement the reinforcing details given in Fig. 3.1, Fig. 4.8(a) shows the layout plan of slab bars. From the cross-section details in Fig. 4.8(b), it is evident that once flexural cracks formed at the top of the beam, they would propagate along the transverse bars which served as crack-inducers. Also, since the steel content in the longitudinal direction (D10 bars) was very small (ρ_s = 0.224%), the concrete between the transverse cracks was able to transfer the tensile forces from the D10 bars (see Section 4.5). Therefore few large transverse cracks were to be expected.

Type 3 cracks formed as a result of tensile strains developing in the transverse D16 bars. This should be expected to result from gravity loading on the continuous slab in the prototype structure. In the test unit, the slab carried its own weight only as a double cantilever. The moments resulting at the beam faces were, however, too small to produce any cracks. There were no visible cracks present in the slab before the commencement of the beam loading. Therefore it is concluded that the simulated earthquake loading must have generated additional transverse tension, sufficiently large enough to produce, together with the gravity moments, these type 3 cracks at the top surface of the slab. The phenomenon is studied further in Section 4.5 and in Chapter 7.

Cracks at the underside of the slab had a pattern generally the same as that of the top surface, with the exception of type 3 interface cracks which did not appear, as can be expected from earlier discussion. Widths of the cracks were not as pronounced as those at the top of the slab.

Type 4 diagonal cracks were also caused by the tensile stresses in the transverse slab bars which, in conjunction with the longitudinal bars under tension, produced tensile diagonal tensile strains in the concrete. In Chapter 7, when discussing the behaviour of slabs in beam-columns joint assemblies, it is postulated that between these diagonal cracks, diagonal concrete struts were mobilised to act as load paths for the slab tension forces to be transferred to the beam and partly to the joint.

At the end of cycle 13, it was felt that further loading of the test unit would only increase concrete crushing and spalling in the beam plastic hinges, as well as the buckling of the beam compression bars, but the joint

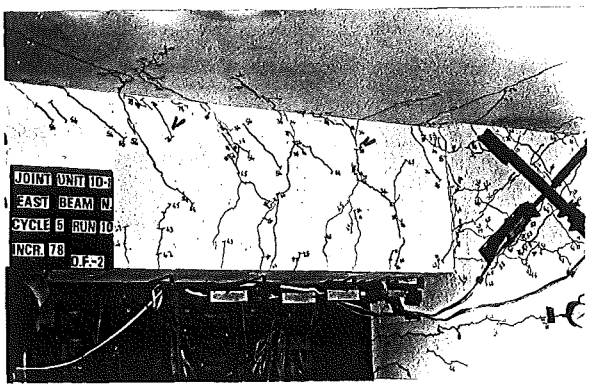

Fig.4.1 - East beam of Unit 1D-I in cycle 5 to ductility of μ = 2

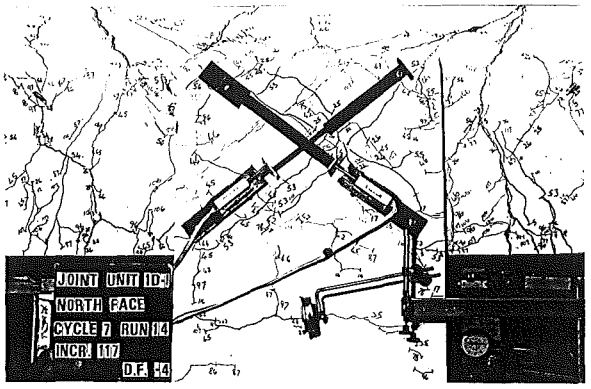

Fig.4.2 - Joint of Unit 1D-I in cycle 7 to ductility of μ = 4

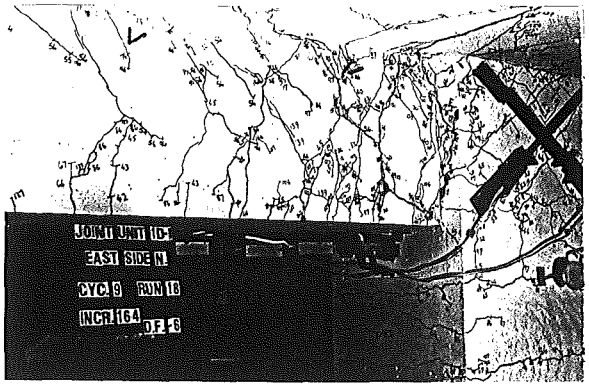

(a) East beam at the peak of 2nd cycle to μ = -6

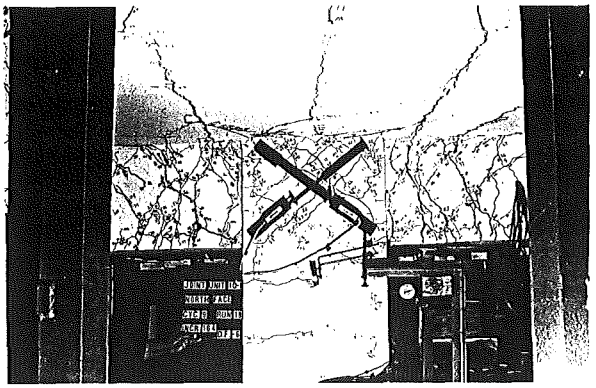

(b) Joint at the peak of 2nd cycle to μ = -6

Fig.4.3 - Unit 1D-I in cycle 9 to ductility of μ = 6

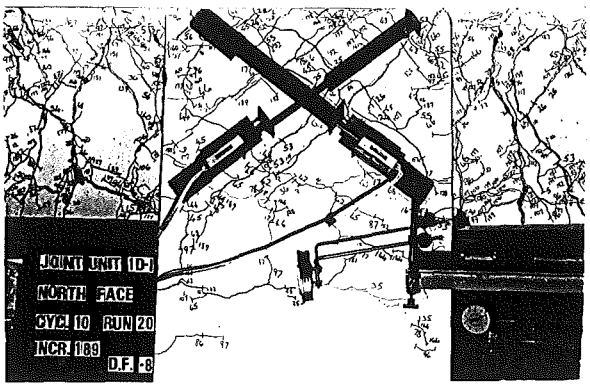

(a) Joint at the peak of 1st cycle to μ = -8

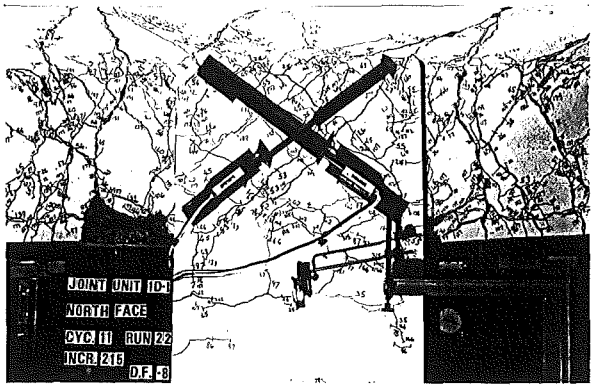

(b) Joint at the peak of 2nd cycle to μ = -8

Fig.4.4 - Unit 1D-I in cycles 10 & 11 to ductility of μ = 8

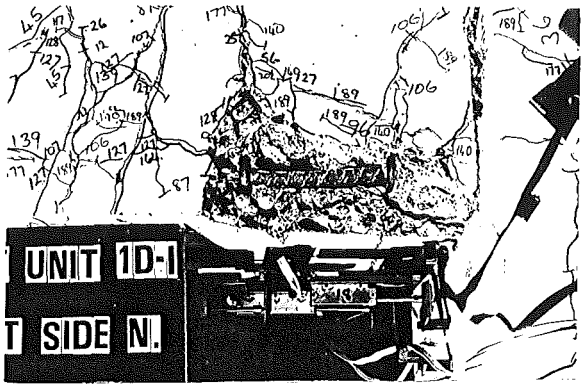

(a) Buckled D24 bar in east beam during the 2nd cycle to μ = -8

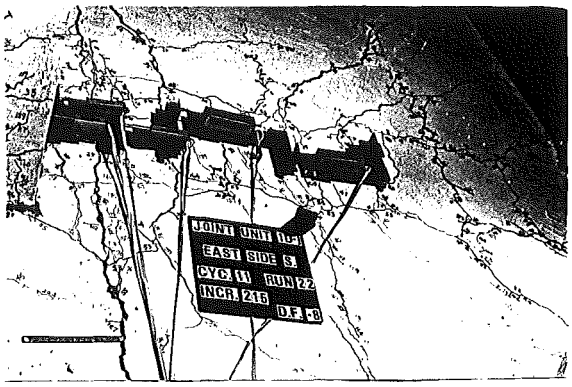

(b) East slab at the peak of 2nd cycle to μ = -8 (view from south)

Fig.4.5 - Features of Unit 1D-I in cycle 11 to ductility of μ = 8

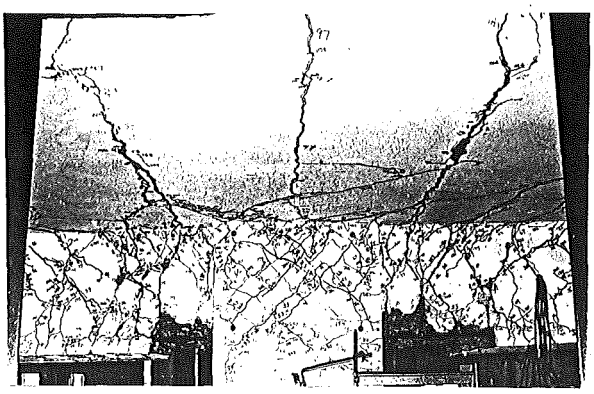

(a) Joint at the end of 2nd cycle to μ = -10

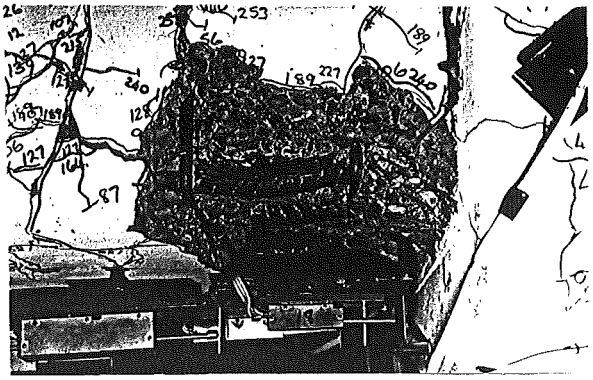

(b) Buckled D24 & D20 bars in east beam at the peak of 1st cycle to μ = -10

(c) Buckled D24 bar in west beam at the peak of 2nd cycle to μ = 10

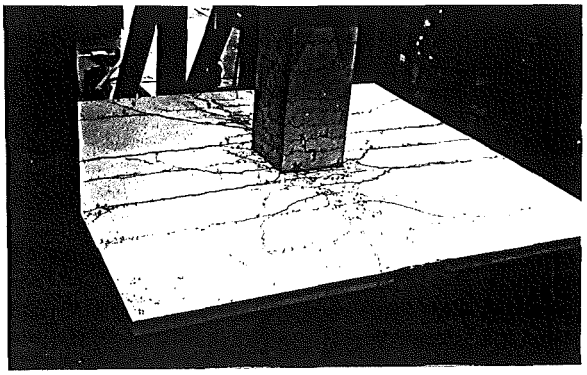

(d) Slab and upper column after test (view from south-east)

Fig.4.6 - Unit 1D-I in cycles 12 & 13 to ductility of μ = 10

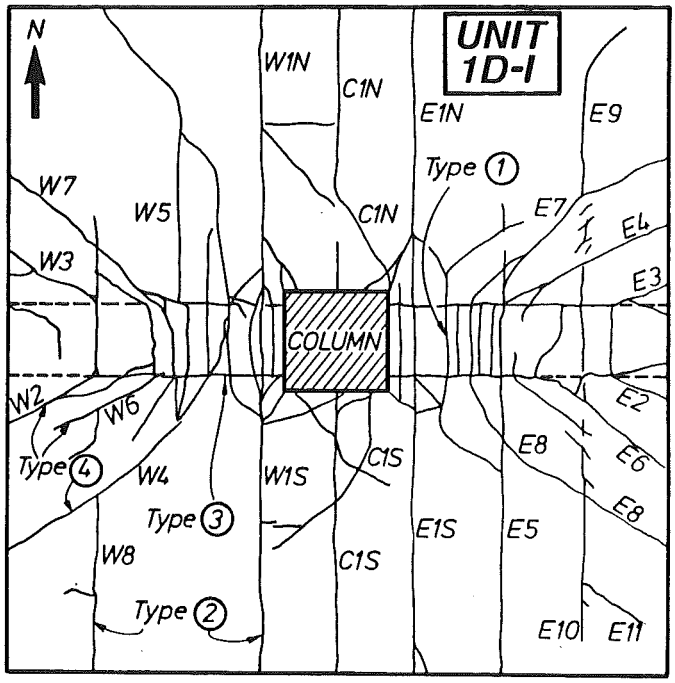

Types of cracks = (1) Beam flexural cracks
(2) Transverse slab cracks
(3) Beam-slab interface cracks
(4) Slab diagonal cracks

Fig.4.7 - The pattern of major cracks at top surface of slab of Unit 1D-I

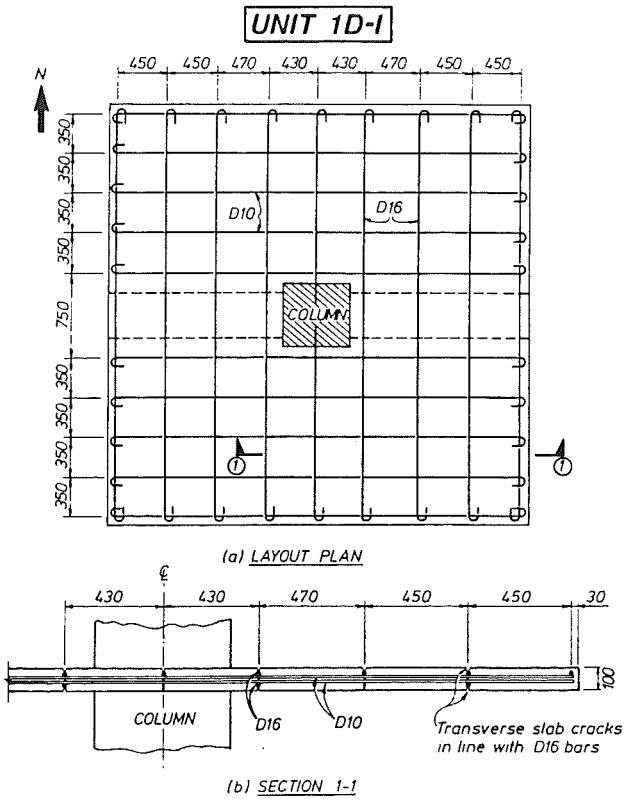

Fig.4.8 - Reinforcing details of slab of Unit 1D-I

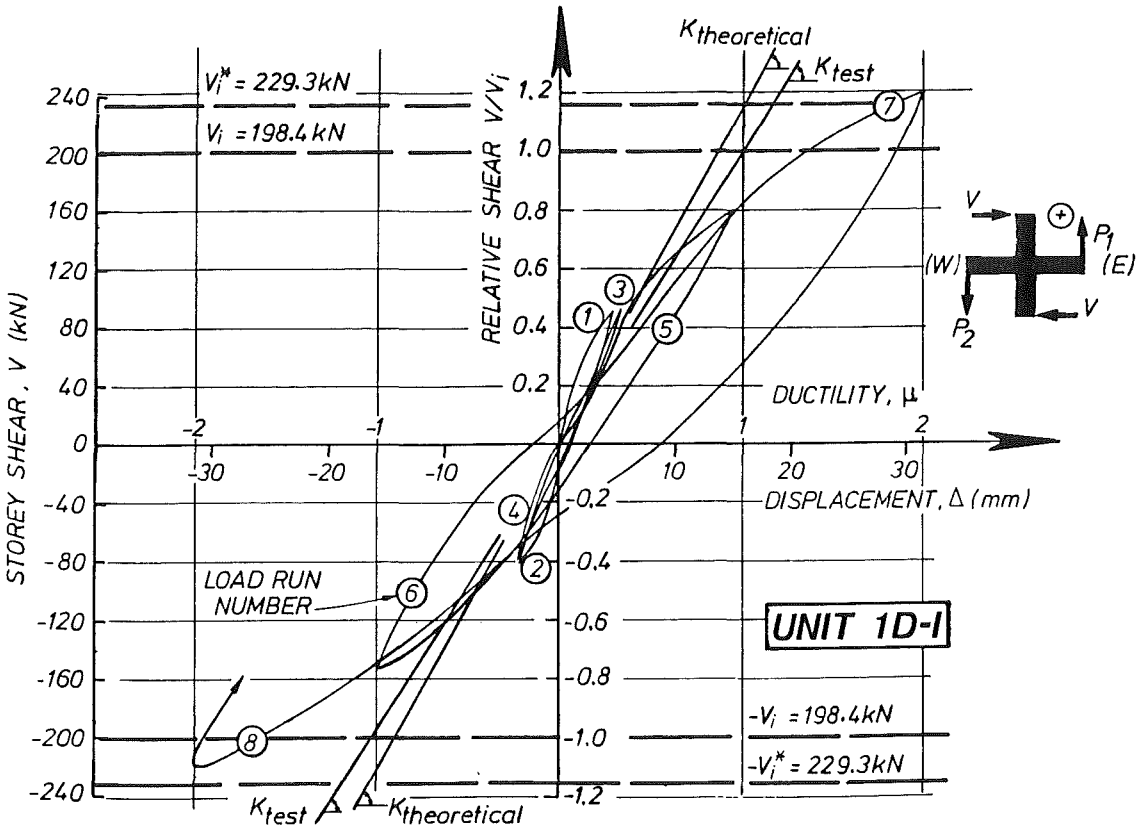

Fig.4.9 - Storey shear-displacement response - elastic cycles

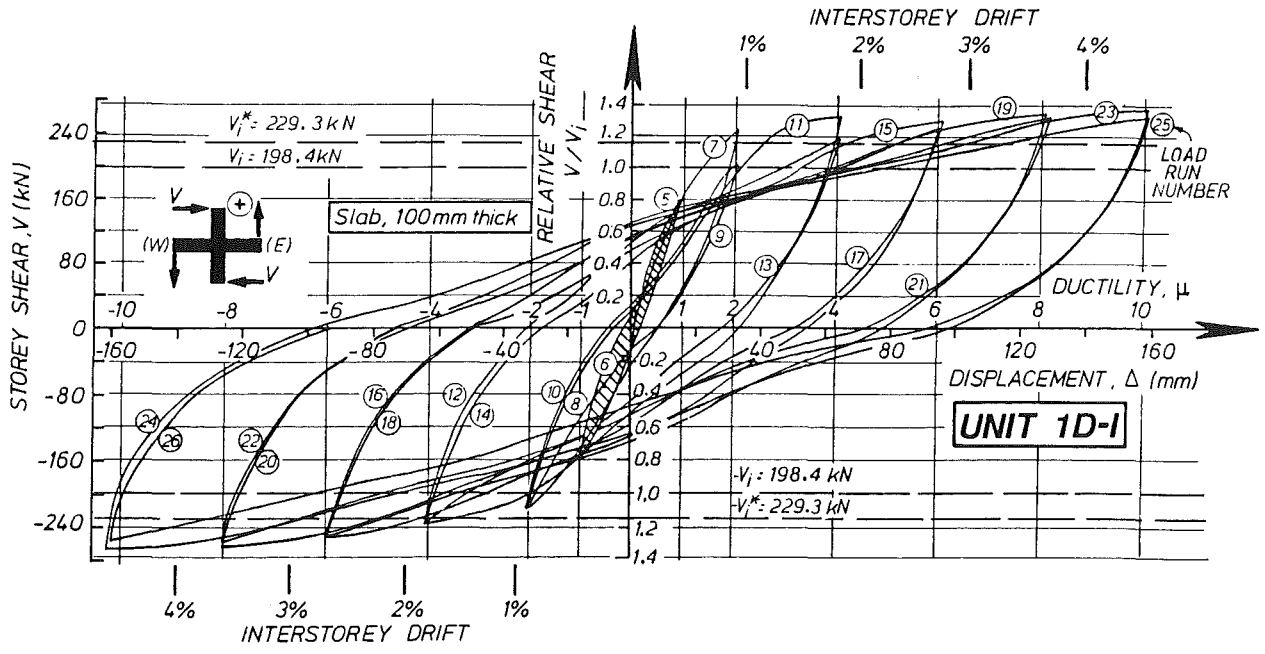

Fig.4.10 - Storey shear-displacement response - inelastic cycles

was not likely to fail. The test was therefore terminated at this stage. In the following section, the strength capacity of the test unit is discussed in association with ductility demand. Reference strengths have been defined in Sections 3.2 and 3.8 and are estimated in Appendix B.3.

4.2 FORCE-DISPLACEMENT RESPONSE

4.2.1 General

The column (storey) shear versus displacement curves are plotted in Fig. 4.9 for elastic cycles and in Fig. 4.10 for inelastic cycles while the force-displacement curves for the east and west beams are given in Figs. 4.11 and 4.12 respectively. The storey shear plots provide an overall measure of the behaviour of the whole beam-column joint assembly and forms a basis for comparison with other test results. Fig.4.10 combines the different degrees of degradation in the east and west beams under opposite loadings, and that of the joint. It is therefore useful to examine also the plots drawn only for beam displacements and forces. They assist in identifying the behaviour of the individual components. In order to avoid confusion, the numbers drawn inside circles in Figs. 4.9 to 4.12 are referred to as load runs rather than semicycles. As shown previously in Fig.3.17, the loading history for this test consisted of 26 load runs. Cycles mentioned in this report are meant to be full cycles, thirteen in total in this test.

In these figures, it is seen that with increasing ductilities, the maximum strength of the test unit as a whole, or of each individual beam component, also increased. This was caused by an increasing contribution of slab bars in tension and strain hardening in both the beam and slab longitudinal tension bars. To indicate the extents of strength enhancement, the reference strengths estimated in Appendix B.3 are included in the figures.

The first-yield displacement of the test unit, $\Delta_{y,test}$ was determined to be 15.7 mm (i.e. 0.45% of storey height) in the first half of cycle 3 when the east beam was subjected to upward force and the west beam to downward force. Applying Eq.(3.25), the measured stiffness was found to be 198.4/15.7 = 12.6 kN/mm. This is 86.9% of the estimated "code" stiffness of 14.5 kN/mm, the derivation of which is given in Appendix B.4. It indicates that the test specimen was more flexible than expected. However, this information needs to

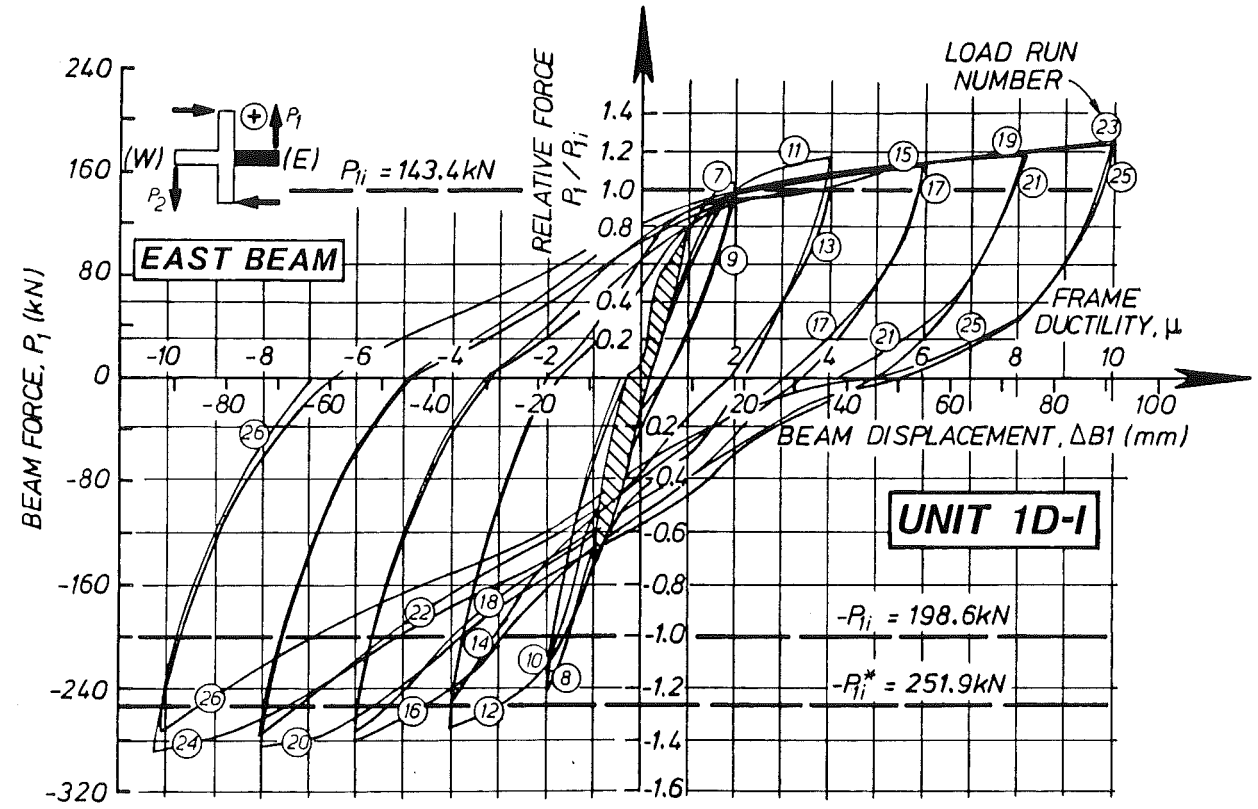

Fig.4.11 - Force-displacement response of east beam

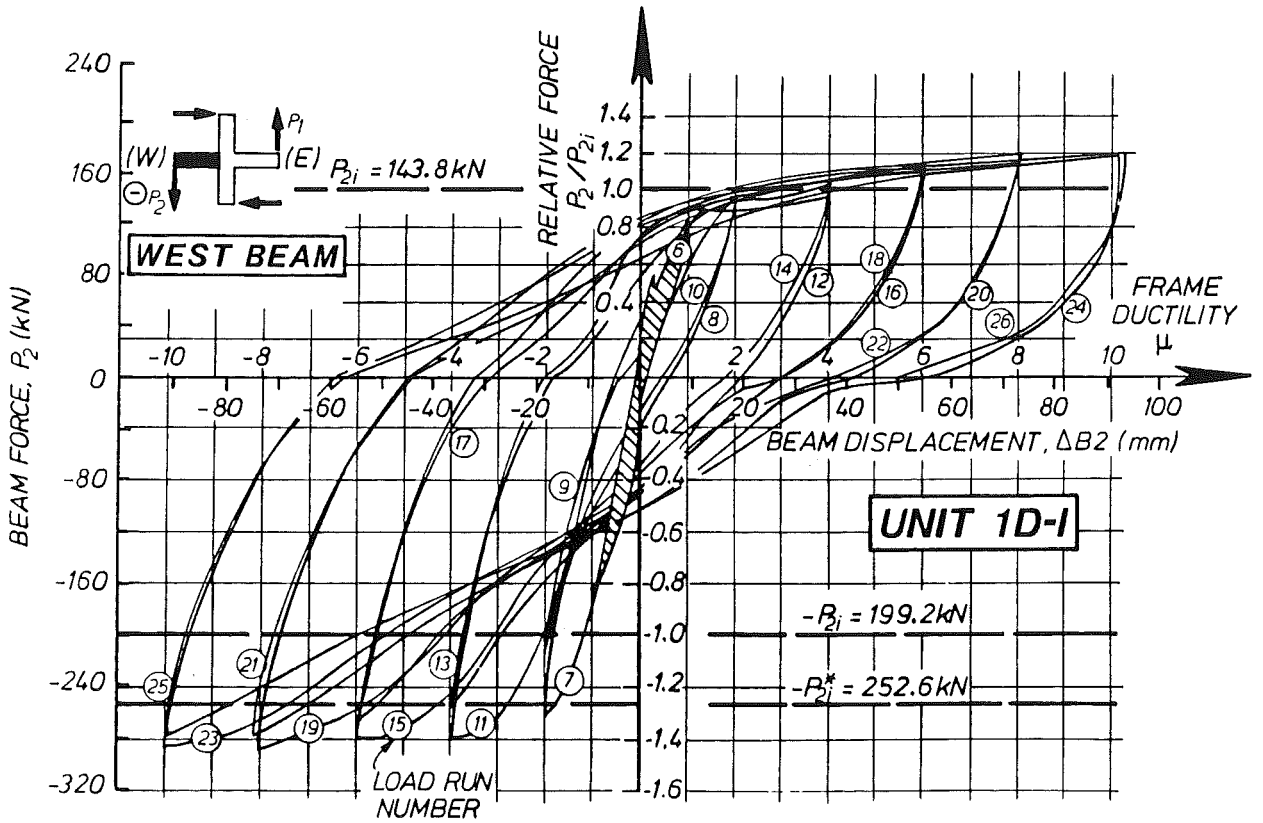

Fig.4.12 - Force-displacement response of west beam

be adjusted in order to bring it in line with the intents of code recommendations for the control of drift, as discussed in Section 1.3.2. Therefore from Eq.(1.5b) the ratio of the calculated ideal strength to the required strength is obtained as

$$\frac{V_{i(test)}}{0.9\ V_{i(design)}} = \frac{198.4}{148.9} = 1.33$$

The limiting interstorey deflection of the prototype frame under code specified seismic forces can therefore be inferred, applying Eq.(1.4b), as 15.7/1.33 = 11.8 mm. This corresponds to an interstorey drift of 0.34%, which is comparable with the code [6] recommended value of 0.32%.

The ductility scale drawn in Figs.4.11 and 4.12 for beams was based on the corresponding displacements relevant to frame ductilities, since equal beam rotations were deliberately imposed in the test (Fig.1.4). If a beam is studied independently, its stiffness may be different from that of an assembly, because beam test would exclude joint distortion and bar slips. For practical purposes, the frame ductilities were considered convenient indicators and therefore used as reference.

4.2.2 Elastic Cycles

For reasons explained in Section 3.6, in the first two cycles of loading, the unit was subjected to approximately one half of the force corresponding to the ideal flexural strengths of the beams, i.e. 0.5 V_i. In the negative load runs (i.e. runs 2 and 4), inadvertently forces slightly less than 0.5V_i were imposed. Consequently the east beam experienced less downward force than the west one, and this was reflected in the crack pattern. However, a similar crack pattern at the east side developed after cycle 3 (ductility $\mu = \pm 1$). It is considered that the test had not been affected by this slight deviation.

It can be seen in Fig.4.9 that loading during the second cycle resulted in relatively little hysteresis. Little additional cracking occurred. As expected, flexural cracking in the beams developed first near the column faces. Cracking of the upper column started early in cycle 1 while cracking of the lower column was noted only in the second half of cycle 2. The likely reason for this was that the concrete in the upper column had lower strength

(see Table 3.6) and that it was not subjected to axial compression. The first transverse (type 2) cracks in the slab had already appeared in load run 1 when the west beam was being pushed downwards. They developed about 120 mm away from the west column face and were in line with a D16 slab transverse bar. These cracks are labelled as W1N and W1S in Fig. 4.7. They extended from the beam to the middle of the slab. Diagonal cracks, labelled W2 and W3 in Fig. 4.7, also developed and reached the west edge of the slab. No cracking had yet appeared in the east slab. Joint cracking during the elastic cycles was slight. The first diagonal joint crack appeared on the south face during run 3.

In the third cycle which was to impose displacement ductility factor of one (μ = 1), the yield displacement and stiffness were determined. Both the estimated stiffness, $K_{theoretical,}$ and experimental stiffness, K_{test}, are plotted in Fig. 4.9. It is seen that in run 6 (μ = -1), the observed stiffness is slightly less than K_{test} determined in run 5. Stiffnesses for both runs were about the same during unloading.

In load run 5, more cracks were noted in the west slab. As cracks W1N and W1S extended to the edges, new crack W4 (Fig.4.7) almost reached the west edge. Crack W5 was about halfway in the slab. In run 6, cracks in the east slab developed in a pattern similar to that in the west slab. Cracks E1N and E1S almost reached the edges. E2, E3 and E4 also formed at the end of the load run while crack E5 was only halfway to the south edge. More diagonal joint cracks formed in accord with the loading directions.

4.2.3 Inelastic Cycles

As seen in Figs 4.10 to 4.12, throughout the subsequent inelastic cycles, the observed beam end forces and the derived storey (column) shear kept increasing and exceeded reference strengths by a considerable margin. Hence the code strength requirement [6] (see Section 1.3) was satisfied.

A distinct feature of the response of ductile frames is that the progressive rise in storey shear (i.e. the frame strength) with increasing ductilities would be accompanied by a gradual degradation of stiffness. This is seen in Fig.4.10. The hystersis loops, however, show stable energy dissipation. The slight pinching at the early stage of each load run reflects the major contribution from the beams to the overall behaviour of the unit.

Although there was a steady reduction in overall stiffness as the imposed ductility was increased, the unit responded to resistance immediately upon load reversals, a feature often absent in the results of similar tests with poorly performing joints.

Curves depicting the force-displacement response of the east and the west beams are given in Figs. 4.11 and 4.12 respectively. Hysteresis relationships similar to those in Fig. 4.10 confirm that most of the energy dissipation ability of the test unit was through inelastic deformations of the beams. For both beams the average stiffnesses in the positive (i.e. upward) bending case were usually higher than those in the negative (i.e. downward) bending case, reasons for which are reviewed in the following.

In the negative bending case, the bottom beam reinforcement in compression had to yield, unless bond deterioration occurred, when previously formed flexural cracks closed to allow the required concrete compression to be mobilised. This involved a considerable reduction in the previously developed inelastic tensile strains in the bars, and was necessitated by the large tensile forces developed in the top reinforcement. Also some bond slip of the bottom beam bars inside the joint core would have augmented this action. The negative response curves for the beams suggest that approximately the first half of the beam force in each load run was resisted by a steel couple only. In the second half stage, concrete in compression at the bottom fibres began to contribute to the negative flexural strength. The negative response curves for the beams of all three test units had a common feature. Up to a ductility of $\mu = 8$ stiffness during the second half of a load run were consistently greater than that in the first half. This indicated the commencement of the contribution to flexural compression of the bottom concrete as downward displacement of the beams progressed. The phenomenon of pinching was more noticeable when a beam was at the early stage of downward displacement, commencing from run 18 for the east beam (Fig.4.11) and run 19 for the west beam (Fig.4.12). It is likely that this was due to bond deterioration along the bottom bars which by then should have been subjected to very large inelastic strains, both in tension and compression. A certain amount of slip might have been necessary before the bottom bars could be engaged by the surrounding concrete, also subjected to some spalling, to carry compressive forces. This agrees with the truss mechanism of shear resistance in beams, as was discussed in Section 2.3.4.

The response curves for upward loading exhibited greater initial stiffnesses. The "seismic" steel-couple concept (see Section 3.8.2) assumed that the top steel did not have to yield when in compression. It is evident, however, from the observed stiffnesses seen in Fig.4.11 and 4.12 that a contribution of top concrete in compression to the flexural resistance, as expected in normal T-beams, was effective at early stage of each load run. This feature was supported by the measured shortening of the top fibres, as reported in Section 4.3.2, and the observed closing of flexural cracks across the top of the beam and the adjoining slabs. This indicated the existence of a flange subjected in part to concrete compressive stresses. Flexural analysis of doubly reinforced T-beams shows that the neutral axis usually lies near to the top fibre. This is confirmed in calculations presented in Appendix B.2 for the ideal positive flexural strength of a beam section, beased on a reasonable effective flange width.

The measured upward acting tip beam forces consistently exceeded by a considerable margin the magnitude of the theoretical "seismic" force $(+)P_i$ = 111.7 kN (case (a) in Table B.3, deriving from the ideal flexural strength of beam section based on steel-couple only), even at a ductility as low as μ = 1, as can be seen in Figs.4.11 and 4.12. When the east beam forces are compared to the reference theoretical force inclusive of flange contribution in compression, namely $(+)P_{1i}$ = 143.4 kN (case (d) in Table B.3, deriving from the ideal flexural strength of beam section based on ACI stress block method and an assumed flange width in compression as explained in Section 3.8), the maximum excess is 27% in run 23 (μ = 10). In Section 3.8.1, it was suggested that the material overstrength factor relevant to measured strength, $\lambda_{o,m}$, be taken as 1.18 (i.e. +18%). It appears therefore that the effective flange width in compression may be much larger than that assumed in case (d). Strengths computed for cases (e) and (f) with larger effective flange widths are also listed in Table B.3.

Under downward bending, both beams showed even greater increase in peak strengths, since there were a larger number of additional slab bars to provide additional tension reinforcement. From the normalised scales in Figs. 4.11 and 4.12, the increase is seen to be quite significant. The maximum strength attained in load run 19 (μ = 8) for the west beam was 45% above the ideal downward force $(-)P_i$, or 14% above the probable maximum force $(-)P_i^*$. Because of the different top and bottom reinforcement contents (see Table 3.1), the extent of strain hardening in tension of the top beam bars and

parallel slab bars is expected to be less than that of the bottom beam bars. This indicates therefore that more slab reinforcement than that recommended by NZS 3101 [4] (Fig.3.6) should be included in estimating the flexural overstrength of the beam when large inelastic displacements are to be expected.

In the last two cycles to μ = 10, the peak storey shear was 137% of V_i or 119% of V_i*, and the storey drift was 4.5% of the storey height. A ductility of approximately μ = 4.5 corresponded to a storey drift of 2%. The overall response resulted primarily from the contribution of the east and west beams. Major sources of deformations originated also from shear distortion of the joint core. These features are discussed in Section 4.3. In a well designed beam-column joint assembly, such as this test unit, joint distortions should not be excessive.

As flexural cracking in the beams and column continued, diagonal cracks at the mid-depths of the beams also appeared. These are seen in Fig.4.1 and Fig. 4.3(a). As expected, the inclination of these cracks was larger when downward force was applied to a beam end. Concrete crushing and spalling were noted in the plastic hinge regions. The D24 bars in the bottom of the east beam were exposed first during load run 22 (second cycle to μ=-8). A buckled bar is seen in Figs. 4.4 (b) and 4.5(a). On load reversal the bars straightened again. It was evident then that these bars were effectively anchored in the joint core. In run 23 (first cycle to μ = 10), all bottom bars in the beams at both sides of the column were exposed (Figs.4.6 (a) to (c)). At this stage these bars buckled between the first two stirrup ties, which were initially spaced at 120 mm, i.e. six times the bar diameter of D20. The efficiency of recommended spacing [4] of stirrups to restrain main bars under compression from buckling at lower ductilities was verified in this test. Flexural cracks were evenly distributed over the whole column height. There was never any sign of distress within the column.

In the west slab, cracks W6 and W7 (shown in Fig. 4.7) formed in run 7 (first cycle to μ = 2). At the same time, crack W8 developed from crack W4 and proceeded gradually to reach the south edge in run 15 (first cycle to μ = 6). In the east slab, diagonal crack E6 formed in run 8 (first cycle to μ = -2). Crack E7 started simultaneously but propagated slowly, and reached the edge of the slab in run 12 (first cycle to μ = -4). At this stage it branched out to form crack E9. The propagation of crack E9 stopped, however, in run 20

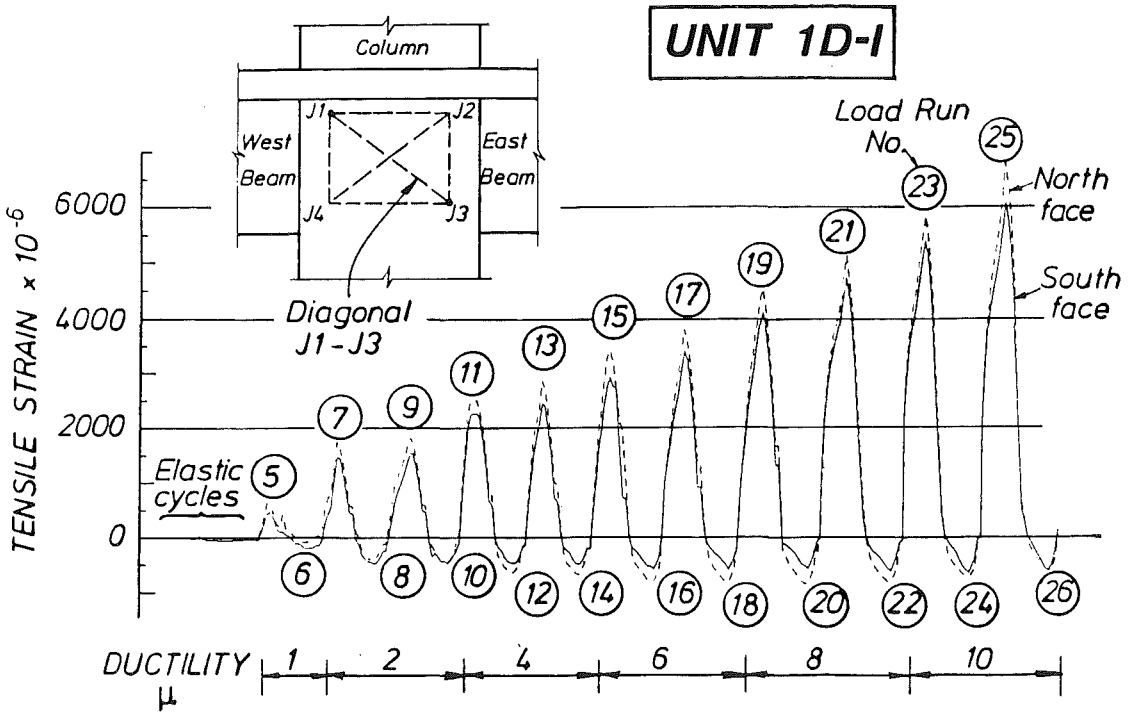

Fig.4.13 - Variation of strains along diagonal J1-J3 of the joint panel

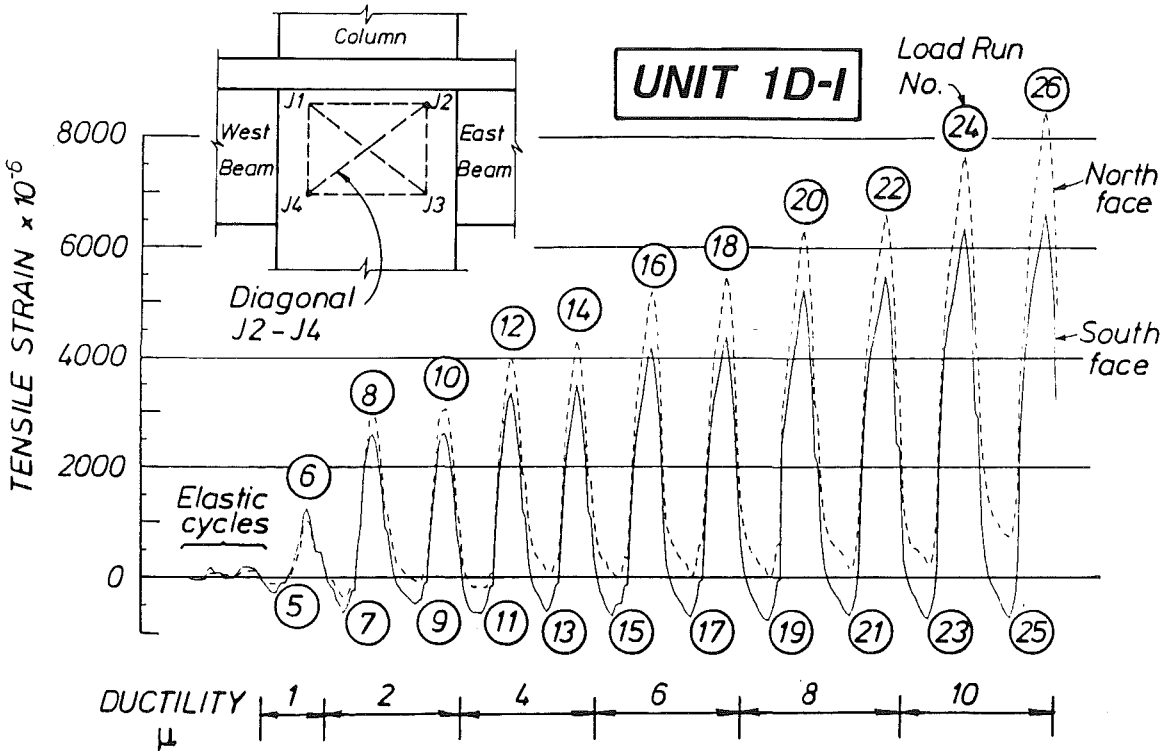

Fig.4.14 - Variation of strains along diagonal J2-J4 of the joint panel

(first cycle to μ = -8). Crack E8 was first noted in run 16 (first cycle to μ = -6). It branched into cracks E10 and then E11 in run 20. The transverse cracks along the centre-line of the slab, C1N and C1S, started from the column faces in run 8. They were primarily affected by downward displacements at the east beam. Crack C1N reached the north edge in run 12 (first cycle to μ = -4) while crack C1S reached the south edge at run 14 (second cycle to μ = -4).

The width of the diagonal cracks in the joint area ranged from 0.5 mm to 1.0 mm at μ = 8. In the last two cycle of μ = 10, a maximum crack width of 1.3 mm was detected. All joint cracks were found to close as load reversed. Sliding shear displacements along diagonal joint cracks, observed visually, were very small.

4.3 DISPLACEMENT COMPONENTS

4.3.1 Joint Deformations

Deformations at the north and south faces of the joint core were measured by the method described in Section 3.9.4 and summarised in Eq.(3.19). The instrumentation enabled the changes in linear strains along the two diagonals, namely J1-J3 and J2-J4, as indicated in the insets in Figs.4.13 and 4.14, to be measured. Variations of measured strain, read on both faces on the joint, are shown in the two figures. Positive (tensile) strains represent elongation of the diagonal while negative (compressive) strains refer to shortening of the diagonal. The relatively large and progressively increasing magnitude of tensile strains and the consistently small and approximately constant magnitude of compressive strains verify that the joint core was predominantly being dilated. This gradual expansion of the joint core can be readily explained with the aid of the postulated truss mechanism of shear resistance, discussed in Section 2.3. It should be noted that elongations and expansion (i.e. tensile strains) were controlled primarily by steel tensile strains developed within the joint core, whereas the small compressive strains resulted from the essentially elastic response of the concrete which was subjected to diagonal compression forces within this core.

Corresponding joint shear strains γ, representing progressive distortions at the north and south faces of the joint core, are plotted in Fig.4.15. The shear strain response is also shown in Fig.4.16, this time

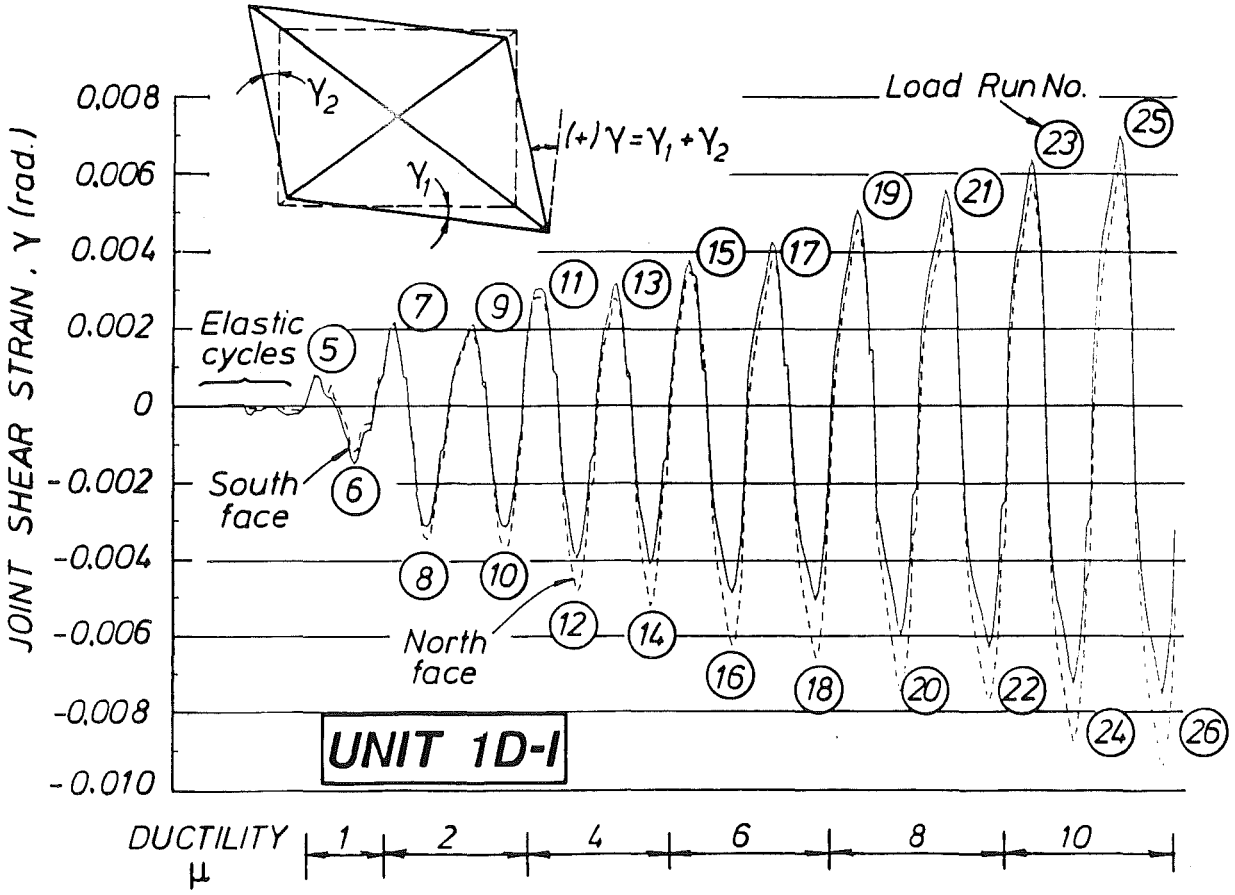

Fig.4.15 - Shear strains within the joint panel

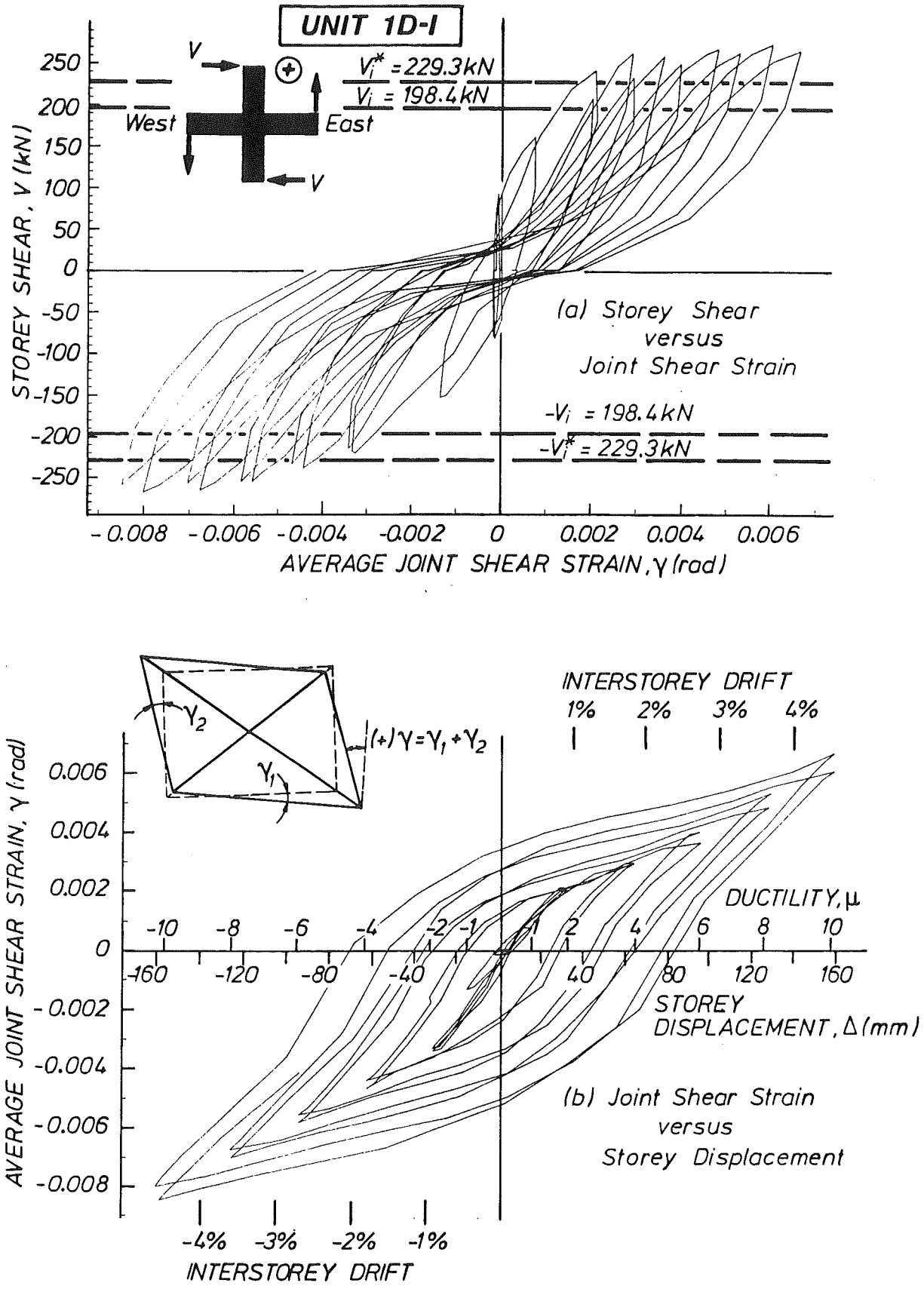

Fig.4.16 - Behaviour of joint panel in joint assembly response

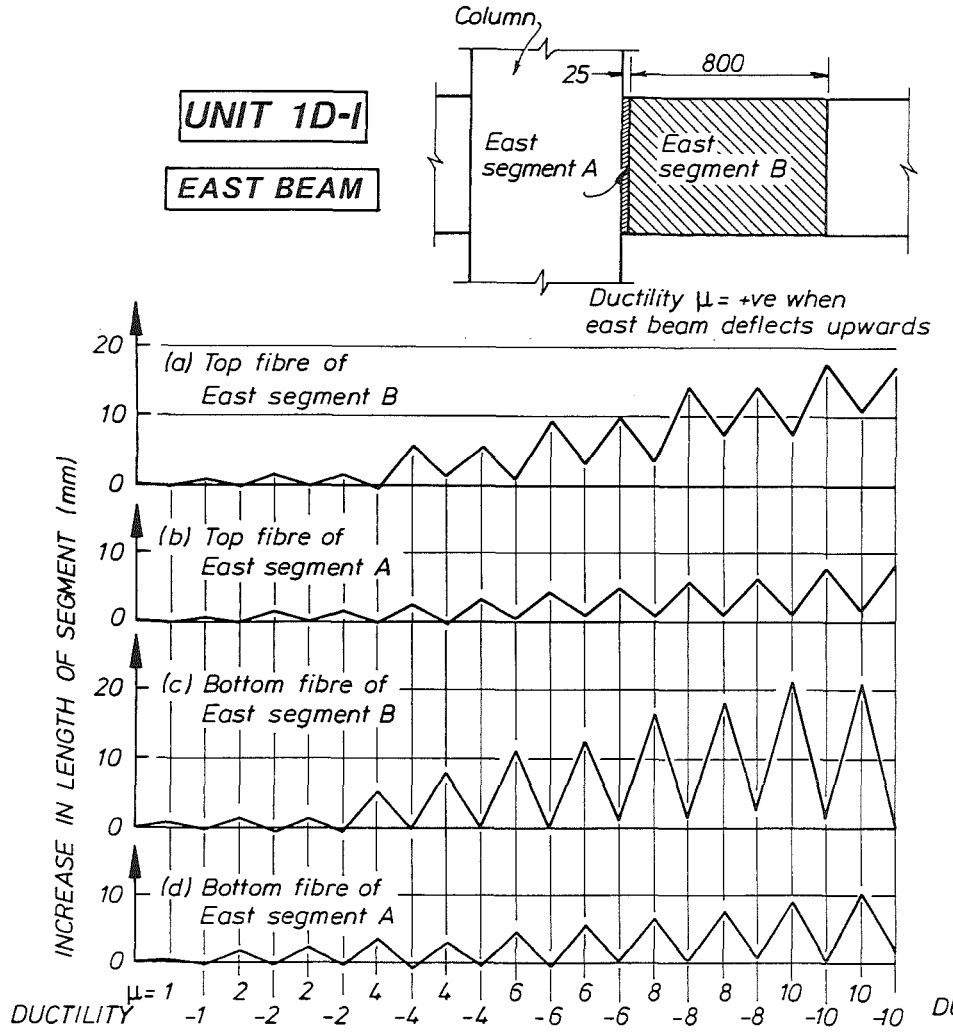

Fig.4.17 - Measured longitudinal movements in segments of east beam

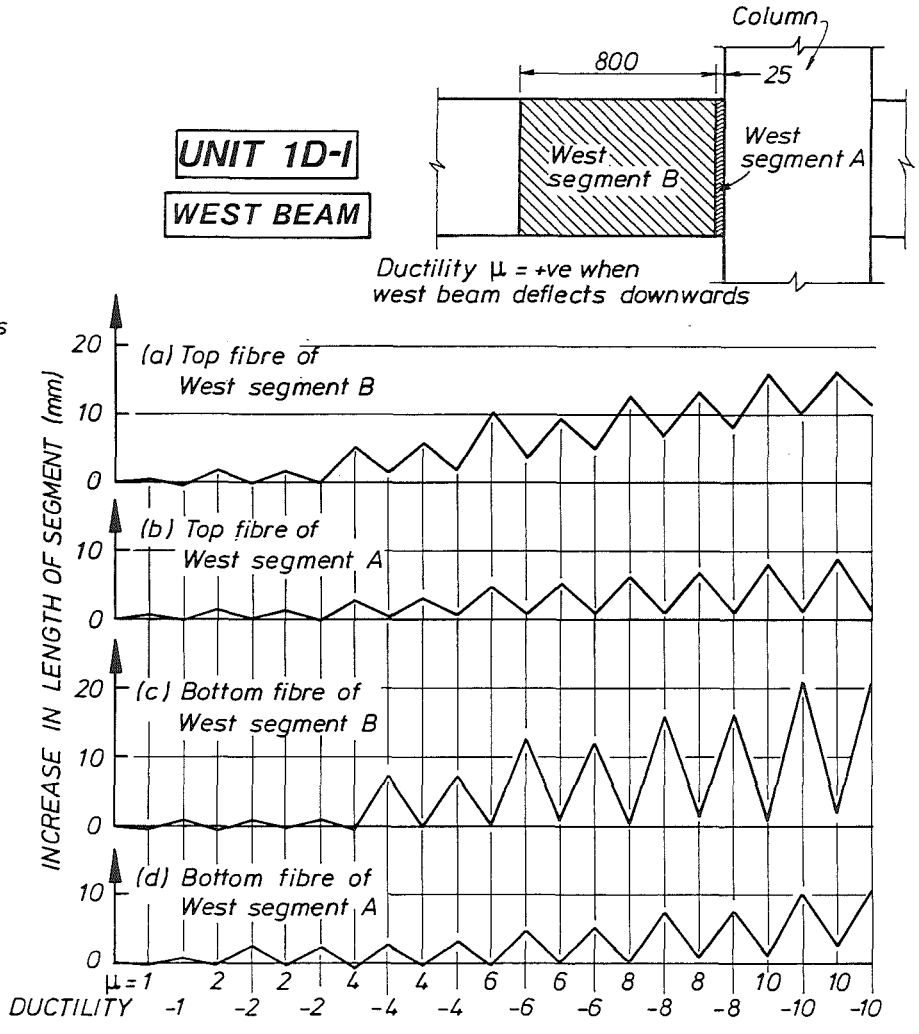

Fig.4.18 - Measured longitudinal movements in segments of west beam

in terms of the average strains and storey shear forces or storey displacements. The pinched loops in Fig.4.16(a) suggest that joint distortions contributed to the stiffness degradation of the test specimen. On the other hand the spindle-shape response loops in Fig.4.16(b) indicate the dilation of the joint core being in proportion to the magnitude of imposed interstorey displacements.

The effects of joint distortions on the total deformations of the test assembly are discussed in Section 4.3.3.

4.3.2 Beam Deformations

Using the method described in Section 3.9.2, the longitudinal movements of the critical parts of the east and west beams relative to the column were derived and these are shown in Figs.4.17 and 4.18. In general, the top and bottom fibres lengthened, corresponding with the opening of cracks in the concrete, and shortened, corresponding with closing of cracks when the concrete would have been subjected to compression. These were in accordance with the loading directions as indicated by the ductility levels. An observation of interest is that even at a ductility as high as 10, at segments A of both the east and west beams (Figs.4.17(b) and (d) and Figs. 4.18(b) and (d)) the residual lengthening was smaller than 2 mm when the concrete was in compression. This implied that the cracks caused by tension in segments A closed upon load reversals. This is particularly significant for the top fibres, bearing in mind that the top beam reinforcement content was almost twice of that in the bottom of the beam. The tensile elongations in both top and bottom fibres of segment A were at this stage in the range of 10 mm. For a reduction in length of 8 mm at one face of the column, there should be a drop in tensile strain of the order of 5%. This appears impossible in view of the strain results presented in Section 4.4. It is therefore surmised that local bond-slip of the beam bars within the joint, coupled with the rotation about the beam bars, both of which having been discussed in Section 2.3.4, in fact took place and enabled cracks to close at the column faces. Estimation of the bond-slip is presented subsequently in this section.

There is a greater difference between the movements of the top and bottom fibres of segments B (Figs.4.17(a) and (c) and Figs.4.18(a) and (c)). The bottom fibres were subjected to larger strain reversals, corresponding to distinctive opening and closing of cracks. This was due to the difference in

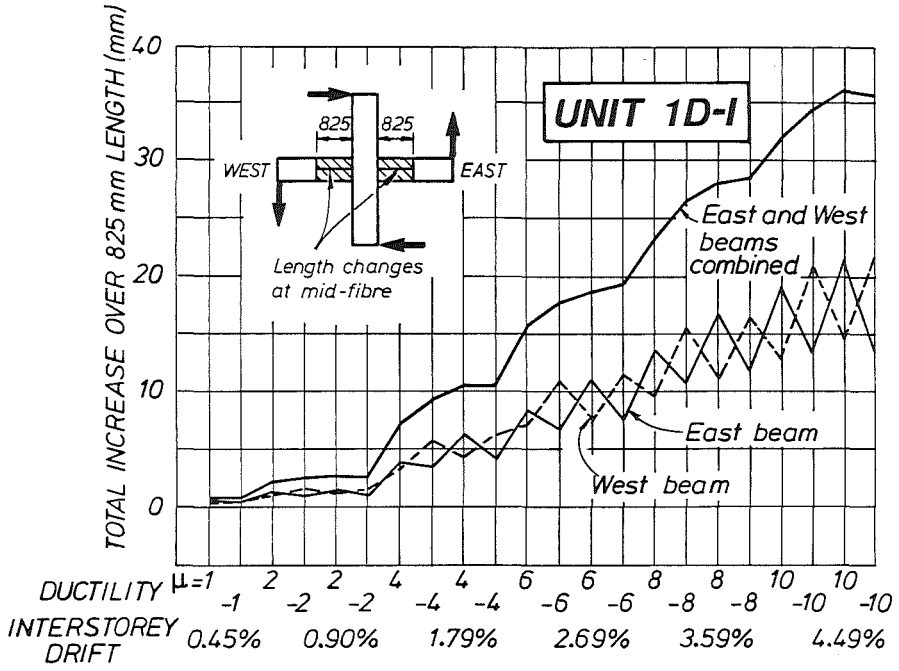

Fig.4.19 - Measured lengthening of east and west beams

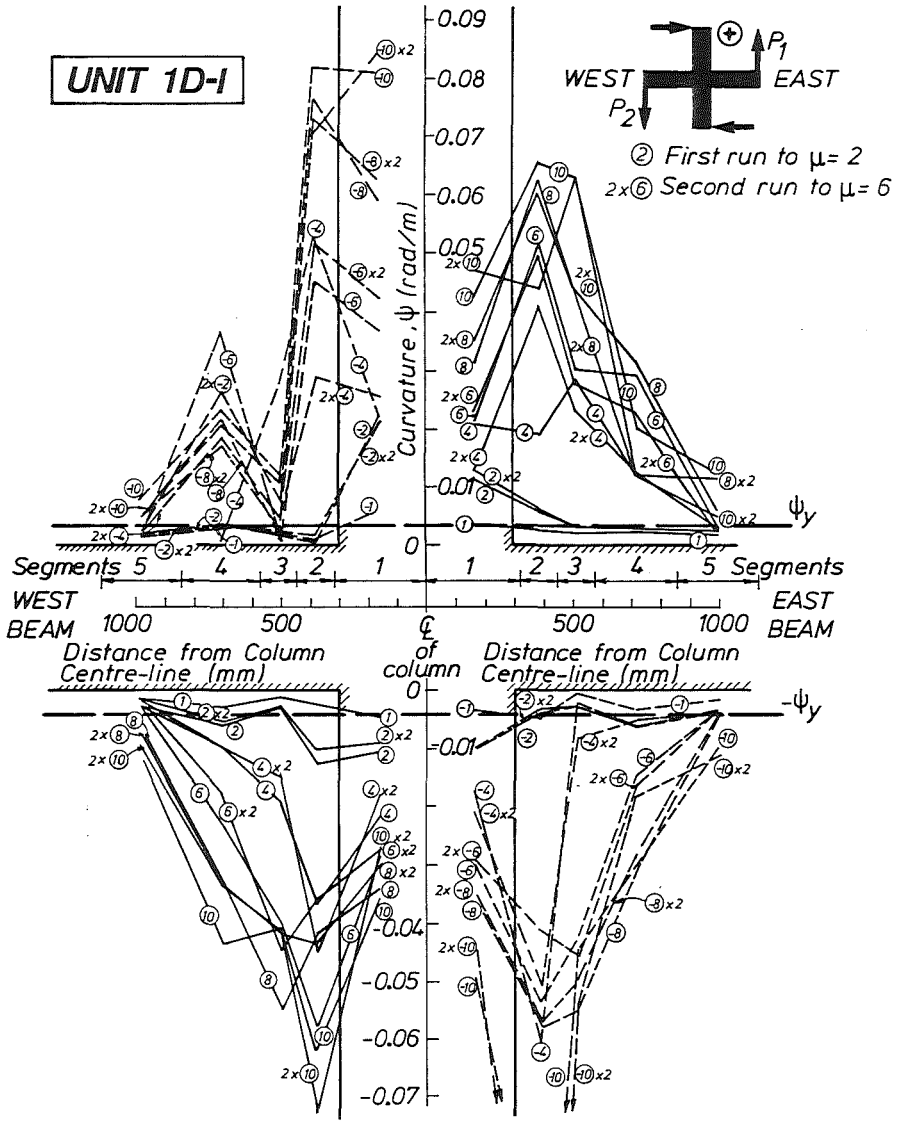

Fig.4.20 - Curvature profiles of east and west beams

beam reinforcement contents. Nevertheless, it is observed that between ductilities of μ = 4 and 6 (or in terms of interstorey drifts of 1.87% and 2.7%), the largest residual lengthening in the top fibres was 4.9 mm.

Components of the lengthening of beams are summarised in Fig.4.19, in which the total changes in length of the mid-fibres of both the east and west beams at the peaks of inelastic displacement levels are shown. The summations of the lengthening of segments in each of the two beams, giving the total elongation of the unit due only to the segmental lengthening are also seen in Fig.4.19. It is evident that inelastic displacements results in considerable elongation of the beams, a feature which, in terms of structural design, requires further consideration.

Strain distributions at the top and bottom layers of the beam bars, derived from linear potentiometer measurements, are shown in Figs.4.27 and 4.28 of Section 4.4.

Curvatures over the $1.5h_b$ region of each beam (Fig.3.23) are presented in Fig.4.20 at the centre of each gauge length for all load runs at their peaks. As explained in Section 3.9.2, the average curvatures of the first segment, ψ_1^*, were calculated according to Eq.(3.10(b)). At low ductilities, distributions of observed curvatures were fairly consistent. At high ductilities, however, curvatures within the first segment, ψ_1^*, were generally smaller than those over segment 2. It should be noted that Eq.(3.10(b)) assumed that strain over the whole length of segment 1 was uniform. This, however, is not the case, as has been demonstrated in Section 3.10. Furthermore, as a result of the spreading of plastic hinges associated with the continuing increase of inelastic tensile strains from the column faces into the free ends of the beams, the curvatures over segments 2 and 3 should increase significantly.

Some other irregularities in the curvature distributions are believed to have been caused by crack developments within a gauge length. Features given in Section 3.10 regarding strain variations, as determined by linear potentiometers, are also applicable to the interpretation of curvatures.

Slips, i.e. rigid body movements, of the beam bars within the joint core were estimated according to the method described in Section 3.10. The results are presented in Figs.4.21 and 4.22 for the top and bottom layers

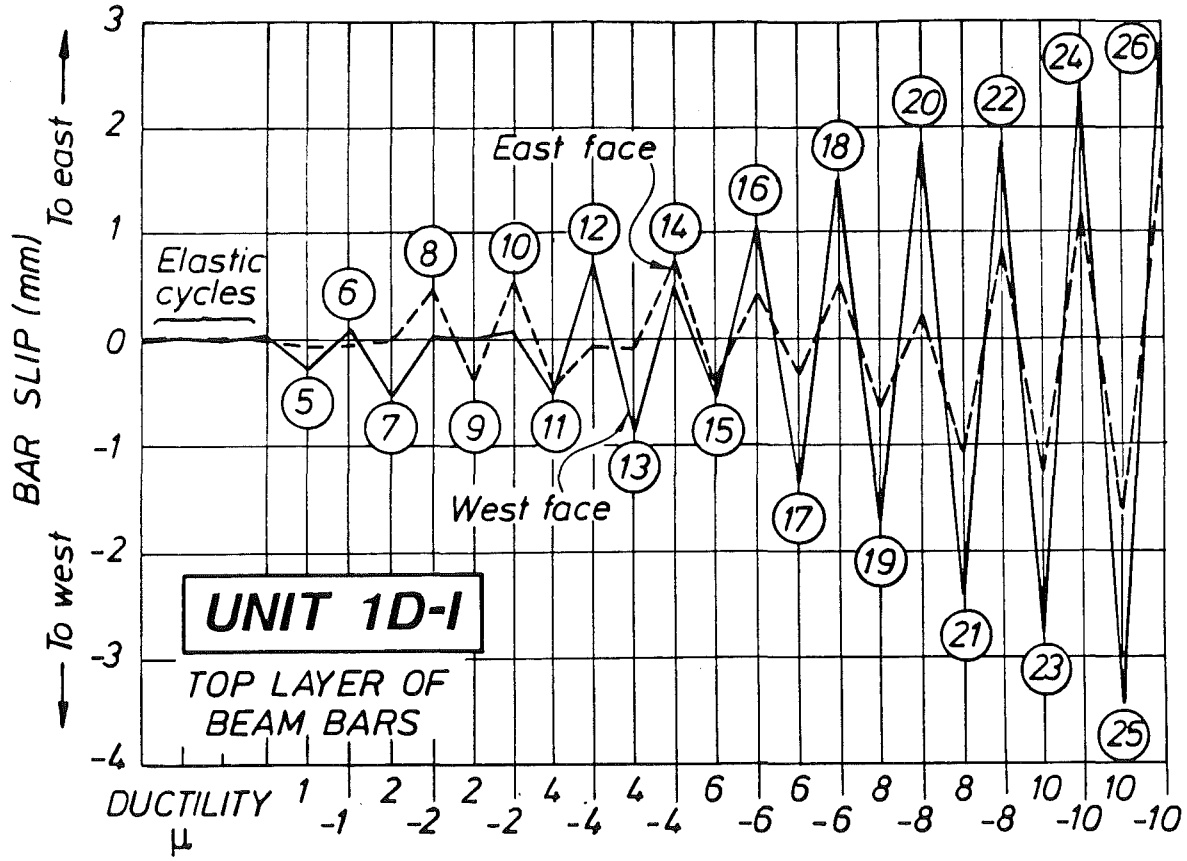

Fig.4.21 - Estimated slips of the top layer of beam bars within joint core

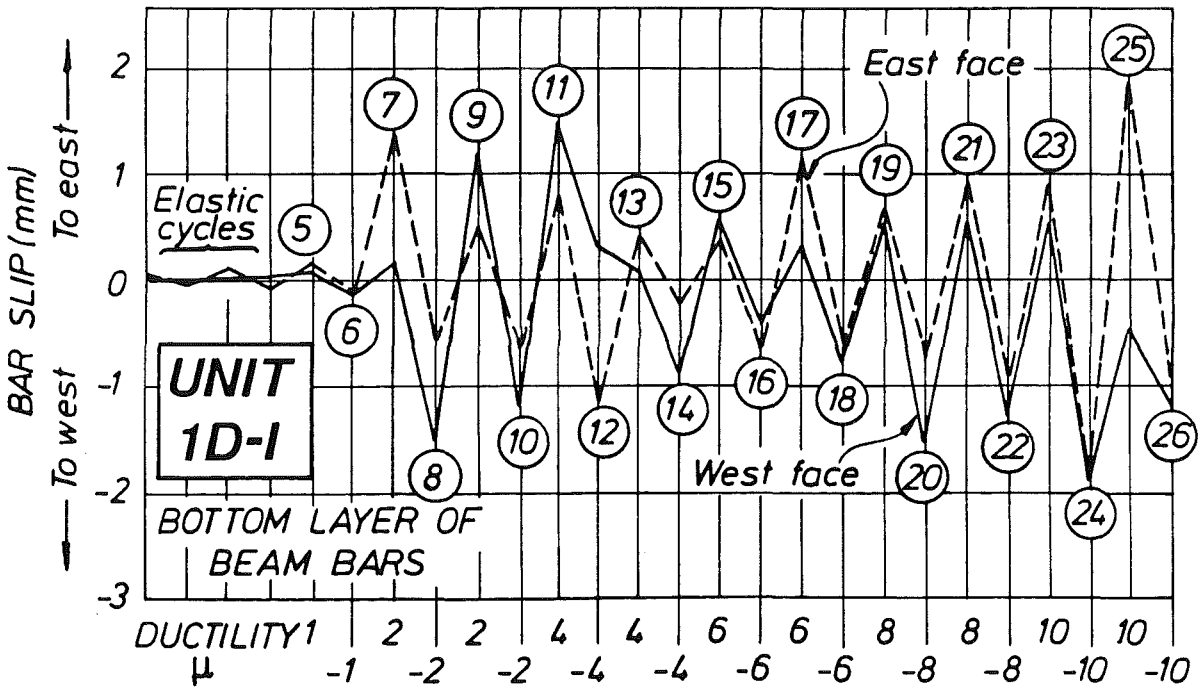

Fig.4.22 - Estimated slips of the bottom layer of beam bars within joint core

respectively. As can be seen, results from the west beam and east beam measurements do not match closely. Because of the numerous idealisations and simplifications made in the calculations (see Section 3.10) this can be expected. However, the trend of gradual increase of slip is evident. Slips of the top layer bars were larger probably because bond deterioration was more severe with more bars provided. Also by considering the sedimentation and hardening processes after concreting, it appears that the bottom layer bars had a better environment to develop bar anchorage. It can be concluded that during large cyclic attacks, slips can amount to 1 to 2 mm in a well designed one-way beam-column joint.

4.3.3 Decomposition of Displacements

In Figs.4.23 to 4.25, various displacement components at successive loading stages are expressed as percentages of the total observed beam deflections or in terms of the derived equivalent column drift. The principles of calculations have been given in Section 3.9.

As seen in Figs. 4.23 and 4.24, results for the first two elastic cycles are fluctuating because inevitable errors affect small readings much more significantly. In low ductility cycles (μ = 1 to 4), some "excessive" deformations were derived for the west beam (Fig.4.24). Nevertheless the graphs give a general and reasonably convincing picture of how the different components affect overall displacements. As the elastic column and beam deformations ($\delta_{1,c}$ and $\delta_{1,b(others)}$) account for a relatively small proportion of the total beam displacements, more sophisticated estimation of these will not change the percentage distribution significantly. The important conclusion drawn from Figs. 4.23 and 4.24 is that while joint distortion accounted for about 26% of total beam displacement at μ=2, this proportion decreased to less than 20% at higher ductilities. This is considered to have been due to adequate joint reinforcement which had been provided to carry the shear forces in the joint while remaining essentially elastic. Another point to note is that joint deformations, normally neglected in the analysis of elastic structures, are particularly significant, while the structure was still elastic, i.e. when μ = 1 was being approached. This signifies the necessity of having to make some allowance for joint distortions, if the stiffness of frames is to be realistically estimated for the purposes of the definitions of drift and displacement ductility.

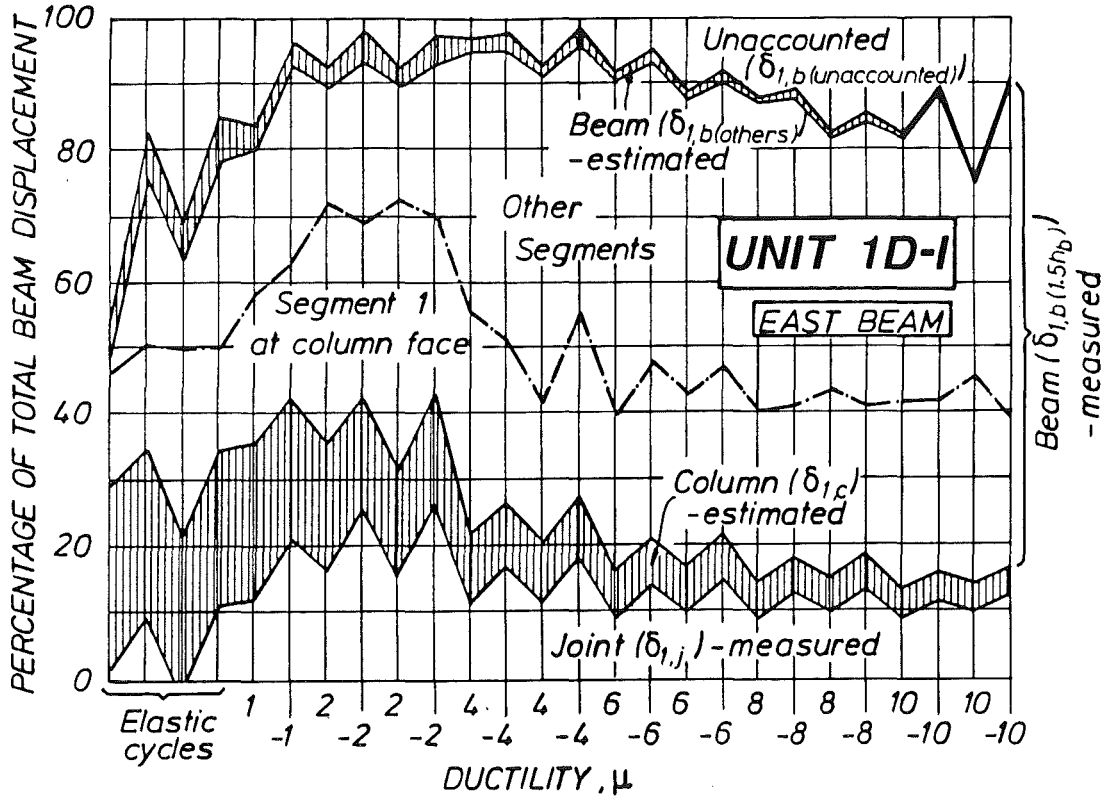

Fig.4.23 - Components of east beam displacements

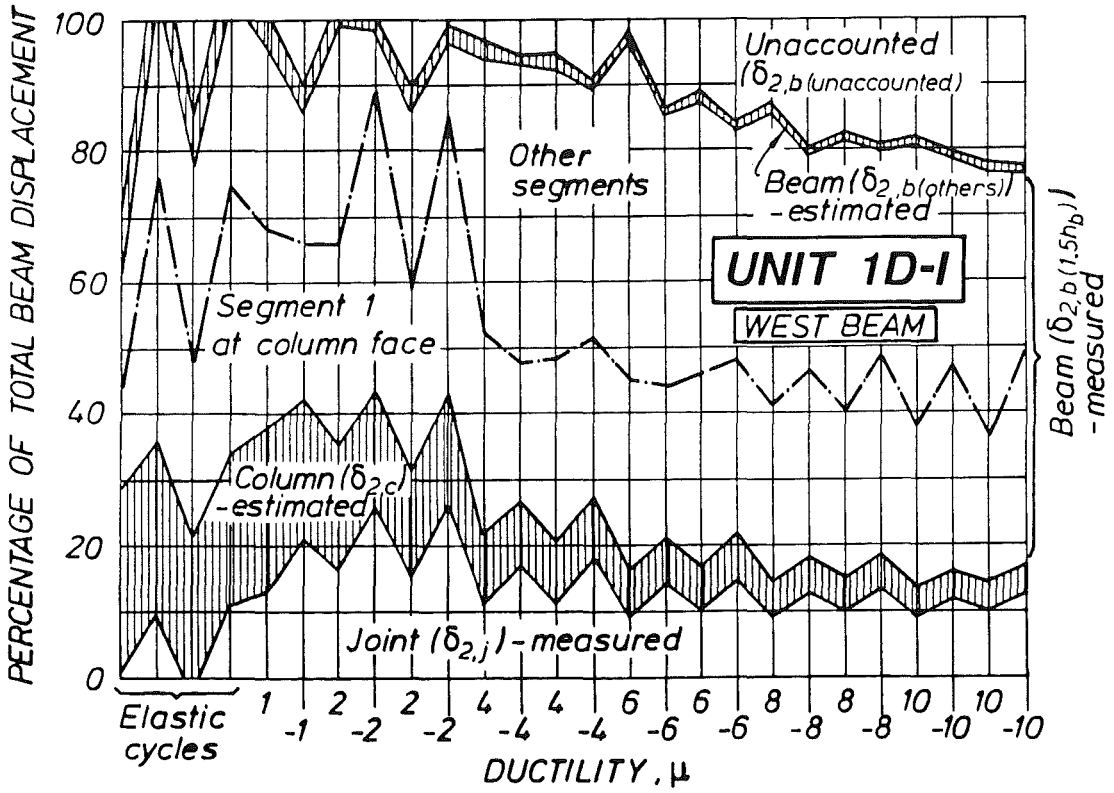

Fig.4.24 - Components of west beam displacements

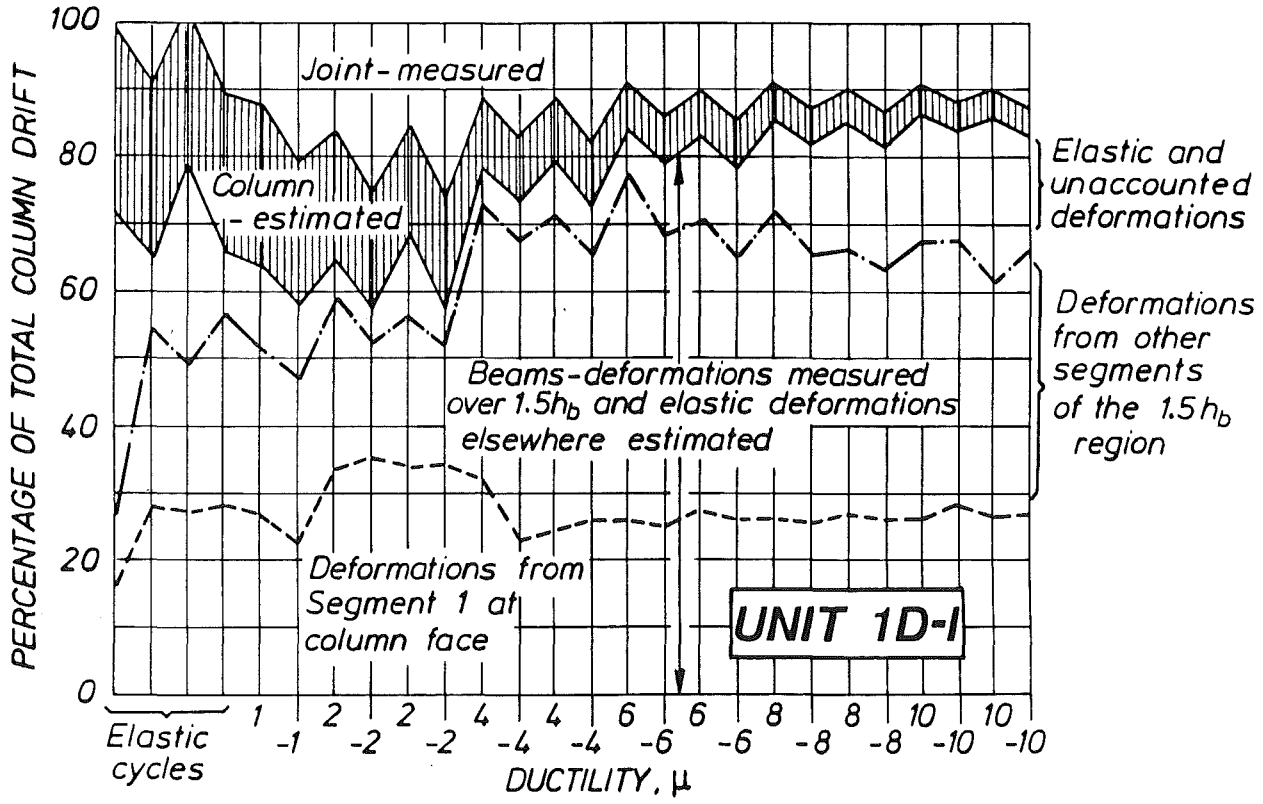

Fig.4.25 - Contributions to interstorey lateral displacements during progressive loading

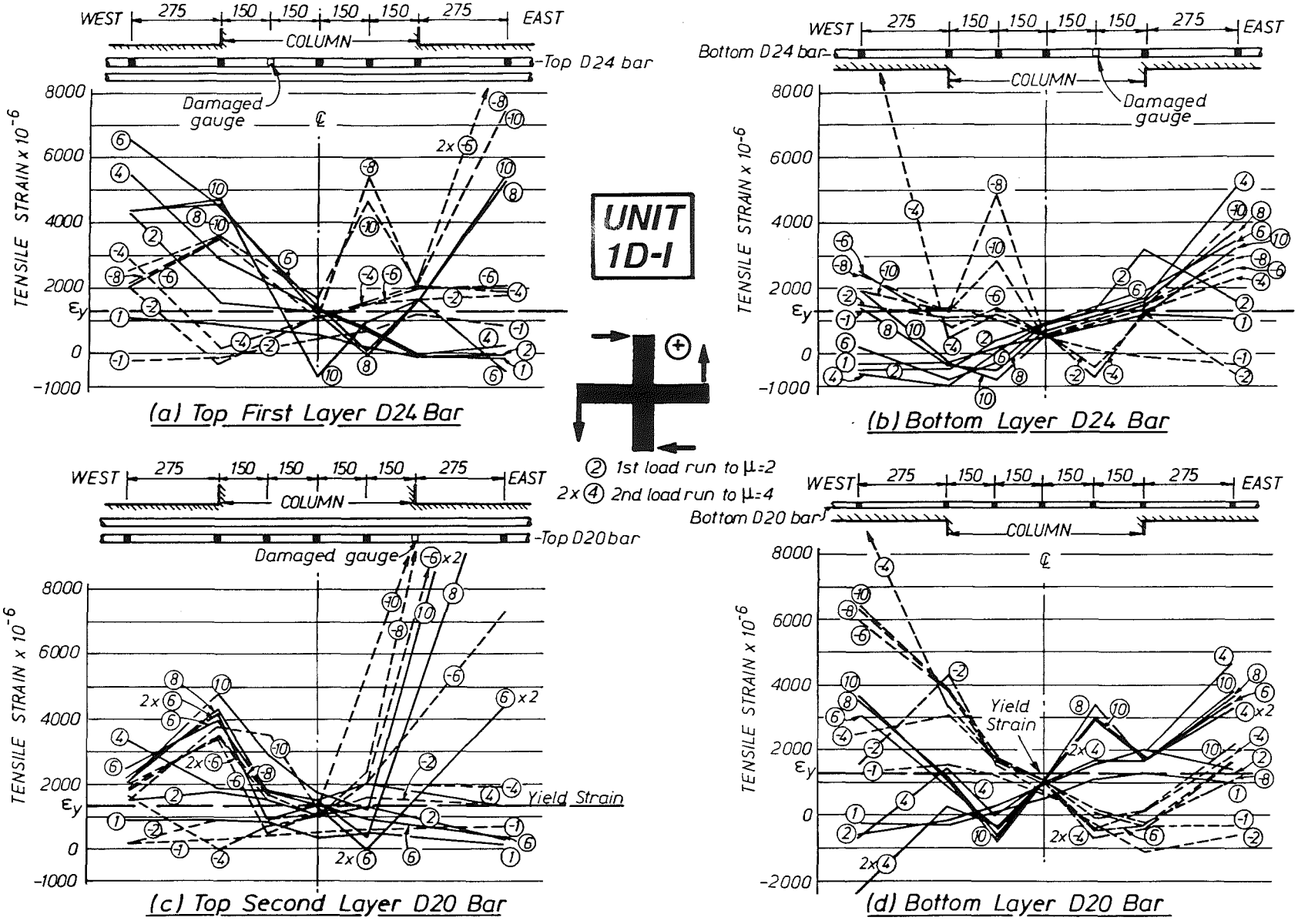

Fig.4.26 - Beam bar strains measured by strain gauges

As applied forces were increased, deformations in the beams continued to contribute most significantly to the total displacements. Some inelastic beam deformations may have also occurred outside the $1.5h_b$ region. These are included in the "unaccounted" parts of deflections. It is of interest to note that of the deflections originating from the $1.5h_b$ length of beams, a substantial part of the displacement was due to bar slip and bar elongation under tensile strain within the joint core, as represented by the part labelled "segment 1" measurement.

In Fig. 4.25 the normalized storey (column) displacements are divided into three major components. The first component is due to the joint distortion as measured during the experiment. The second component involves elastic bending and shear deformations of the column under horizontal shear, estimated by traditional analytical methods. The last component, considered to be due to beam deformations, was taken as the difference betwen the total storey displacement and the first two components (see Eq.(3.8)). The beam component of deformations is further sub-divided into three parts in order to show the relative importance of the sources of deformations contributing to storey drift. These beam deformations have been presented in Figs.4.23 and 4.24. The contributions of component distortions to the total storey drift, shown for the entire loading history in Fig. 4.25, reveal the following pattern :

(1) Joint distortions were well controlled during progressively increasing imposed ductilities, and did not increase disproportionately.

(2) The major sources of storey drifts were beam distortions, as intended. This corroborates the evidence for very good energy dissipation properties for the entire unit, given by the hysteretic response shown in Fig. 4.10.

(3) Columns remained elastic, as intended, and hence their contribution to total deflection diminished as imposed ductilities were being imposed.

4.4 BEAM BAR STRAINS

Of the 28 strain guages installed on the beam bars, three were found inoperative. Results from the remaining 25 gauges are plotted in Fig.4.26 for the entire range of ductilities although it has been concluded in Section 3.10

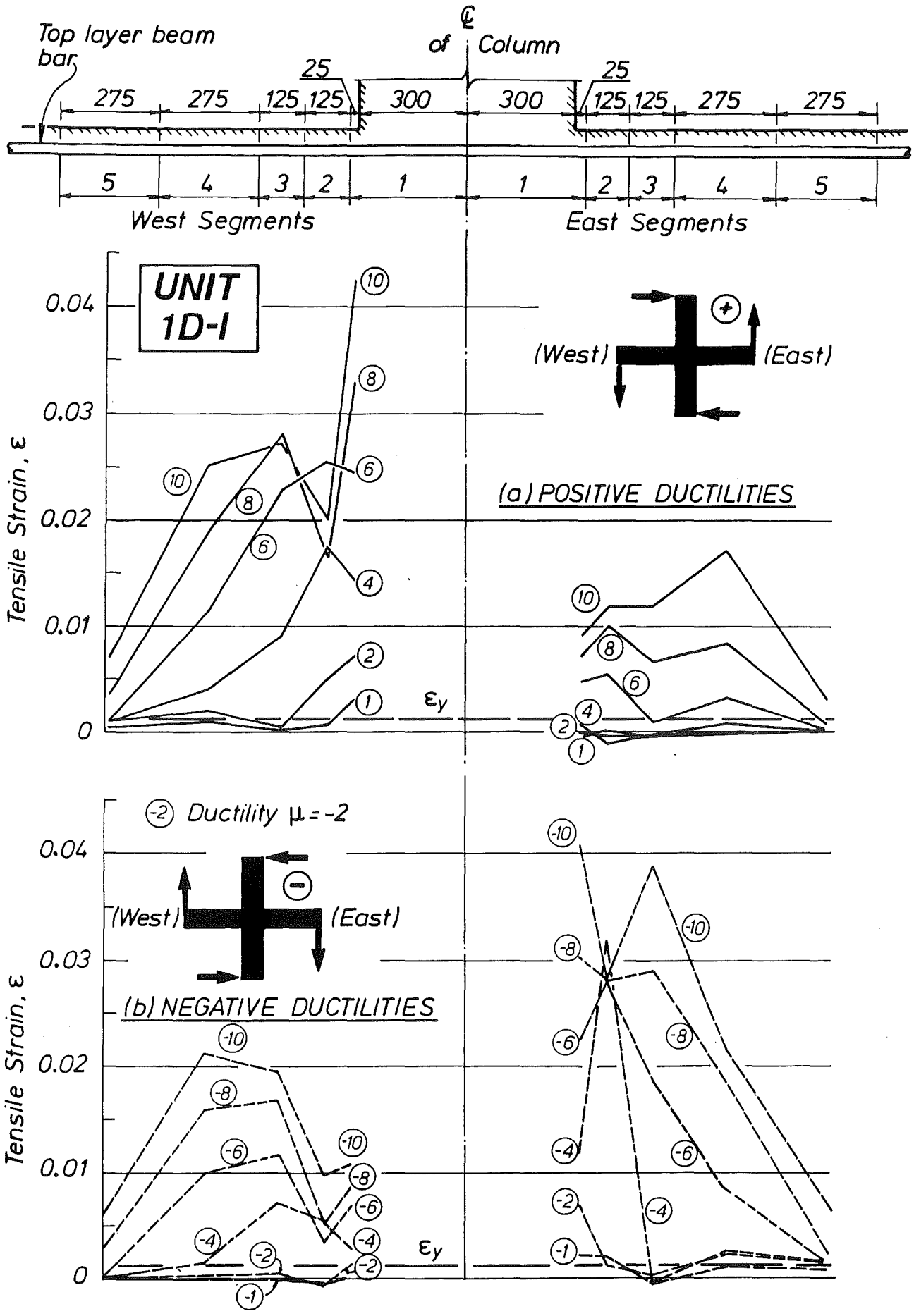

Fig.4.27 - Strain distributions at top layer of beam bars as estimated from linear potentiometers

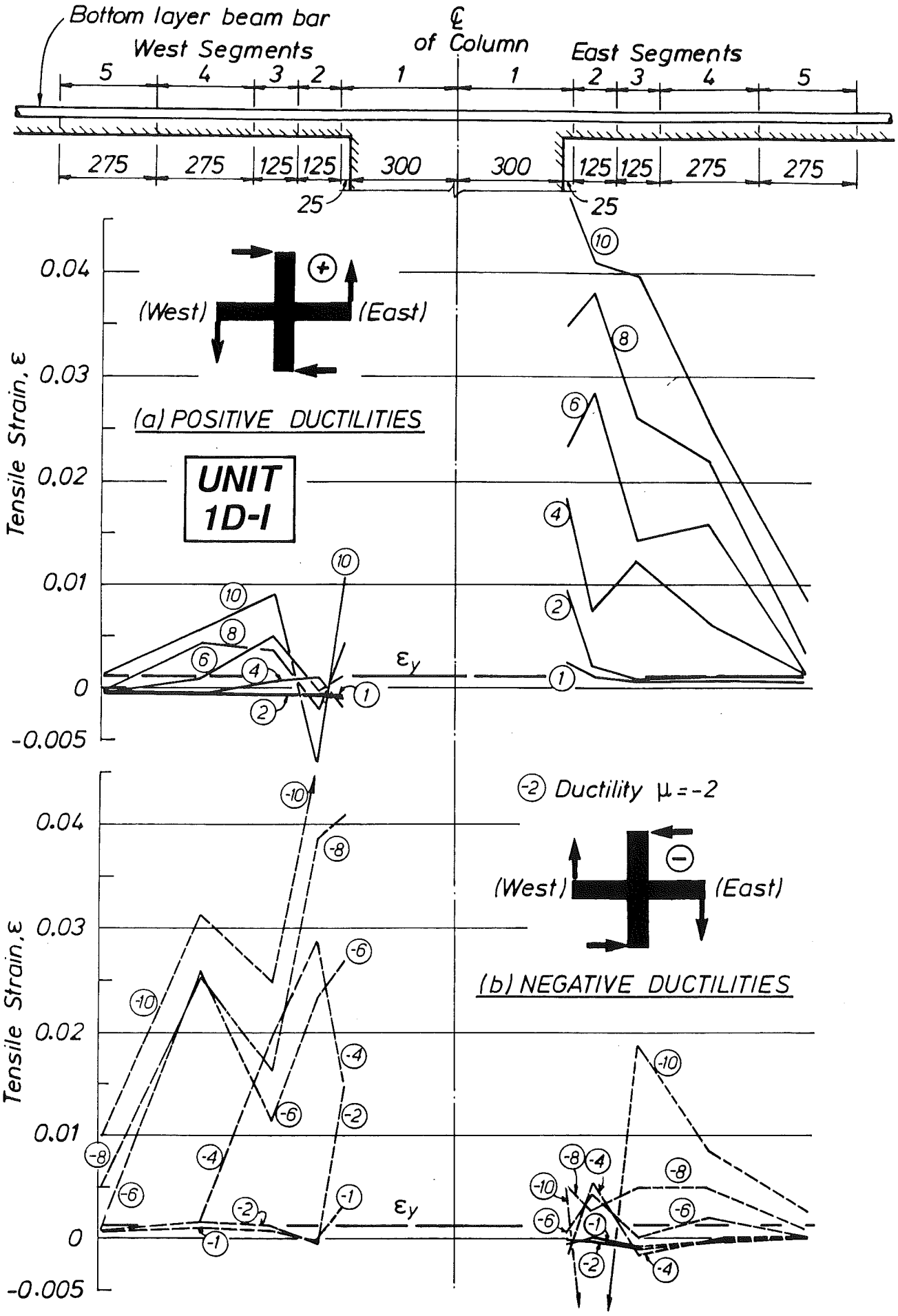

Fig.4.28 - Strain distributions at bottom layer of beam bars as estimated from linear potentiometers

that strains measured at a ductility of four or above were too low and not considered to be correct. The intention of this presentation is to provide further demonstration of the differences with respect to strains derived from linear potentiometer movements, which are shown in Figs.4.27 and 4.28. In Figs.4.26 to 4.28, the solid lines represent strains at positive ductilities, while the broken lines stand for negative ductility results.

The three figures indicate that strain readings consistently showed compressive stresses in both top and bottom bars when the sense of displacement would cause compressive strains in the corresponding fibres. Thus bars passing through the joint had to sustain simultaneously tensile and compressive stresses at opposite faces of the column, although it is not likely that strain hardening in compression would have been attained. From the limited information given in Fig.4.26, which shows consistent low tensile strains at the centre point of the column, it is concluded that despite some bond slips of the beam bars (Section 4.3.2), high bond stresses were sustained and the bars were well anchored. Thus the nominal embedment length of $25d_b$ for the D24 bars proved completely adequate even for this extreme load sequence.

Strain results shown in Figs.4.27 and 4.28 have features similar to the curvature profiles in Fig.4.20 discussed in Section 4.3.2. The spreading of plastic hinges is evident. It should be noted that each time when the loading was reversed, the reductions in tensile strains at column faces were greater for the bottom layer beam bars. This phenomenon is of more significance when considering that the bond-slips estimated in Section 4.3.2 were found to be larger along the top layer bars. Strain changes at the bottom bars were attributed to the difference in beam reinforcement contents. An interpretation from Fig.4.28 is that the maximum compressive steel stress at column face, up to a ductility level of $\mu = 6$, was not likely to exceed f_y, in agreement with the review conclusions of Section 2.3.3. At $\mu = 8$ or more, the continuing crushing and spalling of concrete became more severe so that buckling of beam bars took place before strain hardening of beam bars in compression could be achieved.

Although it is impossible to determine accurately the beam bar stresses in the inelastic range from the test data available, the order of magnitude of the compressive stresses at column faces can be estimated using the ideas developed in Section 2.3.4. The largest positive upward force at

beam tip was measured as 183 kN in the east beam in run 23 at μ = 10 (see Figs.4.11 and 4.12). Applying the simplified 45° truss model for shear transfer in the beam and using the symbols of Fig.2.16(a), the horizontal forces are estimated as follows :

(at bottom) $T_2 = (1533.1)\ 275\ (1.25)\ 10^{-3} = 527$ kN

(at top) $C_{c2} \approx 183$ kN

Thus $C_{s2} \approx 527 - 183 = 344$ kN, corresponding to a steel compressive stress of only f_{s2} = 141 MPa or 0.49 $f_{y,m}$ where $f_{y,m}$ = 290 MPa. However the value of C_{c2} could be even larger, indicating that f_{s2} would diminish further.

On the other hand, under downward displacements, the maximum negative tip force observed was 288 kN in the west beam in run 19 at μ = 8. If the above procedure was repeated by assuming (referring to Fig.2.16(a) for symbols) C_{c1} = 288 kN, the compressive stress f'_{s1} in the bottom beam bars would need to be as high as 1.8 $f_{y,m}$. As discussed earlier, the maximum possible value for f'_{s1} could be 1.0 $f_{y,m}$. In this case, the concrete compression force C_{c1} becomes 663 kN. Using the ACI stress block method (see Section 3.8.2), it is estimated that the neutral axis depth, measured from the bottom fibre of the beam, needs to be 77 mm. This requirement appears to be easily achieved in downward bending of the unsymmetrically reinforced beam.

4.5 SLAB BAR STRAINS

A total of 104 strain gauge were fixed to the longitudinal and transverse bars in the southern half of the slab. Four gauges were not working before test started, and later nine gauges failed to function properly.

Bar strains obtained are plotted in Figs. 4.29 and 4.30 in which slab bar spacing was drawn to scale. For clarity strains at positive (full lines) and negative (dashed lines) peak ductilities were shown on separate graphs. The purpose of extensive instrumentation was to estimate the tensile force distribution across the flange width, and the extent along the beam lengths. It was hoped that the results would assist in the study of the mechanism of force transfer from the slab bars to the joint. It was disappointing to find, however, that the test results did not fully assist in this study. As seen in

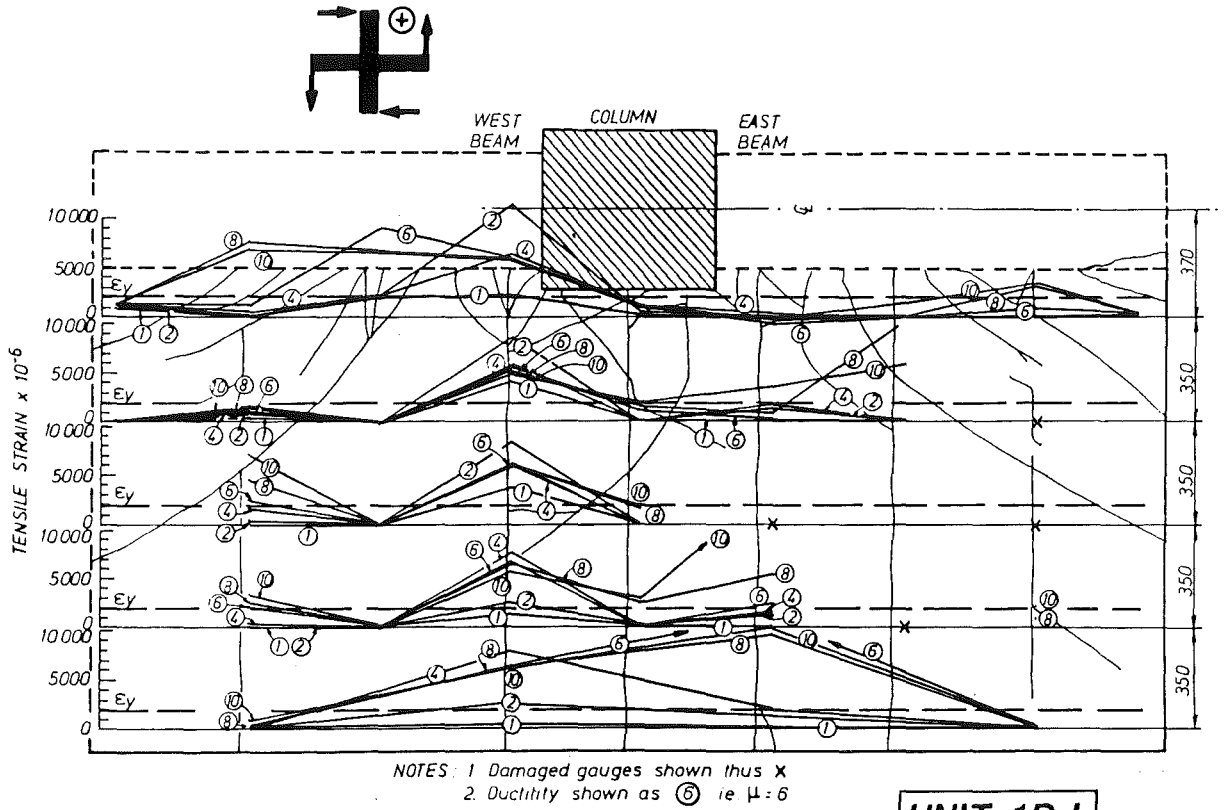

(a) Longitudinal D10 Bars at Positive Ductilities

UNIT 1D-I

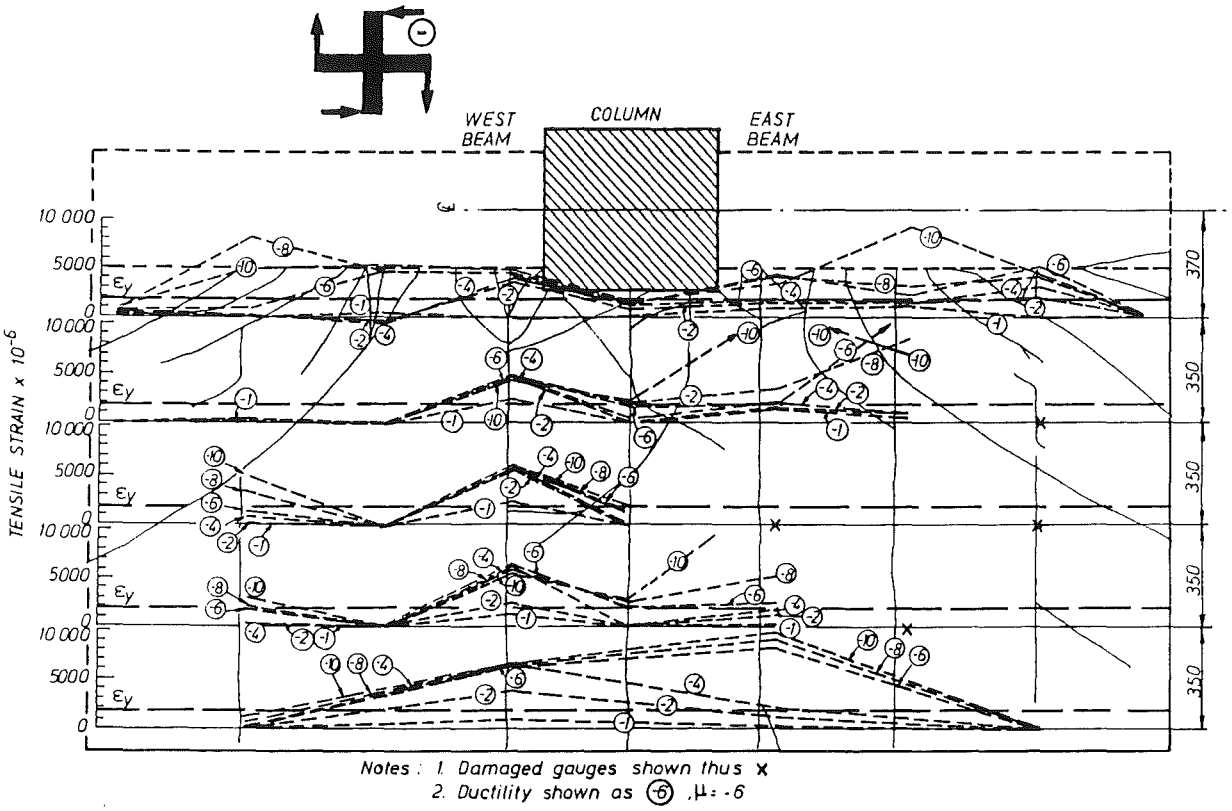

(b) Longitudinal D10 Bars at Negative Ductilities

Fig.4.29 - Longitudinal east-west slab bar strains

Figs. 4.29, not much useful information was obtained for the strain distributions in the east portion of the slab because of failing strain gauges. Some transverse D16 bars exhibited compression strains (Figs. 4.30) which required special examination.

In the figures, the major cracks have also been drawn. It is thus clearly seen that the crack pattern, which was largely affected by the layout and amount of the reinforcement (Fig.4.8), affected strain distribution significantly. Large tensile strains consistently developed at or near cracks. Negligible strains in the longitudinal bars were recorded where the surrounding concrete was not cracked (Fig. 4.29).

The tensile force that can be transmitted by the D10 bars, when developing the measured yield strength at 326 MPa, is 73 kN per metre width of slab. Assuming the tensile strength of concrete to be the same as the modulus of rupture, $f_r = 0.6\sqrt{f'_c}$ [4], the tensile force that the concrete of the slab would carry is estimated to be of the order of 370 kN per metre width. Hence between major cracks (such as cracks W1S and W8 in Fig. 4.7), the concrete slab of the test unit would have been quite capable of transferring in tension the steel tensile forces developed at the cracks, even when the bars entered strain hardening. Indeed, the strain readings suggested that the slab, when in tension according to the sense of loading, could transfer a tensile force equivalent to the area of steel present.

While in general bar strains increased with higher ductilities, smaller local tensile strain were also recorded by several gauges (Figs. 4.29(a) and (b)). As seen in the photograph in Fig.4.6(a) the transverse cracks W1N, C1N and E1N (Fig.4.7) were very wide (varying from 1 mm to 5 mm at $\mu = 4$). The tensile steel strains at those cracks might have been several percent. Strains measured close to but not at the major cracks, even though rather large, are not likely to be indicative of local curvature or actual slab deformation. As cyclic loading progressed, bond along the D10 bars, at either side of a large crack, would have deteriorated. This in turn would have allowed yielding along these bars to spread, resulting in reduced tensile strains. Relatively large tensile strains were recorded in the transverse D16 bars near to the beam tips (Figs.4.30(a) to (d)) especially at ductility levels larger than 6. At these advanced stage of the test, shear displacements of the slab at the beam tips were observed, as shown in

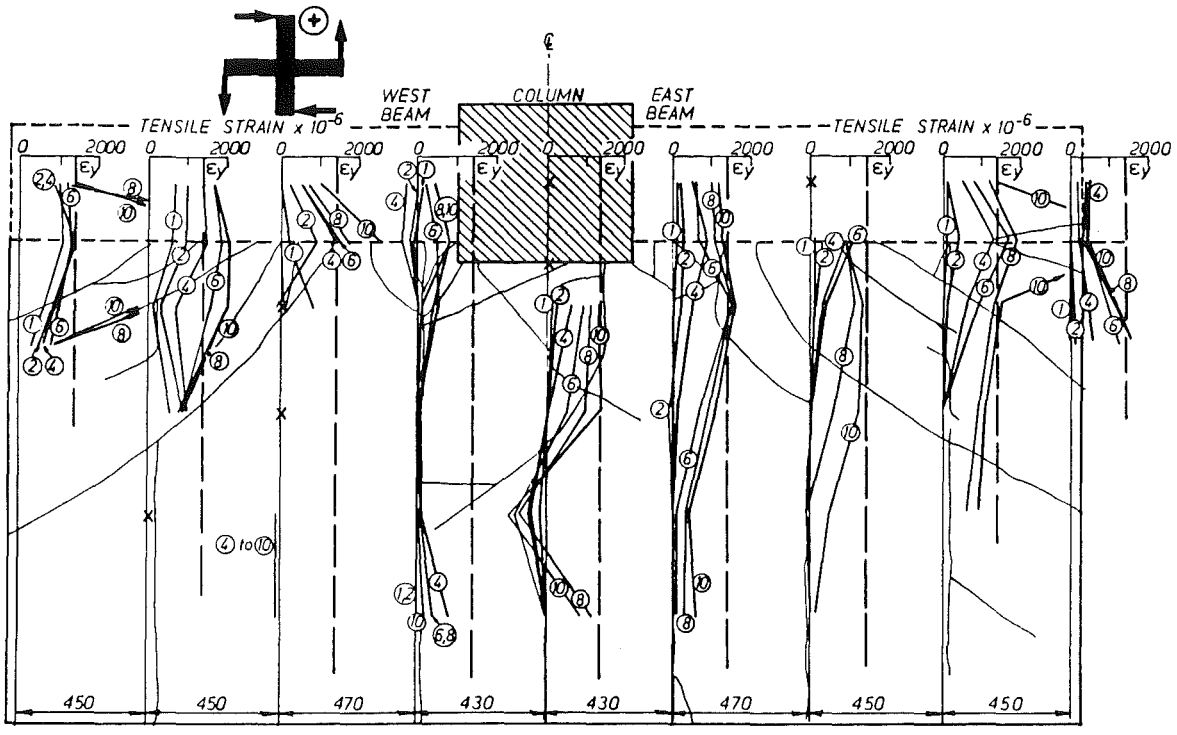

Notes : 1 Damaged gauges shown thus X
2 Ductility shown as ⑥ ie. μ = 6

(a) Transverse Top Layer D 16 Bars at Positive Ductilities

UNIT 1D-1

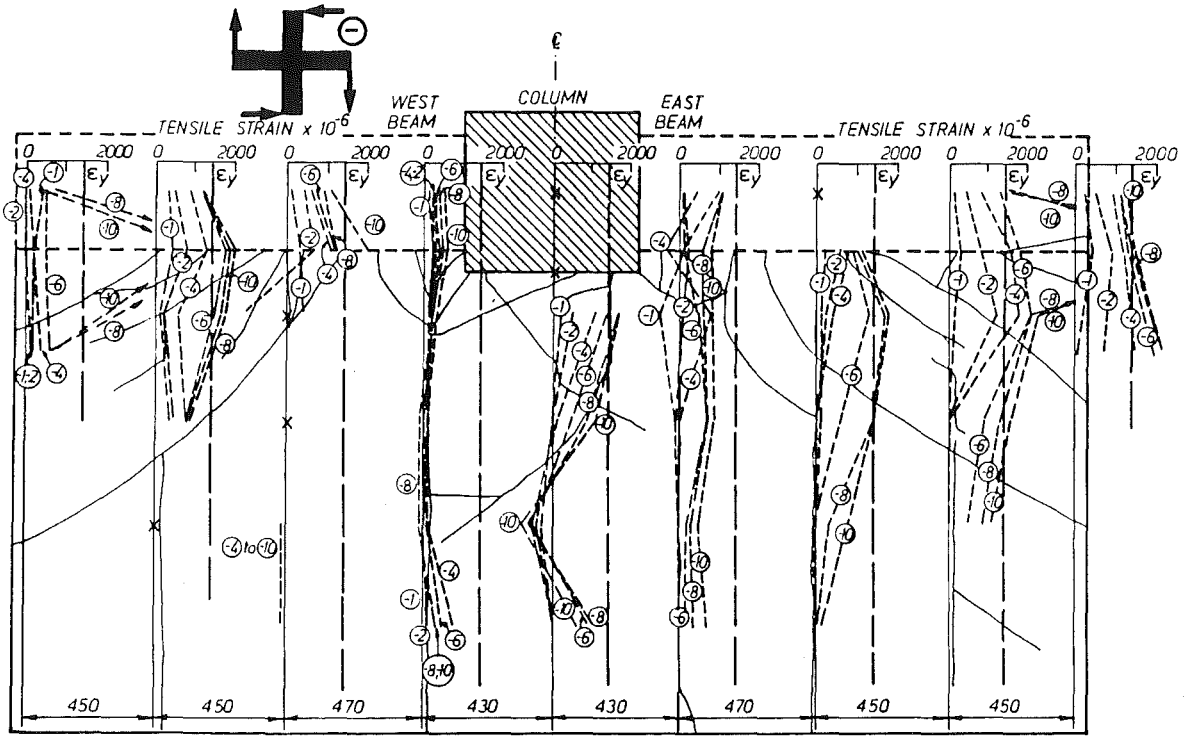

Notes : 1. Damaged gauges shown thus X
2. Ductility shown as -⑥ ie. μ = -6

(b) Transverse Top Layer D16 Bars at Negative Ductilities

Fig.4.30 - Transverse north-south slab bar strains

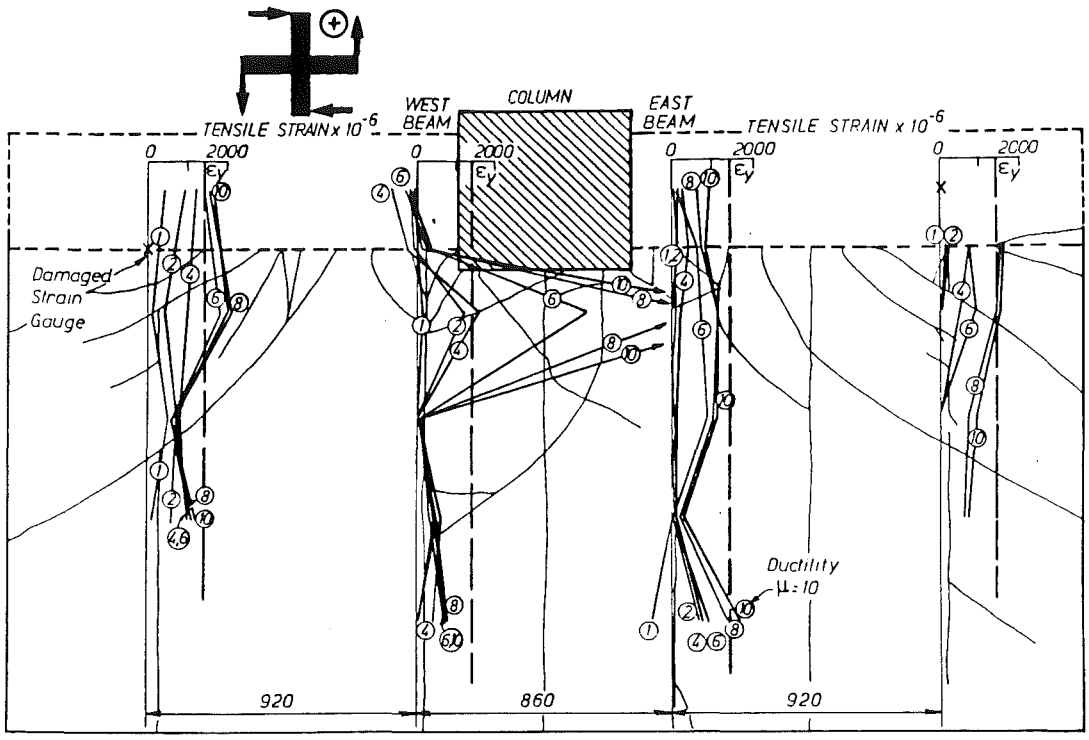

(c) Transverse Bottom Layer D16 Bars at Positive Ductilities

UNIT 1D-I

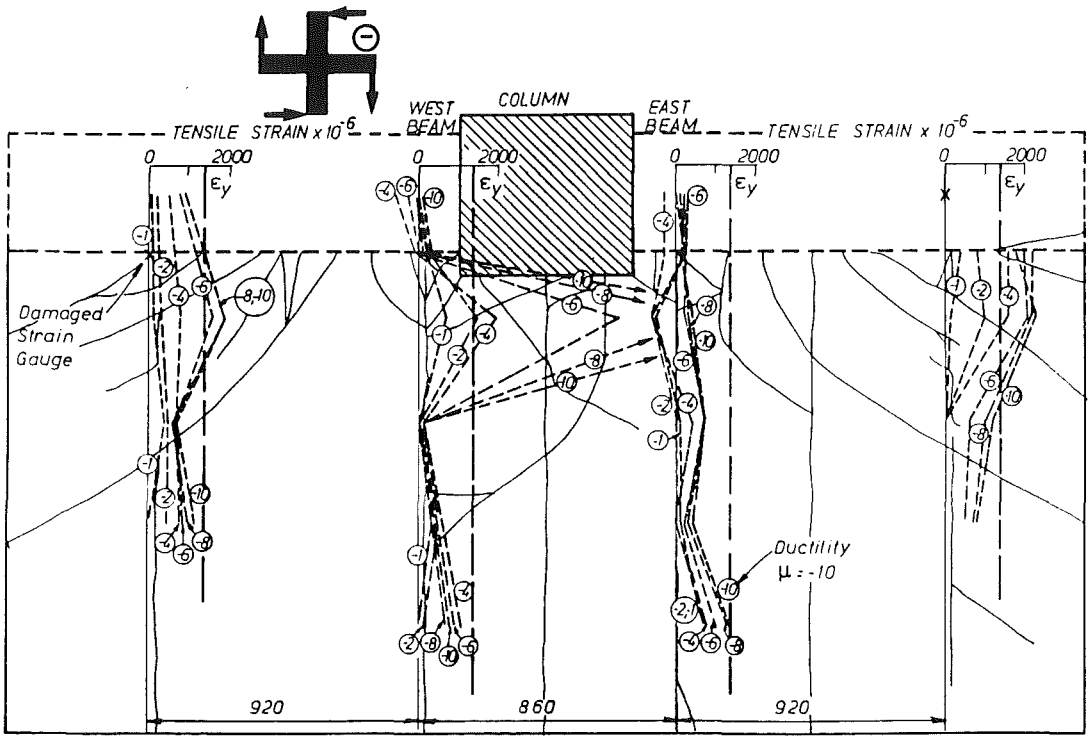

(d) Transverse Bottom Layer D16 Bars at Negative Ductilities

Fig.4.30 - Transverse north-south slab bar strains (continued)

Fig.4.31. This caused wide cracks to form through the slab which introduced dowel shear forces to the transverse slab bars.

Despite significant irregularities in the distribution of observed strains noted above, the following generalisations can be derived from Figs.4.29 and 4.30 :

(1) The longitudinal D10 slab bar nearest to the column was greatly influenced by the flexural action of the beams, as can be expected from considerations of strain compatibility (Fig.4.29).

(2) Consistent tensile strains were also observed in the longitudinal D10 slab bars placed further away from the column (Fig.4.29). Strains generally increased with increasing imposed ductilities, as expected.

(3) Tensile strains developed also in the transverse D16 slab bars (Fig.4.30), with a general tendency of strains increasing from the southern free edge of the slab towards the beam-slab interface. Furthermore, within the range of $\mu = 1$ to $\mu = 4$, tensile strains in the transverse bars near to the beam ends were conclusively larger than those in the bars near the column. Distinct deviations from these observations were found in the top layer bar (Fig.4.30(a)) and the bottom layer bar (Figs.4.30(c) and (d)), both at the west face of the column. However, it is believed that these and other small irregularities were more likely caused by the cracks in the slab.

A major task aimed at in this project was the assessment of the role of the cast-in-place floor slab in the overall response of a beam-column joint test assembly. As expected, it was difficult, and in fact impossible, to obtain a full set of reliable and consistent strain data so as to quantitatively evaluate the different aspects of slab behaviour. Nevertheless, a meaningful interpretation of the steel strain measurements can still be made by relating the results qualitatively to some structural models to explore the mechanisms of slab actions. These models are postulated in Chapter 7 following further presentation of test results for Unit 2D-I in Chapter 5 and Unit 2D-E in Chapter 6. The primary purposes of such study are to understand, and assess, the beam flexural strength enhancement through slab acting as tension flange, and the consequent introduction of additional shear forces to the beam-column joint.

4.6 COLUMN BAR STRAINS

There were 16 strain gauges fixed on to the column main bars. Two had been damaged during concreting and two more were found faulty at the start of test. Figs. 4.32(a) and (b) show the distribution of bar strains at the first peaks of successive ductilities. It was very unfortunate that some strain gauges failed, especially the three which were positioned to show the strain variations of the intermediate bars C2 and C3. The column intermediate bars have been considered to play an essential part in the resisting mechanism of vertical joint shear (Fig.2.4).

At low ductilities (μ=4), some tensile strains remained at levels 1 and 4 (Fig. 4.32(a)) in the exterior bars C1 and C4 despite the loading condition that should cause compression. It has been observed in previous tests[39] that the strains measured in column bars next to the beam bars were affected by the action of intersecting beam bars and particularly the local high bond forces from the beam bars. At ductility of μ = 6, strains in the west and east column bars (C1 and C4 respectively) had reached or slightly exceeded yield level. This was observed at the top as well as the bottom end of the joint region (Fig.4.32(b)). Strains continued to increase but only slightly, as expected, at higher ductilities.

As for the intermediate bars, C2 at level 4 showed tensile strain after the load run to μ = -1. However, this was always below yield value. This tensile strain always decreased to a smaller value at positive ductilities, for which case the bar should be subjected to compression. For both bars C2 and C3 in the mid-depth region of the joint (i.e. between levels 2 and 3), even larger strains were found. The moment patterns shown in Fig. 2.17 suggest that the column moment along the centre-line of the beams should be zero. The observed strain distributions just described therefore implies that the intermediate bars, which at this level should exhibit negligible

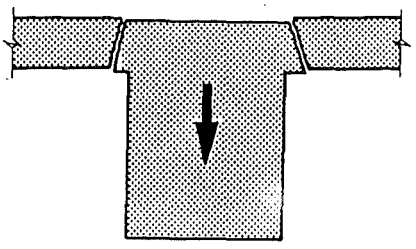

Fig.4.31 - Slab shear displacement near beam tip at large ductilities

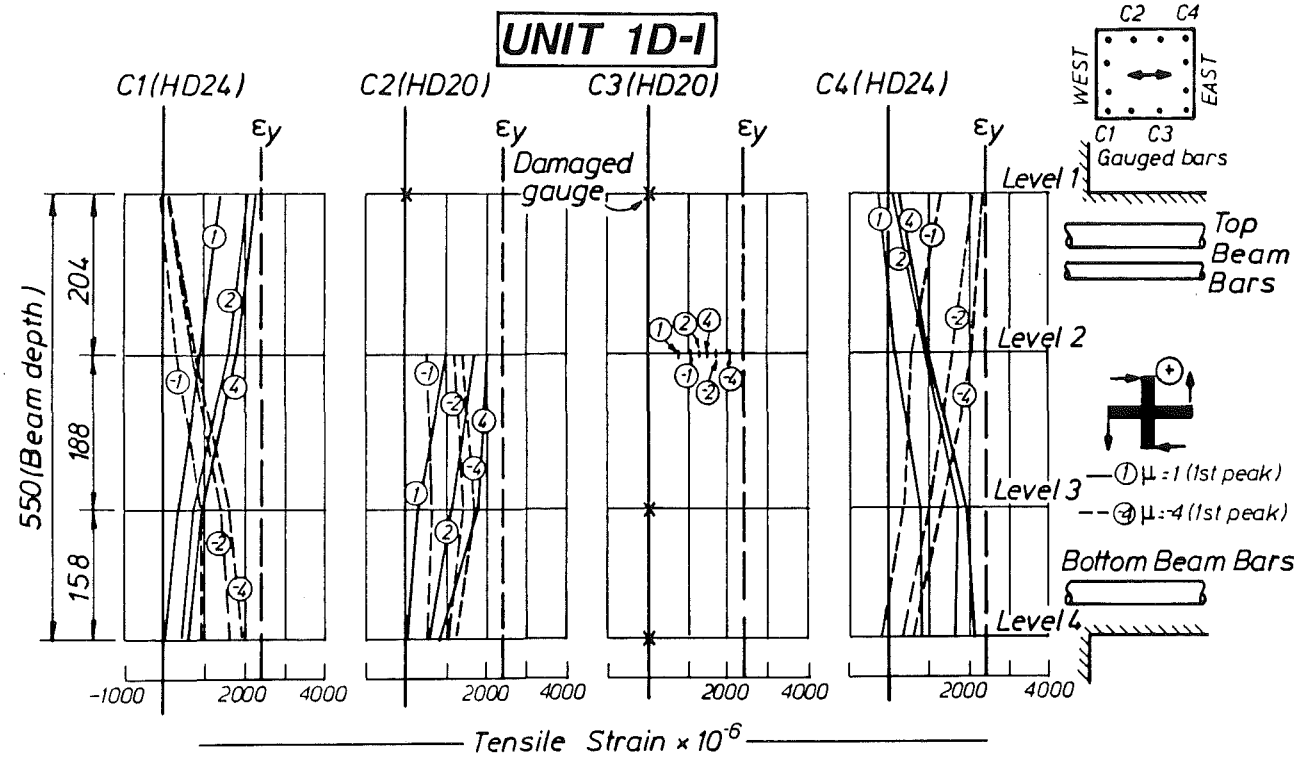

(a) From Cycles of μ=1 to μ=4

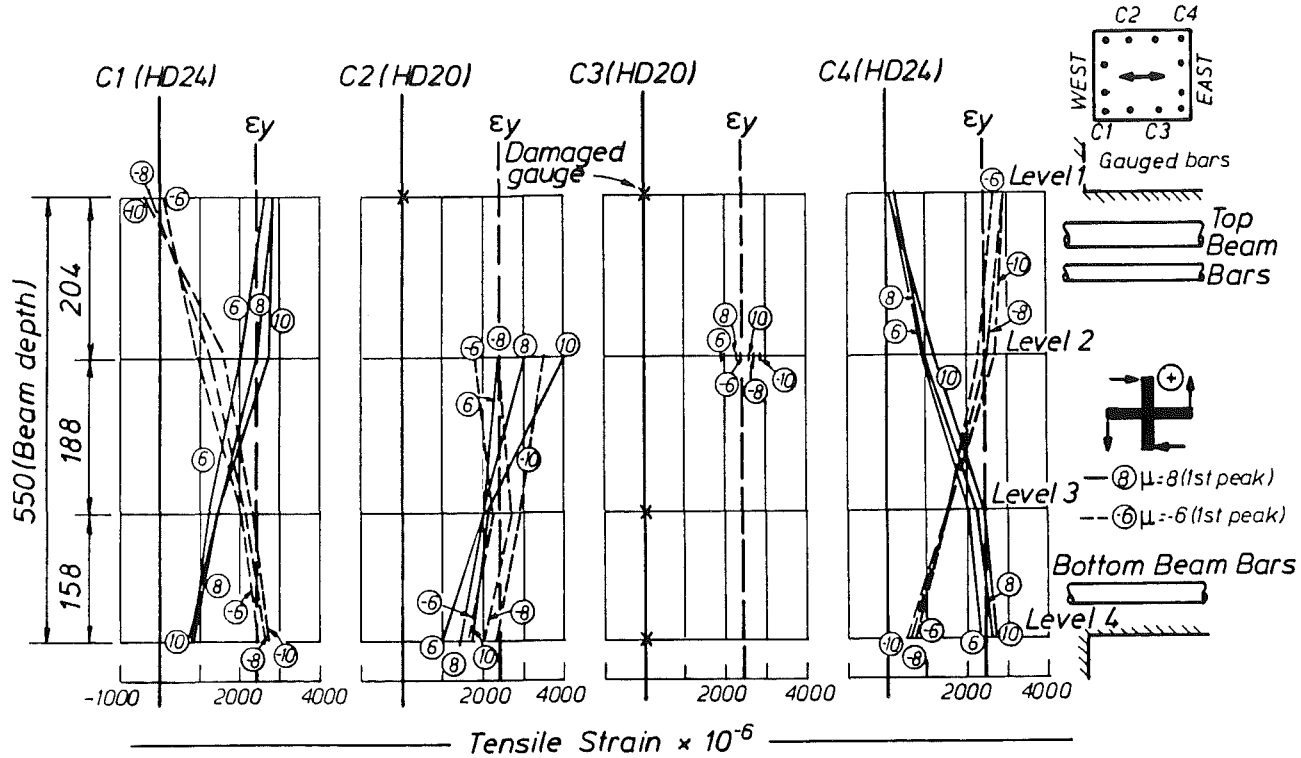

(b) From Cycles of μ=6 to μ=10

Fig.4.32 - Column bar strains in the joint core

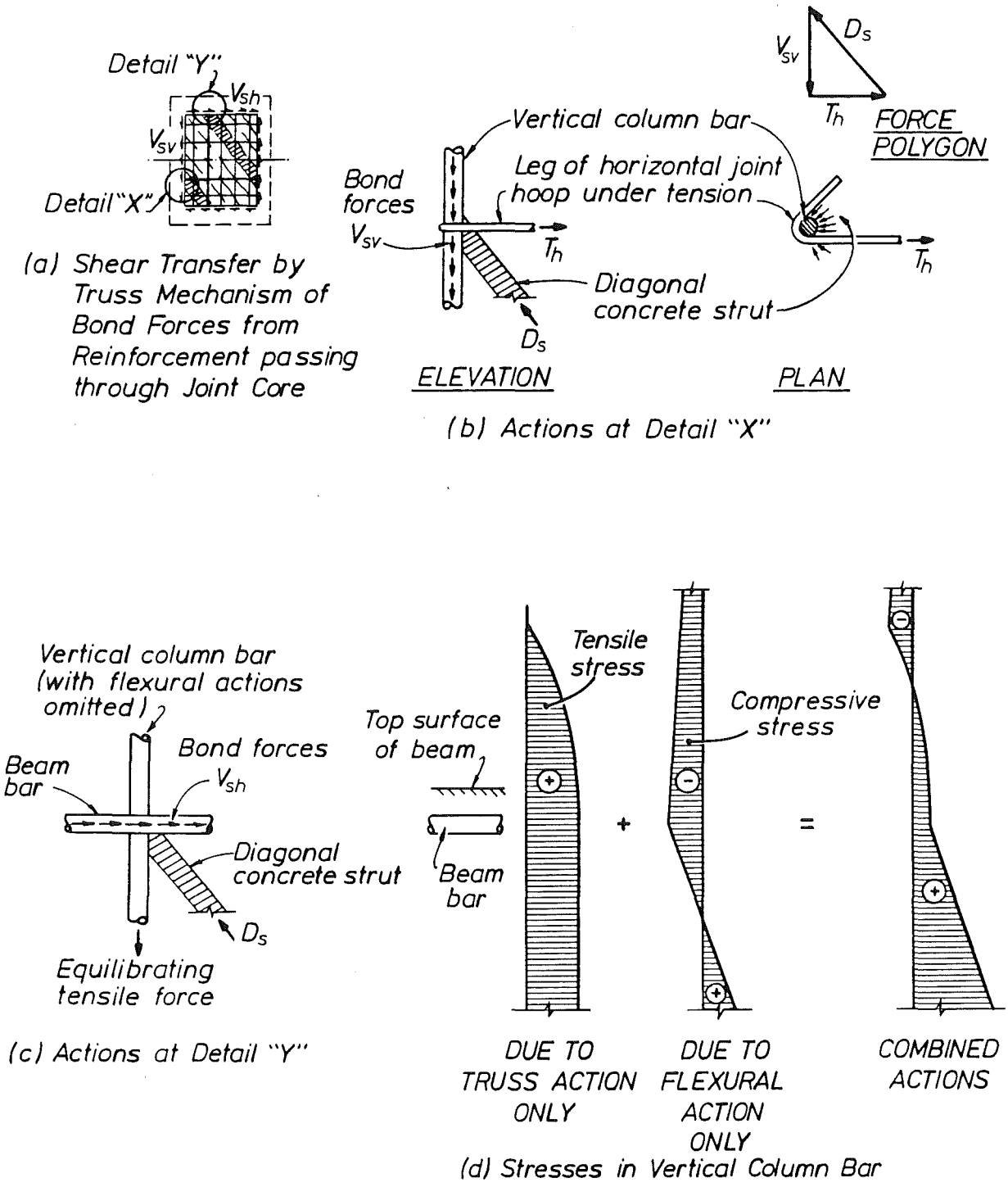

Fig.4.33 - Development of tensile strains in column bars participating in truss mechanism of joint shear resistance

strains according to the moment diagram, participated in the mechanism of joint shear resistance.

That tensile strains existed in column bars but did not conform with the sense of flexural actions can be explained using the models in Fig.4.33. The truss mechanism illustrated in Fig.2.4(d) is reproduced in Fig.4.33(a). At a node of this truss, such as the one shown in Fig.4.33(b), vertical bond forces are sustained by a diagonal concrete compression strut and a tensile force in the leg of the transverse joint hoop. This tensile force can be readily developed by means of a 135° hook. Similarly horizontal bond forces are to be resisted by a similar mechanism (Fig. 4.33(c)). Bar forces due to flexural actions are not considered in Fig.4.33(c). To develop the tensile force in the column bar due to truss action it needs to be anchored beyond the edge of the joint core (i.e. in the column above the joint) by means of bond forces. The idealized distribution of stresses necessary to sustain this truss action together with flexural stresses are shown in Fig.4.33(d). The pattern of the resulting combined stresses in Fig.4.33(d) is similar to that measured during the test. The participation of the intermediate column bar in truss action accounts for the significant tensile strains at middepth of the joint core.

It is evident that the role of vertical intermediate column bars is the same as that of the horizontal joint ties. The significant difference in joint action in the vertical direction arises from the contribution of the column at the boundaries of the joint core. The relevant column sections are expected to remain elastic at all times. hence vertical flexural concrete compression stresses may be assumed to be transmitted to the core at all stages of the inelastic response of the frame (Fig.2.4). Moreover, as tensile stresses in the intermediate column bars at and beyond the horizontal edge of the joint core have increased, as seen in Fig.4.33(d), increased flexural concrete compression forces must be developed in the column, as dictated by equilibrium criteria. This will enhance the functioning of the strut mechanism shown in Fig.2.4(c). It is for this reason that code provisions [4], summarized in Appendix A, assigned one half of the vertical joint shear force to each of the two joint mechanisms. When no axial load is applied onto the column, the observations also agree with the design procedure proposed in Section 8.3.

At high ductility of μ = 10, it was estimated that the exterior bars C1 and C4 were subjected to tensile stress of 447 MPa at the face of the joint core. This is near the yield strength of f_y = 500 MPa for HD24 bars. Using the assumption of $V_{ch} = 0.5\ V_{jh}$ [4], the tensile stress in each of the four intermediate bars such as C2 and C3, would have to be about 570 MPa, i.e. 18% above the measured yield strength f_y = 482 MPa for HD20 bars. This stress level agrees well with those implied by the strain variations for bars C2 and C3, shown in Figs. 4.33(a) and (b).

4.7 STRAINS IN THE JOINT TIES

It was disappointing to discover that four out of fourteen strain gauges failed to give complete strain readings. Readings from these gauges were considered more meaningful because plain round bars were used for ties, thus readings were less likely to be affected by bond stresses and more likely to indicate average strains in tie legs. However, in later tests when a pair of strain gauges was used, one mounted to the top and the other to the bottom surface of a bar, to measure the strains in a tie leg of Unit 2D-I or 2D-E (Chapters 5 and 6), the difference between readings was sometimes considerable.

Strain results are presented in Fig.4.34. It is seen that legs of type B ties were subjected to significantly larger tensile strains, especially at midheight (layers 2 and 3) of the joint. Yield strain ϵ_y was reached at layer 2 during the cycle with μ = 2. Outer legs of type A hoops showed lower strains. Strains in these legs approached yield level only at higher ductilities, i.e. at μ = 8 or 10. Legs of type C hoops were subjected to the smallest strains.

The fact that the legs of type B hoops were more highly stressed than those of type A hoops may be attributed to the beam width (400mm) being smaller than the column width (550mm). This is illustrated in Fig. 4.35. Horizontal joint shear is introduced by the beam bars through bond stresses (see Section 2.3) It is evident that the inner tie legs were under the influence of all beam bars, while the outer tie legs were affected primarily by outer two bars.

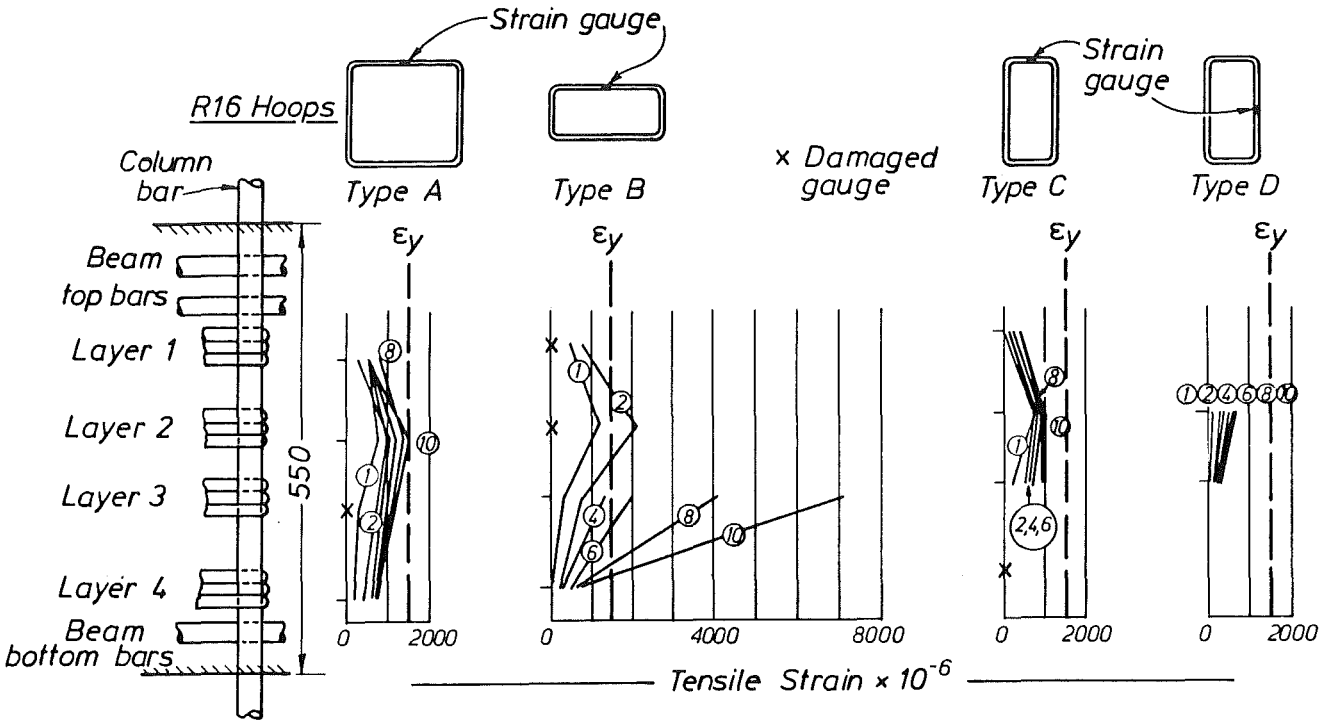

(a) Bar Strains at Positive Ductilities

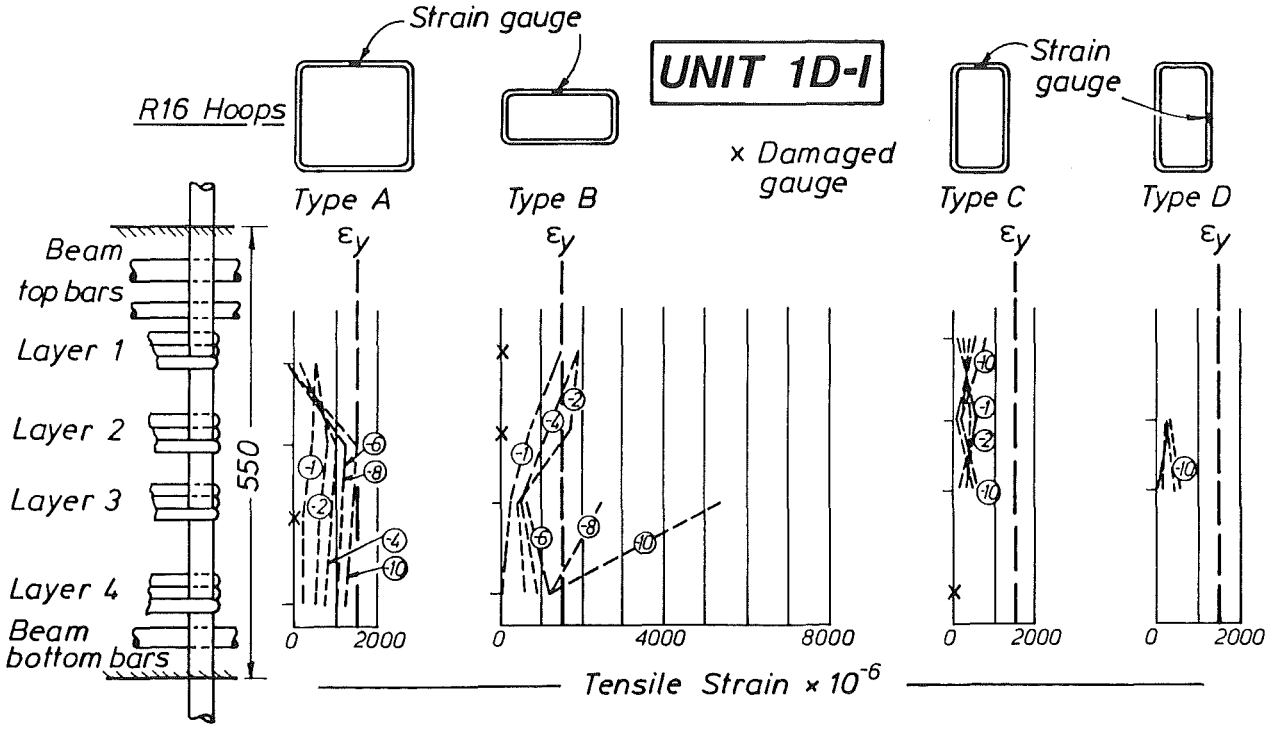

(b) Bar Strains at Negative Ductilities

Fig.4.34 - Joint horizontal hoop strains

The two principal mechanisms of shear resistance of an interior joint core in a planar frame have been reviewed in some detail in Section 2.3. It was shown that with the formation of diagonal cracks in the joint core, as observed in this test (Figs.4.1 to 4.6), the horizontal joint shear resistance was redistributed from the strut to the truss mechanism. The gradual but consistent increase in tensile strains in the horizontal ties, shown in Fig.4.34, indicates such a transfer of joint shear resistance. Also by considering a more realistic distribution of bond stresses of beam bars due to the effect of yield penetration with intensities at the central region well above the theoretical average, as suggested in Fig.2.8, it may be concluded that the central parts of the horizontal and vertical truss members will have to resist larger forces. As seen in Fig. 4.34, the centre two ties (layers 2 and 3) were indeed consistently more highly stressed than those near the top or bottom beam bars (layers 1 and 4). When presenting column bar strain distributions in Fig. 4.32 it was also shown that intermediate bars C2 and C3 were more highly stressed at levels 2 and 3. The experimental results give strong support for the postulated functioning of the truss mechanism. An implication of the above observation is that, to utilise the capacity of all joint hoops more effectively, they should be placed closer to the middle region. The straining of ties in the immediate vicinity of beam bars is likely to be governed by the strains along these beam bars. Therefore the efficiency as ties of a truss mechanism is reduced.

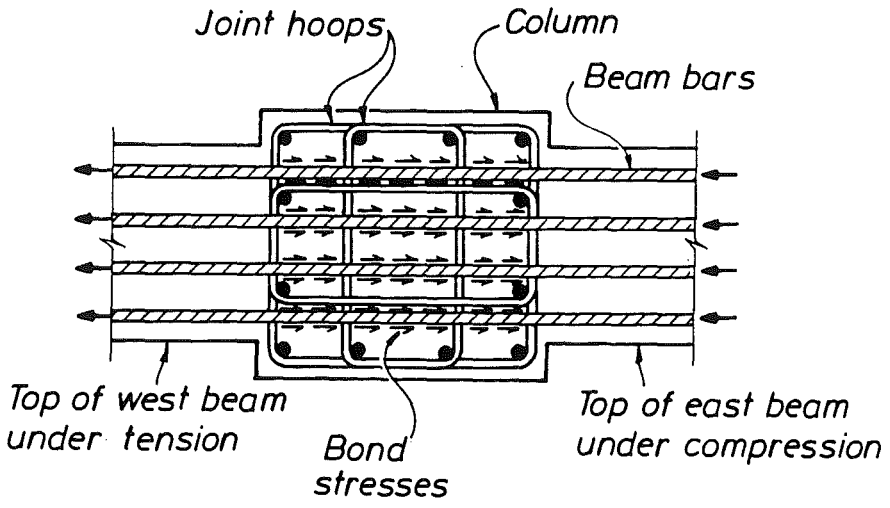

Fig.4.35 - Transfer of bond forces from beam bars to the joint core

Strains in the transverse legs of type D hoops were moderate. This indicates that the joint did not require significant confinement. Some tensile strains in transverse ties must necessarily result from the transfer of large anchorage forces at the corners, resulting in the legs parallel to the beam bars.

In summary, this test showed that the horizontal joint reinforcement played an active and important role in the resistance of joint shear. It supported the finding that beam bars were well anchored and that shear forces introduced by beam bars to the joint core were primarily by means of bond within the joint, as was intended by established design practice [4]. Transverse reinforcement provided has been satisfactory in that the strain distributions observed did not indicate unrestricted yielding of all ties. This could be related to the controlled joint shear distortions discussed in Section 4.3. The predominantly elastic response of joint shear reinforcement even at large ductilities suggests that the amount of this reinforcement might be somewhat reduced. This is considered in Chapter 8.

CHAPTER 5

TEST RESULTS OF UNIT 2D-I

5.1 GENERAL BEHAVIOUR

Eighteen cycles of loading up to a displacement ductility factor of eight were completed in about three weeks. In terms of maintenance of strength and ductility capacity the test unit performed satisfactorily, although the response was not as good as that of Unit 1D-I. Test observations are similar to those made in the first test, such as plastic hinging in the beams at all column faces, fine flexural cracks developing in the column indicating elastic behaviour of the column, and propagation of cracks in the floor slab. The test unit at progressive stages of loading is shown in Figs.5.1 to 5.6 as well as Fig.3.5(b). Since there were four beams meeting at the column, cracks in the joint area could not be recorded, nor could the joint distortion be measured. However, at the 100 mm wide exposed face of each side of column corners, a limited number of fine diagonal cracks near to the beam edge, approximately at an angle of 45° could be identified as presumed extensions of interior diagonal joint cracks. Their widths never exceeded 0.5 mm. They closed on load reversals. Some horizontal cracks in these regions stareted from the edges of the column. These were obvious flexural cracks due to column bending. Some of these diagonal and horizontal cracks, developed at a ductility level of one, can be seen in Fig. 5.1. At larger ductilities (e.g. Figs. 5.4 (c) and 5.5 (c)), there was no significant increase in the number of these cracks. Flexural cracks of the beams at the column faces obscured somewhat the observation of these cracks. At the extreme case (Figs. 5.6(a) and (c)), spalling and crushing of concrete in the plastic hinge regions of the beams extended into the column and caused the column corners to fall off. Even the north-west corner above the slab (Fig. 5.6(b)) fell off.

Cracks in the slab of this unit was more densely and evenly distributed than in the first unit. In addition to the photographs reproduced, Fig.5.7 shows the pattern of the major cracks at the top surface of the slab. The cracks may be grouped into the same four types previously

defined in Section 4.1. Of special importance is the larger number of diagonal cracks observed, an evident result of symmetrical reinforcement layout in two-way slab.

Similar to Unit 1D-I, cracks at the underside of the slab followed the top side's pattern, although the crack widths were much smaller and crack formation in the first few cycles of small ductilities was not significant. Bending of the slab quadrants could be considerable at early stage of the load history, but at advanced ductilities this became insignificant.

Starting from the first two cycles to uni-directional ductility of $\mu = 8$ (north-south, and then east-west), stretching and buckling of the beam bottom bars became visible after the spalling of concrete. A buckled bar in the north beam at the end of cycle 18 can be seen in Fig. 5.6(a). In the last run, the D24 and D20 bottom bars of the east and west beams slipped completely inside the joint.

In addition to monitoring the movement of the unit consistent with the direction of loading, attention was also paid to the out-of-plane movements at the joint level by analysing the readings from the total twelve dial gauges at the north and west faces of the column. Under uni-directional loading, an absolute movement of the joint of less than 1 mm in the perpendicular direction was recorded. This was similar to the observation made in the test of Unit 1D-I. It was not considered to have affected the test results.

This monitoring was further supplemented by installing four dial gauges, one at the side of each beam end. As explained in Section 3.5.2, the purpose was to give an indication of the horizontal movements of beam ends relative and transverse to the joint region. Since the dial gauges were placed at approximately the middepth of the beams, it was hoped that any twisting of transverse beams would not significantly influence these readings. The results were assessed in conjunction with the readings on twelve dial gauges mentioned above. It was concluded that :

(1) Under uni-directional displacement some horizontal rigid body rotation about the vertial axis of the column took place. This was catered for in the test rig design and did not affect the test.

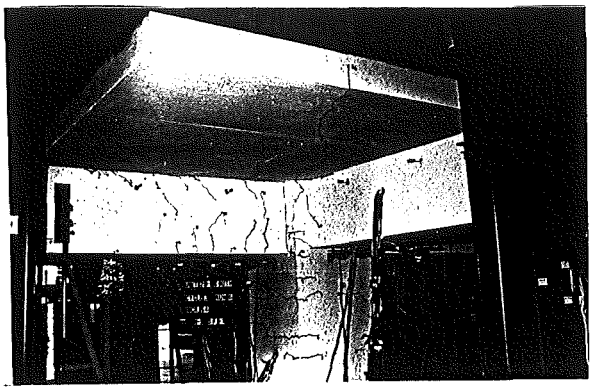

Fig.5.1 - South and east beams of Unit 2D-I in cycle 3 to ductility of μ = 1 (NS)

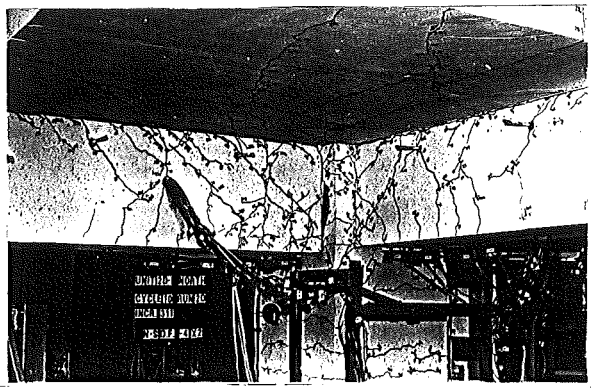

(a) North and west beams at the peak of cycle 10, 2nd cycle to μ = 4 (NS)

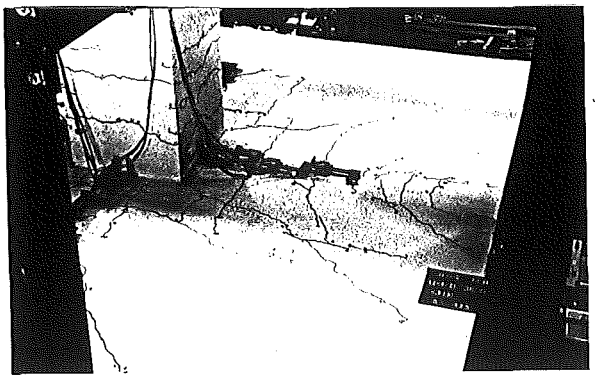

Fig.5.2 - Slab of Unit 2D-I viewed from south-east in cycle 4 to ductility of μ = 1 (EW)

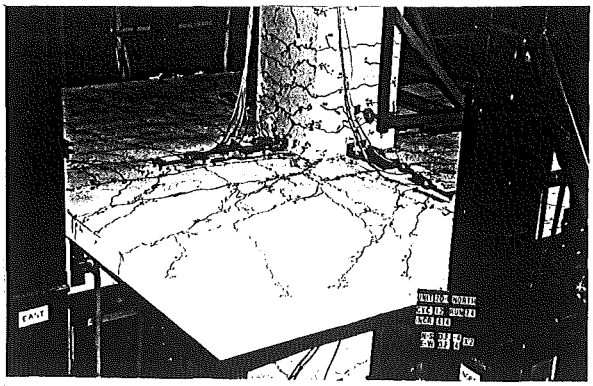

(b) Slab viewed from north-east at the peak of cycle 12, 2nd cycle to μ = -4 (NS) and 4 (EW)

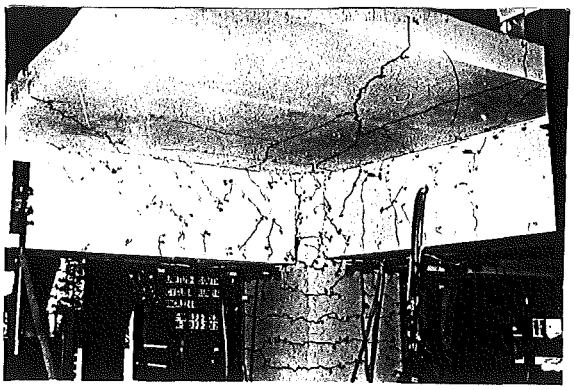

Fig.5.3 - South and east beams of Unit 2D-I in cycle 8, 2nd cycle to ductility of μ = 2 (biaxial)

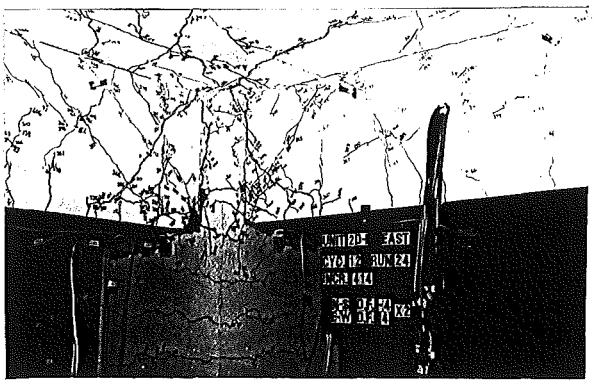

(c) South and east beams at the same ductility as (b)

Fig.5.4 - Unit 2D-I in cycles 10 and 12 to ductility of μ = 4 (uniaxial and biaxial)

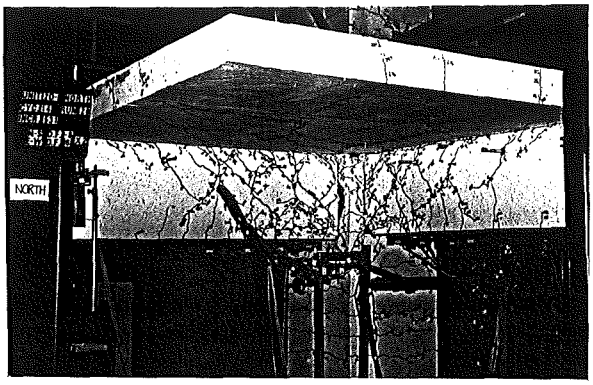

(a) North and west beams at the peak of cycle 14, 2nd cycle to μ = -6 (NS) and 6 (EW)

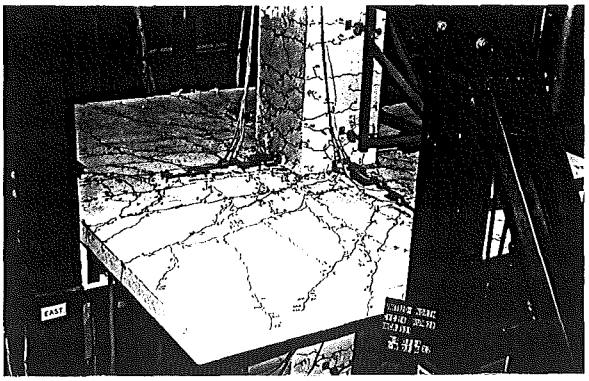

(b) Slab viewed from north-east at the same ductility as (a)

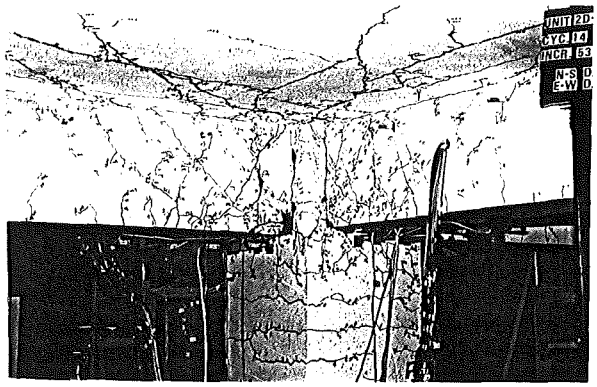

(c) South and east beams at the same ductility as (b)

Fig.5.5 - Unit 2D-I in cycle 14 to ductility of μ = 6 (biaxial)

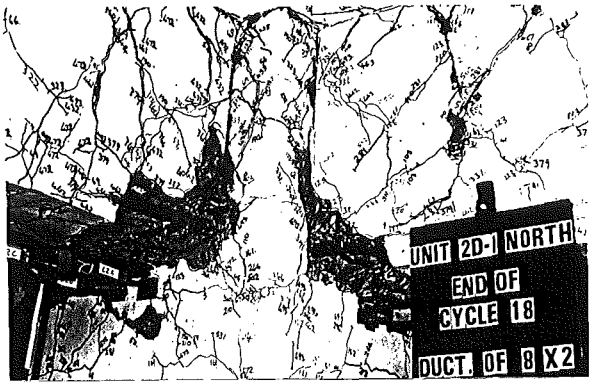

(a) East and north beams

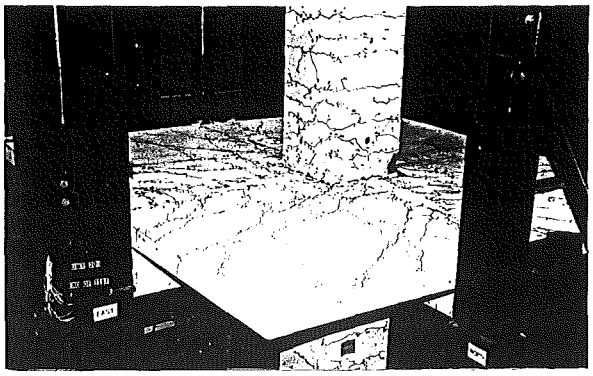

(b) Slab viewed from north-east

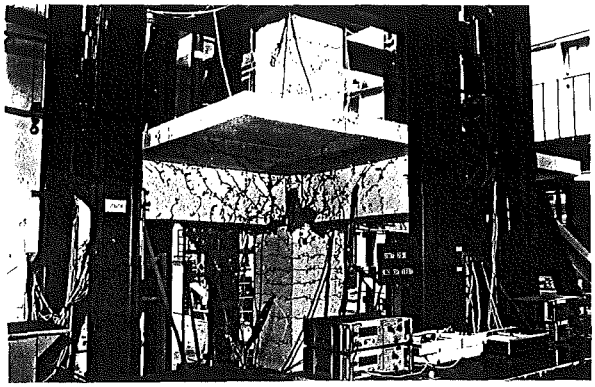

(c) South and east beams

Fig.5.6 - Unit 2D-I at the end of cycle 18, after two cycles to μ = 8 (NS) and two to μ = 8 (EW)

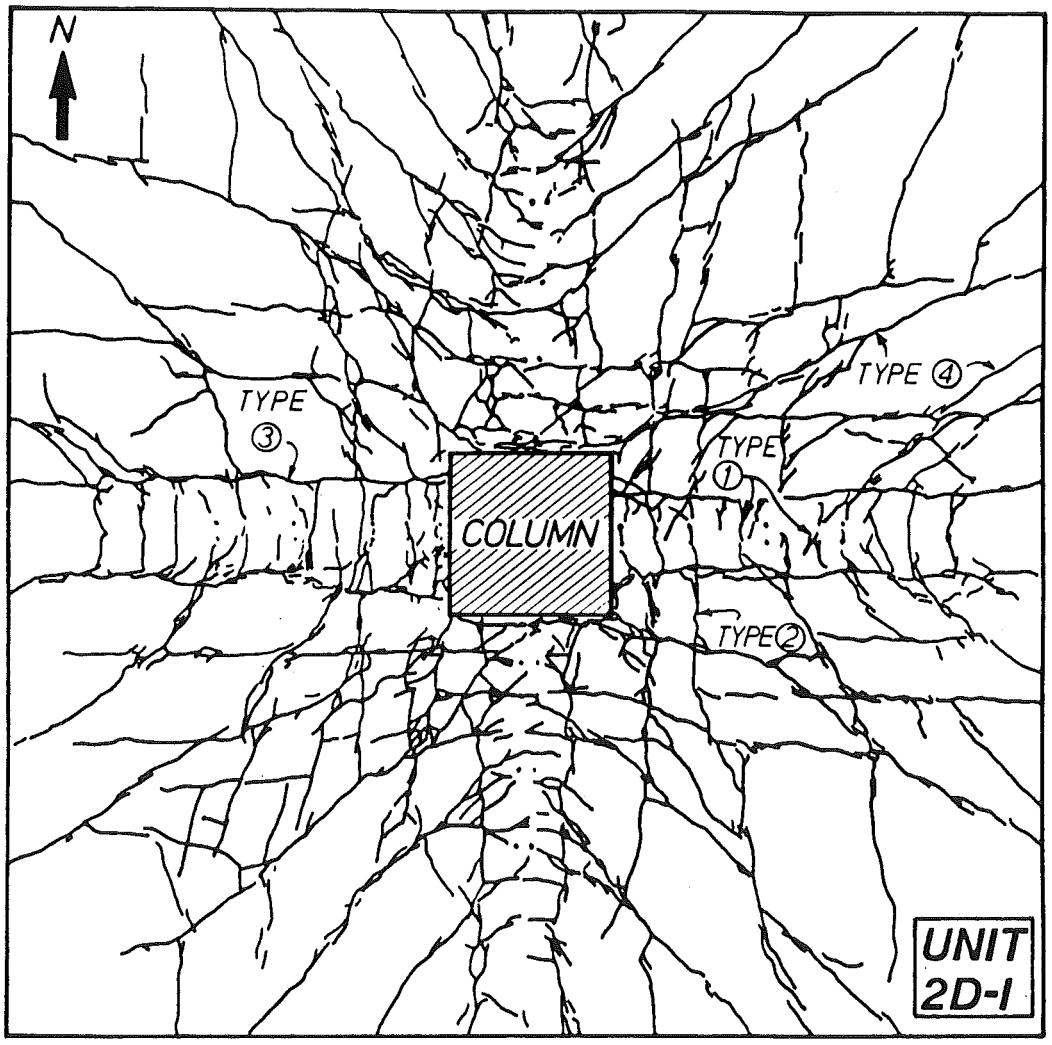

Fig.5.7 - The pattern of major cracks at top surface of slab of Unit 2D-I

(2) The far ends of the transverse beams moved slightly towards the longitudinal beam which was being subjected to downward force. For instance, when the south beam was displaced downwards, both east and west beams swung about the column towards the south. The largest magnitude of this kind of movement at beam ends ranged from 2 to 3 mm at a ductility of six, after the rigid body rotations about the column axis was accounted for. This suggested that slab bars in tension caused the transverse beams to move and that some of the tension force from slab bars may have been transmitted by anchorage to these beams. The effect of this on the flexural strength and behaviour of the beams was considered to be negligible.

5.2 FORCE-DISPLACEMENT RESPONSE

5.2.1 General

The column (storey) shear versus displacement curves are ploted in Fig. 5.8 for the three elastic cycles in the north-south direction and in Figs. 5.9 and 5.10 for subsequent inelastic cycles in the north-south and east-west directions respectively. The load history for this test, shown previously in Fig. 3.18 and explained in Section 3.7, consisted of 18 cycles, six of which included loading in both east-west and north-south directions. In summary, the north-south frame was subjected to much more severe loading history with a total of thirty load runs (i.e. semicycles), whereas the east-west frame underwent just eighteen load runs. As for the responses of the four beams, they are presented in Figs.5.11 to 5.14. Calculations for various possible ideal strengths are given in Appendix C.2. The approach for assessing hysteretic response follows that used in Section 4.2 for Unit 1D-I.

The experimentally observed yield displacement and stiffness were determined during run 5 (μ = +1 NS) at 75% of the ideal strength. Both the estimated stiffness, $K_{theoretical}$, and experimental stiffness, K_{test}, are plotted in Fig.5.8. In run 6 (μ = -1 NS), the observed stiffness is slightly less than K_{test}. Frm the curves in Fig.5.8 and other hysteresis graphs, stiffness degradation is seen to be inevitable under the action of cyclic loading.

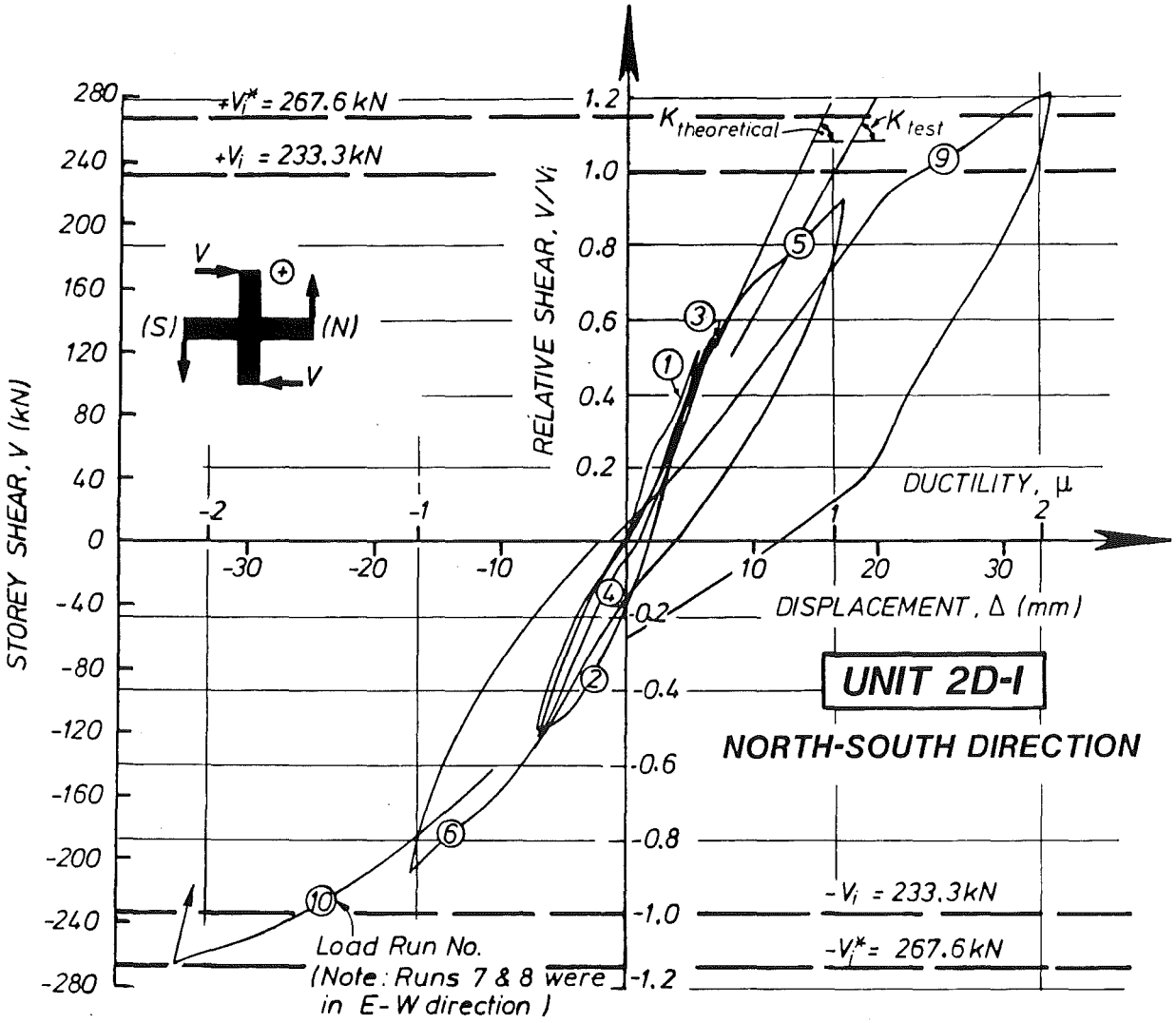

Fig.5.8 - North-south storey shear-displacement response - elastic cycles

The reference displacement at first yield of the test unit, $\Delta_{y,test}$, was found to be 16.5 mm (i.e. 0.47% of storey height). This is slightly larger than the value observed in the first test (Section 4.2.1) which amounted to 15.7 mm. The associated stiffness of 14.1 kN/mm is therefore only 82.5% of the theoretical 17.1 kN/mm estimated in Appendix C.3. However using the reasoning as in Section 1.3.4, $\Delta_{y,test}$ may be compared with the code implied interstorey drift, Δ_e, by Eqs.(1.4) and (1.5) as with Unit 1D-I. Hence with

$$\frac{V_{i(test)}}{0.9V_{i(design)}} = \frac{233.3}{0.9\ (184.5)} = 1.40$$

the drift due to code design load, Δ_e, should be of the value of $\Delta_{y,test}/1.40$ = 16.5/1.40 = 11.8 mm (0.34% of interstorey height). This compares favourably with the code [6] recommended value of 0.32%.

5.2.2 Elastic Cycles

The first two cycles brought the test unit to about one half of the force corresponding to the ideal flexural strengths of the beams in the north-south direction. In the first run to + 0.5 V_i, fine flexural cracks appeared at the north face of the lower column as well as at the south face of the upper column, in accord with the loading direction. Flexural cracks at the bottom of the north beam were evenly distributed, following the spacing of the stirrups. As expected, the major crack was at the column face. At this stage the south beam and slab was subjected to tension at the top. Instead of east-west transverse cracks, diagonal cracks developed and propagated into the slab from the flexural cracks initiated at the top of the south beam. Subsequent strain gauge results showed that at this stage both the east-west and north-south slab bars were in tension. Crack formation in the slab indicated the extent of this diagonal tension field. A certain width of the slab on either side of the beam acted as a tension flange of the beam. Also observed were the relatively large strains in the top layer north-south slab bars, and the longer cracks which developed at the top surface of the slab.

In the second run to -0.5 V_i, cracking proceeded in the same pattern except that it occurred at the top side of north beam and slab, at the bottom of south beam, as well as at the two faces of the column, as expected. A diagonal crack appeared at the underside of the south-east slab, which originated from the corner of the column.

Cycle 2 saw the extension of the existing cracks with little formation of new cracks. As can be seen from the hysteresis loops in Fig. 5.8, less energy was dissipated in runs 3 and 4. Cracks began to appear at the junctions of the slab underside and the beams near the force application points. Subsequently, as forces increased with higher ductilities, there were significant relative vertical displacements between the stem of the beams and the adjoining slab particularly near the free ends of the beams, as previously mentioned in Section 4.5 and Fig.4.31. The largest displacement recorded was 3 mm.

In run 5 in the third cycle which imposed a displacement ductility of μ = 1 (NS), more flexural cracks and inclined flexural-shear cracks were noted in the beams. The column corner cracks at the joint area extended diagonally downward to the east and west beam (Fig. 5.1). This was identified as diagonal cracking of the joint which was obscured by the transverse (east and west) beams. Since the south beam was subjected to a higher (downward) load, cracking in this beam was more severe. Cracks in the south slab were mainly of diagonal type close to the beam, but further away to the edges, they changed to transverse east-west cracks. This is probably because the east-west slab bars had lost anchorage there and the tension effect of the north-south slab bars became more significant. At the interface between the south slab and west beam, both top and bottom slab cracks were formed, again showing the tension in the slab bars. At the north-west slab quadrant, where diagonal cracks did not extend, a long interface crack at the bottom of the slab and the north face of the beam developed. These observations provided evidence that the slab bent upwards in accord with the adjoining beam action.

In run 6 to μ = -1 (NS), more cracking took place in a similar but reverse pattern. A special crack can be seen in Fig. 5.1 which extended at the underside of the south slab to the east edge of the unit. Previously in run 5, when the north beam was being pulled upwards, a similar diagonal crack at the underside of the north slab started from the north-east corner of the column.

East-west loading of the specimen to μ = ±1 was carried out in cycle 4. By comparing the envelopes of hysteresis loops in Fig. 5.9 for runs 5 and 6 with those in Fig. 5.10 for runs 7 and 8, it is seen that the east-west

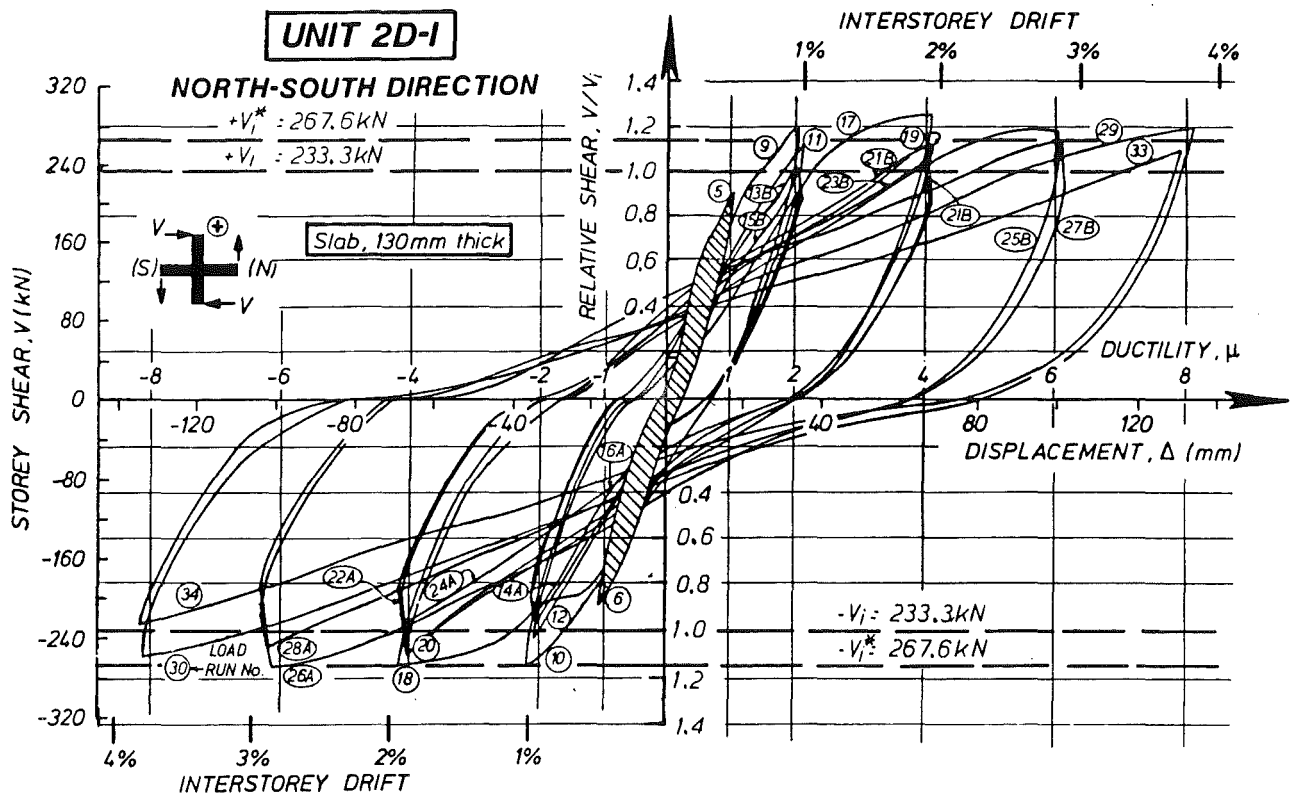

Fig.5.9 - North-south storey shear-displacement response - inelastic cycles

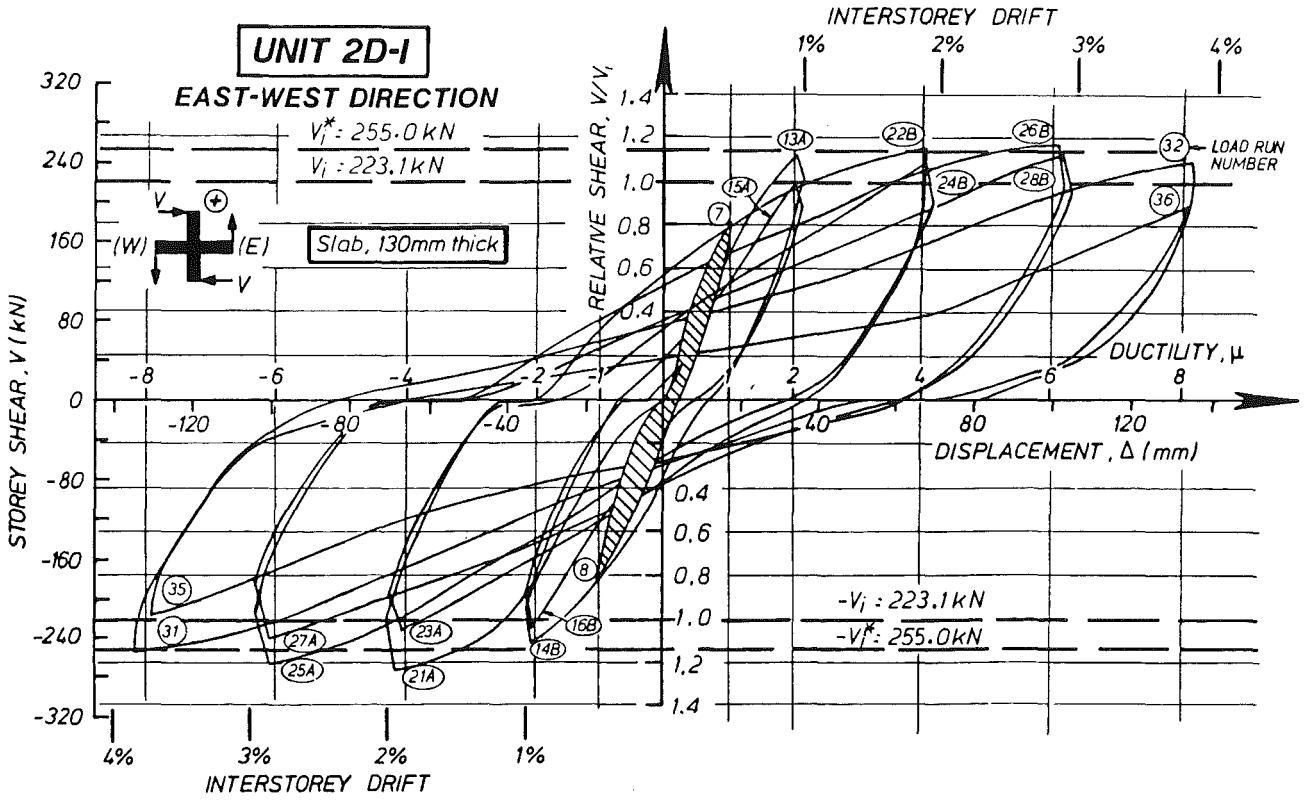

Fig.5.10 - East-west storey shear-displacement response

frame was somewhat more flexible. This resulted in a smaller resistance being developed at the imposed displacement to μ = -1.

Cracks were formed in a manner similar to that observed in previous cycles. Residual deformations already existed in the north and south beams. Hence the final crack pattern, especially in the slab, reflected this effect. In addition to diagonal cracks, transverse and beam-slab interface cracks also developed in the slab (Fig. 5.2). Also since the north and south column faces had already cracked, more east-west joint cracks appeared at the exposed portions of the column.

5.2.3 Inelastic Cycles

The inelastic response of this test unit is considered as being very satisfactory. However, when the hysteresis curves (Fig.5.9 and 5.10) are compared with those of the first one-way unit (Fig.4.10), the performance of this two-way unit is seen to be distinctly inferior. That is to say, identically reinforced beam-column joint assembly under one-way action would perform better than under two-way actions.

Fig. 5.9 shows the overall response of the test unit in the north-south (N-S) direction. The storey shear (i.e. strength) remained fairly constant. Although, as expected, there was a gradual degradation of stiffness, energy dissipation was stable as can be seen from the hysteresis loops. This is especially significant considering the severity of the loading history imposed (Section 5.2.1). On the other hand, it is evident that biaxial loading reduced the peak strengths. Finally, from the relatively flat and pinched run 34 loading curve, it appears that beam bar slippage was about to take place. As a matter of fact, in the subsequent cycle 18 in run 36 (Fig. 5.10), the east-west beam bottom bars slipped completely. Since the first test (Chapter 4) confirmed that throughout the entire test the beam bars were effectively anchored in the one-way frame, this test suggests that two-way action subjected the beam bars to a higher degree of bond deterioration.

As Fig. 5.10 shows, in the east-west direction, stiffnesses of the unit were generally less than those shown in Fig. 5.9. This can be expected because the east-west beam depth was smaller (550 mm) and the preceding north-south loading cycles had already caused considerable cracking in the slab. Nevertheless, as perceived from the two figures, the peak strength and energy

dissipation capacities in orthogonal directions are comparable.

The hysteresis curves in Figs.5.11 to 5.14 drawn separately for the four beams have similar shapes. Like Unit 1D-I this feature indicates that most of the energy dissipation within the test unit was through inelastic deformations of the beams. The particularly flat curves of east and west beams in run 36 (Figs. 5.13 and 5.14) confirm the occurrence of slippage in that direction of the beam bottom bars through the joint.

A common feature of the hysteretic response of two-way units is the reduction of resistance after the attainment of the predetermined displacement ductility in a biaxial loading cycle. This has been covered in some detail in Section 3.7.2 with the aid of Fig. 3.20. In Fig. 5.10, for instance, in runs 21A and 23A at μ = -4, a reduction of peak storey shear in the E-W direction by 20% and 17% respectively, is indicated by the straight and nearly vertical portions of the corresponding curves. This occurred while similar successive displacements were imposed in the N-S direction in runs 21B and 23B (Fig. 5.9). The phenomenon was repeated at the unloading stage. Unloading took place first in the E-W direction first (i.e. 21A and 23A in Fig. 5.10). As the E-W storey shear became zero, the peak N-S resistance at the same time dropped by 19% and 18% for runs 21B and 23B in Fig.5.9 respectively. The shear orbit diagram in Fig. 3.20(a) for cycle 7 illustrates this strength reduction phenomenon in another form.

Similar features are also evident in Figs. 5.11 to 5.14 for the response of the beams. However, it should be noted that the strength reduction of a beam was much more affected by loading of the transverse beams, when the top flange of the beam were in tension. This is evident when peak values of hysteresis curves, consistent with positive loading, are compared with those for negative loading. This suggests that transverse loading had a more significant influence on the contribution of slab reinforcement to the enhancement of "negative" flexural strength of a beam. This issue is examined further in Chapter 7.

Another feature, reported earlier in Section 3.7.2, is that the drop in peak resistance during orthogonal action was accompanied by a slight change, usually an increase, in the corresponding peak displacement. However, this change was small when compared with the large magnitudes of imposed inelastic displacements. As can be inferred in Figs. 5.9 and 5.10, say the

curves of runs 21A and 23A referred to in an earlier paragraph, resistance could decrease further if displacement was to be restored to its original "peak" value. Therefore no attempt was made to adjust the peak displacements during bi-directional testing.

For all four beams (Figs.5.11 to 5.14) the average stiffnesses in the positive upward bending case were usually higher than those in the negative downward bending. Similar observations were made in the first test. It was suggested in Section 4.2.3 that the top concrete in compression contributed to the positive flexural resistance.

In the storey shear-displacement responses (Figs. 5.9 and 5.10), the observed peak shear forces at ductilities of two or more consistently exceeded by more than 20% the theoretical "seismic" shear (203 kN) estimated by the "mixed" approach based on the contribution of an internal steel couple and explained in detail in Section 3.8.2. The theoretical values are given under cases (a) and (g) in Tables C.2 and C.5. Further in Figs. 5.11 to 5.14 showing the beams' response curves, the experimental positive (upward) tip forces were found to be much larger than the theoretical "seismic" (case (a)) strength of 112 kN estimated by the steel-couple method, even at a ductility of μ = 1. For instance in run 5 (μ = 1), the measured peak force on the north beam (Fig. 5.11) was 173.9 kN. In Section 5.4, it is seen that the D24 bottom bar was already strained to above yield level. From Table C.3 the peak strength should fall between the case (d) theoretical values of P_i = 162.9 kN and 1.18 (162.9) = 192.2 kN at flexural overstrength. At this stage no long transverse cracks were formed at the top surface of the north slab; the existing cracks were found to have closed. The compressive stresses recorded in the strain gauges NT1 and NT2 in the slab bars (see Section 5.5) provided further evidence that some width of the floor slab must have acted as a compression flange.

In run 6 (μ = -1), the observed positive force on south beam was 154.1 kN (Fig. 5.12). In this case, both the D24 and D20 bottom bars were strained to below yield level. Again the compressive stresses noted in the strain gauges on the two slab bars close to the beam showed the existence of a compression flange. The effective flange width appeared to be smaller than in the northern flange width (in run 5). This is believed to have been due to the presence of early extensive cracking in the south slab, as reported in Section 5.2.2.

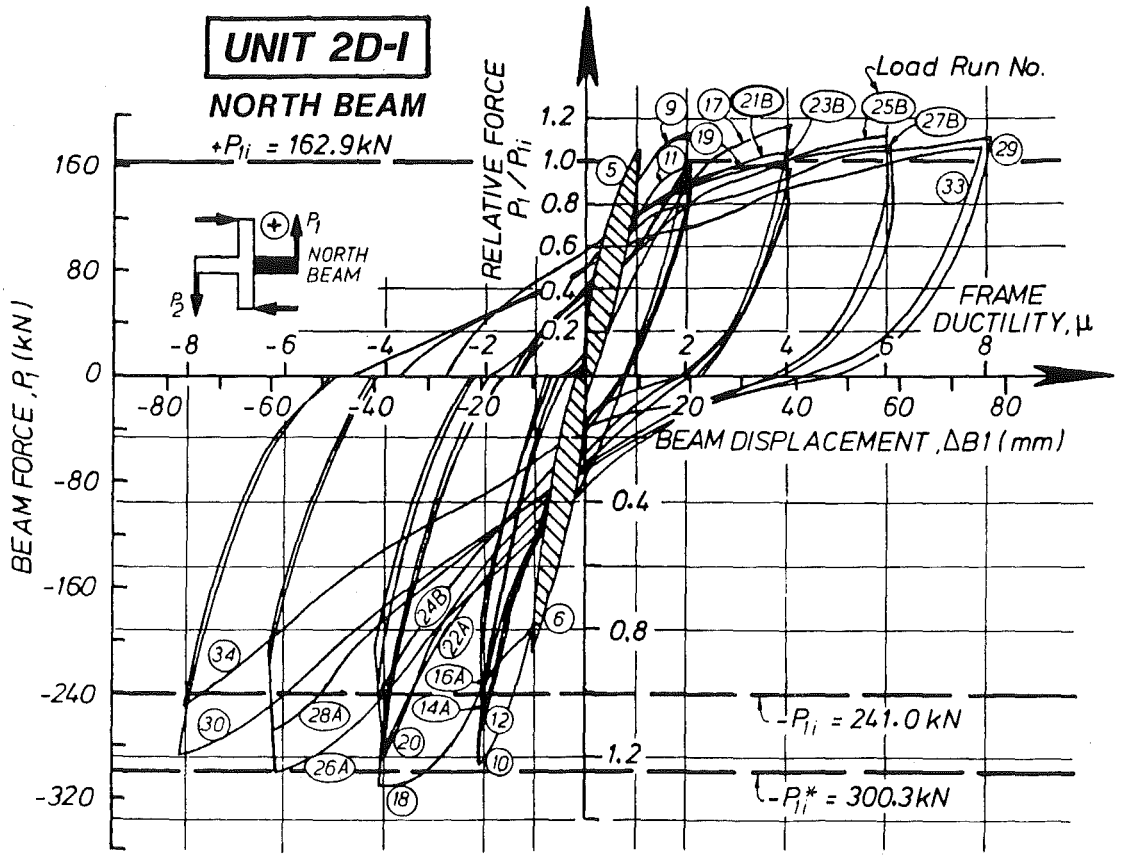

Fig.5.11 - Force-displacement response of north beam

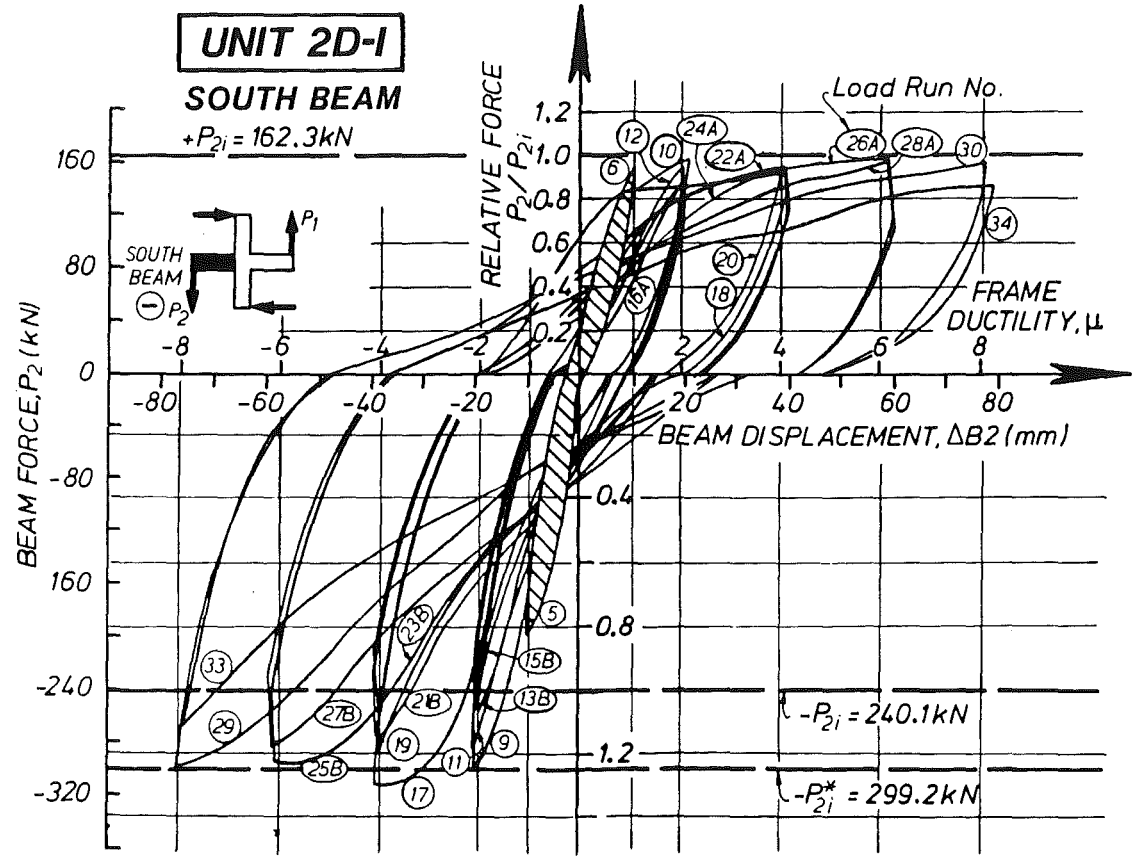

Fig.5.12 - Force-displacement response of south beam

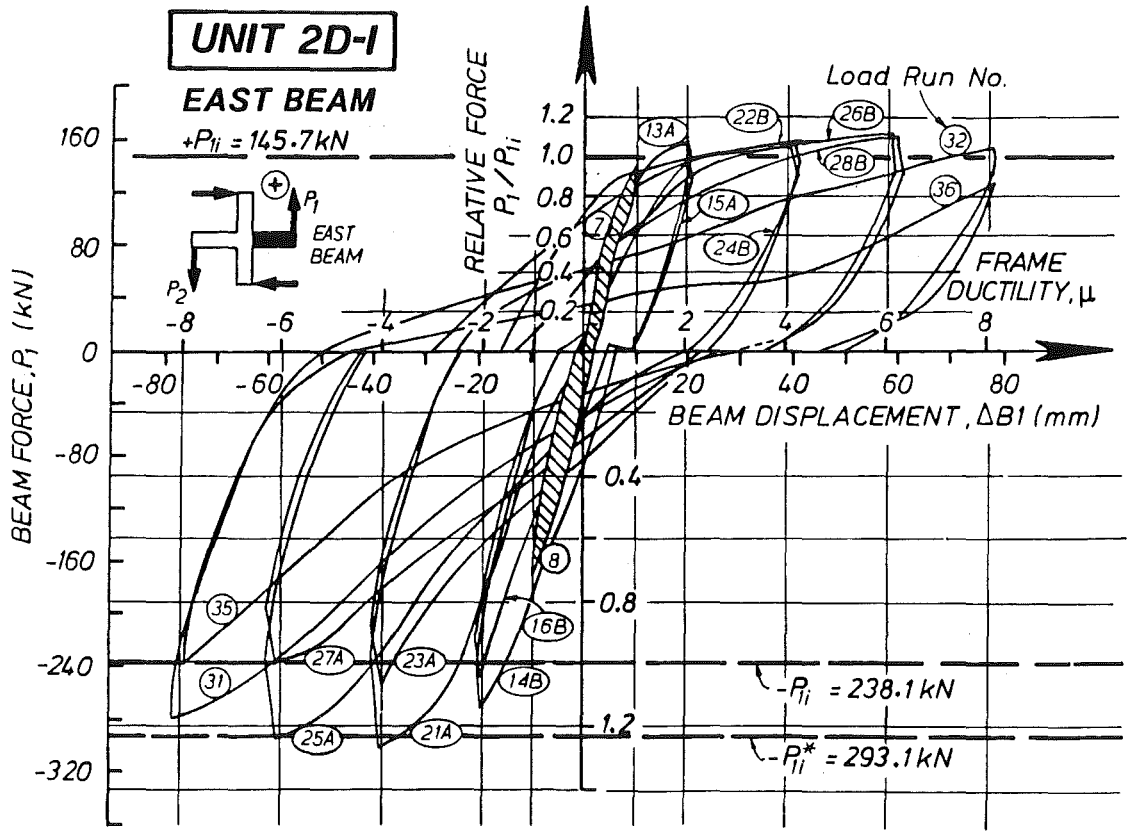

Fig.5.13 - Force-displacement response of east beam

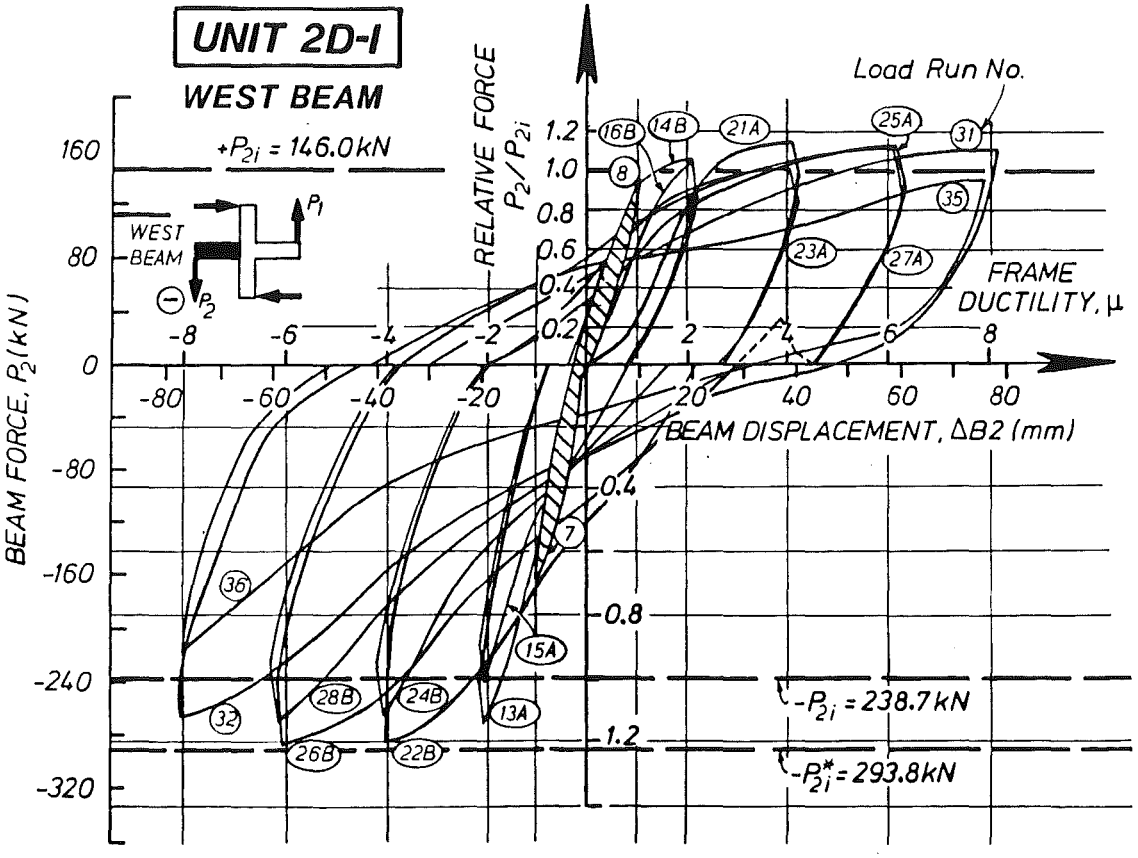

Fig.5.14 - Force-displacement response of west beam

Positive forces for the east beam in run 7 (Fig. 5.13) and the west beam in run 8 (Fig. 5.14) can be assessed in a similar way. Both cases suggest that the beam flange in the east-west direction was less effective in compression. From the strain gauge results only one E-W slab bar on each side of the column was considered to be in compression. From the pattern of cracks at the slab top surface, preceding N-S actions must have reduced the subsequent effective compression flange width of the E-W beam.

Results for the negative downward beam forces in runs 5 to 8 (Figs. 5.11 to 5.14) were more straightforward. The bottom bars were in compression as was the bottom concrete, as evidenced by the closing of flexural cracks during downward displacements of the beams. Together with the top beam bars, almost all longitudinal slab bars were stressed in tension (Section 5.5). However, since at this stage stresses were still below yield level, the theoretical tip force, $(-)P_i$, was not exceeded. As the ductility level increased to 2 or further, this negative theoretical force based on an effective tension flange with width as specified in NZS 3101 [4] denoted by $(-)P_{1i}$ or $(-)P_{2i}$, was consistently exceeded. Run 36 (Fig.5.14) was an exception, in which the E-W bottom beam bars slipped. The experimental forces sometimes exceeded even $(-)P_i^*$, the possible maximum theoretical forces which considered a greater number of slab bars yielding in tension (App.C.2). However the level of theoretical flexural overstrength, $1.25P_i^*$ was never attained. The slab bar strain results in Section 5.5 suggest that more slab bars than those estimated in App.C.2 could be considered as tension reinforcement.

There is a significant difference between the positive peak force of north beam (Fig. 5.11) in run 9 (P_1 = 185.9 kN > P_{1i}) and that of south beam (Fig.5.12) in run 10 (P_2 = 164.6 kN $\approx$ P_{2i}). This difference agrees with the relative magnitudes of tensile strains developed in the top bars, as shown in Section 5.4. The pattern of the cracks is further supported by this phenomenon. Run 9 is the first semicycle to a ductility of two. There were not many new flexural cracks at the bottom of north beam; the width of the major crack at column face was, however, about 3 mm. The existing cracks at the top surface of the northern slab closed, while a transverse crack at the bottom of the north-eastern slab quadrant opened up to reach the east edge of the unit. It appears that quite a wide and thin compression flange developed in the northern slab. On the other hand, the southern slab in run 9 was

displaced downwards. More slab cracks and flexural-shear cracks were noted (Fig. 5.3). It is therefore apparent that when the loading direction was reversed in run 10, the possible contact area available in the southern slab to engage in compression was greatly reduced. At the same time, transverse and diagonal cracks developed in the northern slab. Further in run 11, the north beam peak force reduced drastically to 165.6 kN, indicating continuing reduction in size of the compression flange.

The peak force of the north beam in run 17 was 192.1 kN = 1.18 P_{1i}, the highest upward force measured in the test. This is the first semicycle to a displacement ductility of four. The reasoning in the paragraph above, appears applicable. Furthermore, the strain-hardening of the bottom bars of the north beam must have caused this enhancement.

During subsequent cycles, there was little change in the behaviour of the beams. Their hysteretic responses shown in Figs. 5.11 to 5.14 were considered satisfactory. The final pattern of cracks of the test unit has been described in Section 5.1. The maximum shear deflection in the beams was about 2.5 mm.

5.3 DISPLACEMENT COMPONENTS

5.3.1 Beam Deformations

The measured horizontal movements of the critical parts of the four beams of Unit 2D-I are shown in Figs.5.15 to 5.18. When they are compared with Figs.4.17 and 4.18, it is seen that in terms of longitudinal beam deformations, Units 2D-I and 1D-I have common features. Bi-directional loading to Unit 2D-I did not cause any significant changes. Therefore the discussions in Section 4.3.2 for Unit 1D-I also apply here.

Other results derived from beam deformations, in a pattern similar to those in Section 4.3.2, are shown in Figs.5.19 and 5.20 for beam lengthening, and in Figs.5.21 and 5.22 for beam curvatures. Slips of the beam bars within the joint core, plotted in Figs.5.23 and 5.24, appear to be larger than those estimated for Unit 1D-I (Figs.4.21 and 4.22). This can be expected because Unit 2D-I was subjected to simulated seismic actions in orthogonal directions and this should have affected the anchorage of beam bars in the joint core.

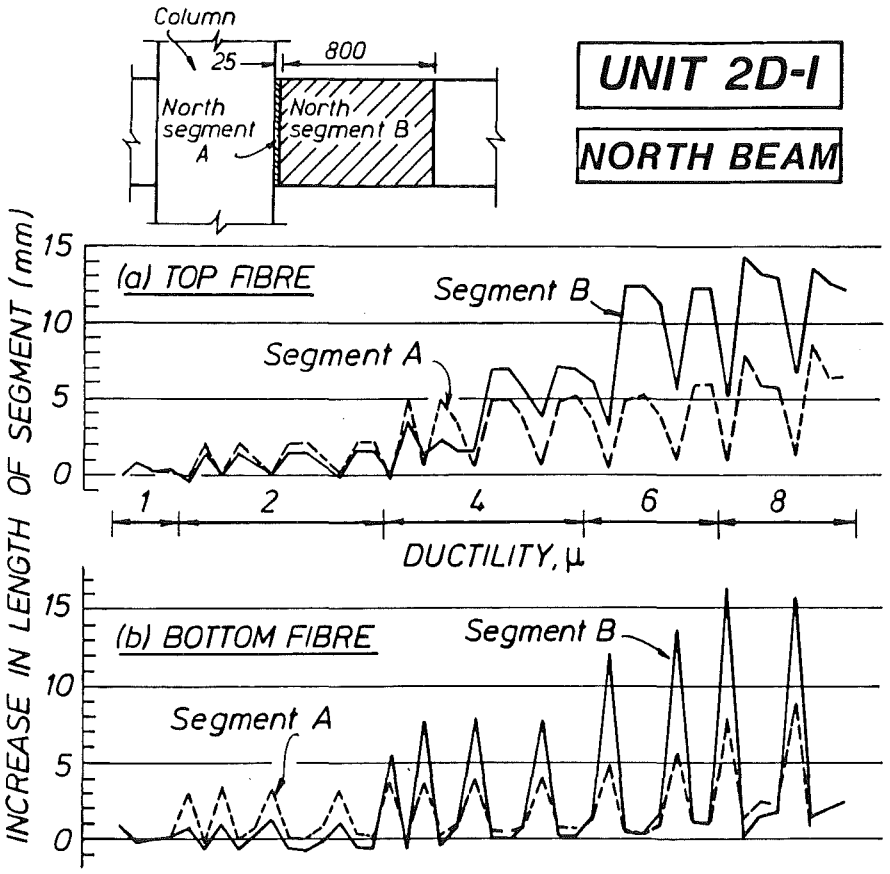

Fig.5.15 - Measured longitudinal movements in segments of north beam

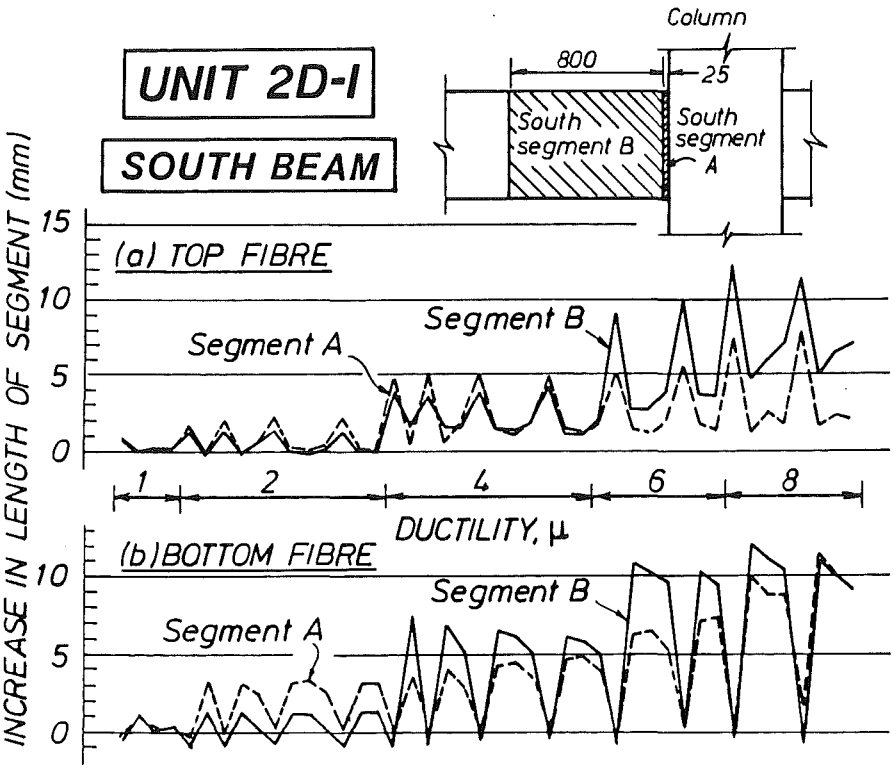

Fig.5.16 - Measured longitudinal movements in segments of south beam

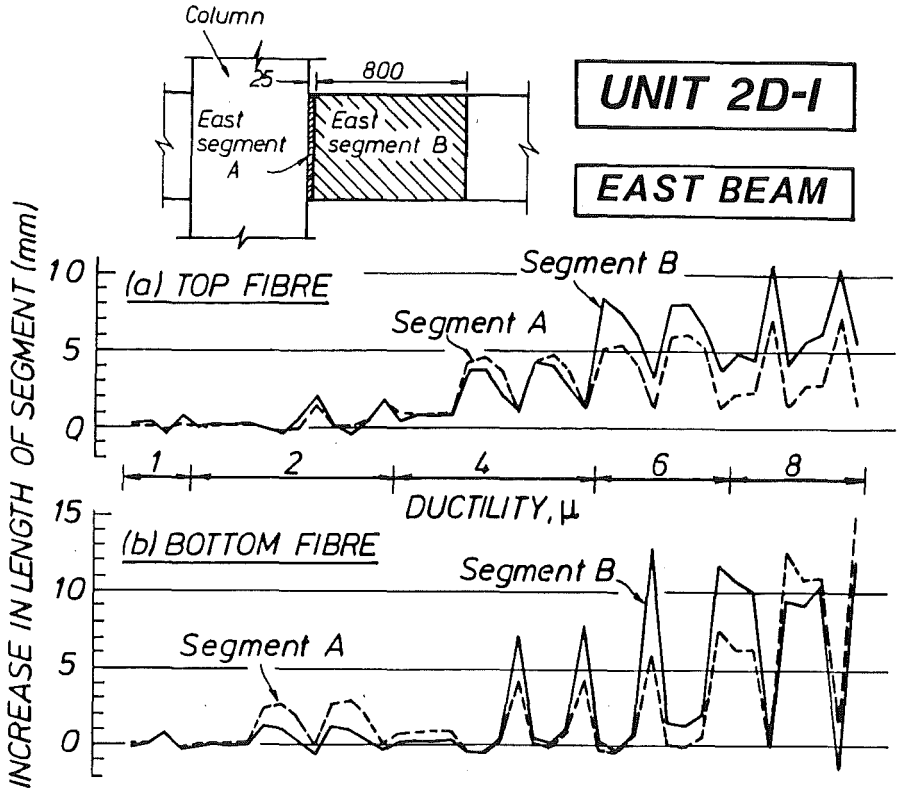

Fig.5.17 - Measured longitudinal movements in segments of east beam

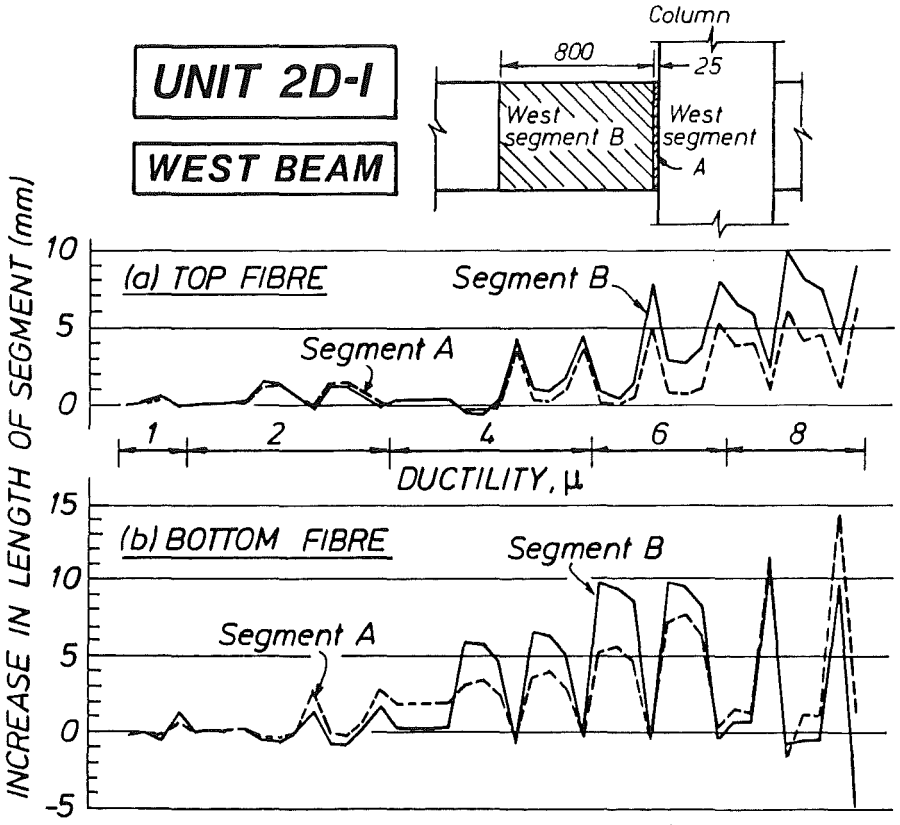

Fig.5.18 - Measured longitudinal movements in segments of west beam

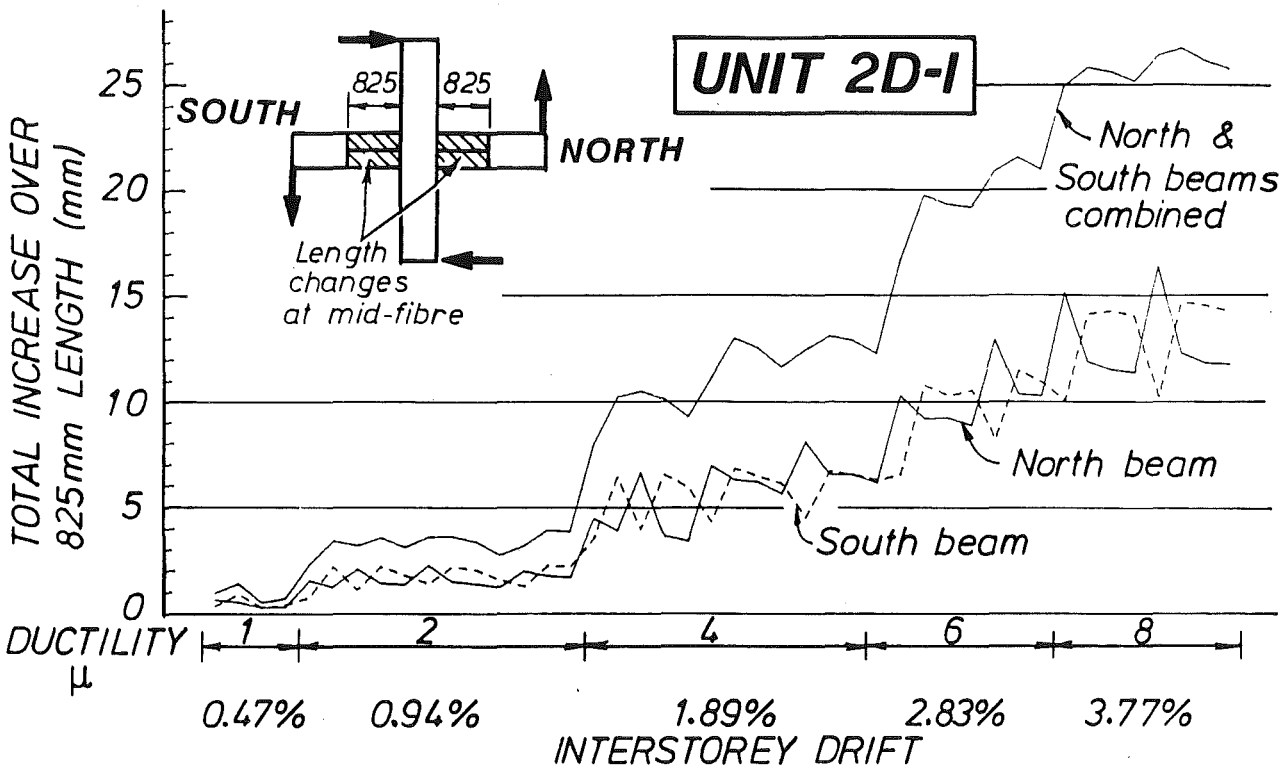

Fig.5.19 - Measured lengthening of north and south beams

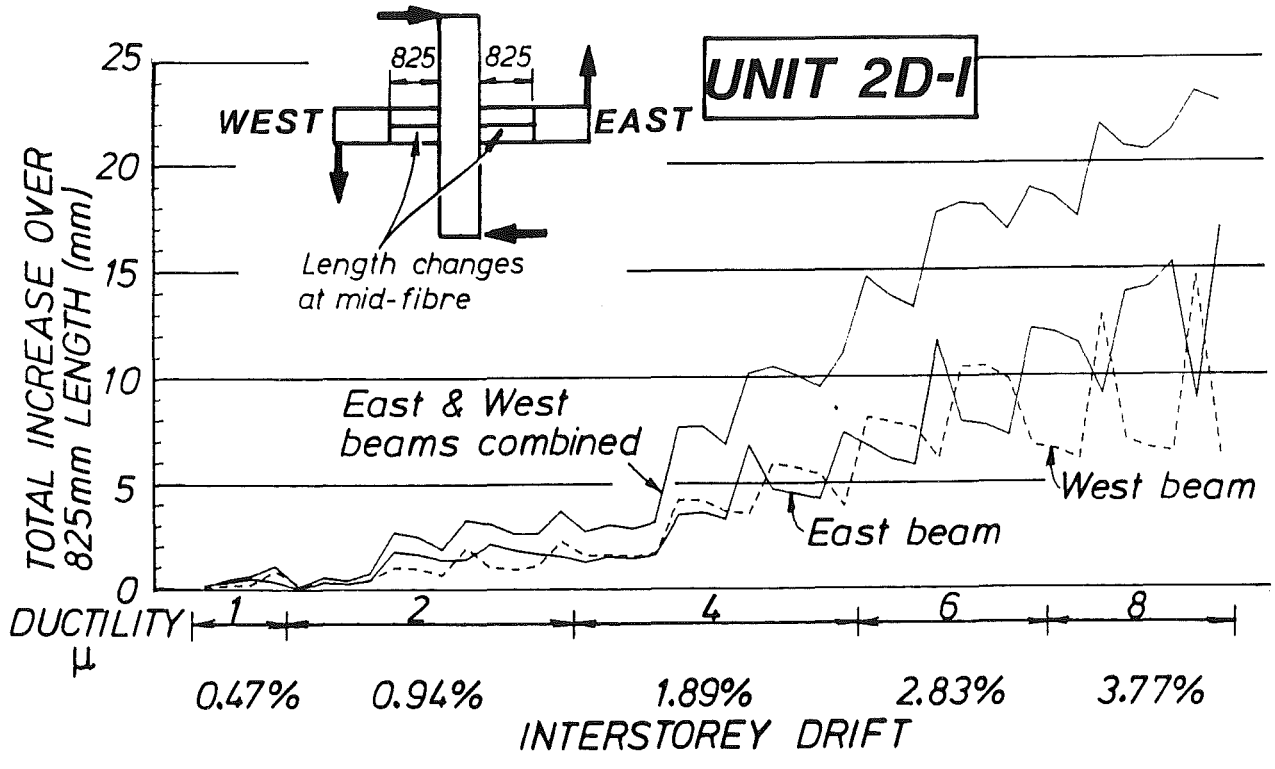

Fig.5.20 - Measured lengthening of east and west beams

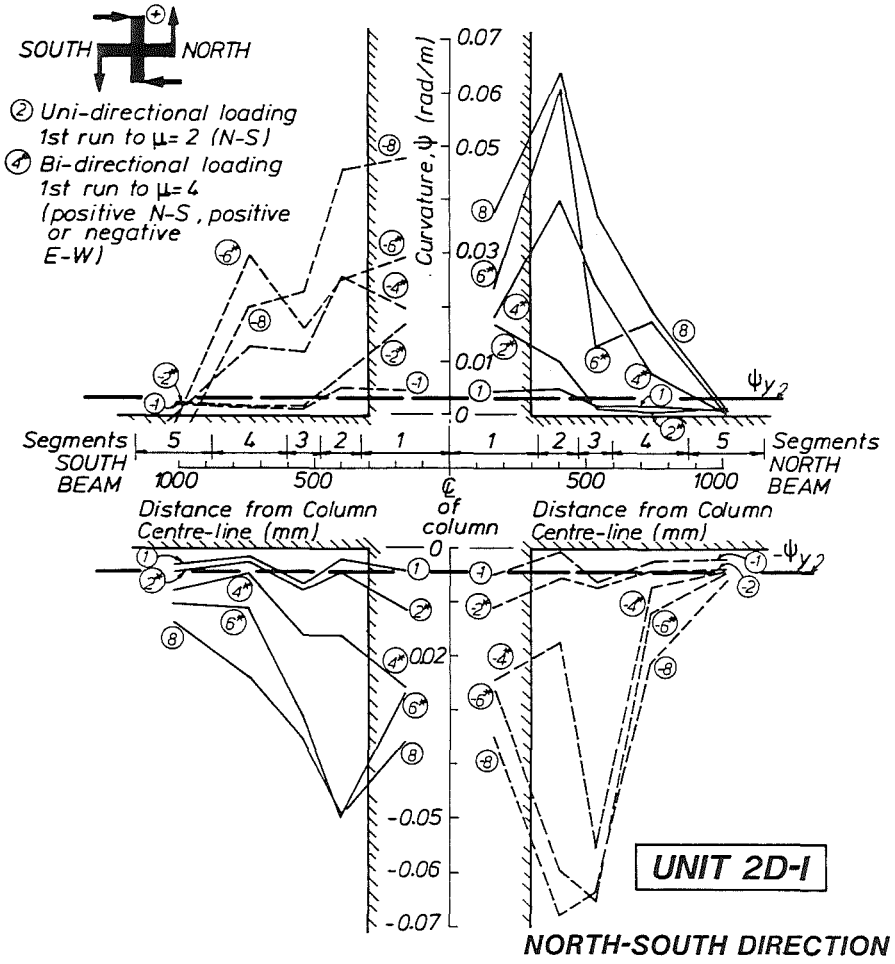

Fig.5.21 - Curvature profiles of north and south beams

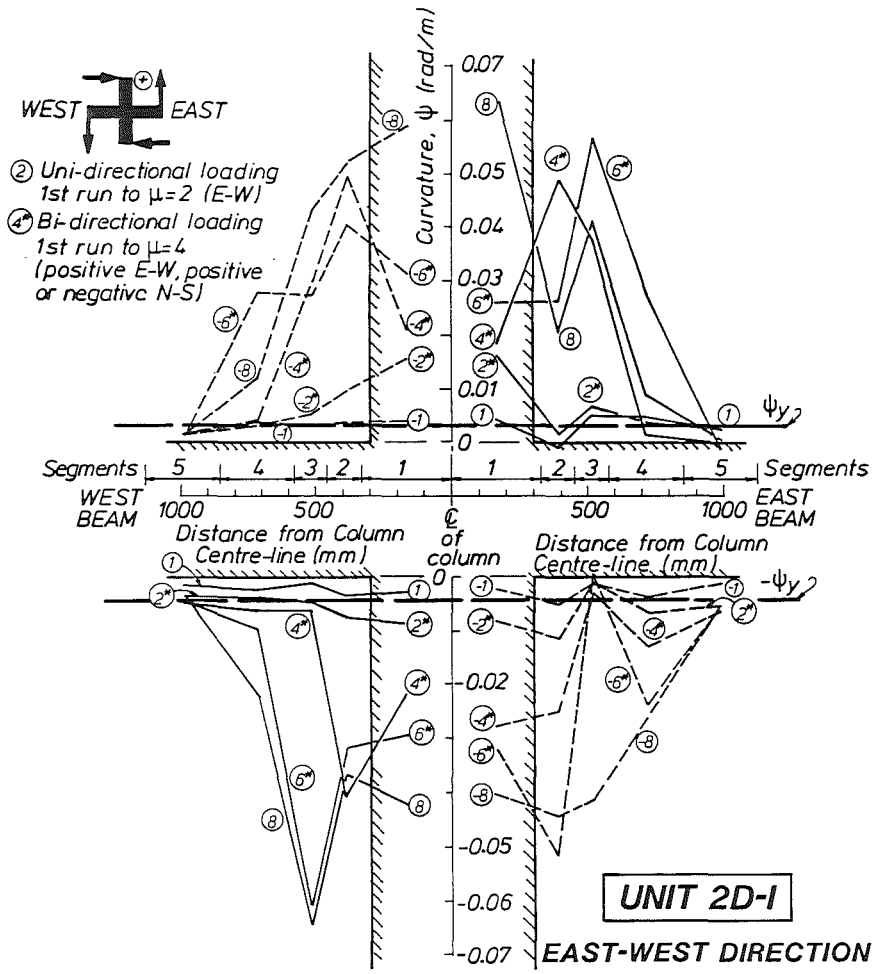

Fig.5.22 - Curvature profiles of east and west beams

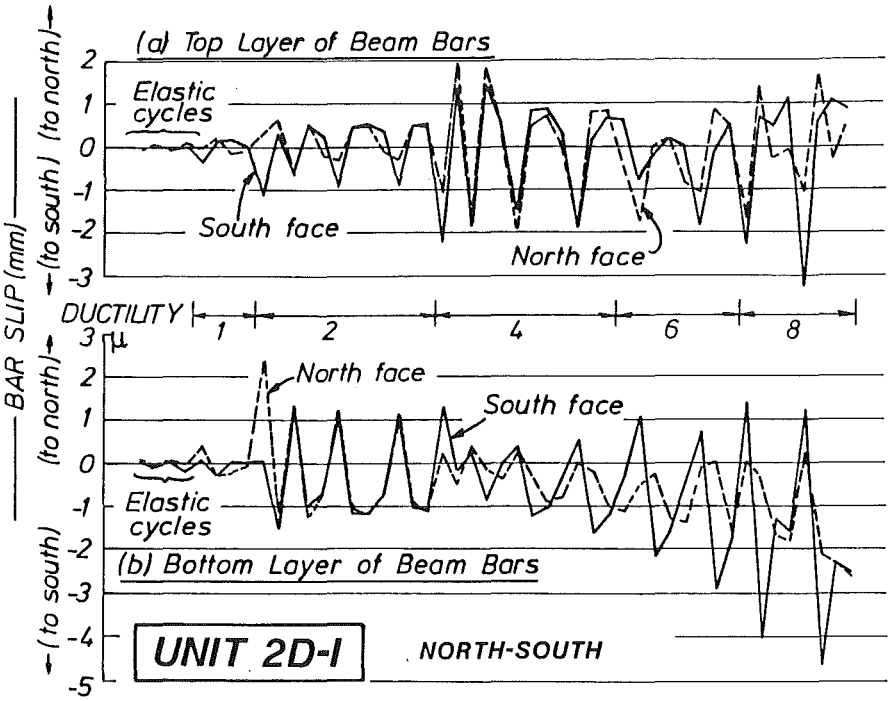

Fig.5.23 - Estimated slips of the north-south beam bars within joint core

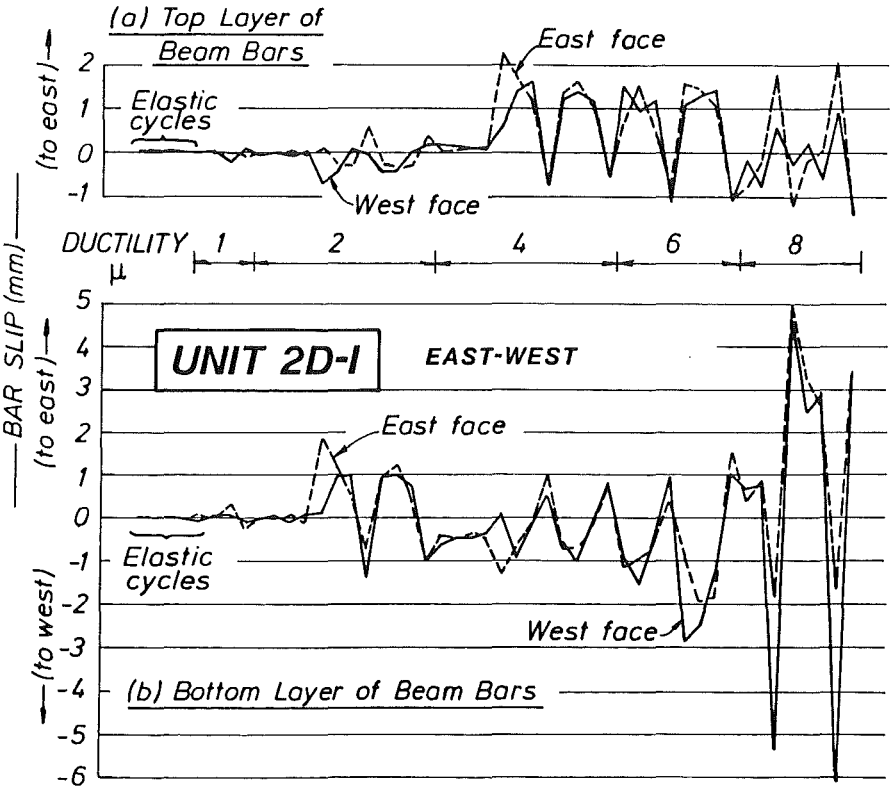

Fig.5.24 - Estimated slips of the east-west beam bars within joint core

In particular, slips in the east-west bottom layer beam bars (Figs.5.24(b)) could be as large as 4 to 5 mm. Complete slippage of these bars was noted in the last load run, as previously reported in Sections 5.1 and 5.2.

5.3.2 Decomposition of Displacements

Using the approach of Section 3.9, the major components of the total beam or storey displacements could be assessed. The results are given in Figs.5.25 to 5.28, highlighting the behaviour of the beams and the whole unit. However, it must be noted tht the component of displacement due to joint shear distortions, δ_j, could not be measured in this unit. Therefore it was assumed to be equal to the difference between the observed total displacement and the sum of the other displacement components due to beam and column deformations. Hence the results for the joint component for this unit do not necessarily match those for Unit 1D-I (see Section 4.3). By referring to Figs.4.23 to 4.25 for the first unit, it is seen that some "unaccounted for" beam displacements, due to inelastic shear deformations and unequal beam properties in the positive and negative sense, could amount to as much as 20% of the experimentally observed total displacement at the very large displacement ductility of ten. However, they were rather small at ductilities of two to four. Therefore, it is necessary to make allowance for these "unaccounted displacements" when interpreting the effects of joint distortions, as presented in the graphs.

Apart from the major difference just described, the discussions presented in Section 4.3.3 are considered also relevant to this test unit and hence are not repeated. In view of the similar behaviour of the beams, the beam component of total displacements is not sub-divided into two or three parts as was done in Figs.4.23 to 4.25.

5.4 BEAM BAR STRAINS

A total of 56 strain gauges were installed on the beam bars. Results for the north-south beam bars are plotted in Fig.5.29 for the range of ductilities between $\mu = 1$ and $\mu = 4$. Gauge strains in the east-west beam bars showed a similar pattern and are therefore not presented here. Like Fig.4.26 for Unit 1D-I, Fig.5.29 again demonstrates that strain gauges, particularly those at the column faces, gave readings significantly lower than realistic

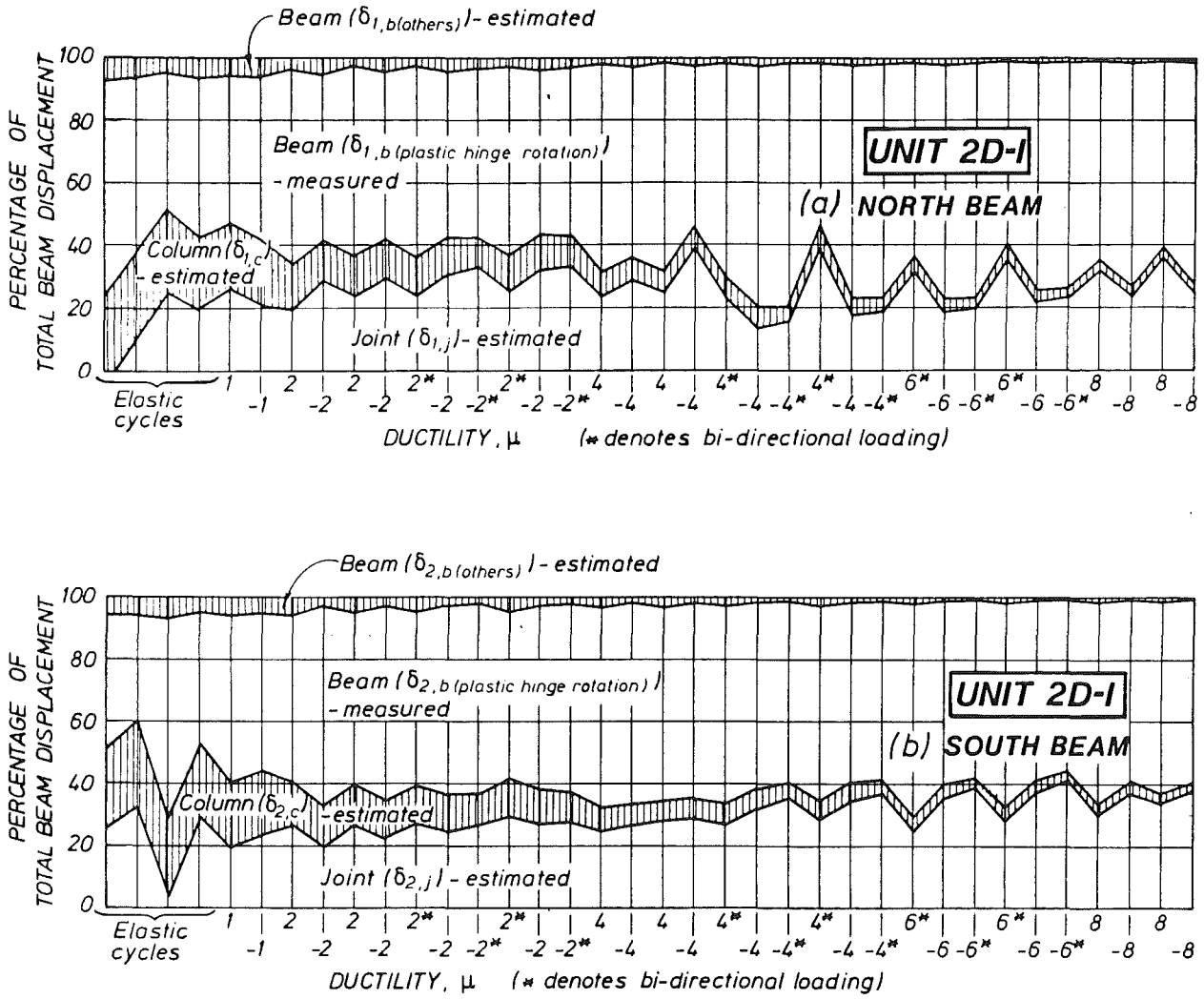

Fig.5.25 - Components of north and south beam displacements

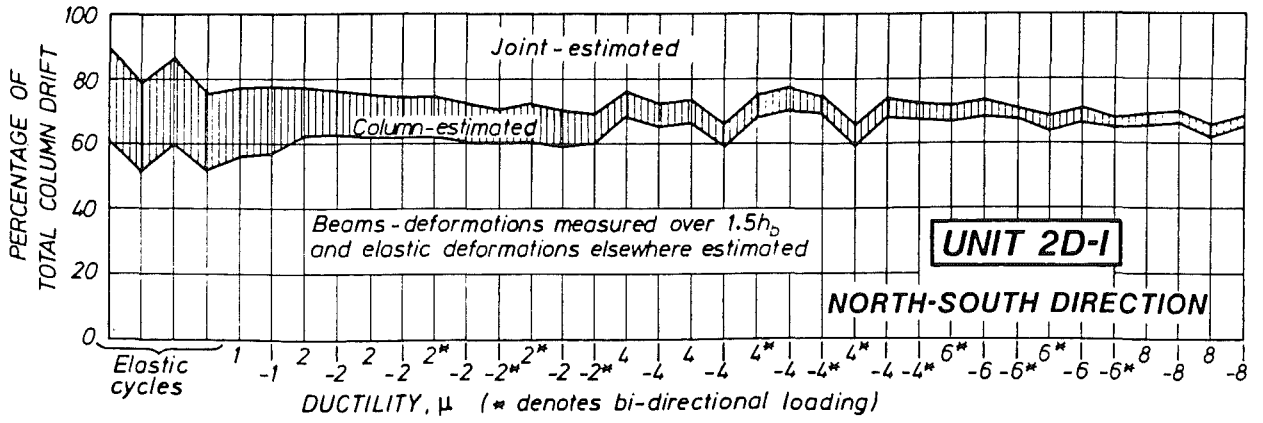

Fig.5.26 - Contributions to north-south interstorey lateral displacements during progressive loading

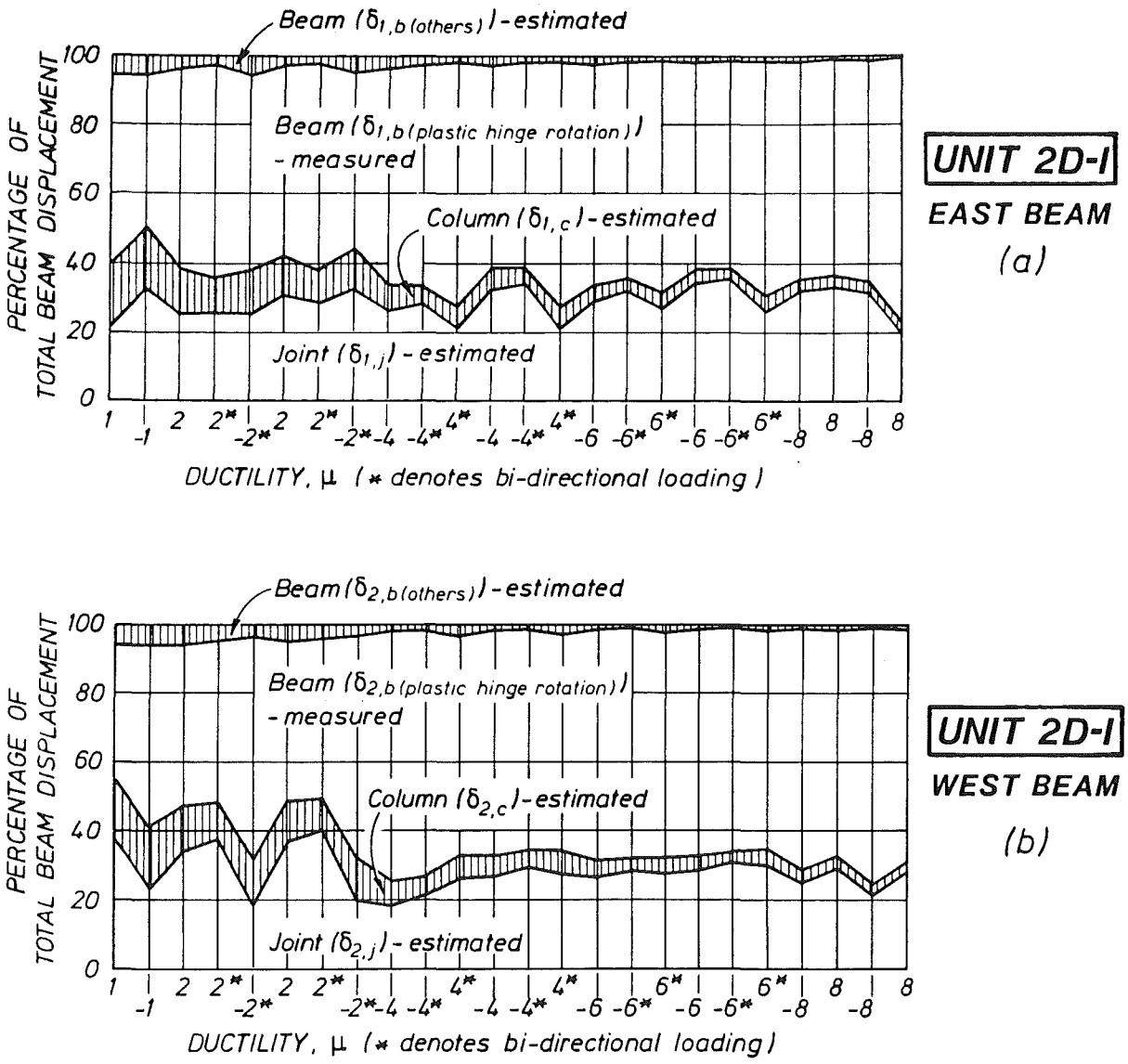

Fig.5.27 - Components of east and west beam displacements

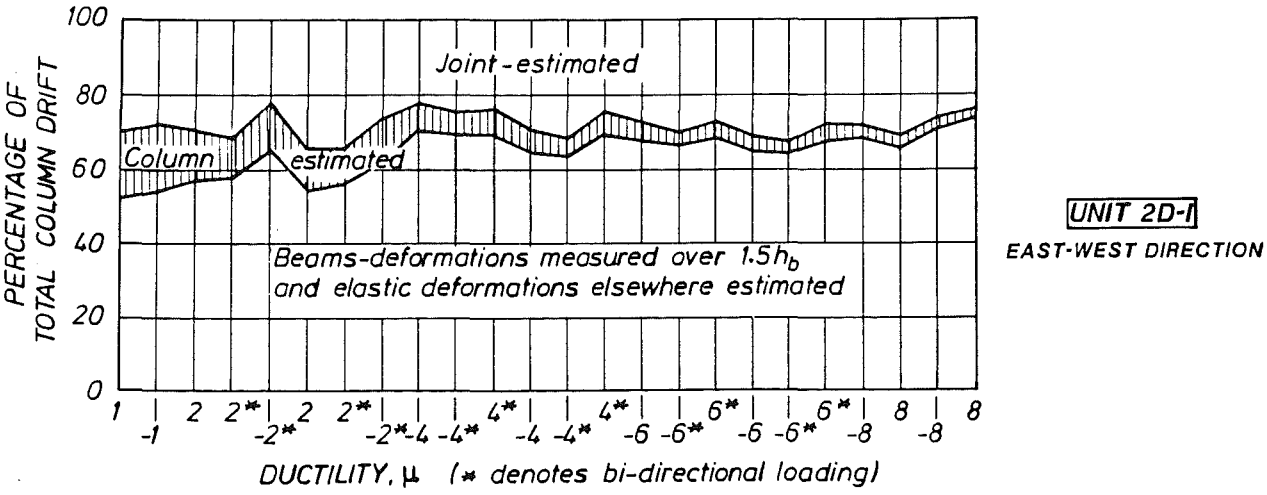

Fig.5.28 - Contributions to east-west interstorey lateral displacements during progressive loading

values. More "realistic" strains at beam bar levels in the plastic hinge regions of the beams, derived from linear potentiometer measurements, are shown in Figs.5.30 to 5.33 for beams in the north-south and east-west directions. Although more irregular the strain patterns are similar to those shown in Figs.4.27 and 4.28 for Unit 1D-I. It is evident that bi-directional loading on this Unit 2D-I did not drastically change the strain patterns. Nevertheless the bond strength of beam bars within the joint core deteriorated more rapidly, as evidenced by the complete slippage of the east-west bottom beam bars in the second cycle to ductility $\mu = 8$. Other conclusions, as in Section 4.4, are also drawn, namely :

(1) While compressive stresses in the beam bars were developed, strain hardening in compression did not materialize. Since the applied vertical forces at beam tips were approximately the same as those observed with Unit 1D-I, it is estimated that the maximum compressive stresses in the beam bars at the column faces were of the order of $0.5f_y$ at top and $1.0f_y$ at bottom.

(2) As inelastic displacements increased, the plastic hinge spread towards the free end of each beam.

5.5 SLAB BAR STRAINS

Reasons for extensively strain gauging the slab bars of the first unit were given in Section 4.5. Difficulties in obtaining reliable results for quantitative analysis were also discussed. Despite this experience, practical restrictions permitted only 38 strain gauges to be attached to the slab bars of this Unit 2D-I, in the south-west quadrant at the beam-slab interface as can be seen in Fig.3.15. Strain results are presented in this report only for the north-south top (Fig.5.34) and bottom (Fig.5.35) layer D10 slab bars up to a ductility level of $\mu = 4$. Strain at higher ductilities are considered more erratic because of severe disintegration of concrete and the relatively large vertical displacements between the beam web and the slab (see Fig.4.31). Strain patterns for the east-west slab bars were found to be similar. Conclusions regarding the strain distributions in the slab bars shown in Figs.5.34 and 5.35, relevant to the discussions in Chapter 7, are similar to those discussed in Section 4.5. They are itemised as follows :

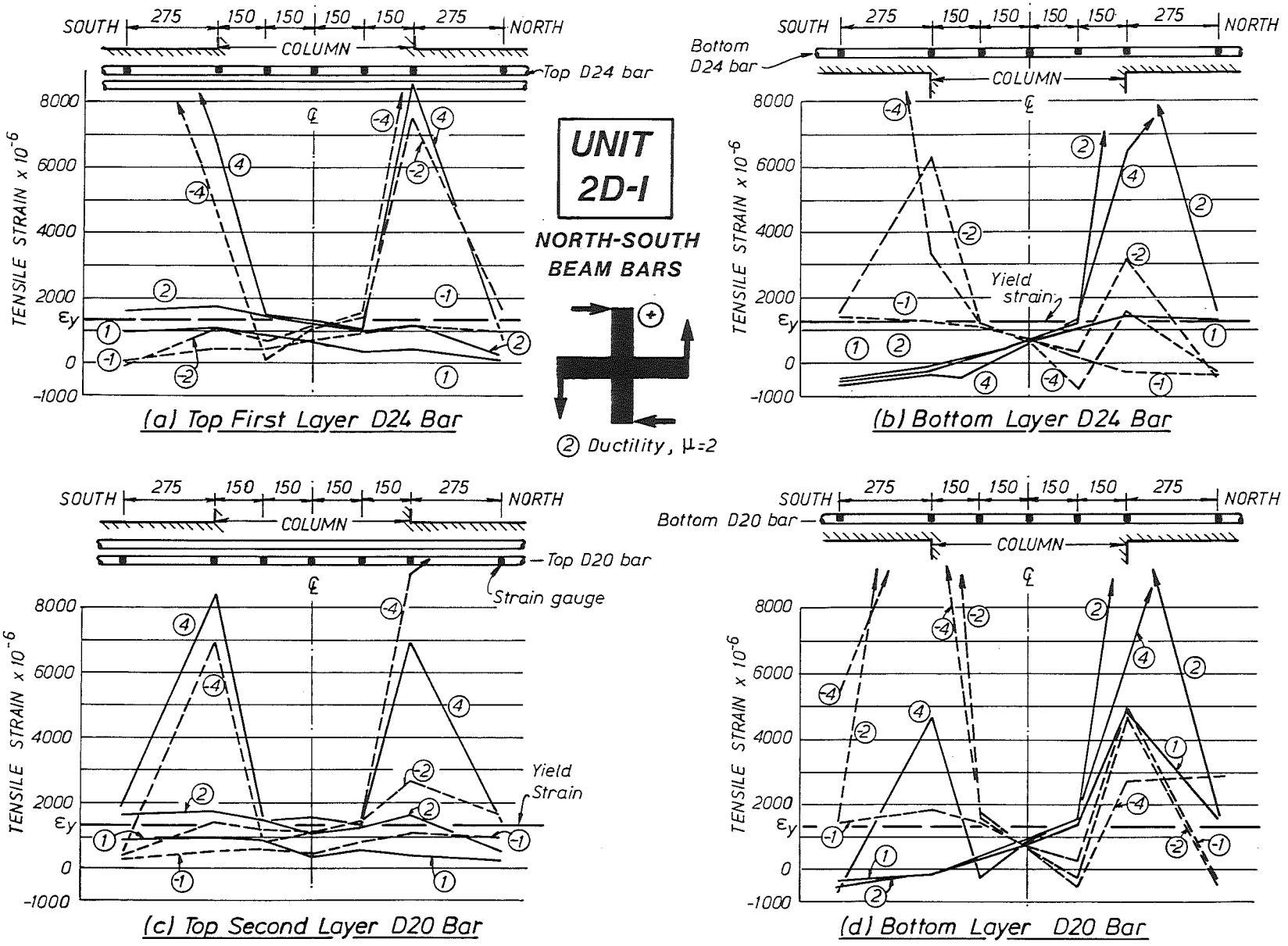

Fig.5.29 - North-south beam bar strains measured by strain gauges

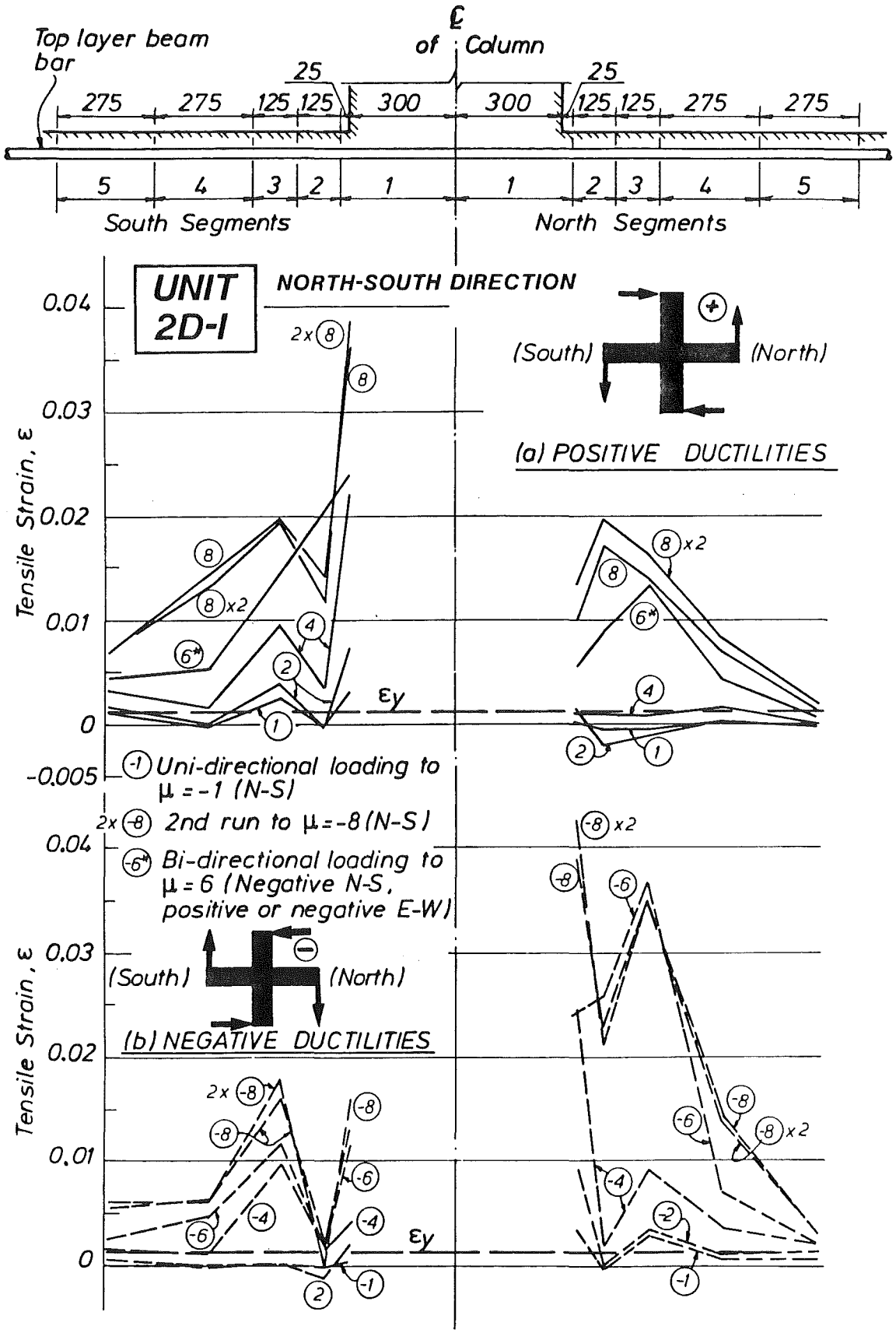

Fig.5.30 - Strain distributions at top layer beam bar level as estimated from linear potentiometer measurements (north-south direction)

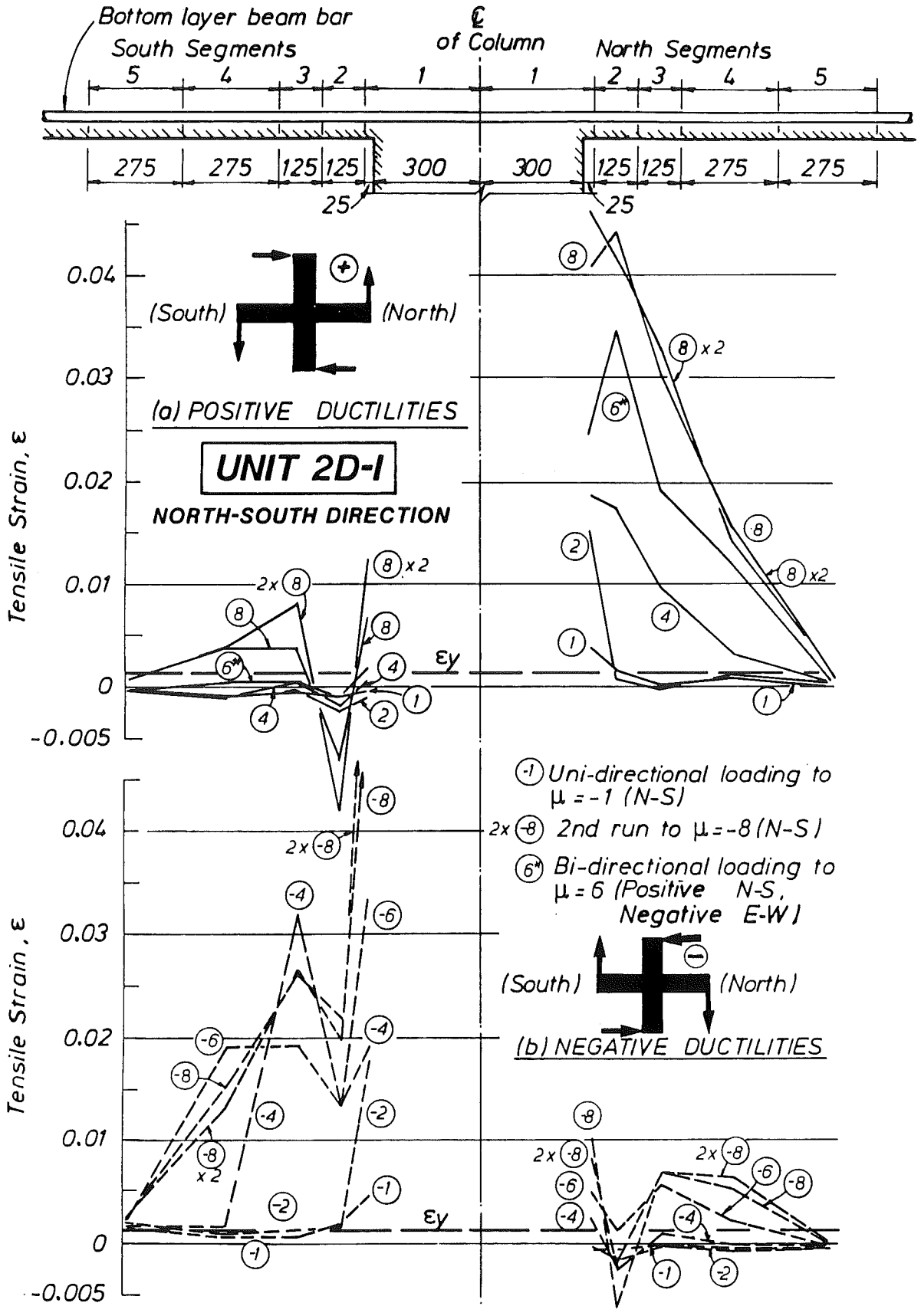

Fig.5.31 - Strain distributions at bottom layer beam bar level as estimated from linear potentiometer measurements (north-south direction)

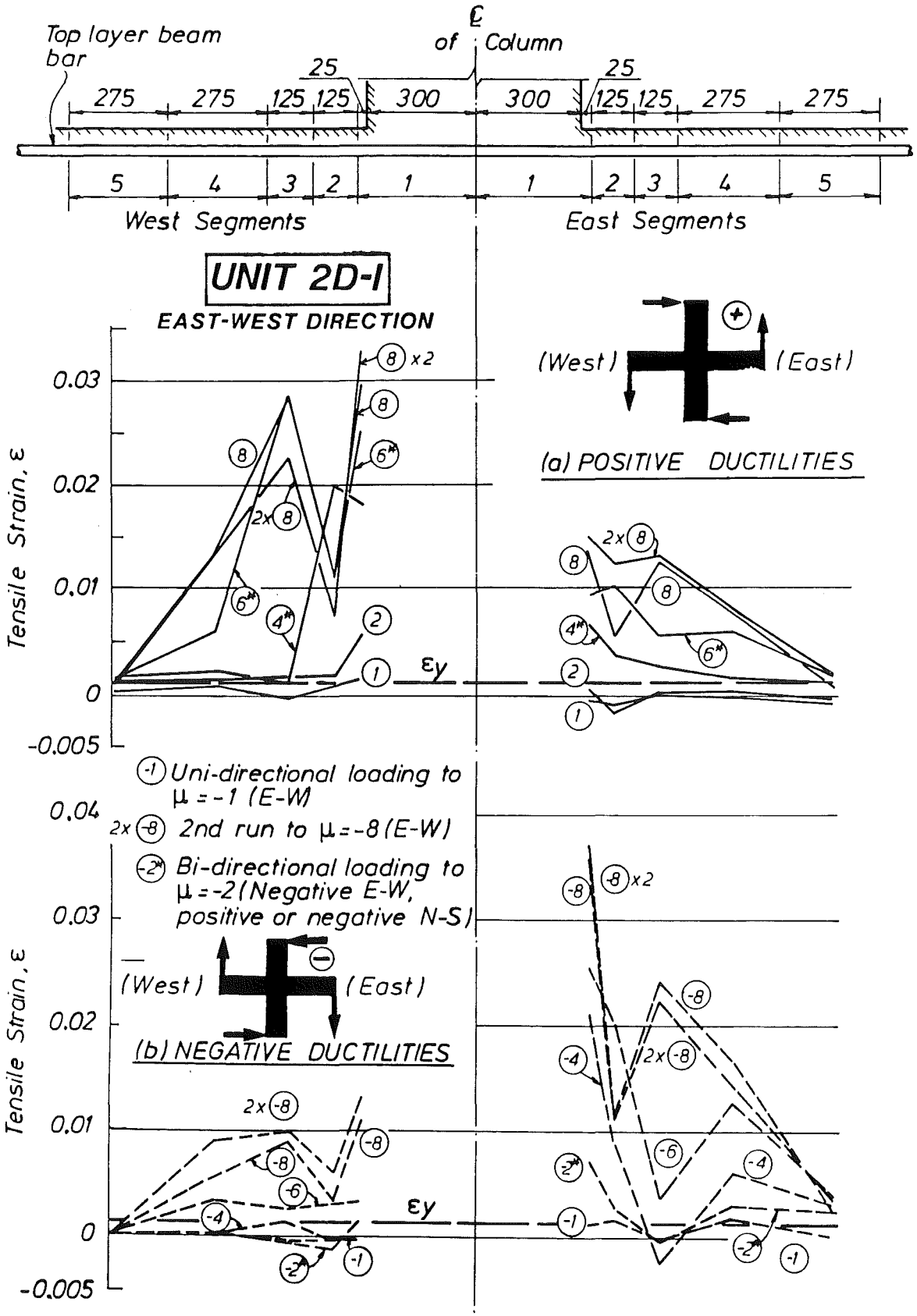

Fig.5.32 - Strain distributions at top layer beam bar level as estimated from linear potentiometer measurements (east-west direction)

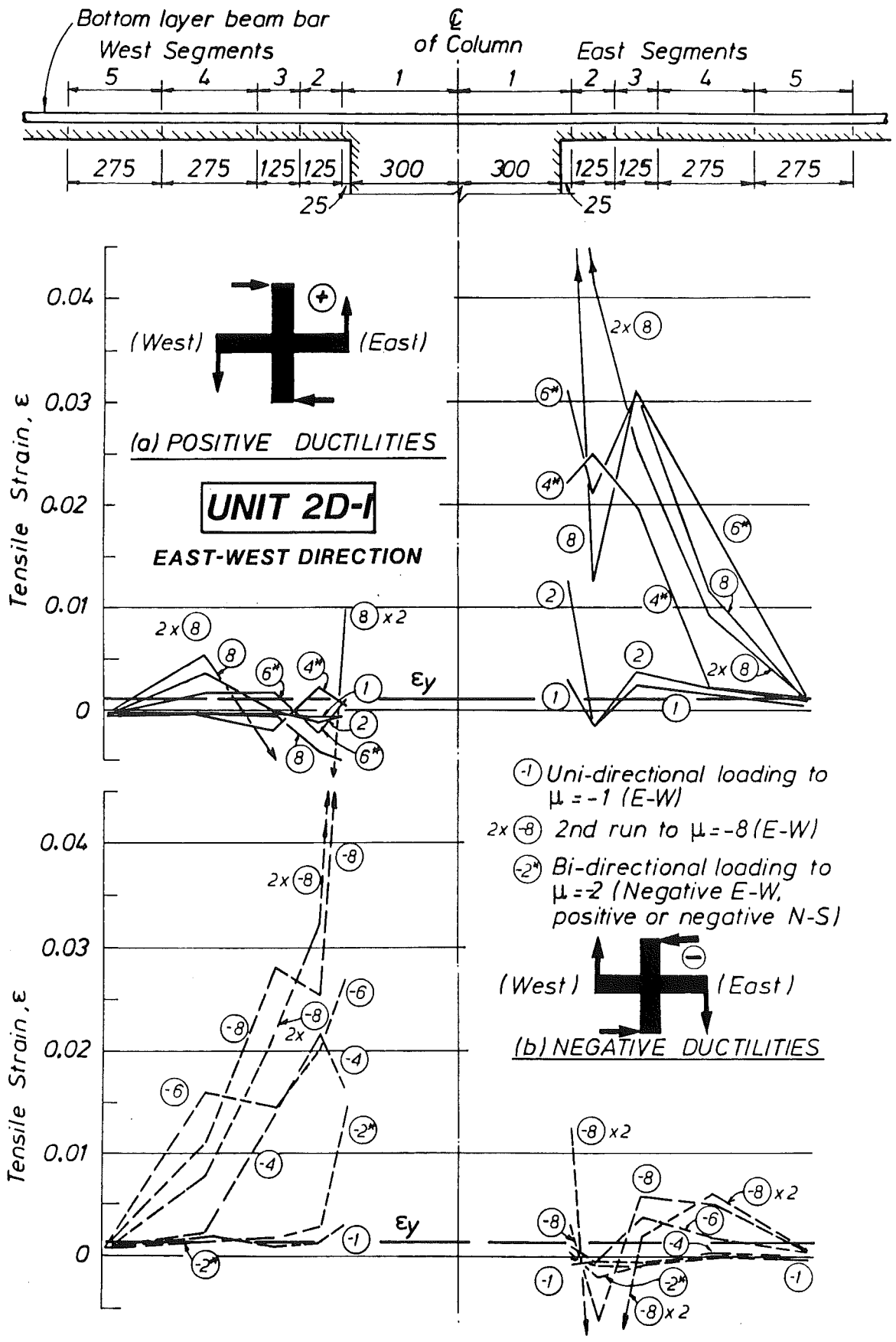

Fig.5.33 - Strain distributions at bottom layer beam bar level as estimated from linear potentiometer measurements (east-west direction)

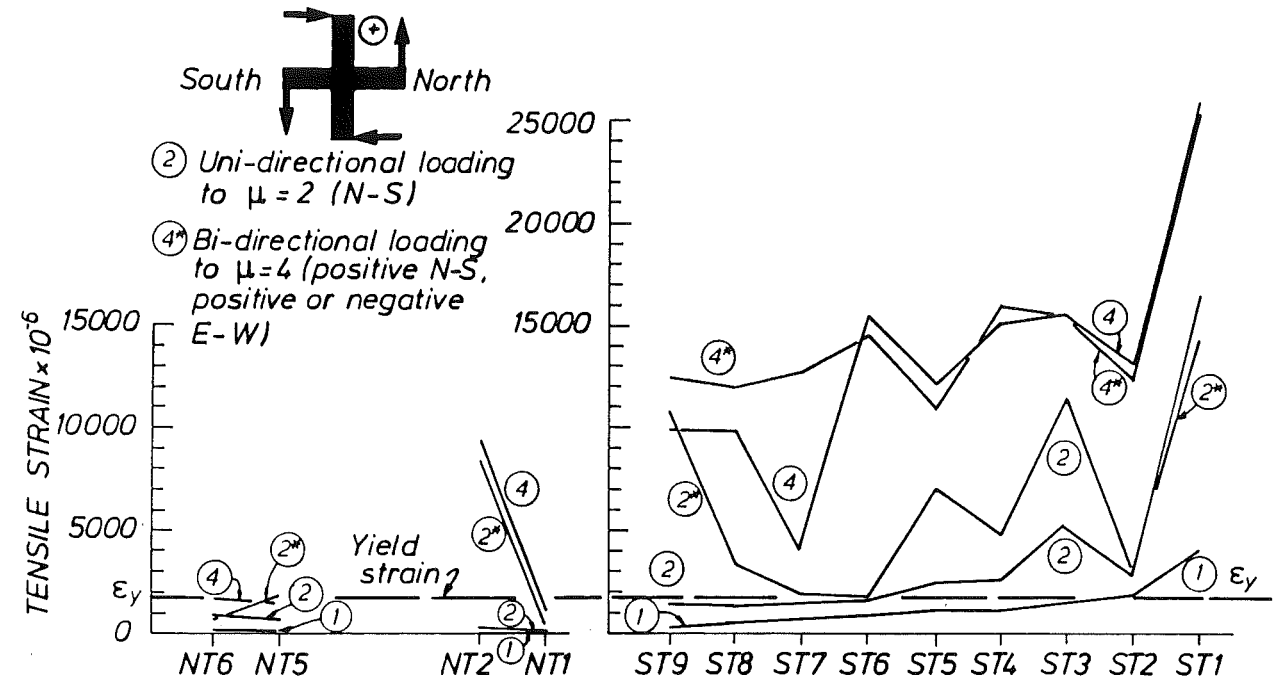

(a) POSITIVE DUCTILITIES

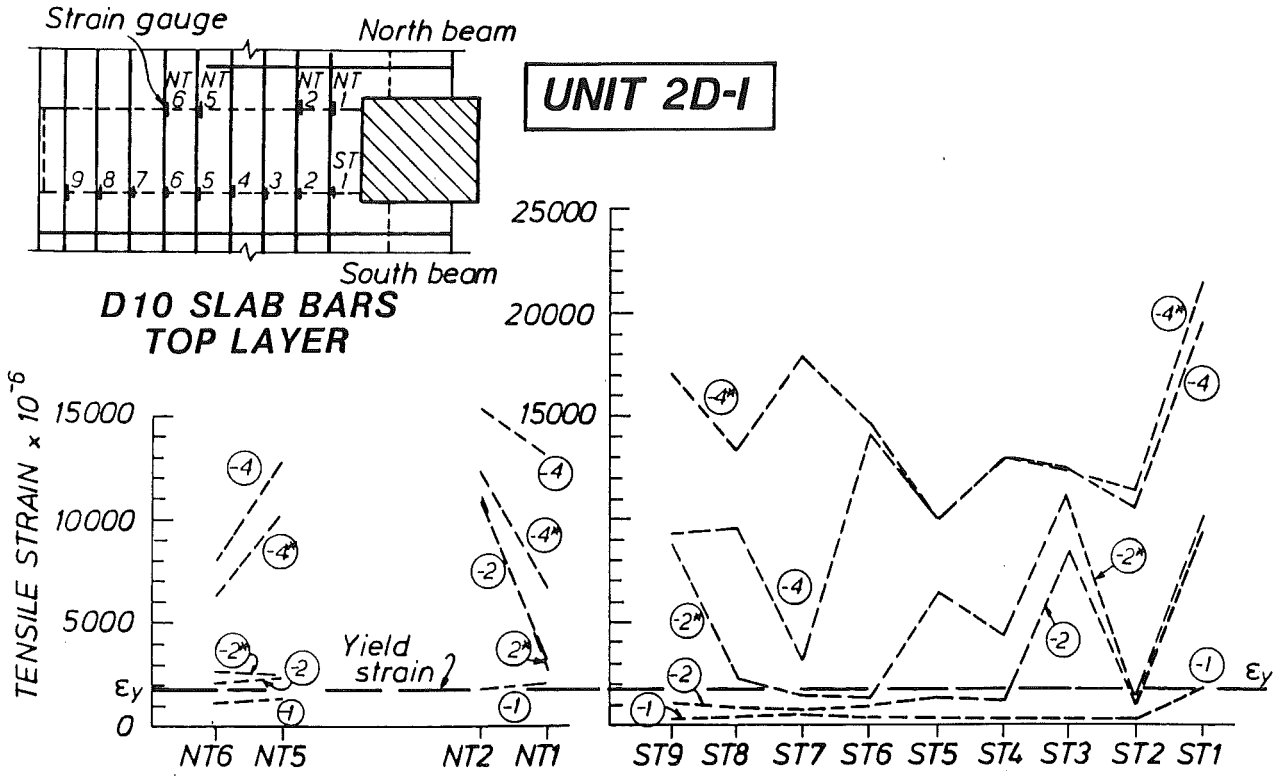

(b) NEGATIVE DUCTILITIES

Fig.5.34 - North-south top layer slab bar strains

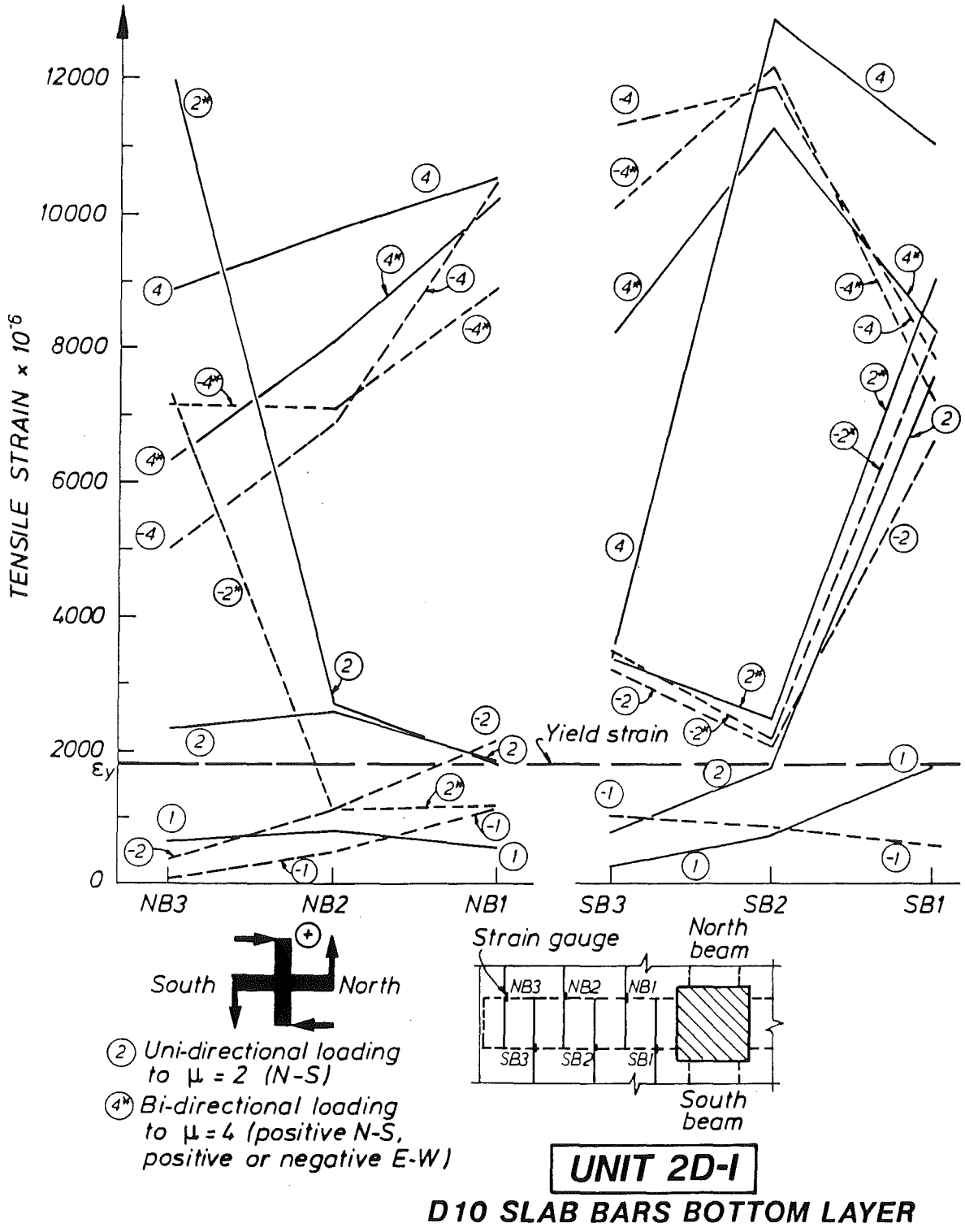

Fig.5.35 - North-south bottom layer slab bar strains

(1) Strain changes in the top layer slab bars near to the column, in particular the two monitored by strain gauges ST1 and ST2 (Fig.5.34), indicate that the bending actions of the north and south beams dominated the behaviour of these bars. This is expected from the consideration of strain compatibility. Although no compressive strains were observed, the differences in strains between positive and negative ductilities suggest that compressive stresses were developed in the bars in the vicinity of the column. This implies that when the south or north beam bent upwards, a compression flange was formed. However, it appears that with increasing ductilities, this compression flange became less conspicuous.

(2) As with Unit 1D-I, under uni-directional north-south loading, tensile strains in the tension flange decreased towards the (west) free end of the slab. When bi-directional loading was applied, however, the smaller tensile strains, for instance in bars ST9, ST8 and ST7 (Fig.5.34), increased by a large amount. It should be noted that under east-west loading, the north-south slab bars acted as transverse reinforcement to develop a diagonal compression field in the plane of the slab.

(3) The top layer slab bars in the middle strip, such as those represented by ST3 to ST6 in Fig.5.34, appeared to be consistently in tension even though the beam was subjected to upward bending. This can be related to the tension flange action to be discussed in Chapter 7.

(4) The flexural behaviour of a slab, in agreement with the sense of bending of the adjoining beam, can be quite significant at ductilities of $\mu = 1$ to $\mu = 2$. However, at higher ductilities this bending action of slab appeared to have diminished. This follows from point (3) above and the strain variations in the bottom layer slab bars in Fig.5.35.

5.6 COLUMN BAR STRAINS

In the region of the joint a total of 36 strain gauges were mounted to seven of the longitudinal HD28 bars along the west and north faces of the column. The numbering system for the column bars is self evident from Figs. 5.36 and 5.37 which show strain variations at various ductilities. Results for the corner bar C4 have been partly duplicated, but the ductilities are denoted in different directions in the two figures and accordingly interpretation should take this into account. Additional gauges were provided to the intermediate bars, namely C2, C3, C5 and C6, at levels 1A and 4A. These were meant to supplement gauge readings taken at levels 1 and 4, where strains would be affected by the truss mechanisms of joint shear resistance (see Fig.4.33) as well as by actions resulting from the anchorage of intersecting beam bars.

In Fig. 5.36(a), strains in columns bars C1 to C4 are shown when the column was subjected to loading in the north-south direction only. The observed strain variations in bars C1 and C4 generally agreed with the loading conditions. Tensile strains were recorded in these corner bars over the full height of the joint at ductility levels 2 and higher. According to the loading, compression strains are to be expected at one end.

Compressive strains, recorded at levels 1A and 4A in bars C5 and C6, (not shown in these figures), which were subjected to the same north-south loading as was bar C4, appear to justify the propostion [39] that the deviation from expected compression strains was caused by the action of intersecting beam bars and particularly local bond forces introduced by the beam bars. Strains under north-south action of column bars C5, C6 and C7 (Fig. 5.37) are not presented here. It is also to be noted that on many occasions, strains at levels 2 and 3 of bars C1 and C4 (and also bars C5 to C7, which are not shown) were higher than the corresponding strains at levels 1 and 4. Bi-directional loading effect might aggravate this strain irregularity. From the results for column bars C4 and C7 under east-west loading, conclusions drawn are similar to those for bars C1 and C4 when north-south loading was applied.

For intermediate bars C2 and C3 under uni-directional north-south loading, consistent tensile strains of significant magnitudes, though below yield level, were obtained (Fig. 5.36(a)). Irrespective of beam bar effects

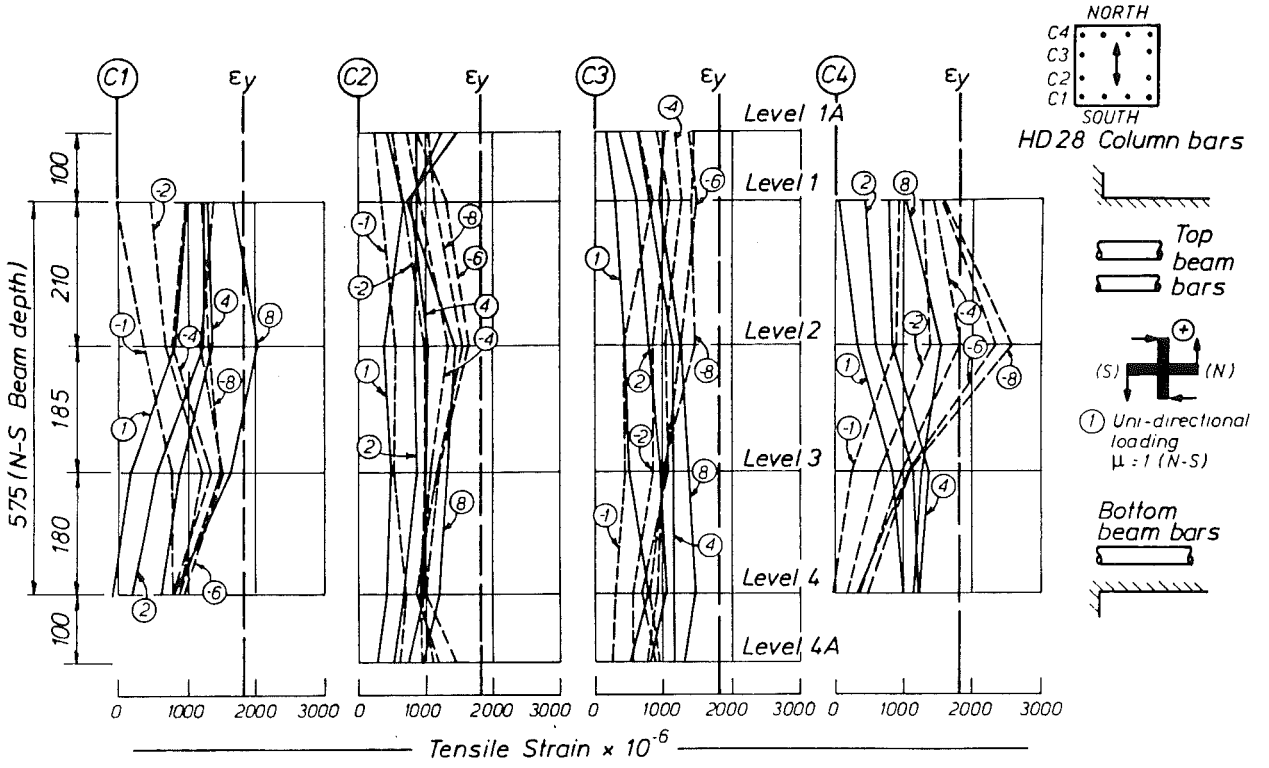

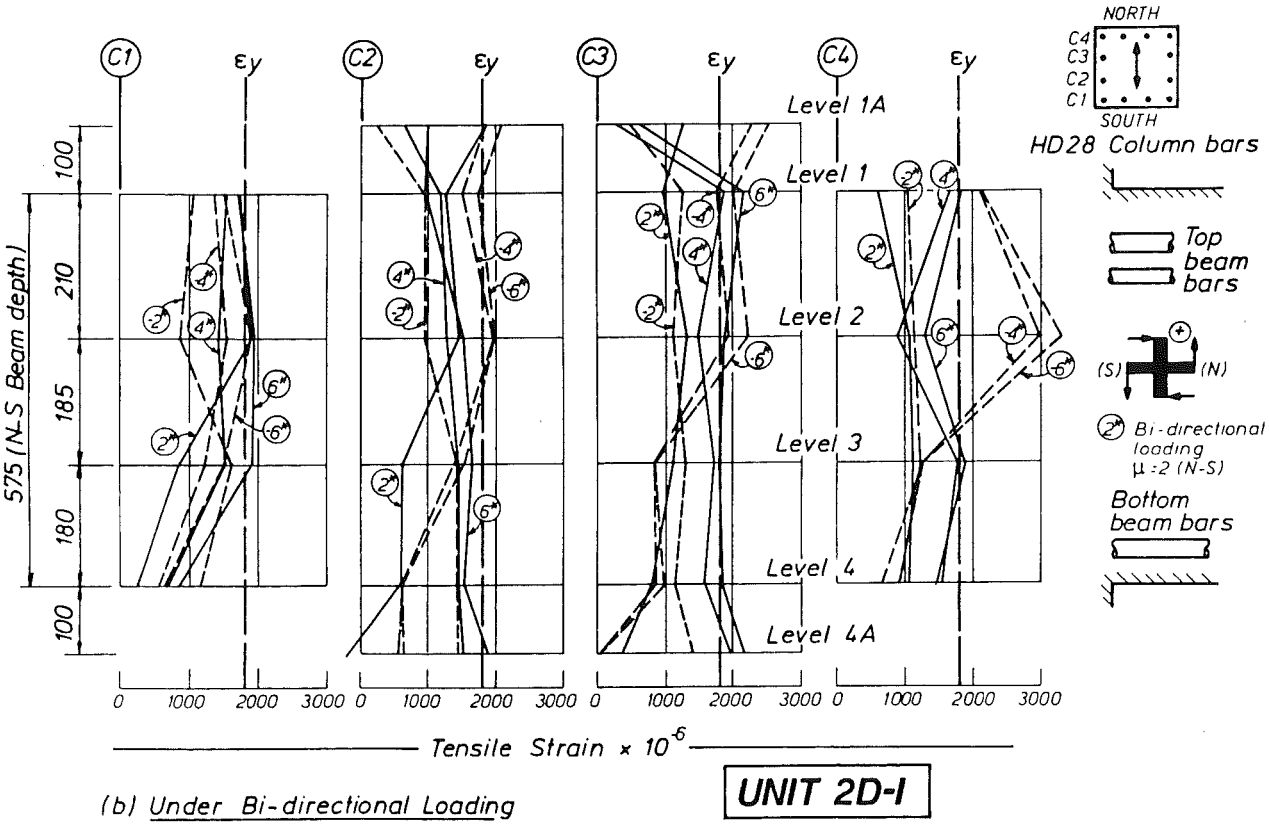

Fig.5.36 - West face column bar strains in the joint core

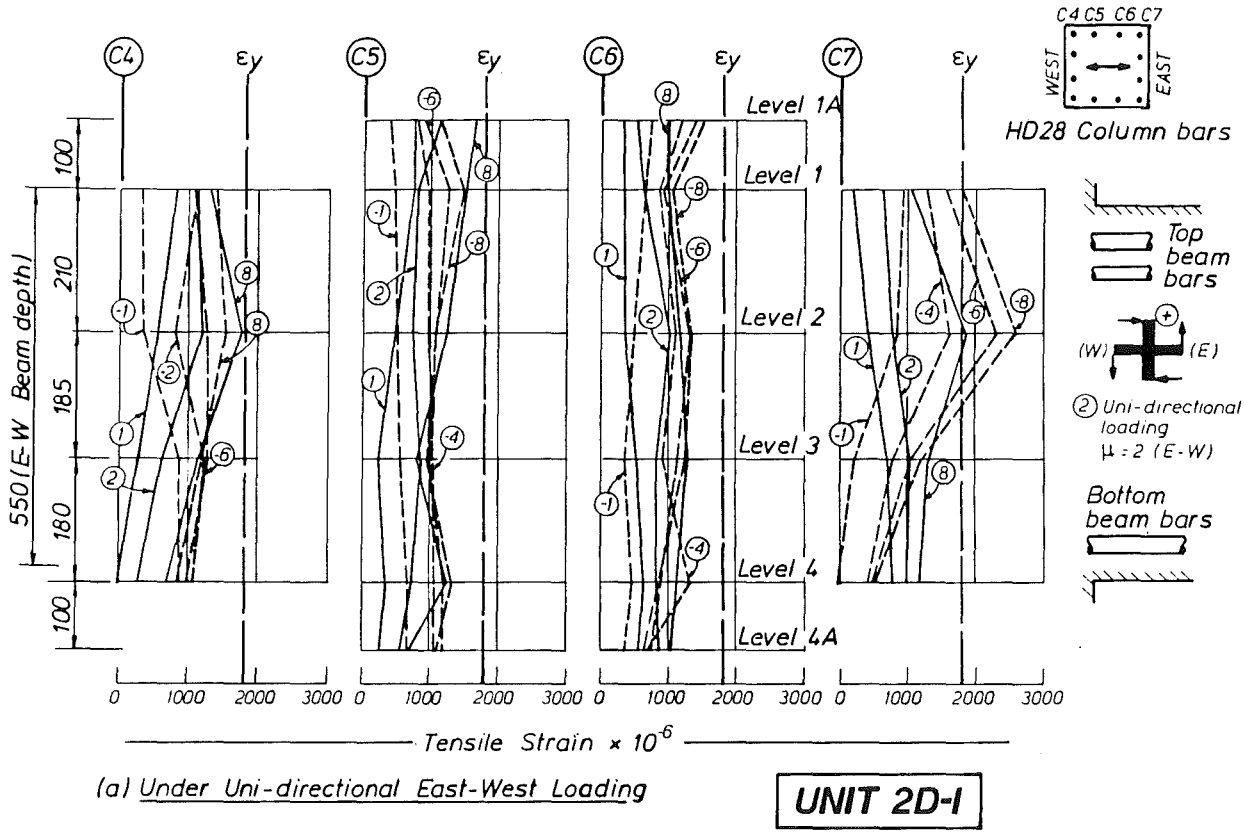

(a) Under Uni-directional East-West Loading

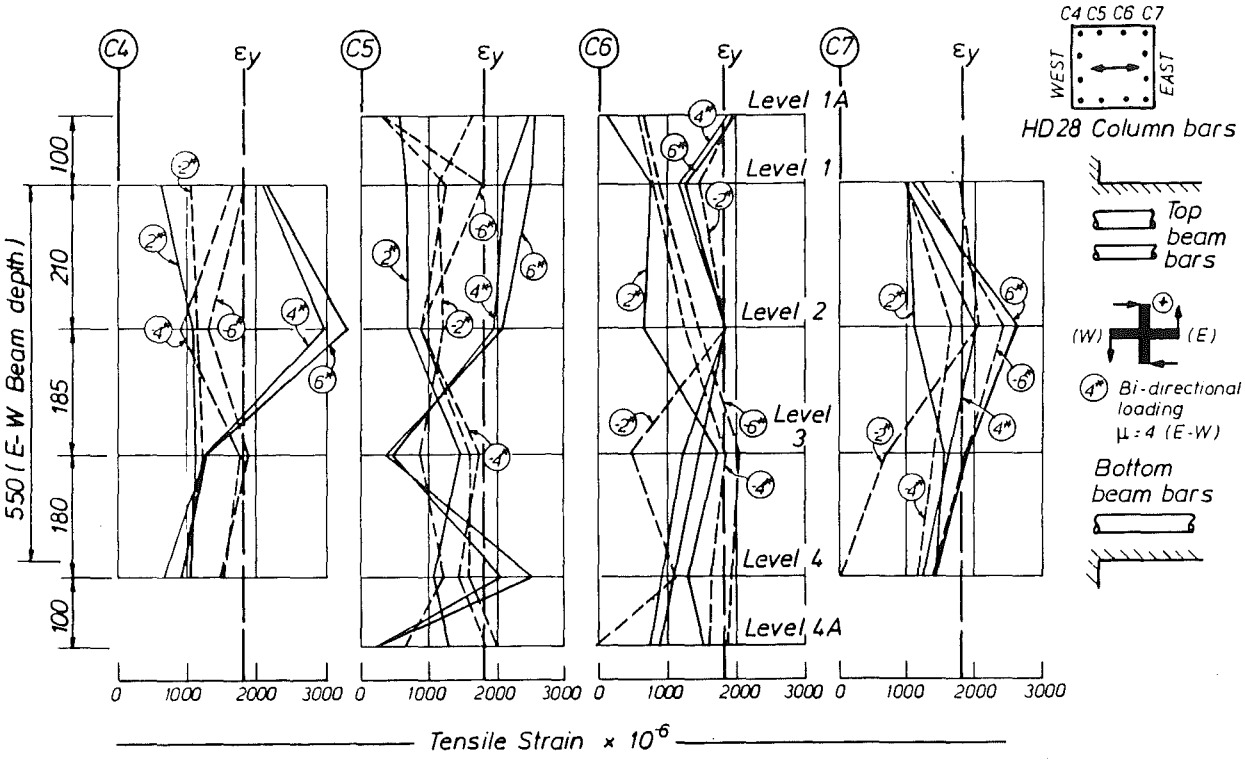

(b) Under Bi-directional Loading

Fig.5.37 - North face column bar strains in the joint core

mentioned above, the strains at levels 1A and 4A also confirmed this tensile state. It is to be remembered that, because of the absence of axial compression, the columns acted as vertical beams. Thus intermediate column bars, such as C2 and C3, are expected to be in tension at levels 1 and 4. Strain distributions for the interior bars C5 and C6 under east-west loading are similar (Fig. 5.37(a)). The participation of the intermediate bars in resisting vertical joint shear is therefore evident. As has been explained in Section 4.6, their contribution is essential in the truss mechanism to develop the necessary diagonal compression field.

Strain patterns shown in Figs. 5.36(b) and 5.37(b) for bi-directional loading depict more irregularity. This is to be expected. However, the reasons for the development of tensile strains in all column bars within and in the vicinity of the joint are basically the same as those considered for uni-directional loading. The considerably higher strain values generated under biaxial loading and shown in the figures, sometimes exceeding yield level, indicate that under this condition the column bars were subjected to a more severe tensile stress state. Therefore, if column hinging is to be avoided, the consideration of biaxial effect in the vicinity of a joint, within the capacity design approach, becomes even more important.

While these findings highlight the functioning of the joint shear mechanisms, it is to be remembered that interior columns of this type, and hence joint cores, will always be subjected to axial compression due to graity loads. Such compression forces will reduce, or even suppress, tensile stresses generated in column bars within and near the joints.

5.7 STRAINS IN THE JOINT TIES

As seen in Figs. 5.38 and 5.39, the R16 joint ties were extensively strain gauged. For easier comparison, strains at positive and negative ductility levels are presented separately. It was mentioned in Section 3.5.3 that hoop ties in layers 2 and 3 had a pair of strain gauges placed at each location, one being at the top side and the other at the underside of the bar. From the test, it was found that differences of as much as 50% in readings for two such gauges were quite common. This is thought to have been caused by bending deformations which occurred in the horizontal ties due to dowel action when diagonal cracks crossed these bars. In some cases, principally under

biaxial bending conditions the differences during large imposed ductilities could even be 200%.

The following observations can be made with respect to the patterns shown in Fig. 5.38 which records strains in the north-south legs of the ties when these are subjected to loading defined in terms of north-south ductilities. These observations are similar to those made previously in Section 4.7.

(1) Tensile strains indicate that the horizontal ties were active. It is believed that tie forces were utilized to resist joint shear forces rather than to provide confinement to the core concrete within the joint. The column required no confinement, as there was no axial compression load applied to it. Moreover, the theoretical flexural compression zones of the sections above and below the joint were not large. Tie strains increased gradually and consistently with increased ductility levels. This phenomenon is believed to match with the postulation that, as cyclic inelastic loading progresses, the truss mechanism, relying on internal transverse tension forces, becomes more significant than the strut mechanism.

(2) Under uni-directional (north-south) loading, the mid-depth ties (layers 2 and 3) were generally subjected to larger strains than the outer ties (layers 1 and 4). This is to be expected when using the concepts of the truss mechanism in resisting joint shear. Some of the bi-directional (both north-south and east-west) loadings changed this pattern, but the overall trend remained the same.

(3) Type F legs exhibited larger strains than types D and E. The likely reasons for the differences in the contributions of parallel tie legs to transverse tension were discussed previously in Section 4.7 and Fig.4.35.

(4) Type E legs exhibited strains comparable to those measured in type D ties. All hoop ties appear to have efficiently participated in resisting joint shear forces.

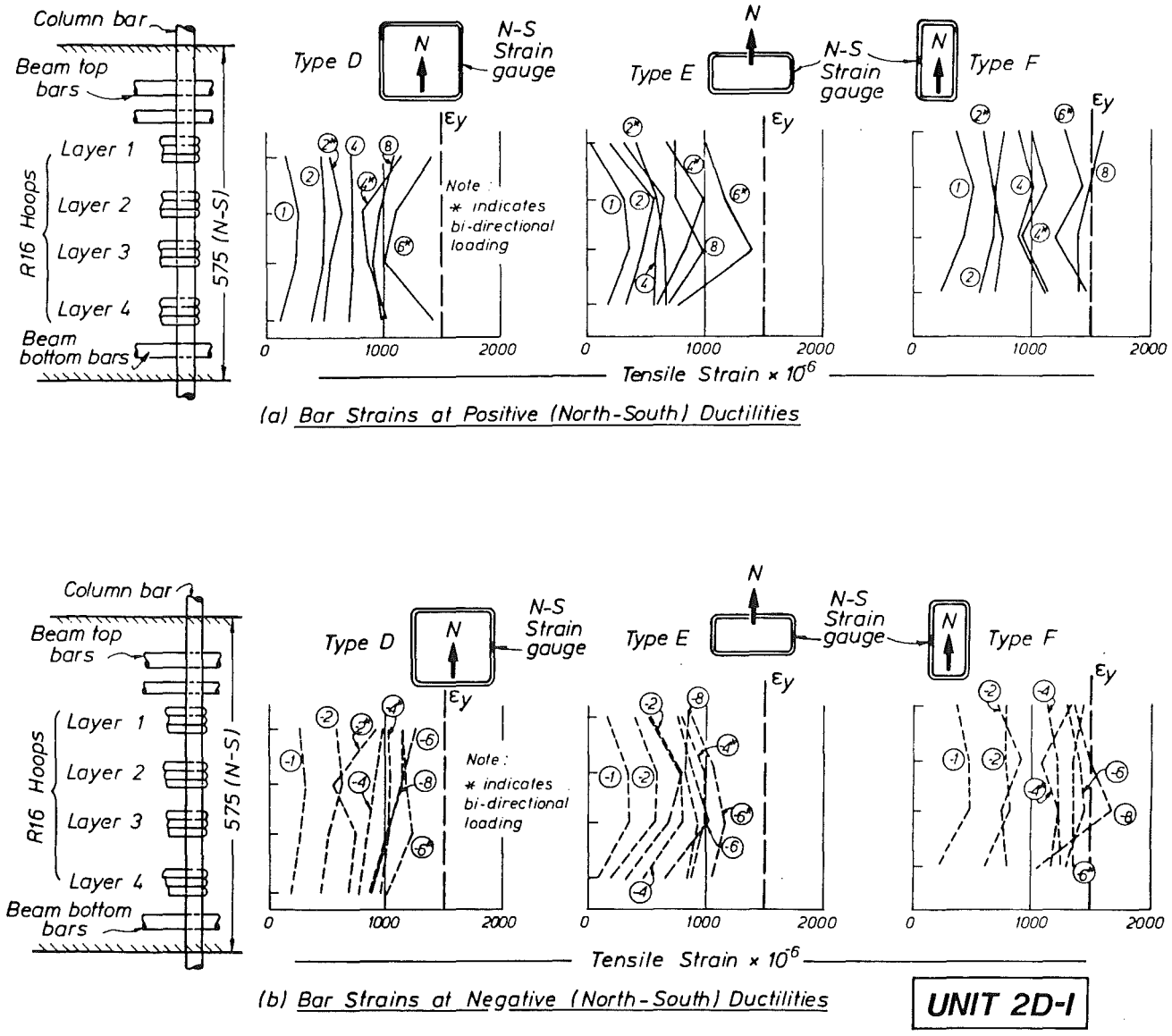

Fig.5.38 - North-south joint horizontal hoop strains under north-south loading

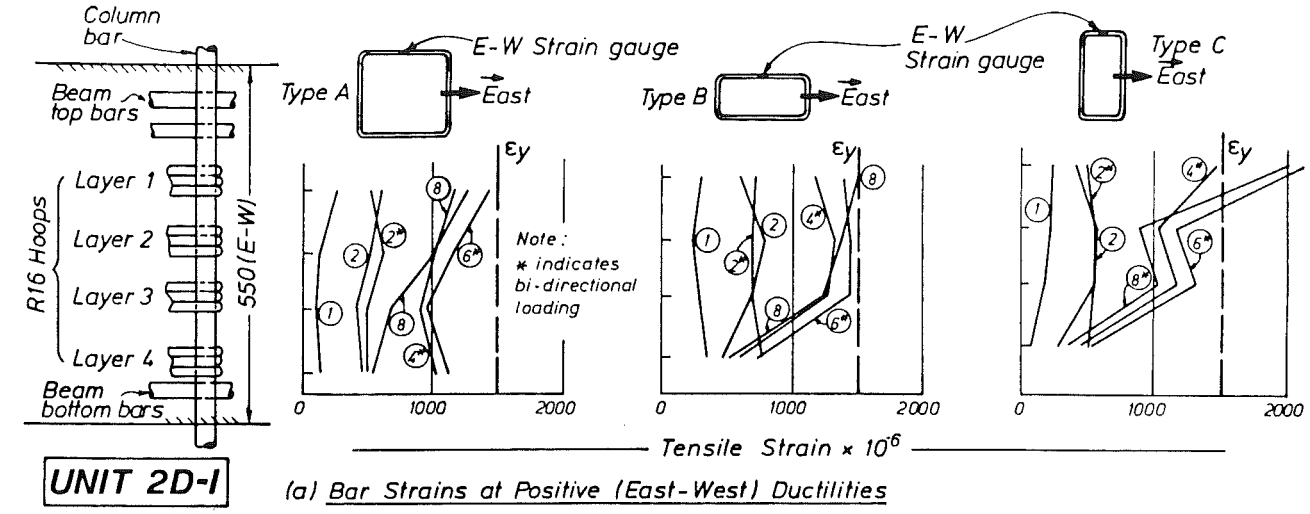

(a) Bar Strains at Positive (East-West) Ductilities

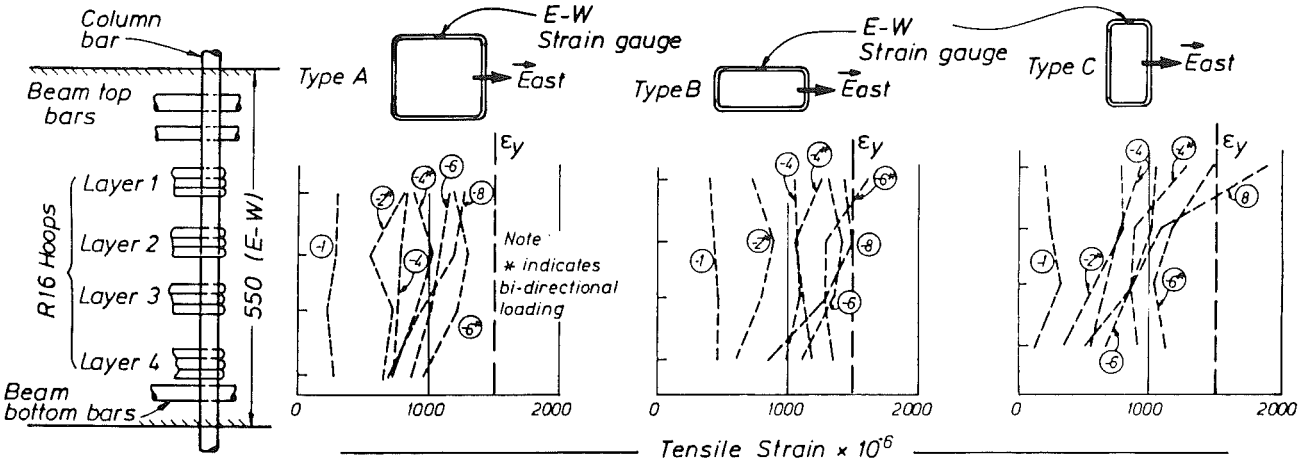

(b) Bar Strains at Negative (East-West) Ductilities

Fig.5.39 - East-west joint horizontal hoop strains under east-west loading

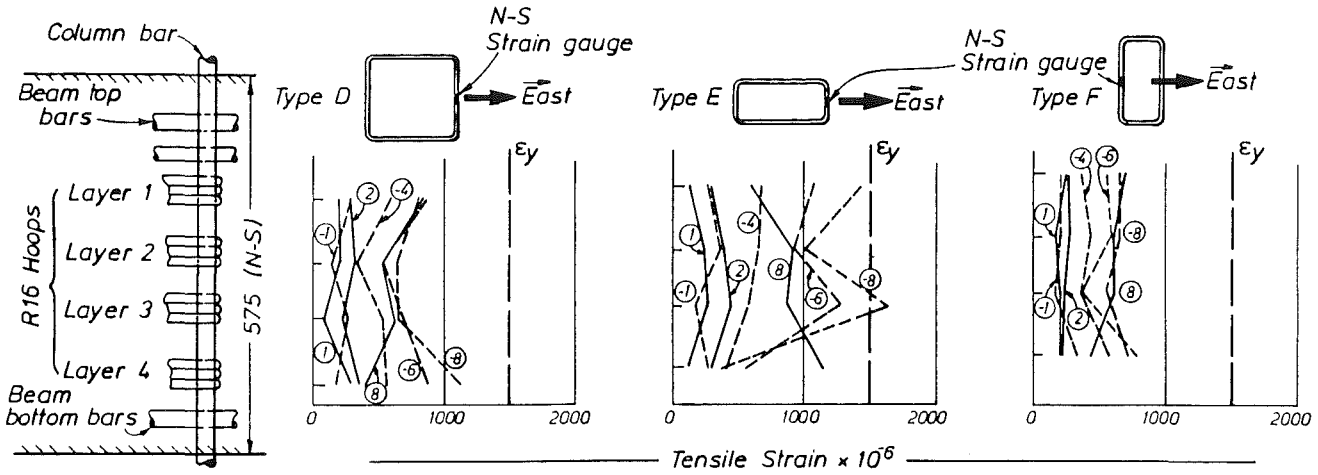

(a) North-South Bar Strains at East-West Ductilities

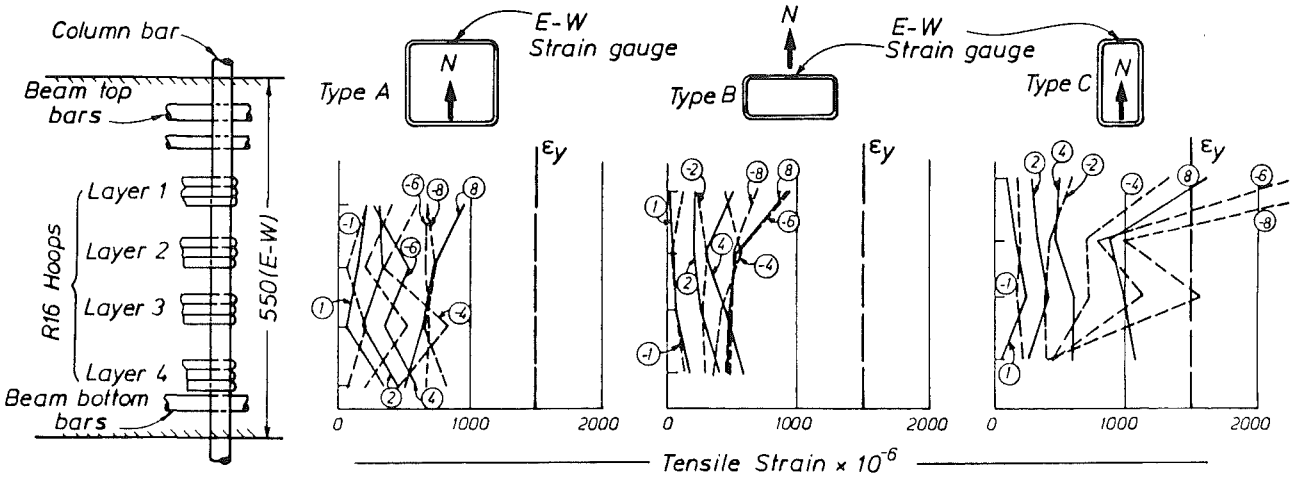

(b) East-West Bar Strains at North-South Ductilities

UNIT 2D-I

Fig.5.40 - Strains in horizontal joint hoops under loading transverse to the orientation of the tie legs

Test results shown in Fig. 5.39 for the east-west legs (types A, B and C) under loading in terms of east-west ductilities are similar and lead to the same observations as discussed above. The only exception is type C tie in layer 1. Unexpectedly the measured strain jumped to 0.0023 at a ductility of μ = -6 (north-south only). Results for subsequent loadings (μ = 6*, ±8) are therefore questionable for this tie.

Strain results were also evaluated for conditions when seismic forces were applied at different angles, as shown in Fig. 5.40. North-south tie legs (types D, E and F) were monitored during east-west loading only. Similarly strains in east-west legs (types A, B and C) were recorded during north-south loading. These are three possible causes for the development of tensile strains in the bars. First, the bond stresses arising from the action of the beam bars could affect the strain readings of layers 1 and 4. Second, the tie legs provided the necessary containment to the joint core which underwent dilation due to diagonal cracks. Finally, in conjunction with the action of containment, residual tensile stresses in the bars should also be considered. With repeated cyclic loading, particularly after the imposition of large ductilities, diagonal cracks, however small, will not completely close after the removal of the load. Thus residual tensile stresses in ties, which have no particular function in terms of load resistance, are inevitable. They will increase with cumulative ductility. Strains of types D, F, A and B were quite moderate (Fig.5.40), the maximum being only of the order of 0.001. Types E and C exhibited somewhat larger tensile strains. This could be an indication of the anchorage stress transferred from the long legs which were resisting joint shear in their directions. The extremely large strains recorded for type C leg in layer 1 at high ductilities (Fig.5.30(b)), should be considered unreliable.

CHAPTER 6

TEST RESULTS OF UNIT 2D-E

6.1 GENERAL BEHAVIOUR

The test of this last unit took about four weeks to complete with twenty cycles of loading up to a displacement ductility factor of thirteen having been attained. In terms of interstorey drifts, however, the displacements imposed in this test are comparable to those relevant to the interior joint (2D-I) test, as explained in Section 3.7.1. In terms of sustained strength and energy dissipation, the overall performance of this test unit 2D-E was better than that of 2D-I, although not as good as that of Unit 1D-I.

The test unit at different stages of loading is illustrated by the photographs in Figs. 6.1 to 6.7 as well as Fig.3.5(c). As expected, plastic hinges formed in the three beams at the column faces. The flexural and flexural shear cracks in the beams were similar to those observed in Unit 2D-I. The maximum deflection due to sliding shear, measured vertically between two lines across a crack, of the east beam was 6 mm while that of the north or south beams was approximately 4 mm. Concrete spalling and crushing became significant starting from a ductility level of eight (Fig. 6.5). Bar buckling took place at a ductility of eleven (Fig.6.6) and thirteen (Figs. 6.7 (a) and (b)). However, no obvious slippage of bars within the joint was noted.

In this test it was possible to observe cracking at the only exposed west face of the joint. As in the first test (Chapter 4), fine diagonal cracks formed and closed in accord with loading directions. The maximum crack width measured was less than 0.5 mm.

The crack pattern at the top surface of the slab can be seen in Fig. 6.8 and also in some of the photographs in Figs. 6.1 to 6.7. When the pattern is compared with that of Unit 2D-I (Fig.5.7), the slab diagonal cracks are seen to be less dense in this exterior joint assembly. This difference is thought to have been caused by the bar curtailments as can be compared in

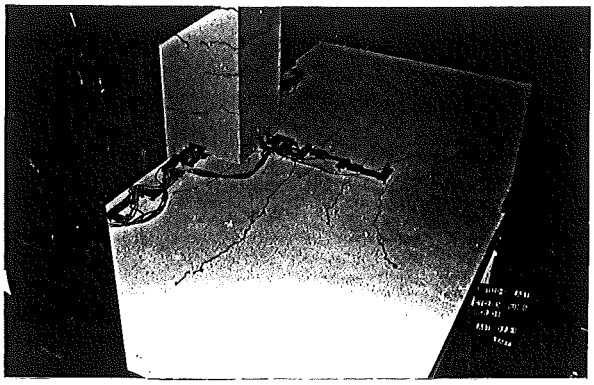

(a) Slab at μ = -1 (EW)

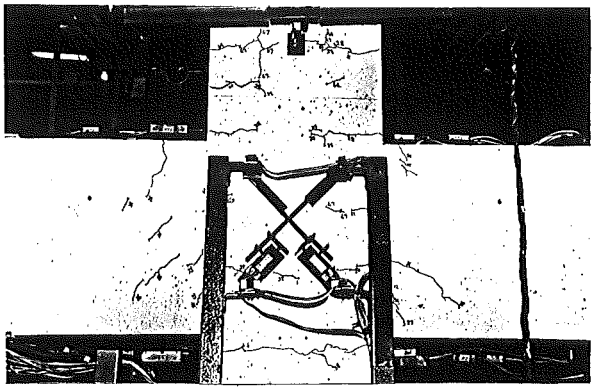

(b) West face joint at μ = +1 (EW)

Fig.6.1 - Unit 2D-E in cycle 3 to ductility of μ = 1 (EW)

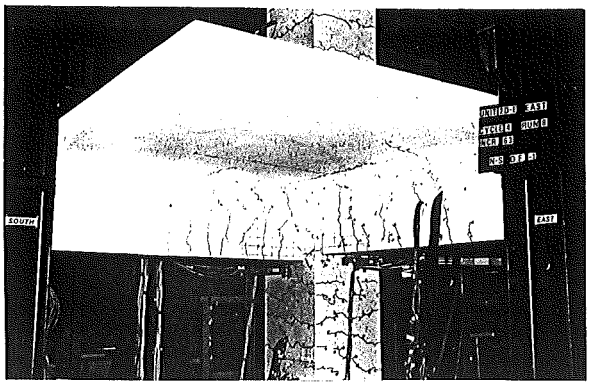

(a) South and east beams at μ = -1 (NS)

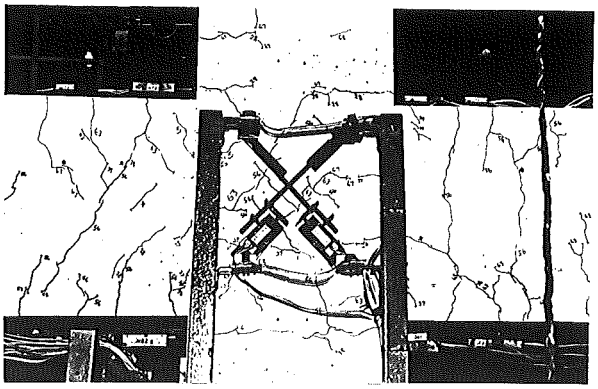

(b) West face joint at μ = -1 (NS)

Fig.6.2 - Unit 2D-E in cycle 4 to ductility of μ = 1 (NS)

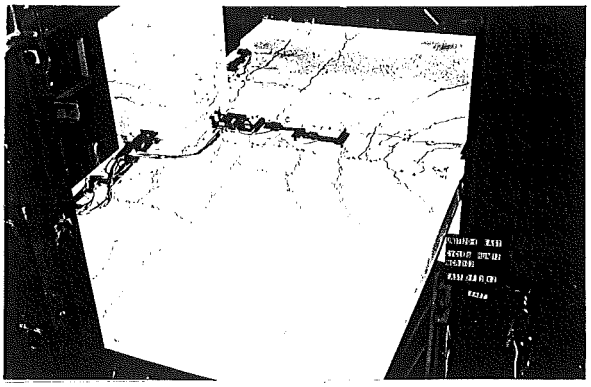

(a) Slab at the end of cycle 6, after two cycles of μ = 3 (EW)

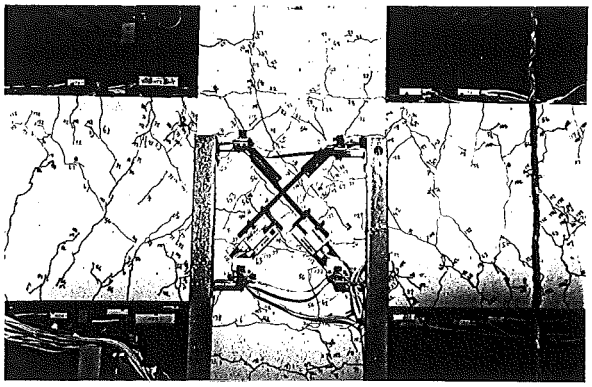

(b) West face joint at the peak of cycle 8 to μ = -3 (NS) and 3 (EW)

Fig.6.3 - Unit 2D-E in cycles 6 and 8 to ductility of μ = 3 (uniaxial and biaxial)

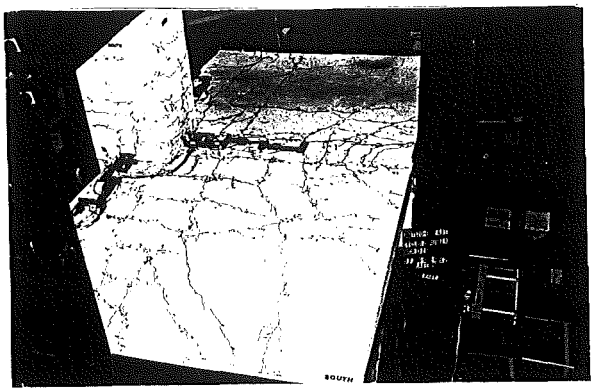

(a) Slab viewed from south-east at peak of μ = -6 (NS) and 6 (EW)

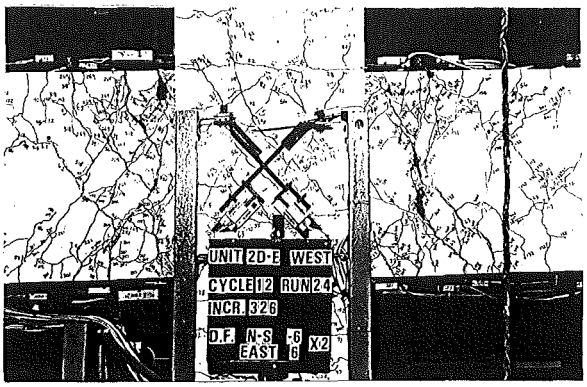

(b) West face joint at the same ductility as (a)

Fig.6.4 - Unit 2D-E in cycle 12 to ductility of μ = 6 (biaxial)

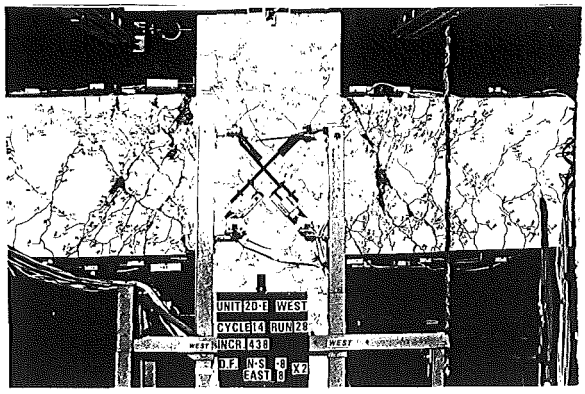

Fig.6.5 - West face joint of Unit 2D-E in cycle 14 to ductility of μ = 8 (biaxial)

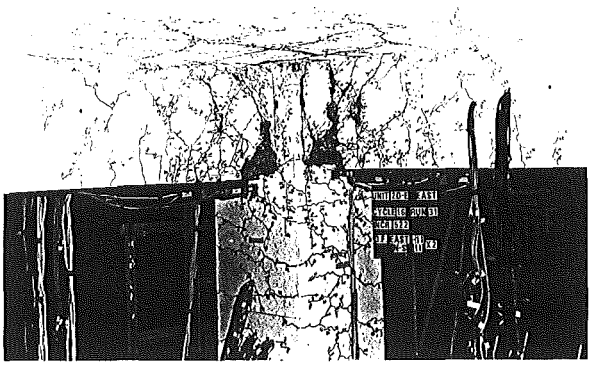

Fig.6.6 - South and east beams of Unit 2D-E in cycle 16, 2nd cycle to ductility of μ = 11 (biaxial)

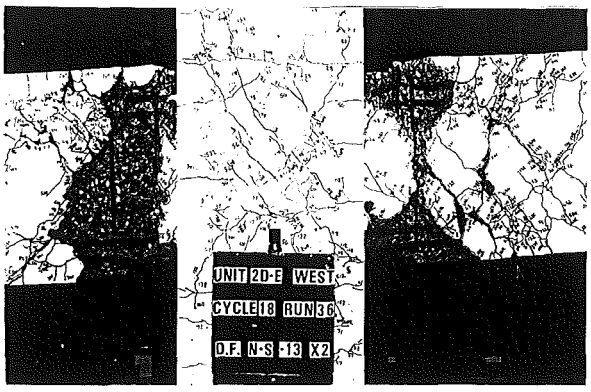

(a) West face joint at the peak of cycle 18, 2nd cycle to μ = -13 (NS)

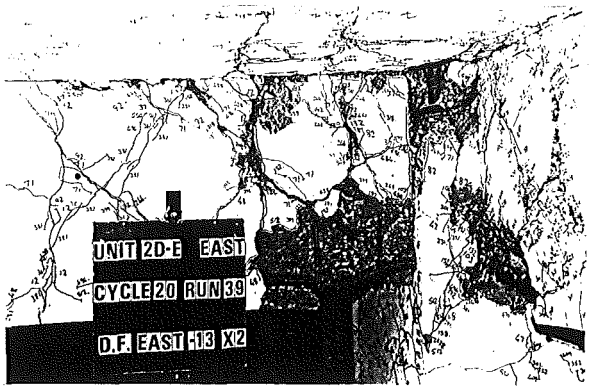

(b) East and north beams at the peak of cycle 20, 2nd cycle to μ = -13 (EW)

Fig.6.7 - Unit 2D-E in cycles 18 and 20 to ductility of μ = 13 (uniaxial)

Figs.3.15(b) and 3.16(b). Crack pattern at the bottom of the slab was similar to that at the top.

6.2 FORCE-DISPLACEMENT RESPONSE

6.2.1 General

The column (storey) shear versus displacement curves are plotted in Fig. 6.9 for the three elastic cycles in the east-west direction and in Figs. 6.10 and 6.11 for subsequent inelastic cycles in the east-west and north-south directions respectively. The force-displacement responses of the three beams are shown in Figs. 6.12 to 6.14. All essential features of presentation are the same as those used for the other two test units in Chapters 4 and 5. Calculations for estimation of ideal strengths and theoretical stiffness are given in Appendices D.2 and D.3 respectively.

From load run 5 to μ = -1(EW), the first yield displacement $\Delta_{y,test}$ was determined to be 12.1 mm (0.35% of storey height). This corresponded with a stiffness of 9.5 kN/mm. As in previous tests, the measured stiffness was a little less than the theoretical value (Fig.6.9).

6.2.2 Elastic Cycles

The first two cycles (Fig. 6.9) subjected the test unit to one half of the ideal "negative" strength of the east beam, as explained in Section 3.7.1. In the first run to $-0.5\ V_i$, only one N-S transverse flexural crack appeared at the top side of the slab along the east edge of the column. In the succeeding run, which displaced the east beam upwards to the same force level, four flexural cracks developed from the bottom of the east beam to the slab. This relatively extensive cracking can be expected from the fact that the applied upward force was almost 70% of the ideal "positive" strength $+V_i$. Fine flexural cracks also appeared at the column faces, even at the exposed joint area. The crack pattern at the west column face in cycle 3 can be seen in Fig. 6.1(b). No diagonal cracks in the north and south exposed face of the joint were noted even at a ductility level of μ = 1(EW).

In run 5 the east beam was pushed downwards. Transverse and diagonal cracks formed in the slab as seen in Fig. 6.1(a). From the extent of the transverse crack, it can be inferred that at this stage the width of the slab

as tension flange of the east beam was quite large. An important observation was that vertical and diagonal cracks formed at this stage in the north and south spandrel beams as seen in Figs. 6.1(b). As the EW slab bars were stressed in tension, the north and south beams were subjected to both bending about the vertical axis of the beam section and torsion. In subsequent cycles to higher negative ductilities in the E-W direction only, the widths of the diagonal (torsional) cracks remained small. However, under the same ductilities, the vertical flexural cracks at the upper west faces of the north and south beams, especially close to the column, widened. It appeared that bending of the north and south beams with tips deflecting towards the east was more dominant than torsion. Further discussion in this aspect is presented in Section 6.3.4.

In run 6 to positive ductility of $\mu = 1$, a transverse crack extended to the south at the underside of the slab. In Fig.6.9, it is seen that at this stage the measured storey shear approached the theoretical strength V_i which was based on an assumed compression flange, as explained in Section 3.8.2.

North-south loading of specimen to $\mu = \pm 1$ was carried out in cycle 4. The formation of cracks in the slab and the beams was similar to that observed in Unit 2D-I, as can be seen in Fig.6.2(a) when it is compared with Figs. 5.1 and 5.2. Fine diagonal joint cracks at the exposed west face of the column developed during this cycle of loading, as seen in Fig.6.2(b). The photograph also indicates the extent of flexural and shear cracks in the north and south beams. Evidently the "torsional" cracks (Fig.6.1(b)) became insignificant.

6.2.3 Inelastic Cycles

As shown by the hysteretic force-displacement curves in Figs.6.10 to 6.14, throughout the subsequent inelastic cycles, the observed beam tip forces and the derived storey (column) shear forces kept increasing, except at an imposed ductility of thirteen. At this ductility level, corresponding to an interstorey drift of 4.5%, extensive concrete spalling and beam bar buckling took place, as seen in Figs.6.7(a) and (b). Nevertheless, the measured strength still approached the theoretical "seismic" shear strengths estimated by the "mixed" approach (see App. D.2). By comparing these graphs with those

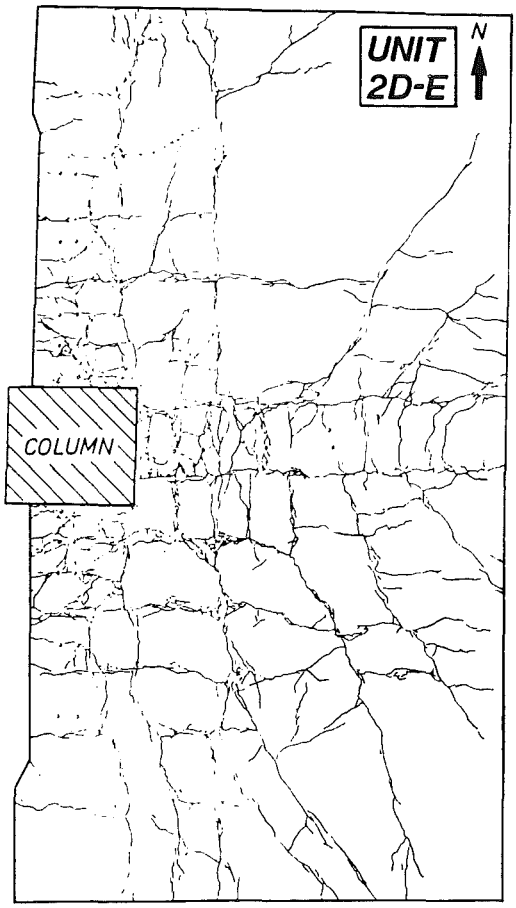

Fig.6.8 - The pattern of major cracks at top surface of slab of Unit 2D-E

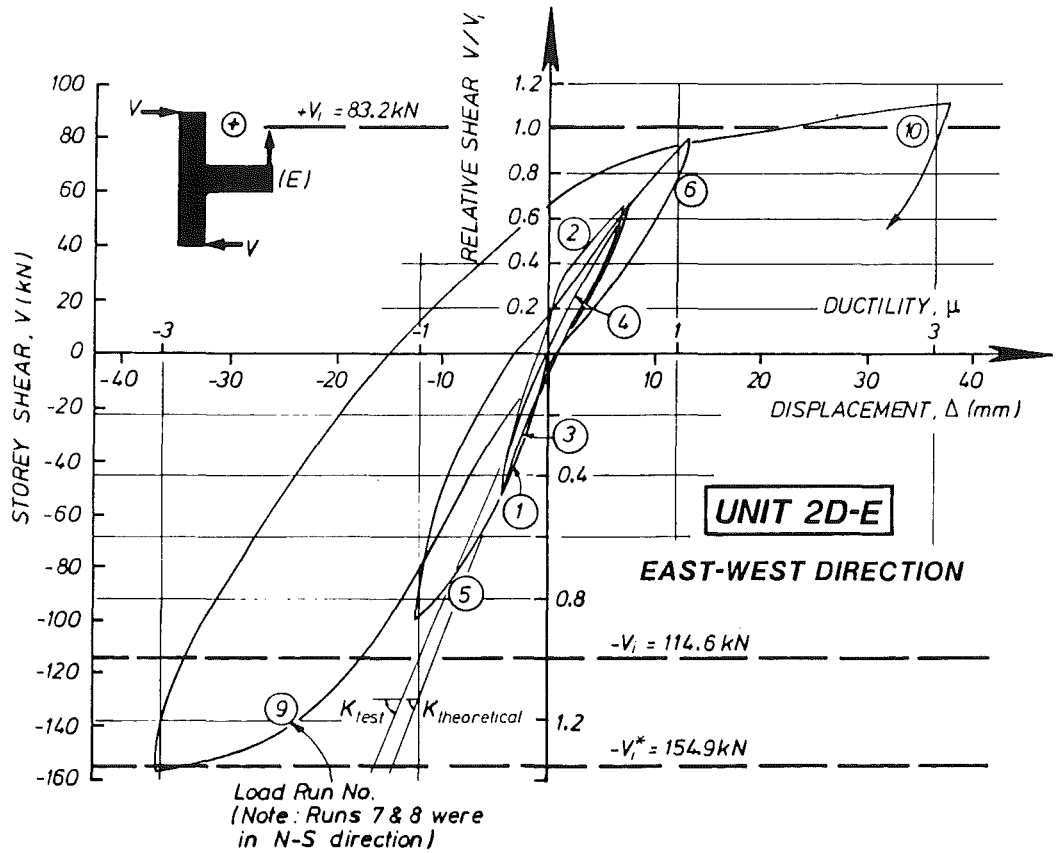

Fig.6.9 - East-west storey shear-displacement response - elastic cycles

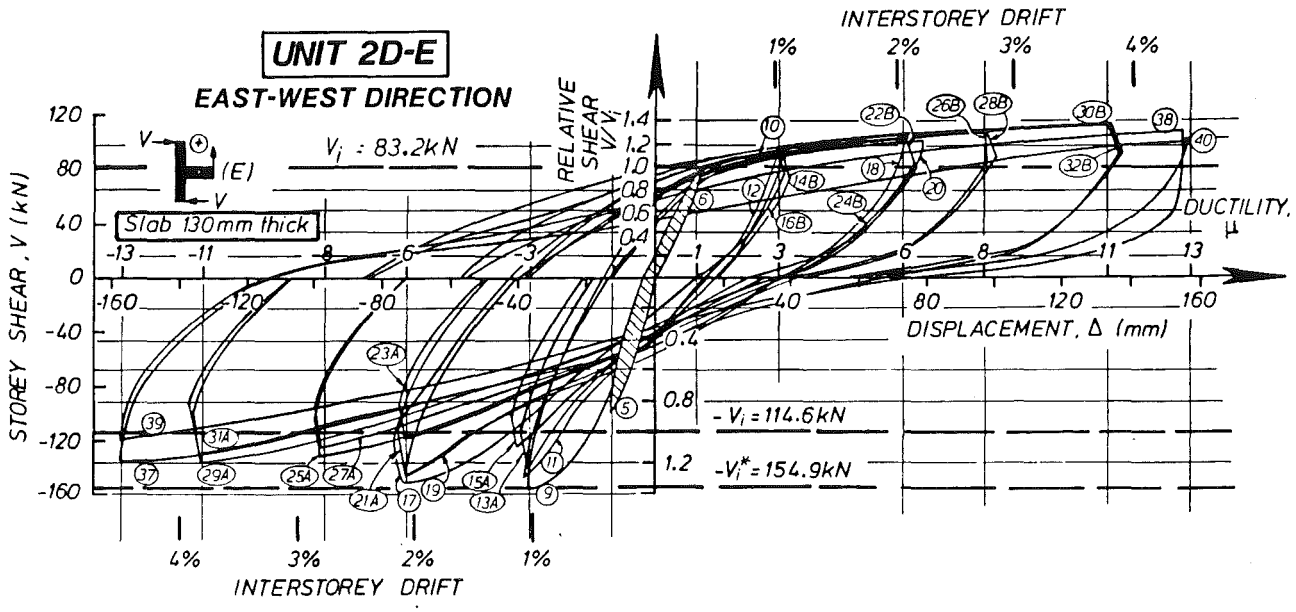

Fig.6.10 - East-west storey shear displacement response - inelastic cycles

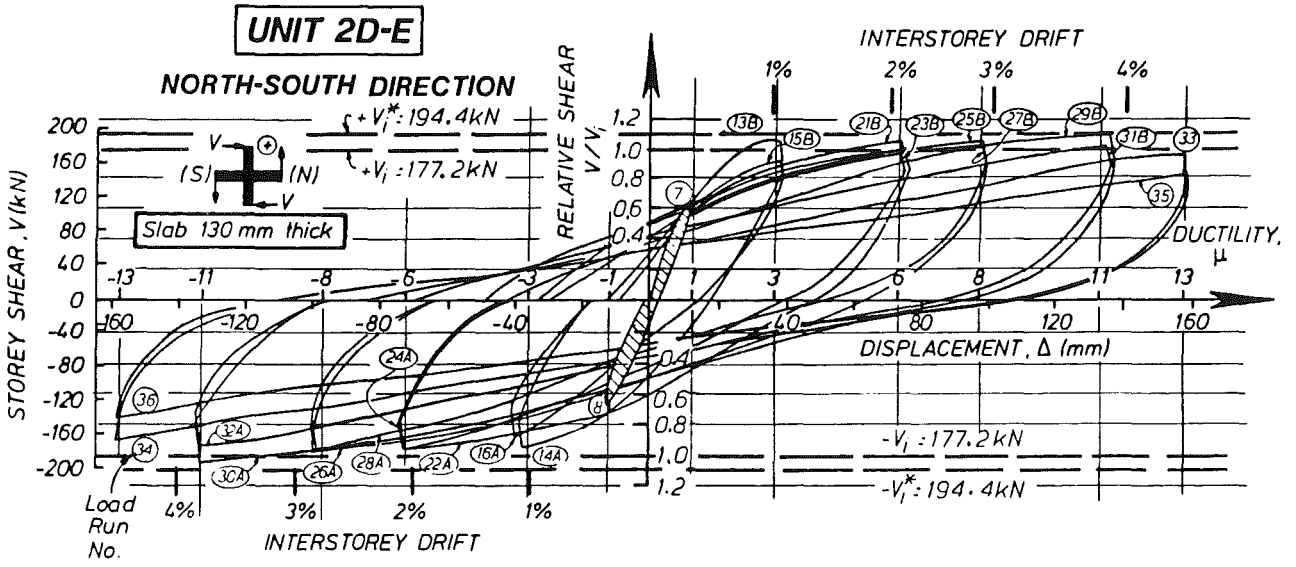

Fig.6.11 - North-south storey shear displacement response

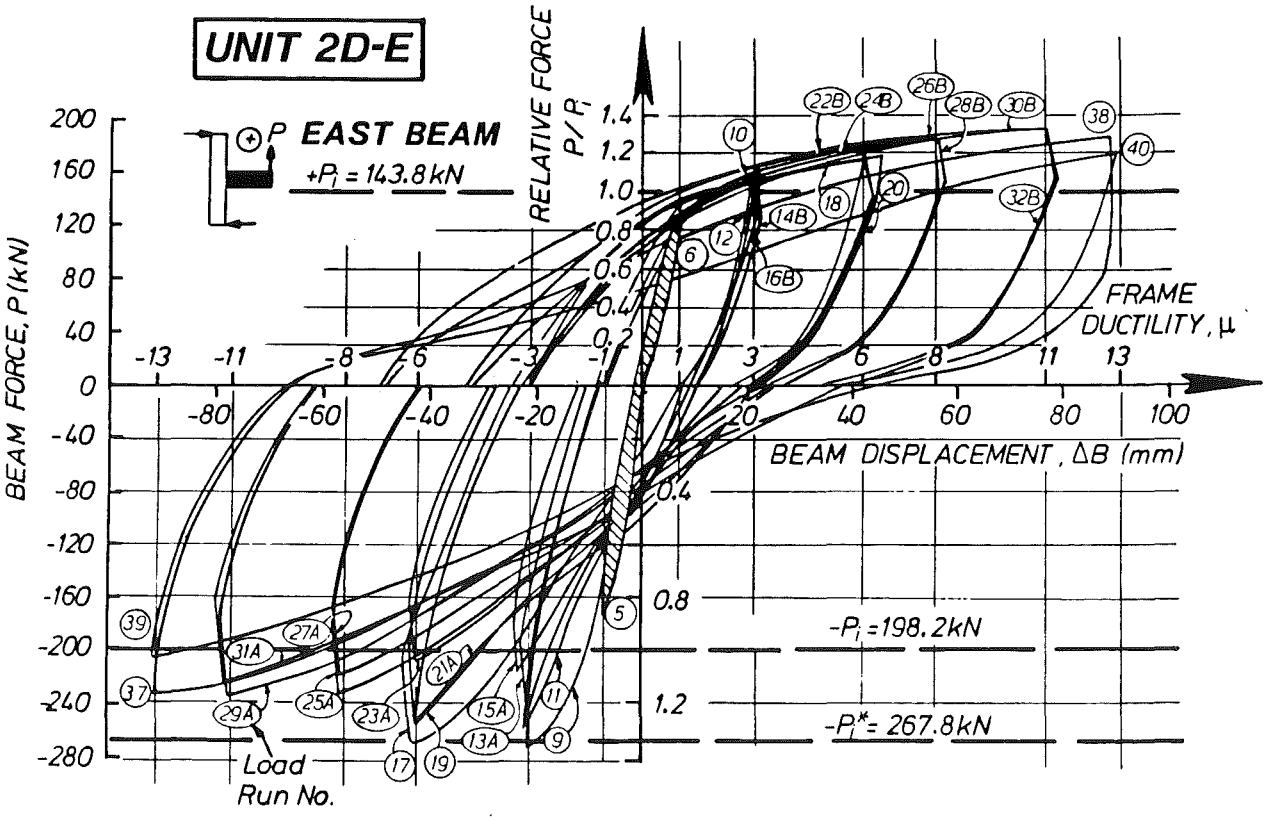

Fig.6.12 - Force-displacement response of east beam

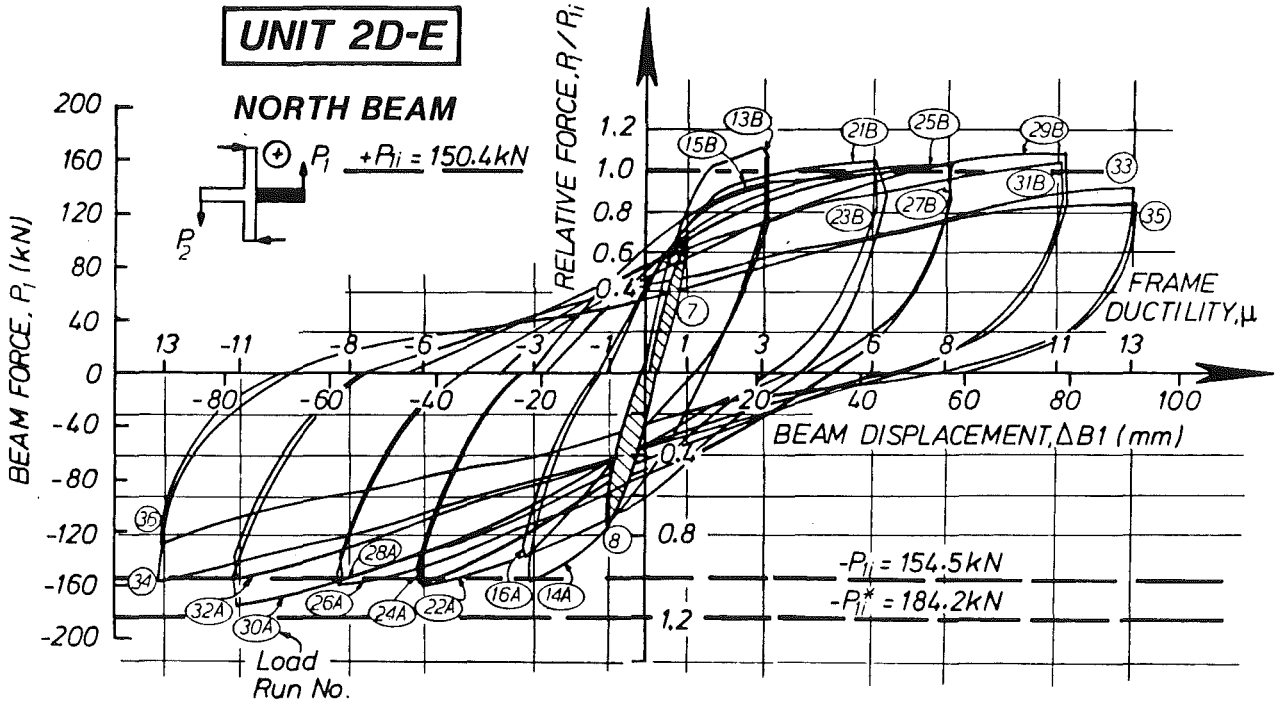

Fig.6.13 - Force-displacement response of north beam

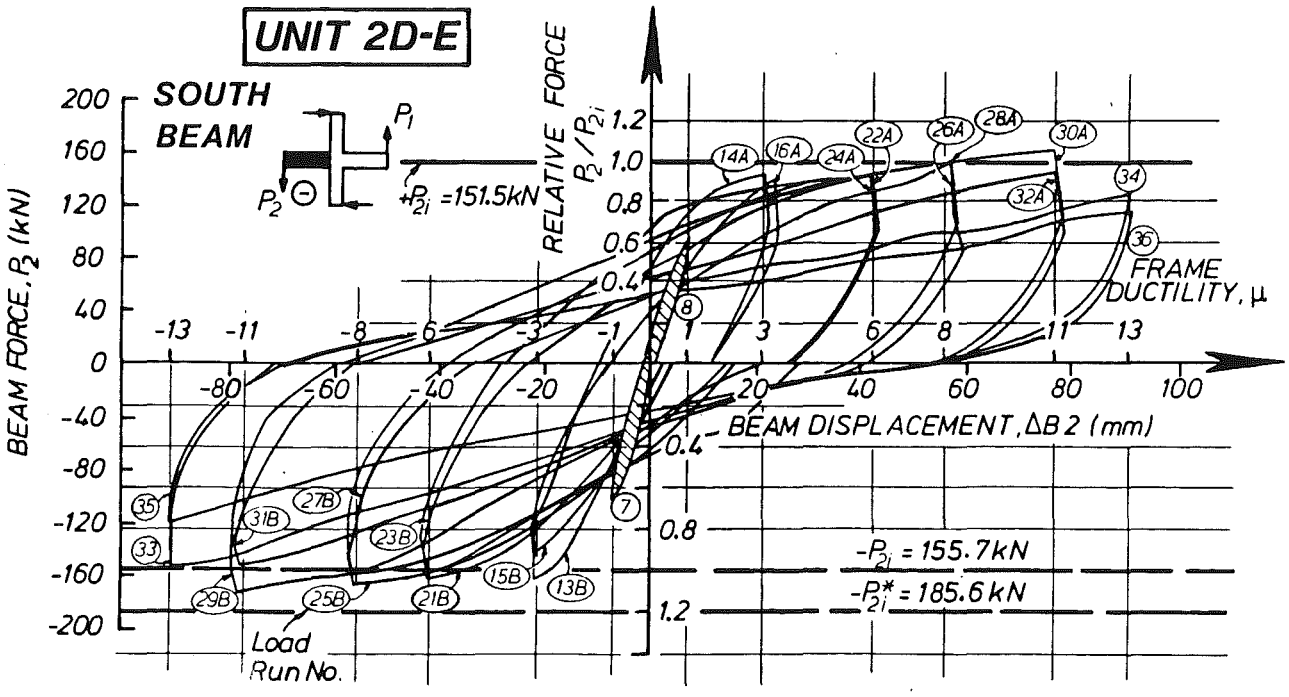

Fig.6.14 - Force-displacement response of south beam

relevant to the interior joint Unit 2D-I (Figs. 5.9 to 5.14), it may be seen that this exterior joint assembly performed better at all stages of the test.

Most of the special features of the hysteresis graphs, described in Section 5.2.3 for Unit 2D-I, are also relevant to this unit. Hence they are not repeated here. However, one point worth mentioning is the steady increase in the measured positive (upward) resistance of the exterior east beam (Fig.6.12). In the sections describing beam and slab bar strains, it is suggested that the top D24 beam bars and some of the east-west top layer slab bars at the corresponding ductilities developed only moderate compressive stresses at the column face. It appears therefore that a certain width of flange participated in compression.

6.3 DISPLACEMENT COMPONENTS

6.3.1 Joint Deformations

For this unit, deformations at the exposed west face of the joint core were measured following the method described in Section 3.9.4 for Unit 1D-I. Variations of the linear strains along two diagonals, J1-J3 and J2-J4 are plotted in Fig.6.15. It was impossible to place linear potentiometers at the east face of the joint.

Fig.6.15 shows two strain responses. Recorded strains along the diagonal J1-J3, represented by solid lines, were as expected. Tensile strains increased consistently according to (positive) ductility levels. At negative ductilities, small residual tensile strains or even compressive strains were recorded. The differences between strains at positive and negative ductilities were considerable. The results for diagonal J1-J3 support the expected development of a diagonal compression field in a cracked joint core. Strains changes along the diagonal J2-J4 (dashed lines) were relatively moderate. Tensile strains at peak ductilities when the diagonal J2-J4 should have elongated extensively were in fact less than half of the tensile strains observed along diagonal J1-J3 in preceding load runs. Furthermore, no compressive strains were observed even when the loading should cause compression along J2-J4.

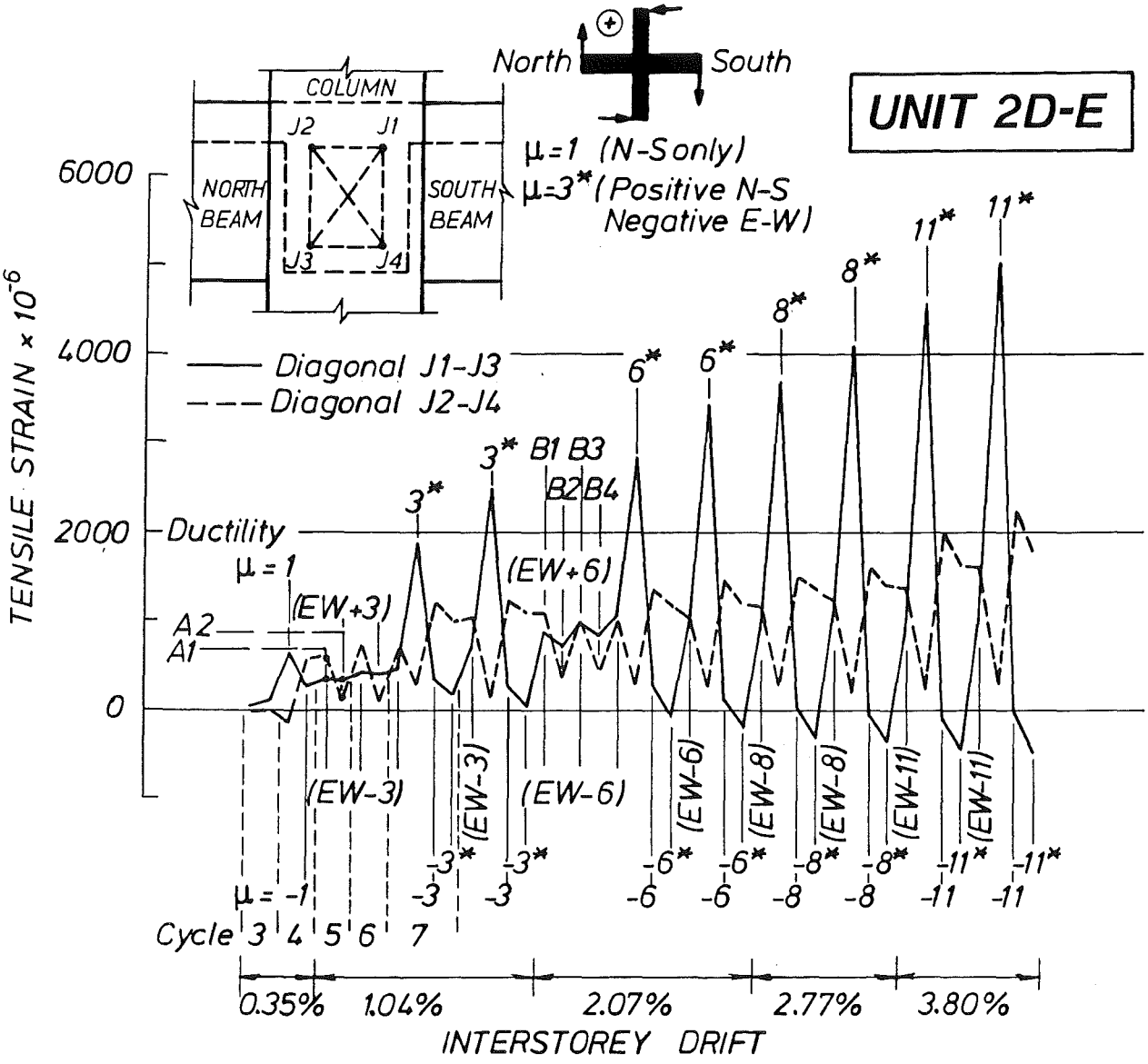

Fig.6.15 - Variations of strains along west face diagonals of the joint panel

Results in Fig.6.15 may be compared with the corresponding results for Unit 1D-I summarised in Figs.4.13 and 4.14 which have been discussed in Section 4.3.1. For Unit 1D-I both the north and south faces of the joint core were instrumented. Figs. 4.13 and 4.14 show a generally regular pattern as expected, and the results are considered more reliable. The measurements of diagonal strains in this Unit 2D-E, showing a different pattern, were likely to be influenced to a significant scale by the behaviour of the east beam. First the hooked bars from the east beam (see Fig.3.3(c)) might interfere with the potentiometer steel rods embedded in the joint core. Second the sense of loading applied to the east beam could also change the diagonal strains observed at the west joint face. When the east beam was pushed by a downward (negative) acting tip force, the north and south beams underwent large lateral deformations because of slab participation in membrane action (see Fig.6.30(a) and Section 6.3.4). The spandrel beams were therefore subjected to horizontal bending about the weak (vertical) axis, resulting in longitudinal (north-south) tensile strains along the outer (west) faces of these beams with maximum values at the column. This bending phenomenon implies that strains along the two joint diagonals should also increase with uni-directional E-W negative ductilities. Alternatively with (positive) upward loading of the east beam, the bending effect on the spandrel beams (Fig.6.30(b)) reduced drastically. In this case only residual tensile strains along both joint diagonals should be recorded.

The expected results suggested in the last paragraph did not fully conform with the observed results depicted in Fig.6.15. For convenience in the following discussions in this section, measured strains along diagonals J1-J3 and J2-J4 are simply referred to as J1-J3 and J2-J4 respectively. The cyclic loading history can be seen in Fig.3.19. In cycles 1 to 6, loading was imposed in one direction only. Results from the first two elastic cycles are not considered.

In cycle 3 (Fig.6.15) when only east-west ductility of μ = -1 and μ = +1 were imposed in successive order, J1-J3 exhibited small tensile strains while J2-J4 were essentially zero. In cycle 4 to unidirectional μ = ±1(NS), both diagonals responded as expected. The residual tensile strains at zero-load, not shown in Fig.6.15, were 224 x 10^{-6} (J1-J3) and 187 x 10^{-6} (J2-J4).

In the first half of cycle 5 to unidirectional μ = -3(EW), indicated by A1 in Fig.6.15, both diagonal strains increased, with J1-J3 slightly to 335 x 10^{-6} and J2-J4 more considerably to 610 x 10^{-6}. However, in the second half

cycle to μ = 3(EW), indicated by A2 in Fig.6.15, J1-J3 remained unchanged while J2-J4 dropped to 86 x 10^{-6}.

Similar response was observed in cycle 6 to the same unidirectional μ = ∓3(EW). There were slight changes in the tensile strains of J1-J3, but more significant fluctuations occurred in J2-J4.

The test unit was subjected to bi-directional loading in cycle 7. The response in terms of observed diagonal strains shown in Fig.6.15 was found not to follow regular patterns. Strain changes along J1-J3 consistently agreed with those expected under the action of north-south loading only. Those strains were enhanced by the additional tensile strains caused by the downward bending of east beam. However, the response of diagonal J2-J4 was less sensitive to N-S loading, while more significant strain changes were recorded as east-west displacement ductilities were imposed. The patterns of strain changes observed in subsequent bi-directional cycles were found to be similar to those described for cycle 7, except that peak strains increased progressively. The simultaneous reductions in tensile strains of J1-J3 and J2-J4 can be clearly seen in Fig.6.15 in the two uni-directional cycles from μ = -6(EW) shown by B1 and B3, to μ = 6 (EW) denoted by B2 and B4.

It was suggested in an earlier paragraph that strain changes recorded at the west face of the joint were associated with the response of the north-south spandrel beams in terms of east-west lateral deflections of these beams. Section 6.3.4 studies this response in detail. It is concluded that bi-directional loading sequences significantly affected the observed results. Hence it is considered that the west face diagonal joint strains did not represent the mean joint distortions in the north-south direction.

6.3.2 Beam Deformations

As in Units 1D-I and 2D-I, longitudinal deformations of each of the three beams of this unit were measured over a length of 825 mm from column face. The horizontal movements of the top and bottom fibres are shown in Figs.6.16 to 6.18 and these can be compared with those shown in Figs.4.17 and 4.18 and Figs.5.15 to 5.18. It should be noted that results at ductility

level of μ = 11 for the north beam of this Unit 2D-E were not given because two linear potentiometers became inoperative at that stage.

The symmetrically reinforced north and south beams acted as spandrel beams of this unit. Observed movements of segments A shown by dashed curves in Figs.6.16 and 6.17 indicate that when bending caused compression in either the top or bottom fibres, at ductility levels of μ =6 or less, the previously opened cracks at column face would close almost completely, once again supporting the assumption that concrete flexural compression forces would be mobilised regardless of reinforcement contents. At higher ductilities, it appears that this crack closure was less effective with larger residual lengthening in segment A being observed. However, other test results such as force-displacement response of the assembly and bar strains reported in this chapter provide further evidence of the existence of concrete compression forces. As for segments B, the changes in length at bottom fibres were comparable to those at top fibres. This again can be expected from the symmetrical reinforcing arrangements. However, the absolute magnitudes of the horizontal movements of the north and south beams were not symmetrical. As spandrel beams of an exterior joint assembly, the north and south beams are characterised by some special behavioural features. Because the linear potentiometers monitored only the central vertical planes of the beams, results presented in Figs.6.16 and 6.17 are considered to give very limited information with respect to those aspects. A more comprehensive treatment of the behaviour of the spandrel beams in terms of lateral (east-west) movements is given in Section 6.3.4.

For the east beam, longitudinal east-west movements are shown in Fig.6.18. it is recalled that the beam bars were anchored in the joint core with end hooks (see Fig.3.3(c)). Fig.6.18 may be compared with figures for other east beams, i.e. Fig.4.17 for Unit 1D-I and Fig.5.17 for Unit 2D-I. While responses appear to be similar, it must be noted that the top fibres of segments A and B of Unit 2D-E (Fig.6.18(a)), when loaded so as to cause compression, resulted in slightly larger residual lengthening. This residual lengthening in segment A at the last cycle to ductility μ = 11 was found to be 3.4 mm and is considered to have resulted from the response of the spandrel beams when subjected to distortions causing rotations about their vertical axis (Fig.6.30).

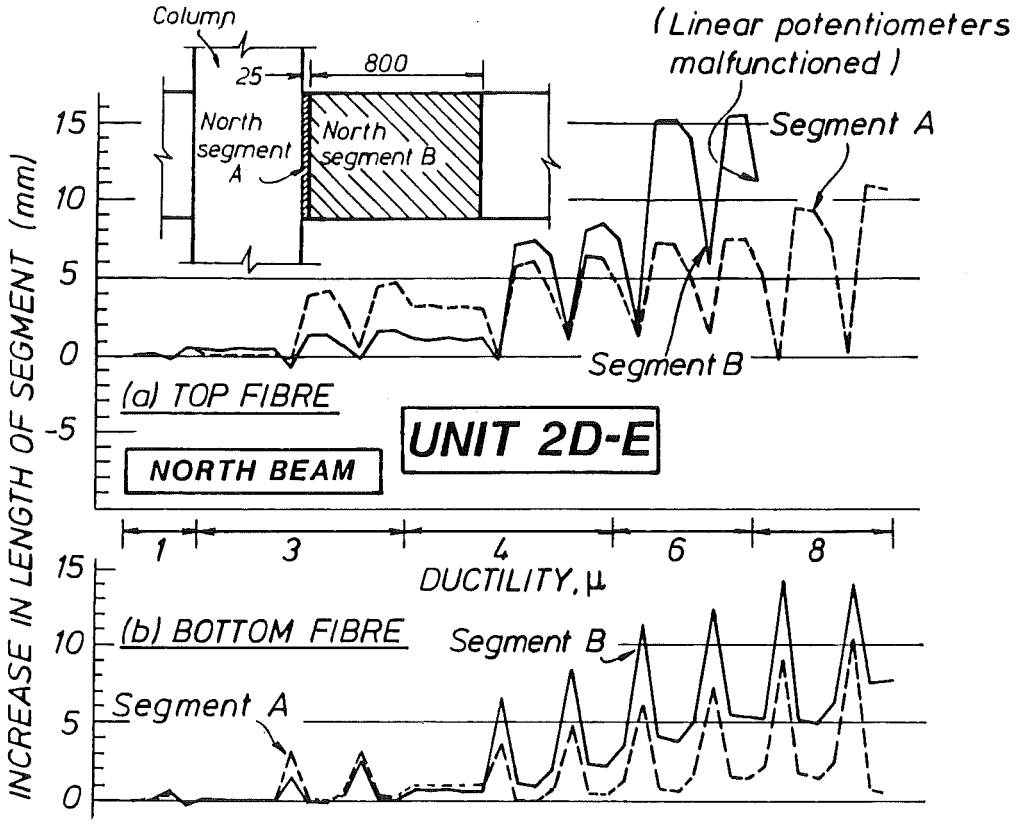

Fig.6.16 - Measured longitudinal movements in segments of north beam

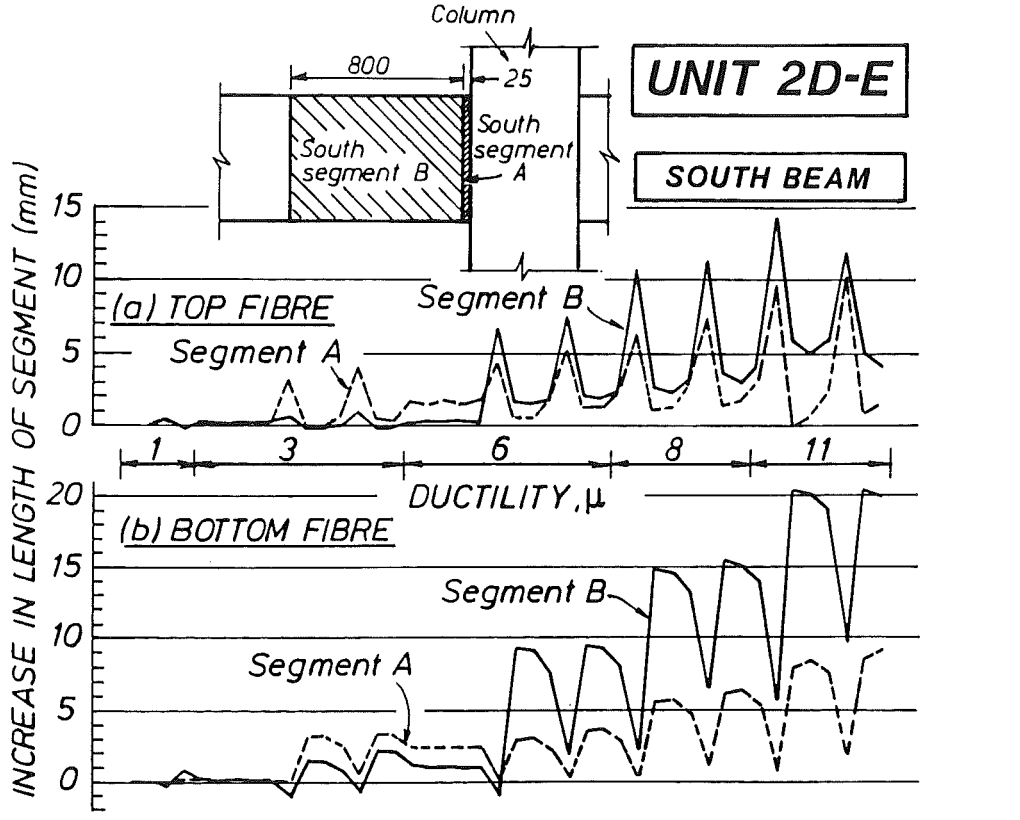

Fig.6.17 - Measured longitudinal movements in segments of south beam

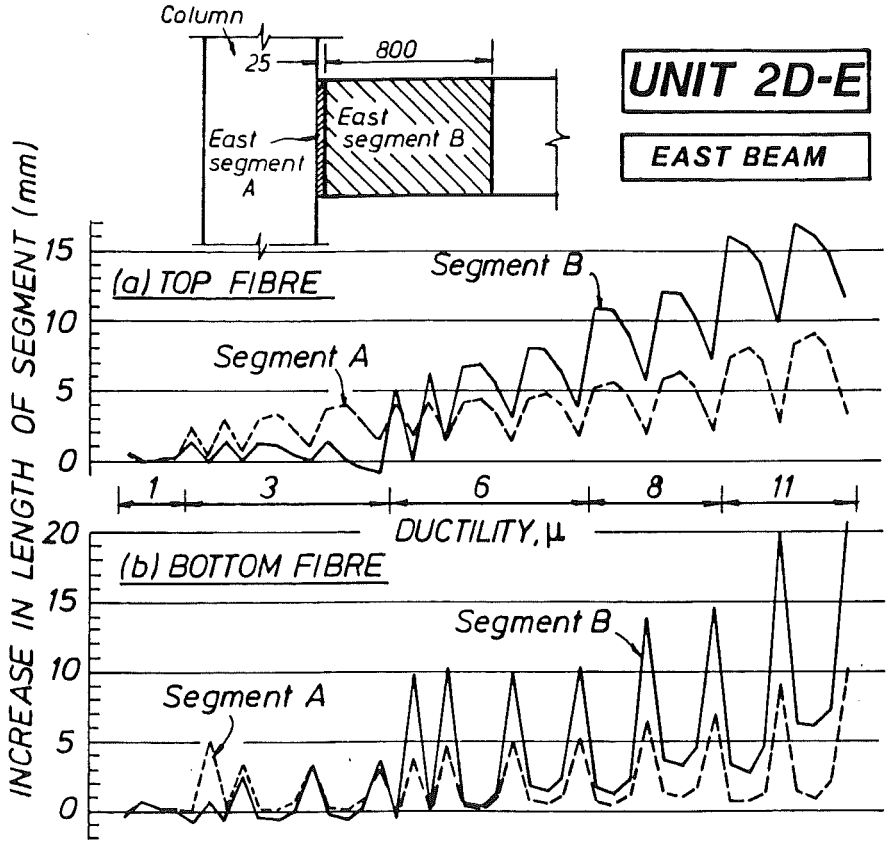

Fig.6.18 - Measured longitudinal movements in segments of east beam

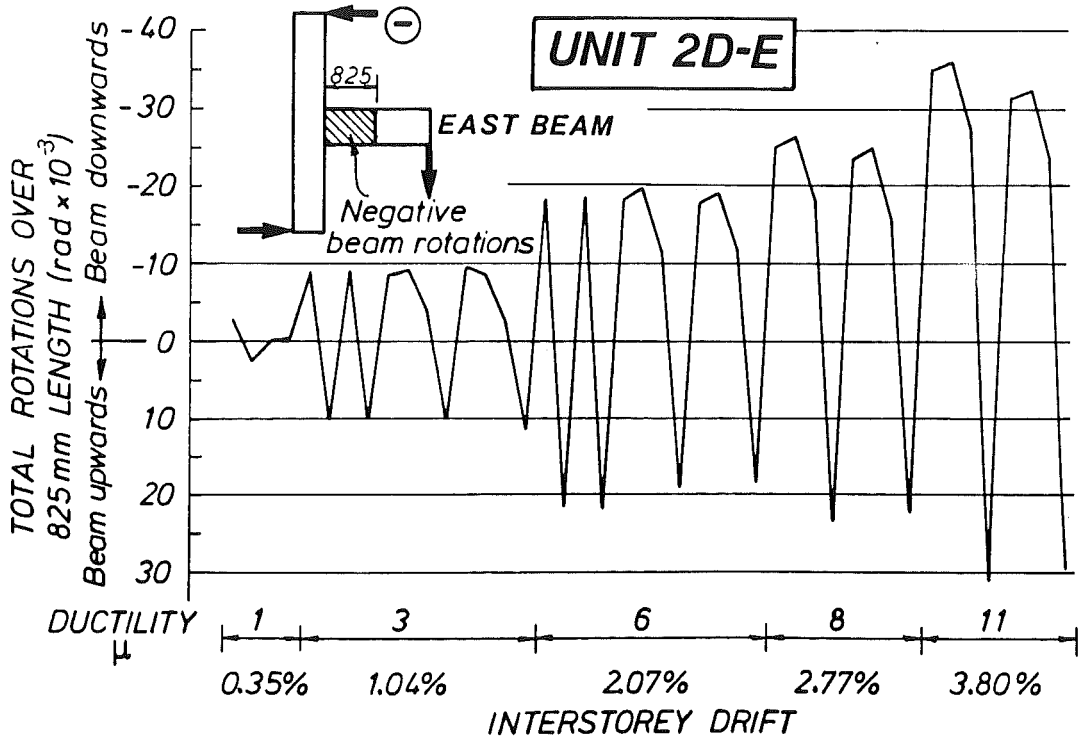

Fig.6.19 - Total rotations in plastic hinge region of east beam

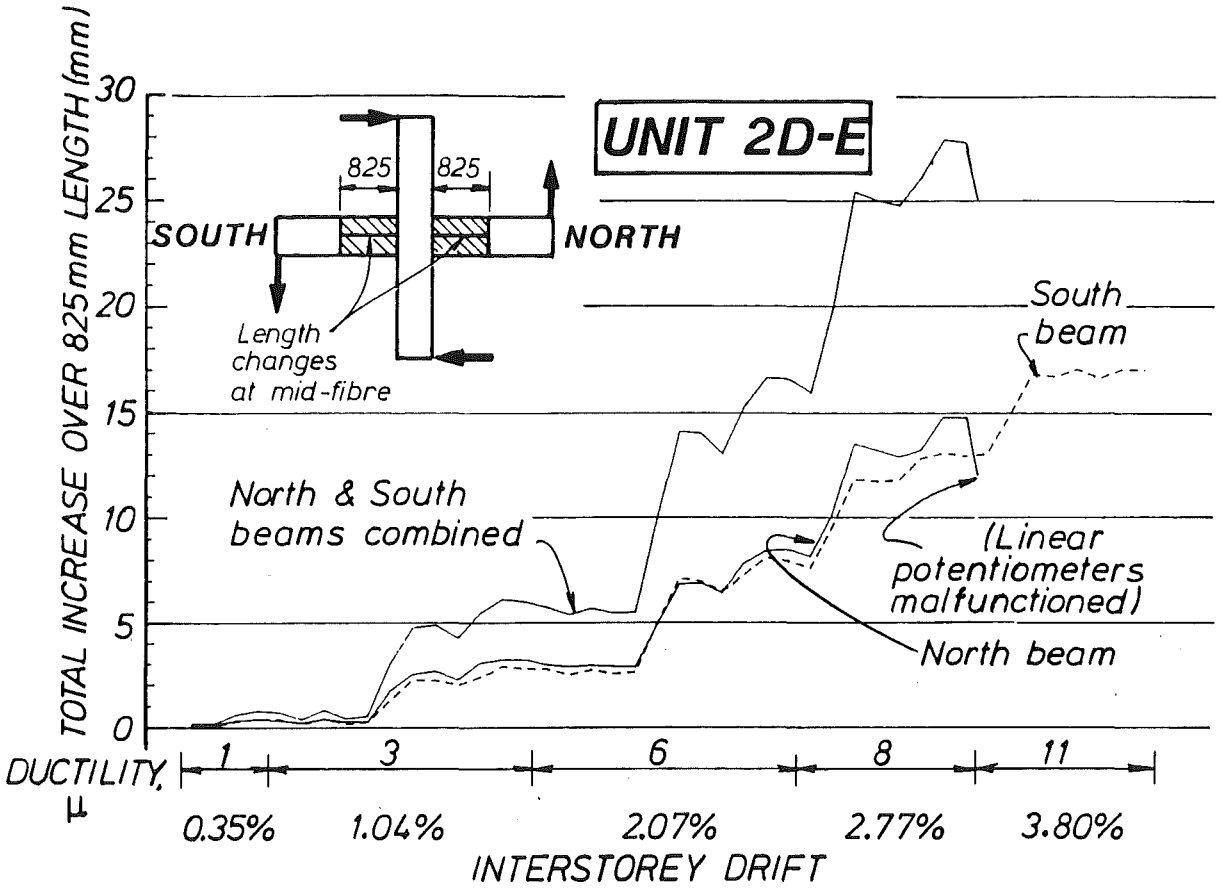

Fig.6.20 - Measured lengthening of north and south beams

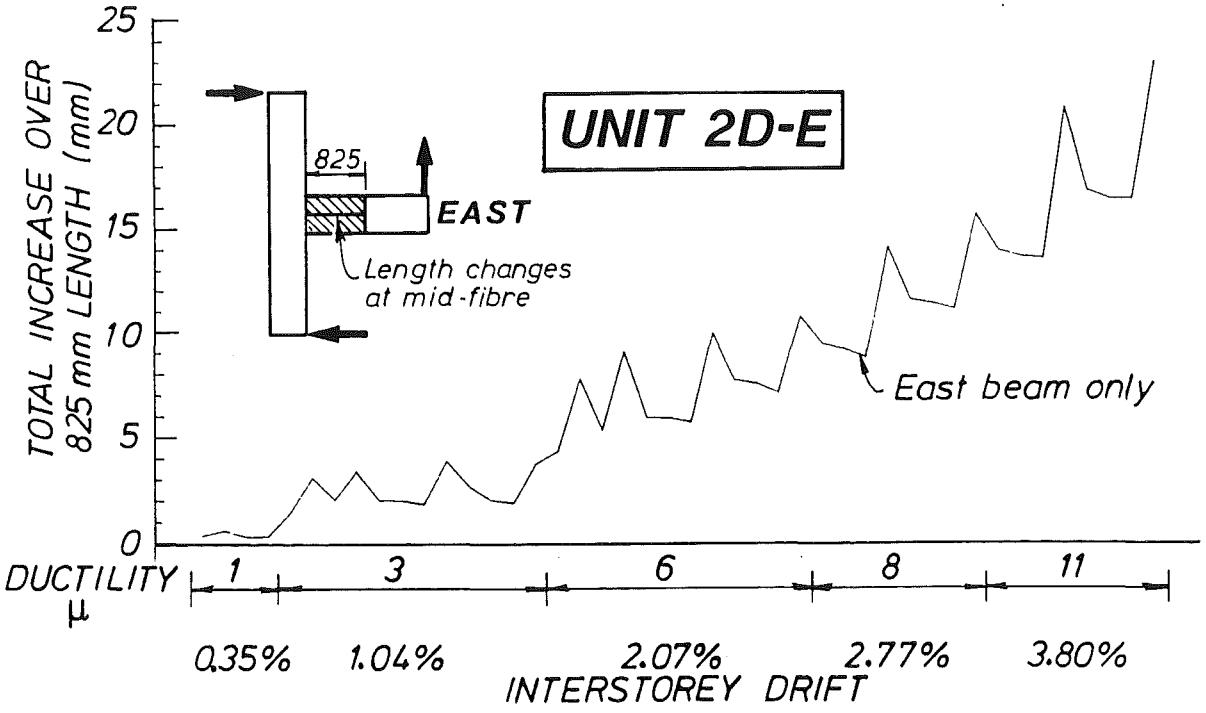

Fig.6.21 - Measured lengthening of east beam

Using the results of Fig.6.18 and applying Eq.(3.9), the total rotations of the east beam over 825 mm length were calculated and plotted in Fig.6.19. This 825 mm length, being equal to 1.5 times the beam depth, was considered to represent the plastic hinge length. Fig.6.19 will be referred to again in Section 6.3.4.

Results of beam lengthening at mid-fibre are shown in Figs.6.20 and 6.21, while those of beam curvatures are presented in Figs.6.22 and 6.23. Patterns are similar to those presented in Sections 4.3.2 and 5.3.1. Estimated slips of the beam bar within the joint core are plotted in Figs.6.24 and 6.25. The slips were comparable to those observed in Unit 2D-I (Figs.5.23 and 5.24). The anchorage of the beam bars was adequate because, as reported in Section 6.1, the bottom beam bars eventually buckled.

6.3.3 Decomposition of Displacements

The major components of the total beam or storey displacements were calculated and these are presented in Figs.6.26 to 6.29 according to the same approach described in Section 4.3.3 and 5.3.2. As explained in Section 6.3.1, joint shear distortions in the north-south direction were not evaluated. The features exhibited in Figs.6.26 to 6.29 are similar to those seen for Unit 2D-I in Figs.5.25 to 5.28.

6.3.4 Lateral Movements of North-South Beams

As reported in Section 3.5.2 and as shown in Fig.3.13, linear potentiometers were mounted to monitor the east-west lateral movements of the north and south spandrel beams and the joint. The data enabled the corresponding rotations and twists of the beam ends be calculated. Appropriate corrections were made for the horizontal rigid-body rotation of the whole specimen. The north-south movement of the joint could not be monitored precisely with linear potentiometers due to practical difficulties. Consequently horizontal rigid-body rotations could only be estimated using data from other dial gauge readings (Fig.3.12(a)). Since the beams also moved vertically under bi-directional loadings, results from the linear potentiometers were further corrected accordingly. Points a, b, c and d, shown in Figs. 6.30 to 6.33, always refer to locations at mid-depth of the slab, i.e. 65 mm from the top surface.

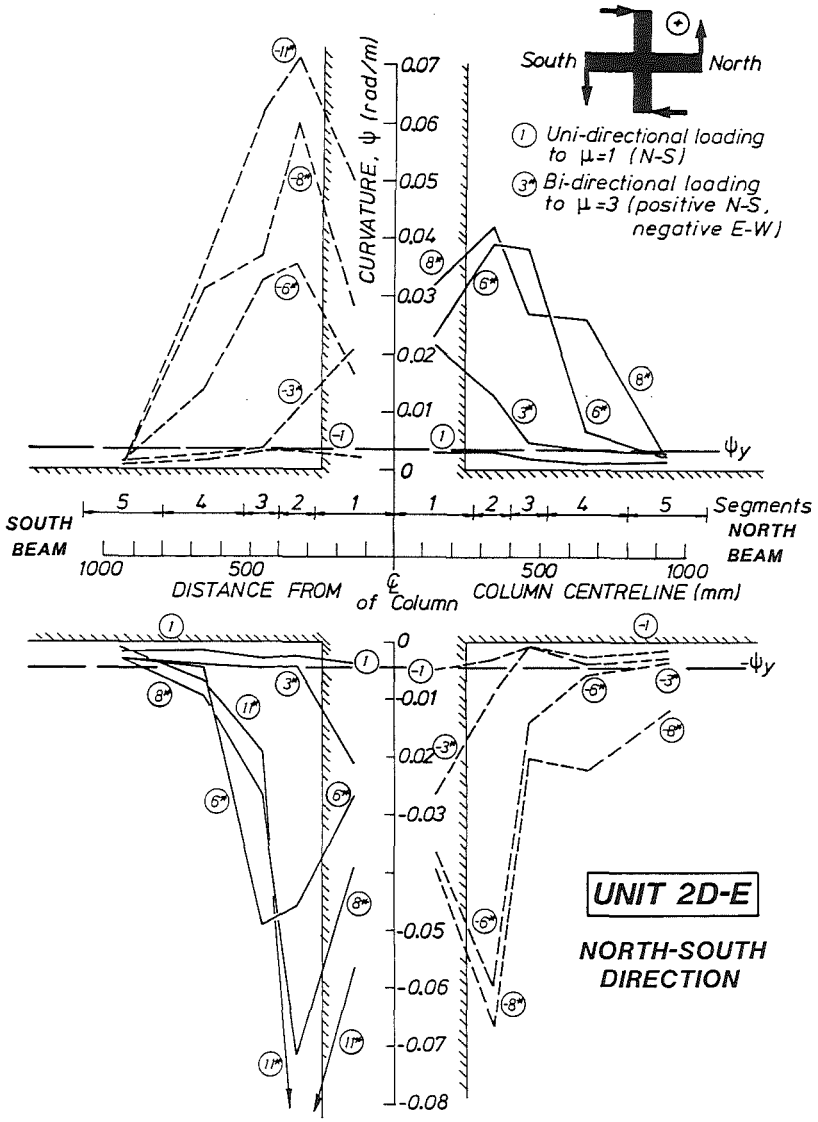

Fig.6.22 - Curvature profiles of north and south beams

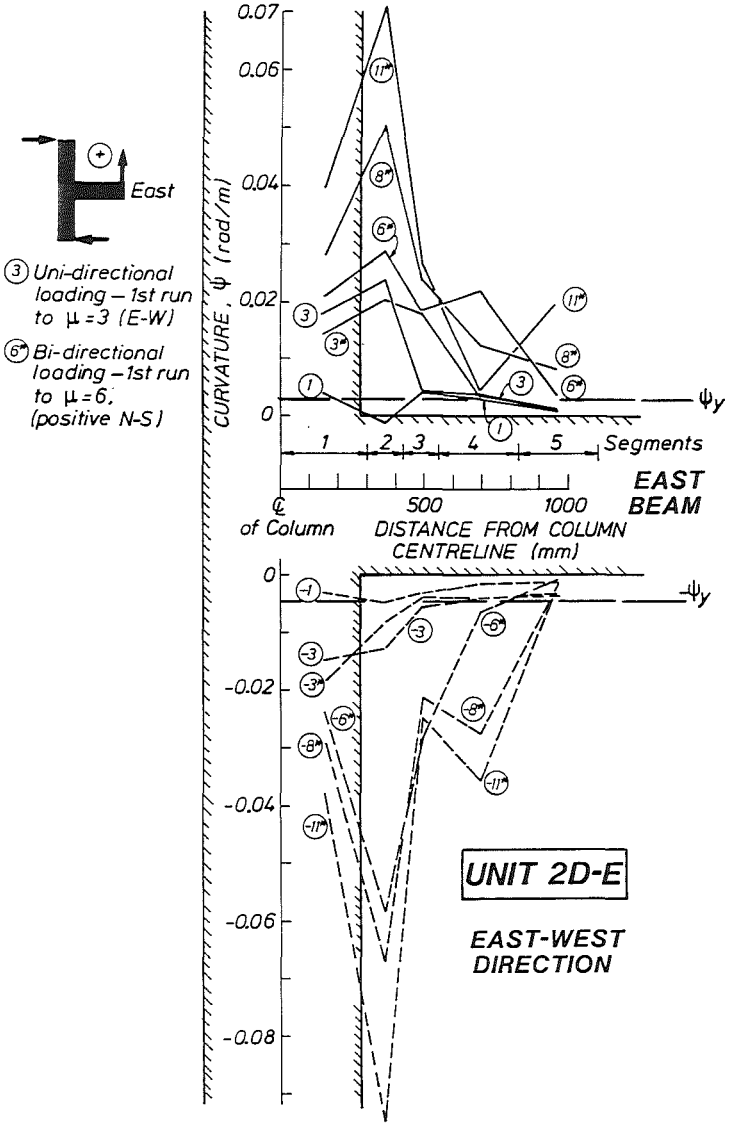

Fig.6.23 - Curvature profiles of east beam

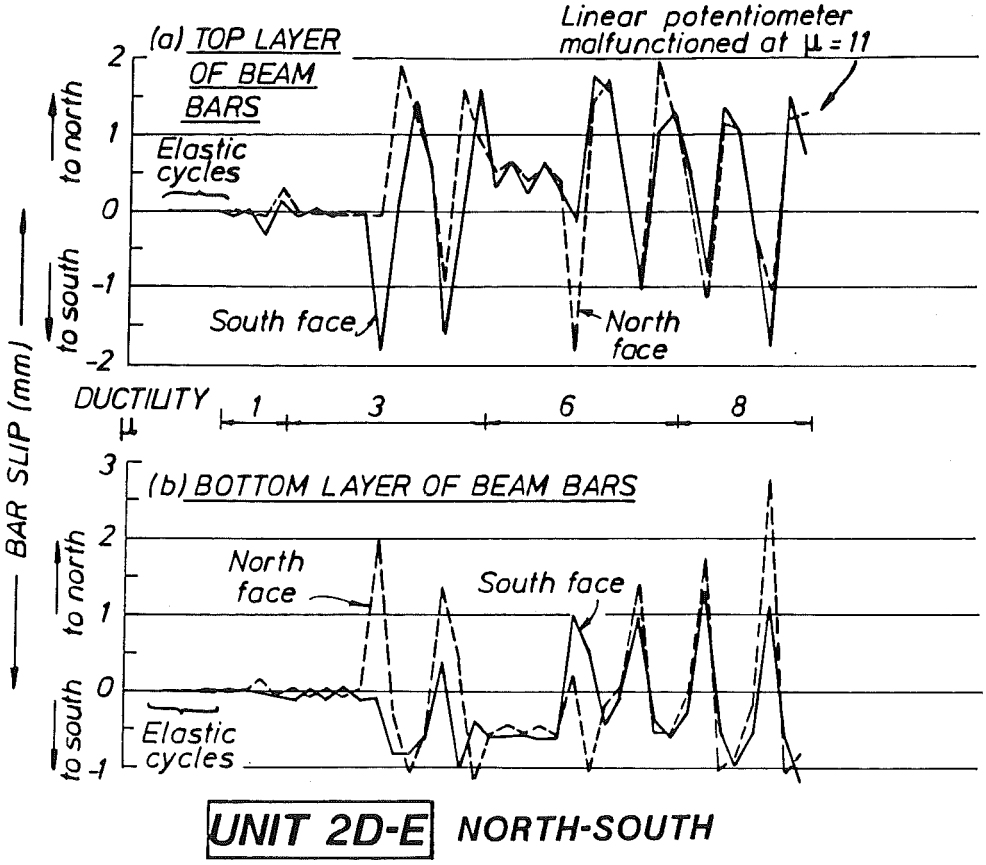

Fig.6.24 - Estimated slips of the north-south beam bars within joint core

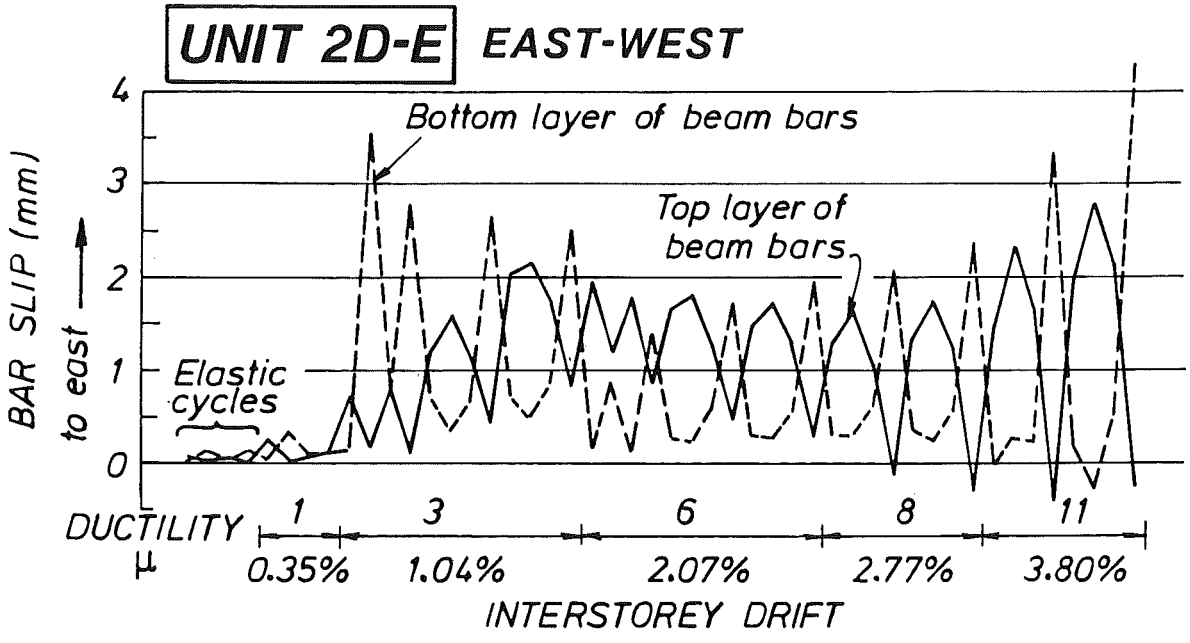

Fig.6.25 - Estimated slips of the east beam bars within joint core

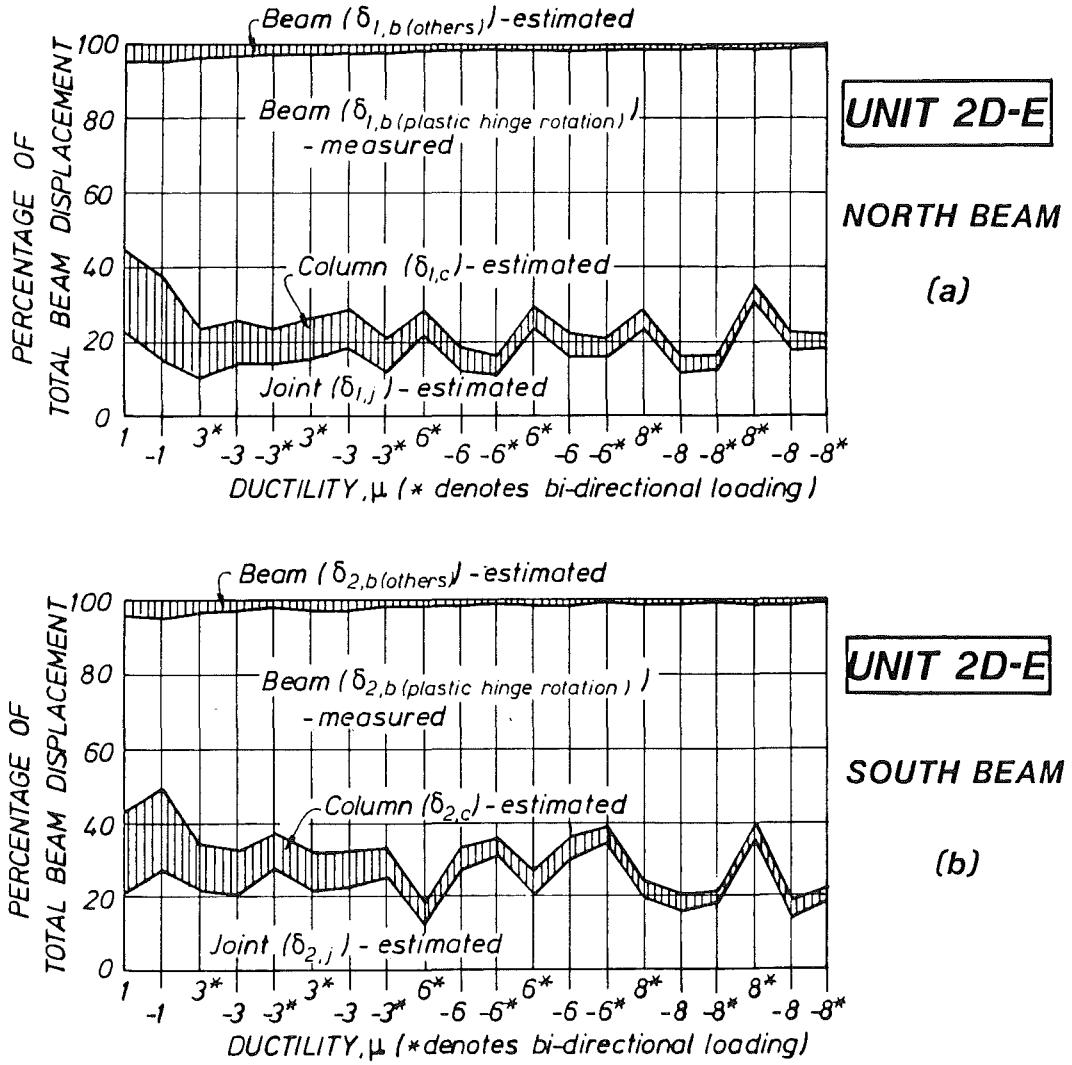

Fig.6.26 - Components of north and south beam displacements

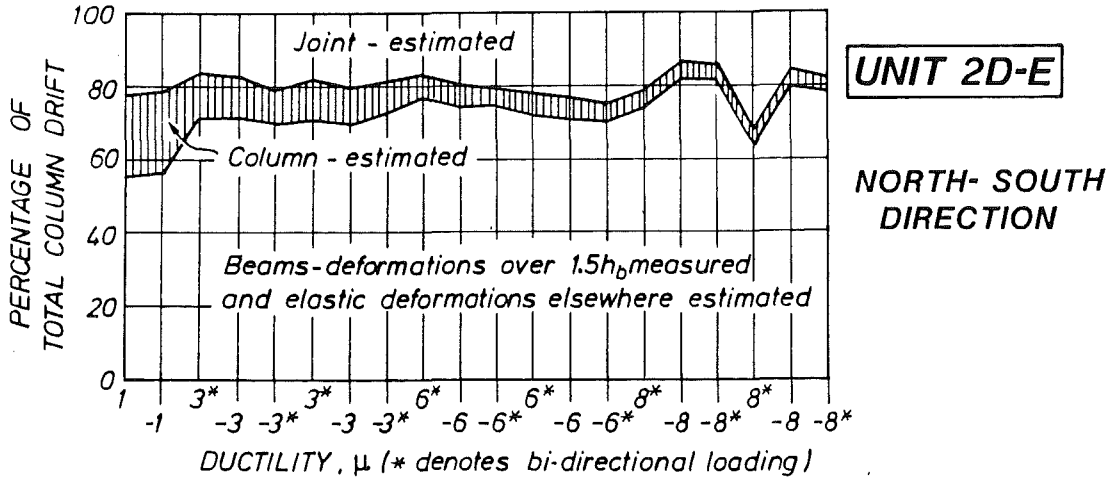

Fig.6.27 - Contributions to north-south interstorey lateral displacements during progressive loading

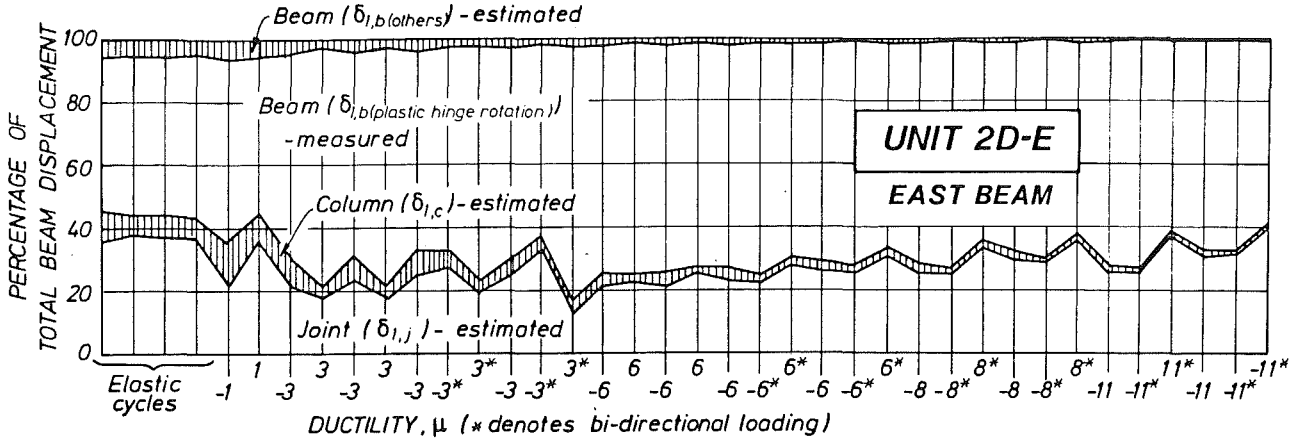

Fig.6.28 - Components of east beam displacements

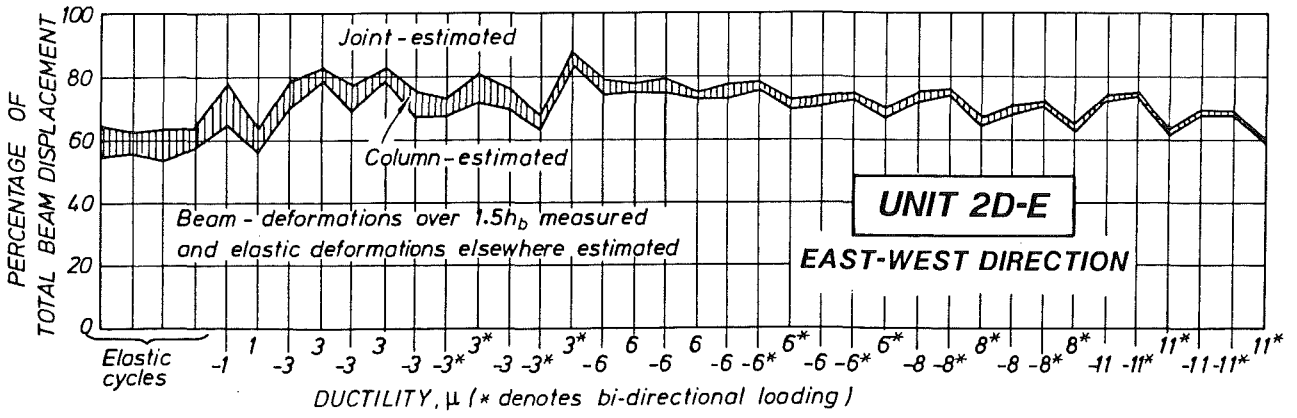

Fig.6.29 - Contributions to east-west interstorey lateral displacements during progressive loading

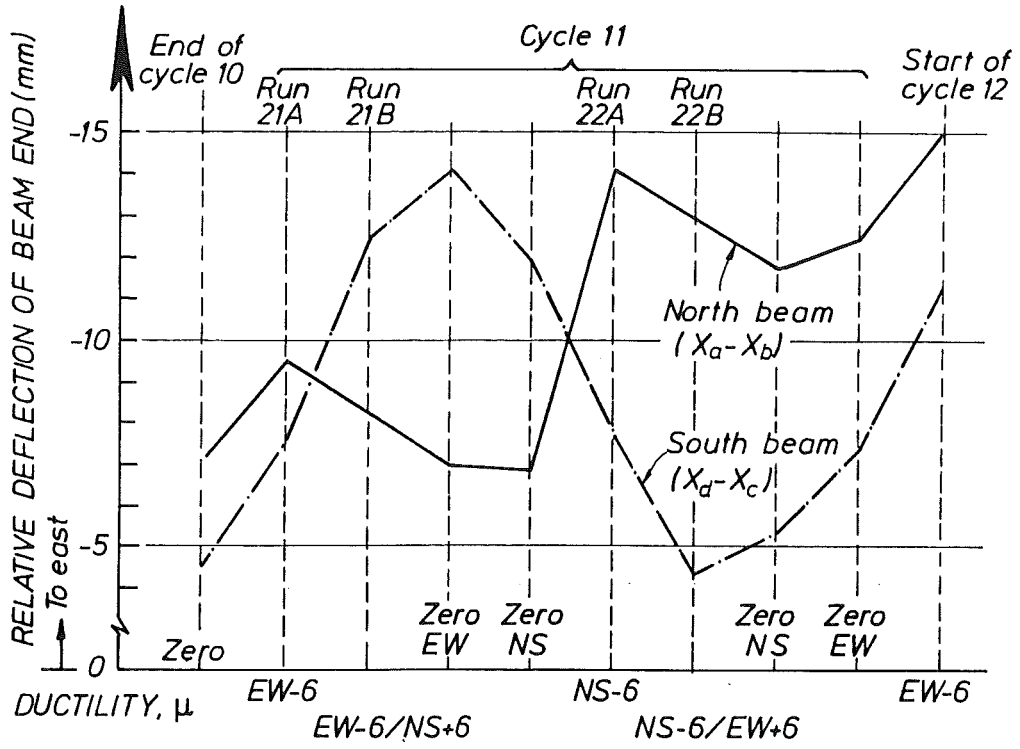

(c) RELATIVE DEFLECTIONS IN CYCLE 11

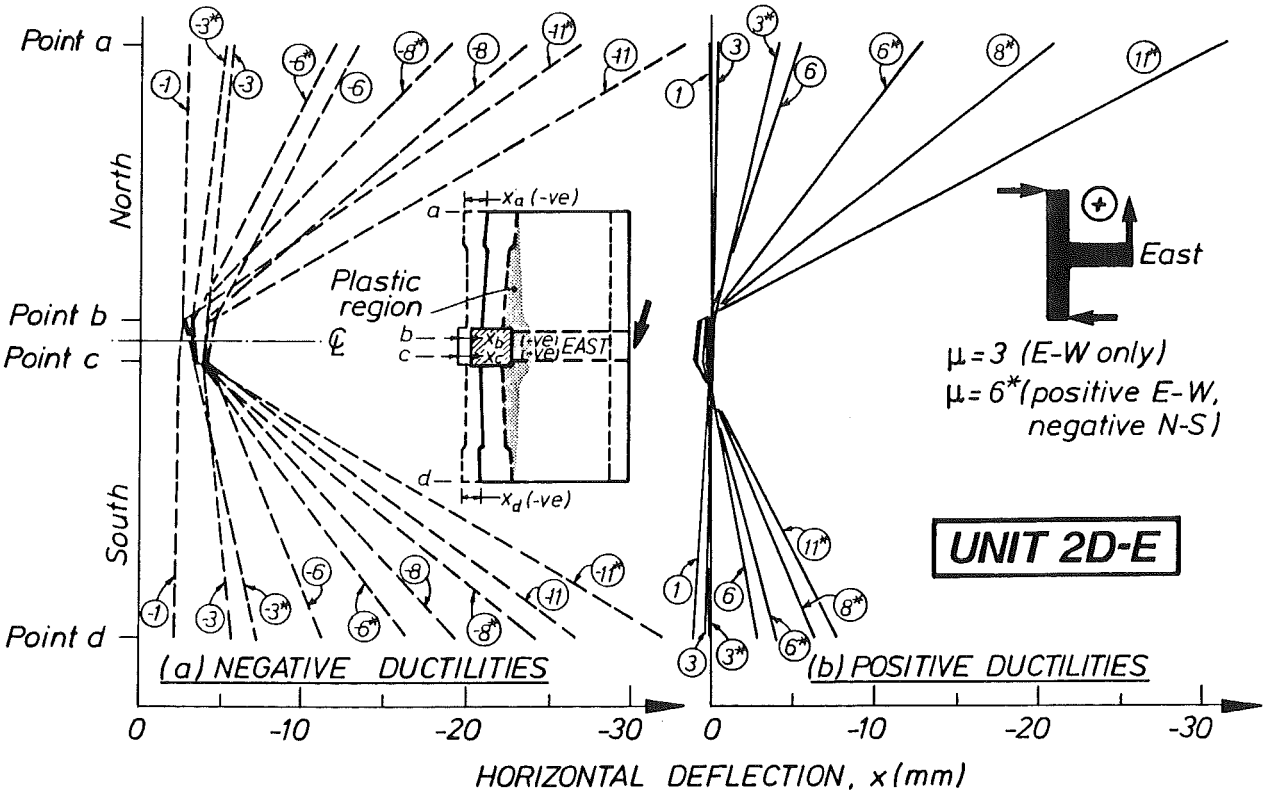

Fig.6.30 - East-west lateral deflections of north-south spandrel beams at 65mm from top surface of slab

Fig.6.30 shows the horizontal east-west deflections at the beam ends and at the joint. It is seen that the north and south beam ends moved laterally significantly with respect to the joint. At negative ductilities when the east beam was being displaced downwards (Fig.6.30(a)), the deflections were generally symmetrical. This pattern is consistent with the participation of the slab bars in tension flange action which is discussed in Section 6.5. However,, there was consistent decrease in lateral displacements at point a (i.e. north end) when proceedings from an imposed uni-directional negative ductility to a bi-directional ductility of the same level (Fig.6.30(a)). This trend was reversed at point d at the south end.

Distortions at positive east-west ductilities (Fig.6.30(b)) were irregular. While the joint (points b and c) moved to the west, residual eastward movements at points a and d remained dominant. The following paragraph attempts to explain the above phenomena by considering the behaviour of the floor slab in this exterior joint assembly. Also the predominant effect of the sequence of applying displacement ductilities is more easily appreciated by reviewing in some detail the measurements recorded in one specific cycle. For this purpose cycle 11 to bi-directional ductility of μ = 6* is chosen.

In Fig.6.30(c), the east-west lateral deflections of the beam ends, relative to the column (joint), at various stages of cycle 11 are shown by a continuous solid line for the north beam and a dashed-dotted line for the south beam.

As can be seen in Fig.6.30(c), at the end of cycle 10 when all external applied forces were removed, there was a large residual deflection at the north end. In load run 21A, the east beam was subjected to negative (downward) ductility of μ = -6(EW). Both spandrel beams moved eastwards in a similar fashion. It is considered that this resulted from the fact that the floor slab acted as tension flange of the east beam. It is reported in Section 6.5 (slab bar strains) and in Chapter 7 (slab behaviour) that the north-south slab reinforcing bars were simultaneously stressed in tension.

The following load run 21B imposed an additional ductility of μ = 6(NS), resulting in a bi-directional ductility referred to as -6* in Fig.6.30(a). As north beam was displaced upwards, its lateral deflection reduced (Fig.6.30(c)). At the same time the south beam moved further to the east whilst undergoing downward displacement. Thus there was an "apparent"

horizontal anti-clockwise rotation of the test specimen about its column axis. Upon unloading in run 21 by first proceeding to zero EW ductility, this "apparent" anti-clockwise rotation continued. However, at the second stage while approaching zero NS ductility, the north beam deflected backwards to the west while the south beam changed little.

In run 21B when the south beam was pushed downwards, the N-S running slab bars in the southern slab panel were stressed more severely than in run 21A. At the same time, tensile stresses in the E-W slab bars in the same panel had to be increased to sustain the diagonal compression field that transmit in-plane shear forces due to the simultaneously applied downward tip forces at east and south beams. Thus in comparison to the north beam, lateral deflection of the south beam increased. The simultaneous upward displacement of the north beam caused compression in the top fibres of the north slab panel close and parallel to the spandrel beam. Consequently the east-west tension in the north slab panel would have reduced. This resulted in the decrease of the E-W lateral deflection of the north beam.

A clockwise rotation of the test unit about a vertical axis, opposite to that reported for run 21, was observed in run 22A to μ = -6(NS). No external force was applied to the east beam. The north beam was pushed downwards and its eastward deflection doubled. Deflection at the south end decreased further as the south beam was lifted upwards. Again it is considered that this resulted from increased tension being generated in the north-south slab bars in the north panel, necessitating also increased tension in the east-west slab bars in order to mobilise a diagonal compression field in that panel.

In run 22B to μ = -6(NS) and +6(EW) causing compression in the top fibres of the east beam at column face, both spandrel beams deflected backwards (i.e. to the west). As can be seen in Fig.6.30(c), the westward movement of the south beam was much larger.

Upon unloading first to zero N-S ductility while maintaining μ = +6(EW), the north end rebound further to the west but the south end deflected again eastwards, both by a small magnitude. Subsequently the E-W ductility was removed, causing both spandrel beams to move eastwards. There were always residual tensile strains in the slab bars.

The results in Fig.6.30 are presented in a condensed format in Fig.6.31 in which the average absolute lateral deflections of the beam tips, relative to the joint, are plotted versus the displacement cycles. The gradual and consistent increase in beam tip movements with progressive ductilities is more easily seen.

The unsymmetrical response of Unit 2D-E, in terms of the "rigid body rotations" implied by the test results of Fig.6.30, is considered to be a feature of an isolated exterior joint test assembly. The phenomenon is not considered to have any significant influence on the overall behaviour of exterior joints, particularly in a real building structure where continuity with adjacent parts of the floor system will inhibit in-plane (rigid body) rotations.

Rotations about the north-south horizontal axis of spandrel beam sections at the same four points, are presented in Fig.6.32. For an easier interpretation of these results, the rotations at locations a and d relative to those measured at b and c, defined as twist, were computed and these are presented in Fig.6.33. Up to an east-west ductility of 6, symmetrical response is evident. Differences of beam twists with larger imposed ductilities are significant and consistent with similar differences in horizontal deflection of the spandrel beams shown in Fig.6.30.

In Section 6.3.2 the total rotations of the east beam over a distance of 825 mm from the column face, considered representative of the plastic hinge rotations, were shown in Fig.6.19. The response throughout the test was nearly symmetrical, although the magnitudes of positive rotations associated with upward bending of the east beam tended to become smaller at ductilities of six or more. However, as far as the spandrel beams are concerned the predominantly negative end rotations shown in Fig.6.33 indicate that these beams were essentially influenced by the downward bending of the east beam. Because of tension flange action this was to be expected. When the east beam was displaced upwards to achieve positive E-W ductilities, large residual negative rotations prevailed (Fig.6.33). This trend is consistent with that observed earlier when the lateral deflections of the spandrel beams were considered.

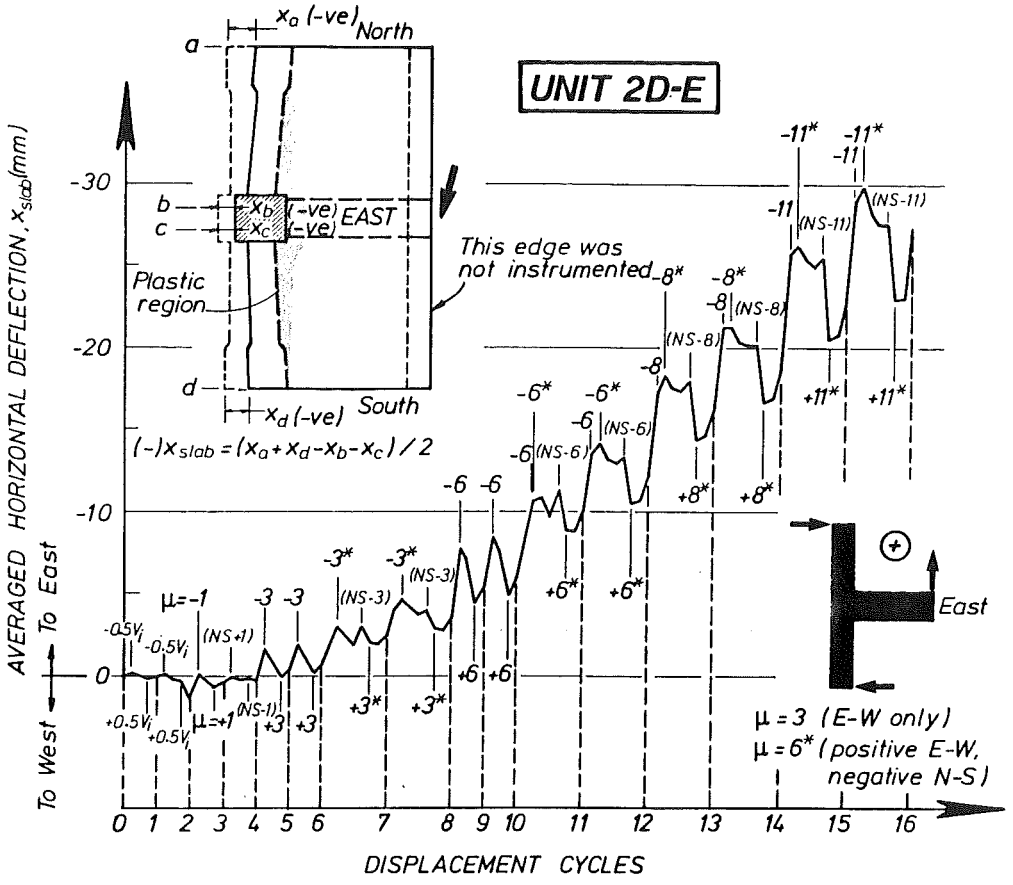

Fig.6.31 - Averaged east-west lateral deflections of north-south spandrel beams relative to column

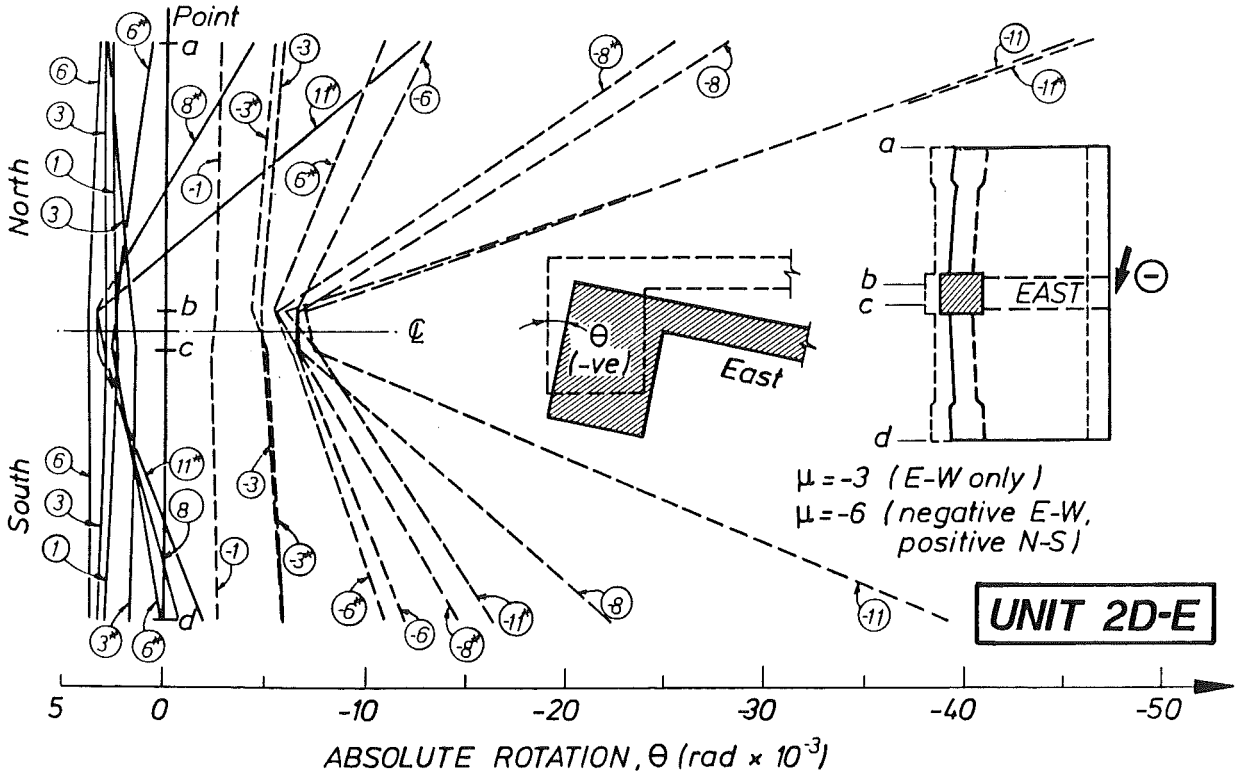

Fig.6.32 - Rotations of joint and spandrel beams about north-south axis

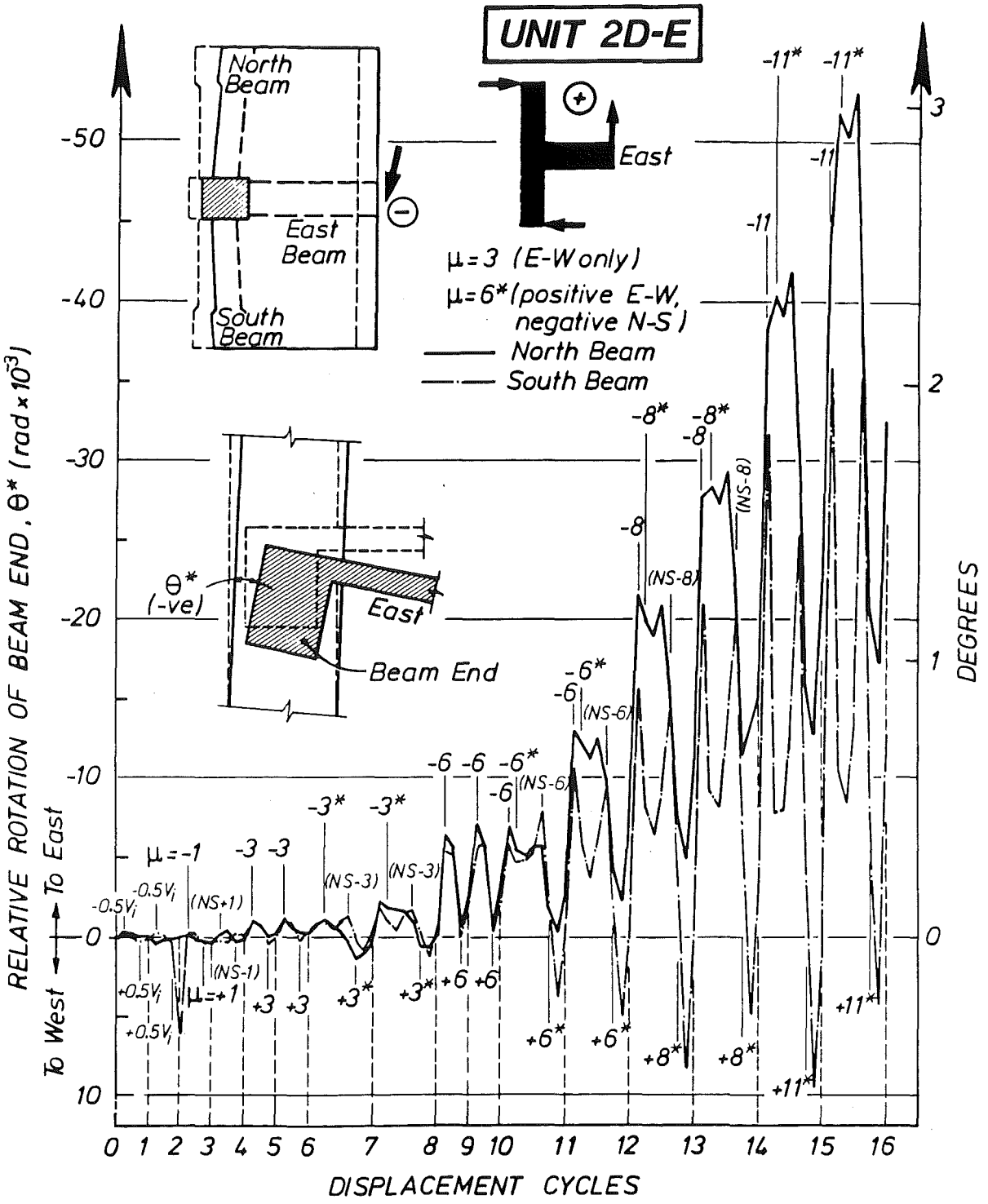

Fig.6.33 - Rotations of ends of north-south spandrel beams relative to joint

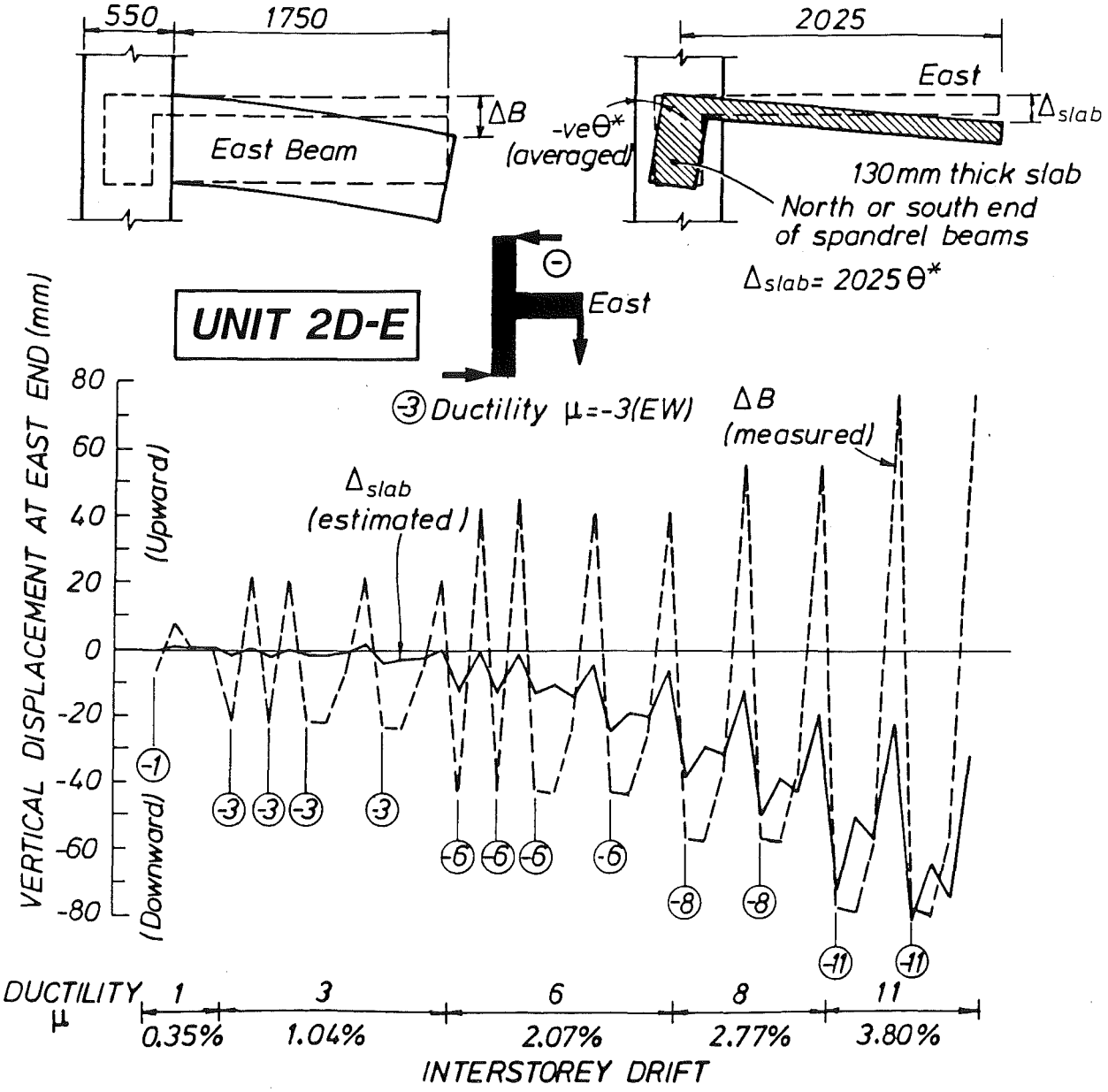

Fig.6.34 - A comparison of measured vertical beam deflections and estimated slab displacements at the east edge of test unit

Fig.6.34 compares the measured vertical displacements at the east beam tip, Δ_B, which are extracted from Fig.6.12, and the estimated slab vertical deflections, Δ_{slab}, due to the twists in the spandrel beams. The twist angle $\theta*$ in Fig.6.34 was taken as the average of the angles found for the north and south beams shown in Fig.6.33. Deflections due to flexure or shear developed in the slab were neglected. The results in Fig.6.34 corresponding with uni-directional negative E-W ductilities are as expected. The displacement Δ_{slab} increased as loading progressed. At ductility μ = -11(EW), Δ_{slab} nearly matched Δ_B. At this stage twists in the spandrel beams appeared to be comparable to the rotations in the east beam.

Using traditional methods [1,4] and treating the spandrel beams having a rectangular section, the cracking torque and ideal torsional post-cracking strength were estimated as 39 kNm and 67 kNm respectively. When all twelve D10 east-west slab bars in one slab panel (Fig.3.16(b)) were stressed to the yield strength of the steel, the torsional moment with respect to the centre of the rectangular beam section would have been 68 kNm. However, the spandrel beams were also subjected to bending about the weak axis and to horizontal shear forces. Moreover plastic hinges developed at column faces under north-south seismic actions. Therefore it is considered that torsional moments, even at large twists due to large east-west negative ductility loading, were very small. The overall performance of the test unit, in terms of strength and ductility capacities, was considered not to have been affected by the twisting of the spandrel beams.

6.4 BEAM BAR STRAINS

Strains in the longitudinal reinforcing bars of the three beams, measured by electrical resistance strain gauges, are summarised in Figs.6.35 and 6.36. In a pattern similar to that observed with the last two units, starting from ductility level of μ = 3 strains became erratic particularly at column faces. More realistic strain distributions at large ductilities at beam bar levels in the plastic hinge regions are given in Figs.6.37 to 6.39.

Throughout the loading history the north-south beam bars were adequately anchored inside the joint core (Fig.6.35). Buckling of the bottom layer beam bars commenced in the second cycle to μ = 11. The limited information in Fig.6.35 nevertheless shows that bar strains within the joint

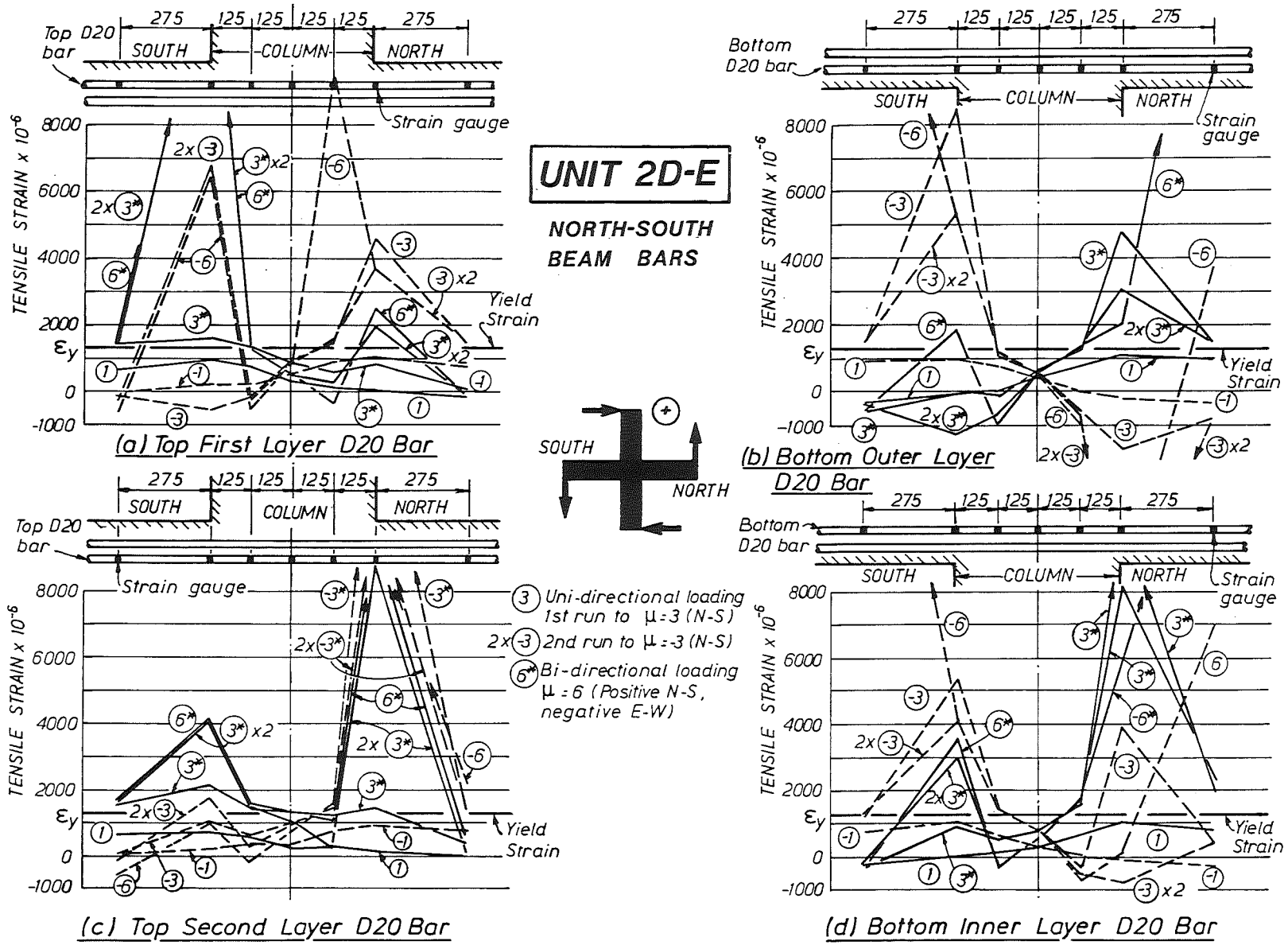

Fig.6.35 - North-south beam bar strains measured by strain gauges

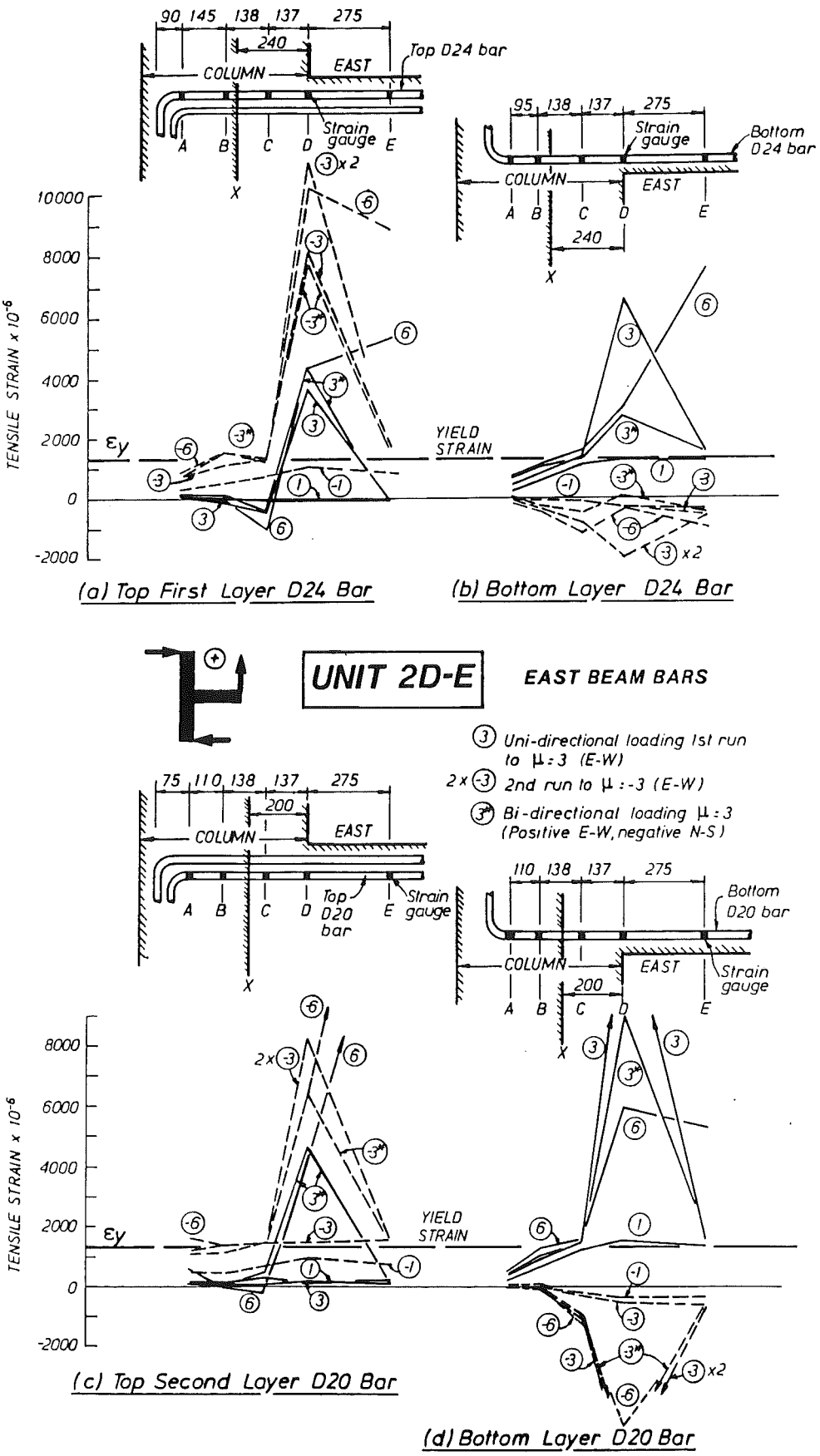

Fig.6.36 - East beam bar strains measured by strain gauges

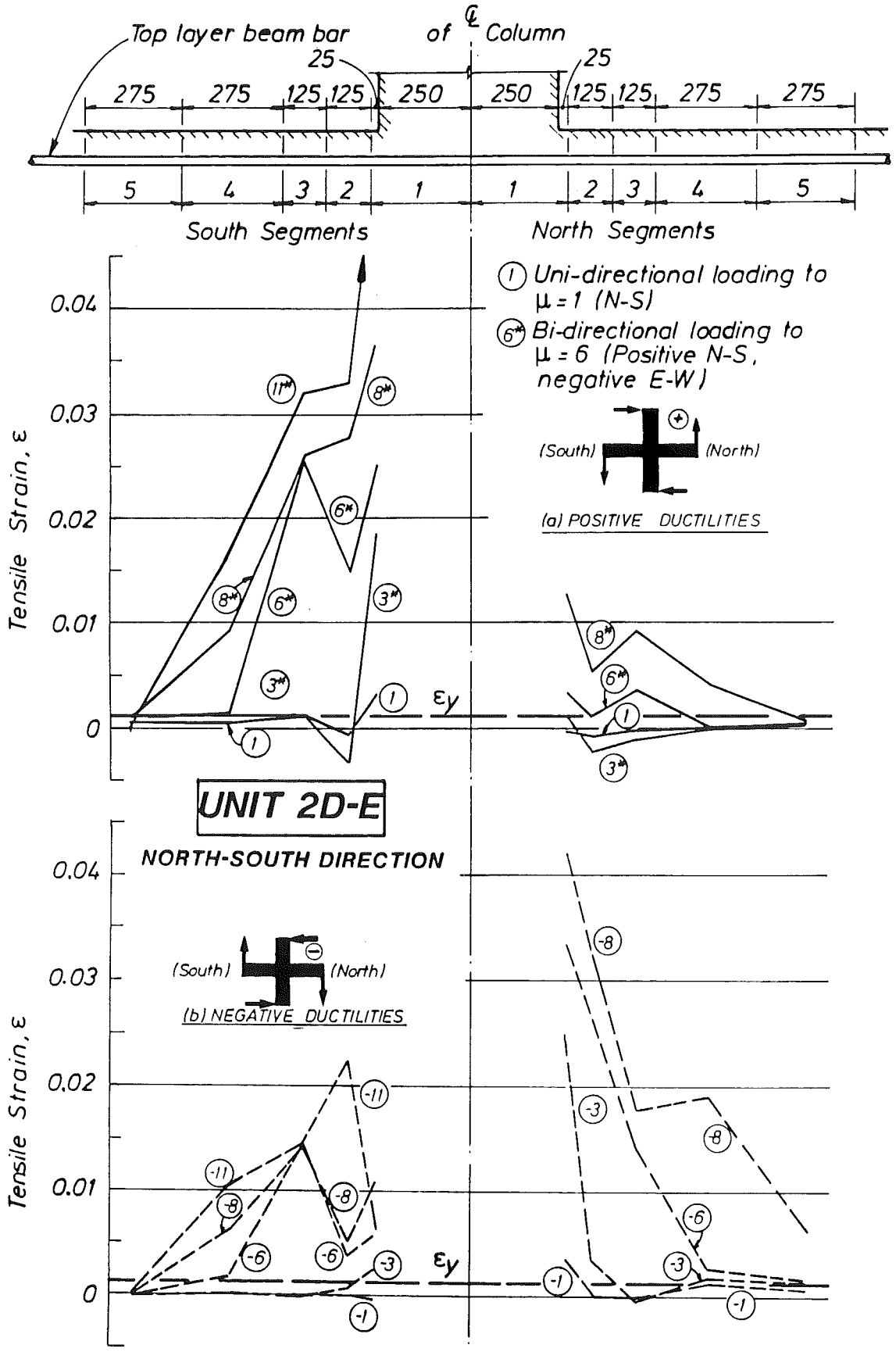

Fig.6.37 - Strain distributions at top layer beam bar level as estimated from linear potentiometer measurements (north-south direction)

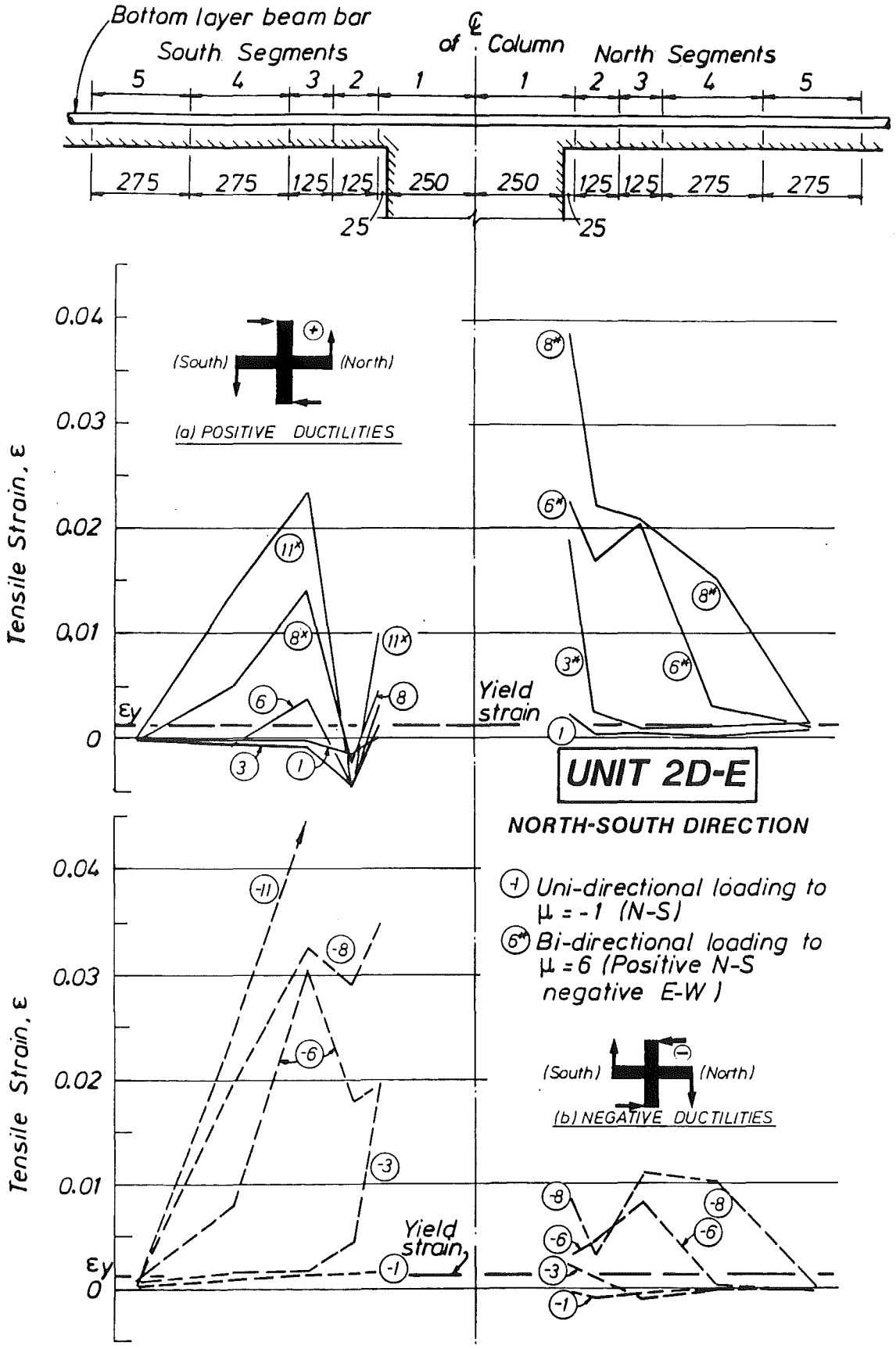

Fig.6.38 - Strain distributions at bottom layer beam bar level as estimated from linear potentiometer measurements (north-south direction)

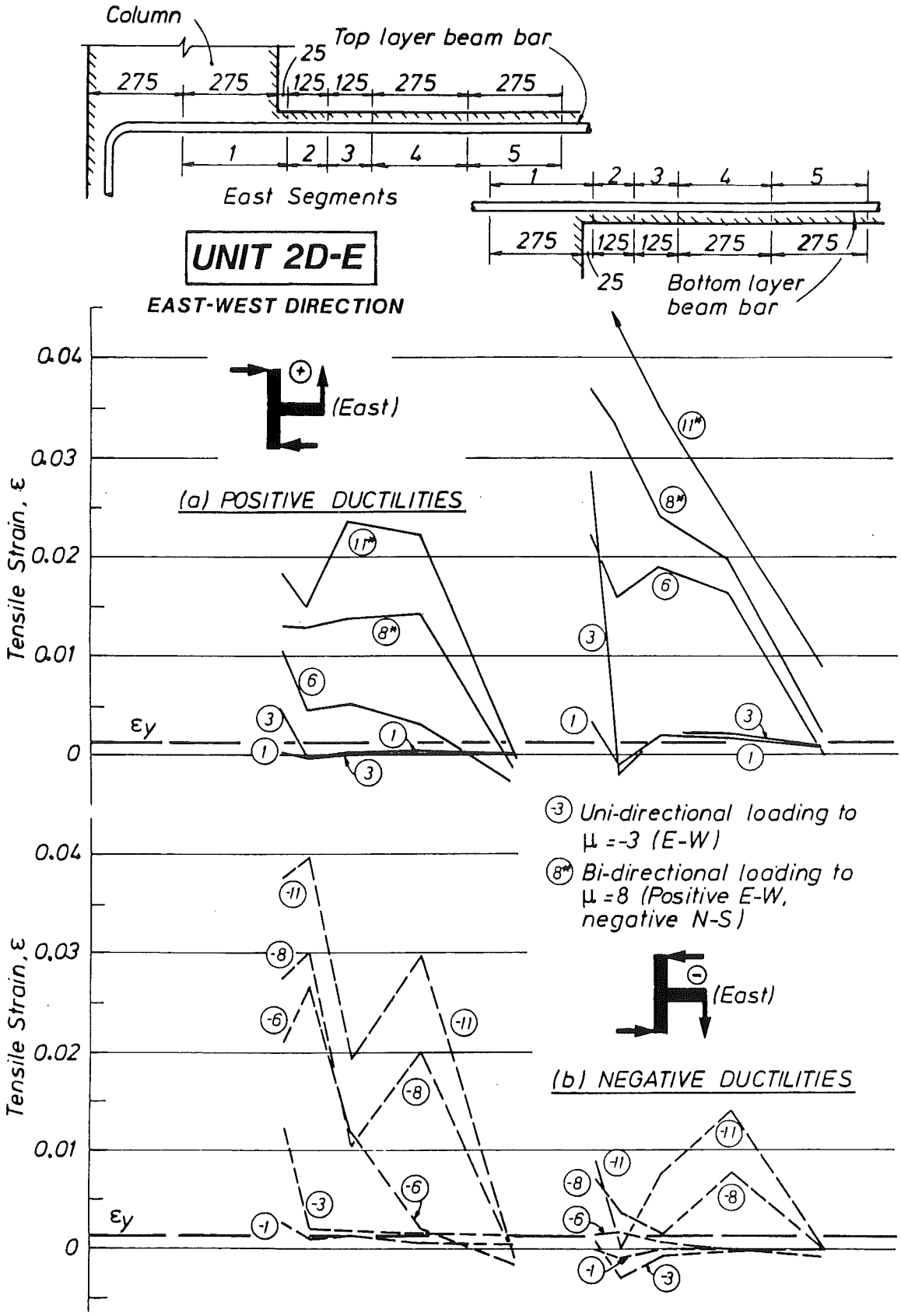

Fig.6.39 - Strain distributions at top and bottom layer beam bar level as estimated from linear potentiometer measurements (east-west direction)

remained predominantly tensile and bond forces were developed over the full depth of the joint core rather than outside the joint.

When Fig.6.35 is studied together with Figs.6.37 and 6.38 for beam strains in the north-south direction, it is concluded that the compressive stresses developed in the beam bars at column faces did not attain strain hardening. The maximum level appeared not to have exceeded yielding in compression. The largest tip forces observed from the response of the north beam (Fig.6.13) were 165 kN (upward) in run 29 to μ = 11 and 174 kN (downward) in run 30 to μ = -11. According to the estimation method based on truss model for the transfer of beam shear (Section 4.4), it is found that the probable steel compressive stresses at column faces were of the order of $0.8f_y$ in the top bars and $0.9f_y$ in the bottom bars of the symmetrically reinforced beams.

Referring to the east beam (Fig.6.36 and 6.39), both the top and bottom bars were provided with 90° standard hook anchorages in the joint core. The beam was initially displaced downwards (i.e. to negative ductility) in each cycle. The pattern of strain distributions shown in Fig.6.39 agrees with those found for Unit 1D-I (Figs.4.27 and 4.28) and Unit 2D-I (Figs. 5.30 to 5.33). This confirms the spreading of inelastic steel tensile strains in the plastic hinge towards the free end of the east beam.

The effect of bi-directional loading on the strains in the east beam bars measured by strain gauges can be seen in Fig.6.36. With allowance for this effect, the strain patterns shown in Fig.6.36 indicate that adequate embedment lengths were provided to anchor the beam bars subjected to cyclic tension and compression forces. Consistently low tensile strains were maintained at gauges A and B. However, larger strains were recorded at gauge C. The hatched lines marked "X" in Fig.6.36 indicate the theoretical position beyond which anchorage for hooked beam bars should be provided in compliance with NZS 3101 [4] provisions. The code suggests that a distance of $10d_b$ = 240 mm (for D24 bars) or 200 mm (for D20 bars), measured from the inner face of the exterior column, should be ignored when estimating anchorage lengths (see Fig.2.5). This recommendation was based on previously obtained experimental evidence confirming yield penetration along beam bars undergoing large ductility reversals. It was observed in this test, and evidenced in Fig.6.36, that anchorage especially in compression was very satisfactory. Therefore some relaxation in the $10d_b$ requirement to a reduced $8d_b$ length is considered permissible. As will be seen in Chapter 8, the concrete strut

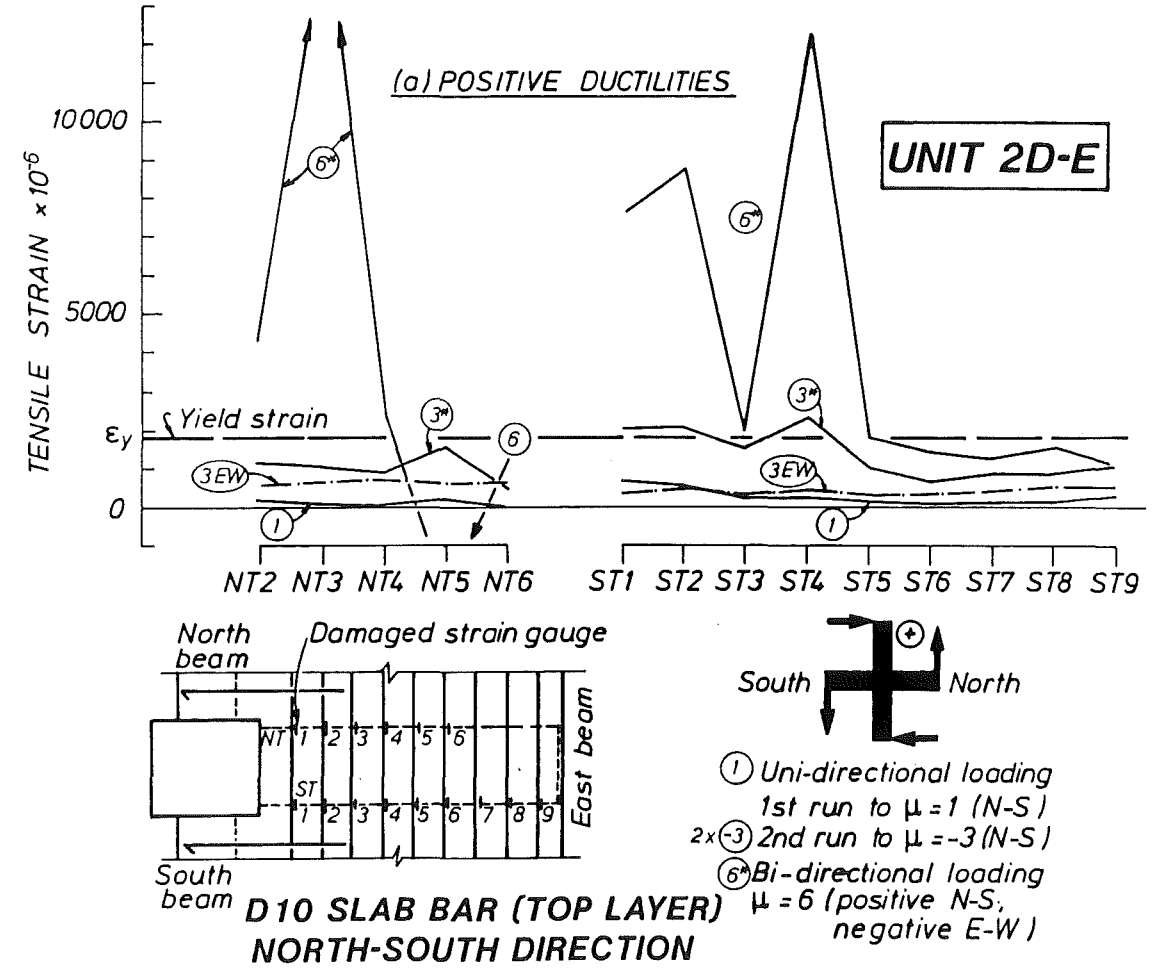

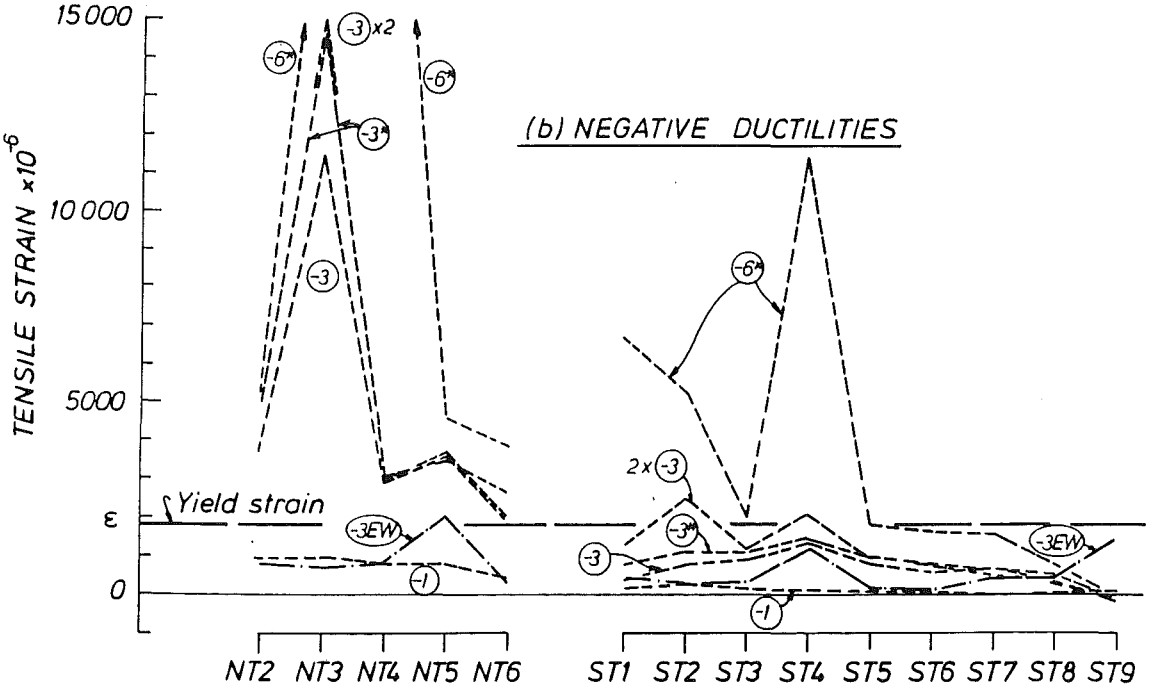

Fig.6.40 - North-south top layer slab bar strains

mechanism of exterior joint shear resistance is enhanced by the anchorage forces at these hooks.

The vertical east beam shear forces measured at the tip (Fig.6.12) were found to be slightly less than those observed for Unit 2D-I. Hence referring to Sections 5.4 and 4.4, the maximum probable compressive stresses in the beam bars were $0.5f_y$ at top and $1.0f_y$ at bottom.

6.5 SLAB BAR STRAINS

Figs. 6.40 and 6.41 show the slab bar strains in the north-south direction. In this direction, the joint assembly behaved as an interior joint assembly like Unit 2D-I. Although the absolute magnitudes of the strains measured were less than those seen in Figs.5.34 to 5.35, the observations and conclusions reported in Section 5.5 for Unit 2D-I are considered equally applicable to this Unit 2D-E. Therefore only essential points are highlighted here. The dominant influence of north-south actions on the five top layer

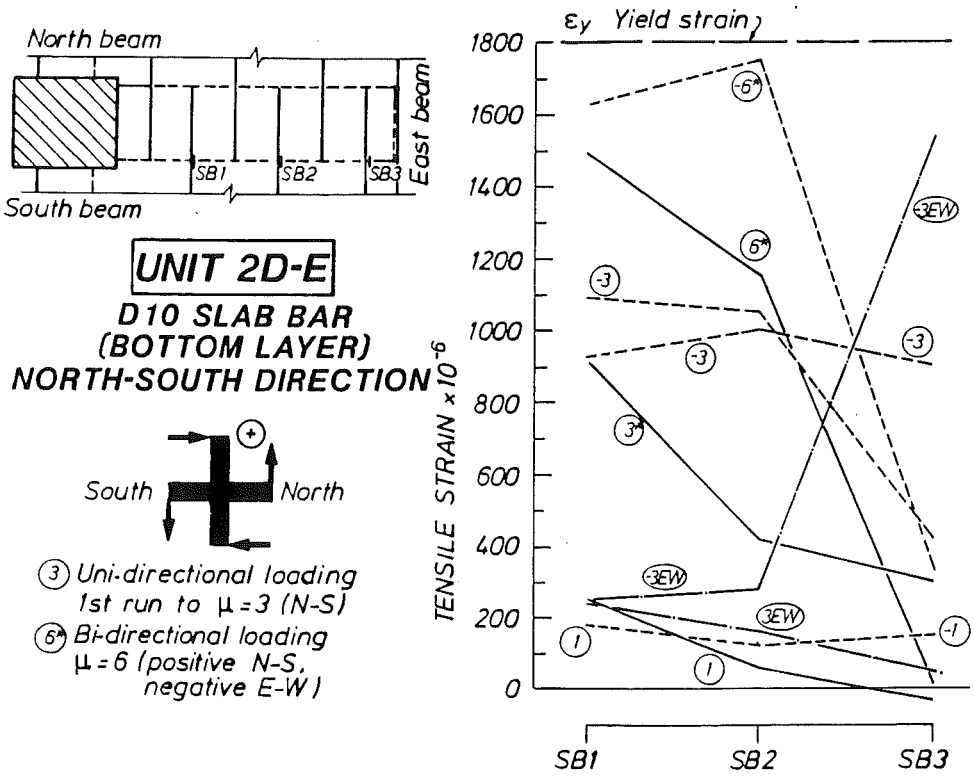

Fig.6.41 - North-south bottom layer slab bar strains

slab bars near to the column is evident in Fig.6.40. The smaller strains observed in this test, when comparing Figs.6.40 and 6.41 to Figs. 5.34 and 5.35, are likely to be caused by curtailing the east-west top layer slab bars (see Fig.3.16). A different mechanism of slab force transfer in the E-W direction as in an exterior joint, to be discussed in Chapter 7, would accordingly affect the transverse N-S slab bars especially at increasing ductilities. To demonstrate the participation of these N-S slab bars in E-W ductilities, strains at $\mu = \pm 3$(EW) are plotted in Figs.6.40 and 6.41. The elastic tensile strains are considered significant.

In the east-west direction, the top layer D10 slab bars (Fig.6.42) had standard hook anchorages as shown in Fig.3.3(b) and in this respect satisfied code [4] requirements. While all twelve bars were strain gauged along and above the inner face of the north-south beam, as shown, it is to be noted that, because the north and south beam ends were enlarged (see Section 3.2), the four outermost slab bars (i.e. ETS6, ETS5, ETN5 and ETN6) were provided with slightly longer embedment length. The same applied to the bottom layer bars EBS6, EBS5 and EBN5 in Fig.6.43.

Under negative east-west ductilities (Fig.6.42(b)), slab bars were strained in tension. Therefore Fig.6.42(b) gives important information regarding the extent of slab bars participating in tension flange action. At uni-directional ductility $\mu = -1$(EW), two slab bars on each side of the column (i.e. ETS1, ETS2, ETN1 and ETN2) attained very high elastic tensile strains. These strains reduced, as expected, when the east beam was displaced upwards as indicated by the strain results for $\mu = 1$(EW) in Fig.6.42(a).

With the advancement of cyclic loading, tensile strains above yield level developed in more slab bars at negative east-west ductilities (Fig.6.42(b)) while at subsequent positive (E-W) ductilities, large residual tensile strains were observed (Fig.6.42(a)). The effect of bi-directional loading on the E-W slab bar strains is more obvious in Fig.6.42(a) showing the positive ductility case, in which the south beam was pulled upwards and the north beam pushed downwards. It has been shown in Fig.6.40(b) and discussed in the first paragraph of this section that tension forces developed in the N-S slab bars. The diagonal compression field mobilised in the slab (see Chapter 7) required that the E-W slab bars be stressed in tension. Hence increased tensile strains under bi-directional loading were consistently noted in Fig.6.42(a). The increase was more uniform in the north slab panel.

In the negative ductility range (Fig.6.42(b)), the effect of bi-directional loading was less obvious. There were increases and decreases in slab bar strains. The changes appeared to be more uniform in the south slab panel. This can be explained by considering the loading history (Fig.3.19) according to which negative E-W ductility was imposed prior to positive N-S ductility of the same magnitude. As the south beam was displaced downwards together with the east beam, the bars in the south slab panel were stressed in tension in both directions.

At ductility of $\mu = 6$ or more (Figs.6.4(b) and 6.5), concrete spalling and crushing in the beams at column faces might have caused some of the slab bars to loose their anchorage. Subsequent strain readings were considered questionable. However, the conclusion drawn from the consistent tensile strain distributions, shown in Fig.6.42(b), is that at least four bars on each side of the column were subjected to tension at yield strength when the east beam was displaced downwards. This observation agrees with that made in Fig.6.12, in which the measured negative (downward) beam tip forces ranged between the theoretical $-P_i$ (which considered only two slab bars in tension, according to code [4] recommendations) and $-P_i^*$ (which included all the twelve top layer slab bars in tension, as a hypothetical extreme case).

When the east beam was pulled upwards to positive ductilities, the reductions in tensile strains as can be inferred from Fig.6.42(a) suggest that probably four slab bars on each side of the column were subjected to compression. In particular compressive strains were measured in the bars marked ETS1 and ETN1. The results can be correlated with the discussions presented at the end of Section 6.2.3 which suggested that a flange under compression existed at the top of the slab.

The bottom layer east-slab bars (Fig.6.43) were embedded in the spandrel beams each with a straight length of 260 mm. Despite the absence of anchorage hooks, it is evident from Fig.6.43 that slab bars close to the column were also stressed in tension.

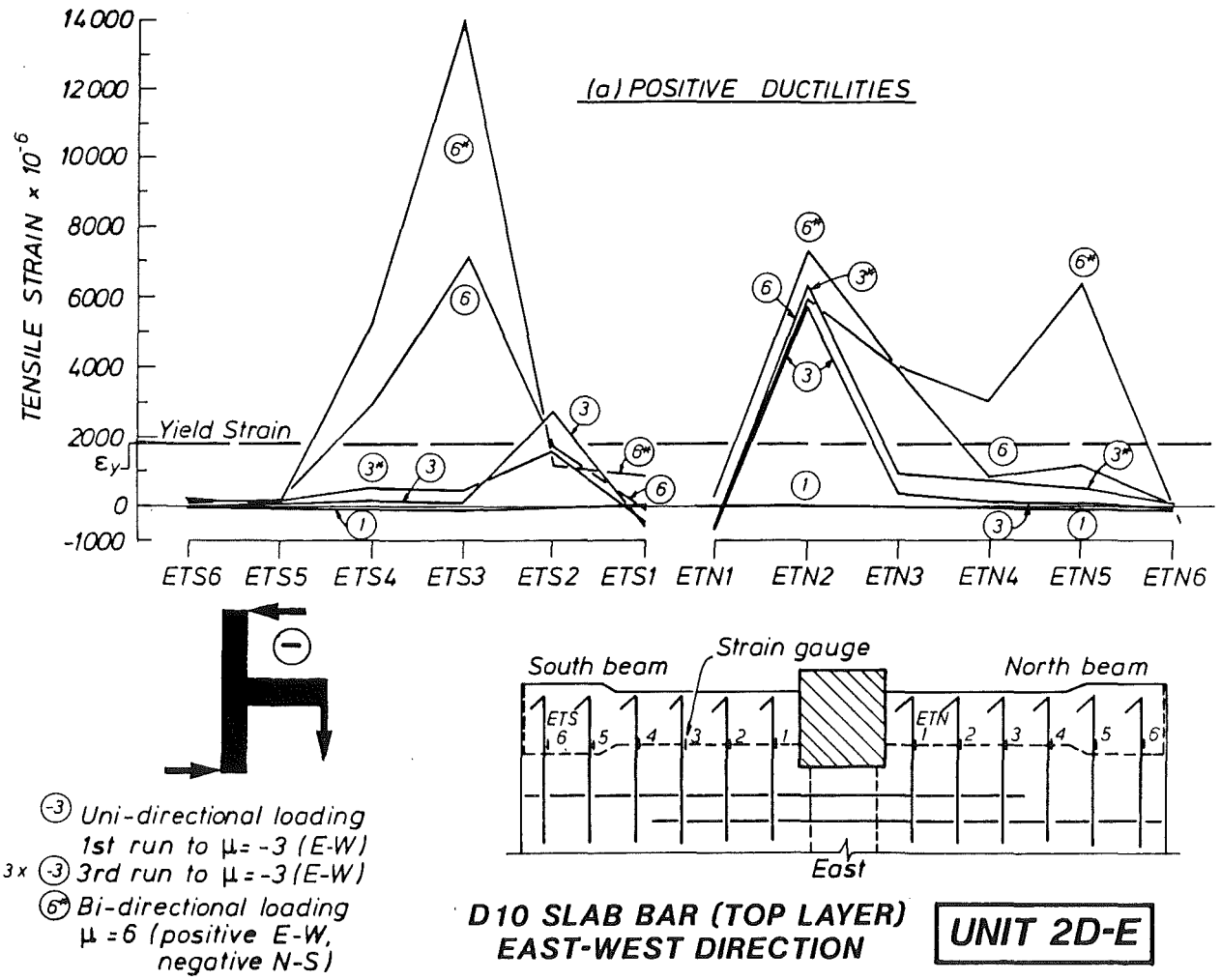

Fig.6.42 - East-west top layer slab bar strains

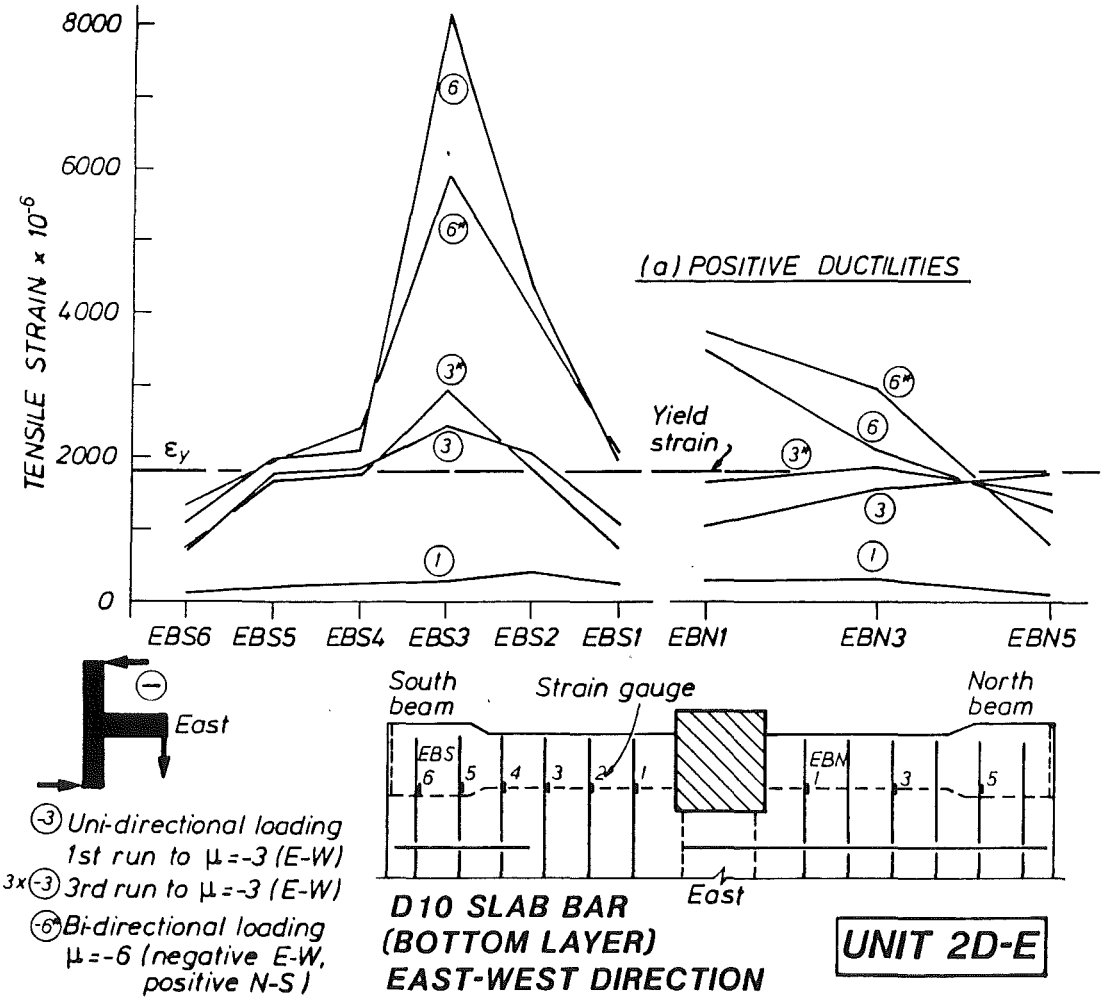

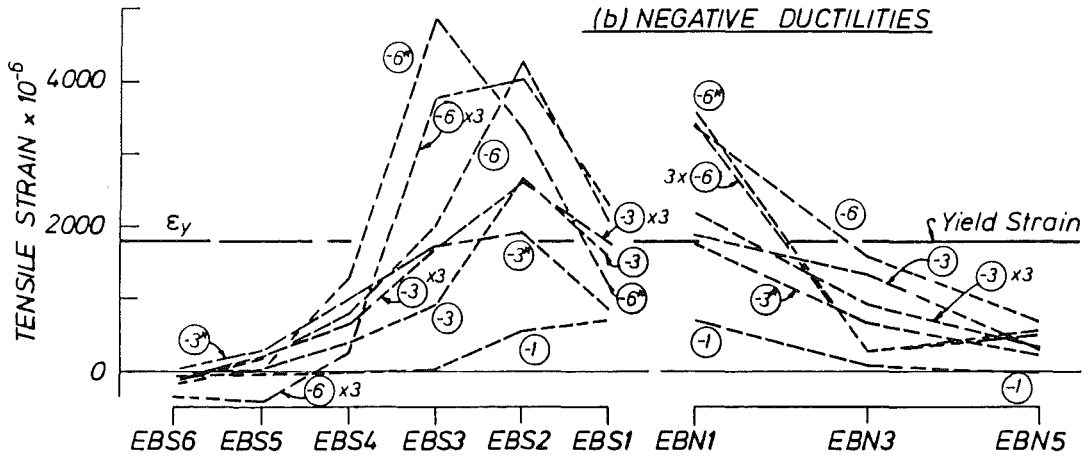

Fig.6.43 - East-west bottom layer slab bar strains

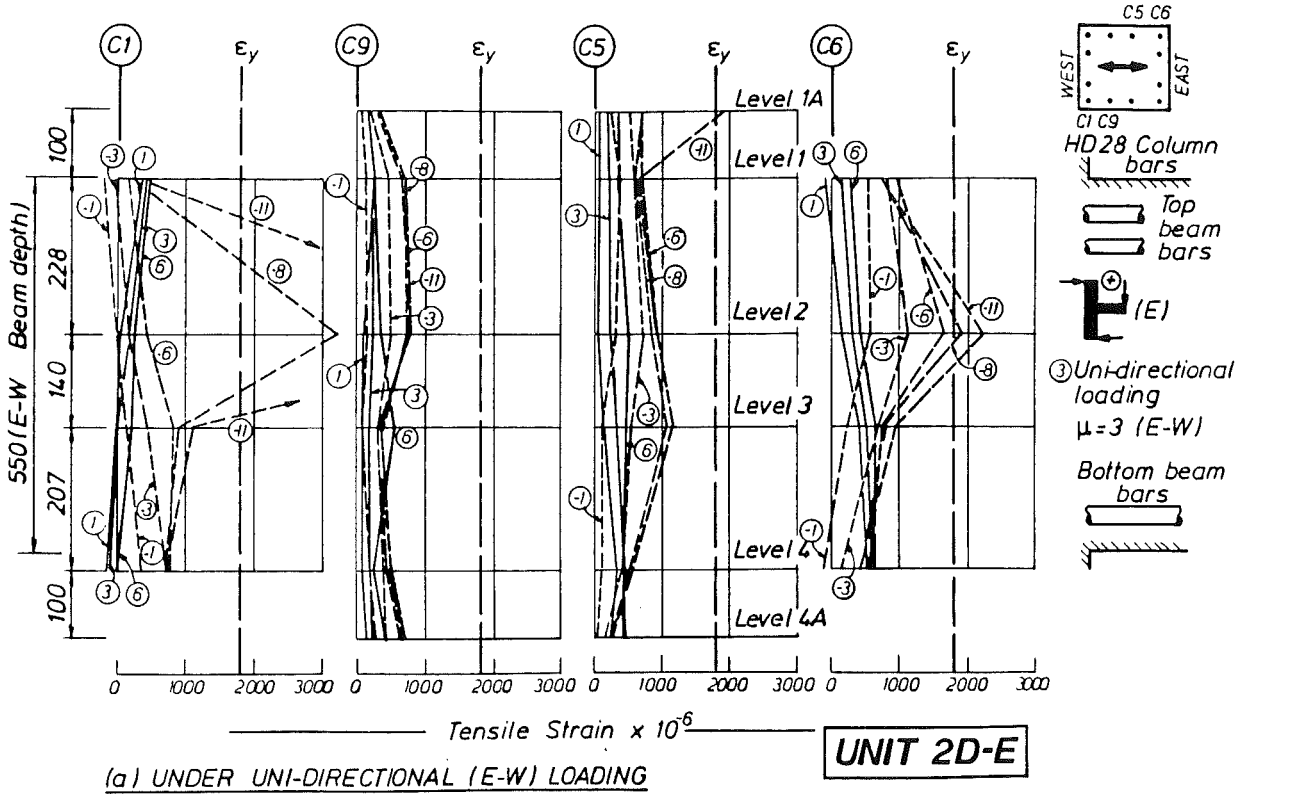

(a) UNDER UNI-DIRECTIONAL (E-W) LOADING

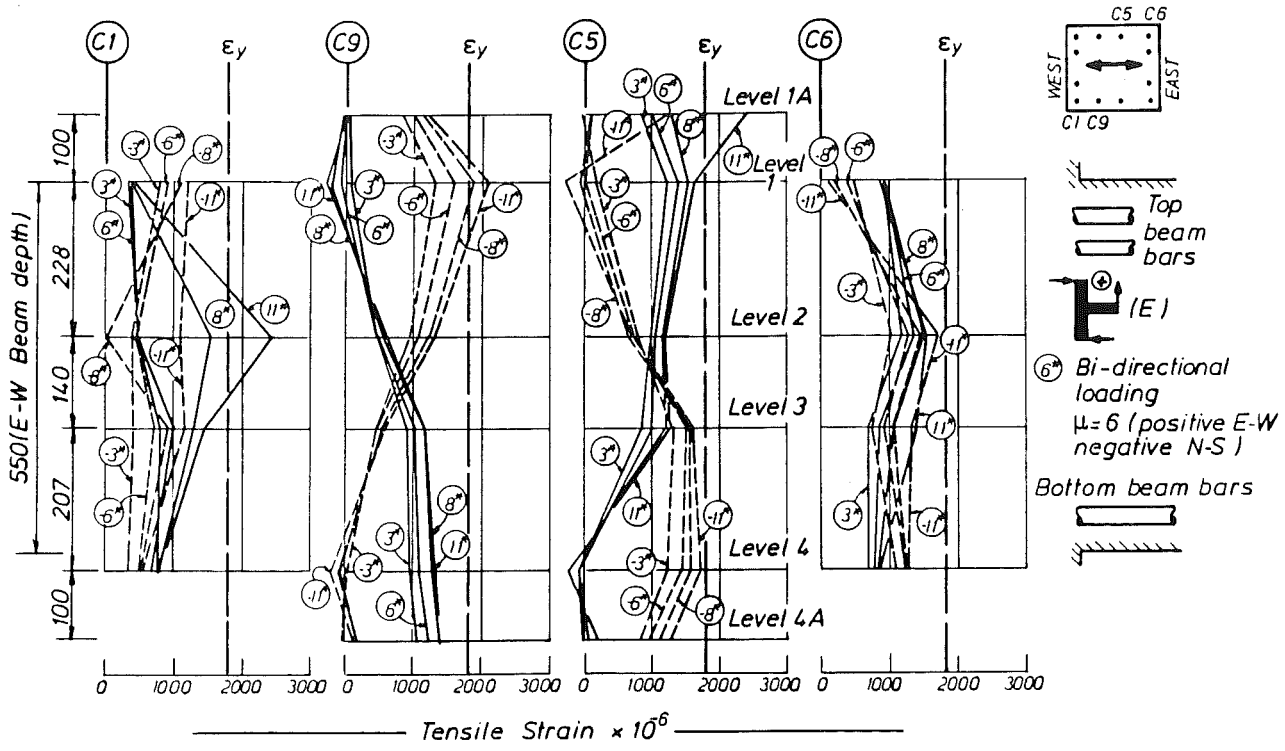

(b) UNDER BI-DIRECTIONAL LOADING

Fig.6.44 - Column bar strains within the joint core showing east-west loading effects

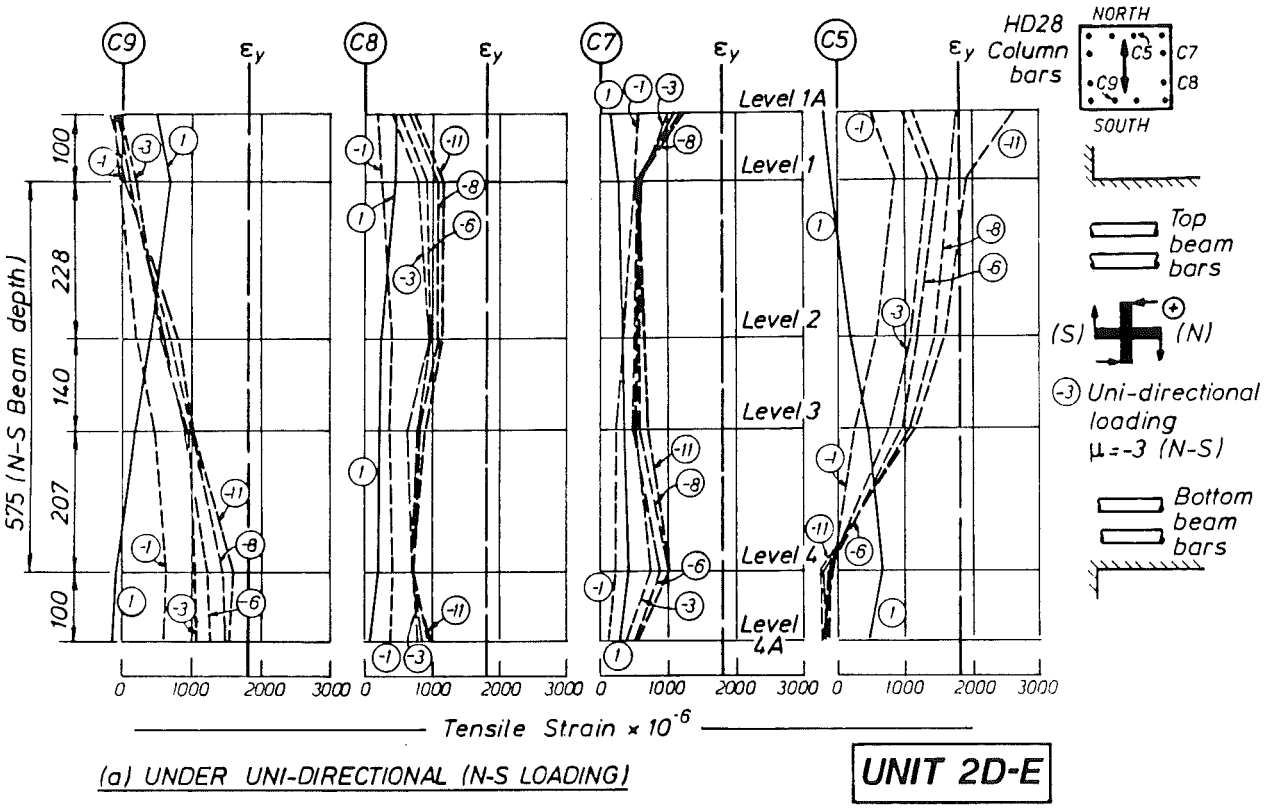

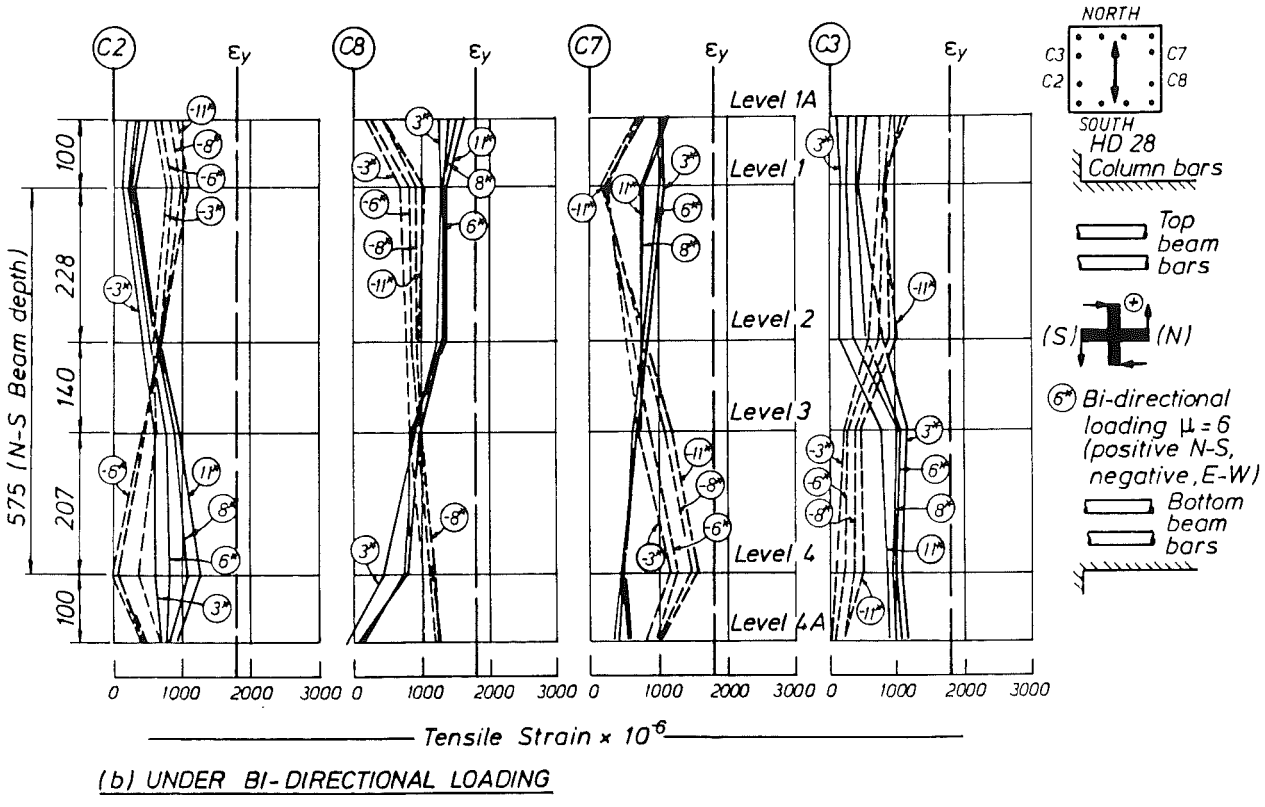

Fig.6.45 - Column bar strains within the joint core showing north-south loading effects

6.6 COLUMN BAR STRAINS

Strain results shown in Figs.6.44 and 6.45 for the column bars confirm that the column sections remained elastic throughout the test. In view of the similarity to results observed in the other tests, only selected results are presented here. In general the column's performance was superior to that of Unit 2D-I's interior column discussed in Section 5.6. A comparison of the design and flexural strengths of the columns estimated on the basis of specified material properties can be seen in Table 3.3 of Section 3.2.

Under unidirectional east-west loading (Fig.6.44(a)), the exterior column bars C1 and C6 showed predominant tensile strains in agreement with the loading direction and ductility levels. The tensile strains were generally low. The very high tensile strains at level 2 in both of these bars at ductilities of μ = -8 and μ = -11 were unexpected and could not be explained. However, reference can be made to column bars C2, C3, C7 and C8 in Fig.6.45(b) in which bar strains at bi-directional ductilities are presented. These do not show similar irregularities. Hence the high tensile strains at level 2 of bars C1 and C6 have been disregarded.

For the intermediate column bars C9 and C5 (Fig.6.44(a)), the tensile strains recorded were consistent and gradually increasing, particularly at levels 2 and 3. This is seen as a moderate participation of the column bars in the truss mechanism of shear resistance of the (exterior) joint core in the east-west direction.

While for the column bars in Fig.6.44(a) relatively low tensile strains under uni-directional E-W loading were recorded, Fig.6.44(b) for the same bars under bi-directional loading show higher tensile strains. The strain variations of bars C9 and C5 at levels 2 and 3 are consistent with the predominance of loading in the north-south direction and indicate that the column bars were well anchored inside the joint. It should be noted that contrary to the predictions of a routine analysis of the critical column sections at levels 1 and 4, only negligible compression stresses were recorded in bars C5 and C9.

Fig.6.45 shows column bar strains in terms of north-south loading. Similar conclusions as above are drawn. Because column bars C9 and C5 have been included in Fig.6.44, Fig.6.45(b) shows two alternative bars C2 and C3

under bi-directional loading. Fig.6.45(b) supports the assumption relevant to the participation of vertical column bars in the truss mechanism of joint shear resistance (see Section 4.6) The tension imposed on these column bars within the joint manifests itself in the virtual absence of compression strains at the boundaries of the joint, as seen in Fig.6.45.

6.7 STRAINS IN JOINT TIES

In the calculations in Appendix D.1, it is shown that just enough horizontal joint reinforcement was provided for the predicted shear inputs from both E-W and N-S directions to satisfy code [4] requirements. The strain results for the north-south running legs of the joint hoops under ductilities defined in the N-S direction are presented in Fig.6.46, while results for the east-west legs at E-W ductilities are given in Fig.6.47. Fig.6.48 shows the bar strains under loading transverse to the orientation of the tie legs. This presentation format is identical to that used for Unit 2D-I in Section 5.7. Conclusions similar to those for the other units can also be drawn, although strains measured in this unit were smaller. It appears that the strain patterns seen in Figs.6.46 and 6.47 are not significantly different even though the joint in the E-W direction functioned as an exterior joint as opposed to an interior joint in the N-S direction. The only noticeable exception is the results for type B hoops at negative ductilities (Fig.6.47(b)). Tensile yield strain was exceeded in ties in the upper half of the joint because there was larger shear input from the top bars of east beam under negative (downward) bending. It is evident that of types A, B and C hoops, only the capacity of the type B hoops were fully utilised. The joint core remained essentially elastic, as desired.

In summary, the general strain pattern shows a gradual but consistent increase in tensile strains with ductility levels. This indicates the gradual deterioration of joint shear resisting mechanism via concrete compression strut. In the east-west direction (Fig.6.47), higher readings for the bars during imposed bi-directional ductilities (e.g. results between $\mu = \pm 3$ and $\mu = \pm 3^{*}$), did not suggest the existence of any confining effect, as claimed sometimes, to improve joint performance. It is considered that strains in the short legs of types C and E ties are primarily due to anchorage required to be provided for the development of consistently higher forces generated in the long legs of these ties.

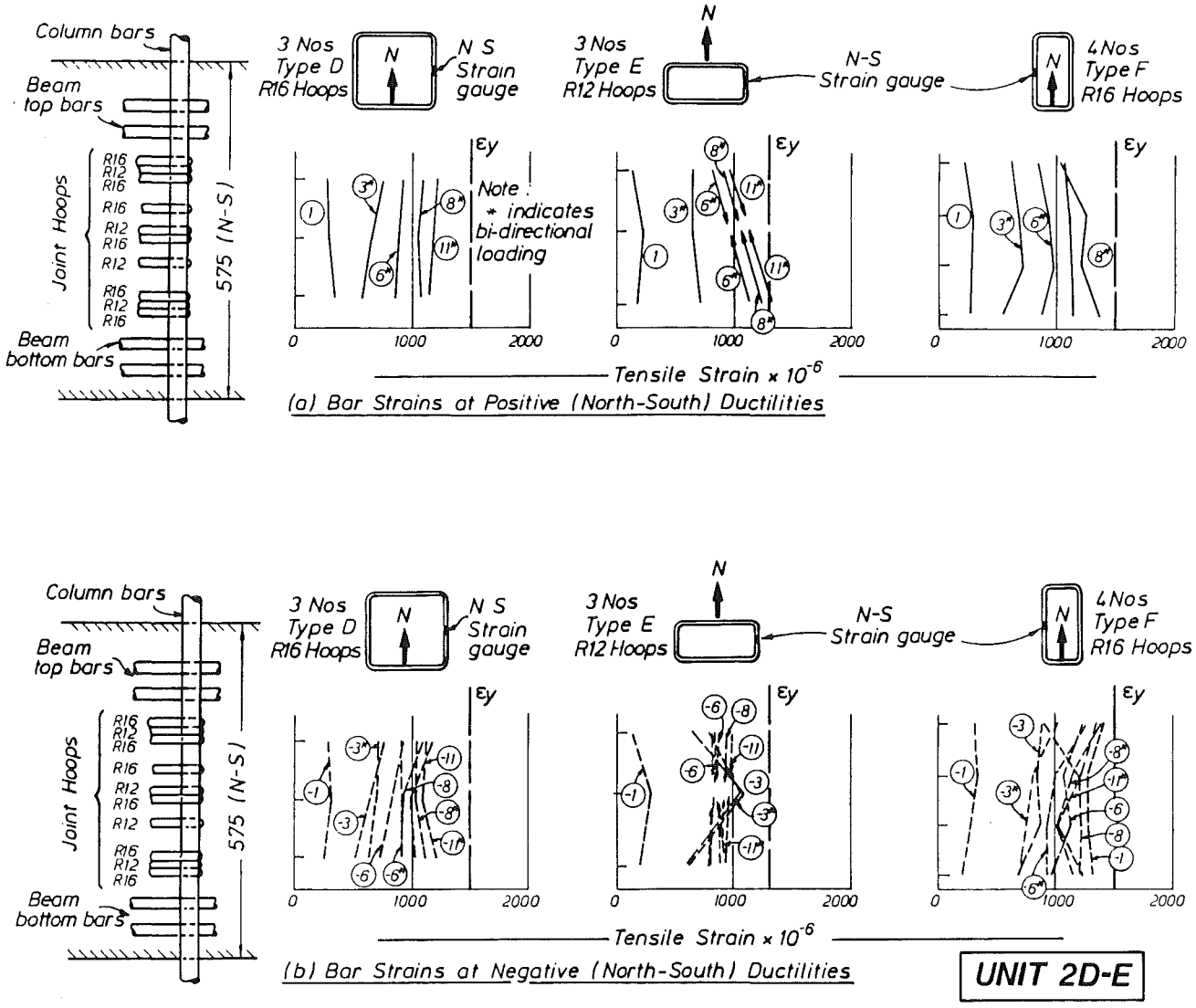

Fig.6.46 - North-south joint horizontal hoop stains under north-south loading

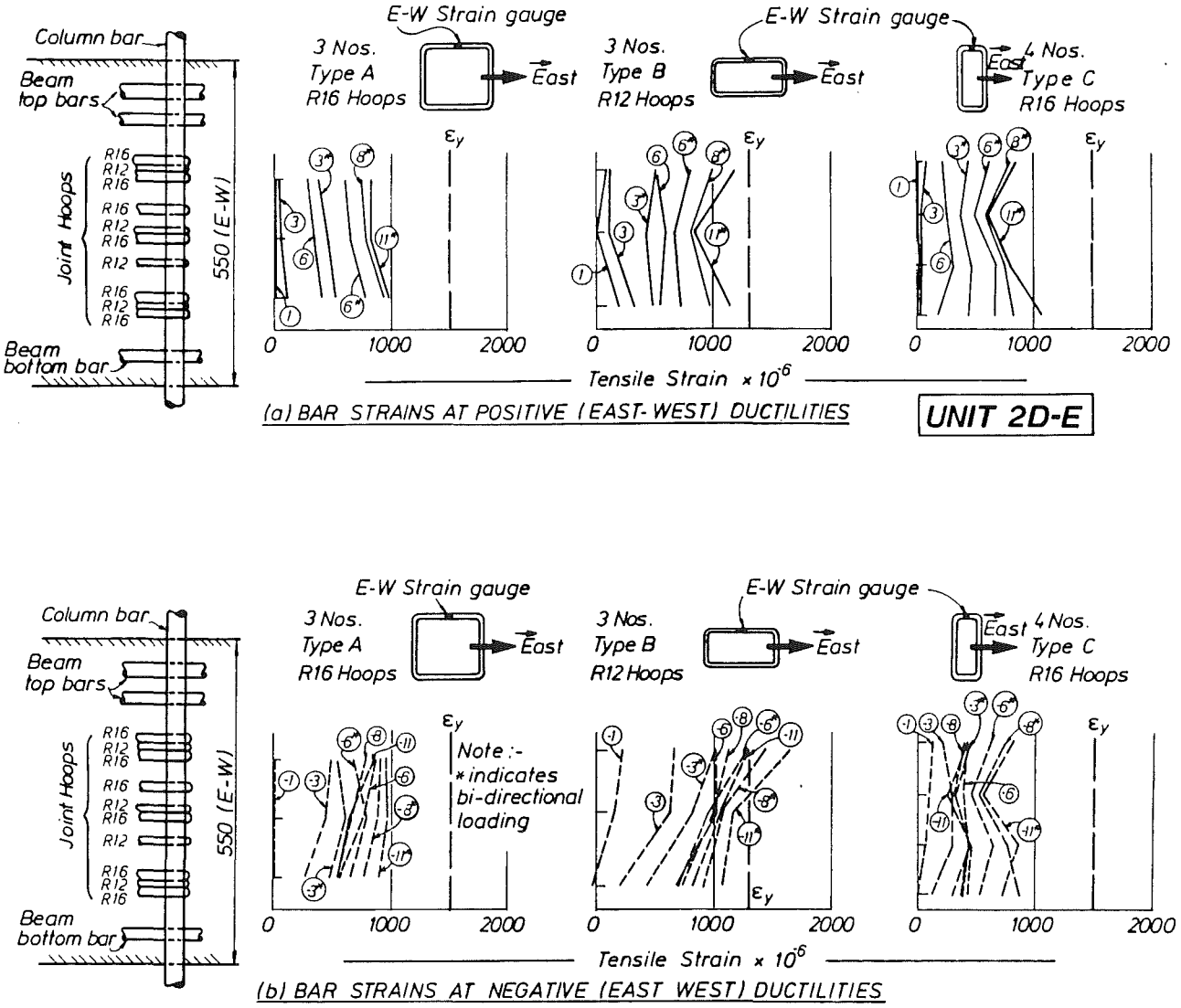

Fig.6.47 - East-west joint horizontal hoop strains under east-west loading

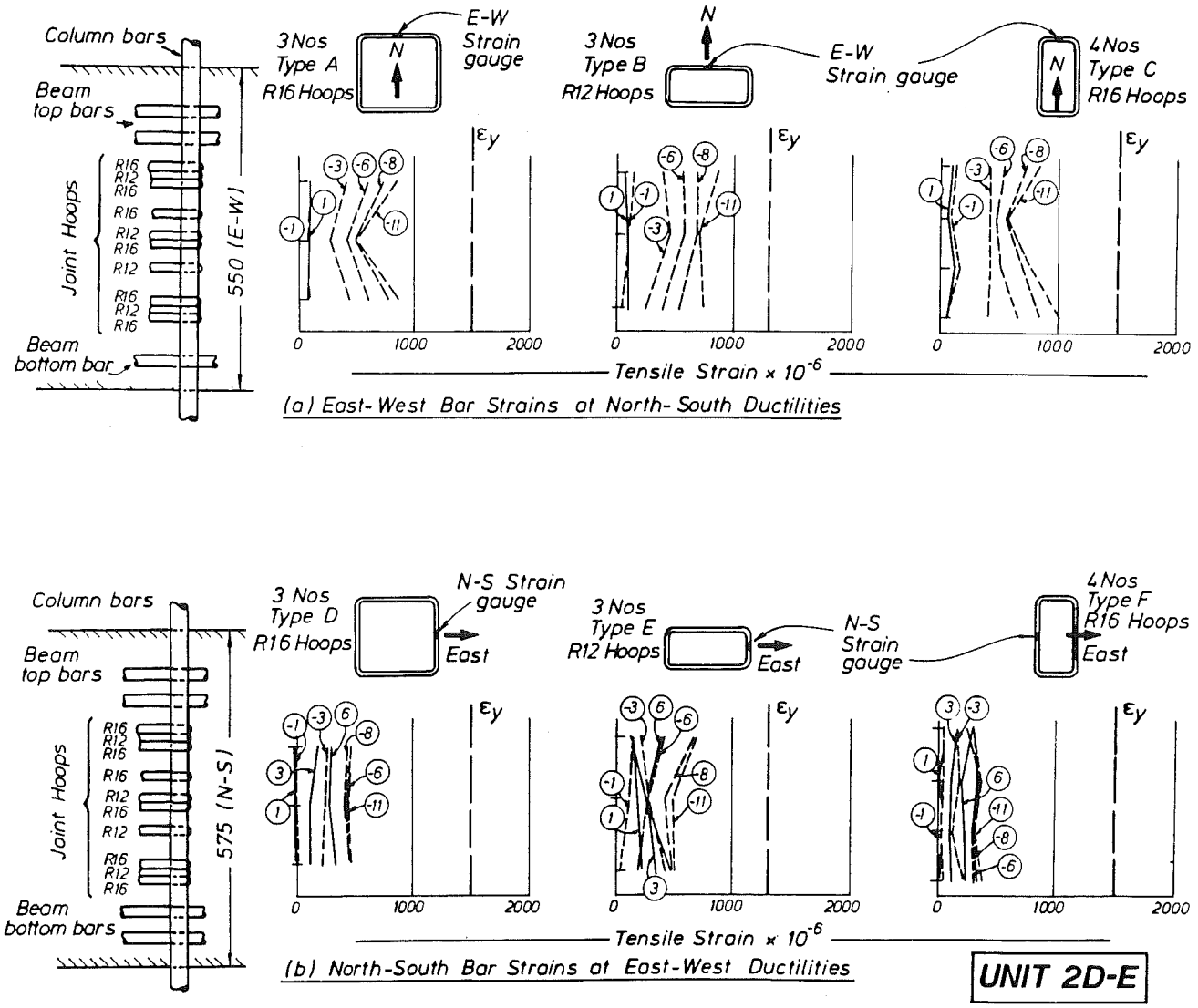

Fig.6.48 - Strains in horizontal joint hoops under loading transverse to the orientation of the tie legs

CHAPTER 7

THE ROLE OF FLOOR SLABS

7.1 GENERAL ISSUES

An important objective of this research project was to identify, and if possible to quantify, the contributions of floor slabs to both the enhancement of the flexural strength of beams and the behaviour of beam-column joints in the inelastic seismic response of reinforced concrete frames. The present state of understanding of these slab contributions, as reflected in code provisions, has been covered in Section 3.8. In this section suggestions are made using relatively simple mechanisms to predict, with an accuracy considered to be acceptable for general design purposes, significant aspects of flange behaviour. The sources of beam strength enhancement are of particular interest, for they need to be considered in the design for shear strength of beams, the flexural strength of the columns, and the shear strength of joints. Reference is also made to experimental evidence to support suggested behavioural models.

In attempting to develop a design strategy for the incorporation of slab effects considered above, the following relevant questions are considered to serve as guidelines :

(1) To what extent is the flexural strength of a beam, considering the presence of horizontal slab bars parallel to such a beam, enhanced by a tension flange? In simple terms, what may be taken as the effective width of a flange in tension?

(2) Having identified the fact that the enhancement of the flexural strength of flanged beams will be greater when ductility demands increase during a major earthquake, what magnitude of strength enhancement should a designer rely on, and what magnitude should be used when considering force input to joints and columns?

(3) How important are the contributions to frame behaviour of transverse beams which are cast monolithically and hence interacting with the floor

slab in torsion, flexure and shear, in terms of the enhancement of the lateral force resistance of ductile frames?

(4) To what extent does increased beam flexural strength affect the desired resistance of beam-column joints? Does the increase of joint shear force due to flange contributions in beams warrant the use of additional joint shear reinforcement?

(5) Does a slab, surrounding partly or fully the top region of a beam-column joint, contribute to the strength and performance of such a joint?

(6) To what extent are slab contributions affected when ductility demands on two-way frames arise simultaneously in both principal directions of the framing system during skew earthquake attacks?

(7) To what extent does beam strength enhancement due to the contribution of slabs affect the desired hierarchy in the design strength of columns and beams?

In attacking the issues, isolated free body models, taken from various parts of the floor system, are extensively used to establish equilibrium criteria for each part. Subsequently attempts will be made to reconcile compatibility of deformations in adjacent free bodies, particularly in the plastic state. The main function of structural models is to offer a rationale for the flow of internal forces from various parts of the floor slab to the joint, where actions in beams and columns must equilibrate each other. In consistency with the experimental part of this research project, the structural models are based on one-way and two-way cast in place beam-column-slab assemblies which are statically determinate. However, the principles developed will be extended to continuous beams of prototype building frames.

7.2 MECHANISMS IN SLABS ACTING AS FLANGES

7.2.1 Bending Effects on Slabs

Earthquake induced lateral forces on two-way slabs simultaneously impose a complex pattern of flexure, torsion and membrane forces. Bending effects and membrane actions in slabs, the latter being considered of prime

importance, are examined as two distinct features of behaviour. Torsional effects, in general not likely to be significant in slabs, can be considered as part of bending.

Fig.7.1(a) shows the deformed shape of an interior flanged beam of a two-way frame which is subjected to lateral forces. Effects of gravity are not considered. Strips of the slab, parallel to but located further away from the longitudinal beam A-B, may be subjected to section curvatures similar to those developed in the beam. The deformation of a strip of slab, such as that shown in Fig.7.1(b), will depend to a great extent on the stiffness of the slab in flexure relative to that of the transverse beams in torsion. Fig.7.1(b) shows the idealized extreme case of a transverse beam at A with infinite torsional stiffness. Such a beam would impose on the slab the same rotation, $\theta' = \theta$, which occurs at the beam-column junction. Consequently, the end moments induced in the slab, m_A and m_B, would then be proportional to either the flexural stiffness of the elastic slab, or equal to the flexural strength provided in these slab sections if the response is in the inelastic range. The latter would depend on the amount of effective bottom or top slab reinforcement respectively at the faces of the transverse beams. These slab moments would need to be transmitted by the transverse beams to the columns by means of torsion, as illustrated in Fig.7.2. The torsional moment M_{ty} from the transverse beam would then be transferred to the beam-column joint. Accordingly, by the development of slab moments the lateral force resistance of the frame would be increased. The beam A-B in Fig.7.1(a) may be assumed to be unaffected by the slab moments shown in Figs.7.1 and 7.2. However, in realistic situations some twisting of the transverse beams would be inevitable, so that $\theta' < \theta$ (Figs.7.1(a) and (b)).

Figure 7.1(c) shows the other extreme of boundary conditions for a slab strip. In this case it is assumed that the transverse beams have no torsional stiffnesses. Hence in spite of the large twist θ, no torque is generated in these beams. The slab in this case is not subjected to curvature and thus no moments are developed in it. Again the strength of the beam A-B (Fig.7.1(a)) is not affected.

A designer would need to use some judgement when estimating the significance of slab contributions due to imposed curvatures which, as the above two examples illustrated, depend predominantly on the torsional response of the transverse beams. If twisting is significant, early diagonal cracking

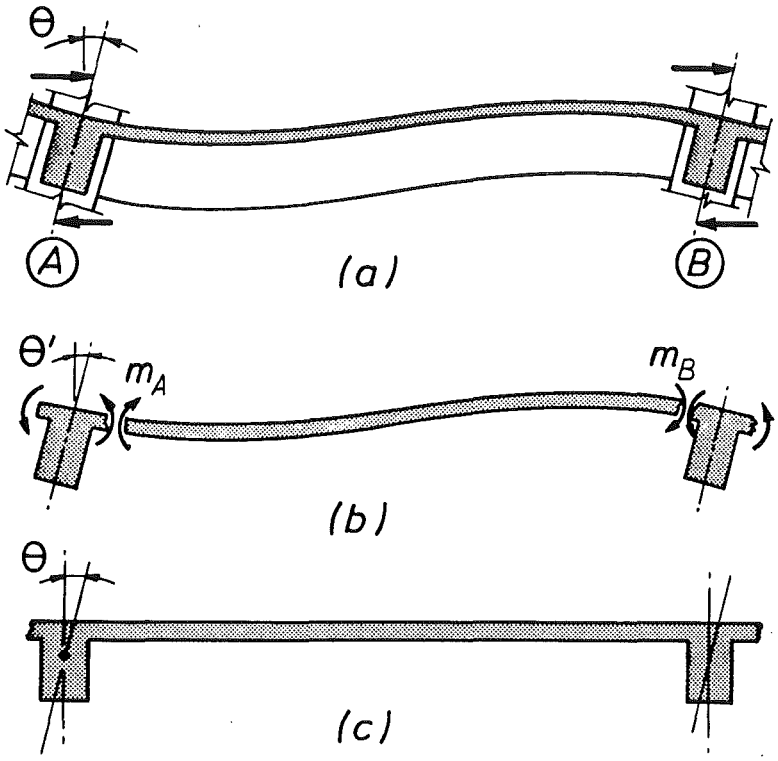

Fig.7.1 - Slab contribution to lateral force resistance due to imposed curvature only

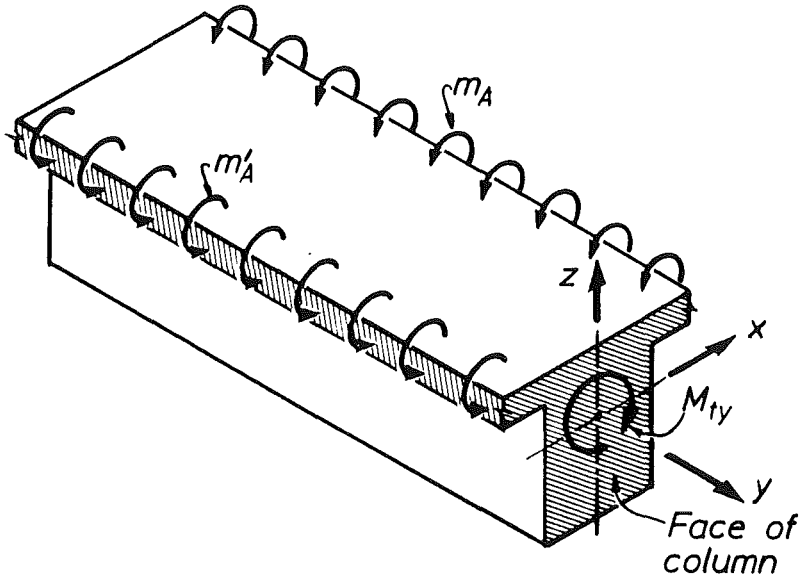

Fig.7.2 - A transverse beam subjected to torsion due to moments introduced by the adjoining slabs

in the beam will result in a large reduction of torsional stiffness. In the case of two-way frames, such as that implied in Fig.7.1(a), the inelastic seismic response of the structure in a direction transverse to the beam A-B will also affect the torsional response of the transverse beams. The ensuing flexural and diagonal cracking, and the formation of two plastic hinges in each span of a transverse beam, are likely to render the beam's torsional stiffness negligible.

During the elastic response of a frame under lateral force, slab participation of the type shown in Fig.7.1(b) is likely to contribute to some enhancement of lateral force resistance of a frame. However, with increasing ductility demands this contribution must diminish for the reasons discussed above. Membrane action, to be discussed in the next section, will lead to further, if not to complete, elimination of flexural contribution (Fig.7.1(b)) of a slab. Consequently, bending effects on slabs are not considered to warrant further considerations in the context of slab contributions to the enhancement of the lateral force resistance of ductile frames.

7.2.2 Membrane Actions in Slabs

After the formation of a plastic hinge, with the top beam reinforcement subjected to tension T_1, very large tensile strains ϵ_s, approximated by the dashed block in Fig.7.3(a), will be imposed on the adjacent slab from consideration of compatibility. Thus slab reinforcement placed parallel to the beam will also be subjected to tensile strains. For reasons to be examined subsequently, these tensile strains reduce in slab strips located further away from the beam-column joint. With large imposed interstorey drifts, slab forces may be associated with yielding of the slab reinforcement. Strength enhancement in frames, due to slabs acting as tensile flanges, is considered to originate predominantly from membrane forces such as T_x in Fig.7.3(b). Therefore the mechanism of this type of membrane action, particularly during the inelastic seismic response of ductile frames, warrants closer examination.

At a certain stage of the frame response, bending moments such as m_B shown in Fig.7.1(b) and axial tension forces such as T_x in Fig.7.3(b), will be developed simultaneously in the slab. As membrane tension increases, the flexural strength of the slab section will diminish. When membrane strains are large enough to cause both the effective top and bottom slab bars to

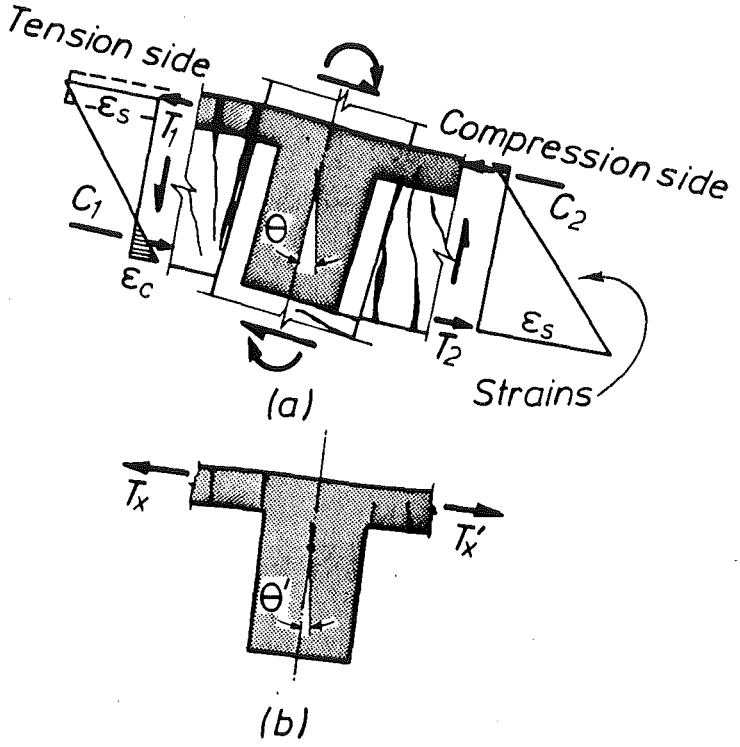

Fig.7.3 - Membrane action in a slab due to beam curvature

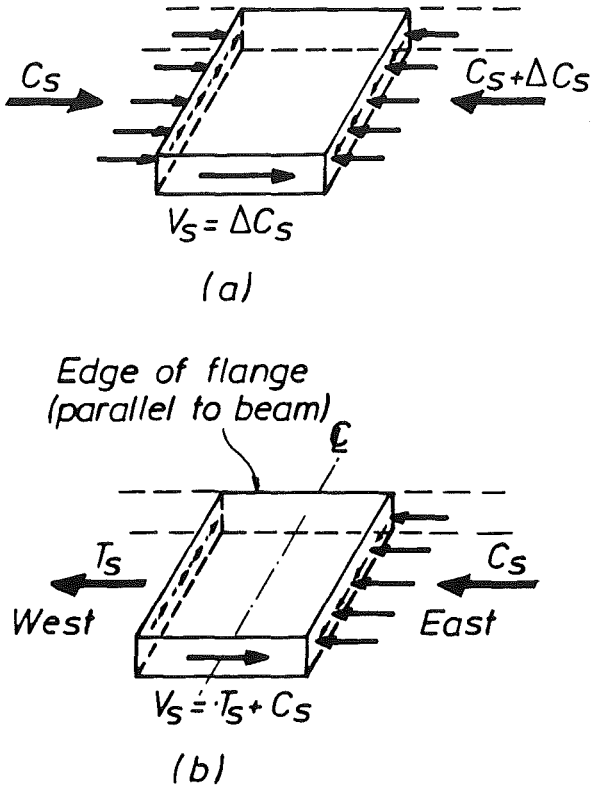

Fig.7.4 - Forces on flange edge elements

yield, moments in the slab (m_B) will vanish. In ordinary floor construction, slabs reinforcement contents are generally 0.2 to 0.3% of the slab sectional area. Bar curtailments are common. Thus m_B is not large.

The behaviour of flanges of homogeneous beam sections is well established. Relevant analyses, such as used to estimate the effective width of the compression flanges of reinforced concrete T or L beams, usually refer to the midspan region of beams where positive moments prevail (see Section 3.8). It follows then from first principles that when a beam is subjected to moment and shear, its flanges, formed by a cast-in-place floor slab, are also subjected to horizontal in-plane shear forces. For example, the horizontal shear force V_s on the slab edge element of a compression flange, shown in Fig.7.4(a), results from the difference of flexural compression forces applied to adjacent sections. When the resulting shear stresses are large enough, cracks due to diagonal tension will develop in such compression flanges. Unless appropriate shear reinforcement, normally placed at right angles to the shear force V_s (Fig.7.4(a)) is provided, the contribution of such a slab to flexural resistance may vanish once diagonal cracks due to in-plane shear develop.

Fig.7.3(a) indicates that during unidirectional seismic attack, which introduces anticlockwise beam bending moments applied to the column, the adjoining slab is subjected to membrane forces. This will cause tension T_1 on one side and compression C_2 on the other side of a transverse beam. This mode of introduction of in-plane forces into a flange is the single most important feature of slab contribution at joints to the strength of frames subjected to lateral forces.

Fig.7.4(b) shows a corresponding element at the free edge of a slab. The centre line shown is that passing through the column of a one-way frame system. The tension and compression slab forces, T_s and C_s, are those which should be developed by the lateral forces on the frame generating beam moments as in Fig.7.3(a). It is evident that a very much larger shear force, $V_s = T_s + C_s$, than that implied in Fig.7.4(a) would need to develop in the slab if equilibrium of membrane forces acting on the slab element of Fig.7.4(b) is to be maintained. The accumulation of membrane shear forces in such a slab strip could not normally be sustained in the vicinity of the column centre-line. It is postulated that with the exceptions of regions very close to the column, compression forces in the slab, shown as C_s in

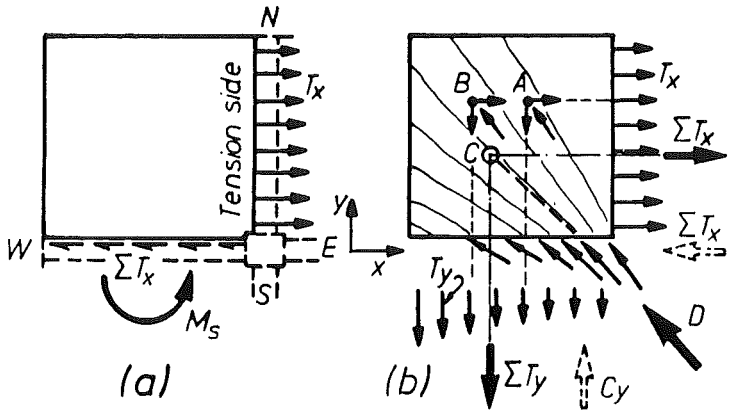

Fig.7.5 - Equilibrium criteria for the mechanism of force resistance in one quadrant of a floor slab acting as the tension flange of a beam

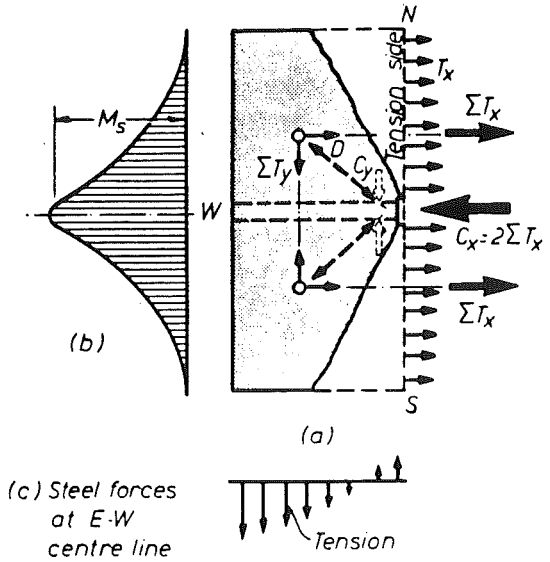

Fig.7.6 - Tension flanges acting as a deep beam

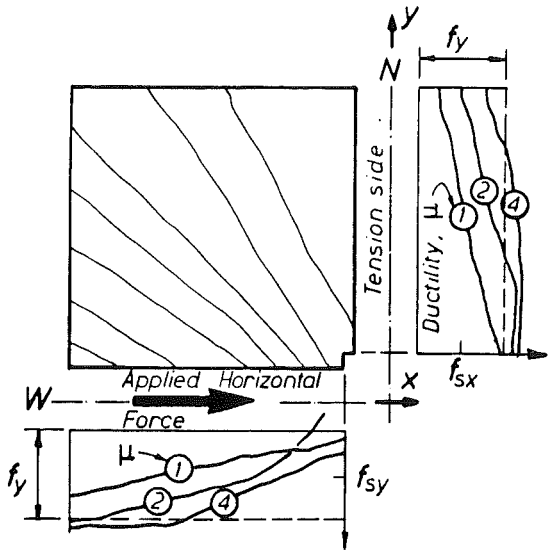

Fig.7.7 - Observed tensile steel stress patterns at slab edges

Fig.7.4(b), cannot be developed when the ultimate lateral force resistance of a frame is being approached. Instead, tensile forces, such as T'_x in Fig.7.3(b), will be present. This feature is more obvious in one-way slabs where transverse beams do not exist. Test results reported in Chapters 4 to 6 support this postulate.

7.3 MECHANISM OF TENSION FLANGES AT INTERIOR JOINTS

7.3.1 Equilibrium Considerations

Fig.7.5(a) shows the plan of an isolated north-west quadrant of a floor slab, situated on the tension side of the east-west beam. It represents a part of a typical isolated test unit such as Unit 2D-I of Chapter 5. When a downward force is applied to the western tip of the beam, tension (membrane) forces T_x will be generated in the slab bars placed parallel to the east-west beam. To maintain equilibrium for the free body in Fig.7.5(a), a shear force equal to the total tension force ΣT_x and a moment M_s must be applied to the south edge of the panel. With the presence of large cracks across the slab, it is assumed that shear transfer across the N-S beam-slab interface is negligible. The horizontal E-W shear forces generated in a homogeneous slab may still be transmitted to the east-west beam by means of concrete shear stresses. However, when ensuing diagonal tensile stresses become large, diagonal cracks will develop in the slab. This was consistently observed in tests (Chapters 4 to 6). For this condition a new mechanism of shear transfer must be mobilized which does not rely on the diagonal tensile strength of the concrete.

The mechanism associated with the transmission of the external forces identified in Fig.7.5(a), within a diagonally cracked flange (slab), is modelled in Fig.7.5(b). The generation of shear forces along the south edge of the panel requires the development of diagonal concrete compression forces, the sum of which is labelled D. Equilibrium can be maintained only if tension forces T_y are simultaneously developed in bars crossing the southern edge of the panel. Equilibrium may thus be satisfied when

$$D = \sqrt{\left[(\Sigma T_x)^2 + (\Sigma T_y)^2\right]} \qquad (7.1)$$

The equilibrium at any point within a diagonal concrete strut, such as points A or B highlighted in Fig.7.5(b), also requires three concurrent inplane forces shown by the smnall arrows. Note that the tension forces are introduced to the concrete by slab bars by means of bond. Thereby a bar force is gradually reduced from $T_x = T_{max}$ at the eastern edge of the panel to $T_x = 0$ at or close to the free western edge. Similar bond forces must be introduced to the concrete strut by bars placed in the north-south direction. The accumulation of the diagonal compression forces from points such as A and B results then in diajgonal compression forces at the southern edge of the panel, as proposed in Fig.7.5(b). It will be appreciated that the inclination of diagonal struts will restrict the plan area of the panel over which (bond) forces can be introduced to the concrete and transferred to the west beam. The components of the diagonal force D, i.e. C_y and ΣT_x are also shown in Fig.7.5(b).

The model in Fig.7.5(b) does not consider the compatibility of deformations. It does suggest, however, that the further a bar carrying a force T_x is situated away from the column, the longer is the load path to the joint. All else being equal, for similar strains a longer load path is associated with larger total deformations. Hence one may conclude that the shorter the load path, the stiffer the associated mechanism will be. In the elastic range of reponse this means that the intensity of the tensile forces T_x should diminish with the distance from the column. The corollary to this principle, when related to the inelastic state, is that with longer load paths strains will reduce. Hence at large imposed ductilities, slab bars close to the column may well enter strain hardening, while those situated near the free edge of the slab may be subjected to only moderate inelastic strains. Observed strains reported in previous chapters suggest that in general, at ductilities of $\mu = 4$ or more, the yield strength of such bars was developed over the entire width of the flange.

The slab reinforcement in the y (i.e. N-S) direction takes part in sustaining tensile forces in the tension flange T_x. Its role may be better appreciated if another free body, consisting of one half of such a unit as shown in Fig.7.6(a) is examined. It models a deep beam. The E-W slab bars are assumed to be effectively anchored only in the shaded area of the slab. This follows from the previous discussion of Fig.7.5(b). Over the width of the column a reactive force $C_x = 2\Sigma T_x$ needs to be applied. A statically admissible disposition of the internal N-S stress distribution of this deep

beam is suggested in Fig.7.6(c). The moment pattern, consistent with the distribution of horizontal tension flange forces T_x, is given in Fig.7.6(b) (see also Fig.7.5(a)). The moment M_s is resisted by the internal couple $\Sigma T_y = C_y$, as illustrated in Figs.7.5(b) and 7.6(a). This mode of flexural resistance suggests that tensile strains in the slab bars placed in the north-south direction should increase with distance measured from the column. Hence across the critical centre section of the model deep beam, internal forces of the kind shown in Fig.7.6(b) are to be expected.

Figure 7.7 shows typical observed tensile stress patterns along two edges of a slab quadrant, derived from strain gauges mounted on slab bars. As expected, stresses in both directions increase with the increase of imposed ductilities. As the postulated mechanism suggests, stresses in the tension flange, f_{sx}, are maximum close to the centrally positioned column. For moderate ductilities, tensile stresses become smaller towards the free edge of the slab. Stresses in the y direction, on the other hand, reach a maximum at the free western edge of the slab and reduce rapidly towards the column. This is consistent with the deep beam action modelled in Fig.7.6(a). Consistent strain patterns were recorded also by other researchers [40,46].

Two important conditions for effective tension flange contribution emerge from this discussion :

(1) In order to develop significant tensile forces in the slab reinforcement to increase the flexural strength of a beam, transverse slab reinforcement of comparable quantity is also required, unless diagonal cracks are absent.

(2) To enable the transfer of tensile forces which act at the critical section of a flange, for instance along the N-S edge shown in Fig.7.6(a), to the joint core, slab bars must be effectively anchored in such a way that a viable diagonal compression field can develop. For this purpose it may be assumed that slab bars are effective only when they are anchored in a suitable region, such as that shown shaded in Fig.7.6(a).

A simple approach to the assessment of the effectiveness of slab bar anchorages, considered to be adequate for design purposes, is proposed in Fig.7.8. This shows the arrangements of the D10 bars in the top (Fig.7.8(a)) and the bottom (Fig.7.8(b)) layers respectively in the northern half of the slab of Unit 2D-I (Chapter 5). The effective anchorage zone was simply taken

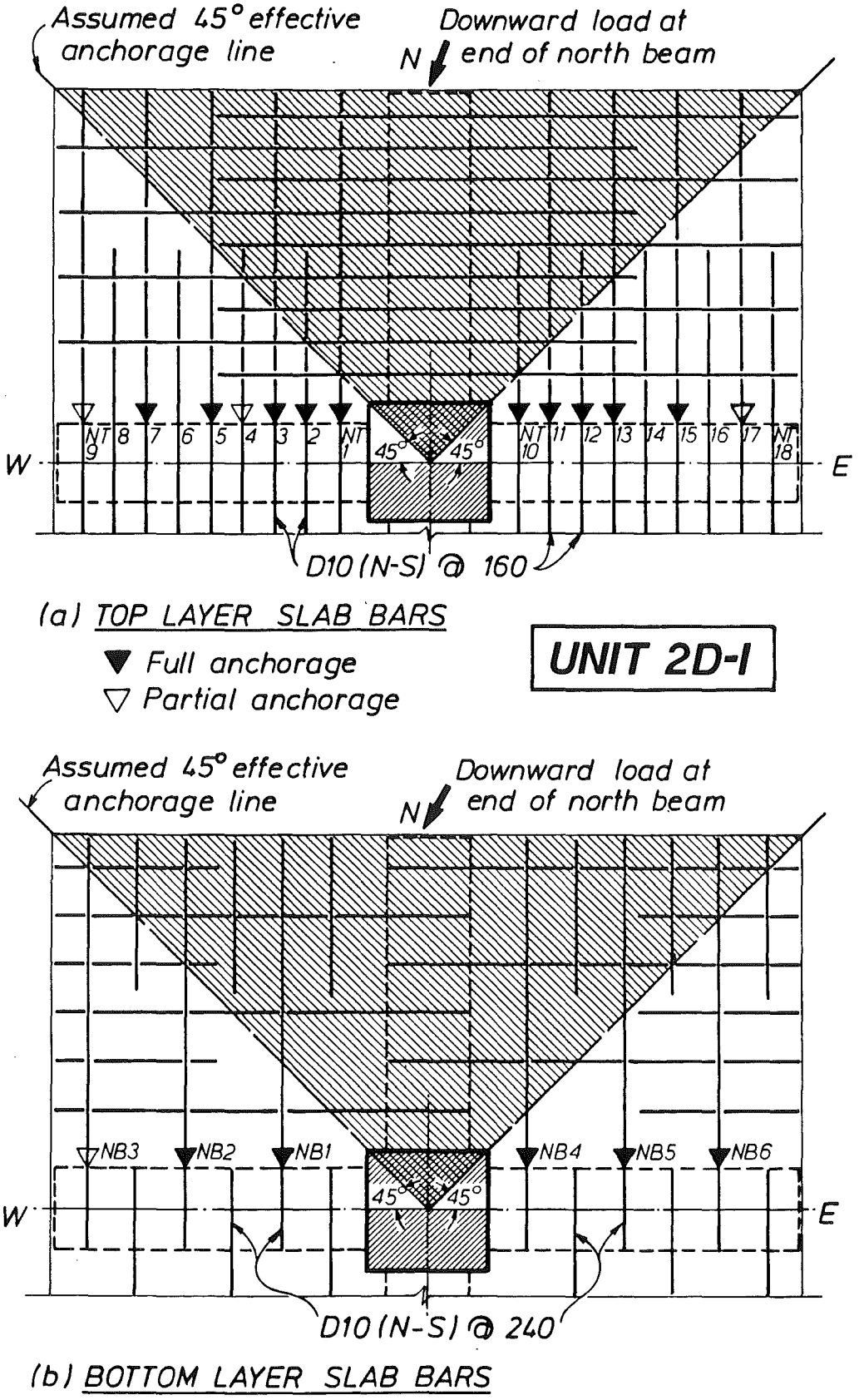

Fig.7.8 - Simple approach in determination of number of longitudinal slab bars effectively anchored

as the shaded area bound by two 45° diagonal lines. A comparison of the extents of anchorage zones, shown in Figs.7.6 and 7.8, indicates that the latter is likely to represent a conservative model. In the model of Fig.7.8 it may be assumed that any bar, extending past the diagonal by a distance less than the customarily code specified development length should be disregarded as being effective. A high degree of precision is not likely to be justified or possible. This modelling suggests that, depending on its position, a bar may develop full, partial or no anchorage from the tension face of the E-W beams. The degree of effectieness is indicated by the small triangles. Thus counting in Fig.7.8 all the top and bottom bars for this unit, the modelling suggests that approximately 70% of the total slab reinforcement (17/24) could be mobilized. Beam moments so estimated will be compared with those encountered during tests as shown by the levels (c) in Figs.7.19 to 7.21.

Similar criteria may be imposed on the N-S slab bars which also are essential parts of the mechanism shown in Figs.7.5 and 7.6. Their prime role is to sustain the bending moments developed in the double cantilever deep beam (Fig.7.6(b)).

There is an exception to the conditions just discussed. When the reinforcement content of the flanges is relatively small, shear stresses in the slab will also be small, even when the slab bars yield. Shear is then transmitted to the E-W beam primarily by shear stresses in the concrete, including diagonal tension. Thereby the anchorage of slab bars in the immediate vicinity of the N-S transverse beam can be activated.

7.3.2 The Introduction of Flange Forces to Joints of One-Way Frames

Equilibrium of a beam-column joint assembly requires that beam moments developed at a joint are balanced by equal and opposite moments generated in the columns. By necessity these moments, consisting of force couples, must be coplanar. However, flange forces discussed in the preceding sections are not generated in the plane of the frame. As the model of Fig.7.5 suggests, flange forces must be transferred by shear stresses or diagonal compression stresses within the slab to the stem of the beam and thereafter to the joint core. The mechanisms of transmission of these forces in one-way frames are discussed in further detail in the following sub-sections, again using an isolated interior beam-column-slab joint assembly as model. As the inelastic response of ductile frames is of prime importance in seismic design,

the model shown in Fig.7.5(b) is considered dominant.

(a) Flange action in one-way slabs

The tensile flange forces, shown as T_x in Figs.7.5 or 7.6 in slabs of one-way frames, can develop only if the slab bars are adequately anchored in another adjacent free body. This suggests that a diagonal compression field of the type shown in Fig.7.8 may be used to model, at least qualitatively, the flange behaviour. In this it is assumed that slab bars are anchored beyond the first diagonal cracks (see Fig.7.6(a)). Fig.7.9 shows a beam-column-slab assembly with one half of the slab not shown for the sake of clarity. The diagonal membrane forces in the slab depict the orientation of the compression field. Hence a shear flow (force per unit length) is introduced to each side of the stem of the west beam, the sum of which is ΣT_x. This should be equal to the shear transferred from the slab by concrete stresses (Fig.7.5(a)). This shear flow enters the stem approximately at the level of the flexural tension reinforcement. The application of a force ΔP at the west end of the beam enables the accumulation of the shear flow to be transferred to the flexural compression zone at the bottom of the west beam section by means of diagonal compression, this being part of the truss mechanism in the web. As Fig.7.6 shows the compression force at the column face is $C_x = 2\Sigma T_x$.

A similar shear flow is introduced to the beam at the east side of the column. As this shear flow enters the east beam stem in the flexural compression zone, its contribution to the enhancement of the flexural strength of the east beam is negligible. The development of membrane tensile forces in the east "compression" slab panel has been justified and shown necessary in Section 7.2.2 and Figs. 7.3 and 7.4. The resultant compression in the top of the east beam at the column face is denoted also as C_x. This implies that the flange actions in the east and west slabs of Fig.7.8 are symmetrical and that no shear forces are introduced to the joint along the north or south face of the column.

It is thus seen in Fig.7.10 that the moment introduced to the column via the joint, as a result of slab participation alone, is zC_x, where z is the assumed internal moment arm. The flexural strength of the west beam is therefore increased by the total moment increment $zC_x = 2z\Sigma T_x$ at the column face. On the other hand, the flexural strength of the east beam remains

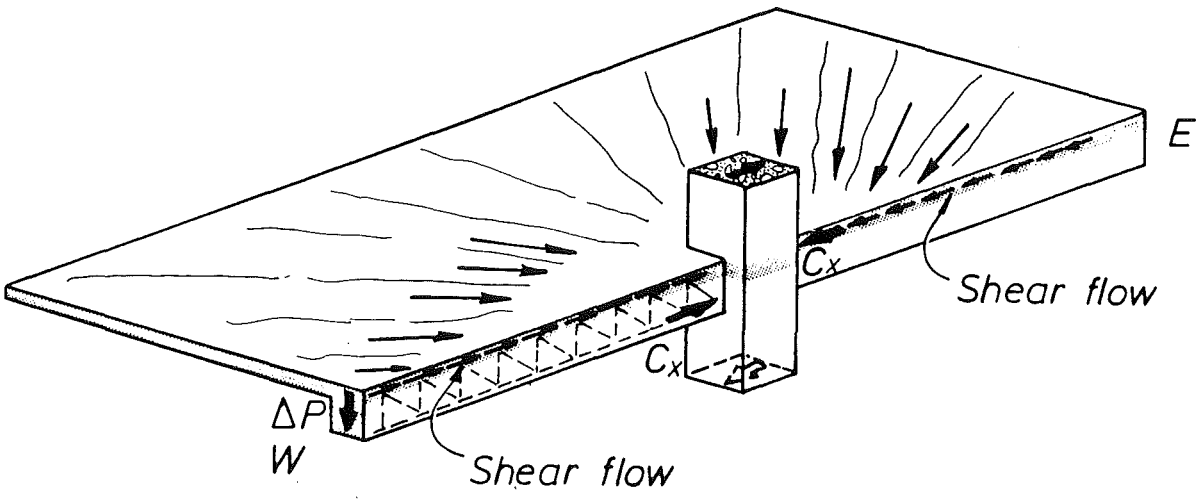

Fig.7.9 - Transfer of flange membrane forces in one-way slabs to beams and columns

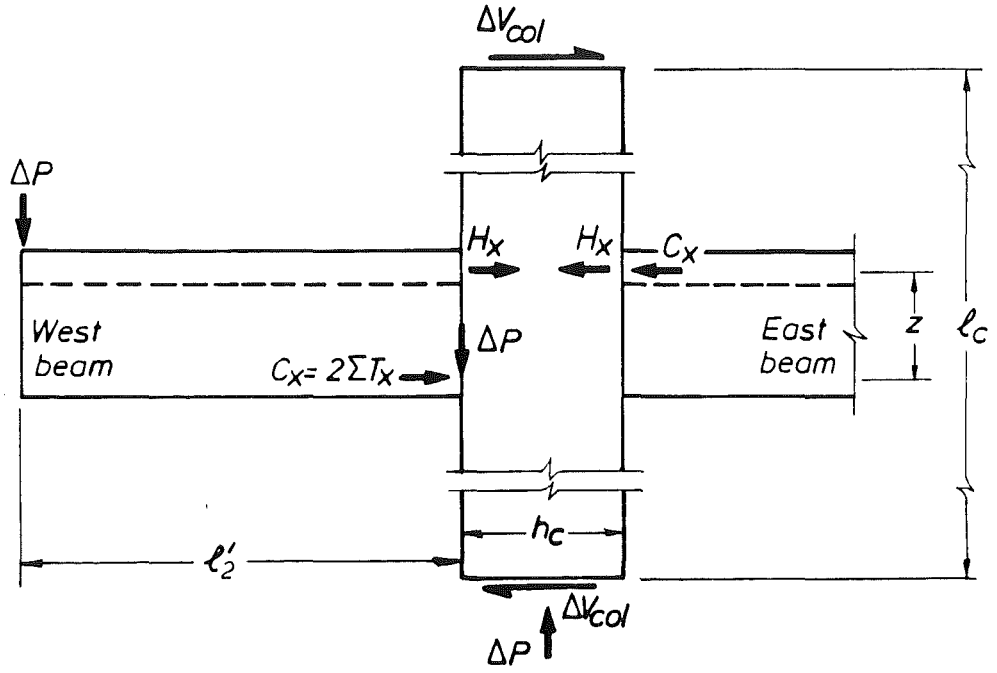

Fig.7.10 - The introduction of slab tensile forces to the joint core of a one-way beam-column assembly

largely unaffected. However, without the introduction of the compression force C_x at the east face of the column, strength enhancement due to slab participation is not possible.

(b) Introduction of flange forces to joint core

The enhancement of the strength of a beam-column assembly from flange contributions may be derived in terms of the column shear forces using Fig.7.10 which summarises the actions discussed in sub-section (a). It can be seen that any horizontal shear forces H_x that may be introduced through diagonal compression (Fig.7.9) directly to the joint will not contribute to the strength enhancement of the unit. With the approximation as discussed before, accepting that $C_x = 2\Sigma T_x$ at both faces of the column, the moment equilibrium with respect to the centre of the joint assembly (Fig.7.10) is

$$2z\Sigma T_x + 0.5h_c\Delta P - \Delta V_{col}\ell_c = 0$$

Because $\ell_2'\Delta P = 2z\Sigma T_x$, the increase of column shear is

$$\Delta V_{col} = \left(2z\Sigma T_x + 0.5\, h_c\Delta P \right)/\ell_c = \frac{z}{\ell_c}\, \Sigma\, T_x \left(2 + \frac{h_c}{\ell_2'}\right) \qquad (7.2)$$

where ℓ_c, ℓ_2' and h_c are lengths indicated in Fig.7.10. Consequently the increase in horizontal joint shear force will be

$$\Delta V_{jh} = 2\Sigma T_x - \Delta V_{col} = 2\Sigma T_x \left[1 - \frac{z}{\ell_c}\left(1 + \frac{h_c}{2\ell_2'}\right)\right] \qquad (7.3)$$

Further discussion of the effect of this joint shear is presented in Section 7.3.3(c).

7.3.3 The Introduction of Flange Forces to Joints of Two-Way Frames

The mobilization of membrane forces in tension flanges of two-way frames was explained in Section 7.3.1 with the aid of Figs.7.5, 7.6 and 7.7. Having considered the mechanisms of transmission of flange forces in one-way frames in Section 7.3.2, this section considers additional parameters necessary for considering the response of two-way frames.

(a) The role of transverse beams

It may be argued that the contribution of transverse beams, such as the north-south beam in Fig.7.5(a), to the enhancement of the strength of an assembly may be significant. therefore the probable role of transverse beams is also qualitatively examined.

Figure 7.11(a) shows horizontal forces which could possibly be introduced by adjacent slabs to a transverse beam. On the left hand (tension) side of the beam the same slab forces (T_x) are shown as those in Fig.7.5(a). On the other (compression) side of the transverse beam, similar tension (T'_x) or compression (C'_x) forces may be introduced. The net horizontal forces, $\Delta T_x = T_x - T'_x$ or $\Delta T_x = T_x + C'_x$, acting on a model cantilever beam, are suggested in Fig.7.11(b). It is reasoned that these forces cannot be very large. Because the very large shear force V_s shown in Fig.7.4(b) cannot be sustained, the slab on the compression side of the transverse beam, though theoretically a compression flange, cannot in general resist compression forces. An exception, to be discussed in sub-section (d) to follow, is the region very close to the column. Thus the net forces ΔT_x, applied to the transverse beam, originate mainly from partial anchorage of the slab bars within this beam, if any. Thereby the tension in a slab bar at one side of the beam is reduced from T_x to T'_x at the opposite side. A model cantilever beam (Fig.7.11(b)) under these conditions would then be subjected to bending moments M_{bz} about the vertical (weak) axis of the beam section, and to shear forces V_x. The magnitudes are shown qualitatively in Figs.7.11(d) and (c) respectively. The deflected shape of the beam would be as seen in Fig.7.11(e). By considering compatibility of horizontal deformations in adjoining slab quadrants such as the one shown in Fig.7.5(a), and of the beam which has much larger flexibility (Fig.7.11(e)), it is likely that the beam could resist only negligible forces with the exception of locations very close to the column. It was reported in Chapter 5 that horizontal tip displacements of transverse beams during the largest imposed ductilities did not exceed 2 to 3 mm. Displacements Δ_x of this order could not generate significant resistance in the beam (Fig.11(e)).

The transverse beam is likely to swing horizontally about a pivot near the face of the column, the movement being to a larger degree affected by the deformations of the adjacent slab quadrants on the compression side,

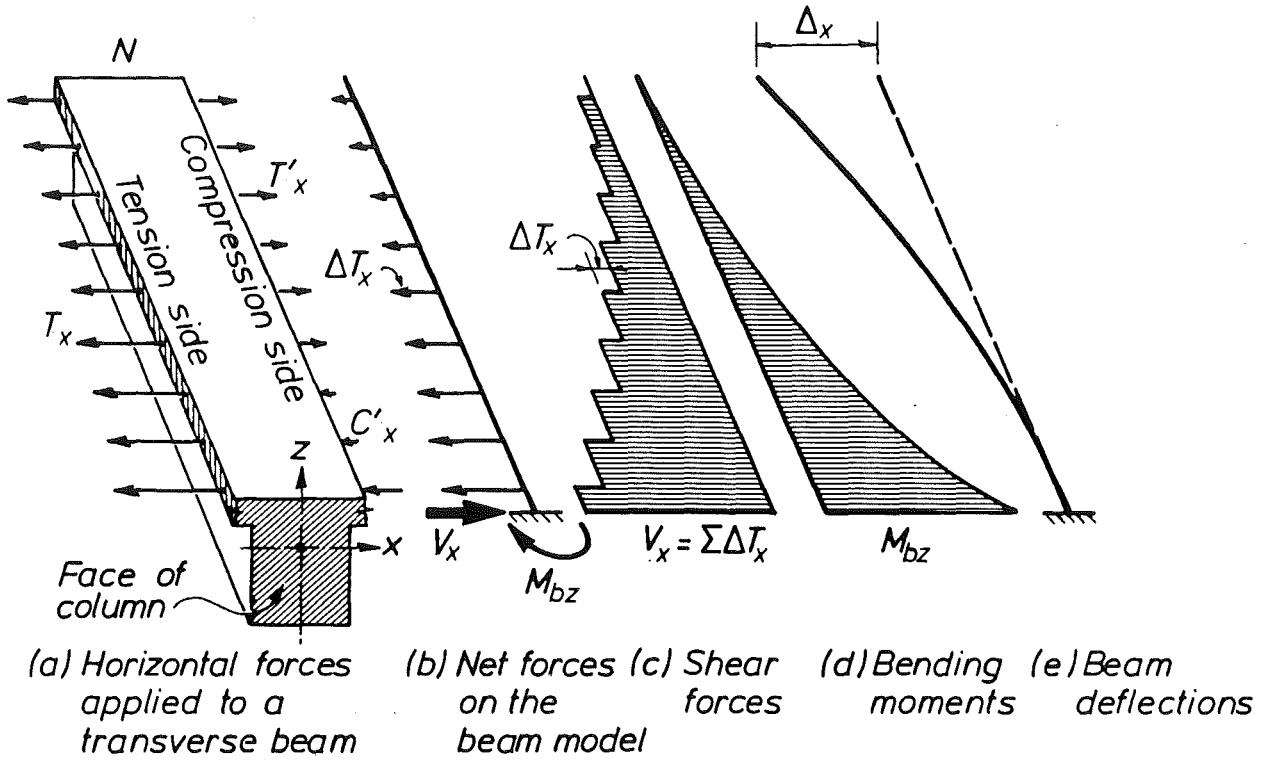

Fig.7.11 - A transverse beam subjected to hypothetical forces in the plane of the floor slab of a beam-column assembly

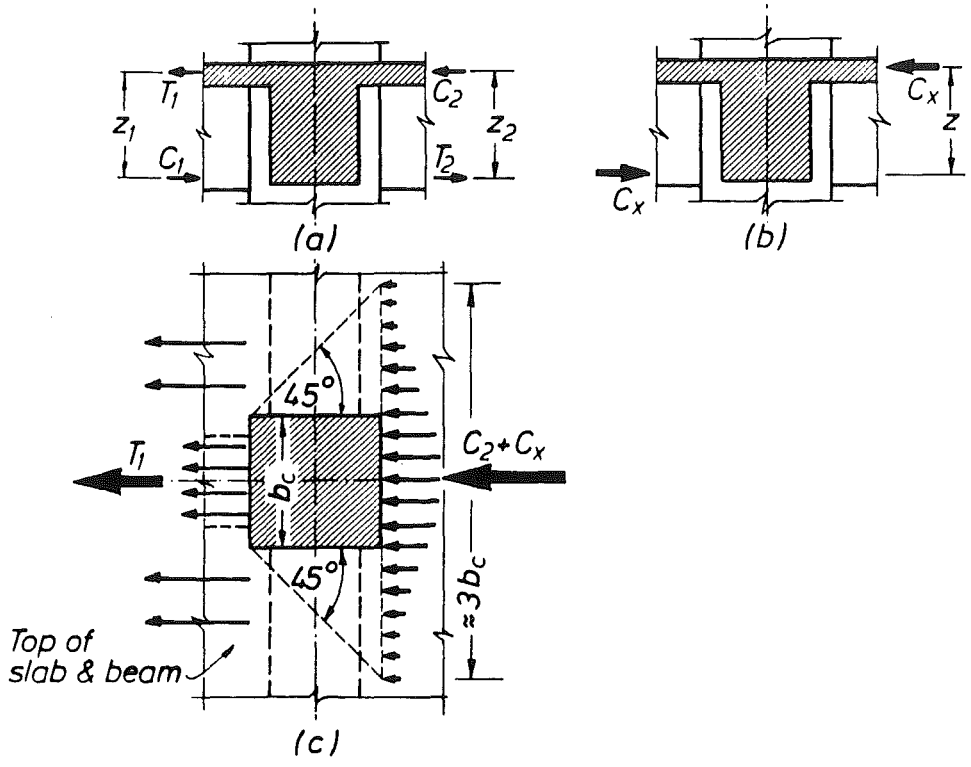

Fig.7.12 - Forces introduced to an interior column by flanged beams of a two-way assembly

without offering resistance of any significance. This was found to be particularly evident at edge beams (Chapter 6). Softening of the transverse beam of Figs.7.5 and 7.11 will be accelerated when inelastic deformations, associated with formation of plastic hinges, are imposed by seismic actions in the north-south direction. No attempt is made here to assess the role of the transverse beams in a fully elastic structure.

(b) The role of a "compression" flange

From the examination of the role of transverse beams, it may be concluded that for the purposes of assessment of the strength enhancement of the longitudinal beams, especially when large displacement ductilities μ are attained, the transverse beams' contribution can be neglected in design computations. This assumption implies that the "compression" slab, located to the east of the N-S beam in Fig.7.6, is required to absorb all the tension forces, $2\Sigma T_x$. This requires the development in the "compression" slab of a diagonal compression field similar to the one for one-way slabs shown in Fig.7.9. With this simplification the mechanism in all four quadrants of an isolated unit is the same as that shown in Fig.7.5(b). It should be appreciated that tension flange contribution based on equilibrium criteria implied by Fig.7.5(a) can always be developed, as long as slab bars carrying the force T_x are adequately anchored in the east beyond the N-S tension edge of the slab quadrant. This anchorage can be more efficiently developed in the opposite and rather stiff east "compression" flange than in the relatively flexible transverse N-S beam.

While the assumption of neglecting the contribution of the transverse beam may be questioned, it should be noted that it does not affect equilibrium criteria and that the assumption does not influence the magnitude of strength enhancement in the beam-column joint assembly by flange actions. The assumption made above simply implies that in this modelling, the relatively small contributions of the transverse beam to strength enhancement are assigned to the slab on the compression side of the transverse beam.

(c) Introduction of flange forces to joint core

Using the simple models presented in previous sections, the strength enhancement of a beam-column joint assembly due to the contribution of tension flanges, simulating a two-way frame under earthquake-type lateral forces, may

be readily quantified in the same way as was done in Section 7.3.2 and Fig.7.10 for one-way frames. The estimate of strength enhancement may also be achieved with a conventional flexural analysis of the affected beam section. The former however enables a better visualization of the mode of additional force transfer to the joint due to flange actions. The approach used in Fig.7.10 is elaborated in Fig.7.12 showing familiar internal beam forces acting at the faces of an interior column, which are generated by clockwise moments in the frame. The tension forces T_1 and T_2 in Fig.7.12(a) are based only on the flexural reinforcement within the stems of the beam section. Thus T_1 does not include any reinforcement in the tension flange. The ideal flexural strengths of these left and right beam sections without flanges are $M_1 = T_1 z_1$ and $M_2 = T_2 z_2$ respectively, where z_1 and z_2 are the appropriate internal lever arms. In accordance with the previously described model (Fig.7.6) the total slab forces generated are $C_x = 2\Sigma T_x$. They represent eccentric axial compression, applied to each of the two beam sections as illustrated in Fig.7.12(b).

It was concluded in Fig.7.10 that an additional anticlockwise moment $\Delta M \approx zC_x$ can be applied at the left-hand beam section. This represents the strength enhancement of the beam on the left due to the contribution C_x from the tension flanges. As indicated in Figs.7.12(a) and (b), the internal forces introduced by the left-hand rectangular beam section to the column are thus: T_1 in tension at top and $C_1 + C_x = T_1 + C_x$ in compression at bottom. The total moment of resistance of the beam to the left of the column is $M^*_1 = M_1 + \Delta M$, as has been derived in Section 7.3.2(b).

Forces developed in beam flanges, C_x, are introduced to the joint core primarily by concrete compression stresses. This is shown in Fig.7.13 for an idealised model. With the moment increment $\Delta M \approx zC_x$ introduced to the joint, corresponding increases of the column and beam shear forces are ΔV_c and ΔV_b respectively. It is seen that as a result of flange contribution no extra horizontal steel forces and corresponding bond forces are introduced to the joint core. It is thus possible to combine the horizontal compression forces from the beam, C_x, with corresponding vertical compression force increments from the column, namely $\Delta C'_c$ and $\Delta C''_c$. The diagonal strut so formed should be capable of transmitting the entire horizontal and vertical joint shear force due to flange contributions alone without the aid of any additional joint shear reinforcement. Unless the total calculated joint shear stress is very close to the maximum considered by codes to be acceptable, the additional

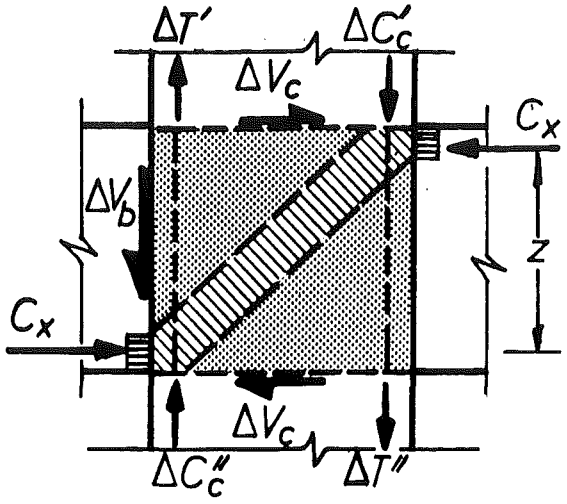

Fig.7.13 - Joint mechanism mobilised to resist additional forces originating from tension flanges

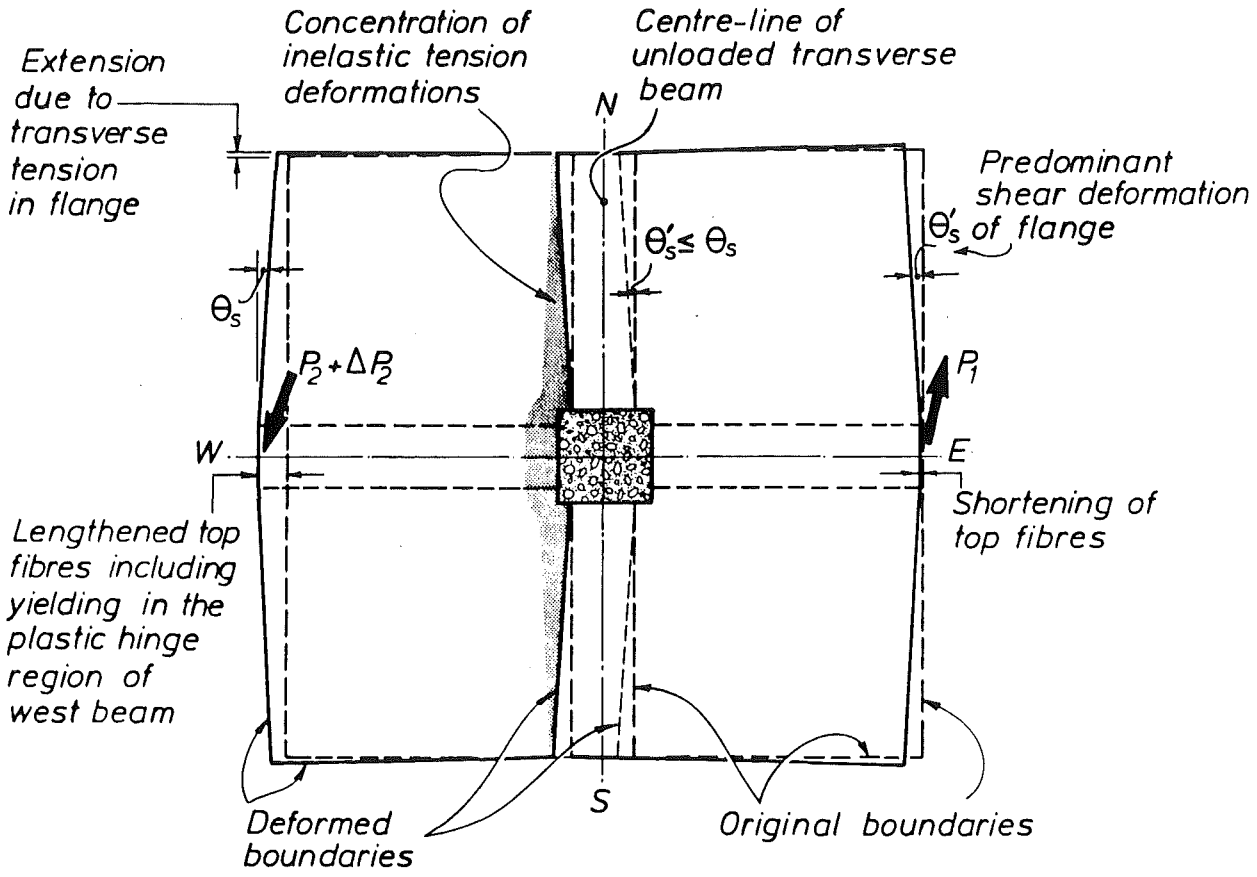

Fig.7.14 - Flange deformations due to lateral forces acting on a two-way beam-column assembly in the east-west direction only

diagonal compression force, modelled by the diagonal strut in Fig.7.13, will be readily accommodated in the joint core. An estimate of the relative magnitudes of the enhanced shear forces across the column (i.e. joint core) can be made using Eqs.(7.2) and (7.3). Noting that the main variable ΣT_x depends on the amount of effective slab reinforcement placed, it follows that these enhanced forces should not be significant in ordinary slabs. With capacity design of ductile frames, columns are expected to remain elastic. Therefore the increase in bond forces along column bars, introduced by additional forces ($\Delta T' + \Delta C_c''$) or ($\Delta T'' + \Delta C_c'$), are not likely to be critical and thus should not require further attention in design.

(d) Membrane distortions

Distortions of the flanges which are compatible with the membrane actions postulated in previous sections are illustrated, by necessity with some exaggeration, in Fig.7.14 for a two-way assembly. Inelastic deformations in both the west beam and slab panels, originating from yielding of the beam and slab bars, are idealized as being concentrated in the shaded strip. These inelastic deformations represent the major source of the elongation of the top fibres of the west beam. Distortions of the west slab panels, acting as two deep beams (as seen in Fig.7.6) are assumed to be approximately symmetrical about the E-W centre-line and are indicated by the shear strain Θ_s. As the north-south transverse beams are assumed to offer no resistance to the E-W seismic forces, as discussed in sub-sections (a) and (b), their deformations must be controlled by those of the slab panels. Fig.7.14 implies that these transverse beams should follow the movements of the east "compression" slab panels. When only flange actions are considered, the east slab panels are subjected to the same tension forces as those in the west slab (Fig.7.12(b)). The shear deformation of the east panels, as indicated by Θ_s', should therefore be of the same order of magnitude as Θ_s.

A review of the postulated mechanisms (Figs.7.9 and 7.12(a) and (b)) suggests that in simplified ideal conditions, the only physical contact between the column and the east slab panels is at the beam-column interface. Full width cracks should form between the east slabs and the north-south transverse beams when flange tensile forces develop in the slab bars. A more realistic form of force distribution in flanged beams in the slab plane is presented in Fig.7.12(c). There T_1 includes some tension forces from longitudinal slab bars which are close to the stem of the west beam. These

slab bars are subjected to compression at the east side. The resulting shear (Fig.7.4(b)) can be sustained in these regions especially in the presence of transverse beams. The simple 45° distribution in Fig.7.12(c) suggests that the total participating slab width should be of the order of $3b_c$ or less, where b_c is the column width. Compression forces, C_2 and C_x, at the west side may be effectively transmitted within this width. The total resistance of the assembly, when expressed in terms of flexural moments, is the sum $T_1z_1 + T_2z_2 + C_xz$. It is evident that in this model T_1 (and hence z_1), z_2 and C_x (and hence z) cannot be accurately and separately calculated due to the uncertainty in determining the effective participating width. Hence in subsequent sections, compromises are made for developing design recommendations.

7.3.4 Slab Contributions to Beam Strengths Under Bi-directional Displacements of Two-Way Frames

The discussion in the previous sections emphasized (Figs.7.5 to 7.7) that lateral forces applied to a space frame in a given direction will generate tensile forces in slabs, acting as flanges, in both orthogonal directions. It follows then that there will be a greater increase of tensile forces in elastic slab bars under a bi-directional (skew) seismic attack.

When the response in both principal axes of a framing system x and y, is moderate ($\mu \leq 1$), a superposition of elastic actions may be possible. This is explained in Fig.7.15. The tensile stresses in the slab bars in the x direction, f_{xx}, are those due to frame displacement in the same x direction. They are similar to those observed (Chapter 5) at a ductility of $\mu=1$, and referred to as f_{sx} in Fig.7.7. The stresses in the x direction due to frame displacement in the y direction, with $\mu=1$, are shown as f_{xy} in Fig.7.15. These are similar to stresses shown as f_{sy} in Fig.7.7. The superposition of the stresses in the x direction due to simultaneous frame displacements in both principal directions, $f_s = f_{xx} + f_{xy}$, is seen in Fig.7.15 to lead in this particular example to nearly uniform stresses close to yield intensity. The example of Fig.7.15 suggests that :

(1) A superposition of slab actions due to bi-directional displacements of a symmetrical assembly of the type studied in this project, to evaluate the enhancement of beam strength in a particular direction, is admissible provided that no more than approximately 50% of the tensile capacity of the effective reinforcement in the full slab

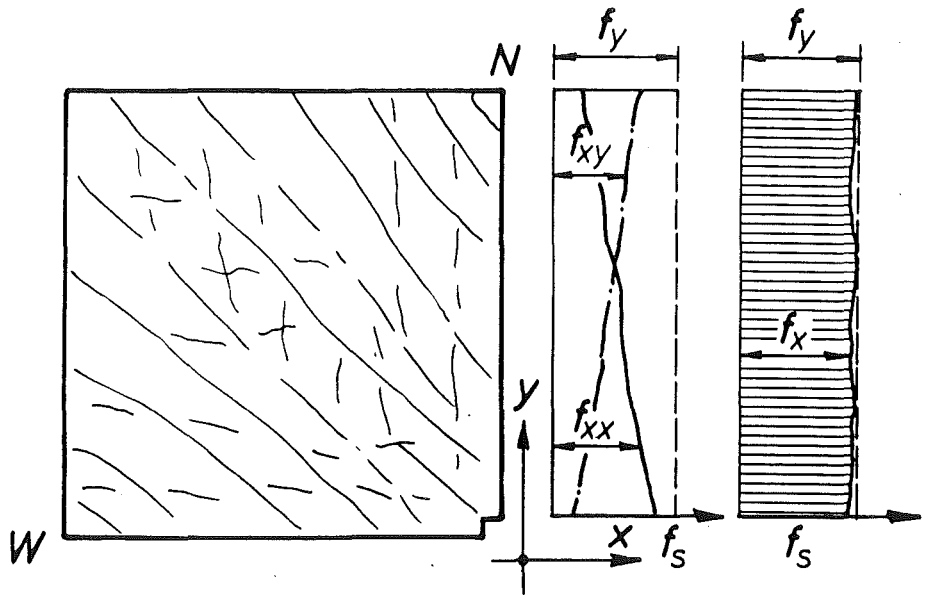

Fig.7.15 - Superposition of flange tension forces during moderate bi-directional seismic actions

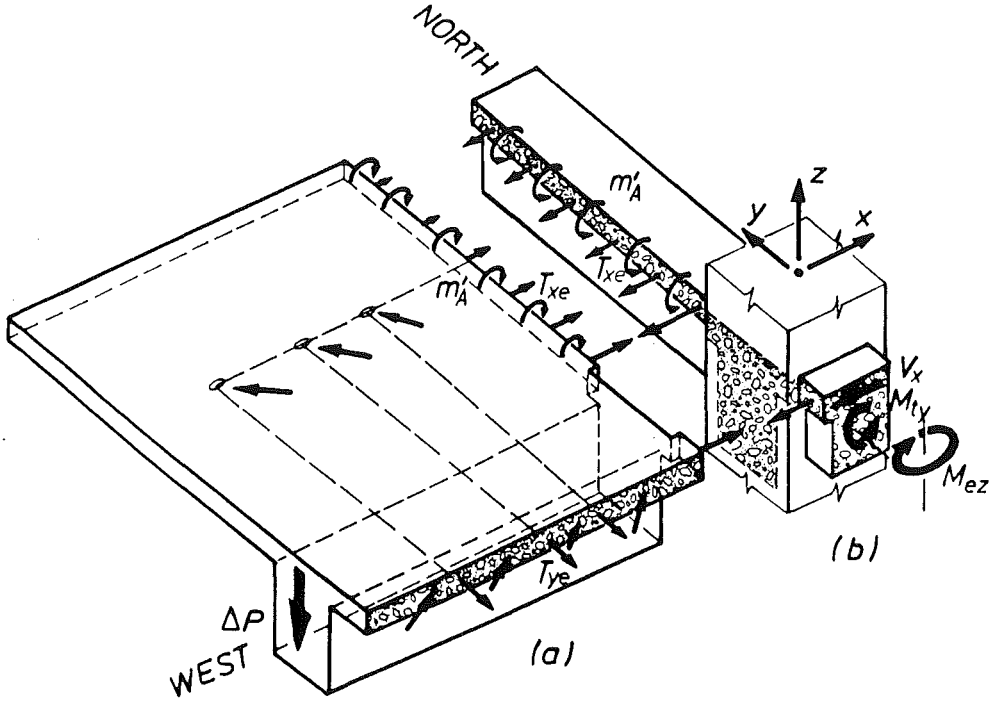

Fig.7.16 - Actions due to tension flange participation at an exterior beam-column assembly

width is taken into account for this purpose.

(2) At displacements corresponding with a ductility of μ=2 or larger in any direction, it is likely that the yield strength of a significant number of slab bars in the direction of attack (see f_{sx} in Fig.7.7) will be developed. Thus a superposition of slab bar contributions, due to displacements in each of the two directions, is no longer admissible. Magnitudes of displacement ductilities as used here refer to frames which satisfy drift criteria in the elastic range of response, when storey drift does not exceed 0.25% of the storey height when approximately 75% of the lateral design forces are applied to the frame (see Section 1.3.2).

(3) At large ductilities, i.e. $\mu \geq 4$, yielding of slab bars over the full width of the flanges may be expected. At this stage it may well be sufficiently accurate to assume that, for example in symmetrically reinforced slabs of the type used in these tests, only 50% of the total tensile capacity of a flange is utilized to enhance the flexural strength of a beam in one of the directions, while the remaining 50% of the tensile capacity contributes to the "deep beam action" illustrated in Fig.7.6. Thereby the flexural strength of the beam in the other direction is similarly enhanced by 50% of the effective slab reinforcement.

(4) During uni-directional seismic attacks, at medium to large ductilities, the maximum enhanced strength of a beam may be developed. However, the strength enhancement of the same beam due to tension flange contribution must immediately reduce when frame displacements occur in the orthogonal direction. This means that the maximum increase in flexural strengths in the orthogonal beams due to tensile flange contributions cannot be developed simultaneously. The phenomenon was consistently observed in tests.

7.4 SLAB CONTRIBUTIONS AT EXTERIOR JOINTS

7.4.1 Equilibrium Considerations

This section examines the possible mechanisms which are associated with a floor slab when acting as a tension flange at an exterior joint. the structure is that shown in Fig.7.16. Only slab interaction with the west beam is discussed. For seismic forces in the y (north-south) direction, the behaviour of the north edge (spandrel) beam with a flange on one side only may be considered to be similar to that of interior beams examined in previous sections.

Actions only due to slab participation as tension flange, to sustain a beam tip load ΔP, are given in Fig.7.16. To study the modes of resistance, two free bodies (Figs.16(a) and (b)) are studied. Only those internal forces which are considered to be important are shown at the interfaces where the structure has been separated into these free bodies, i.e. the edge beam with the column and the remainder of the assembly. These are in-plane (membrane) tension forces T_{xe} and moments m'_A in the slab. Vertical shear force and torsional moments at the slab interfaces have been neglected. Further it is proposed that, for the purpose of estimating the magnitude of the force increment ΔP, when significant ductility demands exist, the slab moments m'_A may also be neglected. A justification for this was presented in Section 7.2 (Figs.7.1 and 7.2). Thus the important component of the exterior beam's strength enhancement (ΔP), because of tension flange action, is assumed to be due to in-plane tension forces in the slab only.

The membrane forces T_{xe} shown in Fig.7.16 will generate shear forces and bending moments in each of the two free bodies. The free body shown in Fig.7.16(a) is similar to one quadrant of an interior slab panel, the contribution of which to flange action has been examined in Section 7.3 (Figs. 7.5 and 7.6). The basic components of the flange mechanism, as suggested in Fig.7.16(a), are steel tension forces in both the x and y directions and corresponding diagonal concrete compression forces.

Figure 7.16(b) implies that the bending moments, shear forces and torsion, generated by the slab actions T_{xe} and m'_A are to be resisted solely by the edge beam. These are similar to those shown in Fig.7.11. The slab moments m'_A induced by the load ΔP are considered necessary from the

requirement of compatibility of slab rotations rather than equilibrium. They may be ignored. As for torsion, it is known that torsional stiffness of an edge beam after the onset of diagonal cracking is typically 5% of that before cracking [66]. The small torsional resistance that may exist can be sustained because reinforced concrete beams are extremely ductile in torsion. Therefore an apparent torsional failure, i.e. large twist, need not significantly affect the strength of an edge beam to resist membrane forces T_{xe} introduced by the slab. Hence reliance on torsional resistance, shown as M_{ty} in Fig.7.16(b), is not necessary. While diagonal cracks, consistent with significant measured twisting of such beams have been observed in the tests (see Chapter 6), no distress due to torsion has been observed. Other tests [44, 45] reported more extensive torsional cracking in the edge beams and emphasized yielding of these beams by torsion. However, there was no direct evidence of any loss of load-carrying capacity of the test assemblies being attributed to torsional effects. Membrane tensile forces of slab bars were consistently noted.

7.4.2 Strength Considerations

Forces introduced to the edge beam by slab bars will generate shear forces V_x, and bending moments M_{ez}, as shown in Fig.7.16(b). Some designers may prefer to consider the horizontal shear, V_x, to act with an eccentricity with respect to the shear centre of the beam section. This would then lead to torsion. As torsional resistance is ignored, the horizontal force V_x must be resisted at the level of the slab.

While it might be possible to resist in the edge beam the shear forces V_x, and the bending moments M_{ez}, it is doubtful whether, on account of its flexibility, efficient beam mechanism could develop. Equilibrium requires that shear forces and moments of exactly the same magnitudes but with opposite sense, should develop in the adjacent free body shown in Fig.7.16(a).

It is evident that the pattern of moments M_{ez} for both free bodies in Fig.7.16 is similar to that shown in Fig.7.6(b). Maximum moments which could be developed about the vertical axis of the critical edge beam section (Fig.7.16(b)) will depend on the beam stiffness and ultimately on the amount of the longitudinal reinforcement near the outer vertical face of the beam. Observed relative deformations of the slab and the edge beam (see Chapter 6) were similar to those shown for the west slab and the transverse beam in Fig.7.14. When, as a result of earthquake forces acting also in the N-S

direction causing plastic hinges to develop in the edge beam, this beam's contribution to sustaining the force ΔP (Fig.7.16) at the end of the west beam of the assembly is likely to be negligible. Also using this approach, it follows that in the absence of edge beams in exterior joint assembly, the enhanced strength, as represented by the development of tensile forces T_{xe} or downward trip force ΔP, is further reduced. The effect of the horizontal flexural strength of an edge (transverse) beam on the development of membrane forces can be verified from other test results [44,45].

The main points of the above discussions are summarised as follows :

(1) In view of its flexibility when compared to slab panels, the edge beam system is likely to transfer slab bar forces which are smaller than those at interior beam-column joints. This means that tensile forces T_{xe} are particularly reduced at locations further away from the column.

(2) In transferring the shear V_x and moment M_{ez} in the edge beam to the north column face (Fig.7.16(b)), it is necessary to develop a horizontal truss mechanism in the plane of the slab. The slab bars, when anchored in the edge beam by means of hooks, are likely to be involved in the mechanism. It follows then that the membrane forces T_{xe} would be reduced.

(3) Strength enhancement, shown as ΔP in Fig.7.16, requires also the development of tensile forces in the north-south slab bars. The contribution of this slab reinforcement to the development of membrane forces T_{xe} will be reduced under simultaneous seismic actions in the N-S direction.

7.4.3 The Introduction of Flange Forces to Joints

The (tension) flange forces developed in the west slab (Fig.7.16(a)) are transferred to the column and joint at the bottom of the east beam by the mechanism as explained in Section 7.3 for interior joint assembly. This results in a strength enhancement represented by the additional downward force ΔP. For the reasons discussed in the last two sections, this enhancement should be less significant than that occurring in interior joint assemblies. Nevertheless this additional force induces shear across the joint. It was

stated in Section 2.3.1 while reviewing joint shear resisting mechanisms that the conditions in a properly detailed exterior joint are less critical. the reaction force is provided by the end hooks of the main beam bars. Therefore it can be appreciated that this additional joint shear arising from flange mechanism in exterior joint assembly can be accommodated easily.

7.5 FLANGE CONTRIBUTIONS IN CONTINUOUS BEAMS

The applicability of the postulated mechanisms of flange contributions to strength enhancement in isolated subunits, such as the three tested in this project, is briefly reexamined in the context of continuous beams and shown in Fig.7.17. To this end a slightly different approach is used.

It is well established that after cracking reinforced concrete beams subjected to seismic forces will become longer. The lengthening of beams in isolated statically determinate beam-column assemblies measured during the imposition of progressive ductilities has been reported in previous chapters. It is evident that when plastic hinges have devleoped, normally at each end of a span of a multi-span frame, and continuing significant displacement ductility is imposed in a storey, beam elongations are far from being negligible. In an idealized form, considering each beam as an incompressible rigid body, these elongations are shown in exaggeration in Fig.7.17(b). The model suggests that beam and slab elongations will be proportional to the depth of the beams. These elongations are compatible with the deformations associated with the flange mechanisms discussed in earlier sections. Fig.7.17(a) suggests the "strut and tie" mechanisms of force transfer acting in the plane of the floor slabs of the example frame of Fig.7.17(b).

The introduction of tension flange forces to beams, resulting in compression forces C_x, occurs principally in the outer (edge) slab panels (i.e. A-B and D-E in Fig.7.17) by means of a diagonal compression field. Tie forces are provided by the slab bars. The actions are the same as those previously described for isolated test assemblies.

As for flange actions in the interior panels B-C and C-D, provided that the effective slab reinforcement is the same throughout the interior panels and is thus capable of developing a tensile force ΣT_x on either side of

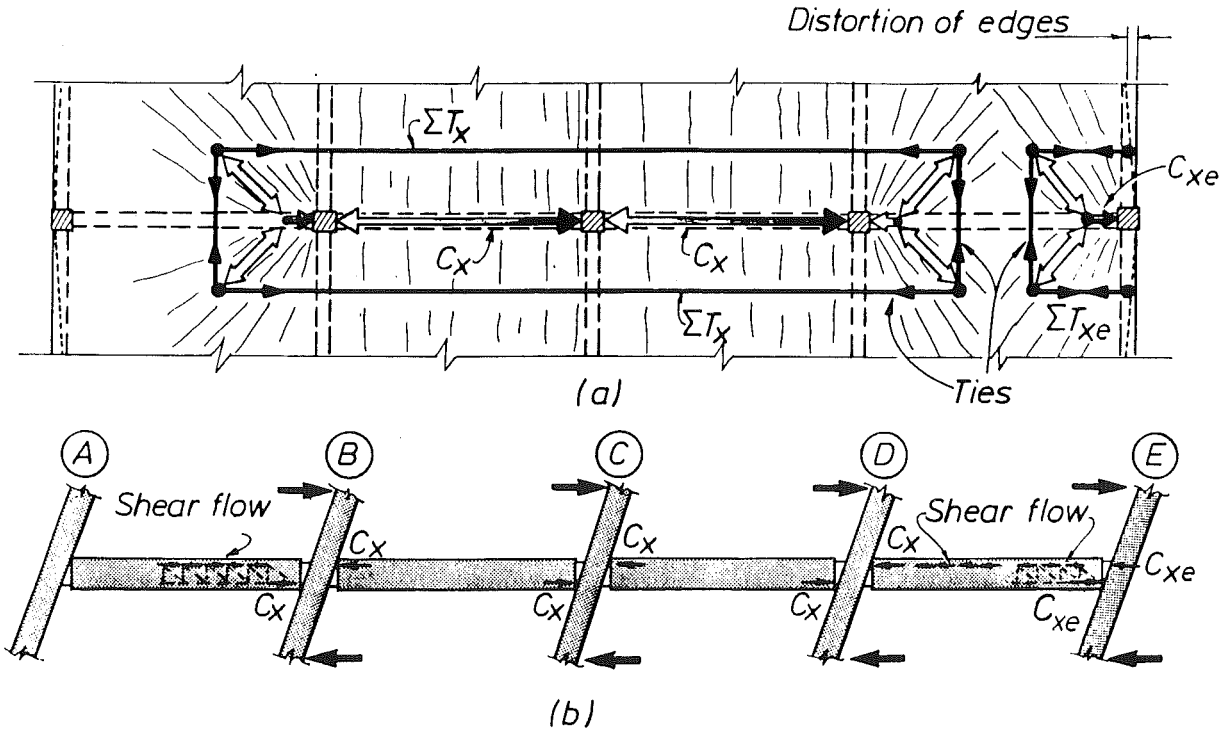

Fig.7.17 - Flange mechanisms in continuous beams

the continuous beams, compression in the beams, $C_x = 2\Sigma T_x$, in the interior spans remain constant. There is negligible or no shear transfer between flanges and the stem of the beams along the interior spans (B, C and D). Consequently transverse cracks consistent only with axial tension in the flange, are to be expected (see Fig.7.17(a)). The complete "strut and tie" mechanism for such a case is illustrated in Fig.7.17(a). It is seen that flanges (slab panels) of interior beams act as ties, while the stems of beams function as struts. The weak links of the mechanisms may be assumed to be the ties.

While all slab panels must elongate, those at the edges of the building will also be subjected to shear deformations. This results in non-uniform tensile strain distribution across the flange with maximum strains close to the longitudinal beams. The resulting horizontal deflections of the edge beams at grids A and E are indicated by dotted lines in Fig.7.17(a). Where slab reinforcement is anchored, as in the edge floor panels, in-plane shear forces are generated and these may lead to diagonal cracking in those panels. Diagonal compression fields are mobilised to transfer compression forces C_{xe} to the exterior column.

In summary there are two independent truss mechanisms, each being in equilibrium. The force transfer around the interior columns (B, C and D) depends on the continuous slab reinforcement developing the forces ΣT_x. The contribution of the other mechanism around the exterior column E depends on the amount of slab reinforcement anchored in the edge transverse beams and the strengths of these beams to transmit the distributed forces ΣT_{xe} to the column by bending and shear. Strength enhancement at each column results from compression forces C_x or C_{xe} being applied to these columns at the point of contact with the beams, i.e. in the flexural compression zones, as shown in Fig.7.17(b). The mechanism of force transfer in the A-B and D-E exterior beams near columns B, D and E, is the same as in isolated assemblies studied in the previous sections. The model in Fig.7.17 suggests that interior transverse beams have no role in enhancing the strength of flanged longitudinal beams.

In a floor system consisting of two-way slabs, in general edge panels must provide the anchorage of slab reinforcement. Hence they are subjected to in-plane shear. Instead of being double cantilevers, as modelled in Fig.7.6, edge panels will act as one continuous deep beam.

The above discussions illustrated the likely strength enhancement in a continuous frame due to tension flange actions, based on the assumptions of constant effective slab reinforcement. In realistic prototype construction, slab bars are usually curtailed. Also top reinforcement can be omitted at the centre of slab panels. In this case some shear and hence cracking may also develop in the interior panels.

After diagonal cracking has formed in the edge panels, longitudinal ties forces ΣT_x and ΣT_{xe} require the development of forces with comparable magntidues also in the (short) transverse ties. When earthquake induced actions are generated simultaneously also in the direction transverse to the frame in Fig.7.17, beam and slab elongations in that direction will introduce additional tensile forces to the (short) transverse ties. Hence their contribution to the mechanisms shown in Fig.7.17(a) will be reduced. Once again it may be concluded that as in the case of isolated units, the full contribution of slab reinforcement to strength enhancement in both orthogonal directions under skew earthquake attack cannot be mobilized simultaneously.

7.6 COMPARISON OF THEORETICAL AND OBSERVED SLAB CONTRIBUTIONS TO STRENGTH ENHANCEMENT OF BEAMS

7.6.1 Bases of Comparison

The theoretical flexural strengths of beam sections at the column faces of the three test units (Chapters 4 to 6) are compared with the bending moments which were developed at the same sections at various stages of the tests. Only negative moments, imposing tension on the top beam bars and on the flange are considered here. The comparisons are presented in Figs.7.18 to 7.21 using block diagrams. Also shown in the figures are the flexural strengths (R) based on design recommendations given in Section 7.7.

At the left-hand side of Figs. 7.19 to 7.21, magnitudes of observed beam moments, derived from measured downward acting forces applied at beam tips, are plotted separately for uni-directional and bi-directional loading patterns used in the tests. Results for uni-directional results are presented in Fig.7.19 because Unit 1D-I simulated one-way frame. The cross-shaded area in each figure represents the range of moments observed when yielding of the top reinforcement was recorded. Low values of flexural strength were measured

at a displacement ductility of $\mu = 2$ or at 0.9% drift (μ=3 for Unit 2D-E) while the maxima corresponded with μ=4 (at approximately 2% drift) or even larger ductilities. The displacements at which maximum and minimum beam strengths were attained may be readily identified in the relevant hysteretic response curves discussed in previous chapters. It should be noted that at large ductilities towards the end of the tests, even smaller moments were sometimes observed due to general deterioration of the units. Those smaller moments were not considered in the assessment of slab contribution.

Theoretical strength predictions are presented for two levels of steel stresses in the right-hand columns of the figures. One set of values is based on the experimentally established yield strength f_y of the tension reinforcement. The other set of moments, based on $1.18\ f_y$ or $1.15 f_y$ is indicative of the order of flexural overstrength due to strain hardening only, which would normally be allowed for when using capacity design procedures. Four bench mark value for theoretical negative moments are used in this comparison. Each level of theoretical flexural strength, labelled (a) to (d), was based on a specific amount of assumed effective flexural tension reinforcement, the estimation of which was made as follows :

(a) Only the top bars within the web width of the beam sections were considered. The ideal flexural strength of this section $M_{i,web}$, with $f_s = f_y$, was used as the reference value to enable the magnitudes of strength enhancements, resulting from the contribution of different amounts of tension reinforcement, to be normalized.

(b) The contribution of slab bars, placed within an effective tension flange width proposed by NZS 3101 [4] as illustrated in Fig.3.6, was included. This additional tributary flange area, labelled (b), is shown in an inset in each figure. This was referred to as M_i in previous chapters.

(c) The contribution to flexural tension of all "effective" slab bars over the entire width of the flange was considered. The effectiveness of each curtailed top or bottom bar in the tension flange was based on the location of its anchorage, using the model of Fig.7.8 recommended in Section 7.7.2. Only those bars which terminated in the shaded area of the panel in Fig.7.8 were taken into account.

(d) The theoretical upper limit of tension flange contribution was based on the participation of all slab bars in the entire width of the slab irrespective of their locations or lengths. This was referred to as M_i^* in previous chapters.

It should be appreciated that in these tests it was not possible to account precisely and separately for the two principal sources of beam strength enhancement, namely the strain hardening of the steel and the fraction of the total slab reinforcement which might have been effective in tension.

When comparisons are made with similar tests in other countries, it should be noted that the arrangement of the top and bottom slab reinforcement in the panels of the two-way slabs of the test units reported here were attempting to simulate realistic conditions, and hence bars were curtailed in both directions as in prototype construction. It is considered that slab reinforcement carried over the full length and width of slab panels, in both isolated subassemblages and continuous floor systems as used in many other tests, should result in greater beam strength enhancement.

7.6.2 Results of Comparison

(A) Unit 1D-I The block diagrams presented in Fig.7.18 show that strengths developed during the test varied between 115 and 155% of the ideal strength $M_{i,web}$, which did not include contributions from the flanges. Special features of this unit, to be noted when a comparison is made with strength enhancements in other units, are :

(i) The amount of longitudinal slab reinforcement being $\rho_s = 0.224\%$ to satisfy code requirements for shrinkage and temperature effects only, was relatively small. The theoretical contribution of all these slab bars parallel with the beam, with $f_s = f_y$ would amount to only 36% strength enhancement ($M_i^* = 1.35M_{i,web}$).

(ii) The effective width of the tension flange, to be considered according to NZS 3101 [4], is rather small. It would account for only 8% of strength enhancement. The reduction of effective slab width in NZS 3101, in comparison with those recommended for two-way frames, was based at the drafting of this code on the assumption that the absence of a transverse beam is likely to reduce the effectiveness of a flange. The level in Fig.7.18, relevant to this case is marked with the letter (b).

(iii) All slab bars extended over the entire slab, hence full anchorage was provided for all bars. Case (c), described in Section 7.6.1, is not applicable to this unit.

(iv) Only uni-directional loading was applied in this test in the east-west direction.

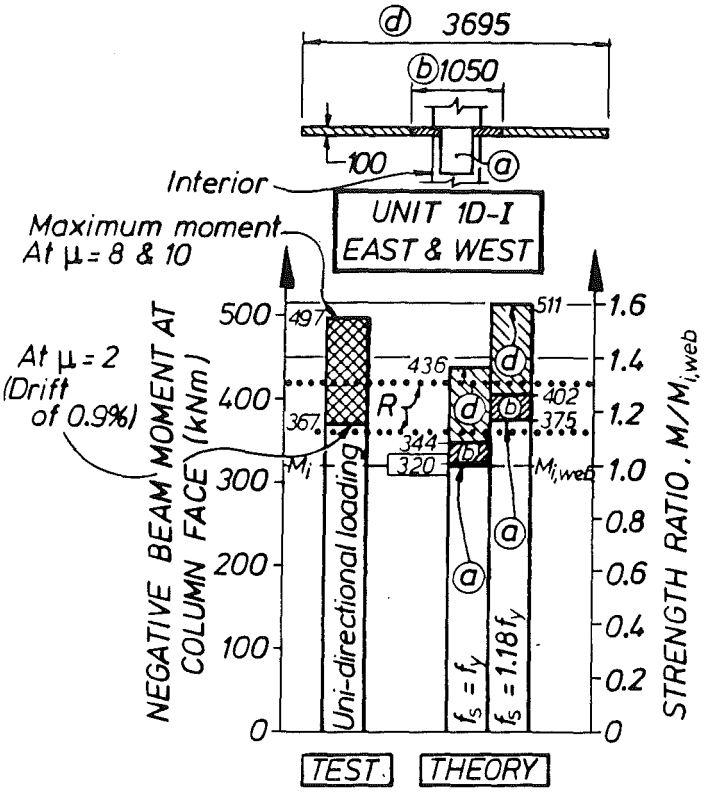

Fig.7.18 - Strength enhancement by tension flange action in beams of Unit 1D-I

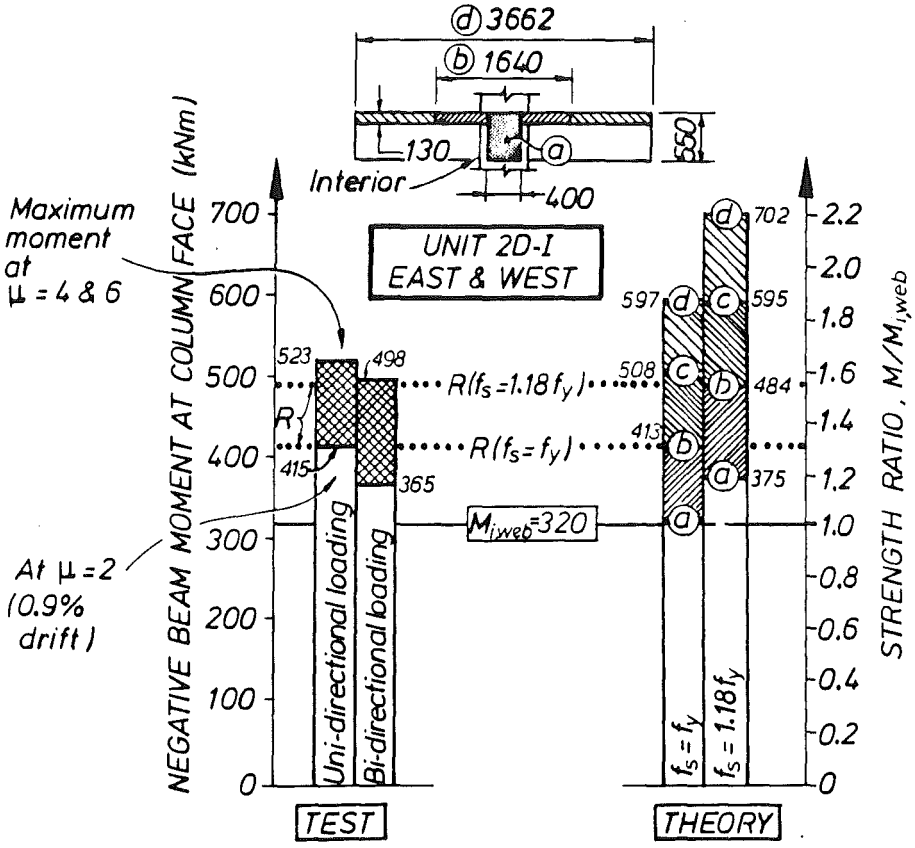

Fig.7.19 - Strength enhancement by tension flange actions in the east and west beams of Unit 2D-I

A comparison of information in Fig.7.18 suggests that current NZS 3101 [4] provisions underestimate minimum slab contribution. It is also evident that, because of the full anchorage of slab bars, at large ductilities the entire slab reinforcement contributed to strength enhancement and most of these bars were subjected also to some strain hardening. As relatively few large cracks developed across the slab (Chapter 4), the effects of tension stiffening were likely to be considerable. Across these large cracks strain hardening would have accounted for larger steel stresses than the assumed value of $1.18\ f_y$.

(B) Unit 2D-I Comparison for the east and west beams of this unit can be seen in Fig.7.19. Results for the north and south beams were very similar with maximum values being 2 to 3% larger than those shown in Fig.7.19. On the other hand the observed minimum strength of these beams at $\mu = 2$ was 2 to 3% smaller than those for the east and west beams.

Observed flexural strengths under uni-directional loading were in the range of 130 to 163% of that based on the beam sections without any slab contributions (case (a) in Fig.7.19). The same measured limits corresponded to 100 to 127% of those used in New Zealand (i.e. case (b)) when no allowance for strain hardening is made. Computed flexural overstrengths, based on $f_s = 1.18 f_y$ for the same case (b), varied between 93 and 117% of the observed values under uni-directional loading patterns.

For the same imposed displacement ductilities strengths developed during bi-directional displacements were always less than those attained during uni-directional displacements. This is considered to have resulted partly from reduced slab participation, as outlined in Section 7.3.4, and partly from deteriorated anchorage conditions for beam bars within the joint core, where transverse tension due to bi-directional loading was also introduced.

Fig.7.19 clearly shows that beam strengths based on the participation of all slab bars over the entire flange width, denoted by strength levels (d), could not be developed in these tests. The fact that some slab bars close to the column would have entered the strain hardening range underscores this observation.

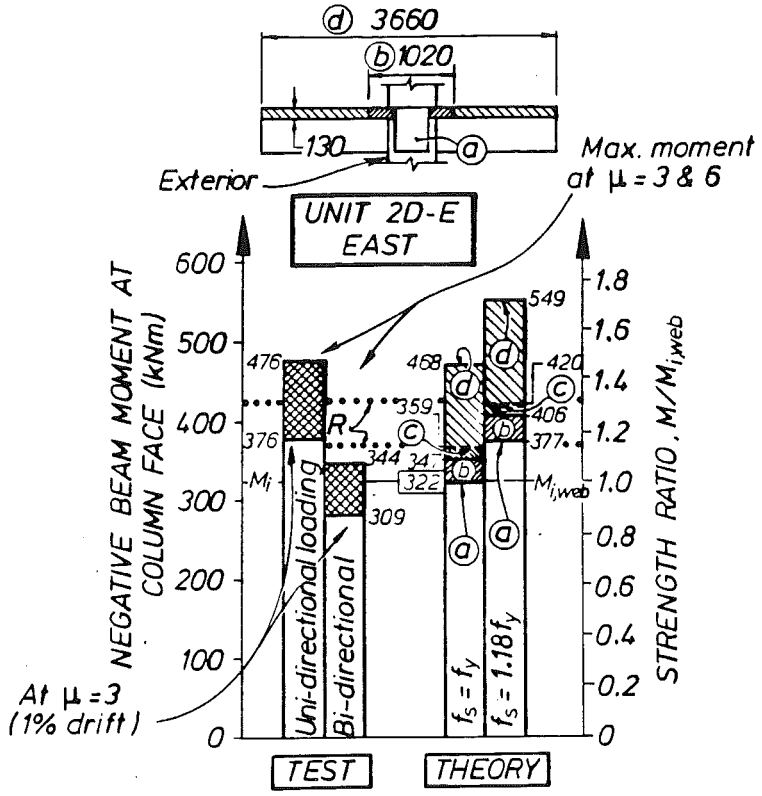

Fig.7.20 - Strength enhancement by tension flange action in the east beam of Unit 2D-E

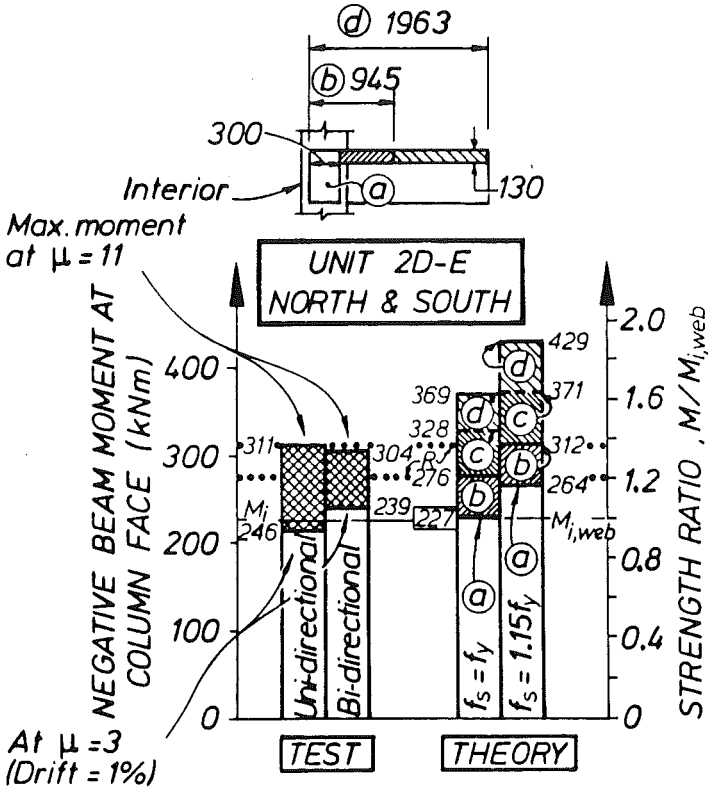

Fig.7.21 - Strength enhancement by tension flange action in the north and south beams of Unit 2D-E

If a comparison is made with theoretical strength enhancements based on the contribution of only those bars which were considered effectively anchored, shown by levels (c) in Fig.7.19, it is found that observed unidirectional strengths varied between 82 and 103% of the theoretical strength so predicted. In this comparison it is assumed that $f_s = f_y$. When strain hardening of the tension steel is taken into account, it follows that only a fraction of all the effectively anchored slab bars could have made a contribution.

It is worth noting that both the top and bottom slab reinforcement contents ($0.252\% < \rho_s < 0.377\%$) were significantly larger than those provided in Unit 1D-I.

(C) Unit 2D-E The correlation between theoretical estimates and experimentally observed enhancements of the east beam of this unit during unidirectional loadings, shown in Fig.4.20, is similar to that established for the other two test units. NZS 3101 [4] recommendations for effective flange width (i.e. case (b)), with steel stress $f_s = f_y$, lead only to 8% strength enhancement with respect to $M_{i,web}$. This is because the top slab bars, which are anchored in the north-south edge beam, are quite widely spaced and the anchorage of the bottom bars within the edge beam is considered inadequate. Also according to the assumption with respect to development length, implied in Fig.7.6, the majority of the short top bars should be disregarded. This case, identified with the letter (c), would suggest a strength enhancement by only 11%. These two ratios may be compared with the observed enhancements of 17% in the fourth cycle to $\mu = 3$ (with interstorey drift of 1.04%) and 48% in the first cycles to $\mu = 3$ to 6. The latter results would have included the contribution of significant strain hardening. Alternatively the enhancements in terms of the measured average strengths are $(434 - 322)/322 = 35\%$ at $\mu = 3$ and $(418 - 322)/322 = 30\%$ at $\mu = 6$ to 8. Four observations emerge from these comparisons :

(i) The effective flange width in tension was considerably larger than that estimated by NZS 3101.

(ii) Strength enhancement due to tension flange action was, as expected, less at an exterior joint than that observed at interior joints.

(iii) Contrary to what was observed at interior joints, strength enhacement due to tension flange action at an exterior joint did not always increase at larger ductilities. This trend can be more easily seen in the force-displacement response curves in Chapter 6.

(iv) For a more accurate estimate of the theoretical strength, the bottom slab bars close to the column could be included as part of the tension reinforcement. Test results in Chapter 6 showed that these bars underwent significant strain changes especially during the early stages of reversed loading.

The reduction of strength enhancement in the east beam during bi-directional loading history was much more profound than in the case of Unit 2D-I, as can be seen in Fig.7.20. In addition to the values shown, it can be derived from the test results in Chapter 6 that the mean bi-directional strength developed at $\mu = 3$ or 6 was of the order of $M_{i,web}$, which is a significant reduction when compared with the $1.3\ M_{i,web}$ overstrength measured under uni-directional loading. This phenomenon is considered to be due to the sharing of the contribution of the east-west slab bars to tension flange mechanisms in both directions (see Fg.7.15).

Finally strengths, relevant to the north-south edge beam of Unit 2D-E are compared in Fig.7.21. Strength enhancements for these beams on the average by 23% (uni-directional) and 20% (bi-directional), in terms of the reference moments $M_{i,web}$, were the smallest in comparison with beams of Units 1D-I and 2D-I. Yet these enhancements are comparable to the mean theoretical prediction of 20% (obtained from 0.5 (312/264 + 276/227) = 120%) based on NZS 3101 [4] recommendations referred to by the letter (b) in Fig.7.21. A likely reason for the modest observed strength enhancement is the small amount of slab reinforcement transverse to those contributing the strength enhancement of the north and south beams. Thereby the strength of the mechanisms, shown in Fig.7.5, in terms of the forces T_x, is limited beacuse of this limited contribution of tension forces in the orthogonal direction, T_y. Under bi-directional loading, slab action in the east direction imposes bending moments on the edge beams with respect to the weak axis, as Fig.7.16 suggests. The resulting bi-axial bending effect must thus reduce the flexural strength of the edge beams with respect to north-south forces.

7.7 CONCLUSIONS

The aims within this study of the role of floor slabs during the seismic response of beam-column assemblies were, to identify and if possible to quantify contributions to the strength of beams, to attempt to find

rational explanations for various features of behaviour, and finally to arrive at recommendations with respect to questions recently raised by design engineers and researchers. Itemized objectives of this research project, relevant to the role of slabs, were listed in Section 7.1. In the following, conclusions complementary to the previously stated seven objective are presented:

(1) A number of parameters affect the magnitude of slab participation as a tension flange. However, a high degree of accuracy in design to predict strength enhancement will not be required unless the amount of the relevant reinforcement in the slab, relative to that in the beams, is large. For most design situations a simple compromise solution in the estimation of the effective width of a tension flange, appears to be adequate. Details of this compromise are presented in the design recommendations in the following section.

(2) The tests reported here support theoretical predictions according to which the contribution of flanges, when subjected to tension, increases due to strain hardening of the flexural tension reinforcement and the spread of inelastic strains further from the stem of a beam, as ductility demands increase. This suggests that a conservative approach, implying modest strength enhancement due to tension flange contributions, may be adopted when the dependable strength of a beam, to meet for example moment demands due to gravity and earthquake effects, is being determined. On the other hand larger flange contributions, and an inclusion of strain hardening phenomena likely to be mobilized during large ductility demands, may be considered when the flexural overstrength of a beam and consequent moment input in a column is being estimated.

Whether this level of sophistication is warranted in the design, depends on the degree of protection which the general seismic design strategy intends to assign to columns. If the intended reserve strength of columns is to be sufficient to ensure only that a so called "soft storey" mechanism does not develop, implied for example by the requirements of ACI code [5], the above two-level strength enhancement approach appears to be justified. However, if columns are to be designed so as to reduce the likelihood of column plastic hinges being developed at any of the upper levels of a multistorey ductile frame, this refinement in the estimate of strength enhancement in beams does not appear to be justified. Current recommendations

in New Zealand [4] for the capacity design of such columns appear to be conservative enough to accommodate significant variations in probable beam strength due to slab participation (see also Eq.(3.1)).

(3) During elastic response transverse beams at interior columns contribute to the complex response of the floor slabs. However, when earthquake induced ductility demands become dominant along both principal axes of the framing system, the stiffness of the transverse beams in terms of both torsion and flexure, relative to the stiffness associated with membrane action of the floor slab, is likely to become negligibly small. Therefore, at the stage when the strength enhancement of beams is of primary interest, the contribution of transverse beams should be ignored. For the purpose of beam strength enhancement, one-way and two-way slabs should be treated in the same way.

(4) The mechanisms of flange action, postulated in Section 7.3 and Fig.7.12(b), indicate that horizontal beam forces due to flange actions alone are introduced to the joint core predominantly by concrete compression stresses (Figs.7.10 and 7.13). Therefore, for the transmission of these forces a strut mechanism within the joint could be utilized which should not require additional joint shear reinforcement.

(5) During earthquake attacks in orthogonal directions, the concrete in the slabs acting as tension flanges will be separated from the columns by large cracks. On the opposite sides of the columns, the slabs will introduce compression forces to joint cores (Fig.7.12(b)). Thus, slabs in two way frames cannot be utilized to resist forces generated within a joint core, and hence they should not be assumed to contribute in a quantifiable manner to joint shear strength or to improved joint performance.

(6) Columns and beam-column joints of two-way frames, designed to sustain forces resulting from simultaneous earthquake attacks along both principal directions of the framing system and development of flexural overstrength of all relevant plastic hinges in beams, will not be affected on account of possible underestimates of beam strength enhancements due to tensile flange actions. Both theoretical considerations presented in Section 7.3.4 and experimental evidence summarised in Section 7.6.2 indicated that the maximum attainable strength of a beam with top reinforcement in tension cannot be mobilized under orthogonal seismic attack. One of the reasons for this is

that slab bars in a given direction are utilized during seismic motions in both directions (Fig.7.15).

(7) With few exceptions a strong column-weak beam strength hierarchy within ductile frames is desired. This requires the knowledge of the strength of the beams as detailed, which could be developed during large inelastic displacements imposed by strong ground motions. Only a realistic estimate of the moment input from a beam to an adjaent column will enable sufficient column reserve strength to be provided, thus ensuring that the intended strength hierarchy can be relied on. In this context the assessment of slab contributions to beam (negative moment) strength, an aspect that has been ignored by most building codes, is important.

7.8 DESIGN RECOMMENDATIONS

(1) If warranted a detailed assessment of slab contributions to tension flange action should take into account the following quantities and features :

(i) The amount of slab reinforcement which can be subjected to tension due to neagive moments developed in beams. In this the curtailment of slab bars in two-way slabs should be accounted for.

(ii) The effectiveness of slab bars in developing their tensile strength, which is influenced by the location of the anchorage of each bar within the edge panel of a floor system. Both top and bottom bars in a slab should be considered effective only if they can develop their tensile strength at or beyond a line extending at 45° from the centre of the relevant column (see Fig.7.8 and Section 7.3.1).

(iii) The amount and arrangement of slab reinforcement in edge panels, transverse to slab bars which contribute to the increase of flexural tension forces.

(iv) Imposed ductility at which strength enhancement is to be considered.

(2) It does not appear to be justified to recommend design equations capable of accounting for each of the above major parameters. This follows from the conclusions (1) and (2) made in Section 7.7. For the sake of achieving some simplicity in design computations, a compromise solution is justified. With particular emphasis being placed on aspects of slab bar anchorages, the following design recommendations are made for the estimation

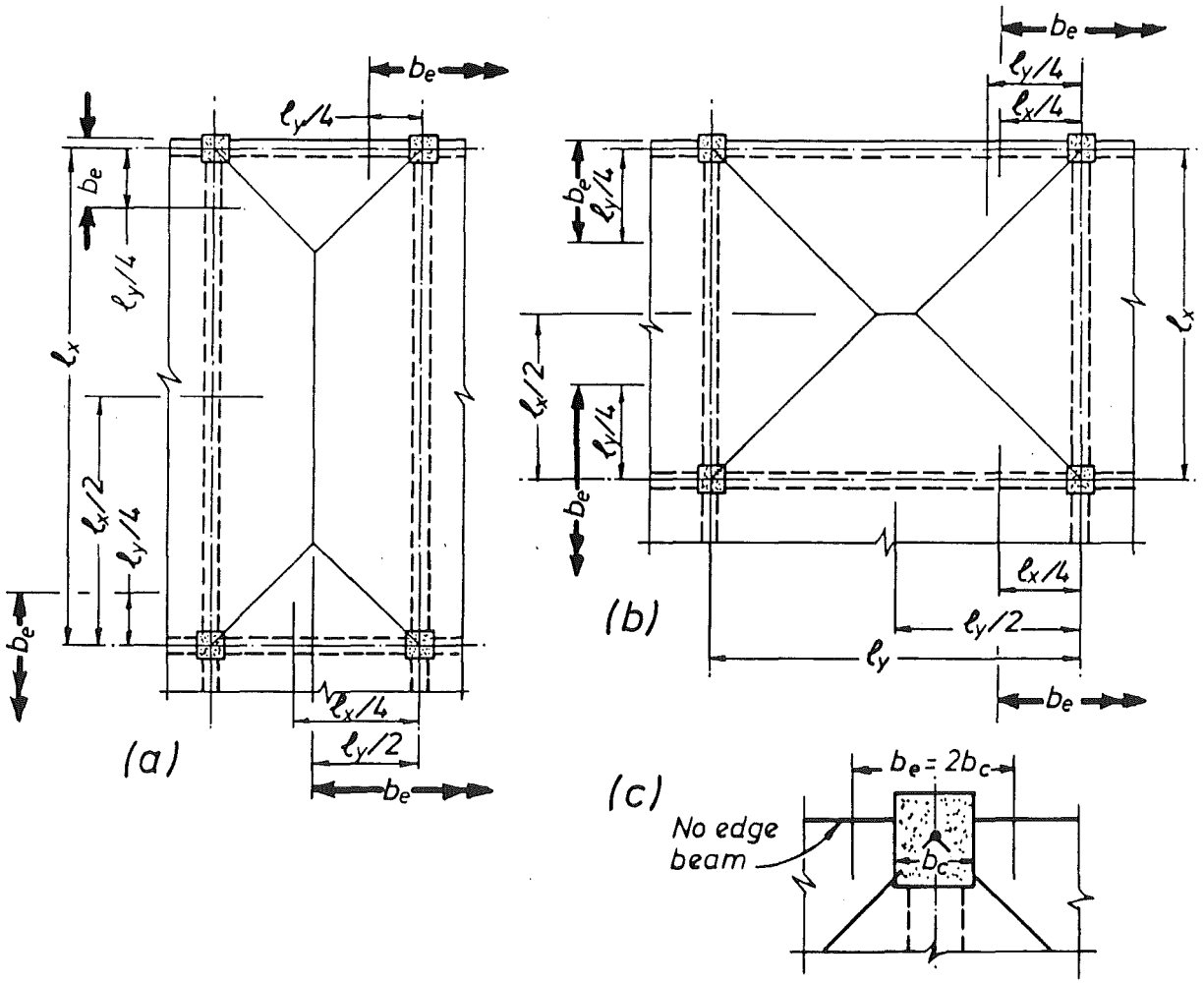

Fig.7.22 - Effective widths of tensile flanges for cast in place floor systems

of the effective flange width, b_e, within which effectively anchored slab bars should be assumed to contribute fully to the negative flexural strength of beams. These are illustrated in Fig.7.22 for various beam-slab arrangements. Accordingly, the flange width b_e, effective in tension, may be taken as the lesser of :

(i) One quarter of the span of the affected beam, extending each side from the centre of the beam section.

(ii) One half of the span of the slab, transverse to the beam under consideration, extending each side from the centre of the beam section.

(iii) Where the affected beam frames into an exterior column, one quarter of the span of the transverse edge beam, extending each side from the centre of the beam section.

(iv) Where the affected beam frames into an exterior column but no transverse beam has been provided, one half of the column width, extending each side from the centre line of the beam section (Fig.7.22(c)).

A high degree of accuracy with respect to the estimation of the number of effective bars within the width b_e is not warranted.

The computed enhanced beam strengths of the three test units, based on these recommendations for effective flange width, b_e, are shown by the pointed lines marked R in Figs.7.18 to 7.21. The larger value refers to the enhancement of flexural overstrength at $f_s = 1.18f_y$ or $1.15f_y$ and is relevant to the capacity design of columns for flexure and that of beams and beam-column joints for shear.

(3) Forces introduced by beams to a joint at the flexural overstrengths of these beams should include the enhanced strengths of the beams which are subjected to negative moments. The uncertainty with respect to force input to joints relates only to the flexural overstrength of a beam, enhanced by tensile flange contributions in excess of that allowed to use in accordance with recommendation (2) above. Because flange contributions to the increase of joint shear force should not require additional joint shear reinforcement (see conclusion (4) in Section 7.7), uncertainty in the estimate of enhanced beam strength due to flange participation only, should not affect joint

design, unless an exceptionally large amount of slab reinforcement could be mobilized.

(4) When members are proportioned in accordance with capacity design principles [4], the same proportion of flange contribution may be assumed for both the determination of dependable strength and the estimation of overstrength in beams.

CHAPTER 8

RECOMMENDATIONS FOR THE DESIGN OF JOINTS

8.1 INTRODUCTION

Test results for the three beam-column joint assemblies reported in previous chapters confirmed that joints designed to current NZS 3101 [4] provisions performed extremely well. In the light of these findings, some relaxations of existing design recommendations will be considered in this chapter. These are based partly on conceptual models of joint behaviour which have been extensively reviewed in previous chapters, and on engineering judgements supported by test observations.

Section 2.3.3 has already presented some aspects of the bond strength requirements, with Section 2.3.2 covering the inter-dependency of bond and shear resisting mechanisms in interior joints. Further in Section 2.3.4, new models for bond-slip and bond stress distribution of beam bars were proposed. Therefore this chapter is an extension of Chapter 2.

8.2 BOND STRENGTH IN INTERIOR JOINTS

8.2.1 Equilibrium Considerations

The discussions in Section 2.3.3 covered inelastic interior joints with symmetrically and unsymmetrically reinforced beams. The relationships between the average bond stress, u_b, and the ratio of beam bar diameter to column depth, d_b/h_c, were expressed by Eqs. (2.8) and (2.9). Test results in this project consistently indicated that in most practical situations the stressing of beam bars in compression will not reach the strain hardening range or even the yield level. Local bond slip of beam bars mainly due to yield penetration in the joint core, and considered in Section 2.3.4 to be inevitable, was detected in the tests. However, they did not appear to aggravate the overall seismic behaviour of the joint test units. Limited loss of the efficiency of beam bars in developing compression stresses at column faces is therefore considered acceptable. The restriction on the allowable

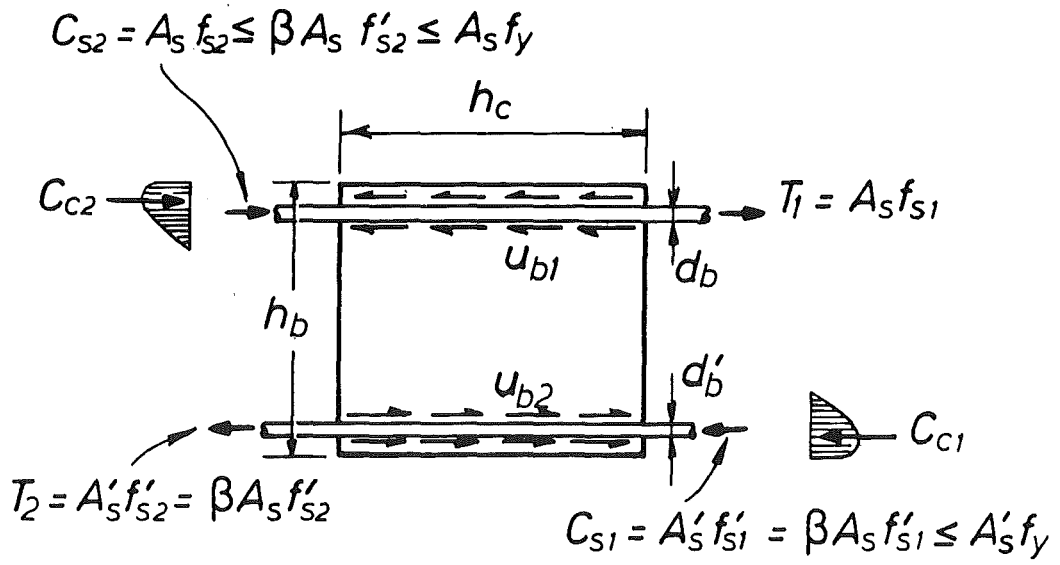

Fig.8.1 - Horizontal steel, concrete and bond forces at an interior joint due to beam moments only

average bond stress u_b implied by codes [4] can therefore be confidently relaxed to that reviewed in detail in Section 2.3.2, i.e.

$$u_b = 1.53 \sqrt{f_c'} \text{ (MPa)} \tag{8.1}$$

By considering horizontal forces only, the two cases considered in Figs.2.12 and 2.13 are generalised in Fig.8.1. The equilibrium of forces for the top beam bar is expressed as

$$A_s f_{s2} + A_s f_{s1} = \pi\, d_b\, u_{b1}\, h_c$$

where the maximum value of f_{s1} and possibly f_{s2} is $\lambda_o f_y$. This expression for the top bars can be simplified to

$$\frac{d_b}{h_c} \leq \frac{4u_{b1}}{f_{s2} + f_{s1}} = \frac{2u_{b1}}{\lambda_o f_y}\, \xi_{m1}$$

where $\xi_{m1} = 2\lambda_o f_y/(f_{s2} + f_{s1})$ is the ratio of the maximum feasible bond force (see Fig.2.8) to the total steel force expected to be developed. It is a convenient parameter to incorporate the effects of the lower stress levels when they are developed in an embedded beam bar at opposite faces of a joint as shown in Fig.8.1.

Similar expressions can be derived for the bottom beam bar of diameter d_b', resulting in $\xi_{m2} = 2\lambda_o/(f_{s2}' + f_{s1}')$. Hence in general an expression in the form of

$$\frac{d_b}{h_c} \leq \frac{2u_b}{\lambda_o f_y}\, \xi_m \tag{8.2}$$

can be formulated to determine the usable diameter of a beam bar. While the factor ξ_m has yet to be determined, it is evident that the larger the value of ξ_m is, the smaller the total bond force in relation to the maximum feasible value, to be introduced to the joint core, is implied. Hence by maintaining the bond stress level given by Eq.(8.1), the bar diameter can be correspondingly increased. Eqs.(8.1) and (8.2) can be compared with Eqs.(2.6) and (2.7) which represent existing code restrictions.

Eq.(8.2) is extended to more general cases by introducing two additional factors, ξ_p and ξ_b, accounting for effects of axial column load and bi-directional seismic actions respectively. By substituting u_b from Eq.(8.1), a convenient design expression to establish the bond (anchorage) requirements for a beam bar in an interior joint is obtained thus

$$\frac{d_b}{h_c} \leq \frac{3\sqrt{f'_c}}{\lambda_o f_y} \xi_m \xi_p \xi_b \qquad (8.3)$$

Because of limited test data, Eq.(8.3) may not be appropriate when concrete compressive strength is outside the range 20 MPa < f'_c < 45 MPa.

8.2.2 Factors Affecting Average Bond Strength

(a) Bi-directional seismic effect (ξ_b)

The factor ξ_b in Eq.(8.3) is intended to recognize the detrimental effect of skew earthquake actions on a joint. For an interior joint with orthogonal framing beams, plastic hinges can form simultaneously at all four faces of the joint. Tension transverse to beam bars will accelerate bond deterioration and eventually reduce strength, and hence will contribute to additional slip of these beam bars. Chapter 5 on Unit 2D-I reported that in contrast to corresponding beam bars in Unit 1D-I, the east-west bottom beam bars lost anchorage and slipped completely within the joint core after a severe history of bi-directional displacement reversals was imposed. Therefore a factor represented by ξ_b is considered to be necessary for designing joints of two-way frames. It is suggested that ξ_b be taken as 0.85, implying a nominal 15% reduction in the effective bond strength. In the absence of experiments, specifically designed to explore this phenomenon, more refined value for ξ_b could not be arrived at.

(b) Axial column load effect (ξ_p)

It is known that transverse confinement significantly improves the bond performance of a bar under seismic conditions [18]. Therefore some allowance for enhanced bond strength is justified when the surrounding concrete over a considerable length of a beam bar is subjected to compression transversely to the beam bar, normally due to column axial load. With an upper limit of 1.25, ξ_p is suggested to include the beneficial effect of axial compression on column, so as to permit in such situations the use of larger diameter bars. In general, even under the minimum design axial compression

load P_e, the ratio $P_e/f'_c A_g$ for a well-proportioned interior column at lower levels of a multi-storey frame could be at least 25% to 30%. Therefore the following expression is suggested:

$$1 \leq \xi_p = 0.85 \left(1 + \frac{P_e}{f'_c A_g} \right) \leq 1.25 \qquad (8.4)$$

Eq.(8.4) is essentially based on engineering judgement and on limited test observations [18]. It is likely that the beneficial effect of transverse compression on bond when $0.1 < P_e/(f'_c A_g) < 0.3$ is underestimated. It could be improved when more test data are available.

(c) Beam moment effect (ξ_m)

Recognizing various possible levels at which beam moments, generating steel stresses, may be introduced to joint cores, a few typical cases are considered for the evaluation of ξ_m, and these are summarised as follows :

(1) When symmetrically reinforced beams (i.e. $A_s = A'_s$ in Fig.8.1) are used and flexural overstrengths are expected to be attained at both joint faces, both top and bottom beam bars may be subjected to the same critical forces as shown in Fig.2.12. At this stage, by referring to Fig.8.1, $f_{s1} = f'_{s2} = \lambda_o f_y$, $f'_{s1} = f_{s2} = f_y$ and hence from the definition given in Section 8.2.1,

$$\xi_m = \frac{2\lambda_o}{1 + \lambda_o} \qquad (8.5)$$

(2) When beams are unsymmetrically reinforced (i.e. $A'_s = \beta A_s$ and $\beta < 1$) and plastic hinges still form at both faces of the joint, the maximum bar forces are as suggested in Fig.2.13. The stresses shown in Fig.8.1 become $f_{s1} = f'_{s2} = \lambda_o f_y$, $f_{s2} = \beta \lambda_o f_y \leq f_y$ and $f'_{s1} = f_y$. Therefore,

(for top bars) $$\xi_m = \frac{2}{1 + \beta} \geq \frac{2\lambda_o}{1 + \lambda_o} \qquad (8.6a)$$

(for bottom bars) $$\xi_m = \frac{2\lambda_o}{1 + \lambda_o} \qquad (8.6b)$$

(3) When gravity loads on beams are significant or dominant in comparison with actions due to earthquake lateral forces, a beam plastic hinge on one side of the column may never develop. This can occur in low-rise building frames particularly with long-span beams, and also commonly in the upper storeys of multistorey frames. Consequently the bottom bars such as the one at the left face of the joint core in Fig.8.1 may remain elastic in all events. This corresponds to $f'_{s2} \leq f_y$. For convenience a stress factor υ_1 is adopted so that $f'_{s2} = \upsilon_1 f_y$ and $\upsilon_1 \leq 1$. It suffices to consider the range $0.8 \leq \upsilon_1 \leq 1$ because smaller values correspond to less critical situations. Substituting $f_{s1} = \lambda_o f_y$, $f'_{s1} = f_y$ and $f_{s2} = \beta f'_{s2} = \beta \upsilon_1 f_y$,

(for top bars) $$\xi_m = \frac{2\lambda_o}{\beta\upsilon_1 + \lambda_o} \qquad (8.7a)$$

(for bottom bars) $$\xi_m = \frac{2\lambda_o}{\upsilon_1 + 1} \qquad (8.7b)$$

(4) When plastic hinges are intentionally relocated away from column faces, neither the top nor the bottom beam bars at the joint faces (Fig. 8.1) will be stressed in tension beyond yield strength while the flexural overstrength of the hinges is being developed. Anchorage conditions will be even less critical. Considering (Fig.8.1) the worst situation when $f_{s1} = f'_{s1} = f'_{s2} = f_y$ and $f_{s2} = \beta f_y$,

(for top bars) $$\xi_m \geq \frac{2\lambda_o}{1 + \beta} \qquad (8.8a)$$

(for bottom bars) $$\xi_m = \lambda_o \qquad (8.8b)$$

Eq.(8.8b) is identical to Eq.(8.8a) when $\beta = 1$, or to Eq.(8.7b) when $\upsilon_1 = 1$.

(5) If more deterioration of beam bar anchorage within an inelastic joint core is accepted, resulting in stress patterns as indicated in

Fig.2.10, the above requirements for bond strength can be further relaxed. As Fig.2.10 shows, bond deterioration manifests itself in decreased compression stress developed in beam bars. The advantage is that as a result the concrete compression strut mechanism V_{ch} is enhanced (see Sections 2.3.2 and 2.3.4), thus reducing the amount of joint shear reinforcement to participate in the truss mechanism V_{sh}. The compressive stresses f'_{s1} and f_{s2} in the bars of Fig.8.1 are quantified by $\upsilon_2 f_y$, where υ_2 is another stress factor of the range $0 < \upsilon_2 < 1$. Note then f'_{s1} and f_{s2} need not be equal. To avoid crushing of the concrete in compression, the values of C_{c1} and C_{c2} (Fig.8.1) should not be excessive although their existence is desirable for V_{ch} to be mobilised. This is identical to the condition that C_{s1} or C_{s2} does not become extremely small or zero. Consequently, υ_2 should be at least 0.5. Considering the maximum bar forces possible, with $f_{s1} = \upsilon_2 f_y$, $f_{s1} = f'_{s2} = \lambda_o f_y$ and $f_{s2} = \beta\lambda_o f_y \leq \upsilon_2 f_y$,

(for top bars) $$\xi_m = \frac{2}{1+\beta} \geq \frac{2\lambda_o}{\upsilon_2 + \lambda_o} \qquad (8.9a)$$

(for bottom bars) $$\xi_m = \frac{2\lambda_o}{\upsilon_2 + \lambda_o} \qquad (8.9b)$$

To facilitate comparisons, Eqs.(8.5) to (8.9) are plotted in Fig.8.2 showing the resulting maximum and minimum values of ξ_m. Fig.8.2(a) applies for the case $\lambda_o = 1.25$ when Grade 275 steel is used, while Fig.8.2(b) with $\lambda_o = 1.4$ is associated with Grade 380 steel. Different values assigned to $\beta = A'_s/A_s$, $\upsilon_1 = f'_{s2}/f_y$ and $\upsilon_2 = f'_{s1}/f_y$ or f_{s2}/f_y are considered to be within the practical ranges.

To demonstrate relevance to a realistic situation, the largest beam bar diameters allowed by Eq.(8.3), corresponding to the largest values of ξ_m, are calculated using an example interior joint core with column depth h_c = 600 mm, concrete compressive strength f'_c = 30 MPa, and factors ξ_p and ξ_b being assumed to be unity. The results are plotted on the right-hand ordinate of Fig.8.2. Also shown are the limits according to current NZS 3101 [4] requirements. As have been covered in detail in Section 2.3.1 and 2.3.2, NZS 3101 provisions were based on the assumptions of $f_{s1} = f'_{s1} = f_{s2} = f'_{s2} =$

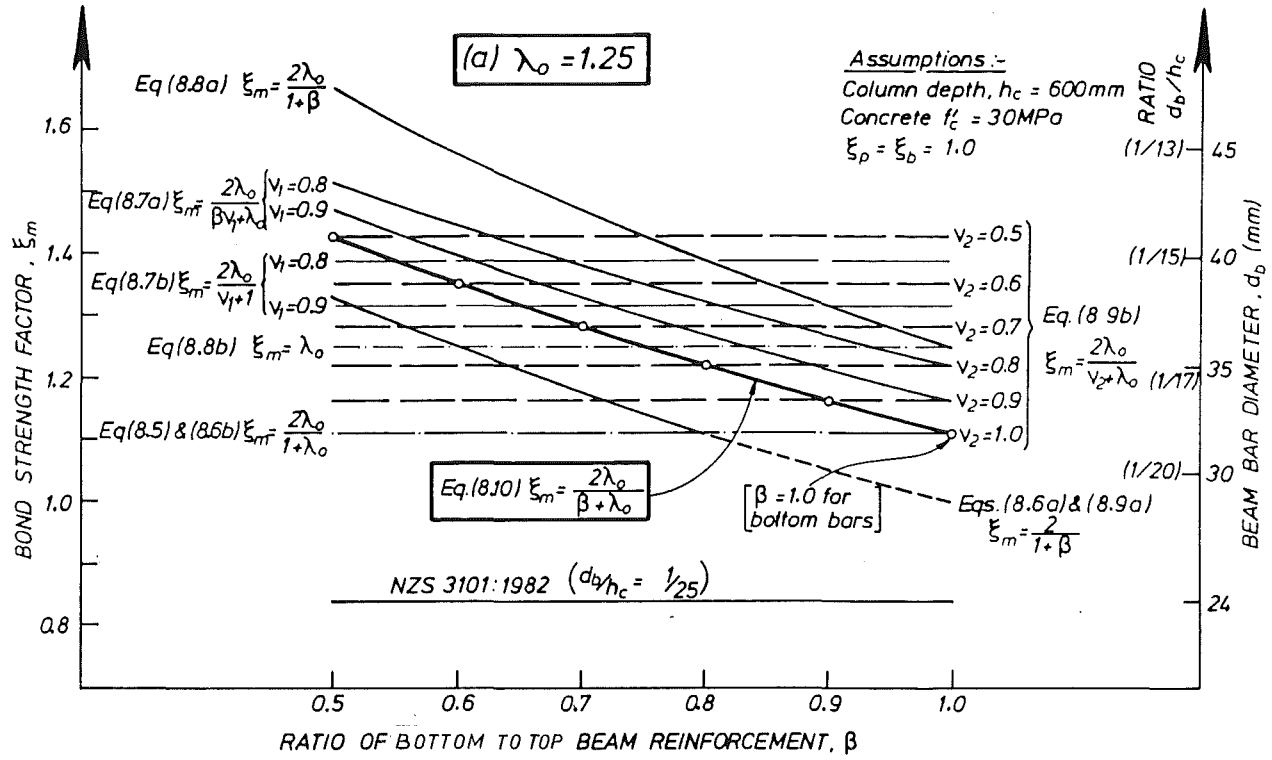

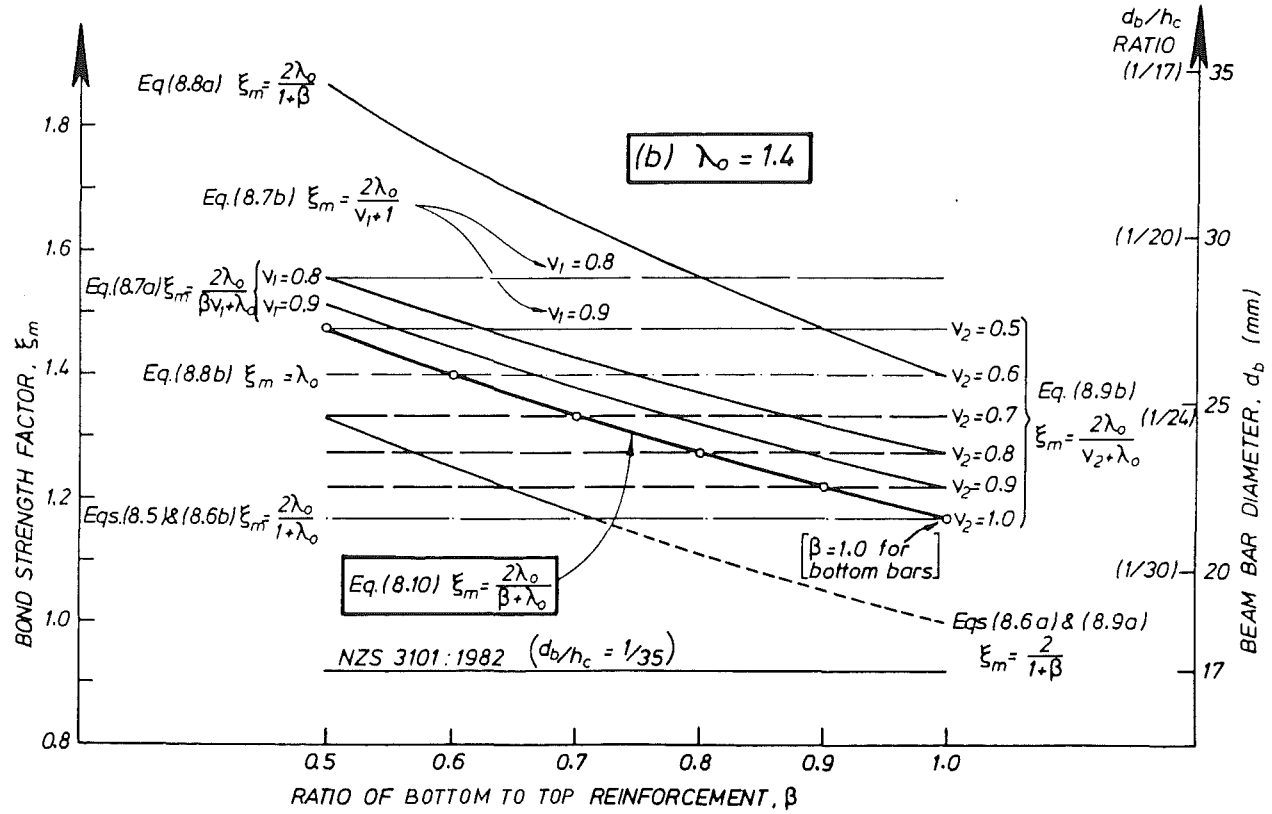

Fig.8.2 - Bond strength factor allowing for beam moment effect

$\lambda_o f_y$ and hence $\xi_m = 1.0$. The code assumed that for all cases $f'_c = 20$ MPa and no allowance was made for the beneficial effects of column axial compression and higher strength concrete.

It is evident from Fig.8.2 that some conditions are more favourable than others for anchorage of beam bars in a joint core. The bond strength factor ξ_m can be determined using Eqs. (8.5) to (8.9) to correspond to a given design situation. However, for routine design work it is desirable to adopt simple rules. Also by recognizing that Eq.(8.3) involves two more coefficients based on judgement, sophisticated rules for ξ_m are therefore not justified. From the test results reported in earlier chapters, the maximum probable compressive steel stresses attained in beam bars at column faces, i.e. f'_{s1} and f_{s2} in Fig.8.1, can be summarised as follows :

(1) For symmetrically reinforced beam sections ($\beta \approx 1.0$), $f_{s2} = 0.8\ f_y$ and $f'_{s1} = 0.9\ f_y$.

(2) For unsymmetrically reinforced beam sections ($\beta \approx 0.5$), $f_{s2} = 0.5 f_y$ and $f'_{s1} = 1.0 f_y$.

Therefore it is proposed that for beam bars in inelastic interior joints :

$$\xi_m = \frac{2\lambda_o}{\beta + \lambda_o} \qquad (8.10)$$

where $0.5 \leq \beta \leq 1.0$. For the bottom layer beam bars, β shall always be taken as unity. Eq.(8.10) is denoted by the heavy lines in Fig.8.2 for the two cases with $\lambda_o = 1.25$ and 1.4.

For elastic joints where plastic hinges are not expected at opposite faces of a joint, Eq.(8.8) may be adopted.

8.3 SHEAR STRENGTH OF INTERIOR JOINTS

8.3.1 General

Section 2.3 has reviewed the two postulated and generally accepted mechanisms of joint shear resistance as well as the influence of bond

performance on these mechanisms. With the notation of Section 2.3 and from Fig.2.4, the shear strength of an interior joint in the horizontal and vertical directions can be derived from the superposition of the two mechanisms as

$$V_{jh} = V_{ch} + V_{sh} \tag{8.11a}$$

and

$$V_{jv} = V_{cv} + V_{sv} \tag{8.11b}$$

It was pointed out in Section 2.3.1 that with some exceptions, code provisions in New Zealand [4] ingore the effectiveness of V_{ch} in inelastic joints. Thus all the horizontal joint shear is assumed to be carried by reinforcement. In Section 8.2.2, a compromise in beam bar anchorage conditions, with due consideration for practicality, has led to relaxation in the requirements for anchoring beam bars in inelastic joints. Therefore it is necessary to evaluate the likely effect of this relaxation on the mechanisms of joint shear resistance.

8.3.2 Contributions of Concrete Strut Mechanism

(a) Horizontal joint shear

The discussions in Section 2.3.3 and particularly Section 2.3.4 on the relationships between bond and shear mechanisms have resulted in the establishment of Eqs.(2.10) to (2.13) which provide a means to quantitatively estimate V_{ch} for inelastic interior joints. Both the postulations and the experimental results in this project suggested that V_{ch} might be considerable. This force can be better appraised by resolving it into two components, namely V'_{ch} and V''_{ch}, so that with the notation in Fig.2.16, Eq.(2.12) becomes

$$V_{ch} = V'_{ch} + V''_{ch} \tag{8.12}$$

where

$$V'_{ch} = C_{c2} - (1 - K_f)V_{col} \tag{8.13a}$$

$$V''_{ch} = \Delta T_c - K_f V_{col} \tag{8.13b}$$

and

$$K_f = C_{s2}/(C_{s2} + C_{c2}) = C_{s2}/T_2 \tag{8.13c}$$

The introduction of the factor K_f ensures that neither Eq.(8.13a) nor Eq.(8.13b) results in negative forces. It is seen that the total value of V_{ch} (Eq.(8.12)) is independent of the assumed allocation of V_{col} to V'_{ch} and V''_{ch}. The likely magnitudes of the factor K_f found from the tests were :

(1) $K_f \simeq 0.7$ for symmetrically reinforced beam sections ($\beta \approx 1.0$), corresponding to compressive steel stress at top layer bars $f_{s2} \simeq 0.8 f_y$ (see also Section 8.2.2).

(2) $K_f \simeq 0.6$ to 0.65 for unsymmetrically reinforced beam sections ($\beta \approx 0.5$), corresponding to $f_{s2} \simeq 0.5 f_y$.

Because anchorage conditions for beam bars change continuously during the elastic and subsequent inelastic response of a reinforced concrete frame, it is difficult, if not impossible, to precisely determine the bond forces ΔT_c relevant to a particular state of a joint. The method proposed in Section 2.3.4, based on simple models and engineering judgements, is considered relatively conservative, yet realistic. It is therefore considered acceptable for design purposes. To estimate the likely magnitude of the horizontal joint shear strength V_{ch}, Eqs. (8.12) and (8.13) can be applied for various combinations of C_{c2} and C_{s2}, bearing in mind that C_{c2} should always exist.

An example based on Fig.8.1 is used to illustrate the effects of the coefficient K_f when h_c = 600 mm. For beam-column joint assemblies of usual proportions, the column shear, V_{col}, is of the order of $0.15(T_1 + T_2)$. The corresponding values of V_{ch}, normalised in terms of the total horizontal joint shear V_{jh}, are plotted in Figs.8.3 and 8.4. Fig.8.3 shows the special case for β = 0.5 and zero column axial load, with the components V'_{ch} and V''_{ch} being separated. Evidently even when C_{c2} diminishes to nearly zero, the case of which as discussed before should not exist, the shear resistance V_{ch} still amounts to 22% of the horizontal joint shear. This results entirely from part of the total bond forces $T_1 + C_{s2}$ being introduced to the diagonal concrete strut, estimated as $\Delta T_c - V_{col}$ (Fig.2.16).

Fig.8.4 shows more general cases by including three possible values of β and also the effects of axial load on the column ($P_e/f'_c A_g$). Also plotted at the top of both graphs are the values of $\upsilon = f_{s2}/f_y \leq 1.0$ for tensile overstrength factors of λ_o = 1.25 and 1.4.

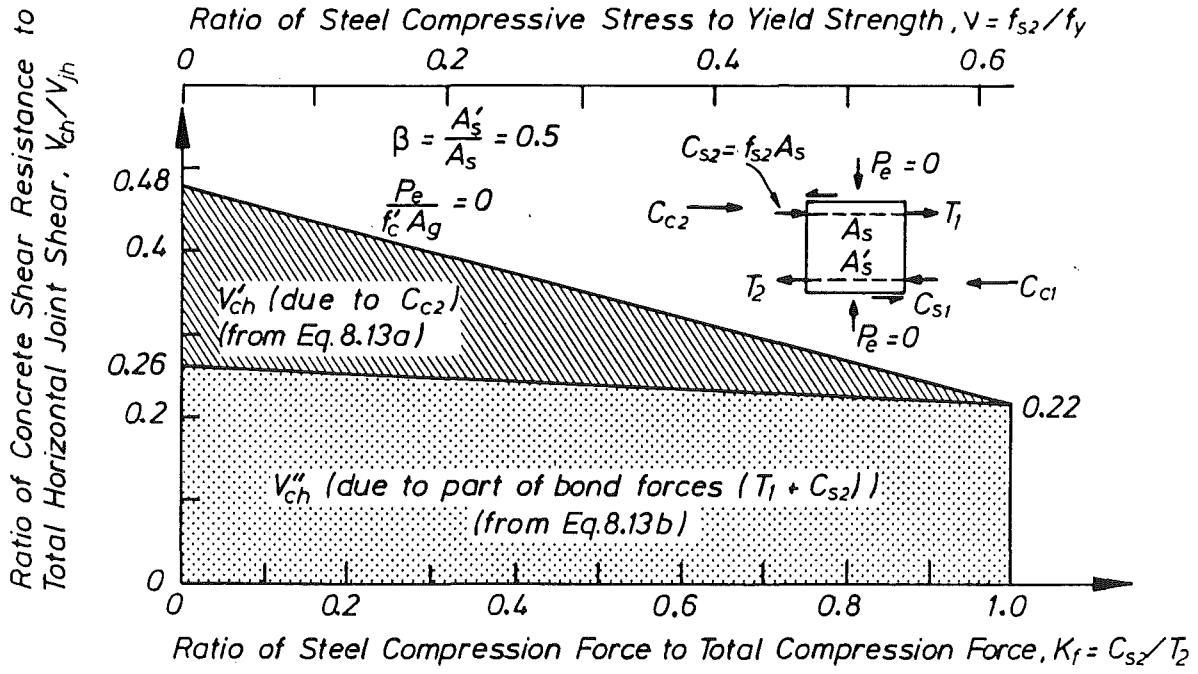

Fig.8.3 - Horizontal concrete shear resistance in an inelastic interior joint assembly with unsymmetrically reinforced beams

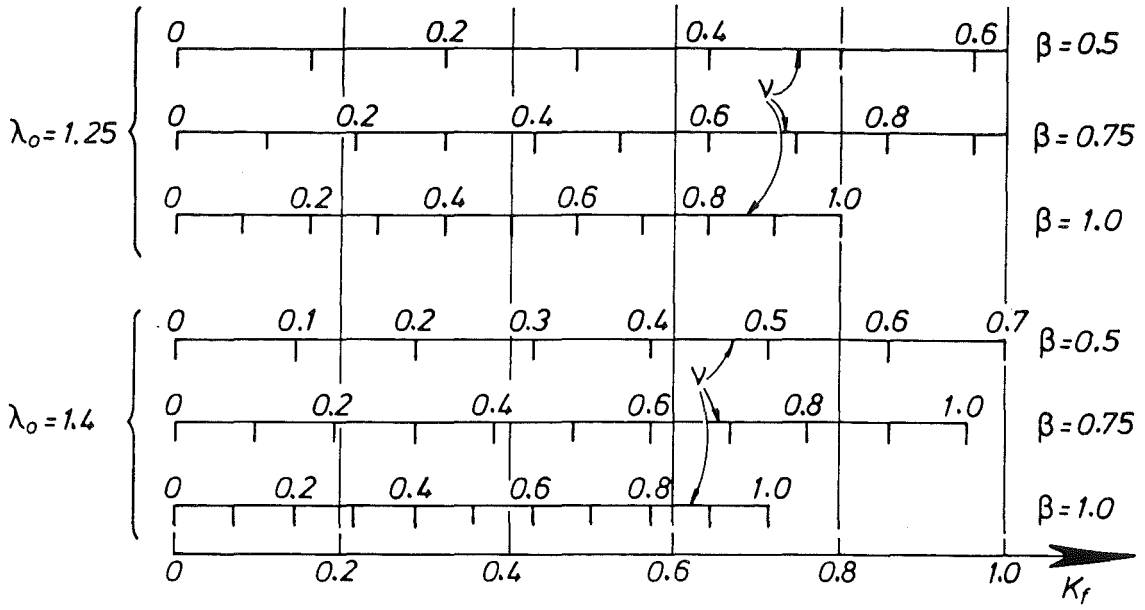

(a) Ratio of steel compressive stress to yield strength for top beam bars, $\nu = f_{s2}/f_y$, as a function of K_f

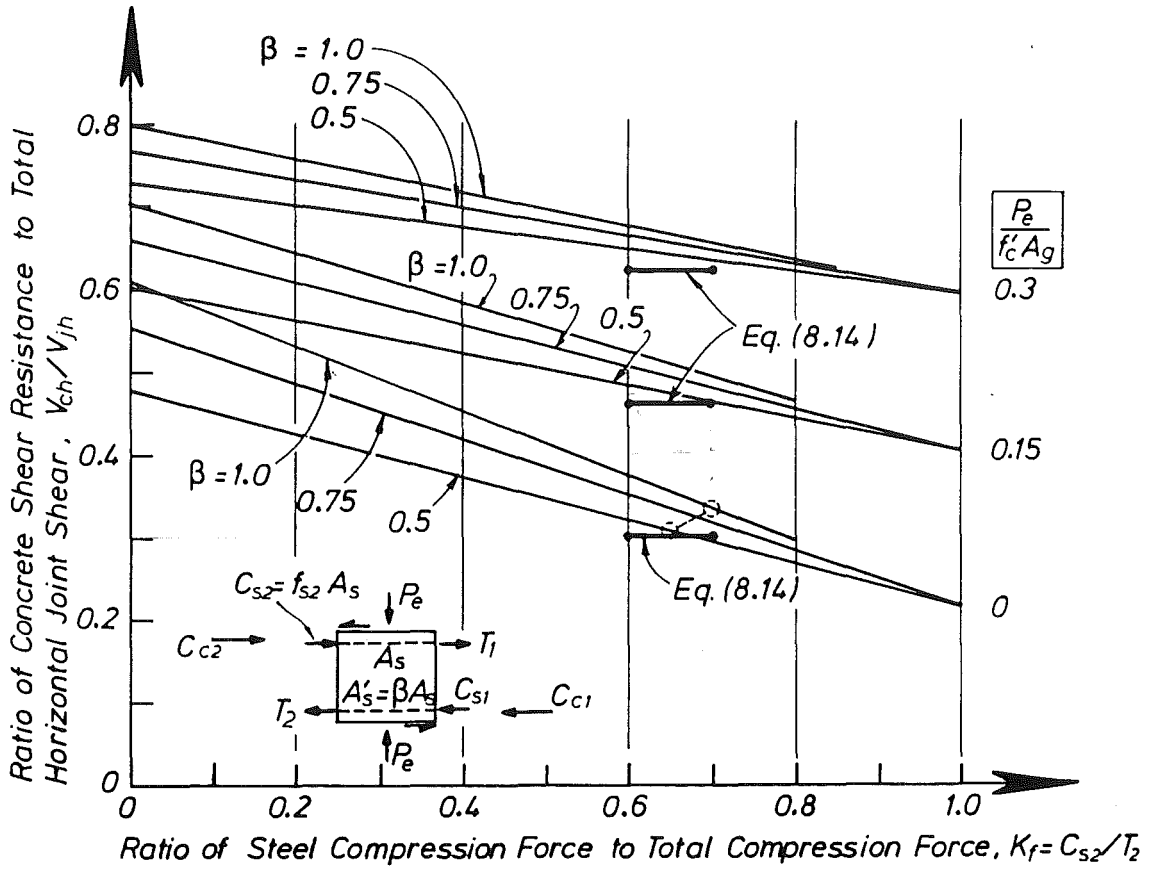

(b) V_{ch}/V_{jh} as a function of K_f and $P_e/f'_c A_g$

Fig.8.4 - The contributions of concrete strut mechanism to horizontal joint shear resistance in an inelastic interior joint

While Fig.8.4 shows that V_{ch} depends to a great extent on the assigned value of K_f, reference is made to the observed values for K_f from the test results as reported in an earlier paragraph. Thus under zero column load, $V_{ch} = 0.31\ V_{jh}$ for $K_f = 0.65$ and $\beta = 0.5$, and $V_{ch} = 0.33V_{jh}$ for $K_f = 0.7$ and $\beta = 1.0$. These are indicated in Fig.8.4 by the dotted circles. For the formulation of a simple design procedure applicable to general cases, a compromise needs to be made. It is suggested therefore, as indicated by the heavy lines bounded by full circles within the range $0.6 \leq K_f \leq 0.7$ in Fig.8.4, to simplify the results to that $V_{ch}/V_{jh} = 0.3$, 0.46 and 0.62 corresponding to the cases when $P_e/f'_cA_g = 0$, 0.15, and 0.3 respectively. The effects of reinforcement ratio β may be disregarded because the relationships in this range of K_f is not sensitive to β. Consequently the simplifications can be expressed by the following equation :

$$V_{ch} = 0.3 \left(1 + 3.5 \frac{P_e}{f'_c\ A_g} \right) V_{jh} \qquad (8.14a)$$

For two-way frames subjected to bi-directional seismic attack, simultaneous development of horizontal joint shear forces V_{jx} and V_{jy} in the two principal x and y directions is inevitable. In this case the beneficial effect of axial column load on joint shear strength will probably be reduced. While little relevant test data are known, an adjustment factor C_j defined as

$$C_j = V_{jh}/(V_{jx} + V_{jy}) \qquad (8.15)$$

is recommended [4] as a multiplier to the column load ratio P_e/f'_cA_g when considering horizontal joint shear in one particular direction. For a symmetrical two-way frame C_j is equal to 0.5.

Test results for the identically reinforced joints of Units 2D-I and 2D-E reported in earlier chapters concluded that the response of a two-way joint core was generally inferior to that of one-way joint. It is therefore prudent at this stage to allow for 15% reduction in the assessed concrete shear strength V_{ch} according to Eq.(8.14a). Hence while Eq.(8.14a) is applicable to joints of one-way frames, the following equation is proposed for estimating V_{ch} in inelastic interior joints of two-way frames :

$$V_{ch} = 0.25 \left(1 + 3.5 \frac{C_j P_e}{f'_c A_g} \right) V_{jh} \qquad (8.14b)$$

(b) Vertical joint shear

The above procedure may be extended to estimate the magnitude of the vertical joint shear resistance by the concrete strut mechanism. Fig.2.4(c) shows the assumption that the angle of inclination of the strut is α. Once the horizontal component V_{ch} of this diagonal force D_c is determined from Eq.(8.14), it is evident that the corresponding vertical component of D_c is

$$V^*_{cv} = V_{ch} \tan\alpha \approx V_{ch} \frac{h_b}{h_c} \qquad (8.16)$$

This vertical component force is denoted by V^*_{cv} so as to differentiate it from the conventional notation V_{cv} (Eq.8.11b) which collectively represents the vertical shear resistance other than that of the vertical joint shear reinforcement.

For design purposes and in the light of previously made assumptions, particularly those with respect to the distribution of bond forces along beam bars, refinements in the determination of angle α in Eq.(8.16) are not justified. As can be seen from Figs.2.4(c) and (d), the angle of inclination of the diagonal compression field within the truss mechanism is assumed to be the same as that of the diagonal strut. Clearly the angle α will increase when axial compression load acting on the column is also to be transmitted through the joint.

Eq.(8.16) is based on equilibrium consideration. It may be readily shown that the vertical forces C''_c and $\Delta T''_c$ at the upper left hand corner of the joint (Fig.2.4(c)) can be easily developed. In view of the expected good bond performance of (elastic) column bars and the small depth of flexural compression zone in the adjacent beam, the component $\Delta T''_c$ is expected to be rather small. On the other hand, the compression reinforcement in an elastic column, without any axial compression as assumed in Fig.2.4, is likely to be subjected to stresses only a small fraction of its yield strength. Hence the contribution of the concrete, shown as C''_c in Fig.2.4(c), will be very significant. Elastic analyses of conventionally reinforced columns also show

that when subjected to flexure only the total flexural compression force (Fig.2.4(b)) invariably exceeds that required to balance the sum of the vertical component of the diagonal strut and the beam shear force, i.e. $C''_c + C''_s > V_{ch} \tan\alpha + V_b$. The resulting excess compression, $\Delta C''$, together with axial compression load on the column, will enable vertical joint shear force, in addition to V^*_{cv}, to be transmitted without the aid of vertical joint shear reinforcement. This is quantified in the following section.

8.3.3 Contributions of Truss Mechanism

Fig.8.5 reproduces the truss model of Fig.2.4(d) with a diagonal compression field inclining at an angle α with the horizontal, where $\tan\alpha = h'_b/h'_c \approx h_b/h_c$. The total joint shear reinforcement in the horizontal and vertical directions is A_{jh} and A_{jv} respectively. From Eq.(8.11a) it follows that the contribution of the truss mechanism to horizontal joint shear can be determined as $V_{sh} = V_{jh} - V_{ch}$, where V_{ch} is given by Eq.(8.14). Thus the shear flow (i.e. force per unit length) around the joint core is

$$v_s = V_{sh}/h'_c \tag{8.17}$$

and the area of the required horizontal joint shear reinforcement is accordingly calculated as

$$A_{jh} = V_{sh}/f_{yh} = v_s h'_c/f_{yh} \tag{8.18}$$

where f_{yh} is the yield strength of the horizontal joint shear reinforcement.

In the vertical direction, as concluded in Section 8.3.2 the joint core is subjected to vertical compression due to the net force $\Delta C'' = C''_c + C''_s - V_b - V^*_{cv}$, over a depth c (Fig.2.4) and also due to axial compression load P_e over a reduced column depth h'_c. These effects can be for convenience approximated by the following uniformly distributed forces (Fig.8.5)

$$p = (\Delta C'' + P_e)/h'_c \tag{8.19}$$

Eq.(8.19) does not account for the fact that there is a larger force transfer between the upper right-hand corner and lower left-hand corner of the joint core (Fig.8.5) due to the concentration of the force $\Delta C''$. However, this

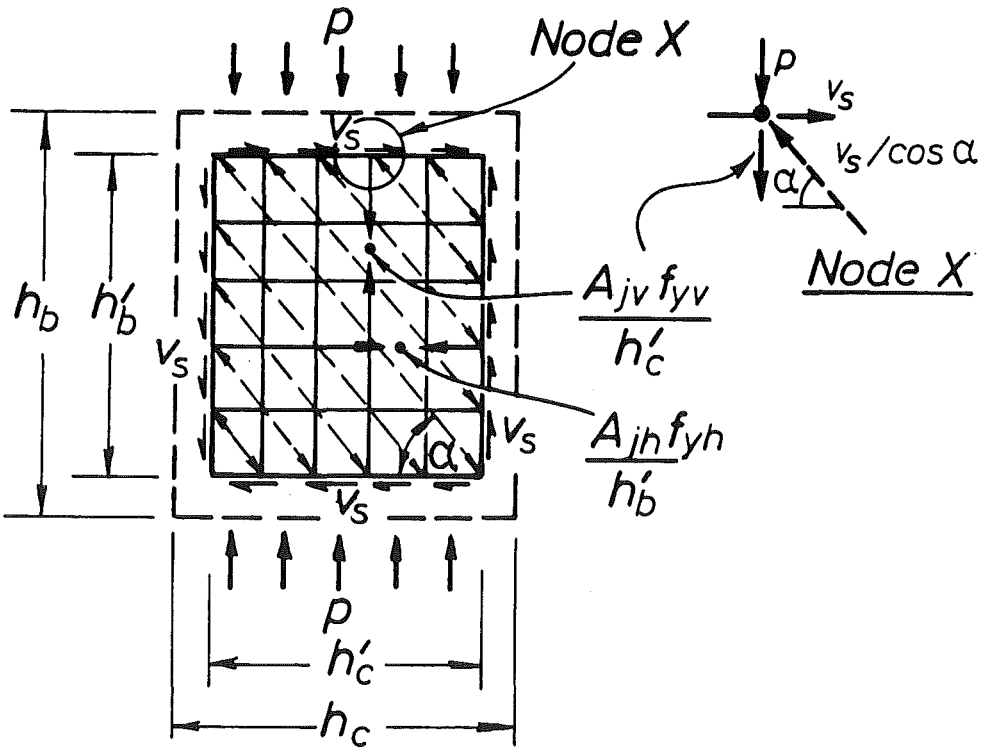

Fig.8.5 - Forces within the truss model for an inelastic interior joint core

assumption of uniform distribution coforms with that implied by the truss model.

Further approximation is taken by assuming that in Fig.2.4(b) each pair of steel compression force and concrete compression force, such as C''_c and C''_s, in each structural member framing into the joint core are acting on the same line of action. Thus the total tensile force in the outer bars of a symmetrically reinforced column behaving elastically, subjected to no axial force as shown in Fig.2.4(b), can be estimated as

$$T''' = T'' \approx 0.5\,[(T + T' - V_{col})\tan\alpha + V_b] \approx 0.5\,[V_{jh}\tan\alpha + V_b] \tag{8.20}$$

The force $\Delta C''$, which acts on the edge of the joint core of Fig.8.5, can now be evaluated by considering the vertical shear flow v_s, which is defined by Eq.(8.17). The equilibrium of the left vertical boundary of the model is satisfied when

$$\Delta C'' = v_s h'_b - T'' \approx 0.5\,[(V_{sh} - V_{ch})\tan\alpha - V_b] \tag{8.21}$$

Alternatively the same result can be reached by referring to the equilibrium conditions implied in Section 8.3.2(b), namely

$$\Delta C'' = T'' - V_b - V^*_{cv} = T'' - V_b - V_{ch}\tan\alpha \tag{8.22}$$

As the beam shear force V_b is relatively small, typically of the order of $V_b < 0.1V_{jv}$, it may be approximated by the average of beam shear forces due to earthquake induced beam moments on either side of the joint.

From consideration of the equilibrium of the vertical forces acting at a node point X in Fig.8.5, the following expression is obtained :

$$p + \frac{A_{jv} f_{yv}}{h'_c} - v_s\tan\alpha = 0 \tag{8.23}$$

where f_{yv} is the yield strength of the vertical joint reinforcement. Hence the required vertical joint shear reinforcement is

$$A_{jv} = \frac{1}{f_{yv}} (h'_c \, v_s \tan\alpha - h'_c p) \qquad (8.24a)$$

Alternatively by substitution from Eqs.(8.17) and (8.19)

$$A_{jv} = \frac{1}{f_{yv}} [V_{sh} \tan\alpha - (\Delta C'' + P_e)] \qquad (8.24b)$$

When $\Delta C''$ is estimated by Eq.(8.21) and by recalling Eq.(2.2b) that $V_{jh}\tan\alpha \approx V_{jv}$, it is found that

$$A_{jv} \approx \frac{1}{f_{yv}} [0.5 \, (V_{jv} + V_b) - P_e] \qquad (8.24c)$$

where all variables are known.

In the presence of some axial compression load on the column the requirement of Eq.(8.24c) is, as a general rule, readily met with the use of intermediate column bars. Particularly in columns which are designed in accordance with the capacity design procedures including the effects of dynamic moment magnification, the vertical reinforcement will have ample reserve strength to absorb the vertical tension forces due to joint shear. Outer column bars may also contribute by restricting the vertical growths of the joint due to shear. In view of this and as stated earlier, the fact that the beam shear V_b is small in comparison with the joint shear, V_{jv}, Eq.(8.24c) may be further simplified to

$$A_{jv} = \frac{1}{f_{yv}} (0.5 \, V_{jv} - P_e) \qquad (8.24d)$$

When the joint is part of a two-way frame, due allowance for the reduced contribution of the axial compression load corresponding to each direction of earthquake attack (Section 8.3.2(a)) should be made with the use of Eq.(8.15).

As was mentioned repeatedly in earlier chapters on test results, strains in horizontal joint ties placed very close to the beam reinforcement are strongly influenced by the elongation of adjacent beam bars. Therefore, for more effective contribution of horizontal joint ties to shear resistance, placement of the ties in a pattern similar to that shown in Fig.8.5 is recommended.

8.4 THE EXTERIOR JOINTS

8.4.1 General

Unlike interior joints, exterior joints were not covered extensively in Chapter 2. As Section 2.3.1 stated, the conditions in an exterior joint are less critical because only one beam acts in a plane. Hence with reference to Fig.2.1(a), Eq.(2.1) for horizontal joint shear force is reduced to

$$V_{jh} = T - V_c \tag{8.25}$$

where $V_c \approx 0.5\ (V_c' + V_c'')$. The vertical joint shear force may be found from equilibrium considerations or approximately estimated by Eq.(2.2b). The mechanisms of shear transfer within the joint core are similar to those postulated for an interior joint. The major deviation is that the presence of the end hooks of beam bars (see Fig.2.1(a)) create more favourable environment to mobilise the concrete strut mechanism. Previous studies on exterior joints [18, 37, 64] asserted that with the assistance of column ties close to and on the outside of the beam flexural reinforcement, and with a certain amount of joint reinforcement, an enhanced concrete strut mechanism would be viable, as illustrated schematically in Fig.8.6. For this reason NZS 3101 [4] permits V_{ch} of considerable magnitude to be assumed in design even for inelastic joints. Test results for Unit 2D-E as reported in Chapter 6 support these conclusions.

8.4.2 Anchorage of Beam Flexural Reinforcement at Exterior Joints

The tension force T developed in the top bars of the beam in Fig.2.1(a) is introduced to the surrounding concrete by bond stresses along the bars and by bearing stresses in the bend of the hooks. According to NZS 3101 [4], in view of yield penetration and subsequent bond deterioration, the basic effective development length for a standard hook, ℓ_{dh}, should be assumed to commence only at a distance of $0.5h_c$ or $10d_b$ from the column face of bar entry, as explained in Fig.2.5. As was discussed in Chapter 6 (Unit 2D-E), the $10d_b$ requirement may be relaxed to $8d_b$. Other requirements shown in Fig.2.5(a) are considered essential.

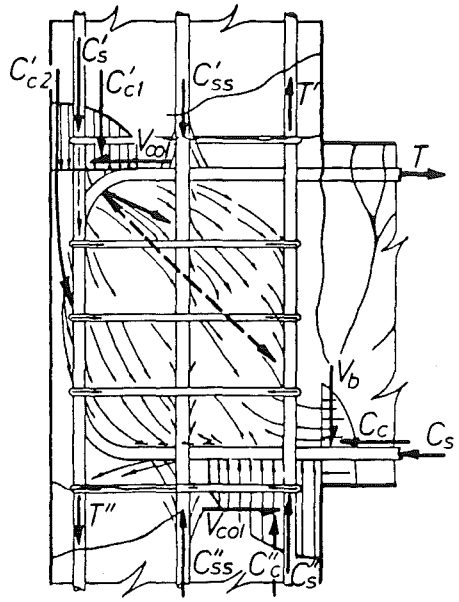

Fig.8.6 - Compression stress trajectories enhancing concrete strut mechanism in an exterior beam-column joint [37]

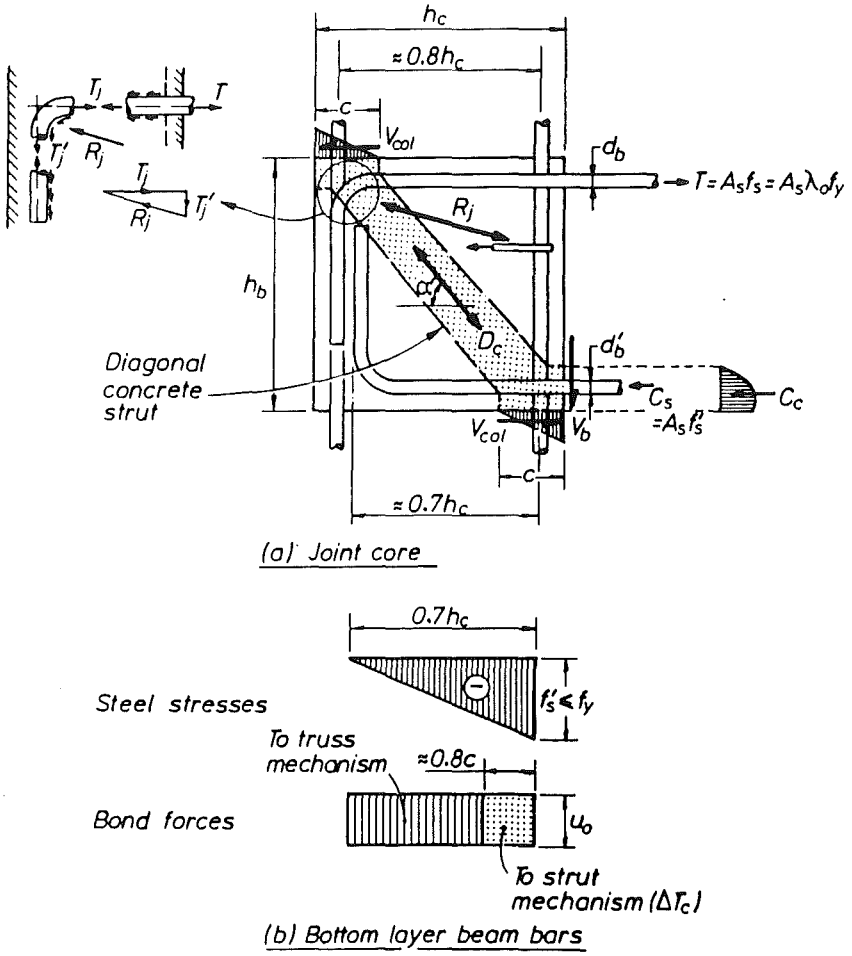

Fig.8.7 - Assumed actions inside an inelastic exterior joint

8.4.3 Shear Strength of Exterior Joints

(a) Concrete strut mechanism

The principles for assessing the contributions of the strut and truss mechanisms follow those for interior joints presented in Section 8.3. However, modifications are necessary to incorporate the features which are different from those considered at interior joints.

Details of the concrete strut mechanism in an exterior joint core are reproduced in Fig.8.7(a). It is evident that in developing the diagonal compression force D_c, associated with tension in the top beam reinforcement, the lower right-hand end of the strut is more critical. As in the case of bars subjected to compressive stress at interior bars, the horizontal component of the strut, estimated as

$$V_{ch} = D_c \cos\alpha' \tag{8.26}$$

at the exterior joint (Fig.8.7(a)) will depend on the extent of the concrete to transmit to the joint a flexural compression force C_c, and also on the distribution of bond forces along the bottom bars which are subjected to compression force C_s. By similarity to Eq.(8.12) the components of $V_{ch} = V'_{ch} + V''_{ch}$ for an exterior joint may be expressed, with the notation in Fig.8.7(a) as

$$V'_{ch} = C_c - (1 - K_f) V_{col} \tag{8.27a}$$

and

$$V''_{ch} = \Delta T_c - K_f V_{col} \tag{8.27b}$$

where

$$K_f = C_s/T \tag{8.27c}$$

and

$$T = A_s \lambda_o f_y$$

Eq.(8.27c) may be simplified to

$$K_f = \beta/\lambda_o \leq 1.0 \tag{8.28}$$

which implies that when $\beta = A'_s/A_s \leq 1.0$ the maximum compressive stress in the bottom bars is restricted to $f_s = f_y$, while the tension reinforcement at the

top develops overstrength $\lambda_o f_y$. Evidence obtained from the test of Unit 2D-E indicated that steel compressive stresses did not exceed f_y.

When the applied moment on the joint in Fig.8.7(a) is reversed, the entire flexural compression force at top may in theory be transmitted to the column by reinforcement only, while the maximum compressive stress in the top beam reinforcement is below yield level. This alternative case is equivalent to taking $\beta = A_s/A'_s \geq 1.0$. Since the total top compression force cannot be larger than the bottom tension force, Eq.(8.28) may result in $K_f = 1.0$. However, as with interior joints discussed in Section 8.3, the concrete compression force C_c should also exist at the top of the beam in this alternative case, and likewise at the bottom of the beam in the case of downward bending as shown in Fig.8.7(a). In Section 2.3.4 and in subsequent discussions of test results, this mobilisation of C_c has been emphasised as necessary and viable. Although anchorage conditions for the beam bars in exterior joints are better than those in interior joints, the reversing cyclic inelastic straining of beam bars nevertheless causes considerable bar elongation and yield penetration. Thus when the exterior beam bars are subjected to compression, a small amount of bond slip still comes into effect to engage the embedding concrete to provide the anchorage of bars. Further plastic rotation of the beam enables C_c to be mobilised. Conclusions drawn from the test results for the east beam of Unit 2D-E were similar to those obtained from the interior test units. When the beam was bent upwards, the maximum steel compressive stress in top beam bars at the column face was of the order of $0.5f_y$. Accordingly the force factor was estimated as $K_f \approx 0.65$ with $A_s \simeq 0.5A_s'$. When the east beam was subjected to downward bending, the K_f factor reduced to a value of approximately 0.5.

By applying Eqs.(8.27a to 8.27c), a sensitivity analysis similar to that in Section 8.3.2 and Fig.8.4 may be carried out. It is evident, however, that for design purposes values for extreme cases are not necessary. From theoretical considerations, an exterior beam with symmetrical top and bottom reinforcement (i.e. $\beta = 1.0$) corresponding with a probable value of $K_f = 0.8$, is most critical. Such beam arrangement was not included in this test series.

From the above discussions, it is concluded that the steel compressive stress and corresponding bond force distributions proposed in Fig.8.7(b) are applicable to both top and bottom beam bars. Bond transfer under transverse compression is more efficient. Hence for the purpose of

estimating V''_{ch} in Eq.(8.27b), the assumed uniform distribution of bond forces over an effective development length of $0.7h_c$, resulting in the unit bond force $u_o = C_s/0.7h_c$, is considered to be conservative. The portion of bond force over an assumed effective depth 0.8c, where c can be estimated using Eq.(2.13), is thus $\Delta T_c = 0.8u_o c$. With typical values of $V_{col} \approx 0.15T$ and $V_{jh} \approx 0.85T$ as discussed in Section 8.3.2(a), and adopting $K_f = 0.8$, the following results are obtained by applying Eq.(8.27) :

(1) When $P_e/f'_c A_g = 0$, $V_{ch} = 0.33\ V_{jh}$

(2) When $P_e/f'_c A_g = 0.15$, $V_{ch} = 0.49\ V_{jh}$

(3) When $P_e/f'_c A_g = 0.3$, $V_{ch} = 0.65\ V_{jh}$

It appears that Eqs.(8.14a) and (8.14b) can be adopted for exterior joints of one-way and two-way frames respectively.

When a moment causes the bottom beam reinforcement (Fig.8.7(a)) to be in tension, earthquake induced beam shear forces will subject an exterior column to axial tension. This will reduce the net axial compression on the column or even result in net tension. In the latter case the term P_e in Eq.(8.14) should be taken as negative. Eq.(2.13) is considered to be still appropriate. For this load condition clearly the ratio V_{ch}/V_{jh} will be much smaller. Therefore the requirements for joint shear reinforcement may be more severe.

Provided that adequate anchorage by a standard hook has been provided for the tension reinforcement, there is no need to investigate at that locality details of the force transfer, V_{ch}, to the diagonal strut. Briefly there are two groups of forces contributing to the strut mechanism in the hook region. The first is due to the anchorage force shown as R_j in Fig.8.7(a). The second group is due to the bond forces introduced from the horizontal part of the top beam bars and also to the vertical compression forces from the column such as C'_c in Fig.2.1(a), and the vertical joint shear reinforcement. This combination allows the total diagonal compression force in the joint core to be resolved into component D_c as shown in Fig.8.7(a) and another component at an angle of inclination much less than α'. This latter force will then engage horizontal joint tie forces in the upper unshaded triangular portion of the joint core as can be inferred in Fig.8.7(a).

(b) The contribution of the truss mechanism

The required quantity of horizontal joint shear reinforcement for exterior joints can be determined using Eq.(8.18) developed earlier for interior joints. As expected, the strategy employed in estimating the necessary amount of vertical joint shear reinforcement in exterior joints should be similar to that presented for interior joints in Section 8.3.2(b). Following the same procedure as in developing Eqs.(8.19) to (8.24), it can be shown that the required amount of vertical joint shear reinforcement is

$$A_{jv} = \frac{1}{f_{yv}} [0.5 \ (V_{jv} + 0.5 \ V_b) - P_e] \qquad (8.29)$$

which for design purposes can be approximated to Eq.(8.24d). When the exterior column is subjected to net axial tension, Eq.(8.29) may indicate a significant increase in the required area of vertical joint shear reinforcement A_{jv}.

CHAPTER 9

GENERAL CONCLUSIONS AND RECOMMENDATIONS FOR FUTURE RESEARCH

9.1 GENERAL CONCLUSIONS

In the experimental part of this research project, three full-scale reinforced concrete beam-column joint assemblies incorporating floor slabs were tested. Test results from these three specimens, which were designed according to the New Zealand concrete design code provisions for ductile moment resisting frames, were very satisfactory in terms of strength and ductility capacity during quasi-static cyclic loading simulating severe seismic actions. The performance of the one-way interior joint (Unit 1D-I) was found to be superior to that of the two-way exterior joint (Unit 2D-E), which in turn was superior to that of the two-way interior joint (Unit 2D-I). The very good performance of the beam-column-slab assemblies was considered to have resulted from the relatively large quantity of joint shear reinforcement provided and the use of sufficiently small diameter longitudinal beam bars to avoid excessive slippage through the joint cores when plastic hinges developed in the beams at the column faces.

There was no evidence during the tests to indicate that the presence of a floor slab or beams in two directions provided confinement to a joint core during bi-directional seismic loading whereby the performance would have been improved. As expected the strengths and stiffnesses of the Units consistently reduced with increasing ductility demands. Under uni-directional loading, a significant portion of slab bars in tension contributed to the negative moment flexural strength of the beams and hence to the enhancement of the strength of each Unit. A mechanism of floor slab contributions to beam flexural strength is postulated and design recommendations to include tension flange effects are made.

Existing design procedures in New Zealand for beam-column joints in ductile frames are based on a concrete strut and a truss mechanism of shear resistance in joint cores. Further review of performance criteria for joints and previous experimental findings suggests that present New Zealand design procedures could be relaxed in terms of both bond and shear strength requirements. Consequently, after detailed consideration of tests results, revised models for bond strengths and shear strengths of joint cores are presented and a set of new design recommendations is proposed.

9.2 RECOMMENDATIONS FOR FUTURE RESEARCH

It was not possible to undertake further testing to verify the appropriateness of the proposed design recommendations. However, it is considered that in future research the following aspects should be given special attention :

(1) The effect of column axial load on both bond and joint shear strengths.

(2) The effect of concrete strength on the bond performance of bars passing through joints.

(3) The effect of deterioration of joint stiffness, usually in terms of the joint core shear deformations, on the stiffness of the test structure.

Test results from this project clearly showed that bond and shear deformations within beam-column joints were significant and that they inevitably reduced frame stiffnesses. Therefore more reliable techniques need to be developed to predict these deformations.

There is still no universally accepted standard to quantify the quality of the seismic behaviour of joints in reinforced concrete framed structures. However it is generally accepted that joint performance must be related to the desired performance of the total structure. Further research is needed to establish more precisely the desired performance criteria.

Most of the experimental work reported in the literature on beam-column joints has been on isolated test specimens. Further studies need to be carried out involving joints in multi-bay frames. Inelastic beam elongations appear to be significant in continuous frames. It has been suggested that at certain levels columns may provide horizontal restraints to beams and hence to joints. The relationships have to be confirmed in tests and the phenomenon studied.

APPENDIX A

Summary of Design Provisions for Beam-Column Joints of Reinforced Concrete Ductile Frames According to NZS 3101:1982

The rationale used in developing the relevant provisions for reinforced concrete beam-column joints in NZS 3101 [4] was discussed in some detail in Chapters 1 and 2. Hence in the following the code provisions are summarized with only a brief reference, when necessary, to the background of a particular requirement. This summary is extracted from an earlier report prepared in 1984 [18]. Symbols and notation are identical to those used in the main text.

Design assumptions

The NZS 3101 code provisions are intended to ensure that joints are designed in such a way that when inelastic lateral displacements occur in ductile frames the required energy dissipation occurs in the potential plastic hinge regions of the adjacent members and not in the joint core regions. Accordingly the joint core should be designed to resist the forces arising when the overstrength of the framing members is developed. That is, the stresses in the flexural steel at the plastic hinges are assumed to be 1.25 times the specified yield strength in the case of Grade 275 steel, or 1.4 times the specified yield strength in the case of Grade 380 steel. The design horizontal shear force V_{jh} and the design vertical shear force V_{jv} are found by rational analysis (see Section 2.2) taking into account the effect of all the forces acting on the joint. When beams frame into the joint in two directions, these forces need only be considered in each principal direction independently.

In determining the shear strength of the joint core using beam overstrength input, the strength reduction factor ϕ is taken as unity. The shear applied to the joint core is assumed to be carried by a mechanism consisting of a concrete diagonal compression strut and a mechanism consisting of truss action from a concrete diagonal compression field and the shear reinforcement (Section 2.3). Shear reinforcement is detailed to carry the design forces in excess of those carried by the concrete.

In order to prevent the concrete diagonal compression strut from crushing, the nominal horizontal shear stress v_{jh} in either principal direction is limited to $1.5\sqrt{f'_c}$ MPa, where

$$v_{jh} = \frac{V_{jh}}{b_j h_c} \qquad (A.1)$$

The effective joint width, b_j, is defined as

(a) When $b_c > b_w$, either $b_j = b_c$ or $b_j = b_w + 0.5\ h_c$, whichever is smaller.

(b) When $b_c < b_w$, either $b_j = b_w$ or $b_j = b_c + 0.5\ h_c$, whichever is smaller.

Horizontal joint shear

The total area of horizontal shear reinforcement placed between the outermost layers of top and bottom beam reinforcement is required to be not less than

$$A_{jh} = V_{sh}/f_{yh} \qquad (A.2)$$

where the horizontal design shear force to be resisted by this shear reinforcement is given by

$$V_{sh} = V_{jh} - V_{ch} \qquad (A.3)$$

In Eq.(A.3), V_{ch} should be taken as zero unless one of the following situations applies :

(a) When the minimum average compressive stress on the gross concrete area of the column above the joint exceeds $0.1f'_c/C_j$

$$V_{ch} = \frac{2}{3}\sqrt{\frac{C_j P_e}{A_g} - \frac{f'_c}{10}}\,(b_j h_c) \qquad (A.4)$$

where $C_j = V_{jh}/(V_{jx} + V_{jy})$ where V_{jx}, V_{jy} = horizontal design shear forces in joint core in the two principal directions (C_j = 1 for one-way frame or 0.5 for symmetrical two-way frame), P_e = minimum axial compressive column load, A_g = gross area of column cross section.

(b) When the design is such that plastic hinging occurs in the beam at a distance away from the column face not less than the beam depth nor 500 mm (Fig.A.1), or for external joints where the flexural steel is anchored outside the column core in a beam stub (Fig.A.2), the value of V_{ch} may be increased to

$$V_{ch} = 0.5 \frac{A'_s}{A_s} V_{jh} \left(1 + \frac{C_j P_e}{0.4 A_g f'_c} \right) \qquad (A.5)$$

where A'_s/A_s should not be taken larger than 1.0. When the axial column load results in tensile stresses over the gross concrete area exceeding 0.2 f'_c, $V_{ch} = 0$. For axial tension between these limits V_{ch} may be obtained by linear interpolation between zero and the value given by Eq.(A.5) when P_e is taken as zero.

(c) For exterior joints without beam stubs at the far face of column, Eq.(A.5) may be used when multiplied by the factor

$$\frac{3h_c(A_{jv} \text{ provided})}{4h_b(A_{jv} \text{ required})} \qquad (A.6)$$

which should not be taken as greater than 1.0. Use of this factor requires that the beam bars be anchored using a 90° standard hook in the joint core (Fig.A.3).

(d) When the ratio h_c/h_b is greater than or equal to 2.0, V_{ch} need not be taken as less than

$$V_{ch} = 0.2 b_j h_c \sqrt{f'_c} \qquad (A.7)$$

Vertical joint shear

The total area of vertical shear reinforcement, normally in the form of intermediate column bars on the side faces of the column, should not be less than

$$A_{jv} = V_{sv}/f_{yv} \qquad (A.8)$$

where the vertical design shear force to be resisted by this shear reinforcement is

$$V_{sv} = V_{jv} - V_{cv} \qquad (A.9)$$

When plastic hinging is not expected to occur in the column above or below the joint core, V_{cv} is given by

$$V_{cv} = \frac{A'_{sc}}{A_{sc}} V_{jv} \left(0.6 + \frac{C_j P_e}{A_g f'_c}\right) \qquad (A.10)$$

except where axial load results in tensile stresses over the column section. When P_e is tensile, value of V_{cv} is interpolated linearly between the value given by Eq.(A.10) when P_e is taken as zero and zero when the axial tensile stress over the gross concrete area is $0.2\ f'_c$.

However, if plastic hinges are expected to form in the column above or below the joint core, V_{cv} should be taken as zero for any axial load on the column.

The spacing of vertical shear reinforcement in each plane of any beam framing into the joint should not exceed 200 mm and in no case should there be less than one intermediate bar in each side of the column in that plane.

Confinement of joint core

The horizontal transverse confinement reinforcement in the joint core should not be less than that required in the potential plastic hinge regions in the adjacent columns. Thus for columns with hoops and supplementary cross ties the total area of transverse steel in each of the principal directions of the cross section should be at least equal to

$$A_{sh} = 0.3 s_h h'' \left(\frac{A_g}{A_c} - 1\right) \frac{f'_c}{f_{yh}} \left(0.5 + 1.25 \frac{P_e}{\phi f'_c A_g}\right) \qquad (A.11)$$

but not less than

$$A_{sh} = 0.12 s_h h'' \frac{f'_c}{f_{yh}} \left(0.5 + 1.25 \frac{P_e}{\phi f'_c A_g}\right) \qquad (A.12)$$

where $\phi = 0.9$. If a capacity design procedure is used to protect columns against plastic hinging, the required quantity of transverse reinforcement in the potential plastic hinge regions may be reduced to one-half of that required by Eqs. (A.11) and (A.12).

In no case shall the spacing of transverse reinforcement in the joint core exceed 10 times the diameter of the longitudinal column bar or 200 mm, whichever is less.

Bar anchorage in interior joints

To keep bond stresses to an acceptable level, the diameters of longitudinal bars d_b passing through a joint core are limited as follows :

(a) Beam bars :

When plastic hinging can occur adjacent to the column face :

$d_b \leq h_c/25$ when $f_y = 275$ MPa, or

$d_b \leq h_c/35$ when $f_y = 380$ MPa.

When plastic hinging is located at a distance from the column face of at least the beam depth or 500 mm, whichever is less :

$d_b \leq h_c/20$ when $f_y = 275$ MPa, or

$d_b \leq h_c/25$ when $f_y = 380$ MPa.

(b) Column bars :

When columns are intended to develop plastic hinges :

$d_b \leq h_b/20$ when $f_y = 275$ MPa, or

$d_b \leq h_b/25$ when $f_y = 380$ MPa.

When columns are not intended to develop plastic hinges :

$d_b \leq h_b/15$ when $f_y = 275$ MPa, or

$d_b \leq h_b/20$ when $f_y = 380$ MPa.

Bar anchorage at exterior joints

The basic development length of a deformed bar in tension terminating with a standard 90° hook (Fig.A.3) is

$$\ell_{hb} = \frac{66 d_b}{\sqrt{f'_c}} \frac{f_y}{275} \qquad (A.13)$$

Where the bar diameter is 32 mm or smaller with side cover not less than 60 mm and cover on tail extension not less than 40 mm, the value may be reduced to $0.7\ell_{hb}$, and where the concrete is suitably confined the value may be reduced to $0.8\ell_{hb}$.

The basic development length for a deformed bar in compression is

$$\ell_{db} = 0.24 d_b f_y / \sqrt{f'_c} \qquad (A.14)$$

but not less than $0.044 d_b f_y$. Where the concrete is suitably confined the value may be reduced to $0.75 \ell_{db}$.

The anchorage is considered to commence within the column at distance $0.5 h_c$ or $10 d_b$ from the column face, whichever is less, except that when the plastic hinge is located away from the column face, anchorage may be considered to commence at the column face (Fig.A.4).

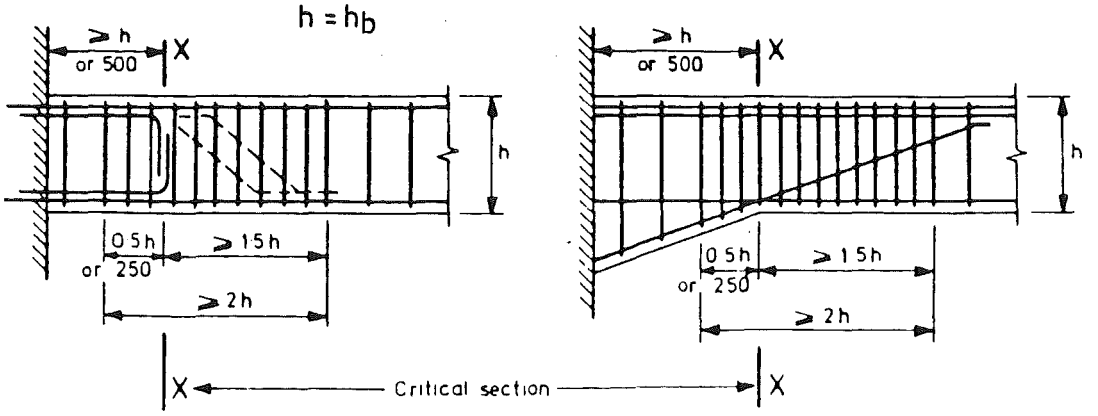

Fig.A.1 - Plastic hinges located in beams away from column faces [4]

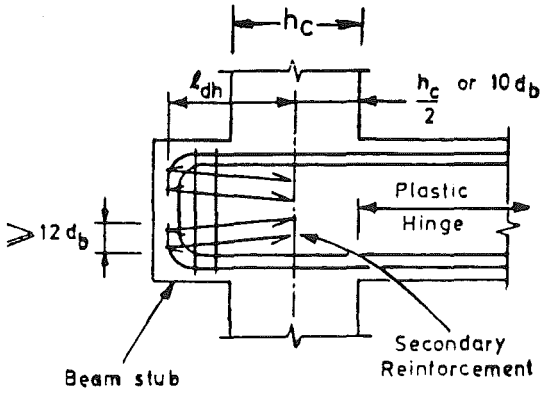

Fig.A.2 - Anchorage of bars in beam stub[4]

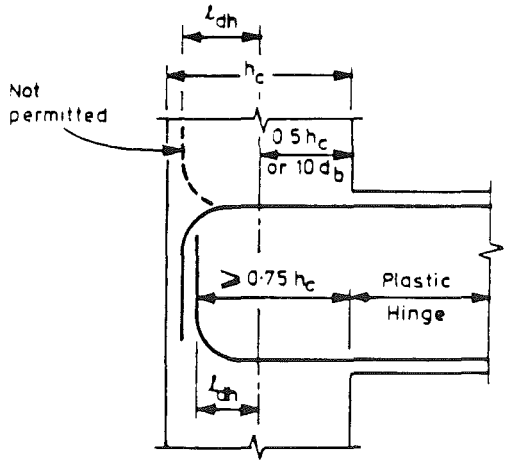

Fig.A.3 - Anchorage of beam bars when critical section of plastic hinge forms at column face [4]

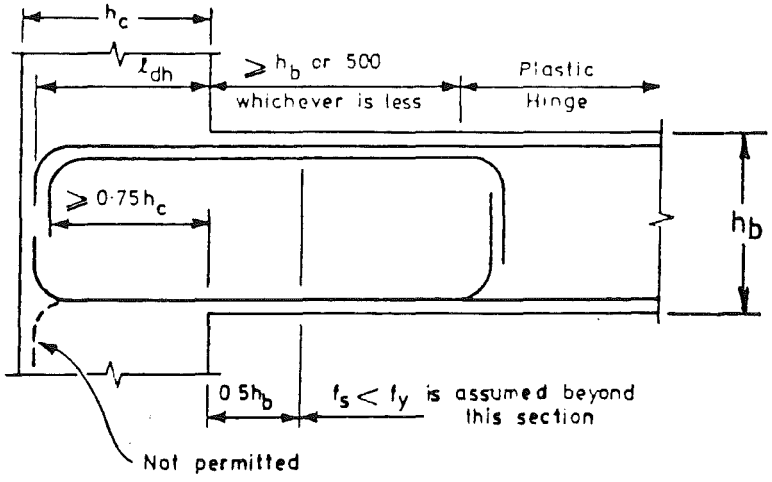

Fig.A.4 - Anchorage of beam bars when critical section of plastic hinge is located at sufficient distance from column face [4]

APPENDIX B

Calculations for Test Unit 1D-I

B.1 Design of Test Unit 1D-I

The final dimensions and reinforcing details for the test unit as constructed are shown in Fig. 3.1. Design was carried out in compliance with the current NZS 3101 [4] code provisions. The following design results have also been summarised in Section 3.2.

(1) The Slab

The 100 mm thick slab was assumed to be equal to the slab between the ribs of the prototype floor to satisfy fire requirements. According to NZS 3101, a minimum of 0.002 of gross concrete area of shrinkage and temperature reinforcement parallel to the beams is required. For this test unit, D10 bars, with a yield strength of f_y = 326 MPa, were provided at 350 mm spacings. The steel content was 0.224%. Though ribs were not included in the test unit, the top flexural reinforcement of the prototype ribbed floor was simulated by providing D16 bars in the transverse direction, which amounted to ρ_s = 0.714%.

(2) The Beams

The largest longitudinal bar used was 24 mm, being equal to 1/25th of the joint (column) depth.

According to the provisions of NZS 3101, the effective slab width in tension was taken as 550 + 2 x 2.5 x 100 = 1050 mm. One D10 slab bar on each side of the beam was therefore included as part of the flexural tension reinforcement. Hence the reinforcement ratio for the beam with Grade 275 steel became

(top bars) ρ = 1.34% (or 0.92% in terms of Grade 400 steel)

(bottom bars) $\rho' = 0.77\% > 0.5\rho$

Alternatively, if all D10 slab bars (10 total) were considered as part of the flexural tension reinforcement, ρ then became 1.66%, which was 24% larger than the value derived from code procedures for flexural design.

From Eq.(3.7) the internal lever arm (434 mm) was taken as the distance betwen the centroids of the top and bottom groups of flexural bars. The ideal (nominal) flexural "seismic" strengths so computed, based on f_y = 275 MPa, were

(-) M_i = 310 kNm and (+) M_i = 183 kNm

These values corresponded to dependable strengths for the prototype structure, with a strength reduction factor of ϕ = 0.9, of

(-) M_u = 279 kNm and (+) M_u = 165 kNm

The alternative nominal flexural strengths of beam sections, calculated by the ACI stress block method (see Section 3.8.2), are given in Appendix B.2.

A consideration for capacity design is that all the longitudinal bars in the beams and slab may be stressed to 1.25 f_y. The maximum beam moments at the column face so derived were then

(-) M_o = 486 kNm and (+) M_o = 231 kNm

The shear forces associated with these maximum moments were considered when designing the beam transverse reinforcement and the column reinforcement.

In the potential plastic zones over 2 x 550 = 1100 mm length on either side of the column, 4 legs of R10 stirrup ties at 120 mm centres (6 times the smaller beam bar diameter) were used as transverse reinforcement. These satisfied requirement of shear strength and minimum tie spacing requirements for confinement and bar stability purposes.

The design strength of the test unit, in terms of the column shear force and based on specified material properties, $V_{i(design)}$, was estimated by Eq.(3.4) as

$$V_{i(design)} = \left(\frac{310 + 183}{1725} \right) \frac{2025}{3500} = 165.4 \text{ kN}$$

The dependable strength became 0.9 x 165.4 = 148.9 kN. With an overstrength factor ϕ_o = 1.25/0.9 = 1.39, the storey shear was estimated as 1.39 x 148.9 = 207.0 kN.

(3) The Column

The largest longitudinal bar used was 24 mm diameter while code requirements allow for Grade 380 steel a maximum bar size of 28 mm (i.e. 1/20th of beam depth).

The required ideal flexural strength of the column section was estimated from the beam flexural overstrengths given. The minimum value of the dynamic magnification factor ω = 1.3 [4] was used. Thus the required ideal flexural strength of the column needed to be 1.3 x (1.25/0.9) = 1.8 times M_{code} = 261 kNm. Thus M_{col} = 427 kNm (see Eq.(3.1)). Accordingly, a reinforcement content of ρ_t = 1.32% was required. Alternatively, considering the case with $(\pm)M_o$ = 355 kNm and taking ω = 1.0, ρ_t = 1.0% was required. The 8-HD24 and 4-HD20 bars gave ρ_t = 1.48% steel content. Hence column yielding during the test was not expected. In a real building some axial gravity load on the column would be present, resulting in a reduction of column reinforcement content.

The design shear force for the column was 1.3 x 207 = 269 kN. However, the transverse reinforcement in the end regions was governed by the minimum spacing requirements for confinement and bar stability.

(4) The Joint

The design horizontal joint shear force across the joint was assessed according to NZS 3101 as

$$V_{jh} = 1.25(275)(2595.4 + 1533.1)10^{-3} - 207 = 1212 \text{ kN}$$

Hence the horizontal joint shear stress was

$$v_{jh} = \frac{1212 \times 10^3}{550 \times 600} = 3.67 \text{ MPa} < 1.5 \sqrt{f'_c} = 8.22 \text{ MPa}$$

Horizontal joint shear reinforcement was assumed to resist the entire shear force, so that

$$V_{sh,required} = 1212 \text{ kN}$$

As shown in Fig. 3.1, four sets of R16 hoops were used. For each set of hoops the number of effective tie legs across the joint was taken as N = 4.8. The shear force that the 4 sets could resist was

$$V_{sh,provided} = 4\ (4.8)\ 201\ (275)\ 10^{-3} = 1061 \text{ kN}$$

which was only 87.5% of that required. However, the measured yield strength of R16 bars supplied was found to be 330 MPa and this corresponded to a shear resistance of

$$V_{sh,provided} = 1061 \times \frac{330}{275} = 1273 \text{ kN} > 1212\text{kN}$$

Following the code recommendations for vertical joint shear,

$$V_{jv} \simeq 1212 \times \frac{550}{600} = 1111 \text{ kN}$$

The concrete mechanism was assumed to carry 60% of the shear force. Reinforcement was to resist the remainder. Therefore

$$V_{sv,required} = 0.4 \times 1111 = 444 \text{ kN}$$

The four HD-20 intermediate vertical bars would provide

$$V_{sv,provided} = 4(314.2)(380)10^{-3} = 478 \text{ kN} > 444 \text{ kN}$$

B.2 Beam Flexural Strengths to ACI Method

The calculation procedure for flexural strength according to the ACI stress block method (Section 3.8.2) follows that explained in standard textbooks [1]. Most of the symbols used in the following calculations and Figs.B.1 and B.2 have appeared in the text and can be referred to in the list of notation. Symbols used only in this appendix are explained as follows :

a = depth of equivalent ACI rectangular stress block
C = resultant internal compression force
β_1 = ratio of a/c (= 0.85)
ϵ_{cu} = ultimate strain in outermost compression fibre of concrete, assumed to be 0.003

(1) Positive Flexural Strength (top fibre in compression)

With reference to Fig.B.1,

b_e = 2(550) = 1100 mm
A_{s1} = 2 (78.5) mm^2 (2-D10 slab bars)
f_{s1} = $\epsilon_{s1a} E_s$ = 0.003 (41-c)200000/c MPa
A_{s2} = 4(452.4) mm^2 (4-D24 top bars)
f_{s2} = $\epsilon_{s2} E_s$ = 0.003(53 - c) 200000/c MPa
A_{s3} = 2(314.2) mm^2 (2-D20 top bars) $f_{s3} = f_y$ = 275 MPa
A_{s4} = 2(452.4) mm^2 (2-D24 bottom bars) $f_{s4} = f_y$ = 275 MPa
A_{s5} = 2(314.2) mm^2 (2-D20 bottom bars) $f_{s5} = f_y$ = 275 MPa

Therefore, $\Sigma C = 0.85 f'_c \beta_1 c b_e$

$$\Sigma T = \Sigma T_{s,top} + \Sigma T_{s,bottom}$$

For equilibrium, $\Sigma C = \Sigma T$. Solving, c = 39.9 mm

The corresponding strains are

ϵ_{s1} = 0.003(41 - c)/c = 0.0001 < ϵ_y ϵ_{s2} = 0.003(53 - c)/c = 0.0010 < ϵ_y
ϵ_{s3} = 0.003(101 - c)/c = 0.0046 > ϵ_y ϵ_{s4} = 0.003(498 - c)/c = 0.0034 < ϵ_y
ϵ_{s5} = 0.003(500 - c)/c = 0.035 > ϵ_y

The ultimate moment of resistance is

$$(+)\ M_i = 10^{-6}\ [0.85\ f'_c\ \beta_1\ c\ b_e\ (c - 0.5\beta_1) + f_{s1}A_{s1}\ (41 - c) +$$

$$f_{s2}\ A_{s2}(53-c) + f_yA_{s3}\ (101-c) + f_y\ A_{s4}\ (498 - c) + f_yA_{s5}\ (500 - c)]$$

$$= 230.5 \text{ kNm}$$

This exceeds the "seismic steel-couple" moment (Appendix B.1) of 183 kNm by 25.9%.

(2) Negative Flexural Strength (top fibre in tension)

With reference to Fig. B.2,

b_e = 550 + 2(2.5) 100 = 1050 mm
b_w = 440 mm
A_{s1} = 2(78.5) mm^2 (2-D10 slab bars) $f_{s1} = f_y$ = 275 MPa
A_{s2} = 4(452.4) mm^2 (4-D24 top bars) $f_{s2} = f_y$ = 275 MPa
A_{s3} = 2(314.2) mm^2 (2-D20 top bars) $f_{s3} = f_y$ = 275 MPa
A_{s4} = 2(452.4)mm^2 (2-D24 bottom bars)
f_{s4} = $\epsilon_{s4}E_s$ = 0.003(c-52)200000/c MPa
A_{s5} = 2(314.2) mm^2 (2-D20 bottom bars)
f_{s5} = $\epsilon_{s5}E_s$ = 0.003 (c - 50) 200000/c MPa

For equilibrium, $\Sigma T = \Sigma C$. Solving, c = 62.8 mm.

The corresponding strains are

ϵ_{s1} = 0.003 (509 - c)/c = 0.021 > ϵ_y ϵ_{s2} = 0.003 (497 - c)/c = 0.021 > ϵ_y
ϵ_{s3} = 0.003 (449 - c)/c = 0.018 > ϵ_y ϵ_{s4} = 0.003 (52 - c)/c = -0.0005 < ϵ_y
ϵ_{s5} = 0.003 (50 - c)/c = -0.0006 < ϵ_y

The ultimate moment of resistance becomes $(-)M_i$ = 323.7 kNm.

When compared with the "seismic steel-couple" moment (Appendix B.1) of 310 kNm, the difference is 4.4%.

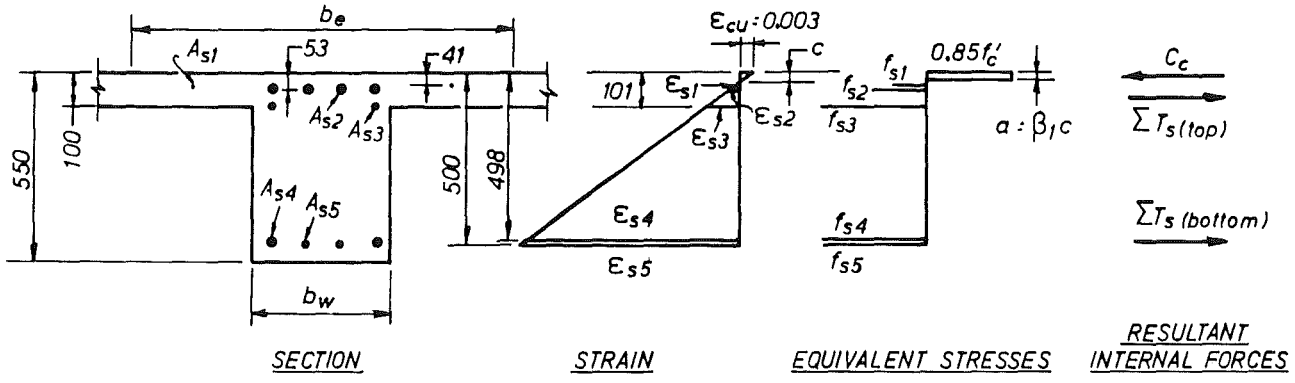

Fig.B.1 - Positive flexural strength of beam section of Unit 1D-I

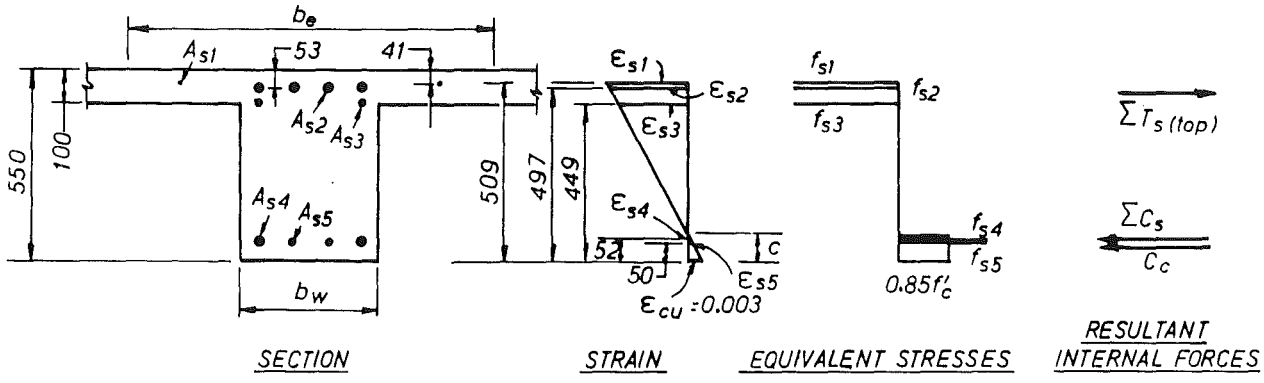

Fig.B.2 - Negative flexural strength of beam section of Unit 1D-I

B.3 Prediction of Strengths of Test Unit 1D-I

The following strength calculations are based on measured material properties. The ideal (nominal) strengths of the T-beam sections so derived at the column faces, $(\pm)M_i$, are calculated for the various cases discussed in Section 3.8.2 and summarised in Fig.3.21. The resulting beam strengths and the corresponding beam end forces and storey shear are summarised in Tables B.1 to B.3. As stated in Section 3.8.2, cases (d) and (g) are taken as reference cases.

TABLE B.1 "EAST-WEST" IDEAL BEAM STRENGTH PROPERTIES

(i) "Positive" Flexural Strength $(+)M_i$ (flange in compression)

Case	a	b	c	d	e	f
b_e (mm)	0	400	550	1100	1500	1650
$(+)M_i$(kNm)	193.3	224.9	230.6	248.0	256.5	258.1

(ii) "Negative" Flexural Strength $(-)M_i$ or M_i^* (flange in tension)

Case	g	h
b_e (mm)	1050	Full slab width
Moment(kNm)	$(-)M_i$ = 343.6	$(-)M_i^*$ = 435.8

(iii) Ideal Tip Forces For Prediction of Stiffness

WEST BEAM	EAST BEAM	COLUMN
Case (g) (-) P_i = 199.2 kN	Case (d) $(+)P_i$ = 143.4 kN	$(\pm)V_i$ = 198.4 kN
Case (d) (+) P_i = 143.8 kN	Case (g) $(-)P_i$ = 198.6 kN	

TABLE B.2 "EAST-WEST" THEORETICAL STOREY SHEAR

Beam Moment	+ve	-ve	+ve	-ve	+ve	-ve	+ve	-ve	+ve	-ve	+ve	-ve
Case	a	g	a	h	b	g	c	g	d	g	d	h
b_e (mm)	0	1050	0	FSW	400	1050	550	1050	1100	1050	1100	FSW
(±)V_i or V_i* (kN)	180.0		211.0		190.6		192.5		198.4		229.3	

Note: V_i from cases (d) & (g) is the reference shear plotted in the response diagrams.

FSW = full slab width

TABLE B.3 "EAST" BEAM THEORETICAL TIP FORCES BASED ON DIFFERENT ASSUMPTIONS

Case	a	b	c	d	g	h
b_e (mm)	0	400	550	1100	1050	FSW
(±)P_i(kN)	(+)111.7	(+)130.0	(+)133.3	(+)143.4	(-)198.6	(-)251.9

Note: "West" beam tip forces are slightly larger due to shorter as-constructed beam length, but the 0.3% differences are insignificant and the results are not shown here for brevity.

FSW = full slab width

B.4 Prediction of Stiffness of Unit 1D-I

(1) Deformations of the Beams

For the east beam, the end deflection is given by Eq.(3.22a) with $P_1 = 0.9(143.4) = 129.1$ kN, $\ell_1' = 1730$ mm, $E_c = 4700\sqrt{f_c'} = 29000$ MPa, $I_e = 3.91 \times 10^9$ mm^4 (Eq.3.13a), $f = 1$, $b_w = 400$ mm, and $h_b = 550$ mm. Thus

$$\delta_{1,b} = 1.96 + 0.18 = 2.14 \text{ mm}$$

The end deflection of the west beam is from Eq.(3.22b) with $P_2 = 0.9(199.2) = 179.3$ kN, and $\ell_2' = 1725$ mm,

$$\delta_{2,b} = 2.71 + 0.24 = 2.95 \text{ mm}$$

The equivalent storey displacement from the contribution of beam deformations (Eq.3.23) becomes thus

$$\Delta_{c,b} = \left[\frac{2.14 + 2.95}{2030 + 2025}\right] 3500 = 4.39 \text{ mm}$$

(2) Deformations of the Column

The elastic flexural and shear deformations of the column is given by Eq.(3.17) with $V_c = 0.9(198.4) = 178.6$ kN, $\ell_c' = 1475$ mm, $E_c = (29000 + 24000)/2 = 26500$ MPa, $I_e = 4.95 \times 10^9$ mm^4 (Eq.3.13b), $f = 1.2$, $b_c = 550$ mm, and $h_c = 600$ mm,

$$\Delta_{c,c} = 2.91 + 0.36 = 3.27 \text{ mm}$$

(3) Total Deformation and Stiffness

By summing up the components including the joint shear strains (Eqs. 3.24 and 3.8),

$$\Delta_e = 4.39 + 3.27 + 0.2\Delta_e$$

Hence $$\Delta_e = 9.6 \text{ mm}$$

With $V_c = V_{code} = 178.6$ kN, the theoretical stiffness, $K_{theoretical}$, of the test unit is estimated according to Eq.(3.25)

$$K_{theoretical} = \frac{178.6}{9.6} = 18.6 \text{ kN/mm}$$

Alternatively, the effective moments of inertia, I_e, can be calculated according to Eq.(3.14). With this expression the estimated deflection components are revised further as follows:

(i) For the east beam, $I_e = 2.67 \times 10^9 mm^4$, $\delta_{1,b} = 3.05$ mm

(ii) For the west beam, $I_e = 3.22 \times 10^9 mm^4$, $\delta_{2,b} = 3.52$ mm

Hence $$\Delta_{c,b} = \left[\frac{3.05 + 3.52}{2030 + 2025}\right] 3500 = 5.67 \text{ mm}$$

For the column, with $I_e = 3.81 \times 10^9 \text{ mm}^4$,

$$\Delta_{c,c} = 4.14 \text{ mm}$$

Allowing for joint distortion, the total equivalent storey (column) deflection is estimated as

$$\Delta_e = 12.3 \text{ mm}$$

The theoretical stiffness of the test unit is then

$$K_{theoretical} = \frac{178.6}{12.3} = 14.5 \text{ kN/mm}$$

This latter value is plotted and compared with the observed stiffness in Fig.4.11.

APPENDIX C

Calculations for Test Unit 2D-I

C.1 Design of Test Unit 2D-I

As explained in Section 3.1, this unit was to simulate a two-way interior beam-column joint. The dimensions and reinforcing details for the test unit are shown in Fig. 3.2.

(1) The Slab

The minimum thickness of a prototype two-way floor slab, to satisfy both NZS 3101 [4] and ACI 318-83 [5] stiffness requirements, is 120 mm. However, in accord with the guidelines of the co-operative research programme, a thickness of 130 mm was adopted. Considering dead weight and live load effects, as in practical design, the top flexural reinforcement at continuous edges (i.e. the beams) consisted of D10 bars at 160 mm centres. This corresponded to a steel ratio of $\rho_s = 0.377\%$ in terms of gross concrete area. At midspan of the slab, D10 bottom bars at 240 mm centres provided a reinforcement ratio of $\rho_s = 0.252\%$. Bearing in mind that the slab reinforcement was based on a nominal yield strength of $f_y = 275$ MPa, as is common in New Zealand, the above steel contents were comparable to the ratios of 0.3% and 0.2% respectively in terms of $f_y = 400$ MPa. Curtailment of the bars, as shown in Figs. 3.2(b) and 3.15(b), satisfied the NZS 3101 requirements.

(2) The Beams

As seen in Fig.3.2, beam depths were specified to be 550 mm in the east-west and 575 mm in the north-south direction. According to the details shown in Fig. 3.2(b), the internal lever arms in the two directions differ only by 1 mm. Hence the flexural strengths of the beams were nearly identical. As with Unit 1D-I (App.B.1) the largest diameter of longitudinal bar used was 24 mm. Thus, for the specified yield strength of $f_y = 275$ MPa, the embedment requirements of NZS 3101 [4] were satisfied.

As recommended in NZS 3101, the effective width of the slab, acting as a tension flange, in association with the beam in negative bending, was taken as $600 + 2 \times 4 \times 130 = 1640$ mm. Noting that only every second bottom bar in the slab passed through the transverse beam (Figs. 3.2(b) and 3.15(b)), a total of eight D10 slab bars were included in the evaluation of the negative flexural resistance of the beam sections. Hence the reinforcement ratios for the beams, using Grade 275 steel, were calculated as:

(top bars) ρ = 1.57% (N-S) or 1.58% (E-W) (or approximately 1.07% in terms of Grade 400 steel)

(bottom bars) ρ' = 0.73% (N-S) or 0.77% (E-W)

Thus $\rho' \approx 0.48\rho$

Alternatively, if all D10 slab bars (24 in total) were counted as part of the flexural tension reinforcement, ρ then became 2.40% (N-S) or 2.44% (E-W), which was about 55% larger than the values derived above from code procedure for flexural design.

For routine design purposes, with good approximation, the internal lever arm in flexure was taken as the distance between the centroids of the top and bottom groups of beam flexural bars. This was estimated to be 435 mm. The ideal (nominal) flexural strengths, based on f_y = 275 MPa, were computed according to Eq.(3.7) as

(-) M_i = 367 kNm and (+) M_i = 183 kNm

These values corresponded with dependable strengths for the prototype structure, with a strength reduction factor of ϕ = 0.9, of

(-) M_u = 330 kNm and (+) M_u = 237 kNm

The shear forces associated with these maximum moments were considered when designing the beam transverse reinforcement and the column reinforcement.

In the potential plastic hinging zones over 2 x 575 = 1150 mm length on the north and south sides of the column, 4 legs of R10 stirrup ties at 115 mm centres were required to resist the shear forces. This also satisfied the requirements of minimum tie spacing for confinement and bar stability purposes.

The design strength of the test unit, $V_{i(design)}$, based on specified material properties, was defined as the corresponding storey shear force when ideal beam flexural moments $(\pm)M_i$ were developed at the column faces. Hence

$$V_{i(design)} = \left(\frac{367 + 183}{1725}\right) \frac{2025}{3500} = 184.5 \text{ kN}$$

The dependable strength, V_{code}, became 0.9 x 184.5 = 166.1 kN. With an overstrength factor ϕ_o = 1.25/0.9 = 1.39, the storey shear was estimated as 1.39 x 166.1 = 230.9 kN.

(3) The Column

The largest longitudinal bar allowed [4] in the column was 28 mm diameter or 1/20th of beam depth, when Grade 380 steel was used.

The required ideal flexural strength of the column section was estimated from the beam overstrengths given in the previous section, and was to be due to a column shear force of $\phi_o V_{code}$ = 230.9 kN.

In accordance with the method described in Section 3.2 the minimum value of the dynamic moment magnification factor, ω, was taken as 1.5 (Eq.3.1). Thus the required ideal flexural strength of the column needed to be at least 1.5 (1.25/0.9) = 2.08 times that of the design earthquake moment M_{code} derived for this column. Alternatively by considering the diagonal flexural strength of a column section (see point 4 in Section 3.2), M_{code} should be magnified by a factor of 2.18. Accordingly, a reinforcement content of ρ_t = 1.58% was required.

It was suspected that, because of the larger participation of slab bars in tension flanges of beams, force input into columns, larger than those derived from the currently codified [4] procedure could result. Since column failure prior to joint failure was not desired, 12 HD28 vertical bars, giving ρ_t = 2.05%, were provided. This would correspond to ω = 1.83.

The test unit is representative of members close to the top of a multi-storey building where gravity induced axial loads on columns are rather small, but dynamic attack due to the contribution of higher modes of vibrations may be more significant. For this situation in a medium rise ductile frame the code [4] recommended value of the dynamic magnification factor would be of the order of 1.7.

The design shear force across the column was 1.6 x 230.9 = 369.4 kN. However, the transverse reinforcement in the end regions was governed essentially by confinement requirement.

(4) The Joint

From details of the beams the design horizontal joint shear force across the joint was assessed as

$$V_{jh} = 1.25(275)(3066.6 + 1533.1)10^{-3} - 230.9 = 1350 \text{ kN}$$

Hence the horizontal joint shear stress

$$v_{jh} = \frac{1350 \times 10^3}{600 \times 600} = 3.75 \text{ MPa} < 1.5\sqrt{f'_c} = 8.22 \text{ MPa}$$

Because of the absence of axial compression load on the column, horizontal joint shear reinforcement was required to resist the entire shear force, so that $V_{sh,\ required} = 1350$ kN. As seen in Fig. 3.2, four sets of R16 hoops were used. For each set of hoops, the number of effective tie legs across the joint was taken as $n = 4.8$. The shear force that the four sets could resist with specified yield strength $f_y = 275$ MPa was

$$V_{sh,\ provided} = 4(4.8)\ 201(275)10^{-3} = 1061 \text{ kN}$$

which was only 78.6% of the estimated maximum acting force. However, realising that the measured yield strength of R16 bars supplied was 330 MPa, the "realistic" shear resistance of the ties was

$$V_{sh,\ provided} = 1061 \times \frac{330}{275} = 1273 \text{ kN}$$

which was 94.3% of 1350 kN. This was considered acceptable.

Following the code recommendations for vertical joint shear, it was estimated that

$$V_{jv} \approx 1350\left(\frac{575}{600}\right) = 1294 \text{ kN}$$

The shear force assumed to be resisted by joint reinforcement was

$$V_{sv,required} = 0.4 \times 1294 = 518 \text{ kN}$$

The four HD28 intermediate vertical bars would provide

$$V_{sv,\ provided} = 4(615.8)(380)10^{-3}$$

$$= 936 \text{ kN} > 518 \text{ kN}.$$

C.2 Prediction of Strengths of Test Unit 2D-I

The ideal (nominal) flexural strengths of the T-beam sections are calculated for the various possible cases summarised in Fig.3.21 of Section 3.8.2. These strength properties and the corresponding theoretical forces, estimated on the basis of measured material properties reported in Section 3.3, are summarised in Tables C.1 to C.6 in a format similar to that used in Appendix B.3.

TABLE C.1 "NORTH-SOUTH" IDEAL BEAM STRENGTH PROPERTIES

(i) "Positive" Flexural Strength $(+)M_i$ (flange in compression)

Case	a	b	c	d	e	f
b_e (mm)	0	400	600	1200	1500	1800
$(+)M_i$(kNm)	192.6	242.7	256.8	280.7	284.5	289.5

(ii) "Negative" Flexural Strength $(-)M_i$ or M_i^* (flange in tension)

Case	g	h
b_e (mm)	1640	Full slab width
Moment (kNm)	$(-)M_i$ = 415.2	$(-)M_i^*$ = 517.4

(iii) Ideal Tip Forces For Prediction of Stiffness

SOUTH BEAM	NORTH BEAM	COLUMN
Case (g) (-) P_i = 240.1 kN Case (d) (+) P_i = 162.3 kN	Case (d) $(+)P_i$ = 162.9 kN Case (g) $(-)P_i$ = 241.0 kN	$(\pm)V_i$ = 233.3 kN

TABLE C.2 "EAST-WEST" IDEAL BEAM STRENGTH PROPERTIES

(i) "Positive" Flexural Strength $(+)M_i$ (flange in compression)

Case	a	b	c	d	e	f
b_e (mm)	0	400	600	1200	1500	1800
$(+)M_i$(kNm)	192.6	224.3	231.7	252.6	255.9	260.4

(ii) "Negative" Flexural Strength $(-)M_i$ or M_i^* (flange in tension)

Case	g	h
b_e (mm)	1640	Full slab width
Moment (kNm)	$(-)M_i$ = 415.2	$(-)M_i^*$ = 508.2

TABLE C.3 "NORTH-SOUTH" THEORETICAL STOREY SHEAR $(\pm)V_i$ or V_i^*

Beam Moment	+ve	-ve	+ve	-ve	+ve	-ve	+ve	-ve	+ve	-ve	+ve	-ve
Case	a	g	a	h	b	g	c	g	d	g	d	h
b_e (mm)	0	1640	0	FSW	400	1640	600	1640	1200	1640	1200	FSW
$(\pm)V_i$ or V_i^* (kN)	203.8		238.1		220.6		225.3		233.3		267.6	

Note: V_i from cases (d) & (g) is the reference shear plotted in the response diagrams.

FSW = full slab width

TABLE C.4 "EAST-WEST" THEORETICAL STOREY SHEAR $(\pm)V_i$ or V_i^*

Beam Moment	+ve	-ve	+ve	-ve	+ve	-ve	+ve	-ve	+ve	-ve	+ve	-ve
Case	a	g	a	h	b	g	c	g	d	g	d	h
b_e (mm)	0	1640	0	FSW	400	1640	600	1640	1200	1640	1200	FSW
$(\pm)V_i$ or V_i^* (kN)	202.9		234.9		213.6		216.0		223.3		255.0	

Note: V_i from cases (d) & (g) is the reference shear plotted in the response diagrams.

FSW = full slab width

TABLE C.5 "NORTH" BEAM THEORETICAL TIP FORCES BASED ON DIFFERENT ASSUMPTIONS

Case	a	b	c	d	g	h
b_e (mm)	0	400	600	1200	1640	FSW
(±)P_i(kN)	(+)111.8	(+)140.9	(+)149.0	(+)162.9	(-)241.0	(-)300.3

Note: "South" beam tip forces are slightly smaller because of longer as-constructed beam length, but the results are not shown here for brevity.

FSW = full slab width

TABLE C.6 "EAST" BEAM THEORETICAL TIP FORCES BASED ON DIFFERENT ASSUMPTIONS

Case	a	b	c	d	g	h
b_e (mm)	0	400	600	1200	1640	FSW
(±)P_i(kN)	(+)111.1	(+)129.4	(+)133.6	(+)145.7	(-)238.1	(-)293.1

Note: "West" beam tip forces are slightly larger due to shorter as-constructed beam length, but the results are not shown here for brevity.

C.3 Prediction of Stiffness of Unit 2D-I

(1) Deformations of the Beams

For the north beam, the end deflection is estimated by Eq.(3.22a) with $P_1 = 0.9\ (162.9) = 146.6$ kN, $\ell_1' = 1723$ mm, $E_c = 4700\sqrt{f_c'} = 28600$ MPa, $I_e = 4.57 \times 10^9$ mm^4 (Eq.3.13a), $f = 1$, $b_w = 400$ mm and $h_b = 575$ mm.

Hence $$\delta_{1,b} = 1.91 + 0.19 = 2.10 \text{ mm}$$

The end deflection of the south beam is from Eq.(3.22b) with $P_2 = 0.9(240.1) = 216.1$ kN, and $\ell_2' = 1729$ mm,

$$\delta_{2,b} = 2.85 + 0.28 = 3.13 \text{ mm}$$

The equivalent storey sway due to beam distortions only is assumed to be the average of $\delta_{1,b}$ and $\delta_{2,b}$. That is, from Eq.(3.23),

$$\Delta_{c,b} = \left[\frac{2.10 + 3.13}{2023 + 2029}\right] 3500 = 4.52 \text{ mm}$$

(2) Deformations of the Column

From Eq.(3.17) with $V_c = 0.9(122.3) = 210.0$ kN, $\ell_c' = 1475$ mm, $E_c = (28600 + 24600)/2 = 26600$ MPa, $I_e = 5.40 \times 10^9$ mm^4 (Eq.3.13b), $f = 1.2$, $b_c = 600$ mm, $h_c = 600$ mm,

$$\Delta_{c,c} = 3.13 + 0.39 = 3.52 \text{ mm}$$

(3) Total Deformation and Stiffness

Applying Eqs.(3.24) and (3.8),

$$\Delta_e = \Delta_y = 4.52 + 3.52 + 0.2\Delta_e$$

Hence $$\Delta_e = 10.1 \text{ mm}$$

With $V_c = V_{code} = 210.0$ kN, the theoretical stiffness, $K_{theoretical}$, of the test unit becomes thus

$$K_{theoretical} = \frac{210.0}{10.1} = 20.8 \text{ kN/mm}$$

With the alternative expression (Eq.3.14) for I_e,

(i) For the north beam, $I_e = 2.82 \times 10^9 mm^4$, $\delta_{1,b} = 3.29$ mm

(ii) For the south beam, $I_e = 3.58 \times 10^9 mm^4$, $\delta_{2,b} = 3.37$ mm

Hence $$\Delta_{c,b} = \left[\frac{3.11 + 3.37}{2023 + 2029} \right] 3500 = 5.60 \text{ mm}$$

For the column, with $I_e = 6.01 \times 10^9$ mm^4,

$$\Delta_{c,c} = 3.92 \text{ mm}$$

Allowing for joint distortion, the total equivalent storey (column) deflection is estimated as

$$\Delta_e = 12.3 \text{ mm}$$

The theoretical stiffness of the test unit is then

$$K_{theoretical} = \frac{210.0}{12.3} = 17.1 \text{ kN/mm}$$

This value is plotted and compared with observed value in Fig.5.8.

APPENDIX D

Calculations for Test Unit 2D-E

D.1 Design of Test Unit 2D-E

This unit was to simulate an exterior beam-column joint as part of the prototype two-way frame modelled by the 2D-I unit. Construction details are shown in Fig.3.3.

(1) The Slab

The required thickness of the slab, with one edge considered to be discontinuous, was 125 mm according to the stiffness criteria of NZS 3101 [4]. A 130 mm thick slab was adopted in conformity with the dimensions of Unit 2D-I. Layout of the N-S slab bars was identical to that of an interior slab. Thus the top layer D10 bars at 160 mm centres and bottom layer D10 bars at 240 mm centres (see also Fig. 3.16) provided reinforcement ratios of ρ_s = 0.377% and ρ_s = 0.252% respectively in terms of gross concrete area. At the west discontinuous edge (i.e. the N-S beams), a nominal amount of top flexural E-W reinforcement was required by the code. This turned out to be D10 hooked bars at 260 mm centres, giving a steel ratio of ρ_s = 0.232%. The bottom layer bars, D10 at 240 mm centres with ρ_s = 0.252% extended into the edge beams in compliance with the code requirements. Again, the above reinforcement contents were comparable to the ratios of 0.3% and 0.2% for the top and bottom layer bars respectively, in terms of higher strength steel of f_y = 400 MPa.

(2) The Beams

In recognition of the different loadings in two directions acting on an exterior bay, the beams were designed separately.

(i) East beam (550 x 400 mm)

The main bars of the east beam were identical to those in the E-W beams of Unit 2D-I, as explained in Section 3.2. From NZS 3101 [4], the width of floor slab acting as tension flange was taken as 500 + 2(2)130 = 1020 mm (Fig.3.21). Therefore one top layer slab bar and one bottom bar on each side of the beam stem should be included as part of the beam's "negative" top flexural reinforcement. In Fig.3.3(b), it can be seen that the bottom E-W slab bars extended into the edge beam by 260 mm. This is less than the code required minimum development length of 300 mm for deformed bars in tension. A designer would be expected to ignore the contribution of such bars.

Therefore in the computation of flexural strength of the east beam section, only the two top slab bars were considered effective. Hence the reinforcement ratios for the east beam, using grade 275 steel, were

(top bars) $\rho = 1.34\%$ (or 0.92% in terms of Grade 400 steel)

(bottom bars) $\rho' = 0.77\% \simeq 0.57\rho$

If all of the top layer D10 slab bars (12 in total) were assumed to be effective tension reinforcement, then ρ became 1.74%, an increase by nearly 30%.

The distance between the centroids of the top and bottom main bars of the beam was 434 mm. The approximate ideal (nominal) "seismic" flexural strength, with $f_y = 275$ MPa, were therefore

$(-)M_i = 310$ kNm and $(+)M_i = 183$ kNm

Applying a strength reduction factor of $\phi = 0.9$, the dependable strengths for the prototype structure were

$(-)M_u = 279$ kNm and $(+)M_u = 165$ kNm

If all the main bars in the beam and the 12 D10 top layer slab bars were stressed to $1.25\ f_y$, the flexural overstrength moments at the column face would increase to

$(-)M_o = 504$ kNm and $(+)M_o = 229$ kNm

It was seen that the flexural strengths were almost identical to those of the east-west beams of Unit 1D-I (App.B.1). The same arrangement of transverse reinforcement was therefore adopted for this unit.

The anchorage length provided for the bottom D24 bars of the east beam, considering the most critical case, was 461 mm measured from the east column face to the end of the 90° hook (Fig. 3.3(c)). The minimum development length estimated from the code (see also App.A) should be 442 mm. This requirement was therefore satisfied. The

"hook lengths" for the D24 and D20 bars are also shown in Fig. 3.3 (c).

(ii) North-south beams (575 x 300 mm)

The smaller column size, typical for all exterior columns, resulted in the beam bar diameter being limited to $d_b = h_c/25 = 20$ mm to satisfy code requirement. In evaluating the negative flexural strength, the effective overhanging part of the flange of the L-shaped N-S beam was assumed to be 125 + 4 x 130 = 645 mm. From Fig. 3.3(b), 3 top layer D10 slab bars and 1 bottom layer bar were within this effective area and therefore considered as part of the tension reinforcement.

The beam properties are summarised as follows:

(top bars) ρ = 1.30%
(bottom bars) ρ' = 1.03% $\simeq$ 0.79 ρ

With the internal lever arm approximated as 415 mm,

(-) M_i = 215 kNm and (+)M_i = 179 kNm
(-) M_u = 194 kNm and (+)M_u = 161 kNm

The alternative case considered all 9 top layer and 3 bottom layer slab bars stressed to 1.25 f_y in tension together with the beam main bars, in which case :

(-) M_o = 358 kNm and (+)M_o = 224 kNm

In the potential plastic hinging zones over 2 x 575 = 1150 mm length on the north and south sides of the column, 3 legs of R10 stirrup ties at 120 mm centres (i.e. 6 times the beam bar diameter) were required as transverse reinforcement according to the minimum tie spacing requirements for confinement and bar stability purposes. This reinforcement also provided sufficient resistance against the maximum beam shear forces.

(3) The Column

As is evident in Fig. 3.3, the column in the N-S direction is an interior column of an exterior frame, while in the E-W direction, it is an exterior column. Actions in both directions were therefore considered. For reasons as used for Unit 2D-I (App. C.1), HD28 bars were used as vertical reinforcement. The design procedures followed those for Unit 2D-I.

(i) Actions in the E-W direction

The storey shear shown at section 2-2 of Fig. 3.3 (a) was defined as positive when the beam was displaced upwards. However, in view of the larger negative flexural strength of the beam section (i.e. $-M_i > +M_i$), the associated negative shear force was taken as the critical case. The corresponding ideal column shear strength based on specified material properties was thus

$$(-)V_{i(design)} = \left(\frac{310}{1.75} \right) \frac{2025}{3500} = 102.5 \text{ kN}$$

The dependable strength became

$$(-)V_{code} = 0.9 \times 102.5 = 92.3 \text{ kN}$$

The corresponding column moment at beam centre line was

$$(-)M_{code} = 92.3 \times (3.5/2) = 161.5 \text{ kNm.}$$

Following the NZS 3101 [4] recommendations, the final design column moment at the critical section (i.e. beam face) to avoid hinge formation in the column, was estimated according to Eq.(3.1). Hence $(-)M_{col} = 302.9$ kNm. This value was smaller than the design N-S moment estimated in (ii) below.

(ii) Actions in the N-S direction

Using similar notation and procedure as in (i) above,

$$(\pm)V_{i(design)} = \left(\frac{215+179}{1.775} \right) \frac{2050}{3500} = 130.4 \text{ kN}$$

(±) V_{code} = 0.9 x 130.4 = 117.4 kN

(±) M_{code} = 117.4 x (3.5/2) = 205.5 kN

(±) M_{col} = 383.4 kNm

It was found that a reinforcement content of ρ_t = 1.91% was required. Similar to the design for Unit 2D-I, it was considered necessary to make allowance for the larger resistance which would result from the action of all slab bars in tension. From practical considerations, 12 HD28 vertical bars (ρ_t = 2.69%) were adopted.

The design shear force across the column was V_{col} = 1.6x1.39x117.4 = 261.1 kN in the N-S direction. Transverse reinforcement was controlled by the minimum bar spacing requirement for confinement of concrete rather than shear.

The design of this column was somewhat unrealistic because, to represent the test situation, no axial load on the column was considered. In the real structures some axial compression would be expected and hence the required reinforcement content in prototype columns would probably be less than that used in these tests.

(4) The Joint

(i) For loading in the E-W direction

The joint in this directions acted as an exterior joint with shear input from the east beam only. The larger design horizontal shear across the joint was estimated as

$$V_{jh} = 1.25(275)(1810+628.3+157.1)10^{-3} - 1.39x92.3 = 763.9 \text{ kN}$$
$$= V_{sh,required}$$

With the arrangement of joint reinforcement shown in Fig. 3.3(c), the contribution of the joint ties was estimated as follows :

- Circumferential R16 ties $6x201x275x10^{-3} = 332$ kN

- Intermediate R12 ties $6x113x275x10^{-3} = 186$ kN

- Intermediate R16 ties $8x\frac{170}{470}x201x275x10^{-3} = 160$ kN

Total $V_{sh,provided} = 678$ kN

Thus $V_{sh,provided}$ was only 88.8% of $V_{sh,required}$. On the other hand, adopting the measured rather than specified strength of the steel bars supplied (see Table 3.5), the shear joint resistance of the ties became $V_{sh,provided} = 807$ kN > 763.9 kN.

(ii) For loading in the N-S direction

For this loading, horizontal reinforcement was to be provided as for an interior joint. The joint shear should be

$$V_{jh} = 1.25(275)(1884.9+1570.8)10^{-3} - 1.25\ (117.4) = 1041.1 \text{ kN}$$

The contribution of the joint ties shown in Fig. 3.3(c) was

- Circumferential R16 ties $6 \times 201 \times 275 \times 10^{-3} = 332$ kN

- Intermediate R12 ties $6\left(\frac{226}{420}\right)113 \times 275 \times 10^{-3} = 100$ kN

- Intermediate R16 ties $8 \times 201 \times 275 \times 10^{-3} = 442$ kN

Total $V_{sh,provided} = 874$ kN

This was only 83.9% of $V_{sh,required}$. Considering the measured steel properties, the shear resistance of the ties increased to $V_{sh,provided} = 1046$ kN > 1041.1 kN.

The vertical joint shear was estimated, following the code [4] recommendations, as

$$V_{jv} \simeq 1041.1 \times \frac{575}{500} = 1197 \text{ kN}$$

Vertical reinforcement was assumed to carry 40% of the shear force. Therefore

$$V_{sv,required} = 0.4 \times 1197 = 479 \text{ kN}$$

The four HD28 intermediate vertical bars would provide

$$V_{sv,provided} = 4(615.8)(380)10^{-3} = 936 \text{ kN} > 479 \text{ kN}$$

D.2 Prediction of Strengths of Test Unit 2D-E

As for Unit 2D-I (App.C.2), the ideal strength properties and the corresponding theoretical forces for Unit 2D-E are calculated for the various possible cases shown in Fig.3.21. The results are summarised in Tables D.1 to D.6.

TABLE D.1 "EAST" IDEAL BEAM STRENGTH PROPERTIES

(i) "Positive" Flexural Strength $(+)M_i$ (flange in compression)

Case	a	b	c	d	e
b_e (mm)	0	400	500	1000	1500
$(+)M_i$ (kNm)	190.9	228.0	232.4	251.5	257.3

(ii) "Negative" Flexural Strength $(-)M_i$ or M_i^* (flange in tension)

Case	g	h
b_e (mm)	1020	Full slab width
Moment (kNm)	$(-)M_i$ = 346.7	$(-)M_i^*$ = 468.5

(iii) Ideal Tip Forces for Prediction of Stiffness

EAST BEAM	COLUMN
Case (d) (+) P_i = 143.8 kN	(+) V_i = 83.2 kN
Case (g) (-) P_i = 198.2 kN	(-) V_i = 114.6 kN

TABLE D.2 "NORTH-SOUTH" IDEAL BEAM STRENGTH PROPERTIES

(i) "Positive" Flexural Strength $(+)M_i$ (flange in compression)

Case	a	b	c	d	e	f
b_e (mm)	0	300	425	700	800	975
$(+)M_i$ (kNm)	191.4	242.8	252.3	268.2	270.2	272.9

(ii) "Negative" Flexural Strength $(-)M_i$ or M_i^* (flange in tension)

Case	g	h
b_e (mm)	945	Full slab width
Moment (kNm)	$(-)M_i$ = 275.5	$(-)M_i^*$ = 328.4

TABLE D.3 "EAST-WEST" THEORETICAL STOREY SHEAR (±) V_i or V_i^*

Beam Moment	+ve	+ve	+ve	+ve	-ve	-ve
Case	a	b	c	d	g	h
b_e (mm)	0	400	500	1000	1020	FSW
$(\pm)V_i$ or V_i^* (kN)	(+) 63.1	(+)75.4	(+)76.8	(+)83.2	(-)114.6	(-)154.9

Notes: $(+)V_i$ from case (d) is the reference positive shear plotted in the response diagrams, while $(-)V_i$ from case (g) is the theoretical negative shear used for reference in the response diagrams and for determination of stiffness.

FSW = full slab width

TABLE D.4 "EAST" BEAM THEORETICAL TIP FORCES BASED ON DIFFERENT ASSUMPTIONS

Case	a	b	c	d	g	h
b_e (mm)	0	400	550	1100	1020	FSW
$(\pm)P_i$(kN)	(+)109.1	(+)130.3	(+)132.9	(+)143.8	(-)198.2	(-)267.8

FSW = full slab width

TABLE D.5 "NORTH-SOUTH" THEORETICAL STOREY SHEAR $(\pm)V_i$ or V_i^*

Beam Moment	+ve	-ve	+ve	-ve	+ve	-ve	+ve	-ve	+ve	-ve	+ve	-ve
Case	a	g	a	h	b	g	c	g	d	g	d	h
b_e (mm)	0	945	0	FSW	300	945	425	945	700	945	700	FSW
$(\pm)V_i$ or V_i^*(kN)	152.2		169.4		168.9		172.0		177.2		194.4	

Note: V_i from cases (d) & (g) is the reference shear plotted in the response diagrams.

FSW = full slab width

TABLE D.6 "NORTH" BEAM THEORETICAL TIP FORCES BASED ON DIFFERENT ASSUMPTIONS

Case	a	b	c	d	g	h
b_e (mm)	0	300	425	700	945	FSW
$(\pm)P_i$(kN)	(+)107.4	(+)136.2	(+)141.5	(+)150.4	(-)154.5	(-)184.2

Notes: "South" beam tip loads are slightly larger due to shorter as-constructed beam length, but the results are not shown here for brevity.

FSW = full slab width

D.3 Prediction of Stiffness of Unit 2D-E

For testing purposes, the theoretical stiffness in the east-west direction, when the east beam is displaced downwards, is taken as reference.

(1) Deformations of the East Beam

Applying Eq.(3.22a) with, $P_1 = 0.9(198.2) = 178.4$ kN, $\ell_1' = 1750$ mm, $E_c = 4700\sqrt{f_c'} = 32460$ MPa, $I_e = 4.01 \times 10^9$ mm^4 (Eq.3.13a), f = 1, $b_w = 400$ mm, and $h_b = 550$ mm,

$$\delta_{1,b} = 2.44 + 0.22 = 2.66 \text{ mm}$$

The equivalent storey sway due to beam distortions is, from Eq.(3.23),

$$\Delta_{c,b} = \left(\frac{2.66}{2025}\right) 3500 = 4.60 \text{ mm}$$

(2) Deformations of the Column

From Eq.(3.17) with $V_c = 0.9(114.6) = 103.1$ kN, $\ell_c' = 1475$ mm, $E_c = (32460 + 30680)/2 = 31570$ MPa, $I_e = 3.47 \times 10^9$ mm^4 (Eq.3.13b), f = 1.2, $b_c = 550$ mm, and $h_c = 500$ mm,

$$\Delta_{c,c} = 2.02 + 0.21 = 2.23 \text{ mm}$$

(3) Total Deformation and Stiffness

Applying Eqs.(3.24) and (3.8),

$$\Delta_e = \Delta_y = 4.60 + 2.23 + 0.2\Delta_c$$

Hence $$\Delta_e = 8.5 \text{ mm}$$

With $V_c = V_{code} = 103.1$ kN, the theoretical stiffness, $K_{theoretical}$, of the test unit becomes

$$K_{theoretical} = \frac{103.1}{8.5} = 12.1 \text{ kN/mm}$$

With Eq.(3.14), considered to be more accurate for I_e, the estimated deflection components are revised as follows :

For the east beam, $I_e = 3.10 \times 10^9 mm^4$, $\delta_{1,b} = 3.38$ mm

and hence $$\Delta_{c,b} = \left[\frac{3.38}{2025}\right] 3500 = 5.84 \text{ mm}$$

For the column, $I_e = 4.60 \times 10^9 \text{ mm}^4$,

therefore $\Delta_{c,c} = 1.80$ mm

Allowing for joint distortion, the total equivalent storey (column) deflection is estimated as

$$\Delta_e = 9.6 \text{ mm}$$

The theoretical stiffness of the test unit is then

$$K_{theoretical} = \frac{103.1}{8.6} = 10.7 \text{ kN/mm}$$

This latter value is plotted and compared with observed value in Fig. 6.9.

CORRIGENDA

p.xvi	11 lines down [Ref.14] - insert "June 1978," between "No.2," and "pp."
p.xvii	20 lines up [Ref.31] - the line should read as follows :
	(ACI 318-71)", American Concrete Institute, Detroit, 1971, 78 pp.
p.xviii	8 lines down [Ref. 40] - "s." -> "S."
p.xix	21 lines down [Ref. 56] - "committee" -> "Committee"
p.5	8 lines down - "eleastic" -> "elastic"
p.7	3 lines down - "disspation" -> "dissipation"
p.10	6 lines down - "repeated" -> "reversing"
p.14	13 lines up - "(1977)" -> "(1971)"
p.15	16 lines down - insert "and" between "NZS 3101 [4]" and "ACI-ASCE 352 [28]"
	1 line up - "can be" -> "was"
p.29	1 line down - "core" -> "concrete"
p.45	16 lines down - "Eq.(2.5)" -> "Eq.(2.4)"
p.61	Table 3.1 - the reinforcement ratios for joints should be as follows :
	(Unit 1D-I) "1.62%" -> "1.86%"
	(Unit 2D-I) "1.62%" -> "1.71%"
	(Unit 2D-E) "1.25%" -> "1.31" and "1.66%" -> "1.72%"
p.94	3 lines up - "whatever" -> "whether"
p.111	7 lines down - insert "(Fig.1.2)" after "Δ_y"
p.120	6,7,11 and 13 lines down - "Eqs.(3.28a) and (3.28b)" -> "Eqs.(3.29a) and (3.29b)"
p.160	12 lines up - ",hence" -> ".Hence"
p.231	14 lines down - "paragraph attempts" -> "paragraphs attempt"
p.267	8 lines down - "Fig.7.6(b)" -> "Fig.7.6(c)"
p.270	6 lines down - "Fig.7.8" -> "Fig.7.9"
	12 lines down - insert "west" between "the" and "beam"
p.273	4 lines down - "therefore" -> "Therefore"
	4 lines up - "Fig.11(e)" -> "Fig.7.11(e)"
p.282	4 lines down - "the" -> "The"
p.287	6 lines down - "mechanisms" -> "mechanism"
p.288	14 lines up - "theoretrical" -> "theoretical"
	7 lines up - "7.19" -> "7.18"
p.302	6 lines up - "slip" -> "slips"
	4 lines up - "was" -> "were"
p.319	1 line down - "coform" -> "conform"

ADDENDUM

The layout of this thesis is such that the reader may get acquainted with various aspects of beam-column joint problems from Chapters 1 and 2 before proceeding to Chapters 3 through 6 which report on the experimental work. In Chapter 2 especially in Sections 2.3.3 and 2.3.4, some new ideas on the behavioural models for joints are developed. These concepts are further elaborated in Chapter 8, resulting in a set of design recommendations. Some readers may find it more convenient to read Sections 2.3.3 and 2.3.4 in conjunction with Chapter 8.